

Fragment-based discovery of HSP70 inhibitors

Suzanne O'Connor

Medicinal Chemistry, Cancer Research UK Cancer Therapeutics Unit
The Institute of Cancer Research
University of London

This thesis is submitted as partial fulfilment of the
requirements for the degree of Doctor of Philosophy.

July 2020



Declaration

To the best of my knowledge the research presented in this thesis is original unless otherwise indicated in the text or references.

This thesis has not been submitted, whether in whole or part, for a degree at this or any other university or institution.

Suzanne O'Connor

July 2020

Acknowledgments

Firstly, I would like to thank my supervisors Ian Collins, John Caldwell and Rob van Montfort for the opportunity to carry out my PhD at the Institute of Cancer Research and for all your guidance, feedback, encouragement and support over the last four years.

I am extremely grateful to the Mair and Franklyn Research Scholarship whose generous donation has funded this PhD.

Thank you to everyone in the Department of Chemistry and the Department of Cancer Therapeutics who has helped me to learn so many new techniques during my time at the ICR. To Martin Rowlands and Jemima Thomas for sharing your SPR expertise. To Mike Carter for helpful computational chemistry instruction. To Craig McAndrew for protein synthesis. To the Structural Chemistry team Maggie Liu, Meirion Richards, Joe Smith and Amin Mirza for your kind advice and assistance. A special thanks to Marc Cabry and Yann-Vaï Le Bihan who solved so many X-ray crystal structures that helped to shape the project and for their contribution to valuable discussions.

I am thankful for a successful collaboration with Atomwise and Jóhannes Reynisson's group at the University of Auckland including Oi Wei Mak and Raina Chand.

I would also like to thank everyone from the Collins' group, past and present for their guidance and encouragement. The ICR has been a fantastic place to learn and I have enjoyed working with you all.

I am grateful to my family and friends, especially my parents, who have always supported me.

To Ashley, for your love and support and willingness for adventures.

Abstract

Heat Shock Protein 70s (HSP70s) are key molecular chaperones that are overexpressed in many cancers and are often associated with metastasis and poor prognosis. Dual silencing of two isoforms, HSP72 and HSC70, using siRNA has shown tumour specific apoptosis. However, it has proved difficult to develop drug-like small molecule inhibitors of HSP70s by traditional methods due to the flexible and hydrophilic nature of the ATP binding site and its high affinity for natural nucleotides. The aim of this work was to identify novel inhibitors of HSP70 using fragment-based drug discovery methods in two parallel approaches.

The first approach focused on the validation of a cryptic, secondary binding site in HSP70 that had been identified by a fragment screen. Multiple methods were used for fragment validation including the synthesis of more soluble fragment analogues and subsequent testing by Surface Plasmon Resonance (SPR). Ligand-observed NMR was used as an orthogonal method to successfully confirm binding. A virtual high-throughput screen against this novel site was carried out by our collaborators to find new hit matter. These compounds were tested by SPR and 11 new fragment hits were identified. As the properties of this novel binding site in HSP70 differ from the ATP binding site it may offer the opportunity to develop inhibitors of HSP70 with better physicochemical properties.

The second approach focused on the development of a quinazoline hit fragment that binds in the ATP binding site of HSP70. Non-nucleotide inhibitors were designed and observed to bind in the phosphate binding region for the first time. Replacement of the quinazoline ring with a naphthyridine, cinnoline, quinoline and pyrimidine cores was also investigated as well as various substitutions around the quinazoline ring. As well as increasing the potency of the quinazoline hit, these compounds have improved our understanding of the nature and flexibility of the ATP binding pocket of HSP70.

Statement of Independent Work

All work in this thesis was carried out by myself except where indicated, work has been carried out by collaborators. The protein was synthesised and purified by Craig McAndrew, X-ray crystal structures were solved by Marc Cabry and Yann-Vaï Le Bihan and QuickShot MS experiments were run by Meirion Richards. The trypsin digest mass spectrometry work was carried out by Fingerprints Proteomics Facility in Dundee. The virtual high throughput screens were run by Atomwise and Jóhannes Reynisson's team at the University of Auckland, Oi Wei Mak and Raina Chand.

Abbreviations

°C	Degrees Celsius
Å	Angstrom
Ac	Acetyl
ADP	Adenosine diphosphate
AIF	Apoptosis inducing factor
ALL	Acute lymphocytic leukemia
Ask-1	Apoptosis signal related kinase 1
atm	Atmospheres
ATP	Adenosine triphosphate
BAG-1	BCL2 associated athanogene 1
Boc	<i>tert</i> -Butyloxycarbonyl
BINAP	2,2'-Bis(diphenylphosphino)-1,1'-binaphthyl
Cbz	Benzyloxycarbonyl
CDI	1,1'-Carbonyldiimidazole
CHIP	C-terminus of HSP70 interacting protein
CML	Chronic myelogenous leukemia
COSY	Correlation spectroscopy
CV	Column volume
Da	Dalton
DBU	1,8-Diazabicyclo[5.4.0]undec-7-ene
DCM	Dichloromethane
DIPEA	<i>N,N</i> -Diisopropylethylamine
DMF	Dimethylformamide
DMSO	Dimethyl sulfoxide
DNA	Deoxyribonucleic acid
EDC	1-Ethyl-3-(3-dimethylaminopropyl)carbodiimide
EGFR	Epidermal growth factor receptor
ER	Endoplasmic reticulum
ESI	Electrospray ionisation
Et	Ethyl
EtOH	Ethanol

Eq	Equivalent
FBDD	Fragment Based Drug Discovery
g	Gram
GRP78	78 kDa glucose-regulated protein
h	Hours
HATU	Hexafluorophosphate azabenzotriazole tetramethyl uranium
HIP	HSP70 interacting protein
HMBC	Heteronuclear multiple-bond correlation spectroscopy
HOP	Heat shock organising protein
HPLC	High-performance liquid chromatography
HRMS	High-resolution mass spectrometry
HSC70	Heat shock cognate 71 kDa protein
HSE	Heat shock elements
HSF1	Heat shock factor 1
HSP	Heat shock protein
HSP72	Heat shock 70 kDa protein 1
HSQC	Heteronuclear single-quantum correlation spectroscopy
HTS	High-throughput screen
IPA	Isopropyl alcohol
IR	Infrared
ITC	Isothermal titration calorimetry
K_D	Dissociation constant
K-RAS	Kirsten rat sarcoma viral oncogene homolog
L	Litre
LE	Ligand efficiency
LLE	Lipophilic ligand efficiency
LC-MS	Liquid chromatography-mass spectrometry
M	Molar
m	Milli
<i>m</i>	Meta
m/z	Mass-to-charge ratio
Me	Methyl
MHz	Megahertz

MeOH	Methanol
min	Minute
mp	Melting point
MS	Mass spectrometry
MW	Microwave
Mw	Molecular weight
nm	Nanometre
NBD	Nucleotide-binding domain
NEF	Nucleotide-exchange factor
NHS	<i>N</i> -hydroxy succinimide
NMP	<i>N</i> -Methyl-2-pyrrolidone
NMR	Nuclear magnetic resonance
NOESY	Nuclear Overhauser effect spectroscopy
<i>o</i>	<i>Ortho</i>
<i>p</i>	<i>Para</i>
PES	2-Phenylethynesulfonamide
Ph	Phenyl
Pi	Inorganic phosphate
proMMP-9	pro matrix metalloproteinase 9
Py	Pyridine
PyBOP	Benzotriazol-1-yl-oxytripyrrolidinophosphonium hexafluorophosphate
pTSA	<i>p</i> -Toluenesulfonic acid
RNA	Ribonucleic acid
RPM	Revolutions per minute
rt	Room temperature
RU	Response units
s	Second
SAR	Structure-activity relationship
SBD	Substrate-binding domain
SBDD	Structure based drug design
Ser	Serine
siRNA	Small interfering RNA

SM	Starting material
S _N Ar	Nucleophilic aromatic substitution
SPhos	2-Dicyclohexylphosphino-2',6'-dimethoxybiphenyl
SPR	Surface Plasmon Resonance
t _{1/2}	Half-life
TEA	Triethylamine
THF	Tetrahydrofuran
TLC	Thin-layer chromatography
ToF	Time-of-flight
TPR	tetratricopeptide repeat
t _R	Retention time
Tr	Truncated
TRIS	Tris(hydroxymethyl)aminomethane
UV	Ultraviolet
vHTS	Virtual high-throughput screen
v/v	Volume per volume
W	Tryptophan
WT	Wild-type
w/v	Weight per volume
μ	Micro

Table of Contents

1	Introduction.....	1
1.1	The burden of cancer.....	1
1.2	The hallmarks of cancer.....	2
1.3	Cancer treatment.....	4
1.3.1	Traditional treatment.....	4
1.3.2	Targeted oncology medicine.....	6
1.4	The heat shock response.....	8
1.5	Heat Shock Protein 70.....	11
1.5.1	HSP70 forms and function.....	11
1.5.2	HSP70 structure.....	14
1.5.3	The role of HSP70 in cancer.....	18
1.5.4	HSP70 inhibition.....	19
1.6	Fragment Based Drug Discovery.....	28
1.7	Hypothesis and Aims.....	34
2	Discovery and validation of a cryptic secondary binding site in HSP70... 36	
2.1	Discovery of a novel binding site in HSP70.....	36
2.2	Cryptic pockets.....	40
2.3	Surface plasmon resonance.....	41
2.4	Validation of the secondary binding site.....	44
2.4.1	Design of Library 1.....	44
2.4.2	Synthesis of Library 1.....	45
2.4.3	Testing of Library 1 by SPR.....	59
2.4.4	Design of Library 2.....	62
2.4.5	Synthesis of Library 2.....	64
2.4.6	Testing of library 2 by SPR.....	72
2.5	Conclusions.....	77
3	Validation of the secondary binding site hits by orthogonal methods.....	79
3.1	Introduction to Ligand-Observed NMR.....	79
3.1.1	CPMG experiments.....	81
3.1.2	WaterLOGSY experiments.....	81
3.2	Hypothesis – the ATP binding site does not exist at the same time as the secondary binding site.....	82
3.3	Testing of fragment hits by Ligand-Observed NMR.....	85

3.3.1	CPMG	85
3.3.2	WaterLOGSY	88
3.4	Introduction to photoaffinity labelling.....	89
3.5	Photoaffinity labelling studies.....	91
3.5.1	Design of a photolabile fragment.....	91
3.5.2	Synthesis of a photolabile fragment	91
3.5.3	Testing of a photolabile fragment by SPR	93
3.5.4	Photoaffinity labelling experiments with HSP72	95
3.5.5	Sequencing of labelled HSP72.....	99
3.5.6	Conclusions from photoaffinity labelling experiments.....	105
3.6	Summary of fragment validation	105
3.7	vHTS screening against the secondary binding site	106
3.7.1	Testing of virtual hits by SPR	108
3.7.2	Conclusions from the vHTS screens and future work.....	123
4	Exploration of the phosphate binding region of HSP70 using structure-based drug design.....	127
4.1	Structure-based drug design.....	127
4.2	Previous work on quinazoline ATP binding site inhibitors	129
4.3	Quinazolines in medicinal chemistry.....	135
4.4	Quinazoline synthesis.....	136
4.5	Targeting the phosphate binding region	137
4.6	Design of hydroxyacetamide analogues	139
4.6.1	Previous work on quinazoline synthesis.....	140
4.6.2	Synthesis of hydroxyacetamides	142
4.6.3	Determination of the major side product by NMR.....	148
4.6.4	Design of an alternative route to hydroxyacetamide 238	152
4.6.5	Testing of hydroxyacetamides by SPR.....	156
4.6.6	Conformational changes observed by X-ray Crystallography....	157
4.7	Library of substituted hydroxyacetamides.....	160
4.7.1	Design and conformational analysis.....	160
4.7.2	Synthesis to explore the phosphate binding region	165
4.7.3	SPR testing of new hydroxyacetamide analogues	169
4.8	Conclusions	175
5	Exploration of the quinazoline fragment hit.....	179
5.1	Previous published and unpublished work.....	179

5.2	Replacement of the quinazoline ring.....	181
5.2.1	Design of quinazoline replacements.....	181
5.2.2	Synthesis of quinazoline replacements	185
5.3	Substitution at the 5 position.....	194
5.3.1	Design at the 5 position.....	194
5.3.2	Synthesis at the 5 position	197
5.3.3	SPR testing of 5 substituted quinazolines	205
5.4	Substitution at the 7 position.....	207
5.4.1	Design at the 7 position.....	207
5.4.2	Synthesis at the 7 position	208
5.4.3	SPR testing of 7-substituted quinazolines.....	211
5.5	Substitution at the 6 position.....	212
5.5.1	Design and synthesis at the 6 position	212
5.5.2	SPR testing and X-ray crystallography.....	214
5.5.3	Analogues of the 6-methyl pyrazole and 6-phenyl quinazolines	215
5.5.4	Extension of 6-methyl pyrazole and 6-phenyl quinazolines	218
5.5.5	Novel analogues at the 6 position	223
5.5.6	Methyl sulfone analogues.....	226
5.6	6-substituted quinazolines with a hydroxyacetamide motif	229
5.6.1	SPR testing of compounds 427 and 428	232
5.7	Conclusions	233
5.8	Thesis conclusion	235
5.9	Future Work.....	237
6	Experimental	244
6.1	Synthetic chemistry.....	244
6.1.1	General methods.....	244
6.1.2	Synthesis.....	247
6.2	Biological Evaluation.....	391
6.2.1	Ligand Observed NMR experiments	391
6.2.2	Photoaffinity Labelling Experiments	391
6.2.3	QuickShot analysis of HSP72-NBD.....	392
6.2.4	SPR experiments	393
7	Appendix.....	396
8	References.....	405

Chapter 1

1 Introduction

1.1 The burden of cancer

Globally, it's estimated that 100 million people around the world had a form of cancer in 2017.¹ This number has more than doubled since 1990 when an estimated 45 million had cancer. In the UK, one in two people will get cancer in their lifetime.²

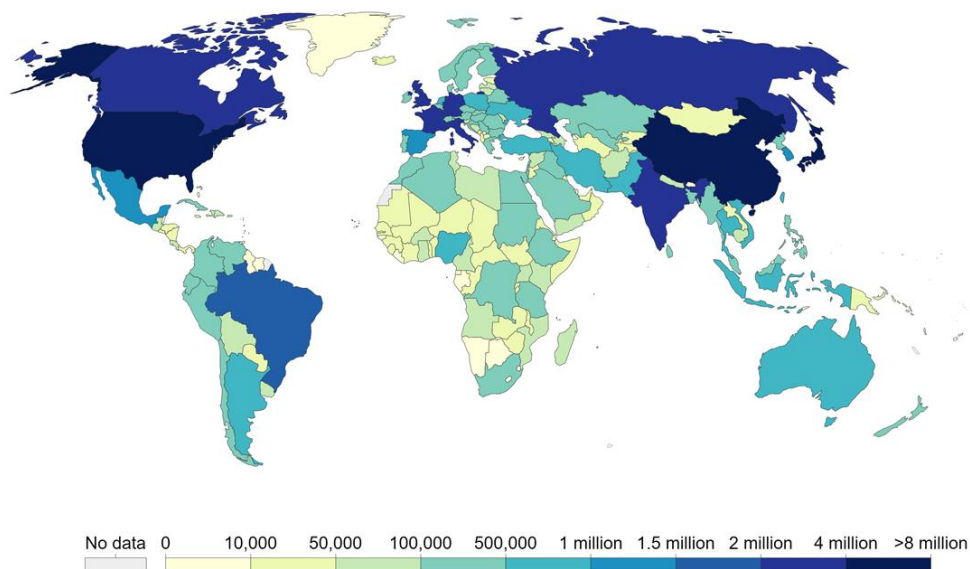


Figure 1.1 – The number of people suffering with any type of cancer in 2017, measured across both sexes and all ages. Reproduced from Our World in Data.³

Cancer is an enormous global health burden and this burden is expected to increase due to the growth and aging of the world's population as well as causes linked with social and economic development.⁴ Today cancer accounts for one in every seven deaths worldwide.⁵ Although cancer is a worldwide problem there is a higher prevalence in higher income countries (Figure 1.1).

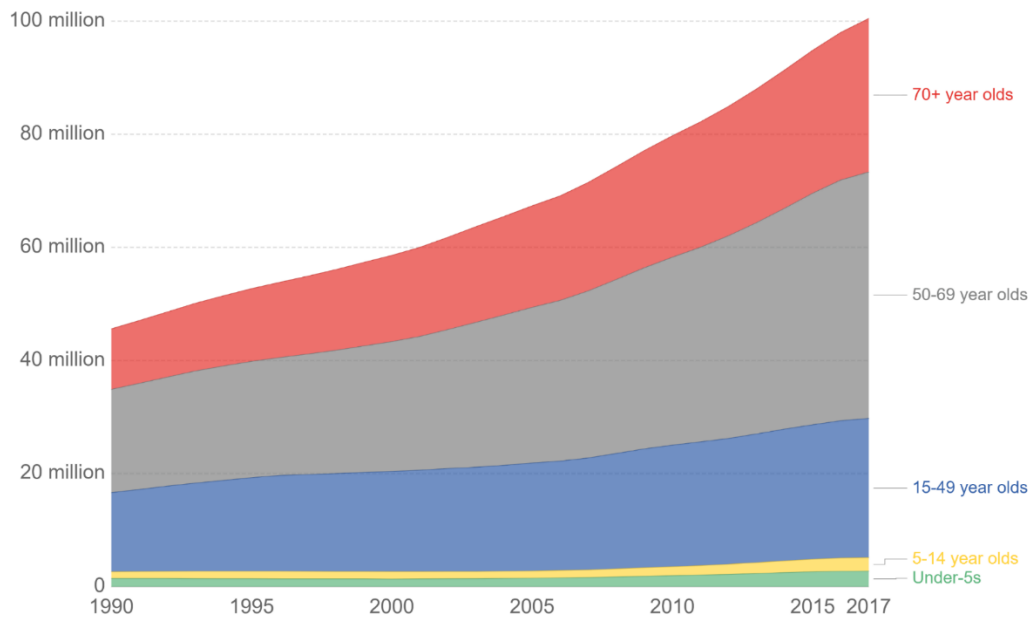


Figure 1.2 – The number of people in the world with cancer by age. Reproduced from Our World in Data.¹

There are more than 200 different types of cancer⁶ and the majority of cancers occur in those aged 50 and over (Figure 1.2). Although the number of people with cancer is increasing, people are much more likely now to survive four of the most common cancer types – lung, colorectal, breast and prostate than they were two decades ago.⁵

1.2 The hallmarks of cancer

Cancer can most simply be described as uncontrolled cell growth. Most cancers are due to genetic changes that occur over a lifetime but these genes can also be inherited. There are five main cancer groups according to the type of cell they start from: carcinomas, lymphomas, leukaemias, brain tumours and sarcomas.⁷

Almost 50 years ago two families of genes were identified, proto-oncogenes and tumour suppressor genes, that regulate cell growth and cell death in healthy cells. Proto-oncogenes can mutate into oncogenes which code for oncoproteins

- faulty proteins that lead to uncontrolled growth and differentiation. Tumour suppressor genes code for proteins that negatively regulate cell proliferation. Mutation of these genes also leads to uncontrolled growth and proliferation.

The hallmarks of cancer, originally proposed by Hanahan and Weinburg in 2000, are the biological capabilities normal cells acquire as they evolve into cancerous cells.⁸ Despite the vast number of cancer cell genotypes, the authors proposed that this complexity could be better understood with the knowledge of the underlying principles. The original six hallmarks are self-sufficiency in growth signals, insensitivity to anti-growth signals, evading apoptosis, limitless replicative potential, sustained angiogenesis, and tissue invasion and metastasis. Recently the authors have added two new emerging hallmark capabilities: avoiding immune destruction and deregulating cellular energetics; and two new enabling characteristics: genome instability and mutation, and tumour-promoting inflammation (Figure 1.3).⁹

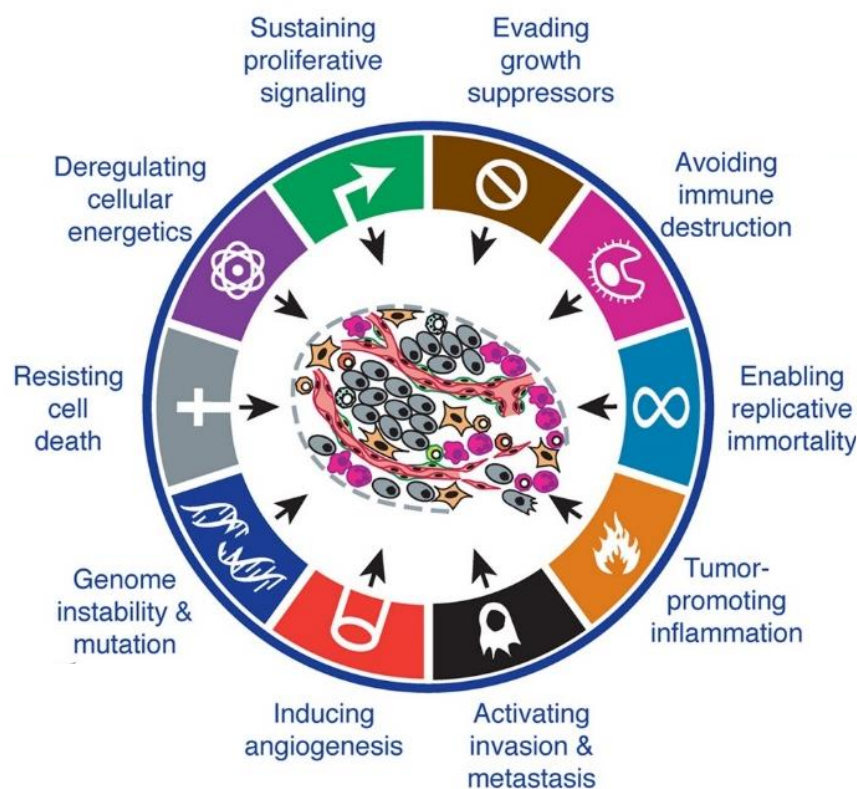


Figure 1.3 – The hallmarks of cancer, proposed by Hanahan and Weinburg. Reproduced from Hanahan *et al.*⁹

1.3 Cancer treatment

1.3.1 Traditional treatment

Cancer appears in medical history as early as 1600 BC in the Edwin Smith papyrus, where the oldest description of the illness exists. Surgery has been the most effective cancer treatment since ancient times, with reports of the use of surgical operations for the excision of cancerous growths going back two thousand years.¹⁰

Shortly after Roentgen's discovery of X-rays in 1895, radiation therapy was found to be a new effective treatment and particularly important when surgery was not an option.¹¹ Ionising radiation damages DNA leading to cell death. Care must be taken to limit the exposure of healthy tissue to this ionising radiation as it does not distinguish between healthy and cancerous cells. This can be done by aiming radiation beams from several different angles. Radiation therapy alone can be curative if the cancer is localised in one area of the body or it can be used synergistically with surgery or chemotherapy.

Chemotherapy has routinely been used in cancer treatment since the 1940s.¹² The premise of chemotherapy is to apply cytotoxic agents that target rapidly dividing cells. Although it can be highly effective this also means chemotherapy kills healthy rapidly dividing cells, such as those in the bone marrow, which results in serious side effects. Chemotherapeutic agents have varying modes of action, some of the most important of which are briefly described below (Figure 1.4).

DNA alkylation

The first chemotherapy drug to be used, mustine, is in the family of nitrogen mustards.¹³ These DNA alkylating agents can form interstrand cross-links leading to cytotoxicity. Platinum complexes such as cisplatin and analogues are also DNA alkylating agents. Their cytotoxicity is thought to be due to the

formation of DNA-platinum adducts which can form crosslinks between bases in the same or opposite strands.

Anti-metabolites

Antifolate drugs such as methotrexate were the first class of antimetabolites to enter the clinic.¹⁴ These compounds resemble folic acid and have a high affinity for the enzyme dihydrofolate reductase which has an important role in thymidine and purine biosynthesis. Inhibition of this enzyme therefore inhibits DNA synthesis.

Microtubule targeting agents

Microtubules are dynamic structures involved in many cellular processes such as maintenance of cell structure, protein transport and mitosis. Microtubule-targeting agents such as the vinca alkaloids and taxanes exert their chemotherapeutic effect by interrupting microtubule function and therefore inhibition of mitosis.¹⁵

Inhibition of Topoisomerase 1

Camptothecin and its analogues have been found to inhibit the enzyme Topoisomerase I, which promotes relaxation of supercoiled DNA by creating single strand breaks, allowing it to unwind prior to transcription.¹⁶ Camptothecin binds to the Topoisomerase I–DNA complex stabilizing it and preventing the religation of the DNA strand.

Hormone therapy

Hormone therapy can be used to inhibit the binding of natural endogenous ligands with their receptors. Steroid hormones are powerful drivers of gene expression in certain cancer cells and changing the levels or activity of a particular hormone can therefore cause that cancer to cease growing or even undergo cell death.

Phosphorylation of target proteins by kinases is tightly regulated and any perturbation to this regulation may lead to a diseased state. Imatinib is a kinase inhibitor used for chronic myelogenous leukemia (CML) and acute lymphocytic leukemia (ALL) that are Philadelphia chromosome-positive (Ph⁺).¹⁸ The Philadelphia chromosome leads to a fusion protein of *abl* with *bcr*, termed *bcr-abl*, which is a constitutively active tyrosine kinase. Imatinib is used to target *bcr-abl* and decrease its activity. EGFR (epidermal growth factor receptor) is a receptor tyrosine kinase that is overexpressed in ~80% of non-small cell lung cancer (NSCLC) and mutated in 20% of NSCLC.¹⁷ Gefitinib is an EGFR inhibitor, effective in cancers with mutated and overactive EGFR, such as NSCLC.

PARP inhibitors, such as olaparib, are used to treat cancers that are more dependent on PARP than normal cells.¹⁹ PARP1 is an important protein for repairing DNA single strand breaks. BRCA1 and BRCA2 are proteins that are important for the repair of DNA double-strand breaks. The Homologous Recombinational Repair pathway is defective in BRCA1 or BRCA2 mutated cancers and the use of PARP inhibitors causes cell damage and death. This is known as synthetic lethality, when two conditions that independently would not cause cell death applied in combination are lethal. Normal cells that don't replicate their DNA as often as cancer cells, and that lack any mutated BRCA1 or BRCA2 still have homologous repair operating, which allows them to survive the inhibition of PARP. As with any cancer treatment targeted therapy is not always effective. Target cells may respond initially to treatment but become resistant over time as the target itself can mutate and/or the tumour can find a new pathway to achieve tumour growth that does not depend on the target.

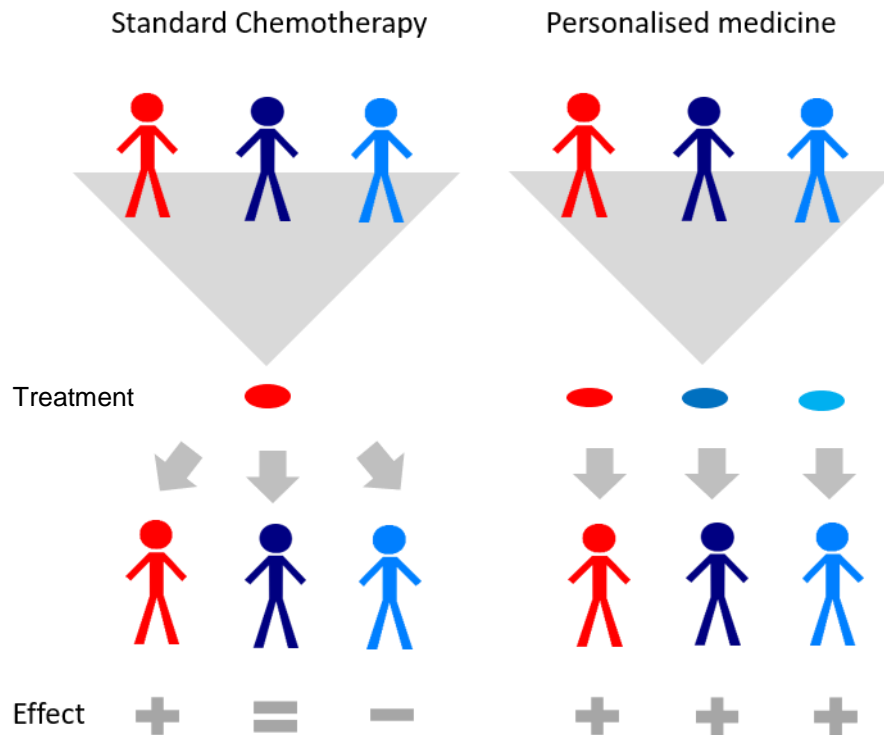


Figure 1.5 - Personalised oncology medicine, when applied correctly, is much more effective than standard chemotherapy. The specific mutations driving the patient's tumour are identified and treated.

1.4 The heat shock response

A number of diseases, including cancer, are caused by an interruption of protein homeostasis. Protein homeostasis is the highly complex and interconnected set of processes that affect the levels and conformational stability of proteins in cells. Maintaining this balance is essential for healthy cells to continue to survive, grow and multiply. Under stress conditions, proteins can become damaged leading to loss of function. Cells have developed an evolutionary cytoprotective response to cope with stress conditions known as the heat shock response.

The heat shock response was first observed by Ritossa in 1962 when experimenting with *Drosophila* larvae.²⁰ Temperatures above 36 °C induced a number of puffs in the chromosomes, associated with gene transcription. The puffs regressed when the larvae were allowed to recover at 25 °C. Since this

first experiment, the heat shock response has been studied in great detail and has been found to be modulated by heat shock proteins.

Heat shock proteins (HSPs) are molecular chaperones that are highly conserved across species, from yeast to human. Molecular chaperones are essential proteins that integrate multiple biochemical networks fundamental for cell survival, proliferation, adaptation and migration and are the main regulators of proteostasis.²¹ HSPs are ubiquitously expressed in all cells and are fundamental to the survival of both stressed and unstressed cells. They are rapidly induced in response to stress such as heat, ischemia, nutrient deprivation, hypoxia, altered pH or heavy metals, resulting in cytoprotection to repeat exposure which would otherwise be lethal.

HSPs are key mediators of the heat shock response pathway. When a heat shock response is triggered, a transcription factor named heat shock factor (HSF) is activated. In humans, there are three heat shock factors which are amplified depending on what stress the cell is responding to. HSF1 is normally present in the cell in its inactive monomeric form but in response to environmental and disease related stress HSF1 trimerises to the active form (Figure 1.6). Activated HSF1 binds to specific regions of DNA leading to a dramatic increase in the production of heat shock proteins.

HSPs are generally grouped into families related to their molecular mass including HSP40, HSP60, HSP70, HSP90, HSP100 and small HSPs. Unlike enzymes, which have very specific active sites, these molecular chaperones have a wide variety of substrates enabling them to carry out their key function in maintaining cellular homeostasis. HSP70 is the focus of this thesis and is therefore described in detail in the following sections. HSP70 is a general term used to describe the family of closely related HSP70 proteins.

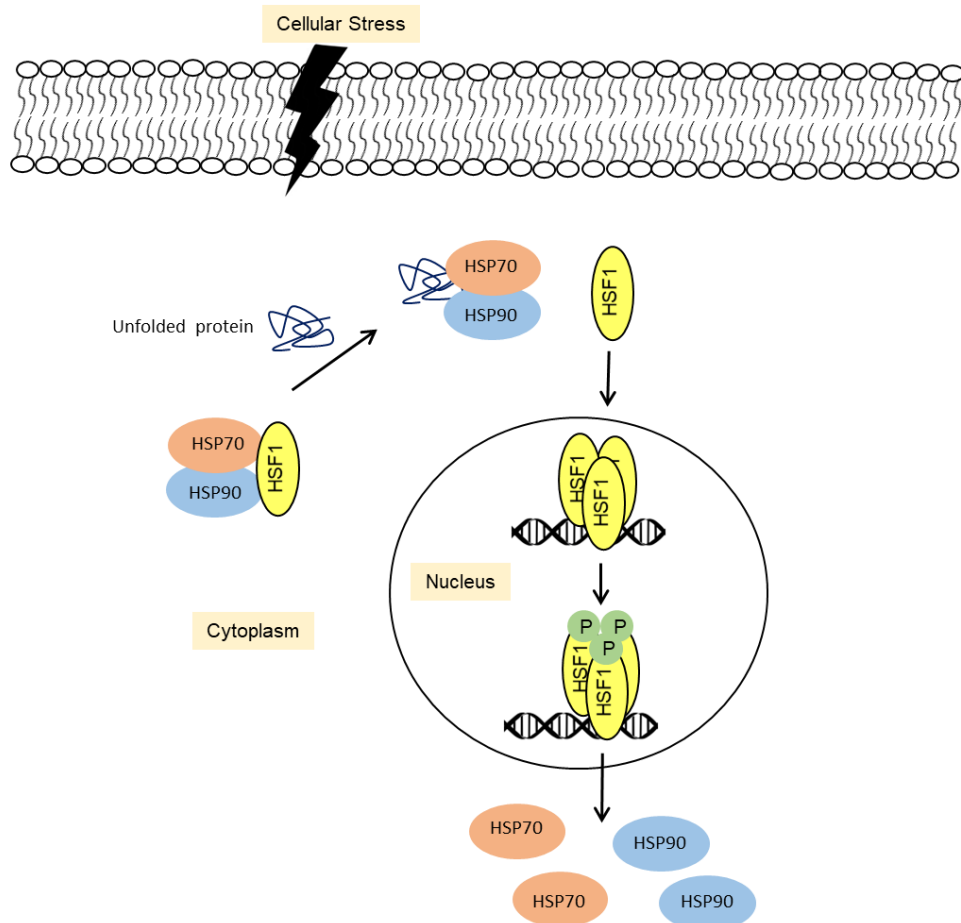


Figure 1.6 – The HSF1 pathway. In normal unstressed cells HSF1 exists as a monomer in the cytoplasm held in a repressed state by an interaction with HSP90 and HSP70. Cellular stress causes an increase in unfolded proteins which leads to the dissociation of HSP90 and HSP70 from HSF1. Monomeric HSF1 is then free to trimerize, translocate to the nucleus and undergo a series of post-translational phosphorylation events. HSF1 activates the transcription of a number of HSP genes, including HSP90 and HSP70. The increased cellular concentration of these chaperones can then inactivate HSF1 by binding to monomeric or trimeric forms of the transcription factor. Adapted from Powers *et al.*²²

1.5 Heat Shock Protein 70

1.5.1 HSP70 forms and function

HSP70s are highly conserved proteins across all domains of life: archaea, eubacteria and eukaryotes. Between *E.coli* and humans there is 53% identity and 68% homology.²³ HSP70 is referred to as DnaK in archae and eubacteria, SSA (Stress-Seventy subfamily A) in yeasts and HSPA in humans. Because of the sequence and structural similarity of these proteins, studies in one system are often used to approximate another.²⁴ Some of the discoveries were made possible by the pioneering work on bacterial DnaK.²⁵ In humans, the isoforms of HSP70 range from 66 kDa to 78 kDa. All share the common domain structure, but each has a unique pattern of expression or subcellular localization (Table 1). The most abundant cytosolic HSP70 proteins are HSP72 (HSPA1A) and HSC70 (HSPA8). HSC70 is generally ubiquitously expressed and performs housekeeping functions in the cell. In contrast HSP72 is expressed at high levels only in response to cellular stress. Some family members function in a specific organelle or tissue such as Grp78 (HSPA5) found in the ER lumen and mortalin (HSPA9) found in the mitochondrial matrix but many others are thought to function redundantly.

Differences in function of the different isoforms are unlikely to relate to the nucleotide binding domain (NBD) as crystal structures have revealed their NBDs to be highly similar.²⁶ For example, there is 89% structural identity between the NBD of HSP72 and HSC70.²⁷ Variations in substrate binding domain (SBD) or accessory proteins may account for differences in function.

Protein	Alternative names	Cellular localisation	Gene	Stress inducible
HSPA1A	Hsp70-1, Hsp72, HspA1, Hsp70-1A, Hsp70i	Cytosol, nucleus, cell membrane, extracellular exosomes	<i>HSPA1A</i>	yes
HSPA1B	Hsp70-2, Hsp70-1B	Cytosol, nucleus, extracellular exosomes	<i>HSPA1B</i>	yes
HSPA1L	Hsp70-1L, Hsp70-hom, Hsp70-1t	Cytosol, nucleus	<i>HSPA1L</i>	no
HSPA2	Heat shock 70kD protein 2, Hsp70.2	Cytosol, nucleus, cell membrane, extracellular exosomes	<i>HSPA2</i>	no
HSPA4	Hsp70-4, Apg-2, HSP70RY	Cytosol	<i>HSPA4</i>	ND
HSPA4L	Hsp70-4L, Apg1, Osp94	Cytosol, nucleus	<i>HSPA4L</i>	ND
HSPA5	Hsp70-5, BiP, Grp78, Mif-2	ER, extracellular exosomes	<i>HSPA5</i>	no
HSPA6	Hsp70-6, Hsp70B'	Cytosol, extracellular exosomes	<i>HSPA6</i>	yes
HSPA7	Hsp70-7, Hsp70B	blood microparticles, extracellular exosomes	<i>HSPA7</i>	yes
HSPA8	Hsp70-8, Hsc70, Hsc71, Hsp71, Hsp73	Cytosol, nucleus, cell membrane, extracellular exosomes	<i>HSPA8</i>	no
HSPA9	Hsp70-9, Grp75, HspA9B, MOT, MOT2, PBP74, mot-2, mtHsp70, mortalin	Mitochondria, nucleus	<i>HSPA9</i>	no
HSPA12A	Hsp70-12A, FLJ13874, KIAA0417	Intracellular, extracellular exosomes	<i>HSPA12A</i>	no
HSPA12B	Hsp70-12B, RP23-32L15.1, 2700081N06Rik	Endothelial cells, intracellular, blood plasma	<i>HSPA12B</i>	no
HSPA13	Hsp70-13, Stch	ER, extracellular exosomes, microsomes	<i>HSPA13</i>	no
HSPA14	Hsp70-14, Hsp70L1	Cytosol, membrane	<i>HSPA14</i>	yes

Table 1.1 - Summary of the human HSP70 protein family

HSP70s directly assist in the correct folding of nascent polypeptides, prevent protein aggregation and help translocate newly folded proteins to their correct location in the cell.²² HSP70s are often described as nanomachines that can change the conformation of their substrate polypeptides by transiently binding to short extended hydrophobic sequences. This can be, for example, during *de novo* protein synthesis at the ribosome, with aggregation prone protein intermediates, with stress denatured proteins or during the assembly and disassembly of protein complexes. They interact with almost all newly synthesised unfolded proteins and are able to recognise such a diverse range of proteins by interacting with a short hydrophobic motif of five amino acids enriched with hydrophobic residues that are found in practically all polypeptides. It has been suggested that HSP70 could bind most sequences in the proteome if the binding sites became accessible. Interestingly, algorithms designed to study *E. coli* DnaK, which has served as a paradigm for the HSP70 family, have estimated that there are potential binding sites approximately every forty residues in the *E. coli* proteome. HSP70s display promiscuity in that they have the ability to bind many different sequences but also selectivity in that they do not bind all sequences in the proteome.

When cells are under stress, proteins can become unfolded and these hydrophobic sequences become exposed. This can cause problems such as loss of protein function and protein aggregation. HSP70s recognise these damaged proteins and allow them to refold correctly or if this is not possible they facilitate their destruction by the proteasomal or lysosomal pathways (Figure 1.7). This interaction between HSP70s and substrate polypeptides is transient and regulated by an allosteric mechanism. Co-chaperones such as HSP40s (J proteins) and nucleotide exchange factors (NEFs) help to regulate the allosteric mechanism, controlling substrate binding and release. HSP40s are co-chaperones with a 70 amino acid conserved J domain that bind to the NBD and stimulate ATP hydrolysis. NEFs bind to the NBD and exchange ADP for ATP which releases the peptide substrate. Together these J proteins and NEFs regulate ATP cycling and control substrate binding. Chaperones also have the ability to independently bind substrates and influence substrate selection.²⁸

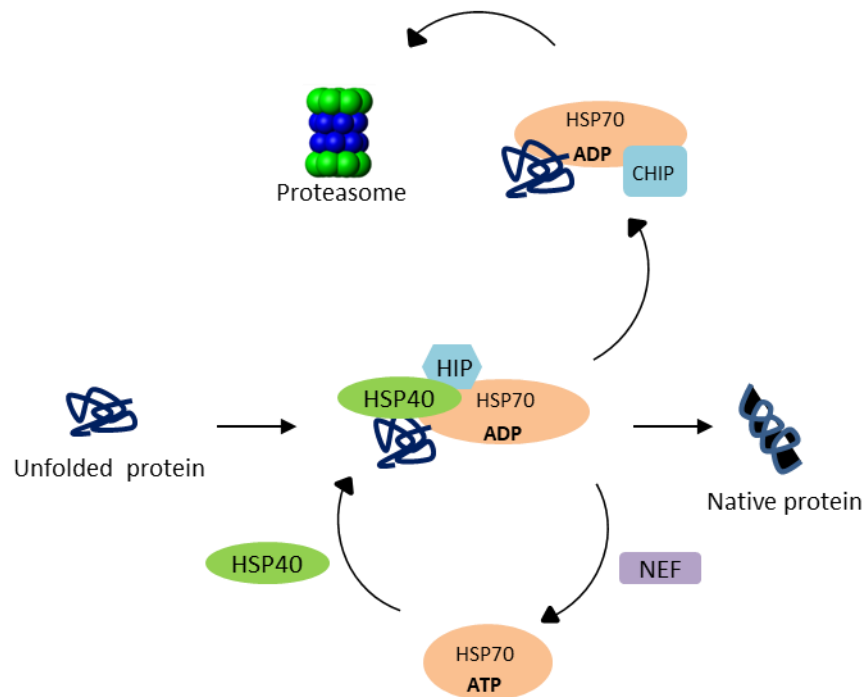


Figure 1.7 - HSP70 and its co-chaperones interact with misfolded proteins. A client protein is presented to HSP70 by the HSP40 co-chaperone. The bound client is stabilised by HSP70 interacting protein (HIP). Binding of the client protein to HSP70 can prevent aggregation of the client protein and allows it the opportunity to refold correctly into the native protein. Release of the bound client is stimulated by a nucleotide exchange factor (NEF) such as Bag-1 or HSPB1. The released client may fold into its native state or enter another cycle of chaperone binding and release. If the client spends too long in the chaperone cycle or if it is recognised by specialized co-chaperones it can be brought by the C-terminus of HSP70 interacting protein (CHIP) to the proteasome for degradation.

1.5.2 HSP70 structure

In general, members of the HSP70 family have two domains – an N terminal nucleotide binding domain (NBD) of about 40 kDa and a C terminal substrate binding domain (SBD) of about 25 kDa connected together via a short linker. HSP70 is a highly flexible protein with extensive communication between these two domains. The NBD is structurally related to actin consisting of two lobes with a deep cleft between them where the nucleotide binding site is located. The NBD can be divided into four subdomains Ia, Ib, IIa and IIb. The SBD has a β sandwich domain consisting of two pairs of β -strands and two sets of protruding loops where the polypeptide binding cleft is located. The binding cleft has five pockets suggesting that HSP70 binds to five amino acid residues of the

substrate polypeptide. The 0th position describes the residue binding in the central pocket which has the highest sequence specificity in HSP70, with leucine being the optimal fit. Isoleucine, valine and phenylalanine can bind here also but these amino acids fit less well. The other four pockets can accommodate a range of amino acids. An α helical lid restricts access to this cleft by docking onto two loops and forming a latch with the other two. The two domains are linked together by a hydrophobic linker that has been shown by NMR and biophysical methods to control ATPase activity by binding in a hydrophobic groove between Ia and IIa subdomains.²⁹

In the nucleotide free and the ADP-bound state, the SBD and the NBD have been shown by NMR studies to tumble independently of each other, only connected by the highly conserved hydrophobic linker between the two domains. In this state, the SBD has a very high affinity for substrate polypeptides and slow association and disassociation rates. The hydrolysis of ATP to ADP causes a conformational change that closes the α helical lid, increasing the affinity of the substrate for the SBD. The α helical lid must dissociate before the substrate can bind or be released.

When ATP is bound a dramatic conformational change in the protein occurs which brings the NBD and the SBD domains together. This increases the association and disassociation rates of the substrate polypeptide by 100 and 1000-fold respectively.

The recently solved structure of the ATP bound open conformation of DnaK has made it possible to understand this mechanism in more detail (Figure 1.8). In contrast to the closed ADP bound conformation, in the open conformation the lobes of the NBD rotate relative to each other, leading to an opening in the crevice into which the linker binds. The SBD α and SBD β dissociate from each other and dock onto two faces of the NBD. The docking of SBD β onto the NBD causes the substrate binding cleft to open which explains the high association and disassociation rates. The NBD is also now locked into the lobe-rotated conformation which is unable to hydrolyse ATP which explains the low rate of

ATP hydrolysis in the ATP-bound state. The substrate polypeptides are able to stimulate ATP hydrolysis through a series of residues that sense insertion of an amino acid side chain into the hydrophobic cleft in the SBD β and transmits the conformational changes to the NBD.

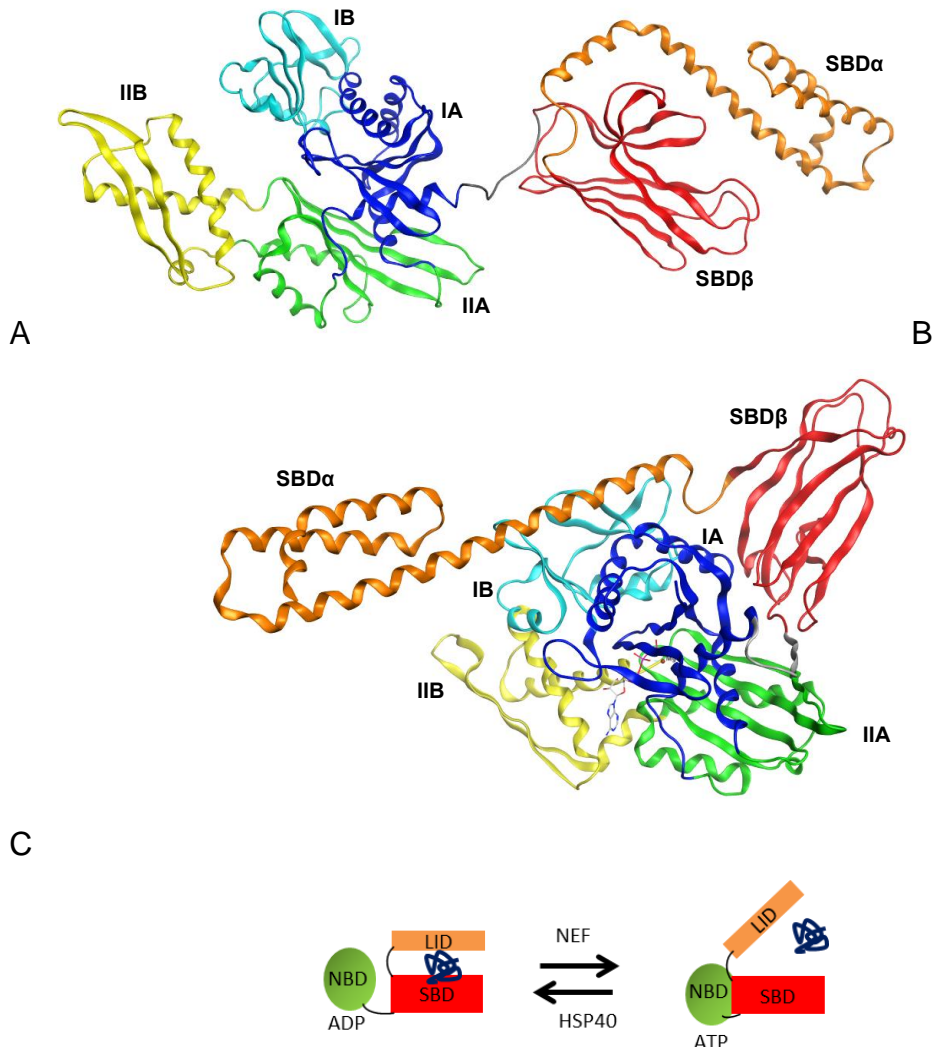


Figure 1.8 - Conformational flexibility of HSP70. (A) NMR-RDC/X-ray structure of *E. coli* HSP70 in complex with ADP (PDB ID: 2KHO). (B) *E. coli* HSP70 in complex with ATP (PDB ID: 4B9Q). The colour code is the following: NBD-IA (residues 4–37, 112–182 and 363–383; blue), NBD-IB (residues 38–111; cyan), NBD-IIA (residues 183–227 and 311–362; green), NBD-IIB (residues 228–310; yellow), linker (residues 384–393; grey), SBD β (residues 394–502; red) and SBD α (residues 503–603; orange), ATP ligand shown in grey, prepared with MOE. (C) When ATP is bound the C-terminal lid SBD α is in an open state and the protein has weak affinity for the peptide substrate, Binding of the peptide stimulates ATP hydrolysis to ADP which causes a conformational change that closes the lid, increasing the affinity for the peptide. These changes are assisted by nucleotide exchange factors (NEF) and the co-chaperones HSP40.

The C terminus has an EEVD motif which can interact with co-chaperones known as tetratricopeptide repeat (TPR)-containing proteins. The C-terminus is the least conserved across isoforms which may allow different family members to interact with different co-chaperones. Co-chaperones that bind the C-terminus can mediate the recruitment and fate of substrates. For example, heat shock organising protein (HOP) bridges HSP70 and HSP90, assisting the transfer between these chaperones by binding to the ADP bound form of HSP70 via TPR1 and TPR2B and to HSP90 via TPR2A. CHIP is another TPR containing protein but instead of assisting in protein folding, it assists in protein degradation (Figure 1.7).

Crystal structures have revealed that NEFs bind at the top of the cleft to residues in the Ib and IIb subdomains which results in an opening of the cleft, distorting the nucleotide binding site. The adenine moiety is enclosed by two solvent exposed arginines, which adopt different conformations upon ligand binding and exhibit high B-factors in the apo structure.³⁰

Crystal structures of ADP bound to the NBD of HSP70 show the nucleotide interacting with subdomains Ia, IIa, and IIb. The adenosine moiety interacts with the side chains of E268, K271, and S275 from IIb, the α -phosphate group interacts with the main-chain amide group of G339 from subdomain IIa, and the β -phosphate group is associated with the main and side chains of T13 and T14 and main-chain of Y15 (Figure 1.9). K71 in HSC70 is the only residue from Ib that interacts with ATP and is essential for catalysis. It is thought that this lysine can activate the water molecule that carries out the nucleophilic attack on the γ phosphate.²⁴ T13 forms a hydrogen bond with the oxygen of the ATP γ phosphate. While mutation of this residue to a valine does not affect hydrolysis it does abolish the communication between the SBD and the NBD.²⁴

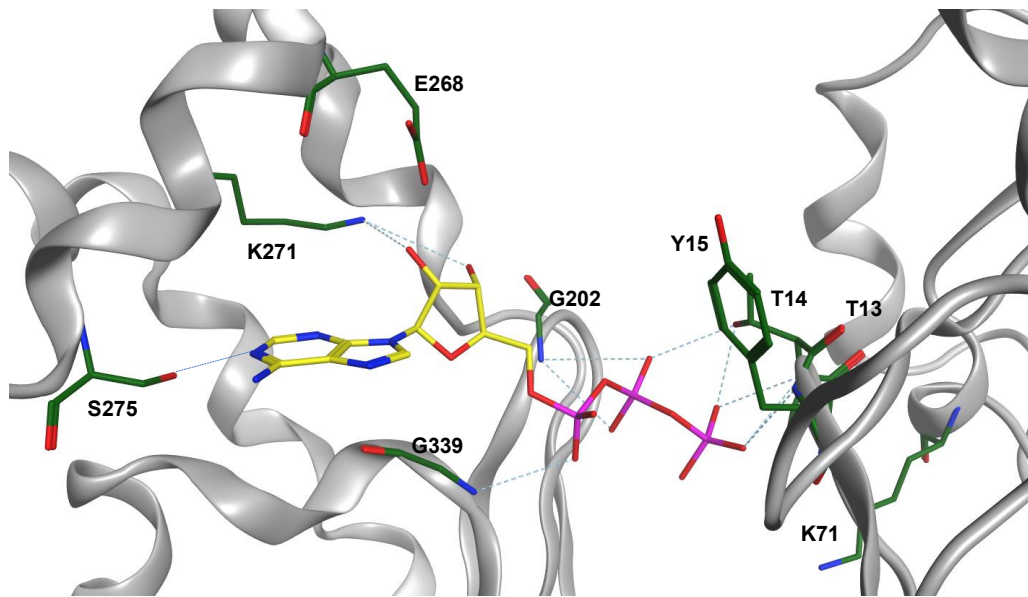


Figure 1.9 – Crystal Structure of HSC70/Bag1 in complex with ATP (PDB ID 3FZF) with key residues highlighted described in the text.

1.5.3 The role of HSP70 in cancer

HSP70s have been implicated in several neurodegenerative diseases which involve misfolded proteins such as Huntington's, Alzheimer's and Parkinson's disease.²³ In cancer, HSP70s enhance cell growth, suppress senescence and confer chemotherapeutic resistance. HSP70 expression is often associated with metastasis and poor prognosis in many forms of cancer including breast, skin and oesophageal cancers and haematological malignancies.³¹ It has been found to be highly elevated in breast, colon, liver, prostate, oesophageal and cervical cancers and has been shown to be critical to the growth and survival of many human tumour cell lines.^{32,26}

In cancer, oncoproteins depend on chaperone activity to maintain their function as they are particularly prone to mistakes in protein synthesis and folding. Many oncogenic proteins rely on chaperones for stability, folding, activation and cellular localisation. As well as carrying mutated proteins, cancer cells can often be subject to stress from hypoxia and nutrient deprivation due to poor blood

supply to the tumour. Chemotherapeutics and radiation therapy put further stress on the cancer cell which leads to further dependence on the HSF1 pathway. This dependence makes heat shock proteins highly desirable anti-cancer targets.

HSP70s are powerful anti-apoptotic proteins. They block mitochondrial translocation and activation of Bax preventing the release of pro-apoptotic factors. HSP70s also inhibit the assembly of the death inducing signalling complex (DISC), bind directly to apoptosis protease activating factor (Apaf-1) and block the recruitment of pro-caspase-9 to the mitochondrial apoptosome.³³ HSP72 interacts with apoptosis inducing factor (AIF) avoiding caspase independent chromatin condensation and apoptosis. It inhibits caspase 3 and regulates kinases in the apoptotic pathway such as JNK, MAPK and ERK. HSP72 uses the E3 ligase CHIP (C terminal HSP70 interacting protein) to promote degradation of Ask-1 (apoptosis signal related kinase 1). Ask-1 activates downstream MAPKs and has a pivotal role in apoptosis. Extracellular HSP72 can also increase proMMP-9 (pro matrix metalloproteinase 9) secretion.³⁴ This zinc metalloproteinase is involved in the degradation of the extracellular matrix, aiding tumour invasion and metastasis.

1.5.4 HSP70 inhibition

Because of its key role in protein homeostasis and its implication in fatal illnesses, understanding the effect of HSP70 inhibition has been of great interest and importance. In genetic studies the knockout of mouse HSC70, the constitutively active form, is embryonic lethal. This is perhaps unsurprising as it is expressed in all cells and performs essential housekeeping functions in the cell. In contrast knockout of mouse HSP72, which is known to play a role in stress induced cell survival, is not lethal but these mice are smaller than wild-type and have stress sensitive phenotypes including genome instability.

RNA interference studies have confirmed the importance of HSP70 in tumorigenesis. Silencing HSP70 with anti-sense RNA induced cell death in breast, lung, oral, colon, prostate, liver and brain cancer cell lines but was non-toxic in non-tumorigenic cell lines.^{35,36,37,38} Inhibiting HSP70 ATPase activity results in the proteasomal degradation of client proteins followed by tumour growth arrest or death.²⁶ Dual silencing of both HSC70 and HSP72 using siRNA has been shown to cause apoptosis in tumour cells as well as degradation of HSP90 client proteins CRAF, CDK4 and ERB2.³⁹ Apoptosis was not induced in non-tumorigenic lines indicating a potential therapeutic window.

Because of the promising anti-cancer potential of HSP70 inhibition, the discovery of selective and potent HSP70 inhibitors has been actively pursued by many groups for more than a decade. This endeavour has proved extremely challenging and has not yet led to a clinical inhibitor. There is, however, much to be learned from previous attempts to drug this challenging target. Designing inhibitors of HSP70 has proven to be much more difficult than targeting HSP90 for example, despite both being in the same target class. There are currently several HSP90 inhibitors in clinical trials for the treatment of cancer. However, treatment of cancer cells with HSP90 inhibitors such as the geldanamycin derivative 17-AAG results in the production of HSP70, likely by activating HSF1, leading to a decrease in the cancer cell death effect of HSP90 inhibitors.⁴⁰ This transcriptional upregulation of HSP70 is a hallmark of HSP90 N-terminal inhibitor activity and an intrinsic resistance mechanism to HSP90 inhibitors.

Computational analysis has been carried out using SiteMap, a programme that ranks the binding sites of a target by giving them a druggability score (Dscore), accounting for the size, shape and the hydrophilic/hydrophobic nature of the pocket. A Dscore below 0.83 is classed as 'undruggable', above 0.98 is classed as 'druggable' and between 0.83-0.98 is classed as 'difficult'. The ATPase site of HSP70 was given a Dscore of 0.95 suggesting a difficult but not undruggable binding site.⁴¹ This is in contrast to the Dscore of 1.04 (druggable) for the ATPase site of HSP90. Analysis of the HSP70 ATP binding site showed a prevalence of hydrophilic residues (Figure 1.10). Although ligands can be

designed to have high affinity with such hydrophilic binding sites, cell permeability then becomes a major challenge.

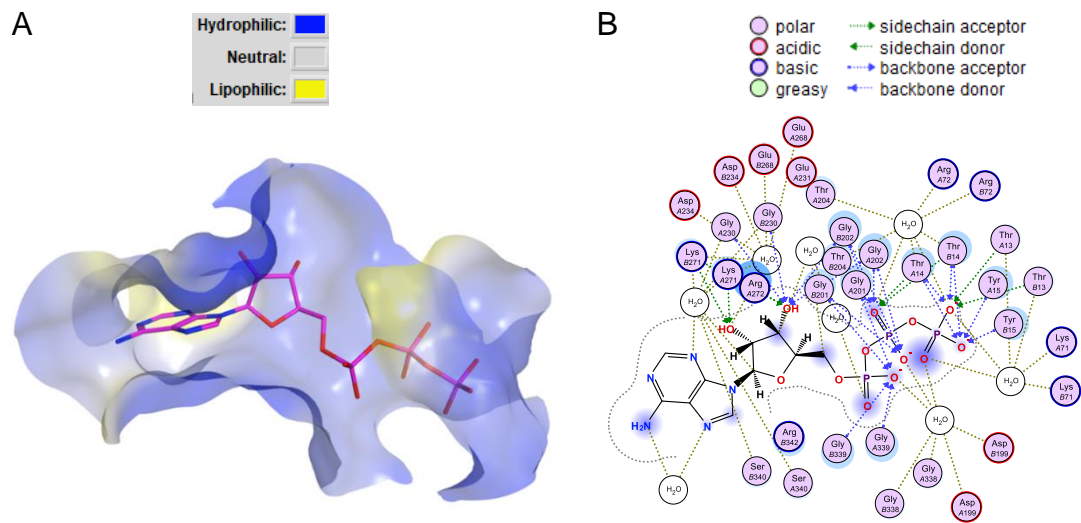


Figure 1.10 – (A) ATP binding site HSC70/Bag 1 in complex with ATP (PDB ID: 3FZF) showing the prevalence of hydrophilic residues. (B) Ligand interaction diagram showing the binding of the β and γ phosphates of ATP are stabilized by interactions with polar amino acids and water in the binding site. Designing a new inhibitor that targets such polar interactions while also maintaining good physicochemical properties is very challenging.

NMR techniques and molecular dynamics have shown HSP70 to be a highly flexible protein in which several residues rotate or move substantially during the catalytic cycle. In particular, residues in the orthosteric site can adopt very different conformations, meaning the size and shape of the ATP binding site changes throughout the catalytic cycle and depending on the ligand bound (Figure 1.11). Publicly available structural data sample a variety of HSP70's conformational states. Structures of the NBD in complex with ATP and the NEF BAG-1 represent the open conformation of the NBD. In contrast, structures with ADP represent the closed conformation. The majority of ligands observed by X-ray crystallography appear to bind an intermediate conformation.⁴²

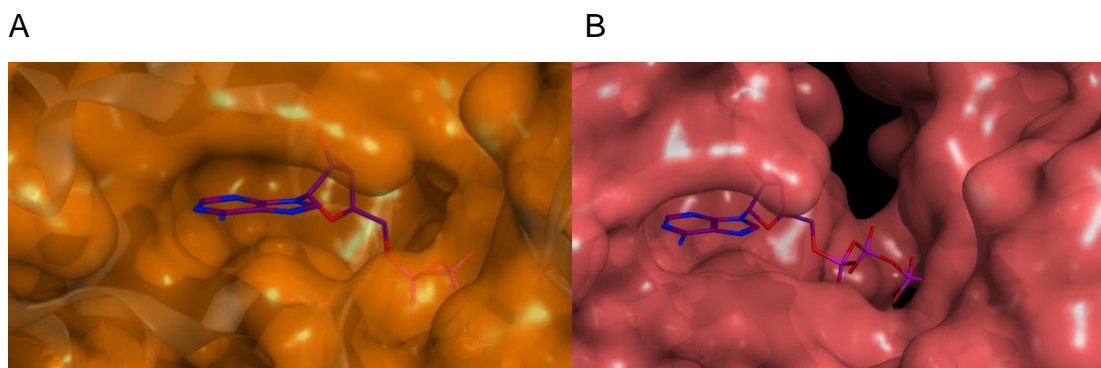


Figure 1.11 – The ATP binding site changes size and shape depending on which nucleotide is bound (A) Structure of HSC70/Bag1 in complex with ATP (PDB ID: 2KHO). (B) Structure of HSC70 NBD in complex with ADP (PDB ID:4H5T).

Fragment hit rate can also be used to measure the druggability of a protein of interest. Studies have shown that the hit rate from a fragment screen correlates well with the hit rate from high-throughput screening (HTS).⁴³ In a fragment screen against HSP90, Vernalis reported a hit rate of 4.4%.³⁰ In comparison, the hit rate against HSP70 using the same screen was extremely low at 0.4%. This low fragment hit rate suggests that identifying high affinity, drug-like ligands for the NBD of HSP70 from novel start points is likely to be challenging. Astex have also carried out a fragment screen against HSP70 and observed by X-ray crystallography fragments binding to four distinct sites outside of the ATP binding site proving the existence of multiple binding sites in the protein.⁴⁴

In cells, the ATP concentration is typically about 1-5 mM. This high concentration of cellular ATP means that ATP competitive inhibitors are much more successful against targets with a low affinity for ADP and ATP. HSP70 has a higher affinity for ADP (K_D 0.3 μ M)³⁰ in comparison to Hsp90 (K_D 15 μ M).⁴⁵ Thus, HSP70 inhibitors will need to have a higher affinity for their target to produce the same effect. In contrast to HSP90 inhibitors where single digit nanomolar affinity has correlated to nanomolar cellular activity, HSP70 inhibitors of 50 nM show cellular activity in the low micromolar range.³⁰

1.5.4.1 SBD inhibitors

Several molecules have been reported to bind to the SBD of HSP70 (Figure 1.12). The first HSP70 inhibitor to be described was a synthetic derivative of the natural product spergualin, 15-deoxyspergualin (15-DSG, **1**) which binds to the C terminal EEDV motif, the same binding site as the TPR-domain co-chaperones.⁴⁶ Unfortunately this compound has low bioavailability and poor stability resulting in insufficient efficacy in a phase II clinical trial. Importantly, 15-DSG also binds to HSP90 with a similar K_D to that for HSC70 so it cannot be excluded that 15-DSG may function via HSP90 rather than HSC70. The structurally related dihydropyrimidines MAL3-101 **2** and NSC630668 R/1 **3** as well as a number of other analogues have improved properties although the sites of action of 15-DSG and dihydropyrimidines have yet to be clearly defined.³⁰

Pifithrin- μ (PES, **4**) is a small molecule identified during a cell-based screen. It interacts with the SBD outside of the peptide binding pocket and effectively inhibits the interaction of HSP70 with various co-factors that interact with the ATPase domain, including J-domain and Bag-domain proteins. It inhibits HSP72 from associating with client proteins APAF1 and P53 and was reported to show specificity for HSP72 over HSC70 and GRP78 although it has since failed to show specific saturable binding in a biochemical study. Schlecht et al. recently showed that pifithrin- μ bound to HSP72 in a non-specific, aggregation-dependent manner.⁴⁷

Novolactone **5** is a fungal metabolite that has been found to irreversibly inhibit the HSP40 stimulated activities of HSP70 in vitro.⁴⁸ In the absence of HSP40, novolactone stimulated ATPase activity in a dose dependent manner but in the presence of HSP40 novolactone inhibited ATPase activity with an IC_{50} of 0.25 μ M. X-ray structures of HSP72 SBD showed the covalent modification of Glu444, a residue that is conserved across mitochondrial and ER associated HSP70s, located at the interface between the β sandwich subdomain and the NBD. The novolactone adduct induces a conformational change that prevents this interaction of the two domains. All known single amino acid replacements of

HSP70s at the interface between the two domains that block interdomain communication have shown an increased basal rate of ATP hydrolysis suggesting this communication is key for the low basal rate of ATP hydrolysis. Novolactone has an interesting and well characterised binding site and it may be a valuable tool compound for studying HSP70 but it does not have suitable drug-like properties to be used in the clinic.

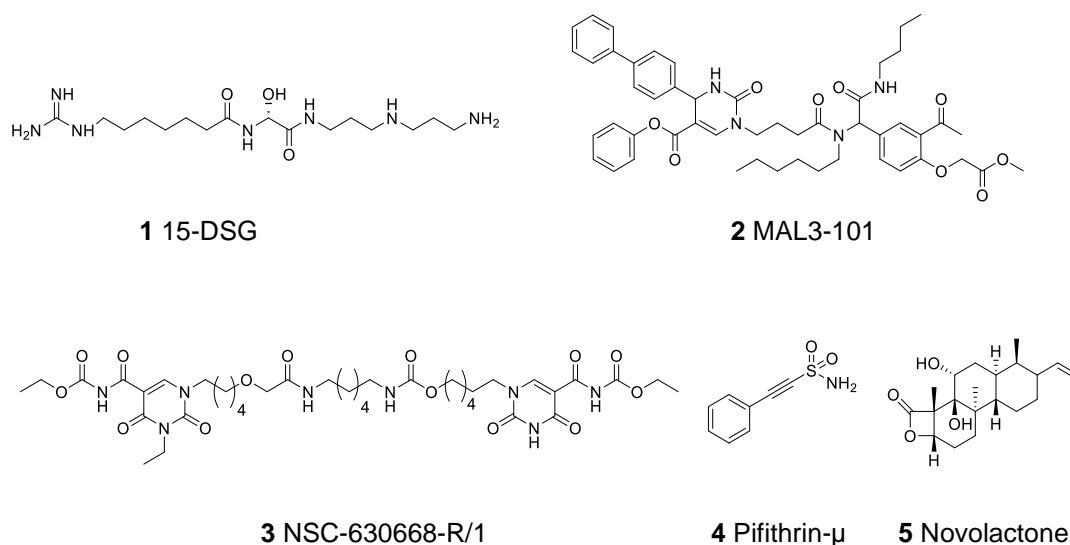


Figure 1.12 – Reported HSP70 inhibitors that bind in the substrate binding domain (SBD).

1.5.4.2 NBD inhibitors

A successful strategy for inhibition of nucleotide dependent enzymes has traditionally been the design of ATP competitive inhibitors. In contrast to HSP90, there were no inhibitors known to bind directly to the ATPase domain of HSP70. Williamson *et al*⁴⁹ therefore used a commercially available ATP analogue as a starting point to design adenosine-based inhibitors. Structure based drug design was applied to generate a series of 8-aminoadenosine ATP competitive inhibitors including VER-155008 **6** (Figure 1.14). VER-155008 phenocopies the genetic knockdown of HSC70/HSP72 and serves as a highly useful control compound in biochemical assays but unfortunately rapid metabolism and clearance observed *in vivo* meant a pharmacologically relevant level was never

reached in tumour tissues. Due to the similarity of the ATPase binding site with actin and other proteins, it was also difficult to achieve selectivity over these off-targets.

Irreversible inhibition is an important strategy for proteins with high-affinity substrates. A recent study aimed to develop an irreversible ATP binding site inhibitor, based on VER-155008, using rational design to target C17.⁵⁰ The inhibitor **7** was instead found unexpectedly to covalently bind to K56. Work is ongoing to develop inhibitors that possess improved reversible affinity for HSP72 and electrophiles that are better matched to the lysine nucleophile.

Starting from adenosine **8**, Cheeseman *et al.* have sought to understand the importance of various parts of the molecule for binding affinity as well as understanding more about the different conformations of the ATP binding site.⁵¹ Removing the 2' or 3' hydroxyl groups or changing their absolute or relative stereochemistry resulted in no measurable binding, as did removal of the 6-amino group or the 3-nitrogen (Figure 1.13). In contrast removal of the 5' hydroxyl was tolerated. Addition of a primary amine to the 8-position resulted in a significant increase in binding affinity (16-fold). Natural product nucleoside derived inhibitors were synthesised with improved affinity for HSP70 than adenosine but none managed to get beyond micromolar affinity. The authors suggested that the complexity surrounding the observed structure activity relationships (SAR) could be due to different conformations of the protein. X-ray crystallography revealed that in contrast to the closed ADP crystal structure, the nucleoside derived inhibitor sangivamycin crystallised in a more open conformation. HSP72-NBD closed conformation observed in the ADP bound structure is presumably brought about by the interactions of the β -phosphate group with the two glycine-rich loops of the phosphate binding region. The absence of the phosphate groups, and in particular the β -phosphate group, in sangivamycin means there is no induced conformational change.

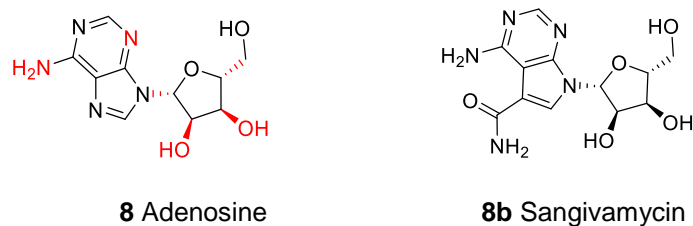


Figure 1.13 – Structures of adenosine and sangivamycin. In a study of adenosine **8** the heteroatoms and stereochemistry highlighted in red were found to be essential for activity.⁵¹

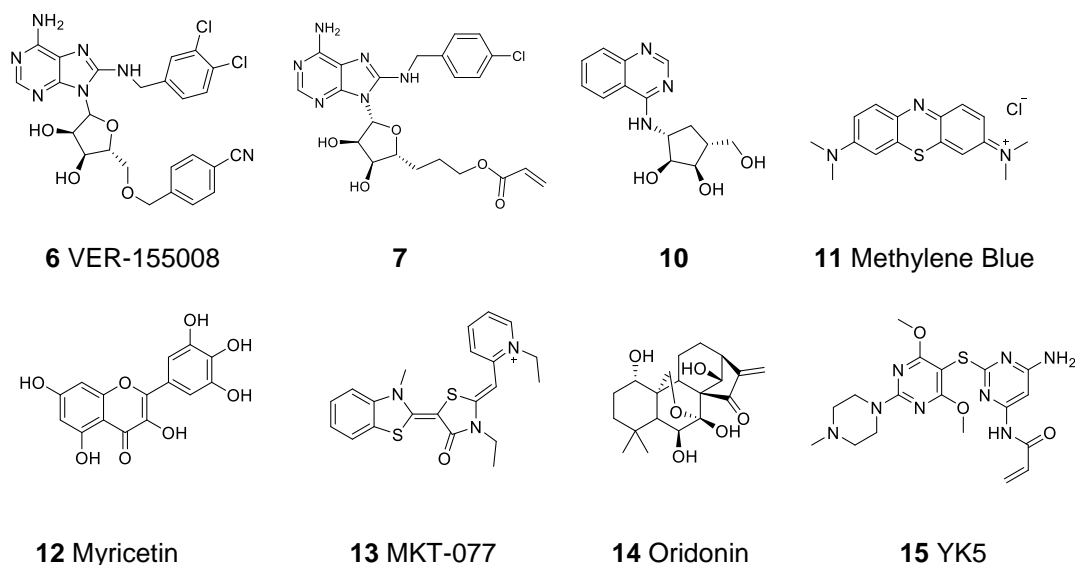


Figure 1.14 – Reported HSP70 inhibitors that bind in the nucleotide binding domain (NBD).

A fragment screen, which was carried out against the NBD of HSC70, identified the first non-adenosine ligand to bind in the ATP binding site.³¹ Development of this quinazoline scaffold will be discussed in more detail in Chapters 4 and 5 but briefly the quinazoline hit **9** was elaborated by growing into the ribose pocket. Ribose 2'- and 3'-hydroxyls form an extensive hydrogen bonding network with ATP binding site residues. Synthetic attempts to directly link a ribose core to the 4-amino position of the quinazoline were unsuccessful but a less polar cyclopenylaminotriol ribose mimic **10** was found to improve the potency seven-fold. (Figure 1.15). Crystal structures of multiple hit fragments confirmed the quinazoline scaffold as stable and an attractive starting point for further exploration.

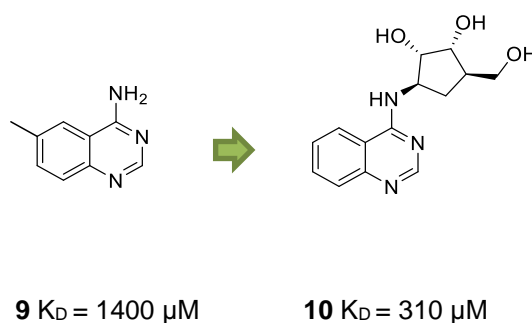


Figure 1.15 – Fragment screening against HSC70-NBD identified a quinazoline hit fragment which was developed into a more potent compound by the addition of a ribose mimic.³¹

Methylene blue **11** abolishes HSP70 ATPase activity by oxidising Cys306 near the ATP binding site and has been explored in a phase II clinical trial for Alzheimer's disease³³ but its specificity for tumour-derived HSP70 remains to be addressed.⁵² Myricetin **12** binds to a non-canonical site on the NBD of DnaK and allosterically blocks the binding of co-chaperone DnaJ but is a highly promiscuous compound.⁵³ The rhodocyanine MKT-077 **13** is an allosteric inhibitor of HSC70 and mortalin that preferentially inhibits the ADP form by binding to a negatively charged pocket near to the NBD.⁵⁴ However, a phase I clinical trial exhibited severe renal dysfunction. It became apparent that MKT-077 is rapidly metabolized, which limits its use as either a chemical probe or potential therapeutic. Oridonin **14**, a diterpene isolated from well-known Chinese medicinal plant has been shown to have a broad spectrum of anti-tumoral activities against a number of human cancers and human cancer cell lines. It has been shown to irreversibly bind to Cys267 of HSP72⁵⁵ but its mechanism of action is not fully understood and it is reported to have other targets such as nucleolin.⁵⁶

Kang *et al.* have developed a homology model of full length HSP70 which they used to design a covalent inhibitor, YK5 **15**⁵⁷ and later the reversible analogues⁵⁸ that they claim bind to an allosteric site in the N terminal domain of HSP70. Like oridonin, YK5 has been reported to form a Michael adduct with Cys267, which is buried deeply in a hydrophobic region requiring significant conformational

change to become solvent exposed. These molecules were identified by phenotypic testing and so require further target validation.

Apoptozole **16** is a small molecule found during a phenotypic screen to induce apoptosis.⁵⁹ The target was identified as the ATP binding site of human HSP72 and HSC70 although this has since been disputed. Evans *et al.* showed that apoptozole was forming aggregates under aqueous conditions that non-specifically interacted with HSP70 proteins.⁶⁰ Using both biochemical and biophysical techniques no experimental evidence was found that apoptozole binds to HSP70 in a specific and developable way.

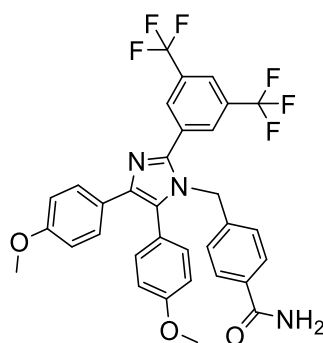


Figure 1.16 – Apoptozole **16** binds to HSP70 non-specifically.

1.6 Fragment Based Drug Discovery

Traditionally the pharmaceutical industry has used high throughput screening to search for starting points for a medicinal chemistry project, however, an alternative approach known as fragment-based drug discovery (FBDD) has emerged in the last 15 years. Fragments are small molecules (less than 300 Da) that can form high quality interactions with the protein, providing attractive starting points for a drug discovery project as they can be grown to improve potency while monitoring physicochemical properties.

Rather than screening hundreds of thousands to millions of compounds to find a lead sized starting point, much smaller collections of much smaller molecules are screened instead. Typical fragment libraries consist of a few thousand compounds. In contrast to the number of drug-like molecules that are possible the number of possible fragments is much smaller; as there are fewer atoms, there are fewer ways they can be arranged. The sampling of chemical space is therefore much more efficient with fragments than with larger molecules.

The probability of finding a match between a molecule and a binding site decays exponentially as the complexity of the ligand increases because there are more ways of obtaining a mismatch.⁶¹ However, the probability of detecting a hit increases with increasing molecule complexity because the larger interaction surface gives tighter binding which increases the assay signal. There is therefore a balance to be struck between molecules large enough to be detected but not so large that there is a high probability that they do not bind to the protein due to unfavourable interactions or shape disparity. Figure 1.17 shows the relationship between the probability of discovering lead molecules from screening and their complexity.

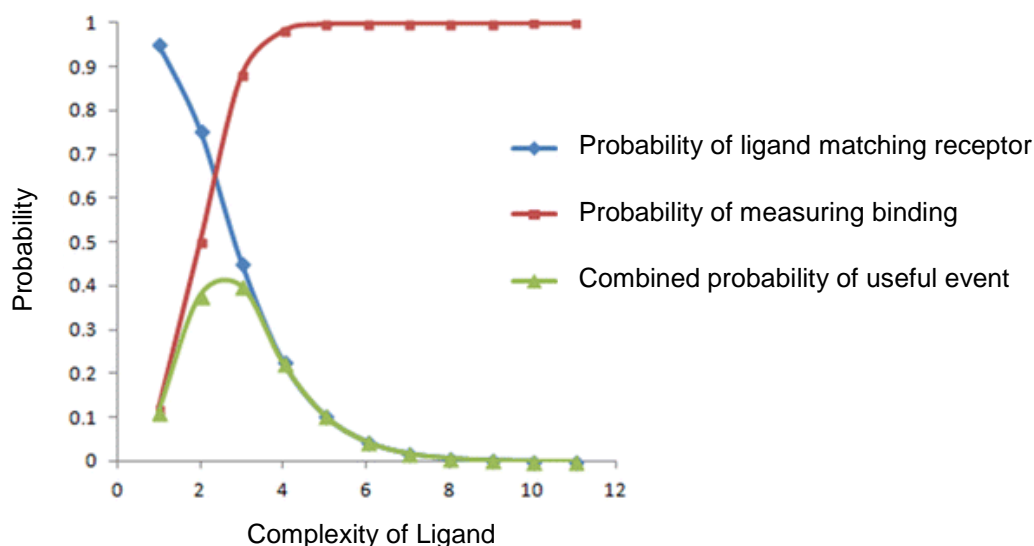


Figure 1.17 - The probability of detecting a hit increases with increasing molecular complexity. Molecular complexity refers to any aspect of a molecule that needs to be matched to the binding site. The probability of finding a match between a molecule and a binding site decays exponentially as the complexity of the ligand increases. Fragment based drug discovery aims to find the balance between these two competing factors. Adapted from Hann *et al.*⁶¹

High attrition rates in clinical trials have been attributed to poor physicochemical properties such as high lipophilicity which can also reduce selectivity and bioavailability. High lipophilicity is also associated with an increased risk of toxicity.⁶² There is concern over the general trend seen across the pharmaceutical industry of the increased average molecular weight and cLogP values of compounds in the pipeline compared to historical oral drugs.⁶³ Often HTS hits are already close to the limits of molecular weight and lipophilicity suggested by Lipinski's rules⁶⁴ making it difficult to adhere to these guidelines. Starting from smaller fragments and optimising for both potency and good physicochemical properties simultaneously should lead to better quality clinical candidates. Similar to Lipinski's rule of five, a rule of three has been useful in fragment library design where ideally the molecular weight ≤ 300 Da, the number of hydrogen bond acceptors ≤ 3 , hydrogen bond donors ≤ 3 and cLogP ≤ 3 , with a particular emphasis on molecular weight and LogP.⁶⁵

Fragments typically have low binding affinities ($>100\mu\text{M}$) and so require more sensitive detection techniques to traditional high throughput screening. The most common techniques used are SPR, NMR, thermal shift, ITC and X-ray crystallography. Although these methods are often lower throughput than biochemical assays they are much more sensitive. Multiple orthogonal methods are used to confirm hits to avoid confusing a weakly binding hit with false positives. Apart from the requirements of specialist detection equipment and confirmation of hits by multiple methods other limitations of FBDD include the necessity for highly soluble fragments and a target protein whose structure can be solved by X-ray crystallography. The techniques used for this thesis - SPR, NMR and X-ray crystallography will be described in detail in later chapters. Figure 1.18 summarises the differences between high-throughput screening and fragment-based drug discovery.

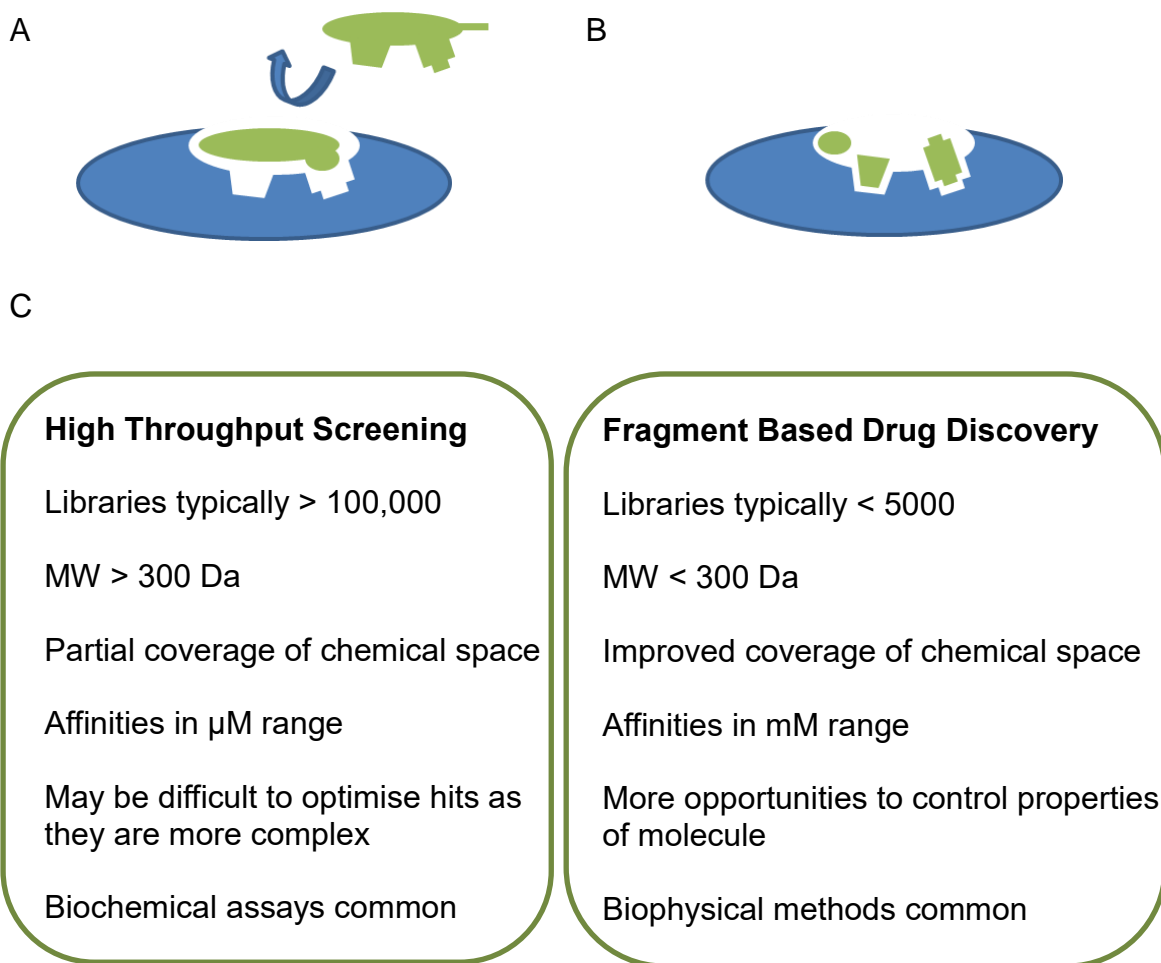


Figure 1.18 – (A) More complex molecules are more likely to form mismatches with the protein. (B) Simple fragments can make high quality interactions with the protein. (C) Summary of fragment-based drug discovery in comparison to high-throughput screening approaches.

For FBDD the emphasis is on the quality of the interactions between the ligand and the protein. Different metrics exist to compare fragments. Ligand efficiency (LE) is often used to assess the quality of the original hits and to justify any additional molecular weight that produces increased affinity when the fragment is grown (Figure 1.19). Lipophilic ligand efficiency (LLE) is the difference between pIC_{50} and lipophilicity and can be useful for factoring in increased affinity, potentially non-specific, due to lipophilicity. Proposed acceptable values of LE and LLE for drug candidates are $\text{LE} > 0.3$ kcal per mole per heavy atom and $\text{LLE} > 5$.⁶⁶

$$LE = \frac{\Delta G}{HAC} = -\frac{RT \ln K_d}{HAC}$$

$$LLE = plC_{50} - c \log P$$

Figure 1.19 - The above formulas are used to calculate ligand efficiency and lipophilic ligand efficiency (where R is the ideal gas constant 1.987×10^{-3} kcal/K/mol, T is the temperature in Kelvin, HAC is the non-hydrogen atom count and K_d is the dissociation constant).

LE or LLE are important but they are not the only criteria that should be used to select which fragments to optimise. The attractiveness of the medicinal chemistry plan, synthetic tractability, solubility, the availability of commercial analogues, and the availability of structural information on the binding mode should also be considered.⁶⁷ The stability of a fragment binding mode is of utmost importance in order to derive meaningful SAR as the fragment is grown. If an inferior fragment is to be developed a clear strategy for improving potency should be identified. For example, in the optimisation of an HSP90 fragment at Astex it was hypothesised that fragment **17** had an unfavourable twist in the bond connecting the pyridine to pyrimidine which would normally be close to planarity. (Figure 1.20). This twist could potentially be induced by substitution of the ring, stabilising the active conformation. This fragment also poorly filled a proximal lipophilic pocket offering a clear direction for fragment optimisation to a good quality lead compound **18**. Fragment **19** also offered the opportunity for fast fragment optimisation. From analysis of the X-ray crystal structure introducing a potential hydrogen bond to a nearby residue was feasible. The lead compound **20** significantly improved both the potency and ligand efficiency.

FBDD has emerged as a successful way to find high quality leads for drug development and has been able to tackle difficult targets for which little or no hits have been found by HTS. It is now well-established in industry and has resulted in more than 30 drugs entering clinical trials.⁴³

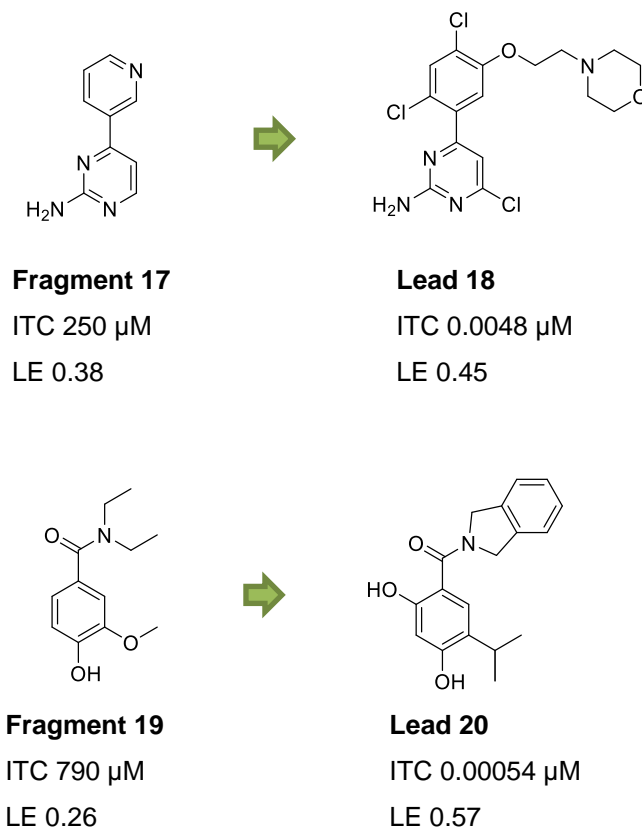


Figure 1.20 – Improving the potency of a fragment can be very successful when there is a clearly identified optimisation plan.⁶⁸ The development of fragment **17** to lead compound **18** was achieved by introducing a favourable twist by substitution of the aromatic ring and by filling a proximal lipophilic pocket. The development of fragment 19 to lead compound 20 was achieved by introducing a substituent capable of forming a hydrogen bond with the protein.

1.7 Hypothesis and Aims

Heat Shock Protein 70 (HSP70) is a key molecular chaperone that is overexpressed in many cancers and is often associated with metastasis and poor prognosis.³³ Dual silencing of both HSP72 and HSC70 isoforms using siRNA has shown tumour specific apoptosis as well as degradation of HSP90 client proteins.⁶⁹ Importantly, apoptosis was not induced in non-tumourigenic cell lines indicating a potential therapeutic window. The NBDs of these two isoforms are extremely similar which could enable both isoforms to be targeted by a single small molecule.³⁰

The discovery of clinical HSP70 inhibitors has been actively pursued for over a decade⁷⁰ but has proven particularly challenging due to the flexible and hydrophilic nature of the ATP binding site and its high affinity for natural nucleotides. There are currently no tool compounds available to determine the anti-cancer effect of HSP70 inhibition *in vivo*.

The overall aim of this work is to identify novel inhibitors of HSP70 using fragment-based drug discovery methods. To achieve this aim, two approaches were proposed:

- 1) Validation and progression of a fragment hit found to bind to a newly discovered secondary binding site in HSP70
- 2) Development of a non-adenosine based ATP binding site fragment through iterative cycles of design, synthesis and testing.

Approach 1, describing efforts against the secondary binding site, will be discussed in Chapters 2 and 3. Approach 2, describing ATP binding site inhibitors, will be discussed in Chapters 3 and 4.

Chapter 2

2 Discovery and validation of a cryptic secondary binding site in HSP70

2.1 Discovery of a novel binding site in HSP70

As discussed in Chapter 1 it has proved highly challenging to design potent inhibitors of HSP70 that have suitable drug-like properties due to the flexibility of the protein which changes the size and shape of the catalytic site, the hydrophilic nature of the ATP binding site and its high affinity for nucleotides ADP and ATP. An alternative approach is to target sites outside of the active site and to incorporate suitable drug-like properties early on in the design of the inhibitor using fragment-based drug discovery (FBDD).

Previous work at the Institute of Cancer Research carried out a fragment screen with 1962 fragments using surface plasmon resonance (SPR) to identify hits.³¹ The screen was carried out against truncated HSC70 (HSC70-NBD) because full length HSP72 gave erratic and difficult to interpret sensorgrams. The use of an ATP binding site mutant S275W allowed differentiation between hits binding in the primary site from those binding in secondary sites (Figure 2.1). This mutation blocks the ATP binding site by changing a key serine residue to a bulky tryptophan. In all available X-ray crystal structures of ligands bound to the ATP binding site of HSP70 S275 forms an anchoring interaction with the ligand. The overlay of the X-ray crystal structures of wild-type HSC70-NBD with the S275W mutant shows that the adenine ring of adenosine overlaps with the new tryptophan residue indicating that there would be no space for adenosine to bind to this mutant. Indeed introduction of this mutation abolished the binding of adenosine by SPR, as expected.³¹ Therefore, hits that bind equally well to both wild type and S275W mutant HSC70-NBD are likely to bind outside of the ATP binding site.

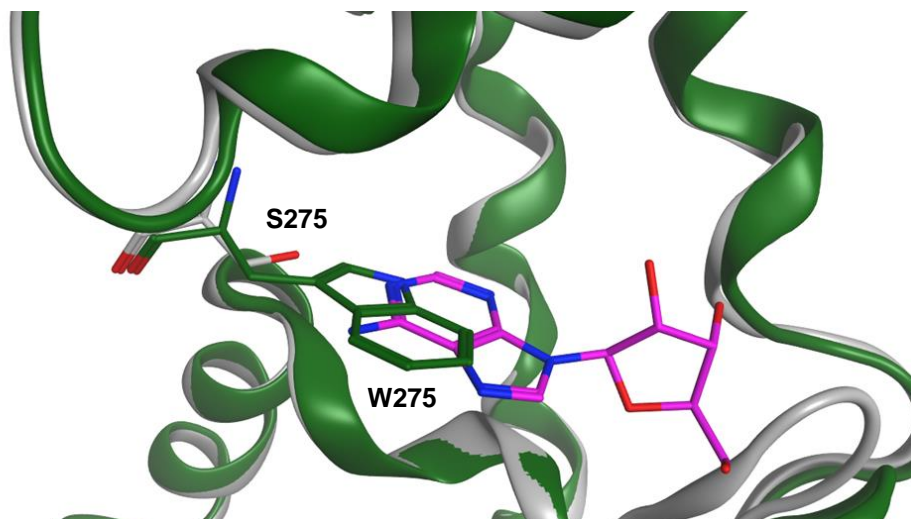


Figure 2.1 – Overlay of wild type HSC70-NBD (PDB ID 5AQF; grey) with the S275 mutant HSC70-NBD (PDB ID 5AQL; green). The large indole group of the tryptophan occupies the space where the adenine ring (pink) would normally bind.

Seven fragments had equal affinity to wild-type HSC70-NBD and the mutant S275W. The X-ray crystal structure of hit fragment **21** with HSP72 NBD was solved to 1.49 Å resolution, revealing the fragment bound in a novel secondary binding site adjacent to the primary site (Figure 2.2). This site has not previously been described and it is not present in apo or nucleotide bound crystal structures. The site is therefore a cryptic pocket, revealed only when the ligand is bound.⁷¹ This cryptic pocket is a long narrow tunnel with a mix of hydrophobic and hydrophilic amino acids, in contrast to the hydrophilic ATP binding site.

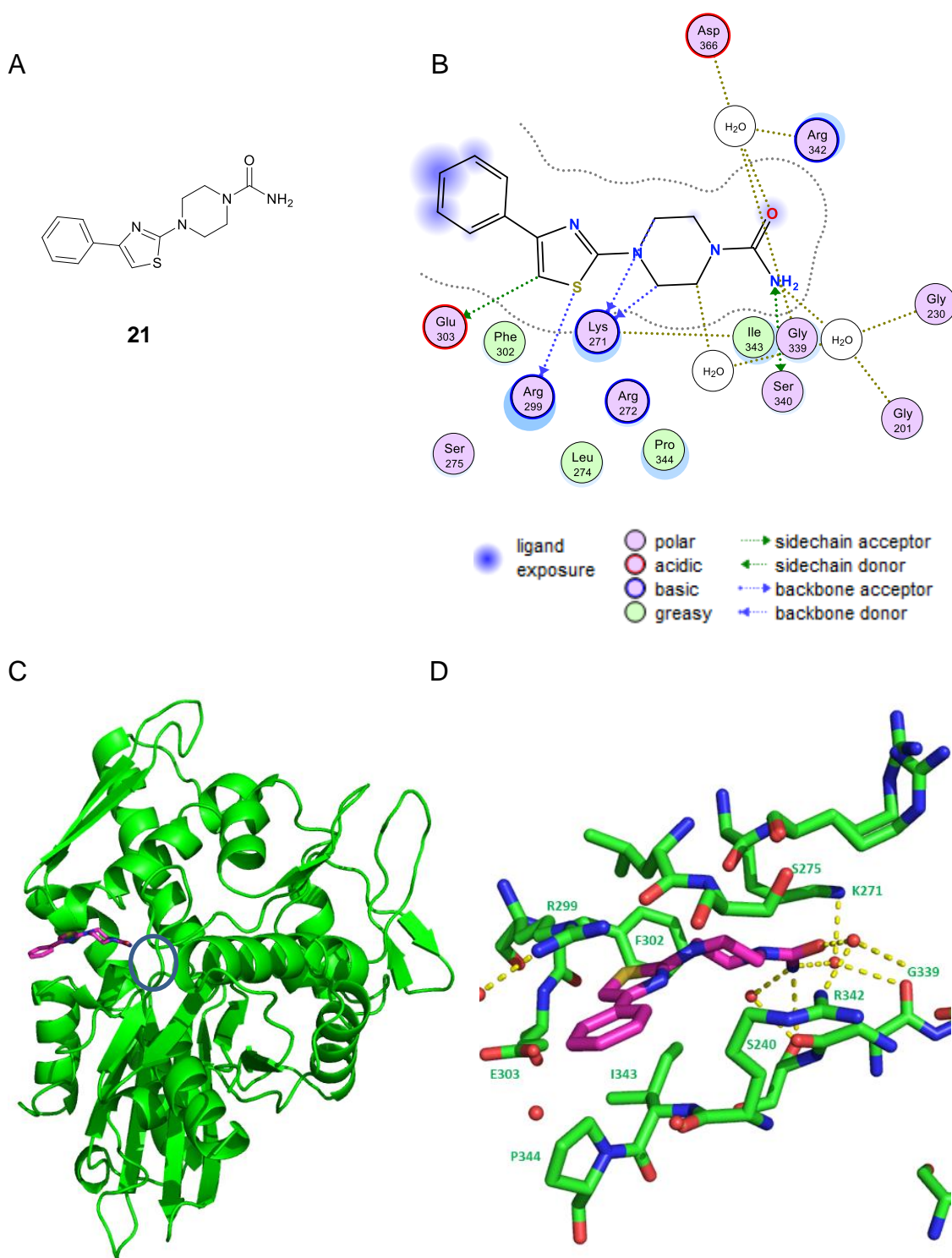


Figure 2.2 – Fragment **21** binds to a novel cryptic secondary binding site in HSP72-NBD. (A) Fragment hit **21**. (B) Ligand Interaction diagram of **21** generated with MOE. (C) X-ray crystal structure of **21** bound to HSP72-NBD with the approximate location of the ATP binding site circled for reference. (D) Expanded view of the binding site.

Commercially available analogues **22** and **23** were purchased and tested by SPR which identified two structurally related hit compounds (Figure 2.3). Further work by a summer student, Ben Williams, identified modifications to the urea **24** and **25** with apparently similar activity. My PhD research began with the aim of confirming and improving the potency of fragment hit **21**, building on this early work.

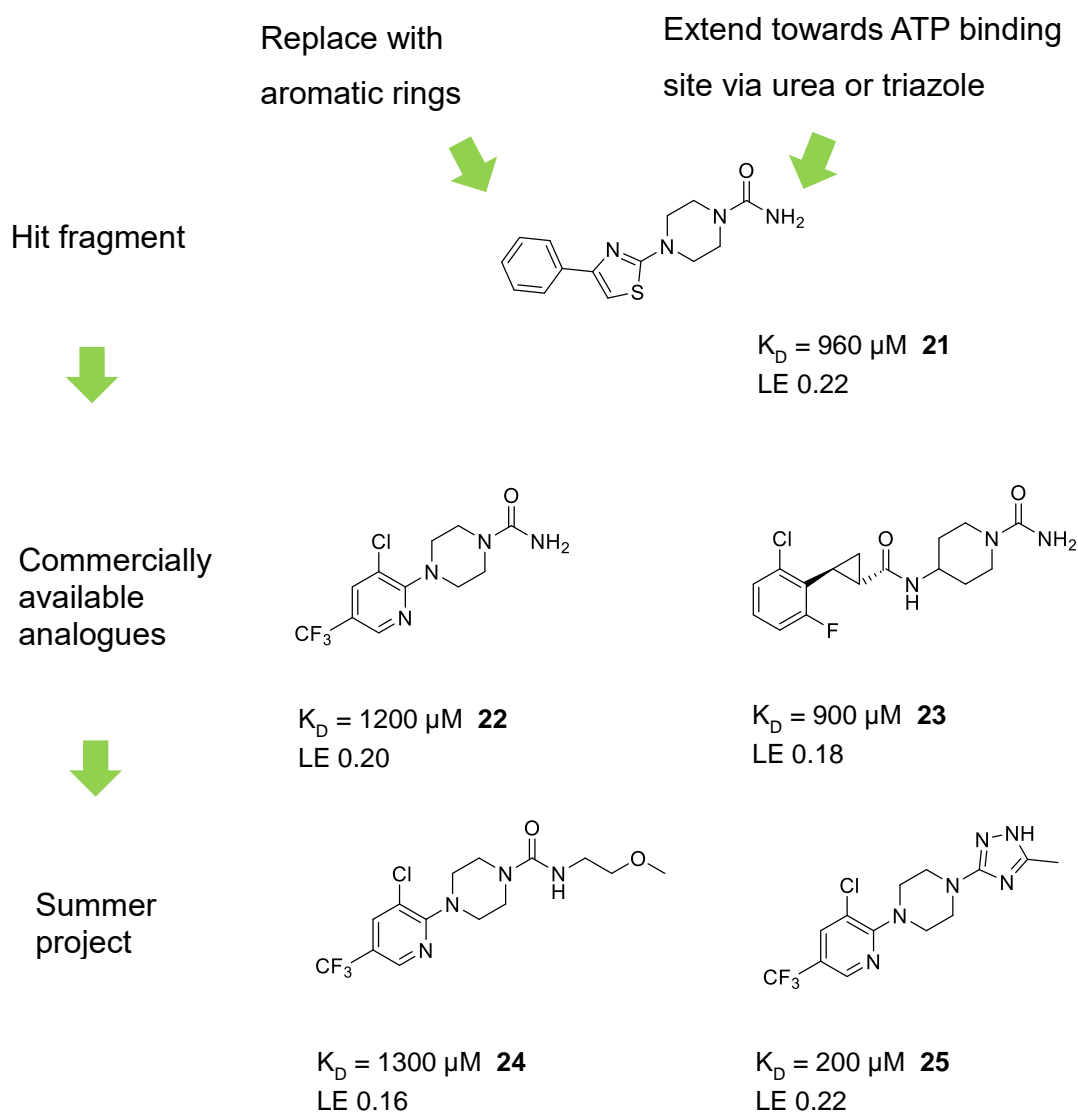


Figure 2.3 – Previous work had identified hit fragment **21**. Two commercially available analogues showed that the aromatic rings could be replaced and the urea could be substituted or exchanged for a triazole ring.

2.2 Cryptic pockets

Cryptic pockets are sites that arise in dynamic regions of the protein that are not obvious in the unbound protein but become apparent once a ligand is bound.⁷¹ Cryptic pocket formation can occur by induced fit, when a binding site is flat in the absence of a ligand and forms in the presence of a ligand, or by conformational selection, when the pocket opens transiently for short periods of time. Such sites can be extensions of an already known pocket or an entirely new site.

From a drug discovery point of view, targeting allosteric cryptic pockets can have the important advantage of selectivity as they are less likely to be evolutionarily conserved and therefore may have reduced off-target effects, and can offer alternative binding sites for difficult to drug proteins. Despite their promising potential there are relatively limited experimental methods that enable direct, detailed structural characterization of the highly dynamic regions from which these cryptic sites arise.⁷² As cryptic pockets require a ligand in order to be identified the majority have been discovered by serendipity. Currently, the only approaches to cryptic site discovery are exhaustive site-directed small-molecule tethering by experiment, long-timescale molecular dynamics simulations by computation, flexible docking and computational tools for identification of small-molecule binding hot spots.⁷³ The use of computational techniques including molecular dynamics to search for cryptic pockets has had some limited success but there is no established method for finding a cryptic pocket as yet.⁷¹

Not all therapeutic targets of interest are druggable but a better understanding of the protein and a search for alternative binding sites can make drugging difficult targets seem more realistic. Many proteins lack druggable pockets but identifying cryptic pockets in these proteins could expand the set of druggable targets. For example, there has been extensive attempts over the last 30 years to develop inhibitors of K-RAS, the most commonly mutated oncogene in human cancers, which led many to believe the target to be undruggable. However, a new cryptic pocket has recently been reported and successfully targeted.⁷⁴

2.3 Surface plasmon resonance

Surface plasmon resonance is a sensitive biophysical technique that can be used to detect the binding of a compound or another protein to the protein of interest. It is able to detect even weakly binding hits of up to millimolar affinity.⁷⁵ Neither ligand nor protein need to be labelled and only a small amount of protein and compound is required. The experiment can provide information on both affinity and kinetics.

In general, when light passes from a dense medium to a less dense medium it bends, known as refraction. As the angle of incidence is increased, the angle of refraction is increased and at a certain point the angle of refraction will become 90° . The angle of incidence at which this occurs is known as the critical angle. When light is shone at an angle greater than the critical angle, total internal reflection occurs; the light does not enter the second media but is instead reflected back. Evanescent waves are formed in the lower refractive index medium under the condition of total internal reflection.

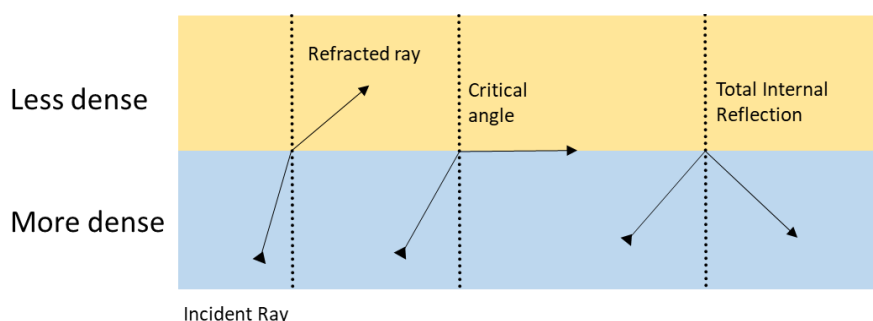


Figure 2.4 – Total internal reflection occurs when the angle of incidence exceeds the critical angle.

In a surface plasmon resonance experiment refractive index changes at a metal surface are used to monitor binding interactions in real time. Biomolecules such as proteins, antibodies, DNA, or RNA are immobilized onto a metal surface.⁷⁶ Polarized, single wavelength light is directed through a glass prism to the bottom of a metal surface and is reflected back to the detector (Figure 2.5). When

polarised light is shone on the metal film at an angle greater than the critical angle, the delocalized electron oscillations in the metal known as surface plasmons, can be excited by the evanescent wave. This phenomenon is known as surface plasmon resonance.⁷⁷ When SPR occurs the intensity of the reflected light decreases sharply. The angle at which SPR occurs depends on the refractive index of the medium. When a ligand binds to a protein immobilised onto the chip it changes the refractive index of the medium and therefore the angle at which SPR occurs which can be measured by a detector. This change in angle measures the amount of bound analyte, its affinity for the protein and the association and dissociation kinetics of the reaction.

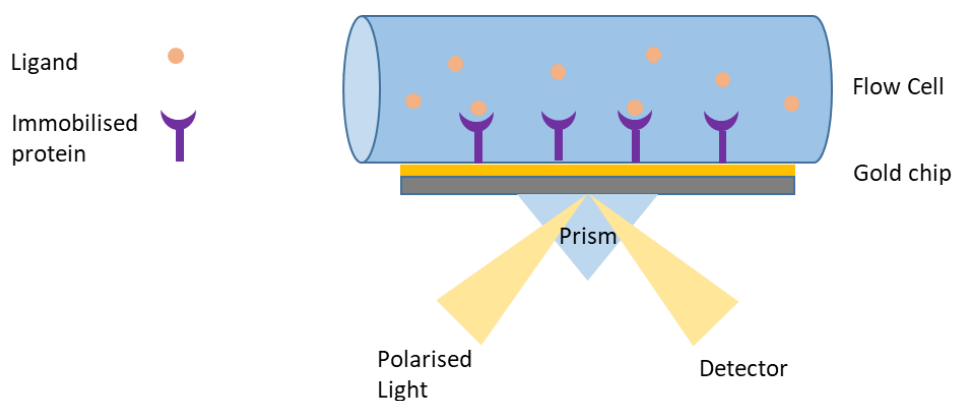


Figure 2.5 – Surface plasmon resonance experiments can be used to measure the binding of a ligand to an immobilised protein of interest.

SPR is highly sensitive technique that can detect weakly binding fragment hits in real time but it requires specialist expertise in experimental design and optimisation as well as expensive equipment. Care must be taken to examine sensorgrams and binding curves which may indicate non-specific binding. The integrity of the immobilised species should also be monitored over time with control samples.

To attach the protein of interest to the chip, a glass surface is coated with an inert metal, usually gold, as it is chemically inert to the solutions and solutes typically used. Onto the gold surface a self-assembled monolayer is deposited

which provides a linker layer to the metal surface and the next layer, which consists of carboxymethylated dextran.⁷⁸ The dextran is a layer of 1,6 linked glucose units that are each modified with one carboxyl group. The protein can then be immobilised onto the chip using amide coupling chemistry.

A mixture of EDC (1-ethyl-3-(3-dimethylaminopropyl)carbodiimide, **26**) and NHS (*N*-hydroxy succinimide, **27**) is used for the coupling reaction. EDC reacts with carboxylic acid groups to form a more reactive intermediate that can be more easily attacked by the nucleophilic lysines of the protein.⁷⁹ EDC crosslinking is most efficient in acidic conditions so for this project sodium acetate buffer at pH 5 was used to couple HSC70-NBD to the chip. NHS is added to improve the efficiency of coupling (Figure 2.6).

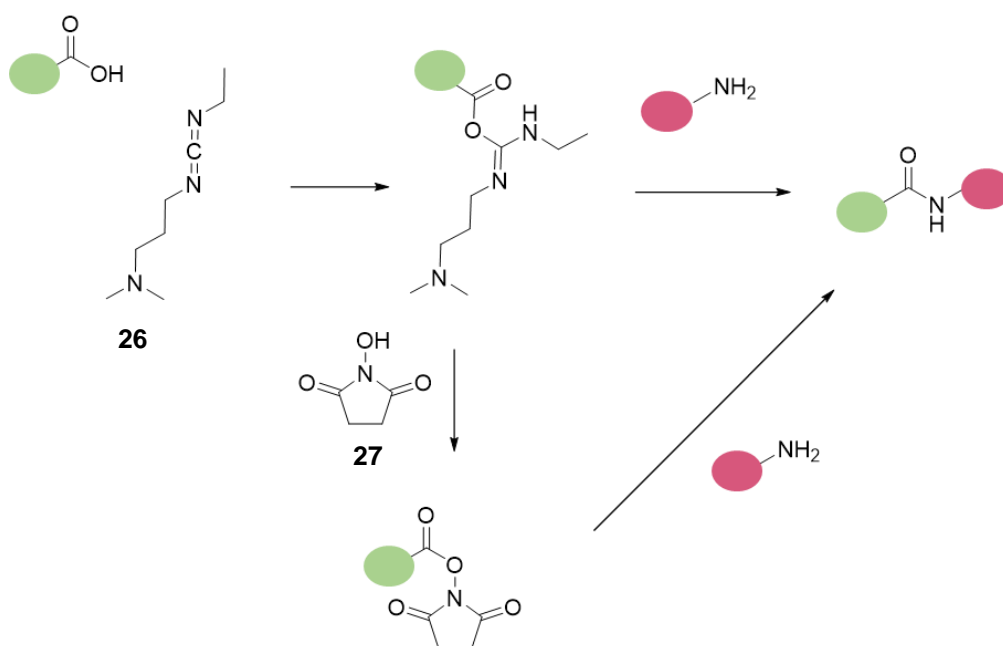


Figure 2.6 – A mixture of EDC **26** and NHS **27** couples the carboxylic acids to the primary amines of the protein by forming reactive ester intermediates.

2.4 Validation of the secondary binding site

2.4.1 Design of Library 1

Previous work had shown that hit fragment **21** could be elaborated by replacing the aromatic rings on the left-hand side of the molecule and by extending towards the ATP binding site with polar groups. My work began with the design and synthesis of a library of compounds based on compounds **21-25** and guided by the X-ray crystal structure. The library was designed to explore new structure activity relationships and to discover what changes were tolerated by the protein. Fragment libraries generally comprise of compounds with molecular weights between 150 to 250 Da and hit fragments generally have a ligand efficiency of greater than 0.3 kcal/mol per heavy atom.⁸⁰ The molecular weight of fragment hit **21** (288 Da) is considered a little high and the ligand binding efficiency (0.21) is less than desirable so determining which elements of the fragment were essential for binding and which could be replaced was an important first step. The changes were designed to be small as it is also desirable to have multiple similar fragments binding to the target to validate the hit fragment.

The core piperazine ring was fixed which allowed two points of differentiation. R¹ was chosen to be either a benzene or pyridine ring with various substituents at the ortho, meta and para positions similar to fragment **22**. Designs with a cyclopropane ring were based on fragment **23**. R² was chosen to be either a substituted urea or a triazole based on fragments **24** and **25** respectively (Figure 2.7).

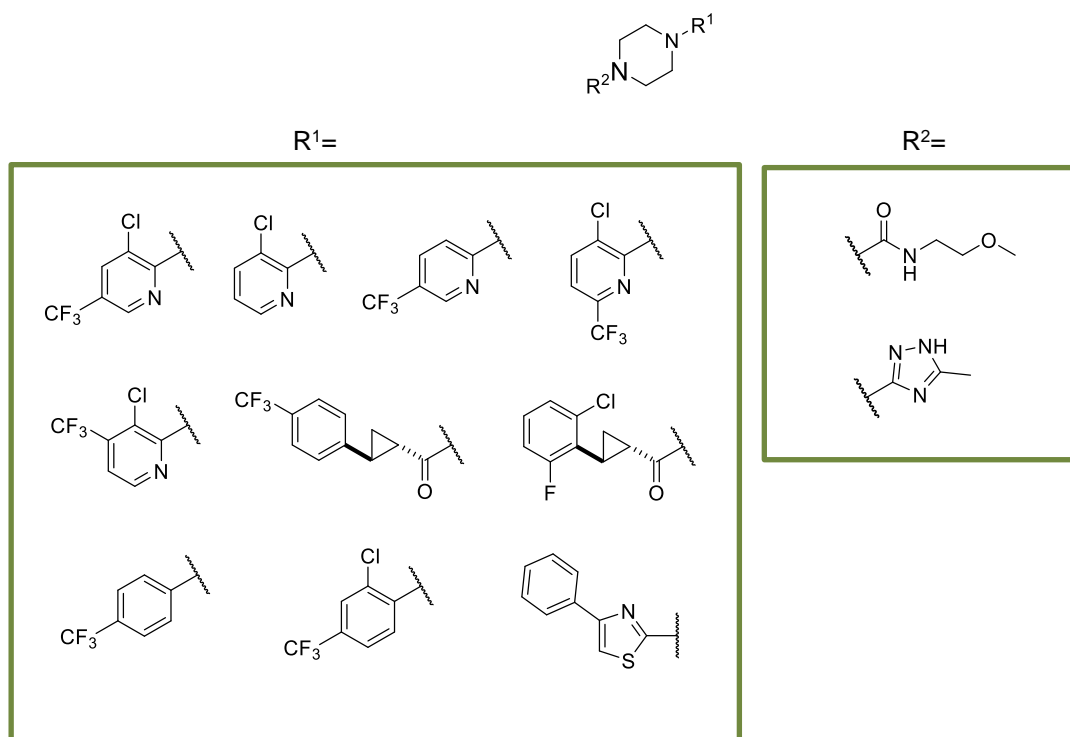


Figure 2.7 - Design of library 1. The core piperazine ring was fixed, the right-hand side of the molecule was chosen to be either a substituted urea or a triazole while the left-hand side of the molecule consisted of a variety of aromatic rings.

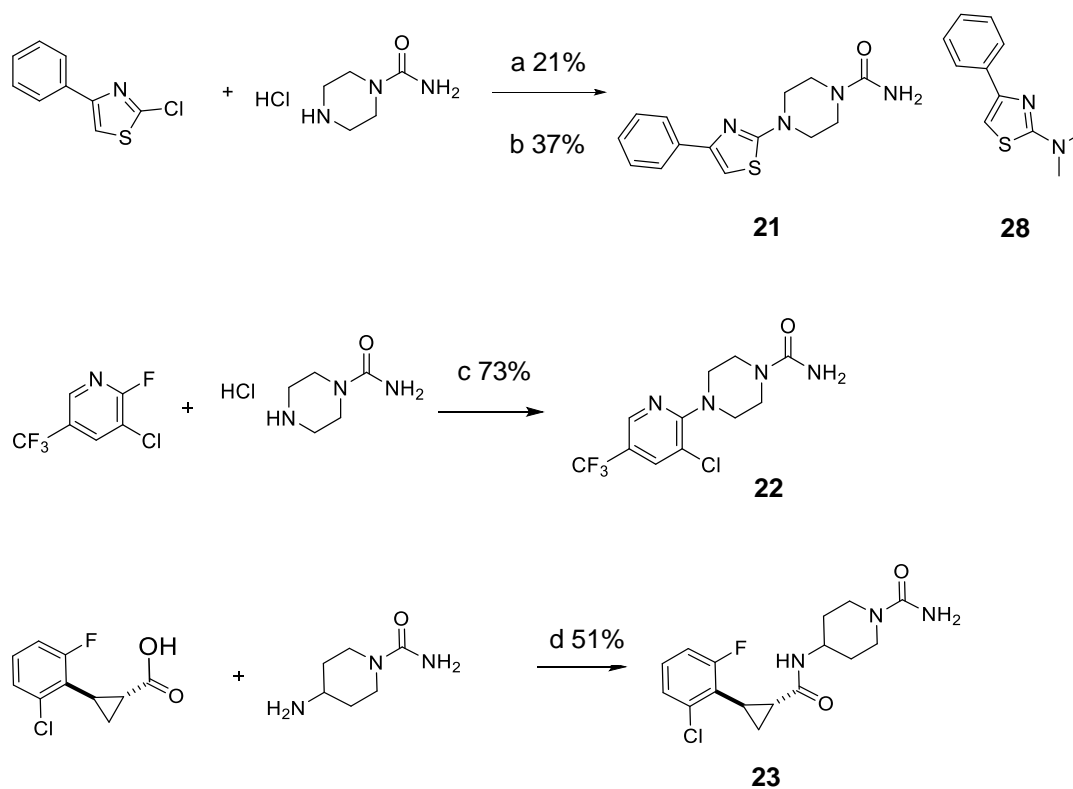
2.4.2 Synthesis of Library 1

2.4.2.1 Resynthesis of hit compounds

Early hit compounds **21**, **22** and **23** are commercially available and were previously bought in for testing. These compounds were now re-synthesised to ensure purity and correct structure. Compounds **24** and **25** were also resynthesised to be used as control compounds in the SPR assay.

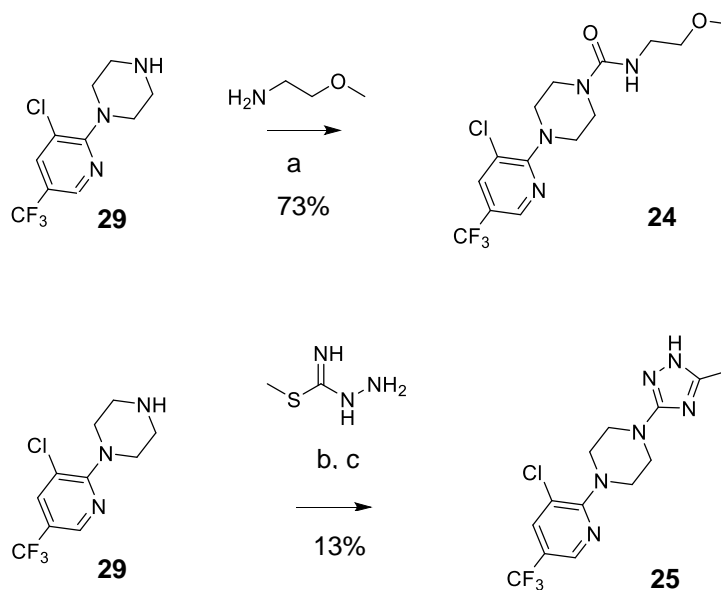
Synthesis of compound **21** was first attempted by S_NAr (nucleophilic aromatic substitution) in DMF. However, the DMF decomposition side product **28** was also observed by LC-MS, which resulted in a low yield. Switching the solvent to DMSO allowed higher temperatures to be used and increased the yield from 21% to 37% (Scheme 2.1). Compound **22** was also synthesised by S_NAr . At high temperatures, the urea decomposed to give a piperazine side product requiring

a balance to be struck between product formation and product decomposition. Highest yields (73%) were obtained in NMP at 100 °C for two hours. Compound **23** was synthesised by amide coupling from the commercially available 2-(2-chloro-6-fluorophenyl)cyclopropane-1-carboxylic acid.



Scheme 2.1 - (a) K_2CO_3 , DMF, 100 °C, 4 h (b) K_2CO_3 , DMSO, 130 °C, 7 h. Isolated yields are shown for compound **21**. Conditions a resulted in a significant amount of side product **28**. Switching to conditions b gave the desired product in better yields. (c) DIPEA, NMP, 100 °C, 2 h. (d) HATU, DIPEA, DMF, rt, 24 h.

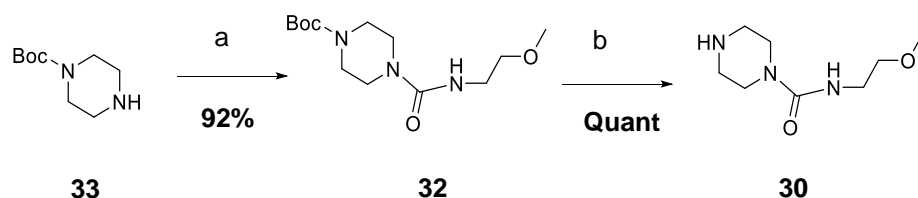
Compounds **24** and **25** had previously been synthesised using the commercially available 1-(3-chloro-5-(trifluoromethyl)pyridin-2-yl)piperazine **29** and were resynthesized using this starting material (Scheme 2.2). **24** was synthesised in one step in good yields with CDI as the coupling agent. **25** was synthesised in two steps with an overall yield of 13%. This is a poor reaction but it supplied enough desired material for testing.



Scheme 2.2 - Resynthesis of previous hit fragments **24** and **25** was carried out for use as control compounds in the SPR assay. (a) CDI, DCM, 0 °C → rt, 22 h (b) water:IPA 1:1, reflux 18 h (c) AcOH, reflux 4 h.

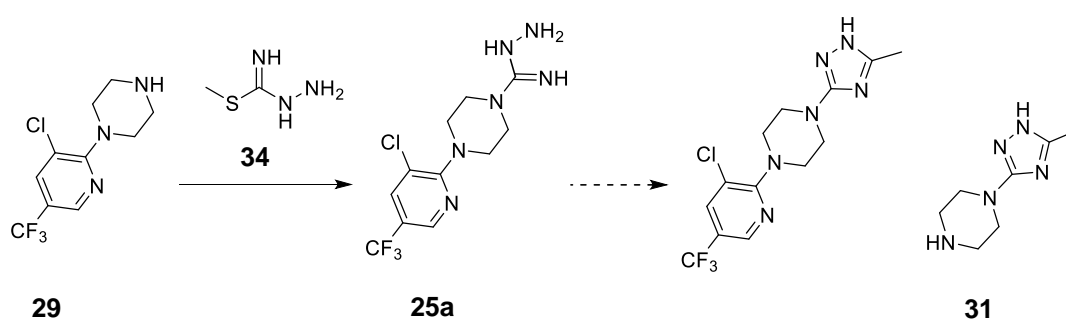
2.4.2.2 Synthesis of key intermediates for library 1

For the new library, a new synthetic route needed to be developed to allow the variable portion of the molecule to be attached at the last step. This required the synthesis of two key intermediates **30** and **31** from which the desired compounds could then be synthesised in one step. The synthesis of intermediate **32** from Boc-protected piperazine **33** proceeded in excellent yields (92%, Scheme 2.3). The Boc protecting group was then removed with standard conditions. Gram quantities of intermediate **30** were synthesised with this route.



Scheme 2.3 – Synthesis of key intermediate **30**. (a) 2-methoxyethan-1-amine, CDI, DCM, 0 °C → rt 18 h (b) 4 M HCl in dioxane, rt, 4 h.

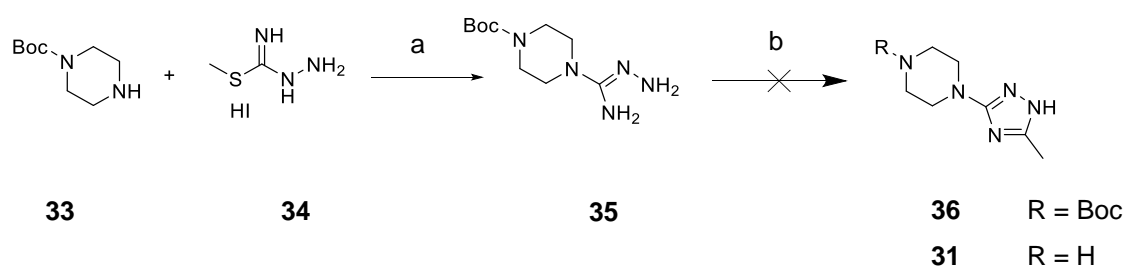
The synthesis of intermediate **31** required significant optimisation. For clarity, only one tautomer of the triazole of **31** is drawn. The route used to synthesise compound **25** was very low yielding (13%). This reaction was optimised as a model system with a UV chromophore with the intention that the optimised conditions could then be used to synthesise **31**. Compound **29** was dissolved in 1:1 IPA:water and heated at 105 °C under conditions according to Table 2.1 and the reactions were monitored by LC-MS.



Expt	Equivalents of 34	TEA	Time (h)	Ratio SM: intermediate 25a
1	1	0	18	3.5:1
2	3	0	18	16:1
2b	3	5	+6	2:1
3	1.5	3	6	3:1
3b	1.5	3	+18	5:1
4	3	5	6	1:1.3

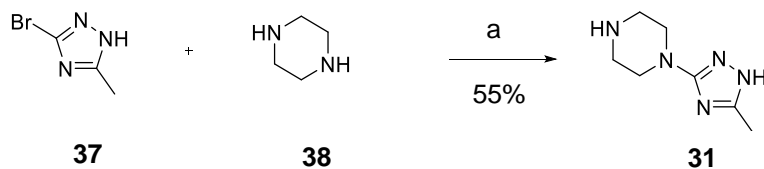
Table 2.1 – Optimising the synthesis of **25a** by varying the equivalents of methyl hydrazinecarbamidithioate, base and time as a model system for the synthesis of intermediate **31**.

Longer reaction times often resulted in lower observed product likely due to product instability as decomposition products were also observed. The product from experiment 4, which was the only experiment that had a higher ratio of product to starting material, was refluxed in acetic acid to give the desired compound **25** in much better yield in comparison to the original conditions (69% vs 13%). These conditions were then used to synthesise intermediate **31**. Refluxing Boc-protected piperazine **33** with methyl hydrazinecarbimidothioate **34** gave the desired product **35** which could be detected by LC-MS. However, refluxing overnight in acetic acid resulted in no desired product **36**, possibly because the Boc group is unstable under these conditions (Scheme 2.4). An alternative protecting group, Cbz, was then investigated. With this replacement protecting group the desired product was formed but in very low yields.



Scheme 2.4 - Synthesis of key intermediate **31** was unsuccessful using conditions optimised for the structurally similar **3** synthesis. (a) TEA, water:IPA 1:1, 105 °C, 6 h (b) AcOH, 120 °C, 18 h.

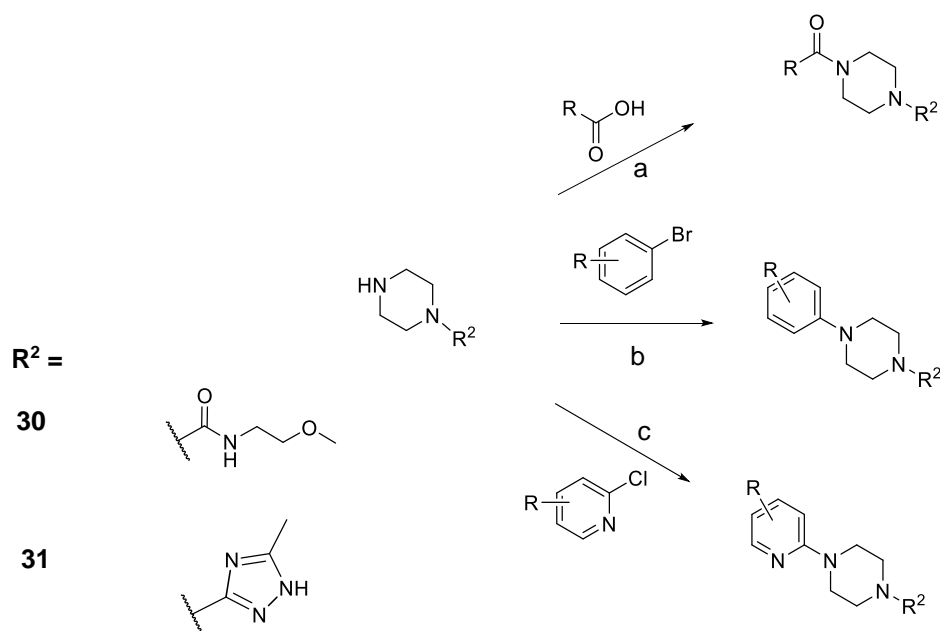
An alternative and more successful approach to make **31** was developed using the commercially available 3-bromo-5-methyl-1*H*-1,2,4-triazole **37** (Scheme 2.5). S_NAr was carried out with five equivalents of piperazine **38** to drive the reaction forward and minimise the unwanted side reaction of the product reacting with the triazole starting material. The desired product was formed but it was extremely difficult to purify from the excess piperazine. The reaction was repeated with three equivalents of piperazine and purified using base modified silica to give a moderate yield of 55%.



Scheme 2.5 - Synthesis of key intermediate **31** from piperazine. (a) NMP, 200 °C, 1.5 h.

2.4.2.3 Synthesis of Library 1 from key intermediates

From the two key intermediates **30** and **31** the desired final compounds were synthesised in one step via amide coupling, Buchwald coupling or S_NAr (Scheme 2.6).



Scheme 2.6 – Synthesis of Library 1 by amide coupling, Buchwald coupling or S_NAr from intermediates **30** and **31** with example conditions. (a) 1.5 eq HATU, 5 eq DIPEA, DMF, r.t. 18 h (b) CS_2CO_3 , BINAP, $Pd(OAc)_2$, toluene, 110 °C, 18 h (c) TEA, ethanol, 150 °C in MW, 1.5 h.

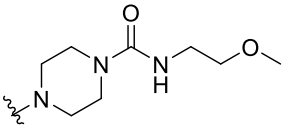
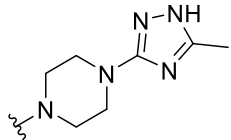
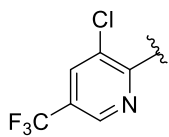
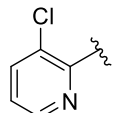
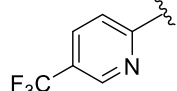
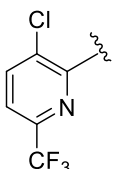
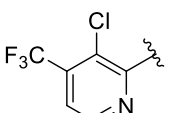
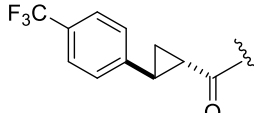
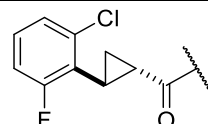
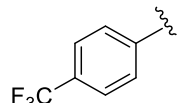
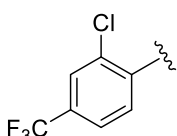
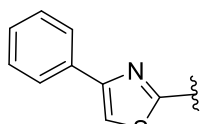
R^1-R^2 R^1	R^2 	
	24 73% Scheme 2.2 ^a	25 13% Scheme 2.2 ^a
	39 15% S _N Ar	47 14% S _N Ar
	40 55% S _N Ar	48 22% S _N Ar
	41 32% S _N Ar	49 45% S _N Ar
	42 33% S _N Ar	50 53% S _N Ar
	43 69% Amide Coupling	51 32% Amide Coupling
	44 72% Amide Coupling	52 27% Amide Coupling
	45 52% Buchwald Coupling	53 n.s.
	46 30% Buchwald Coupling	54 n.s.
	-	55 24% S _N Ar

Table 2.2 – Nineteen compounds based on early hit fragments **21-25** were synthesised. ^aYield and method of synthesis. n.s. not synthesised.

Compounds **39-46** were all synthesised from intermediate **30** using one of three methods – amide coupling, Buchwald coupling or S_NAr . Amide coupling for **43** and **44** proceeded reliably and in good yields. S_NAr for compound **40** proceeded in one hour at 140°C with no starting material remaining, however, for compound **39**, the S_NAr was much slower without the para- CF_3 group and required heating at 200°C for four hours. Compounds **41** and **42** with the CF_3 in the meta position proceeded with yields in between that of **39** and **40** reflecting the expected reactivity of the starting materials. The Buchwald coupling for compound **45** proceeded well and purification by ion exchange chromatography, using an acidic resin, allowed separation from the BINAP ligand. For compound **46**, however, the des-chloro compound was also formed under these conditions. Stopping the reaction after six hours gave the desired product although it was not basic enough to be retained by the acidic resin, resulting in a lower yield.

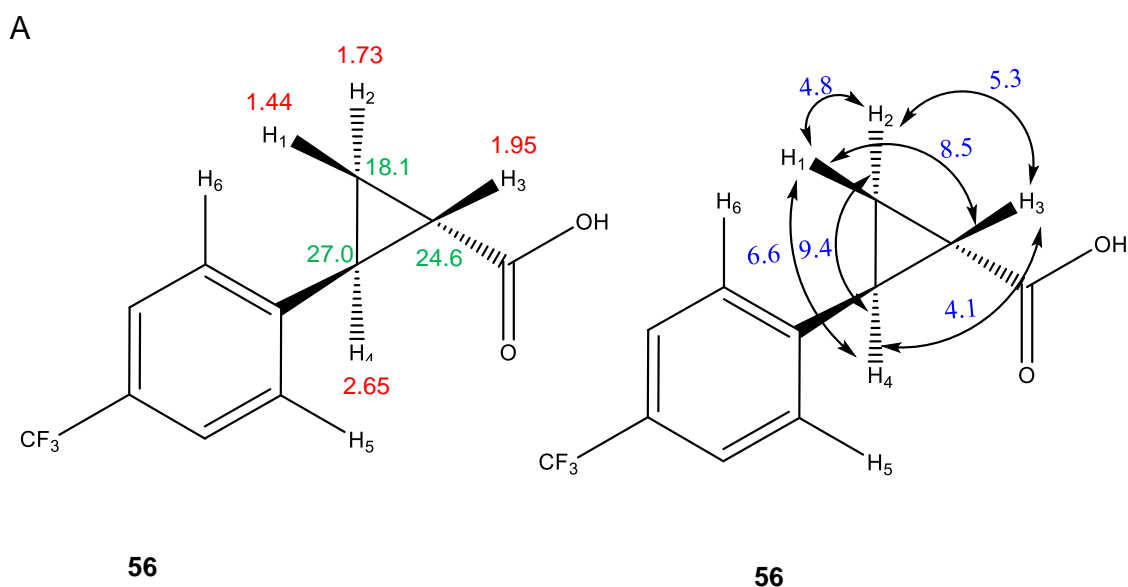
Compounds **47-52** were synthesised from intermediate **31** by amide coupling or S_NAr . Compounds **47-50**, synthesised by S_NAr , co-eluted with a TEA:HCl impurity which was removed using ion exchange chromatography with a basic resin. Amide coupling for compounds **51** and **52** proceeded in reasonable yields overnight. The Buchwald coupling for **53** and **54** using intermediate **31**, however, was unsuccessful despite multiple conditions employed. Compound **55** was instead synthesised by S_NAr .

2.4.2.4 Determination of relative stereochemistry of cyclopropane containing compounds

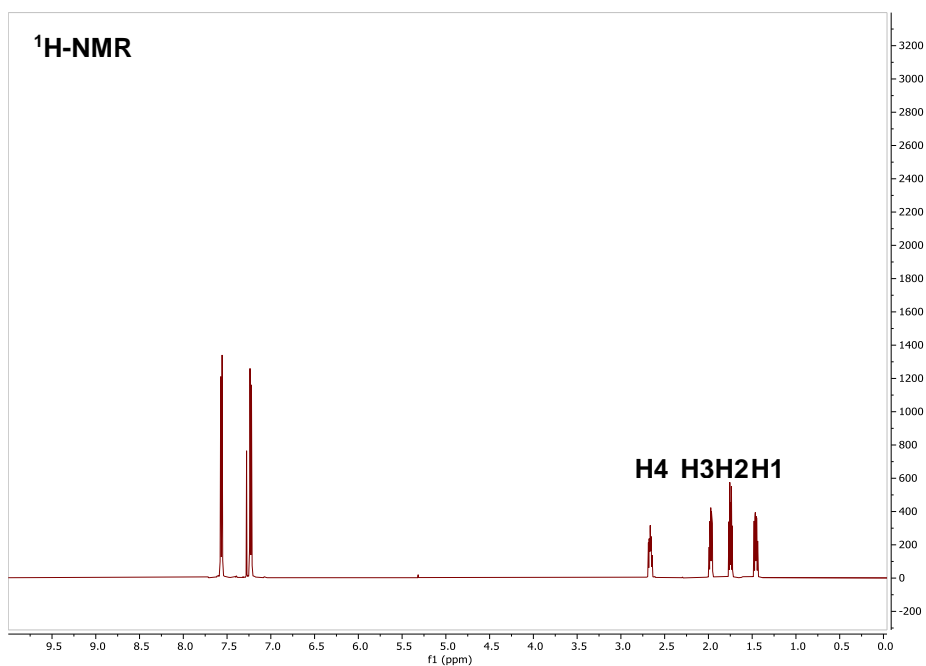
The stereochemistry of the starting materials for compounds **43** and **44** (also **51** and **52**) was not specified and needed to be determined. From the 1H -NMR of **56** and **57** the compounds were single isomers - either *cis* or *trans* (Figure 2.8). ^{13}C -NMR, HMBC, HSQC, COSY and NOESY were carried out to determine which isomer was present. From the HSQC the protons with the two lowest chemical shifts can be identified as H1 and H2 which share a single carbon; H3

and H4 each have their own carbon. H3 and H4 can be distinguished by HMBC - H1, H2 and H4 are all coupled to the carbonyl group but H3 is not.

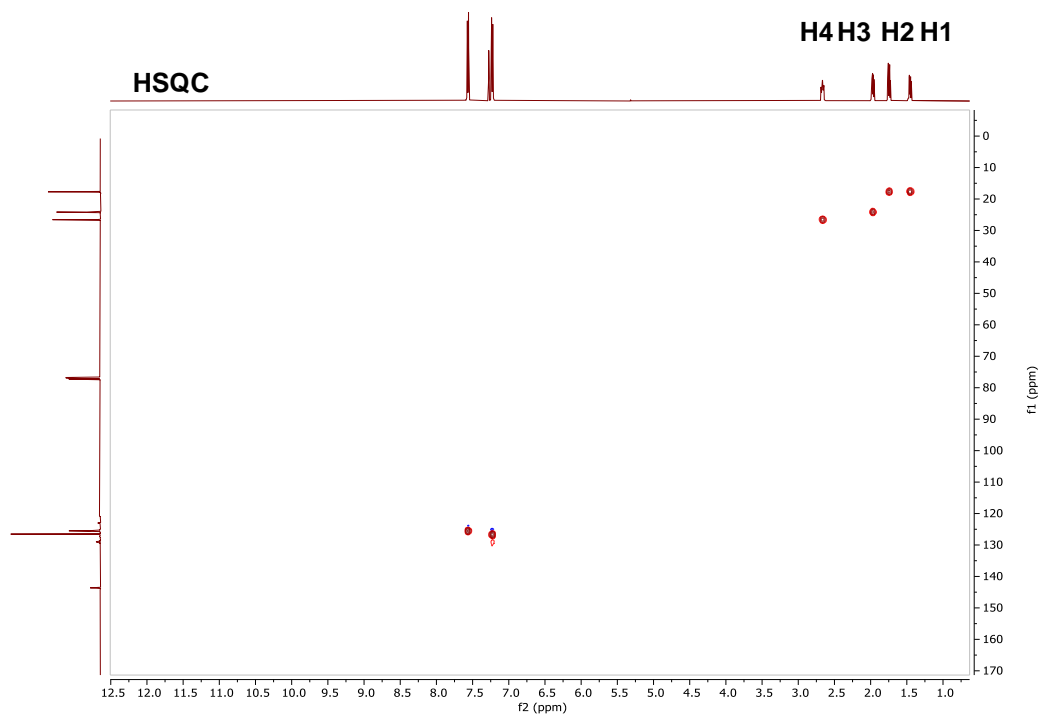
Once each proton was unambiguously assigned, the coupling constants between protons were then determined. Coupling constants for cyclopropane ring systems are quite different to coupling constants for cyclohexane ring systems. Dihedral angles in cyclopropanes are rigidly fixed by the geometry of the ring system. Thus J_{cis} (7-10 Hz) is always larger than J_{trans} (2-6 Hz) in cyclopropane ring systems, and this can be reliably used for structure assignment.⁸¹ Analysis of the coupling constants for **56** showed this compound to be the *trans* isomer. For further confirmation, in the NOESY H1 and H2 are shown to be close in space but H3 and H4 are not, as expected for the *trans* isomer. In the COSY H1 couples to H3 and H2 couples to H4.



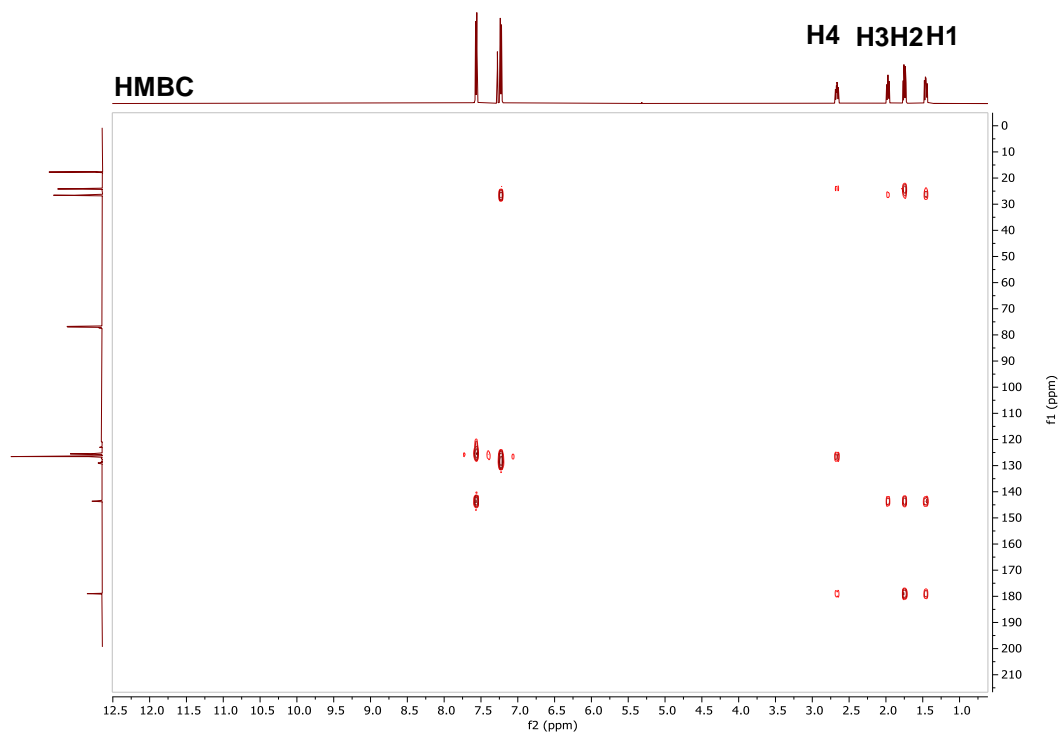
B



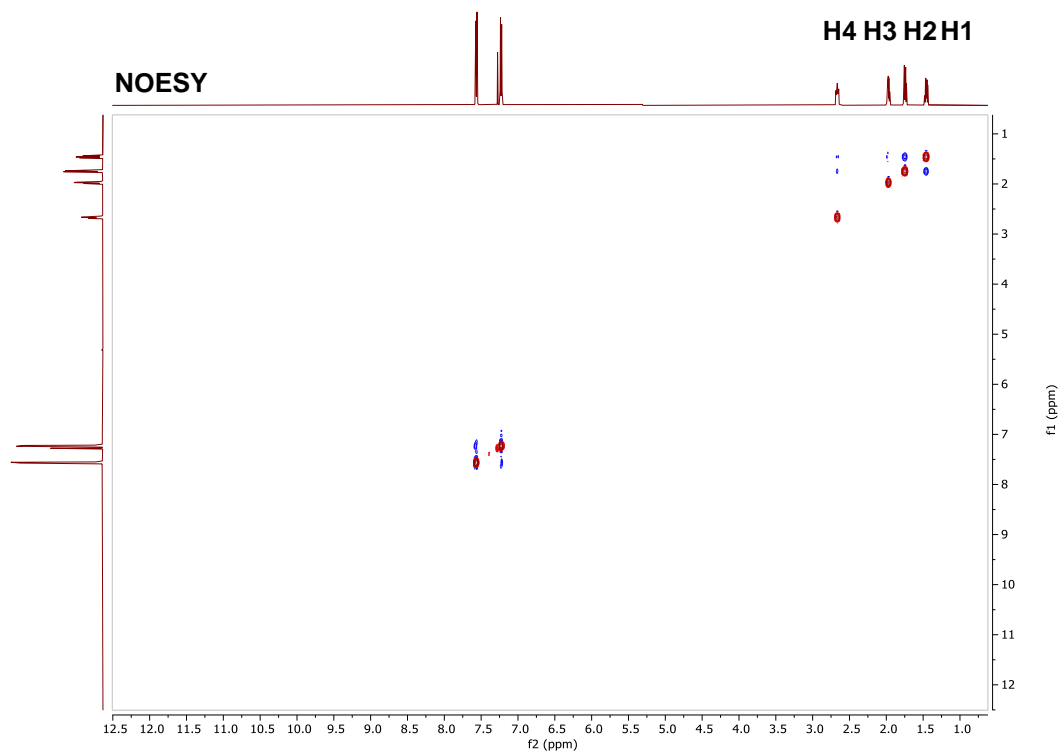
C



D



E



F

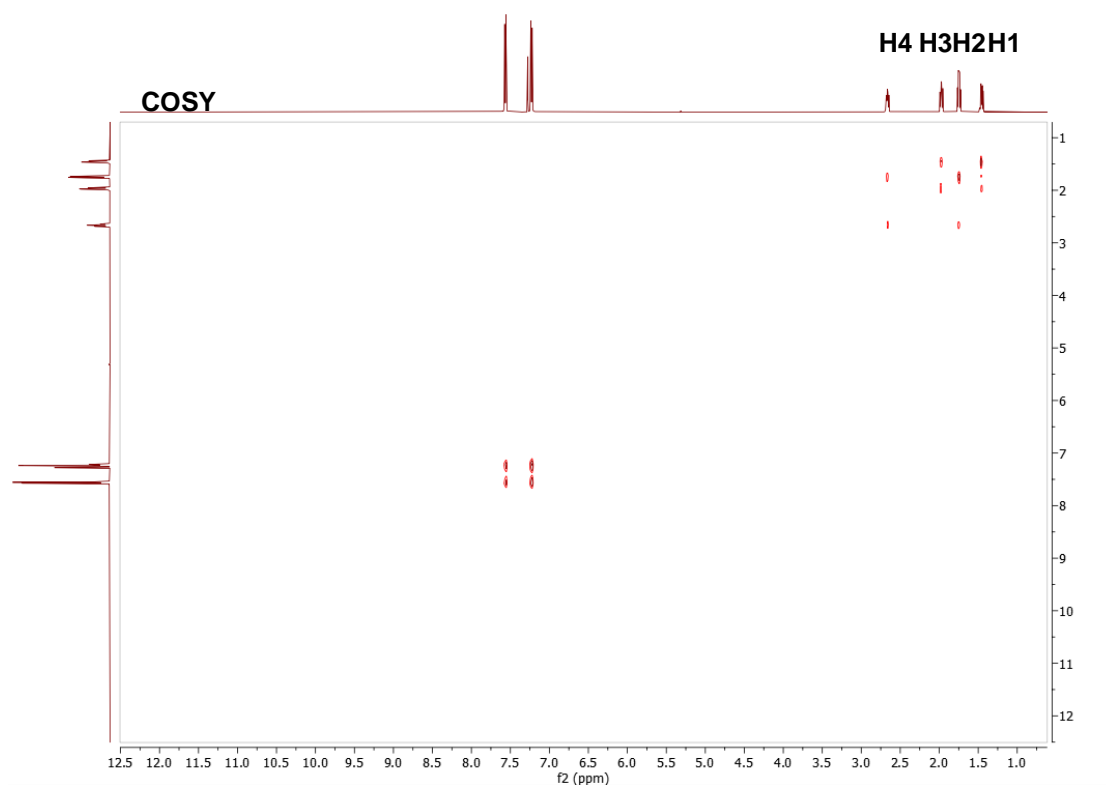


Figure 2.8 – NMR analysis of **56**. (A) ^{13}C -NMR shifts in green, ^1H -NMR shifts in red, coupling constants in blue. (B) H-NMR (C) HSQC (D) HMBC (E) NOESY (F) COSY.

For compound **57** the stereochemistry was also determined to be *trans*, by NMR analysis, carried out in the same way as for **56** (NMR data for compound **57** are in Appendix 2). The coupling constants for the two starting materials are very similar, as expected for such structurally similar compounds with the same stereochemistry. Compounds **43**, **44**, **51** and **52** made from starting materials **56** and **57** were found to have cyclopropane rings with a *trans* configuration, as determined by their coupling constants in the ^1H -NMR.

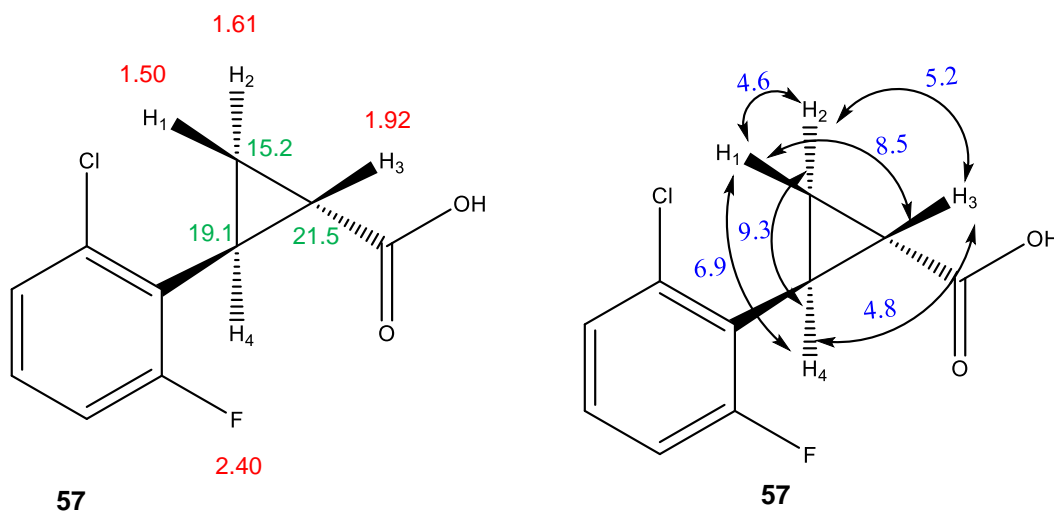


Figure 2.9 – The stereochemistry for **57** was determined to be *trans* by NMR analysis, with coupling constants similar to **56**. (^{13}C -NMR shifts in green, ^1H -NMR shifts in red, coupling constants in blue).

2.4.2.5 NMR analysis of compound **55**

Two quaternary carbon peaks corresponding to the triazole carbons and the triazole's methyl group were not visible in the ^{13}C -NMR for compounds **47**, **48**, **51**, **52** and **55** likely due to tautomerisation. The triazole's methyl group in the ^1H -NMR is very broad consistent with tautomerisation. Adding a drop of HCl to **55** when running the NMR experiments allowed the triazole's two quaternary carbon peaks and the methyl peak to be seen much more clearly in the ^{13}C -NMR and the methyl peak is much sharper in the ^1H NMR (Figure 2.9).

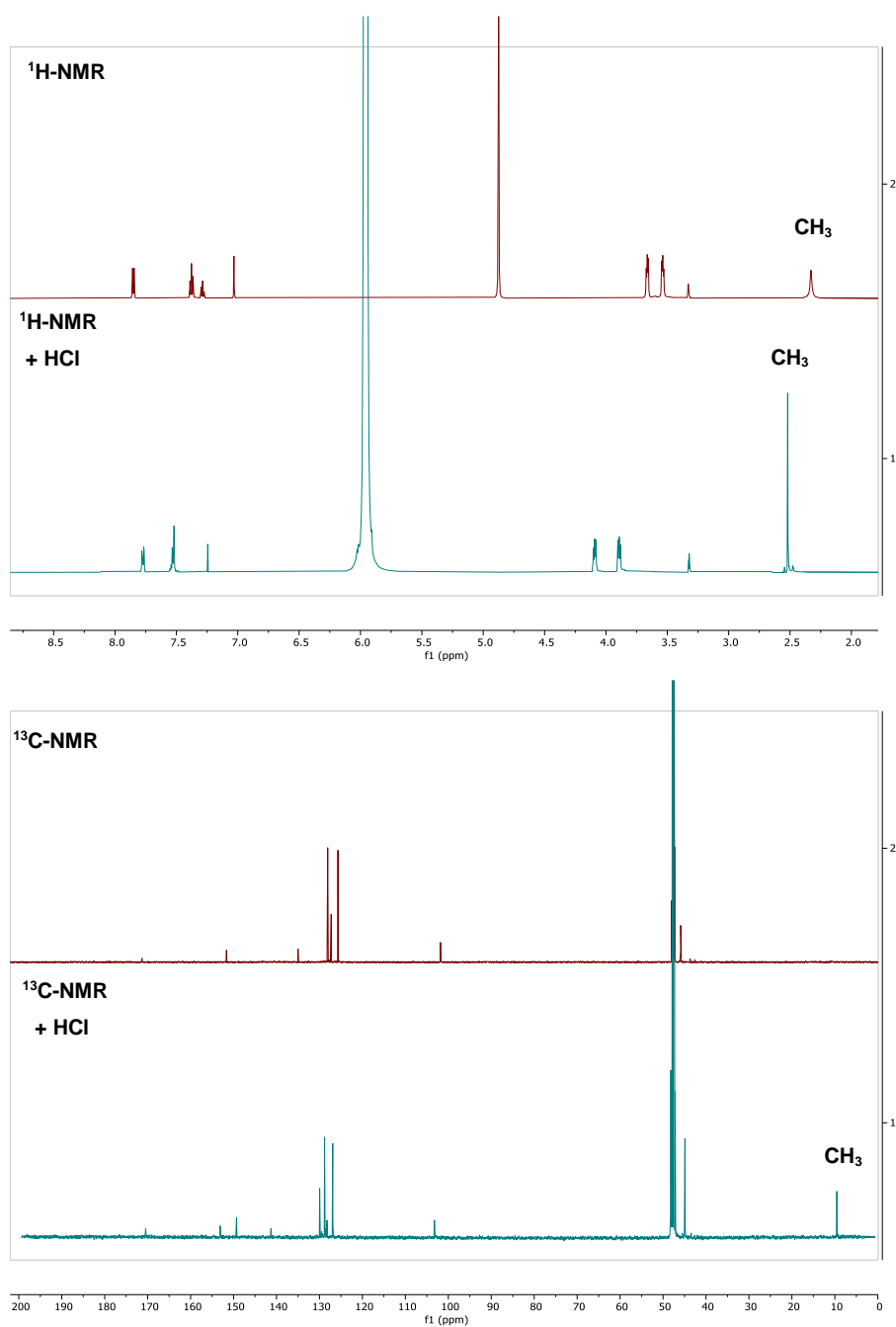


Figure 2.9 - NMR analysis of compound **55**. Quaternary triazole and methyl peaks are not visible in $^{13}\text{C-NMR}$ and the methyl peak is broad in the $^1\text{H-NMR}$ (red spectra). Addition of HCl sharpened the methyl peak and allowed characterisation of the triazole quaternary and CH_3 carbons (green spectra).

2.4.3 Testing of Library 1 by SPR

The library of fragment **21** analogues was tested by SPR against immobilised wild type Tr-HSC70 and the S275W mutant. With increasing concentrations of an inhibitor, there should be increased binding to the protein on the chip until the protein becomes saturated. Control compounds adenosine (fast on/fast off, weak binding) and VER-155008 **6** (fast on/slow off, strong binding) were used for each SPR run and gave K_D values consistent with literature values. Figure 2.10 shows an example of the sensorgrams and binding curves obtained for these controls.

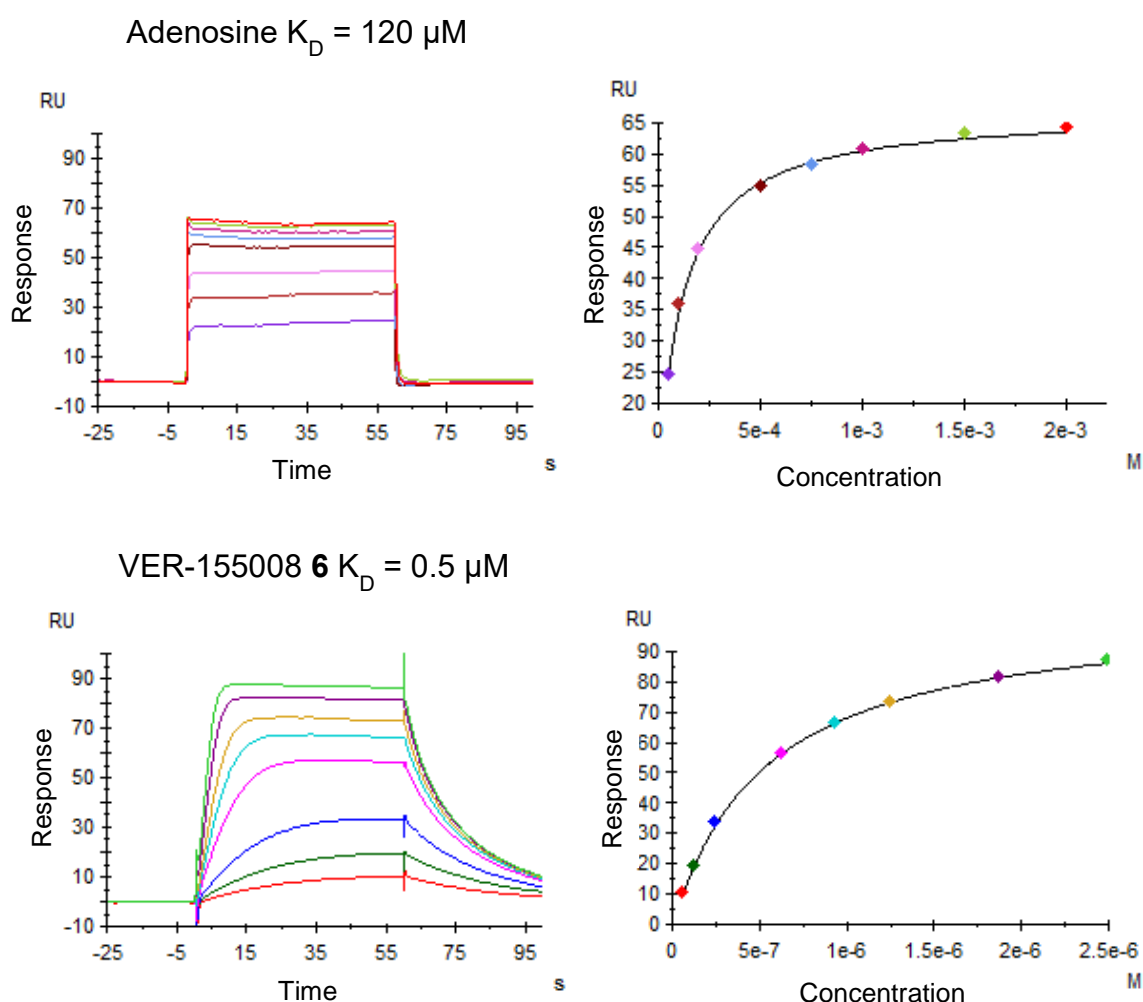


Figure 2.10 - Control sensorgrams and binding curves for adenosine and VER-155008 **6**

SPR testing of compounds **21-52** and **55** gave very surprising results. None of the compounds gave good quality binding curves from which a K_D value could be calculated. Compounds either exhibited very weak binding responses (below 10 RU), straight-line responses where no saturation was occurring even at the highest concentrations indicating very weak or non-stoichiometric binding, or not measurable where compounds precipitated at the high concentrations required to reach saturation (Figure 2.11).

Because the affinity of the fragment for the protein is weak (mM), high concentrations of compound are required for saturation of the binding site. At such high concentrations the compounds were not always soluble in the SPR buffer. It could not be determined if these compounds were non-specific, binding very weakly or were binding but then precipitating at high concentrations. Another concern was that the resynthesized fragment hit **21** was non-stoichiometric in at least two separate experiments. Multiple attempts to repeat the X-ray crystal structure were also unsuccessful.

The focus therefore moved from designing more potent fragments to validating the original fragment hit. We hypothesised that many of the issues with the SPR testing of these compounds could be explained by poor solubility at such high concentrations. The next step therefore, was to design more soluble versions of the original fragment hit to confirm fragment binding.

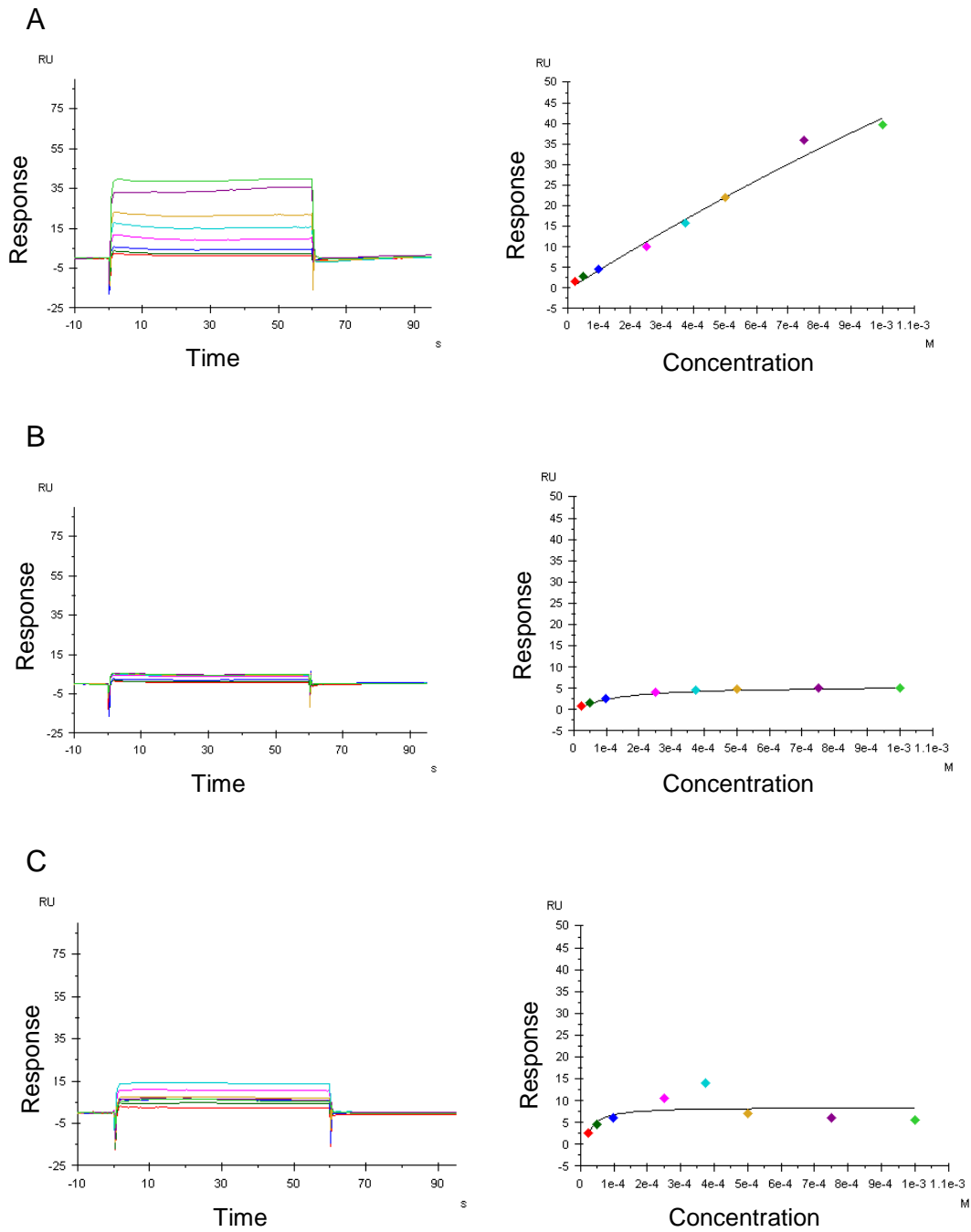


Figure 2.11 – Example sensorgrams from SPR testing of library I. (A) The fragment **21** does not saturate the protein, even at high concentrations suggesting very weak or non-specific binding. (B) The fragment **22** shows a binding curve but the response is very low (<10 RU). (C) The fragment **52** likely precipitates at high concentrations.

2.4.4 Design of Library 2

A second, smaller library based on fragments **21**, **22** and **23** was designed to improve solubility and test their affinity for HSP70. Matched pairs were designed to allow direct comparison between these early hit compounds and the more soluble versions.

A frequently used strategy in medicinal chemistry to improve solubility is the addition of a morpholine ring or other protonatable basic groups.⁸² It was important that any solubilising group added to the fragment would not interfere with fragment binding. Examination of the X-ray crystal structure showed that the para position of the benzene ring is pointing out of the pocket towards the solvent (Figure 2.12). This led to the design of compounds **58** and **59**, the original hit fragment with a morpholine ring attached via an alkyne or ether linker. Similarly, compound **60** was designed to replace the benzene ring with an alkyne from which a morpholine ring was attached and compound **61** was designed as a matched pair to fragment **22** with a morpholine ring.

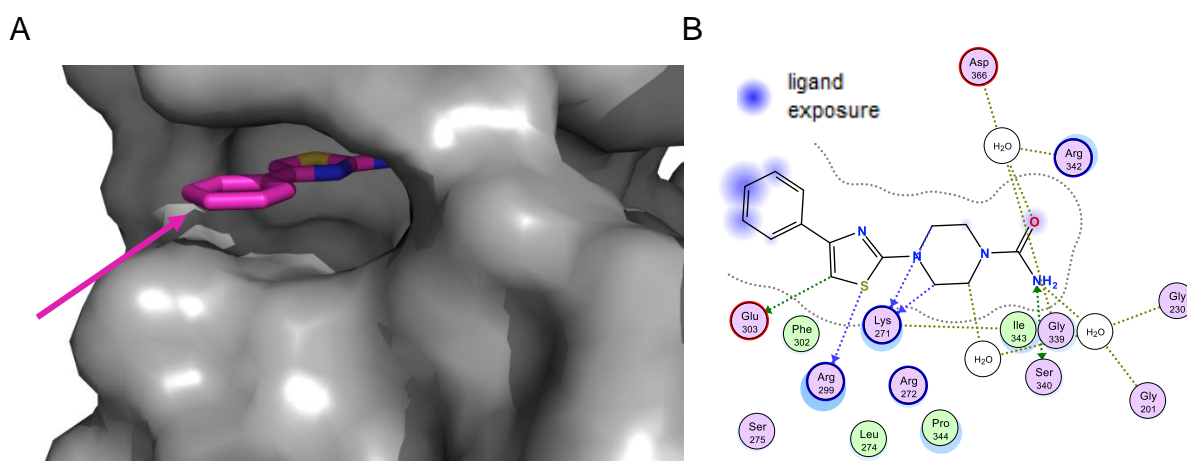


Figure 2.12 – (A) X-ray crystal structure of fragment **21** was used to determine which position to attach the solubilising morpholine group. From this structure, modification at the para position is not expected to interfere with fragment binding. (B) Ligand Interaction diagram generated with MOE showing the solvent exposed regions of the fragment.

Solubility can also be improved by adding polar groups to the molecule, for example by replacing the benzene ring of **21** with a pyridine in compound **62**. Regarding the design of a matched pair for **23**, the 2-(4-bromo-2-chloro-6-fluorophenyl)cyclopropane-1-carboxylic acid is not commercially available, so the closely related fluoro compound **63** and its more soluble version **64** were chosen instead (Figure 2.13). Compound **65** was designed as a more soluble version of **55** to determine if a urea replacement would be tolerated if the solubility was improved.

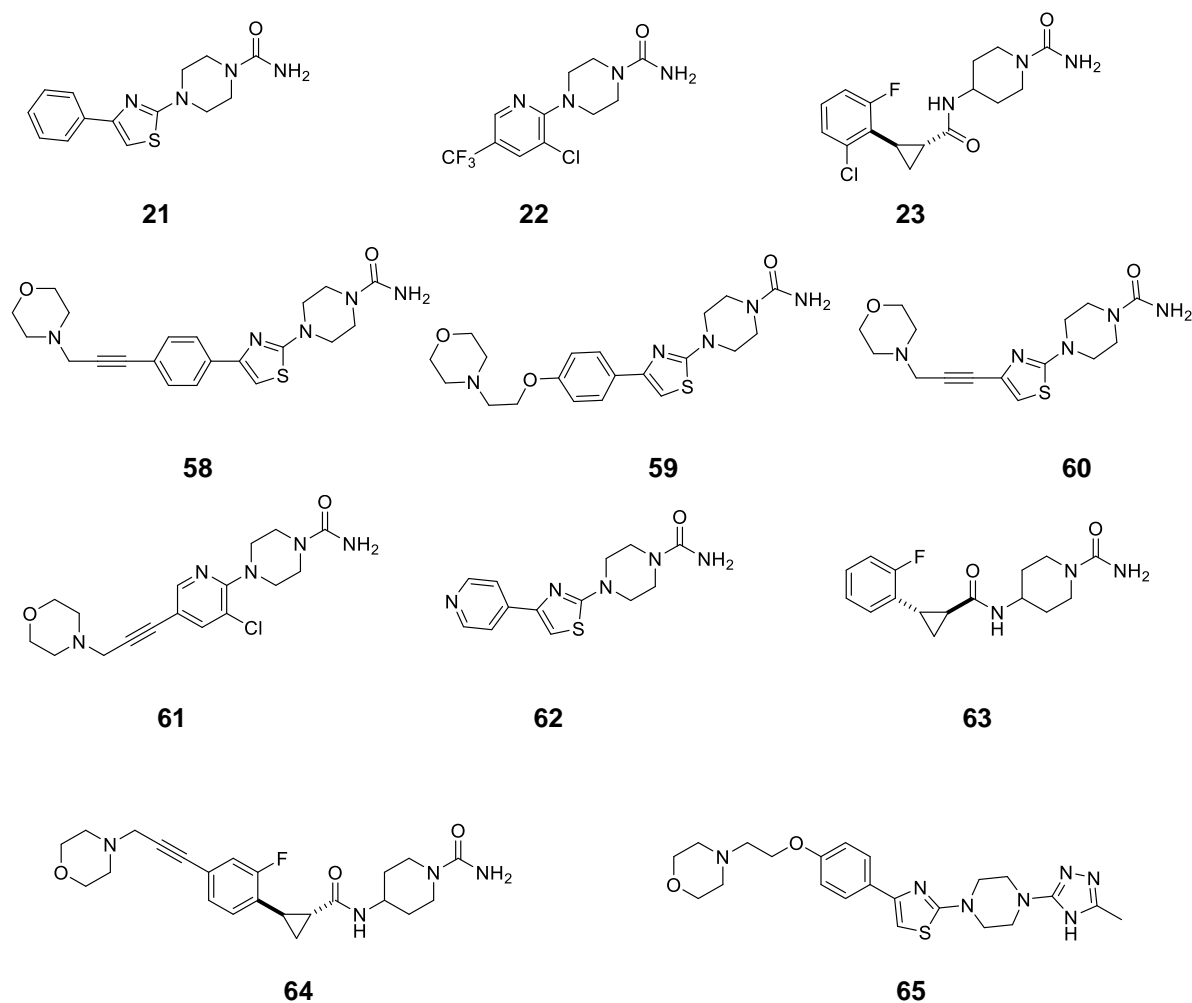
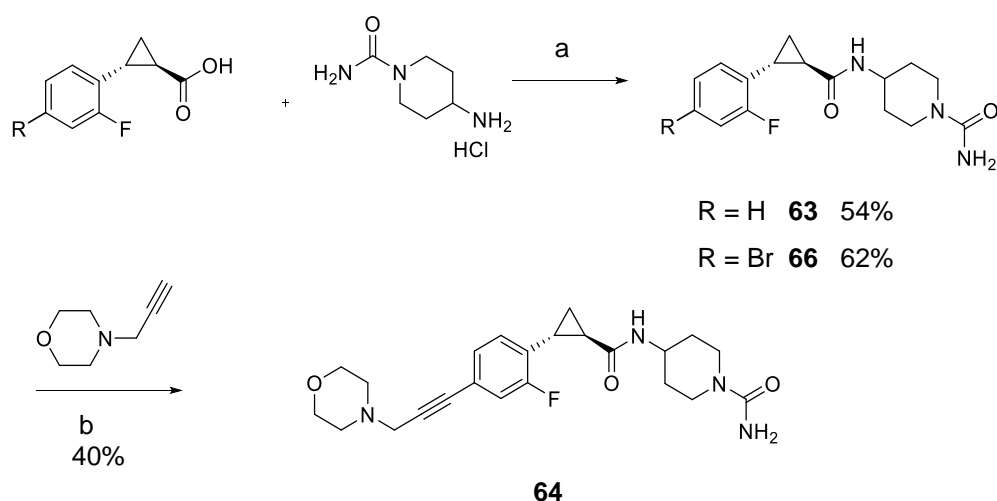


Figure 2.13 - The second library consisted of eight compounds designed to have improved solubility (**58-64**) based on early hit compounds **21**, **22** and **23**.

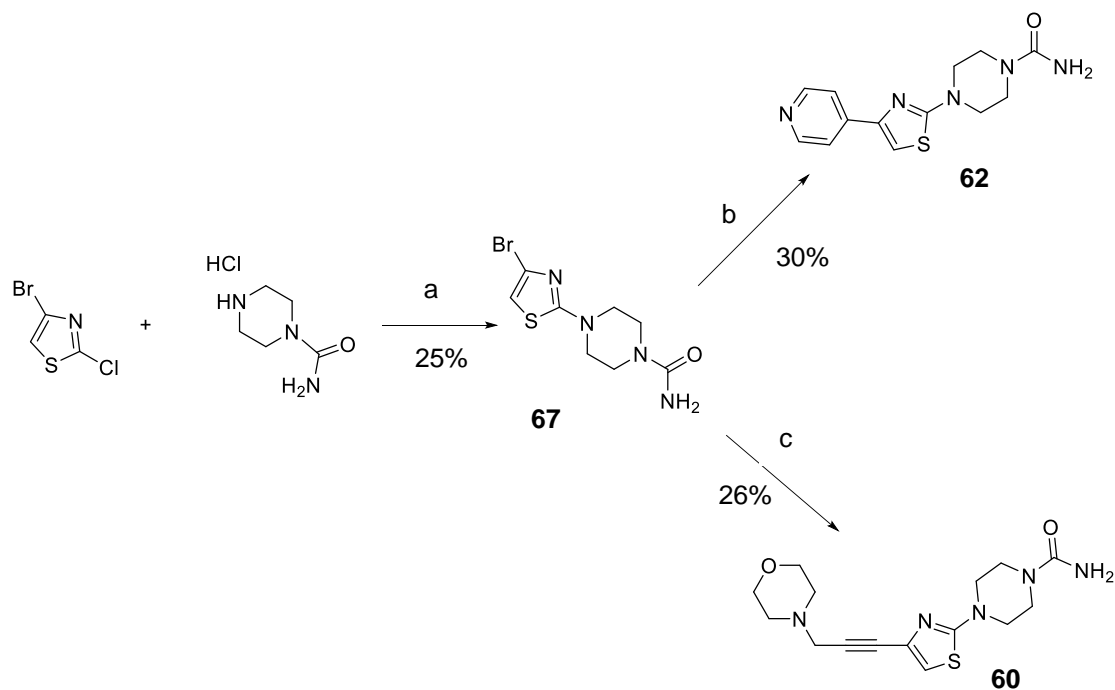
2.4.5 Synthesis of Library 2

Compounds **63** and the intermediate **66** were synthesised by amide coupling using the same conditions as for the library 1 amides. Sonogashira coupling with **66** allowed attachment of the morpholine solubilising group for **64** (Scheme 2.7).



Scheme 2.7 - Synthesis of compounds **63** and **64**. (a) HATU, DIPEA, DMF, rt, 24 h. (b) K_2CO_3 , $PdCl_2(CH_3CN)_2$, SPhos, MeCN, 90 °C, 18 h.

Compound **67**, synthesised by S_NAr , was designed as an intermediate to synthesise both **60** and **62**. For compound **60** no product was observed with the Sonogashira conditions used for **64** but a much shorter reaction time and modified purification gave the desired product (Scheme 2.8). A variety of Suzuki and Stille coupling conditions were trialled to make **62** with the most successful route shown in Scheme 2.8.



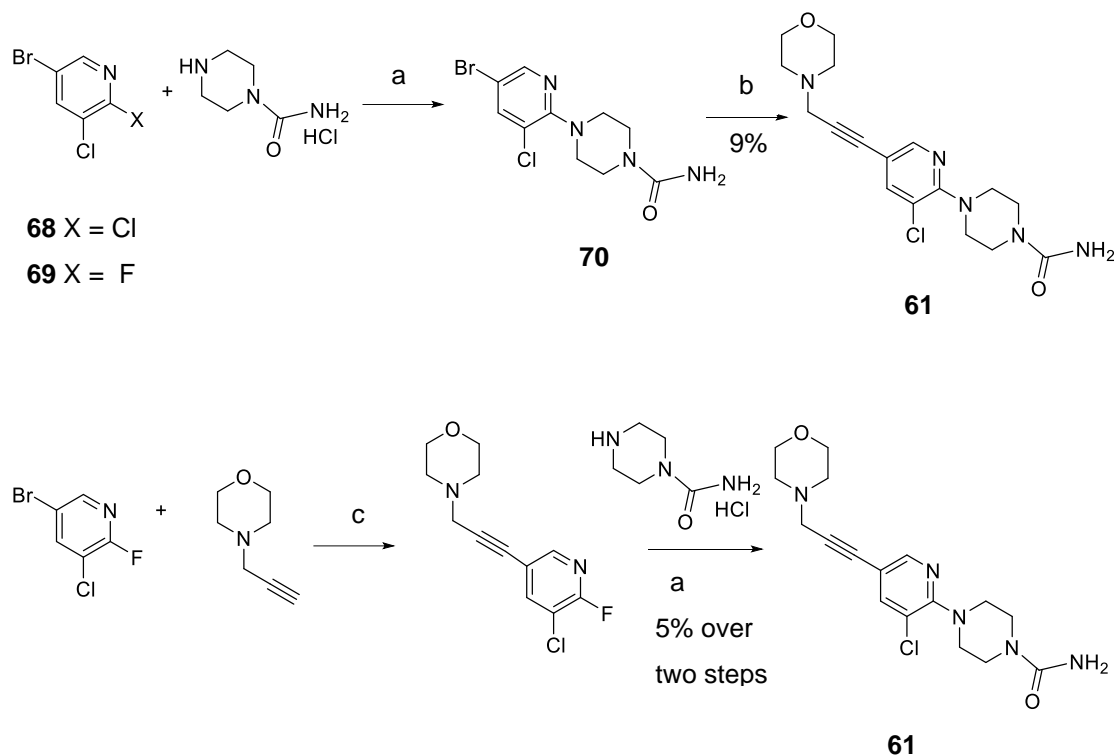
Scheme 2.8 – (a) DIPEA, DMSO, 90 °C, 24 h (b) 4-Pyridineboronic acid pinacol ester, K_3PO_4 , $Pd(OAc)_2$, SPhos, $H_2O:Dioxane$ 100 °C 30 min (c) 4-(Prop-2-yn-1-yl)morpholine, K_2CO_3 , $PdCl_2(CH_3CN)_2$, SPhos, MeCN, 90 °C, 6 h.

For the synthesis of compound **61** a wide variety of conditions were trialed for the first S_NAr step with **68** (Scheme 2.9), however, there were multiple issues with this reaction:

- The product and starting material have the same retention times making it difficult to follow the reaction.
- At shorter times and lower temperatures significant amounts of starting material remained.
- Increasing time or temperature increased the amount of decomposition product.
- S_NAr occurred at both chlorines making it difficult to separate the two products.
- The product was not soluble in MeOH or $CHCl_3$, making purification difficult.

S_NAr was more successful with 5-bromo-3-chloro-2-fluoro-pyridine **69** as the starting material (Scheme 2.9). The reaction was initially attempted in DMSO at 100 °C for 1 hour but the starting materials were not very soluble and the yield was low (16%) with 25% decomposition product observed by LC-MS. Changing the solvent to NMP improved the solubility and decreasing the reaction time to 45 min gave less than 10% decomposition product observed by LC-MS, improving the yield to 30%.

The subsequent Sonogashira coupling proceeded in very low yields and the product was not completely pure. When the Sonogashira coupling was attempted before the S_NAr using 5-bromo-2,3-dichloro-pyridine, the double addition product was observed as the main product after just one hour. The final route to make this compound, shown in Scheme 2.10, began with a short Sonogashira coupling with 5-bromo-3-chloro-2-fluoro-pyridine. However, the product was susceptible to nucleophilic attack at the fluorine and purification by column chromatography gave entirely the 2-methoxy product. S_NAr was therefore carried out with the crude product. The final product required multiple purifications including HPLC resulting in a low overall yield but enough for testing.

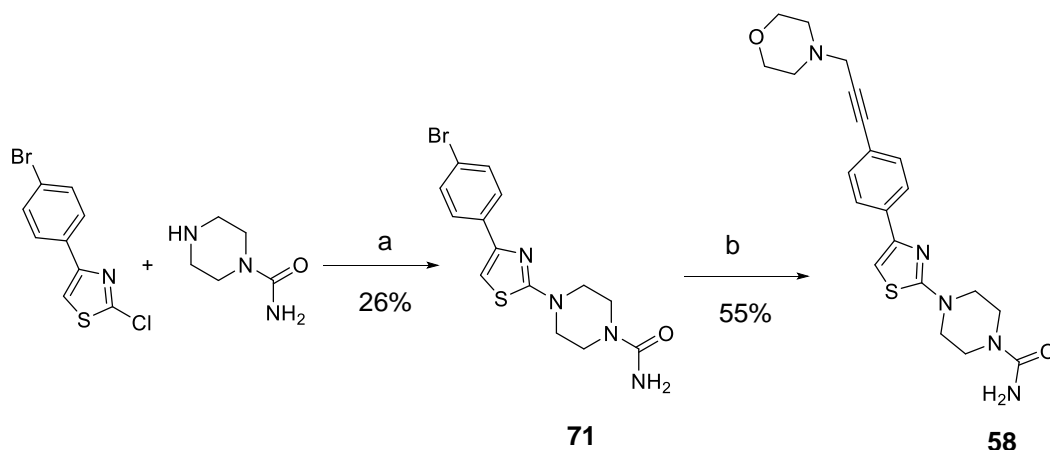


Scheme 2.9 – The S_NAr to synthesise compound **70** could be improved by using the 2-F over the 2-Cl (improving the yield from 10% to 30%). First attempted synthesis of compound **61** resulted in poor overall yields. Reversing the order did not improve the yield. (a) DIPEA, NMP, 100°C, 45 min, MW. (b) 4-(Prop-2-yn-1-yl)morpholine, $PdCl_2(CH_3CN)_2$, SPhos, K_2CO_3 , MeCN, 90 °C, 1.5 h. (c) $PdCl_2(CH_3CN)_2$, SPhos, K_2CO_3 , MeCN, 85 °C, 30 min.

Compound **58** was synthesised by S_NAr followed by Sonogashira coupling (Scheme 2.10). In order to balance product formation with product decomposition to the piperazine different conditions of time, temperature and base were trialled (Table 2.3). All conditions attempted gave similar yields between 21-26%.

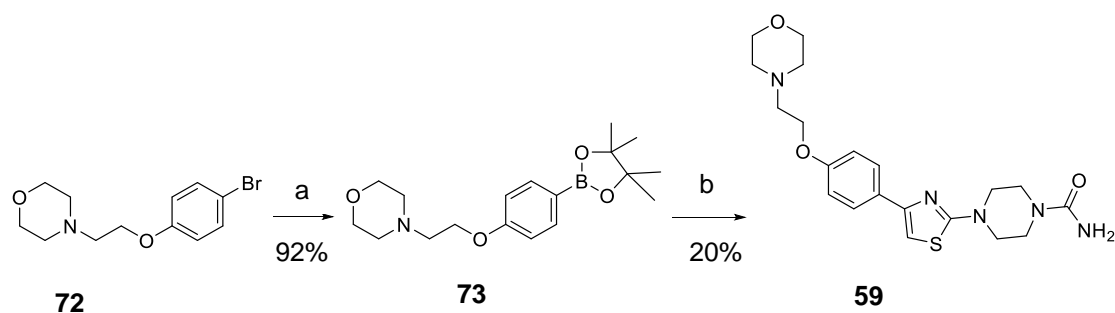
Base	Time	Temp	Yield
3eq K_2CO_3	7h	90	21%
2 eq DIPEA	24h	100	22%
1.5 eq DIPEA	24h	80	26%

Table 2.3 – Various conditions attempted to synthesised **58** gave similar yields.



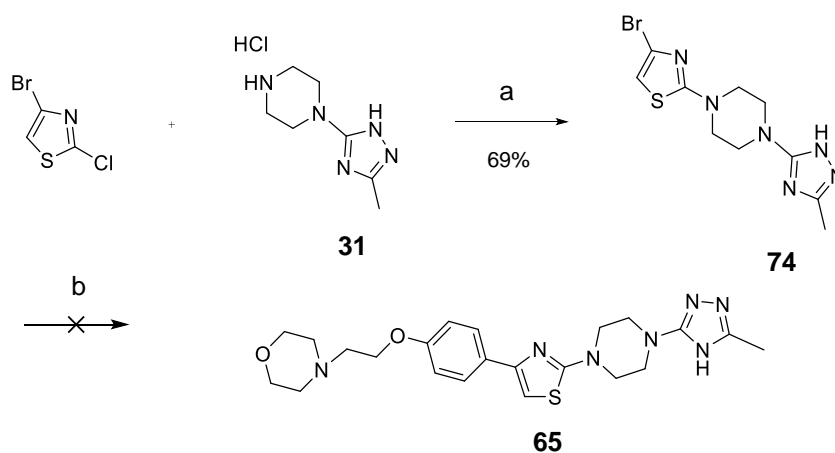
Scheme 2.10 - Synthesis of **58** (a) DIPEA, DMSO, 80 °C, 24 h. (b) 4-(Prop-2-yn-1-yl)morpholine, PdCl₂(CH₃CN)₂, SPhos, K₂CO₃, MeCN, 90 °C, 2 h.

The intermediate **71** was also used for the synthesis of a fragment with a more flexible linker **59** (Scheme 2.11). Miyaura borylation of **72** to the boronic ester **73** followed by Suzuki coupling gave the desired fragment.



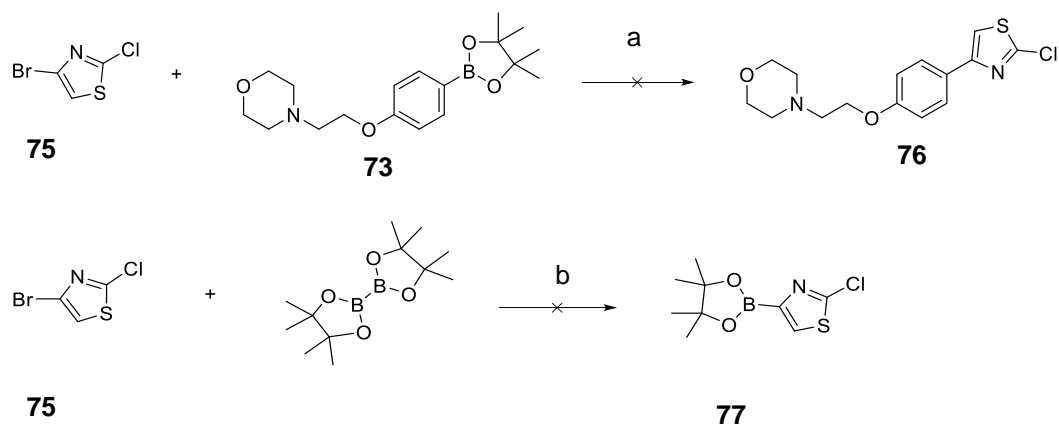
Scheme 2.11 - Synthesis of **59** (a) B₂pin₂, Pd(dppf)Cl₂, KOAc, 90 °C, 18 h (b) Intermediate **71**, Pd(PPh₃)₄, K₂CO₃, 90 °C, 2 h.

In a similar synthesis S_NAr with the piperazine triazole **31** gave the desired bromo intermediate **74** (Scheme 2.12). Coupling with boronic ester **73**, however, resulted in no desired product formation, unlike the synthesis of the urea matched pair **59**. It's possible that the triazole is coordinating to the catalyst, preventing the reaction from proceeding. A literature search on the success of palladium coupling with a triazole group present showed these reactions are generally very low yielding.



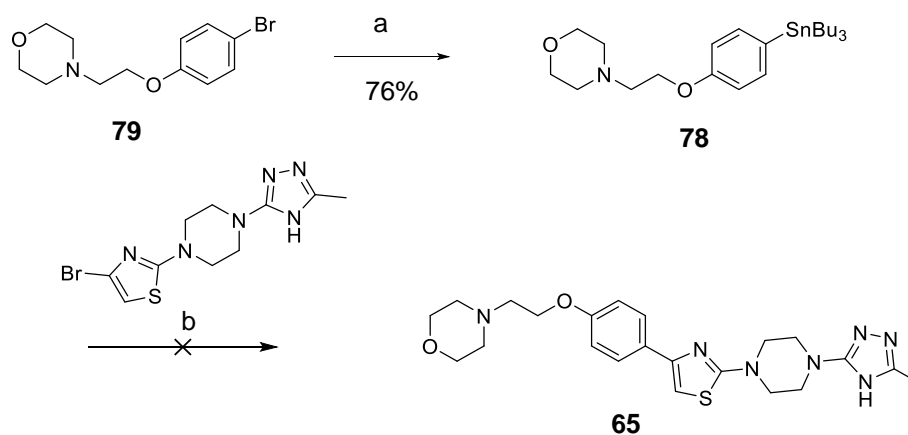
Scheme 2.12 Attempted synthesis of **65** (a) K_2CO_3 , DMSO, 120 °C, 3 h (b) **73**, $Pd(PPh_3)_4$, K_2CO_3 , water, MeCN, 90 °C, 48 h.

An alternative route was designed to swap the order of the S_NAr and Suzuki coupling which would avoid carrying out the Suzuki coupling in the presence of the triazole. However, under these conditions the replacement of the 2-chloro was observed by LC-MS but no desired replacement of the 4-bromo was observed (Scheme 2.13). Attempts to swap the coupling partners by Miyaura borylation of **75** were unsuccessful.

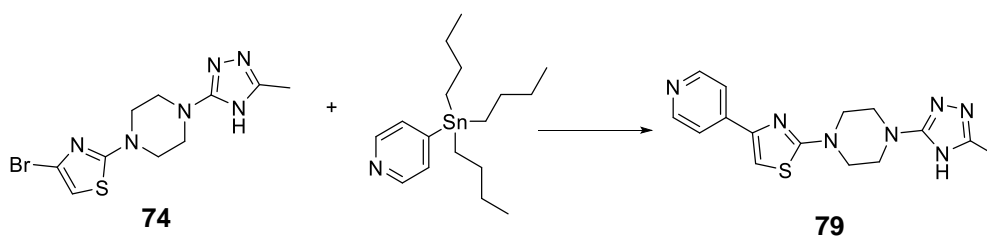


Scheme 2.13 - Attempted Suzuki coupling resulted in no desired product (a) $Pd(PPh_3)_4$, K_2CO_3 , water, MeCN, 90 °C, 2 h. Attempted Miyaura borylation gave no desired product and only starting material was observed by LC-MS (b) $Pd(dppf)Cl_2$, KOAc, dioxane, 90 °C, 48 h.

Stille coupling was then investigated as alternative to Suzuki coupling. The stannane **78** was synthesised from the corresponding bromo starting material **79**. No desired product **65** was formed in the subsequent Stille coupling experiment under standard conditions (Scheme 2.14). The reaction of Intermediate **74** with 4-(tributylstannyl)pyridine was used as model system to optimise these Stille reaction conditions (Table 2.4). Although a variety of conditions were trialled, none gave the desired product.



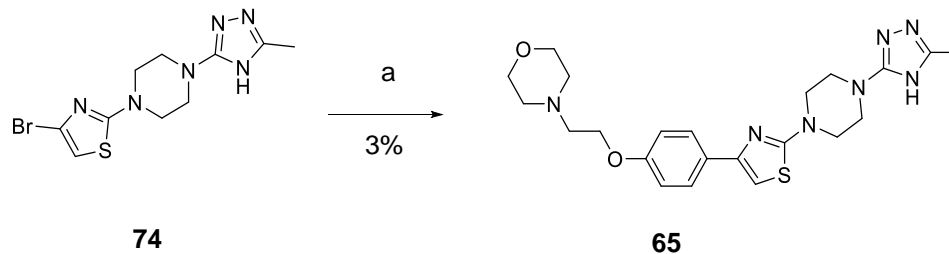
Scheme 2.14 - (a) *n*-BuLi in hexane, SnBu₃Cl, -78 °C, 2.5 h. (b) Pd(PPh₃)₄, CsF, toluene 90 °C, 24 h.



Catalyst	Solvent	Base	Temp	Time	LC-MS
Pd(PPh ₃) ₄	Toluene	CsF	130 °C	1 h	SM
Xant Phos Pd (OAc) ₂	Toluene	CsF	100 °C	1 h	SM
Peepsi-iPr	Toluene	CsF	80 °C	1 h	SM
Peepsi-iPr	Toluene	CsF	100 °C	1 h	SM
Peepsi-iPr	iPrOH	K ⁺ OBu	rt	2 h	SM
Peepsi-iPr	iPrOH	K ⁺ OBu	100 °C	0.5 h	Debromination

Table 2.4 – Synthesis attempts of **79** as a model system to optimise Stille conditions in the presence of a triazole ring **74**.

these conditions were used to synthesise **65** LC-MS analysis showed the desired product among nine other peaks. Enough product was isolated for characterisation and SPR testing.



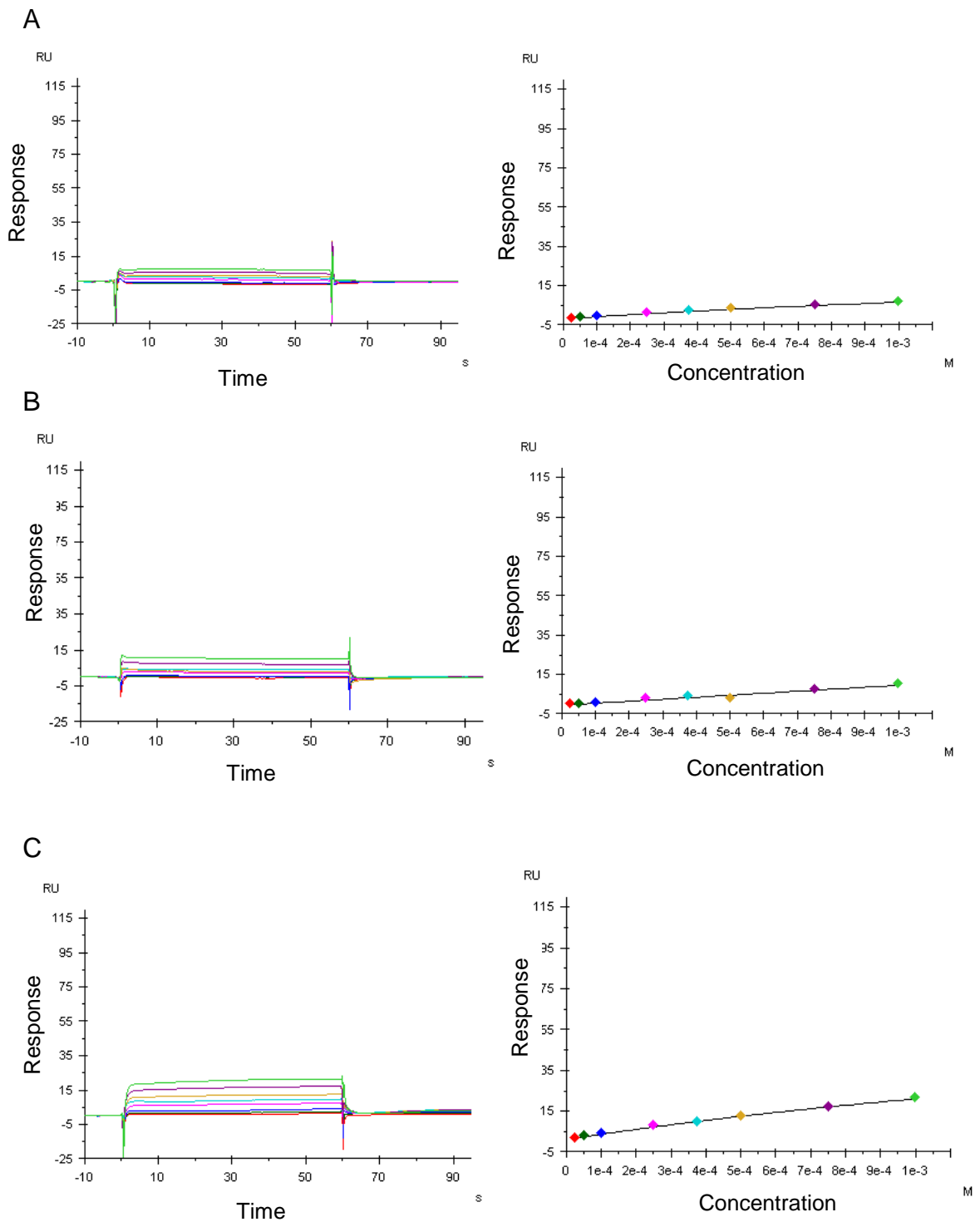
Scheme 2.16 - (a) Pd(PPh₃)₄, dioxane, 100 °C, MW, 20 min followed by addition of stannane **78**, 100 °C, MW, 8 h.

2.4.6 Testing of library 2 by SPR

Compounds **58-65** were tested by SPR using the same methods as for the first library of analogues. Compounds **61** and **62** were found to be inactive by SPR showing binding responses less than 10 RU. Compounds **60** and **63** gave a non-saturating binding response indicating weak or non-stoichiometric binding. Compound **64** showed a failure to wash off the chip completely, resulting in a cumulative response and poor quality sensorgrams (Figure 2.14).

Compounds **58** and **59** are the closest analogues to the original hit fragment with added morpholine rings via a rigid or flexible linker to improve solubility. Both of these compounds gave good quality binding curves from which a K_D could be calculated, giving confidence that these fragments bind in a concentration dependent manner (**58** 388 μ M; **59** 486 μ M; Figure 2.15). These compounds have equal affinity for the S275W mutant as for the wild-type protein, as expected for compounds that bind outside of the ATP binding site. The fragments are fast on and fast off as expected for fragment hits. Other fragments with morpholine solubilising groups **61**, **60** and **59** that had either the phenyl ring removed or the urea exchanged for a triazole were inactive. It became apparent

that there was a strict limit to the changes tolerated by the protein and that small changes in chemical structure led to loss of activity. The focus of the project was therefore moved to further characterisation of fragment **21** binding to the secondary site.



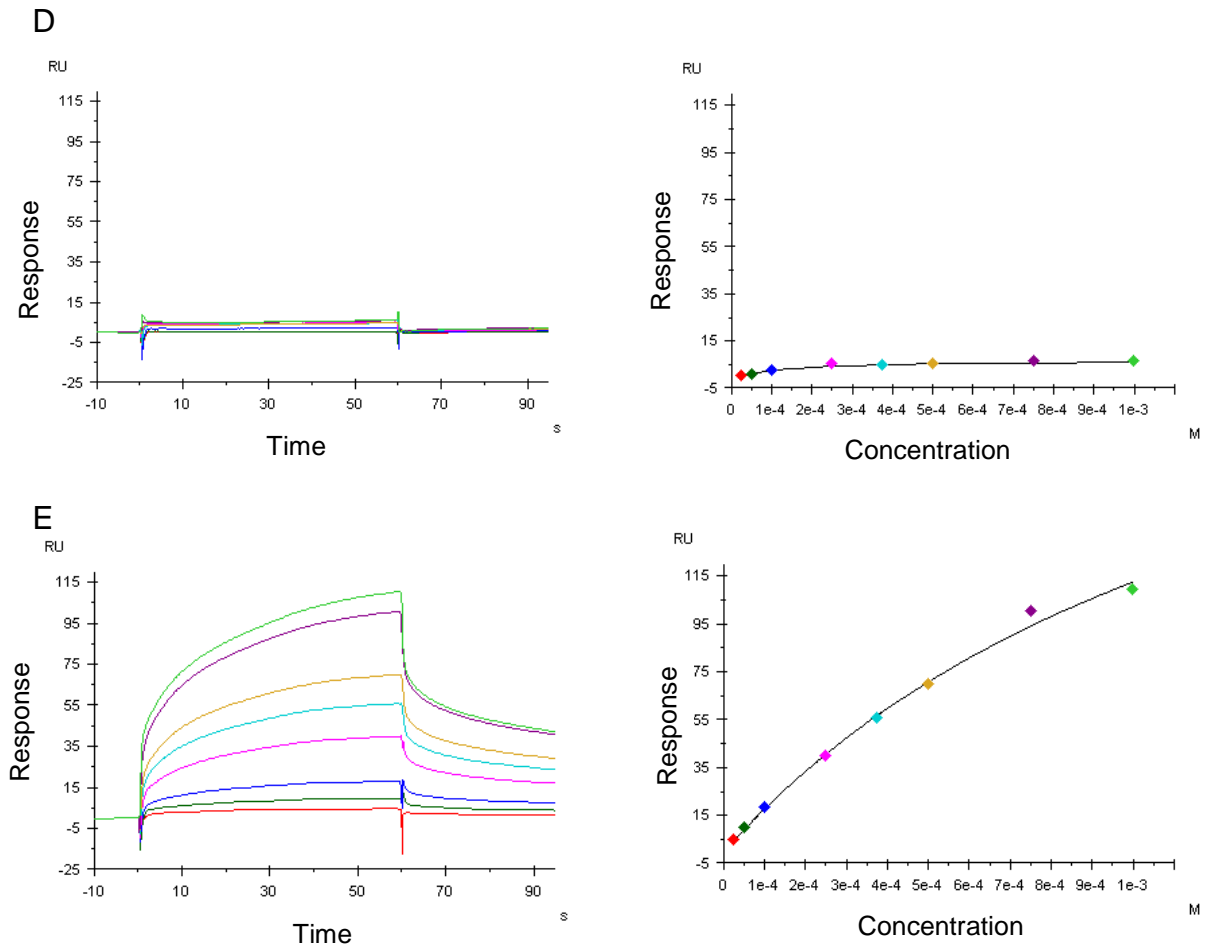
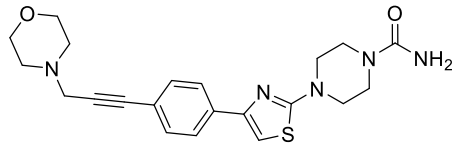
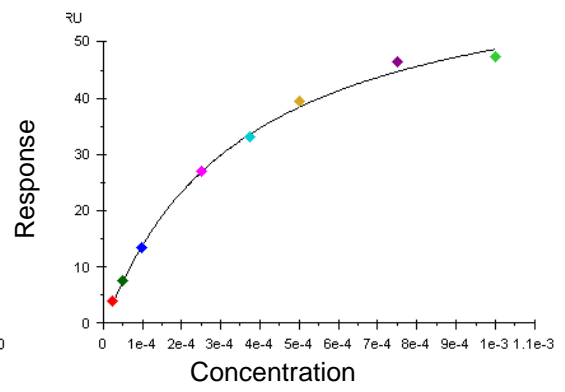
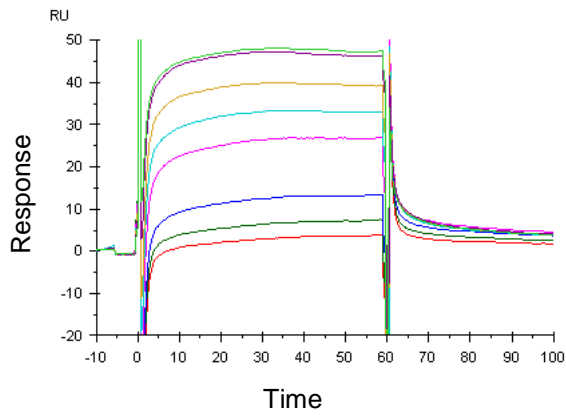
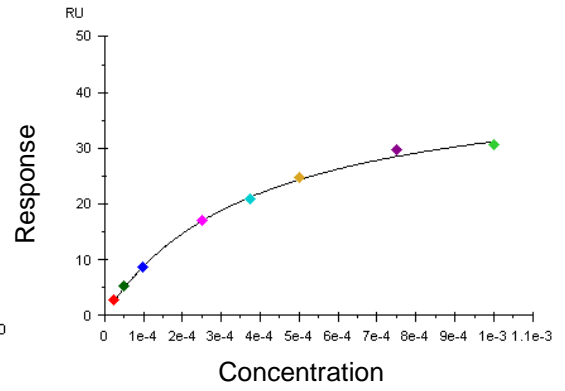
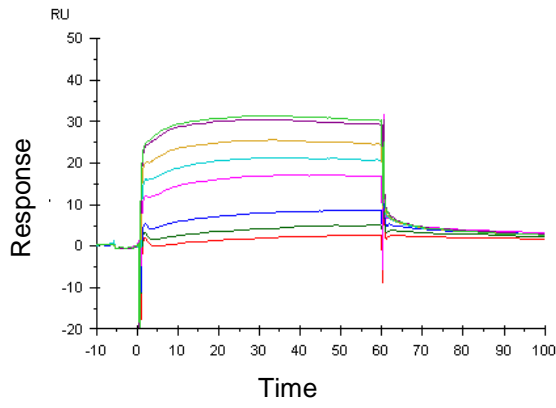
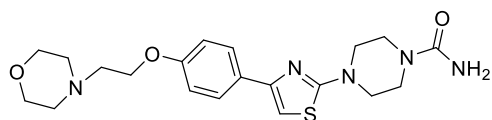


Figure 2.14 – Sensorgrams and binding curves for compounds **61-64**. (A) **61** showed a non-saturating response. (B) **63** showed a non-saturating response (C) **60** showed a non-saturating response (D) **62** was inactive with a response less than 10 RU (E) **64** showed a failure to wash off the chip completely, resulting in a cumulative response and poor quality sensorgrams.

A

**58**WT $K_D = 388 \mu\text{M}$
S275W $K_D = 352 \mu\text{M}$ 

B

**59**

WT $K_D = 486 \mu\text{M}$
 S275W $K_D = 381 \mu\text{M}$

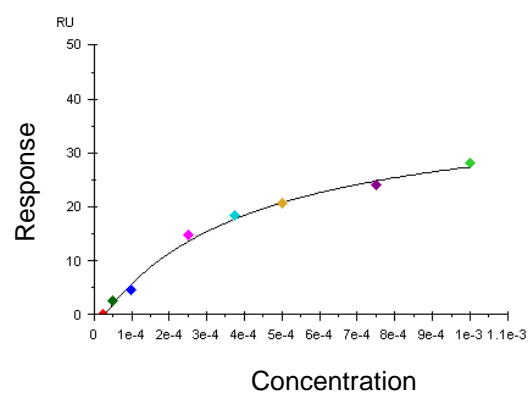
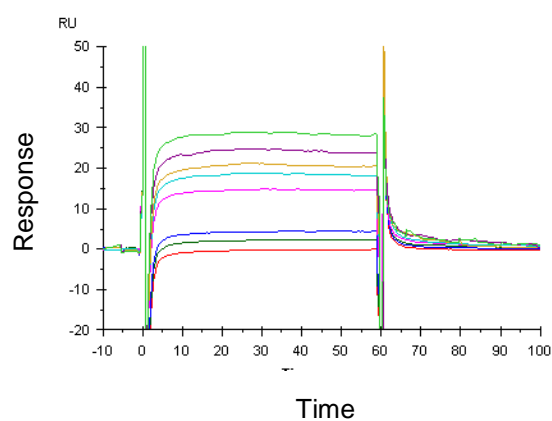
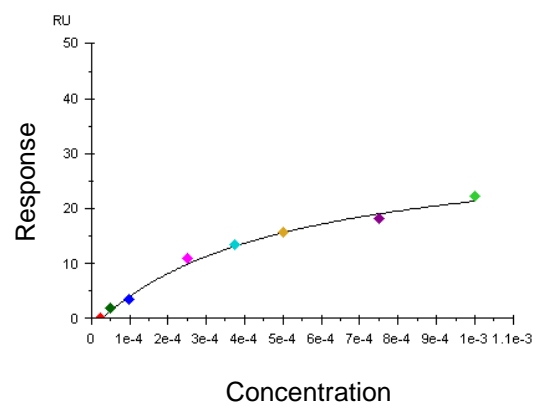
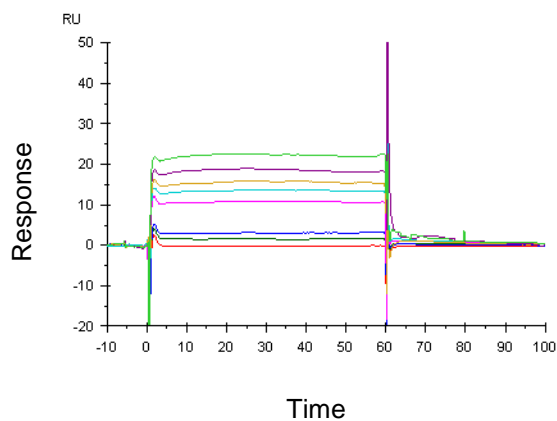


Figure 2.15 – Compound **58** and **59** with morpholine solubilising groups showed good quality binding curves against both wild type and S275W mutant HSC70-NBD when tested by SPR. (A) Sensorgrams and binding curves for compound **58**. (B) Sensorgrams and binding curves for compound **59**.

2.5 Conclusions

This chapter described the discovery of a secondary binding site, adjacent to the ATP binding site, by fragment-based screening and the subsequent synthesis and testing of fragment analogues. Upon testing of the first library of fragment analogues it became apparent that these fragments did not show convincing binding by SPR, likely due to poor solubility at high concentrations which led to non-specific binding or precipitation. SPR testing of Library 1 identified low solubility as a limiting feature of the compound class. More soluble compounds were designed and synthesised using the X-ray crystal structure for guidance. With the design and synthesis of more soluble close analogues of the original hit fragment it became possible to see convincing binding by SPR in a concentration dependent manner.

X-ray crystallography is an extremely useful technique for understanding the key binding interactions and for designing fragment analogues but it does not give a measure of affinity of the ligand for the protein and even very weakly binding ligands may be detected. For fragments that bind to an allosteric cryptic pocket such as fragment **21**, it's possible that the fragment binds via induced fit or by conformational selection or a combination of both. Depending on how frequent the binding conformation exists this can make obtaining X-ray crystal structures quite difficult. HSP70 is a highly flexible protein and it is possible that the binding of fragment **21** to the secondary site occurs infrequently.

This chapter highlights the difficulty of working with a novel cryptic pocket and weakly binding fragments. Fragment validation by orthogonal methods is essential in FBDD because fragments by their very nature are weakly binding and can easily be misinterpreted. It is therefore always necessary to have robust biophysical methods optimised to characterise the fragment further. As the more soluble fragments **58** and **59** showed convincing binding by SPR and the X-ray crystal structure gave information on where the fragment was bound, orthogonal methods were sought to explore the binding of fragment **21** to HSP70 in more detail, which will be described in the next chapter.

Chapter 3

3 Validation of the secondary binding site hits by orthogonal methods

3.1 Introduction to Ligand-Observed NMR

NMR spectroscopy is an analytical tool which is often used to determine the molecular structure of compounds and proteins but it can also be used to detect whether a compound binds to a protein target.⁸⁴ NMR requires nuclei that possess nuclear spin. All isotopes with an odd number of protons and/or neutrons have an intrinsic nuclear magnetic moment and angular momentum. Isotopes with even numbers of both protons and neutrons have zero nuclear magnetic dipole moment and do not exhibit an NMR signal. The most commonly used nuclei in NMR are ^1H , ^{13}C , ^{15}N , ^{19}F and ^{31}P .

In the absence of an external magnetic field, the magnetic field of a nucleus has a random orientation and there is no energetic difference for any particular orientation. When an external magnetic field is applied, nuclei can align with the applied field (the lower energy, α state) or against the applied magnetic field (the higher energy, β state).⁸⁵ The majority of nuclei are in the more stable α state. Applying a radiofrequency energy pulse can excite the nuclei to the higher energy β state. The decay from the excited state to the ground state releases a characteristic radiofrequency signal. This flipping of a nucleus from one magnetic alignment to the other is known as resonance. Not all nuclei resonate at the same frequency due to the shielding effect of the surrounding shells of electrons. Electrons are charged and rotate with a spin that produces a magnetic field opposite to that of the applied magnetic field. Electronic shielding reduces the magnetic field at the nucleus and as a result the frequency required to achieve resonance is also reduced. The relaxation time, which is the time taken by different nuclei to release this energy, varies depending on the environment that the atom is in.⁸⁶ In a ^1H -NMR for example, a signal can therefore be obtained for each hydrogen atom in the molecule.

Ligand based NMR experiments compare the ^1H -NMR spectra of a ligand in solution with the ^1H -NMR spectra of the ligand in the presence of a protein of interest.⁸⁷ They are based on the fundamental difference between proteins and small molecules – their size. Typically, small molecules have a molecular weight of less than 1 kDa while proteins have masses at least ten-fold higher. Small molecules such as ligands have long relaxation times in contrast to large molecules such as proteins which have relatively short relaxation times. Relaxation refers to the restoration of equilibrium magnetisation and random phase. There are two mechanisms of relaxation known as longitudinal (T_1) and transverse (T_2).⁸⁸ T_1 can be similar for both large and small molecules, however, T_2 is quite different. The T_2 relaxation rate of a nucleus is to a first approximation proportional to its tumbling correlation time.⁸⁹ Large molecules tumble slowly in solution and have large relaxation rates and large line widths of NMR signals. In contrast to large molecules, small molecules are characterized by small transverse relaxation rates, weakly positive cross-relaxation rates and large diffusion constants. These differences cause line broadening, changes in the diffusion coefficient and an inversion of the sign of the nuclear Overhauser effect (NOE).⁸⁷ These key differences are used in ligand-observed NMR methods to detect a ligand binding to a protein.

There are several advantages of using NMR in fragment screening.⁹⁰ Compounds can be screened in cocktails allowing several thousand molecules to be screened in a week. These experiments are also highly sensitive and enable the detection of even weakly binding fragments to a protein without the necessity of labelling either the protein or the ligand. The main disadvantages are that pure protein needs to be synthesised in significant amounts which may be difficult for some projects and the protein and ligand tested must be highly soluble in the NMR solvent.

3.1.1 CPMG experiments

CPMG (Carr-Purcell-Meiboom-Gill) is a ligand-observed NMR experiment where time dependent filters are applied.⁸⁷ The protein is a large macromolecule and its signals relax quickly. These signals can be suppressed so that only the ligand signals are observed. When a ligand binds to the protein it behaves like a macromolecule and its signals are also suppressed along with the protein. Only signals for the free ligand in solution are therefore observed and an overall reduction of signal occurs in comparison with the ligand alone. A competitor may be added to displace the ligand from the protein which increases the amount of free ligand, restoring the ligand signals to the original magnitude (Figure 3.1).



Figure 3.1 – The ^1H -NMR signal for a ligand in a theoretical CPMG experiment decreases upon binding to a protein and can be restored by the addition of a competitor molecule.

3.1.2 WaterLOGSY experiments

In a waterLOGSY (water-Ligand Observed via Gradient Spectroscopy) experiment magnetisation can be transferred to the ligand in two ways:

- 1) Transfer to the free ligand from bulk water
- 2) Transfer to the ligand bound to the protein from either water bound in the protein binding site or via exchangeable protons in the protein

When the ligand interacts with water via the protein, we observe Nuclear Overhauser Effects (NOEs) that have a different phase to that of the free ligand⁹¹

(Figure 3.2). The data can be processed in such a way that the absolute NOE signal of a bound ligand can be positive or negative, however, the sign of the NOE signal will be opposite for the free ligand. The spectral region of interest for this experiment is between 6 and 10 ppm which corresponds to the aromatic hydrogens of the ligand. Below 6 ppm, the signal is convoluted by the HEPES buffer, DMSO, glycerol and water, which mask the ligand signal.

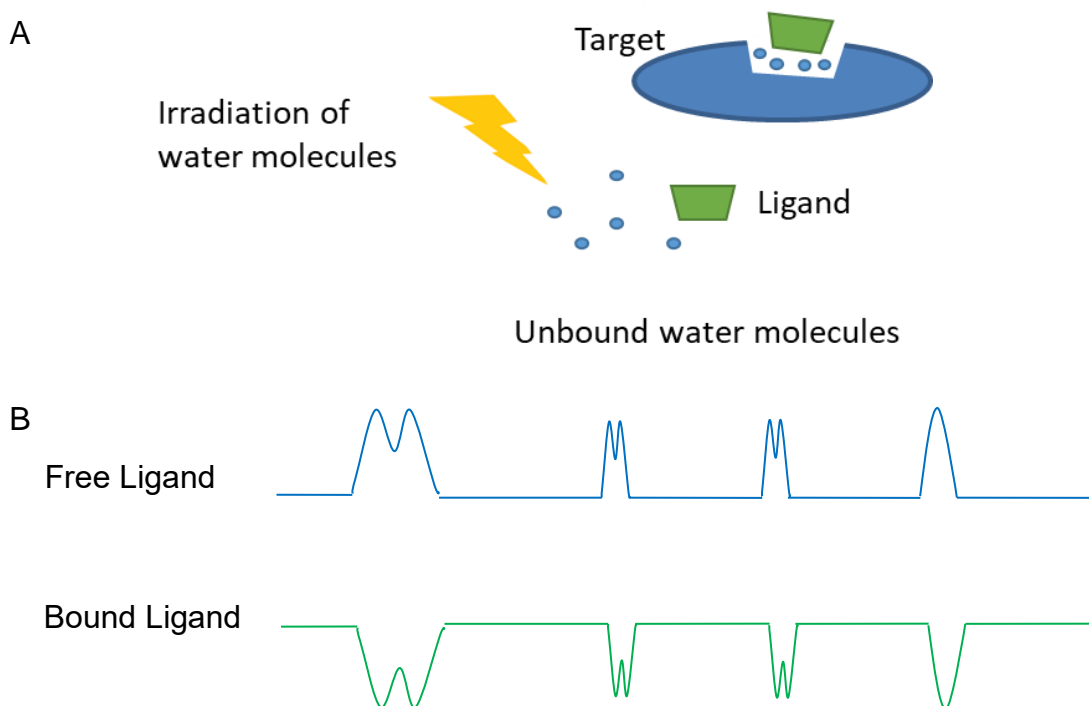


Figure 3.2 - (A) The principle of WaterLOGSY, described in the text and (B) The NOE signal for a free ligand in a theoretical WaterLOGSY experiment has the opposite phase to that of the bound ligand.

3.2 Hypothesis – the ATP binding site does not exist at the same time as the secondary binding site

We hypothesised that fragment **21** would be ATP or ADP competitive by analysing the X-ray crystal structures of ADP bound to HSP72-NBD and fragment **21** bound to HSP72-NBD (Figure 3.3). Every known ATP competitive inhibitor forms a key anchoring interaction with S275.³¹ For example, in adenosine, N1 is

perfectly positioned to interact with the hydroxyl of S275 (Figure 3.3 A). When fragment **21** binds in the secondary site it pushes the alpha helix with S275 out of position, twisting this key serine residue out of the ATP binding site (Figure 3.3 B). Thus, when fragment **21** binds to HSP72, the ATP binding site ligands cannot make this key interaction. From this analysis we expect that the two binding sites do not exist at the same time. Therefore, the binding of the fragment in the secondary site should theoretically be displaced by the binding of ATP or ADP, which have a much higher affinity for HSP72.

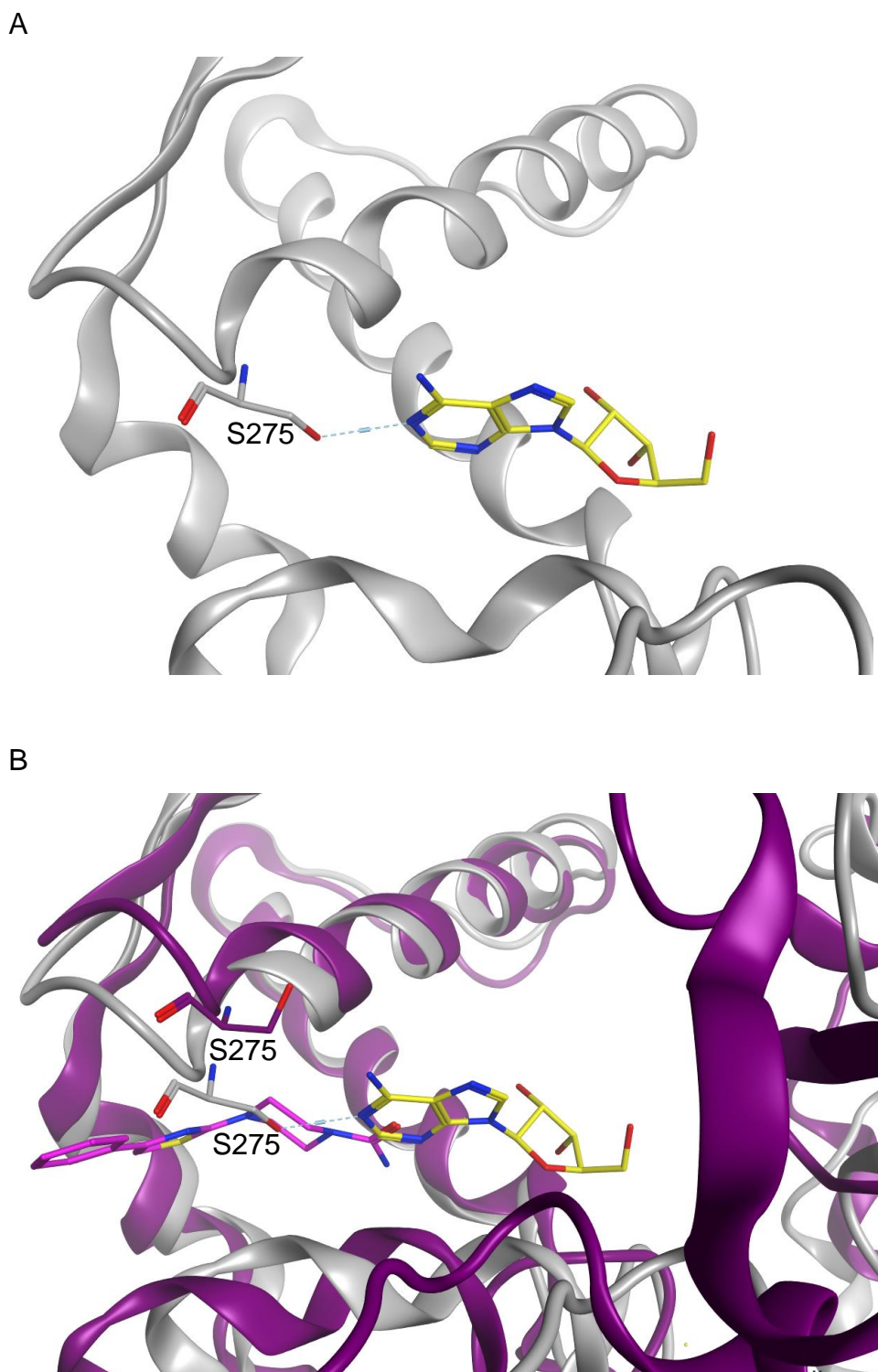


Figure 3.3 – (A) HSP72-NBD with adenosine (PDB ID 5AQY) (B) HSP72-NBD with ADP (grey) overlaid with HSP72-NBD with fragment **21** (purple). S275 moves out of the ATP binding site upon addition of fragment **21** meaning it is unlikely that the allosteric fragment could bind simultaneously with an ATP binding site ligand.

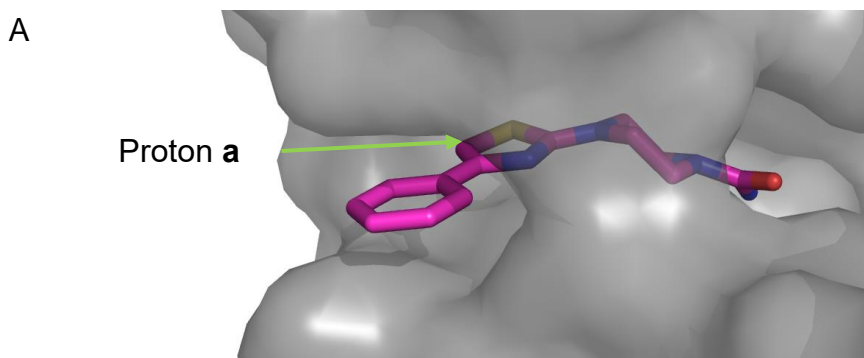
3.3 Testing of fragment hits by Ligand-Observed NMR

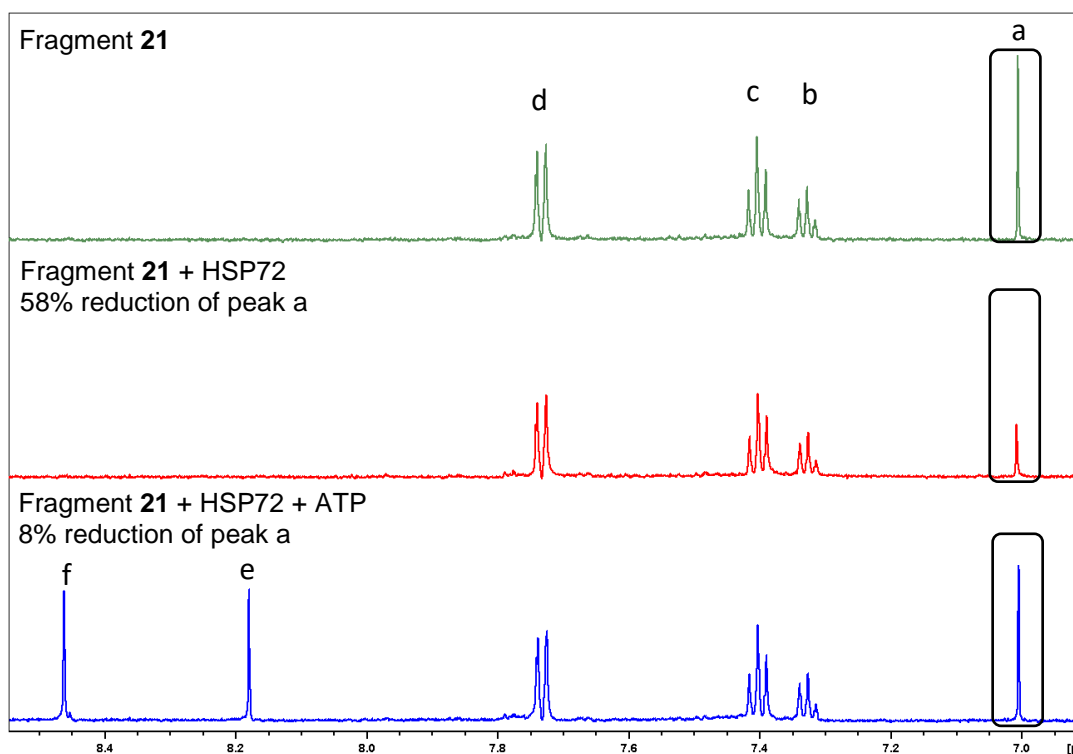
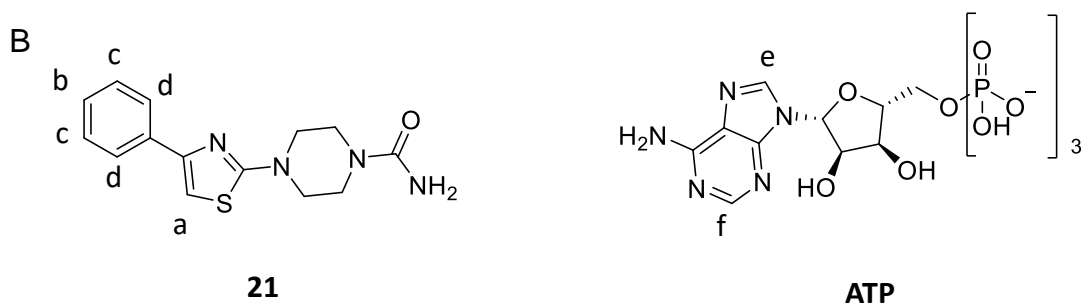
3.3.1 CPMG

Binding of fragment **21** to HSP72 was studied by the ligand observed NMR method CPMG. In this experiment three identical samples with compound **21** were dissolved in DMSO-d₆ and buffer. HSP72-NBD was added to the second sample and HSP72-NBD and ATP were both added to the third sample. The ¹H-NMR spectrum was then measured for each sample with time dependent filters in a CPMG experiment.

In contrast to the protons on the aromatic ring which are solvent exposed, proton **a** on the thiazole ring is buried inside the pocket and was used to calculate the percentage reduction of the intensity of the ¹H-NMR signal upon ligand binding (Figure 3.4 A). When HSP72-NBD was added to fragment **21** a significant reduction (58%) of the intensity of the ¹H-NMR signal of peak **a** was observed in comparison to the ¹H-NMR spectrum of fragment **21** alone, indicating that the compound is binding to the protein (Figure 3.4 B). Addition of ATP as a competitor restores the compound signal to close to its original value as hypothesised. From these NMR experiments fragment **21** was observed binding to HSP72-NBD and was displaced by ATP.

CPMG experiments were then carried out for compound **58**, a more soluble analogue of **21** which had shown good quality binding curves by SPR (discussed in Chapter 2). Compound **58** also showed binding to HSP72-NBD by CPMG and displacement by ATP (Figure 3.5).

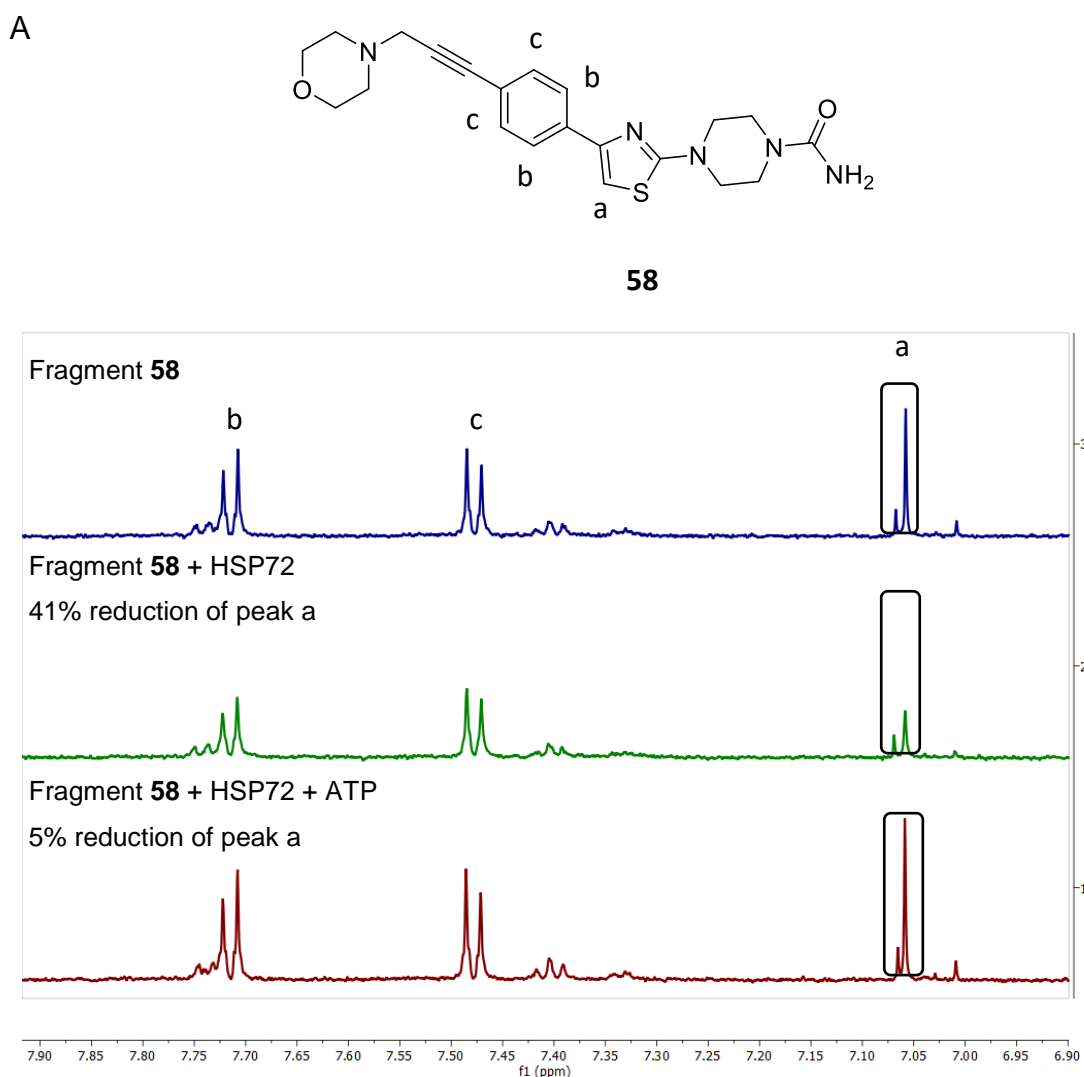




C

	% reduction relative to Fragment 21			
	Peak d	Peak c	Peak b	Peak a
Fragment 21 + HSP72	13%	14%	7%	58%
Fragment 21 + HSP72 + ATP	2%	2%	12%	8%

Figure 3.4 – Binding of fragment **21** to HSP72-NBD was detected by the LO-NMR method CPMG. (A) X-ray structure of the bound fragment shows the phenyl ring is solvent exposed but the thiazole ring with proton a is buried inside the pocket. (B) The proton of peak a is used to calculate the % reduction upon the ligand binding to HSP72. Upon addition of the competitor ATP, this signal is reduced to a much lesser extent. (C) Integration of peaks was performed with MNova.



B

	% reduction relative to fragment 58		
	Peak b	Peak c	Peak a
Fragment 58 + HSP72	36%	31%	41%
Fragment 58 + HSP72 + ATP	22%	7%	5%

Figure 3.5 - (A) Binding of fragment **58** to HSP72-NBD was detected by the LO-NMR method CPMG. The proton of peak a is entirely inside the allosteric pocket and is used to calculate the % reduction upon the ligand binding to HSP72-NBD. Upon addition of the competitor ATP, this signal is reduced to a much lesser extent. (B) Integration of peaks using MNova.

3.3.2 WaterLOGSY

A second LO-NMR method, waterLOGSY, was used to observe the binding of fragment **21** to HSP72. In this experiment four identical samples with compound **21** were dissolved in DMSO-d₆ and buffer. ATP was added to the second sample, HSP72-NBD was added to the third sample and HSP72-NBD and ATP were both added to the fourth sample. The NOE of the ligand is inverted upon addition of HSP72-NBD indicating the ligand is binding to the protein (Figure 3.6). Upon addition of ATP, the compound signals are reduced indicating that ATP is competing with the fragment for binding.

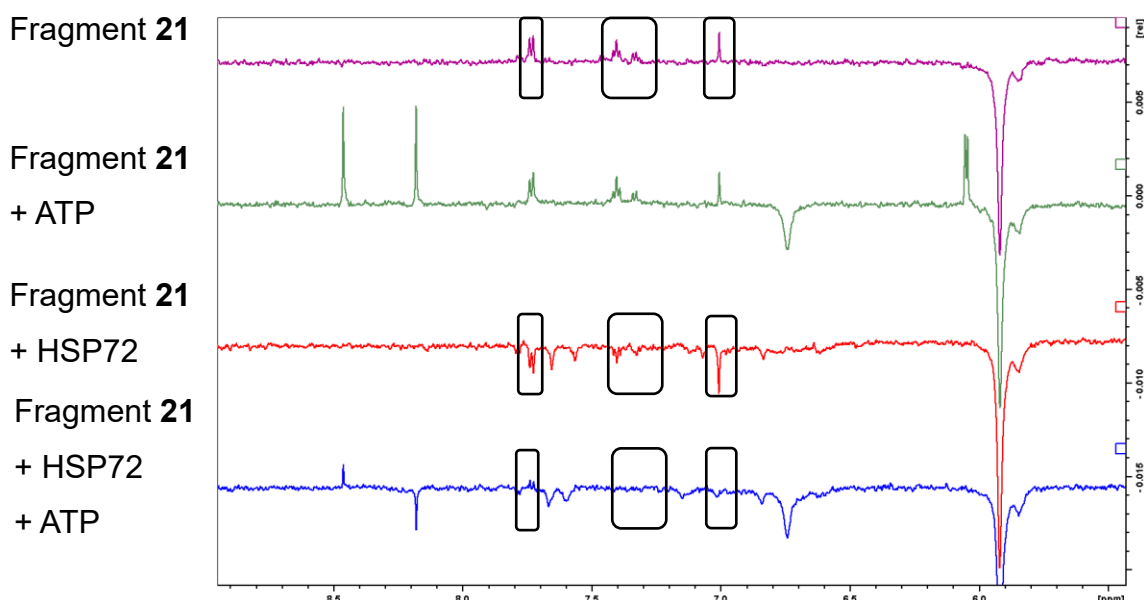


Figure 3.6 - Fragment **21** was tested against HSP72-NBD in a waterLOGSY experiment and showed binding to the protein as well as competition with ATP.

LO-NMR experiments can be used to differentiate between specific and nonspecific target binding due to aggregation. Small molecules can form microscopic aggregates in aqueous buffers, and these aggregates can inhibit diverse drug targets non-specifically.⁹² From the SPR experiments compound **21** showed non-specific binding at high concentrations, however, in the LO-NMR experiments compound **21** does not show aggregation at this concentration (200 μ M).

3.4 Introduction to photoaffinity labelling

Recently Cravatt *et al.* have reported a new technique for fragment-based screening to identify small molecule-protein interactions in cells.⁹³ They treated HEK293T cells with fragment probes that contained photoactivatable diazirine rings which, upon exposure to UV light decomposed to form covalent bonds to cellular or membrane bound proteins (Figure 3.7). The probes also contained an alkyne tag which could react with biotinylated azides using copper catalysed azide alkyne cycloaddition chemistry. These biotinylated proteins were then isolated using Streptavidin beads, digested with trypsin and sequenced by mass spectrometry. Fragments that bound to a protein were therefore identified by chemical proteomics. Protein labelling was not observed in the absence of UV light indicating that the fragment protein interactions correspond to reversible binding events which were converted to covalent adducts by photoreactivity.

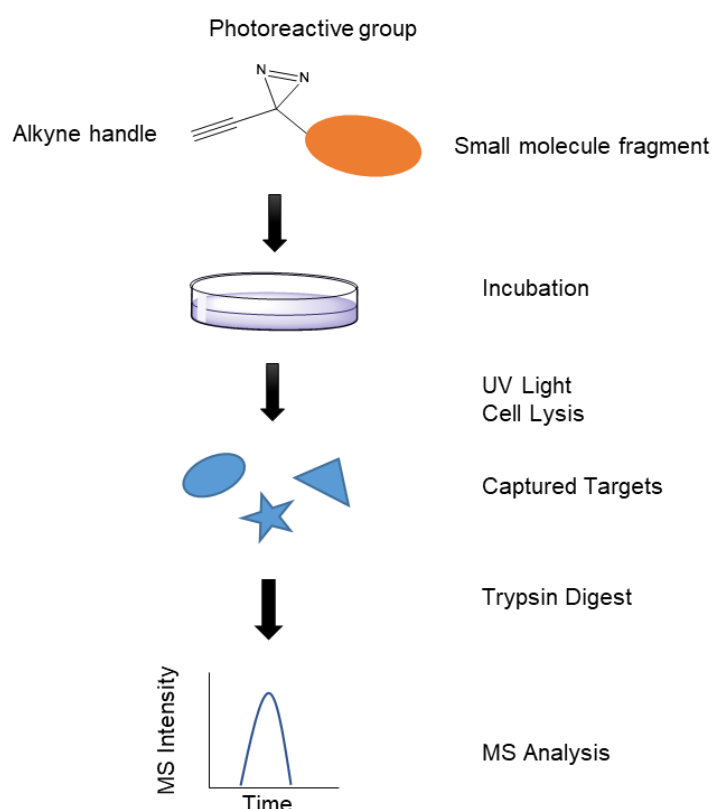


Figure 3.7 – Overview of fragment-based screening methodology developed by Cravatt *et al.* Cells are incubated with small molecule probes that upon exposure to UV light form covalent bonds to the proteins. These proteins are then captured and identified by mass spectrometry.

Inspired by this work and other applications of photoaffinity labelling studies to determine ligand binding sites,⁹⁴ this method was investigated as an orthogonal method to characterise the binding of fragment **21** to HSP72-NBD. The experiment was designed to incubate a photoreactive analogue of fragment **21** with HSP72 to determine by photoaffinity labelling studies if the fragment was bound to the protein and where. As this experiment was not going to be carried out in cells there was no need to include the alkyne tag to retrieve the protein.

This experiment required the synthesis of a fragment with a photolabile diazirine group which upon exposure to UV light decomposes to form a highly reactive carbene that reacts immediately with the nearest X-H bond in the protein, where X is C, N or O (Figure 3.8). Although fragment **21** binds to the secondary site reversibly, addition of this photolabile diazirine ring would allow the formation of a covalent bond from the fragment to the protein which would be detected by LC-MS as the mass of the protein plus the fragment. This would provide information on whether the fragment had bound to the protein and the ratio of the fragment to protein. A trypsin digest can be performed to break down the protein into smaller amino acid sequences which can be analysed by LC-MS/MS experiments to provide information on where the fragment is bound to the protein.

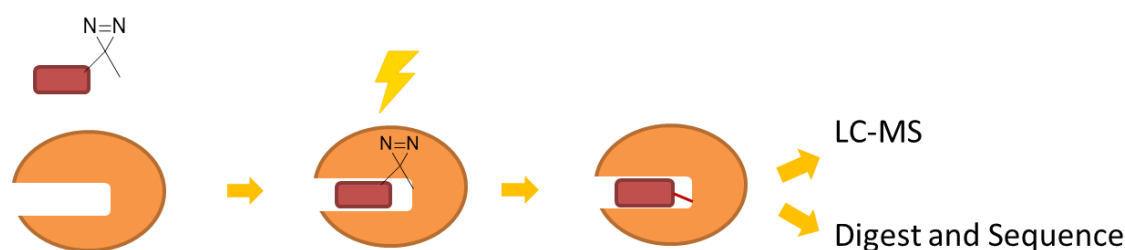


Figure 3.8 – Planned experiment to detect the binding of fragment **21** to HSP72-NBD by photoaffinity labelling studies. The fragment binds to the protein and upon exposure to UV light forms a covalent bond to the protein. Analysis by LC-MS can detect binding by additional fragment mass to the protein mass. A trypsin digest and sequencing by LC-MS/MS experiments could give information on where the fragment is bound.

3.5 Photoaffinity labelling studies

3.5.1 Design of a photolabile fragment

Analysis of the X-ray crystal structure of fragment **21** with HSP72-NBD shows the fragment bound in a long narrow binding site with the phenyl ring pointing towards the pocket opening which is exposed to solvent (Figure 3.9). A key factor in this experiment is that the addition of the diazirine ring does not interfere with the binding of the fragment to the protein. For this reason, the diazirine attachment point was designed in the *para* position of the phenyl ring, to avoid any clash with the protein, in a similar way to compounds **58** and **59** where the morpholine ring was attached to improve solubility (Chapter 2).

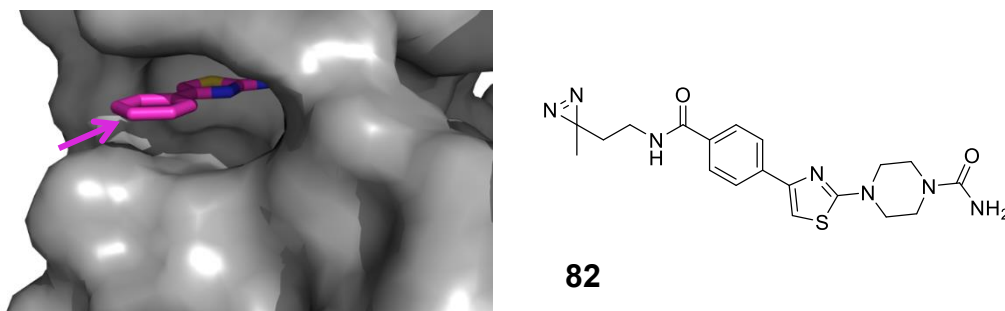
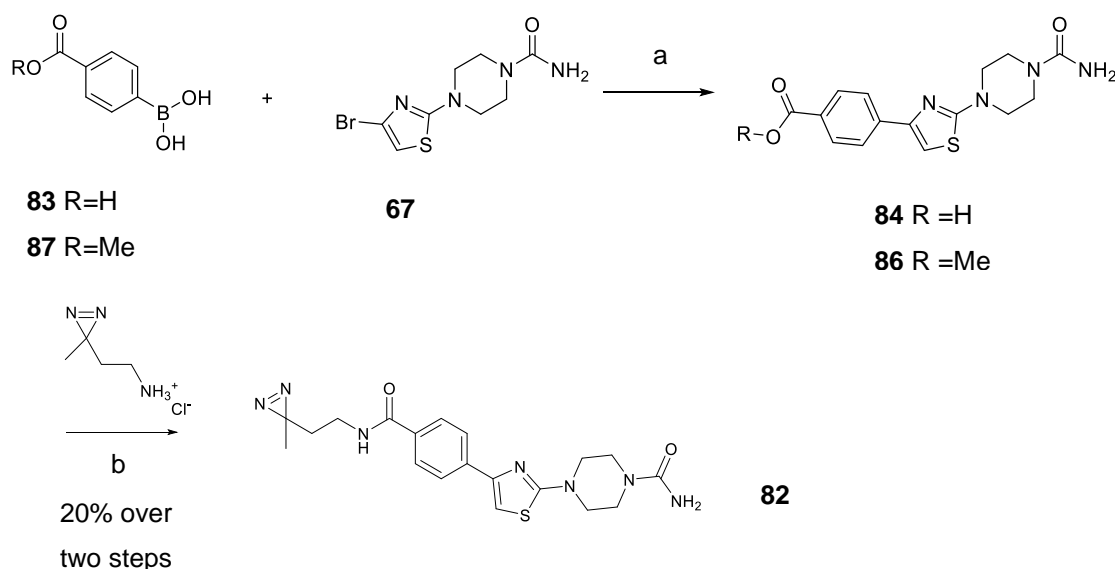


Figure 3.9 – Design of **82**, a photoactivatable analogue of Fragment **21** with a diazirine ring attached via a linker to the *para* position of the phenyl ring to avoid any clash with the protein.

3.5.2 Synthesis of a photolabile fragment

Photolabile fragment **82** was synthesised from **67** (Scheme 3.1; the synthesis of **67** was described in Chapter 2). The first step was a Suzuki coupling with 4-borono-benzoic acid **83**. During the reaction both the desired product **84** and the piperazine decomposition product **85** were observed (Figure 3.10). Isolation of pure product from the reaction mixture was extremely difficult. Attempts to purify by precipitation, reverse phase or normal phase column chromatography, acidic ion exchange or basic ion exchange chromatography were unsuccessful and gave impure product. Because **84** was difficult to purify, an alternative synthesis

of the methyl ester **86** with **87** was investigated instead (Scheme 3.1). Although this would involve an extra step, the purification should be more straightforward with the acid protected as the ester. However, four main peaks were observed by LC-MS after just one hour of reaction, corresponding to the acid product **84**, the ester product **86** coeluting with triphenylphosphine oxide, the acid product with decomposed urea **85** and the ester product with decomposed urea **88**, and no pure product was isolated (Figure 3.10). Because of these purification difficulties the acid **84** was used crude for the next amide coupling step to give the desired photoactivatable fragment **82** (Scheme 3.1).



Scheme 3.1 – Photolabile fragment **82** was synthesised in two steps from intermediate **67** and **83**. (a) K_2CO_3 , $Pd(PPh_3)_4$, MeCN: H_2O 1:1, 90 °C, 18 h (b) HATU, DIPEA, DMF, rt, 4 h. Attempts with **87** resulted in multiple products (Figure 3.10).

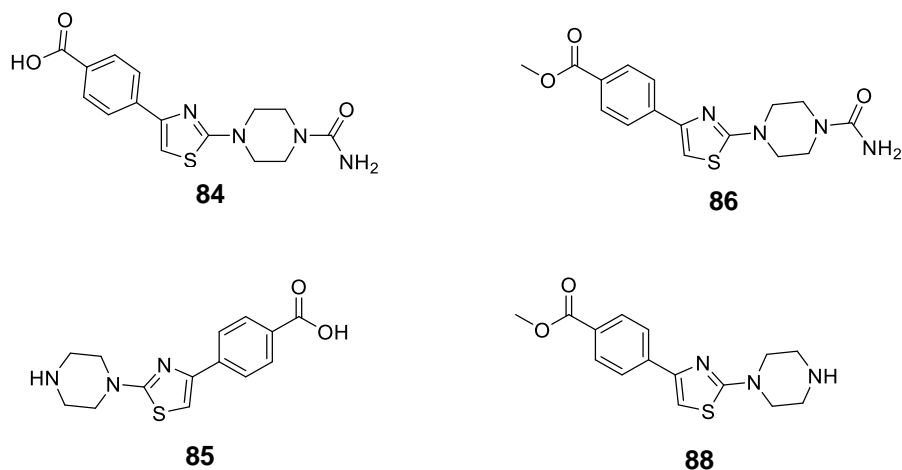


Figure 3.10 – Multiple products were formed in the Suzuki coupling of **87** with **67** (Scheme 3.1).

3.5.3 Testing of a photolabile fragment by SPR

Compound **82** was tested by SPR to ensure that the addition of the diazirine ring did not interfere with binding to the protein. As with the SPR experiments in Chapter 2, two different proteins were used for the SPR experiment - HSC70-NBD and a mutant HSC70-NBD S275W. Mutation of the S275 in the active site to a W275 blocks compounds from binding in the ATP binding site.³¹ Compounds that bind outside of the ATP binding site should bind equally well to the mutant and the wild type protein. Compound **82** was found to bind to HSC70-NBD with an affinity of 378 μM (Figure 3.11). This compares well with the related fragments **58** and **59** which bound with similar affinity (Table 3.1). The compound has an equal affinity for the wild type and the S275W mutant HSC70-NBD as expected for binding to a secondary site.

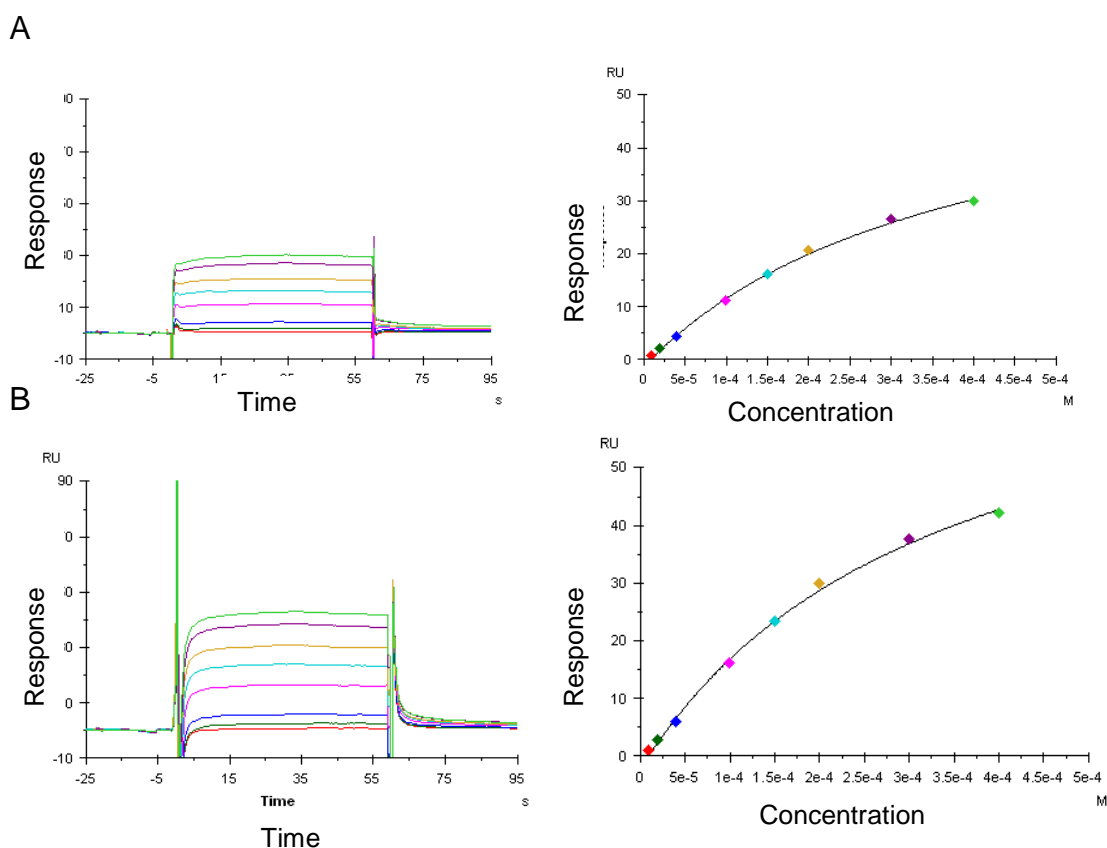


Figure 3.11 - SPR sensorgrams and binding curves of **82**. (A) Binding of **82** to HSC70-NBD. (B) Binding of **82** to HSC70-NBD S275W.

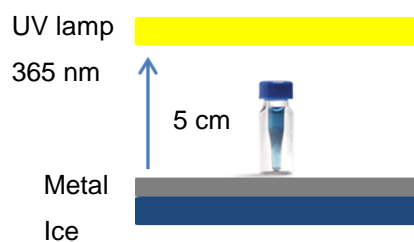
Structure	Compound	SPR HSC70-NBD	SPR HSC70-NBD S275W
	58	388 μM	352 μM
	59	486 μM	381 μM
	82	378 μM	329 μM

Table 3.1 – SPR testing of the photoactivatable fragment **82** showed similar binding affinity to both wild type HSC70-NBD and HSC70-NBD S275W as compounds **58** and **59** indicating that the compound is binding outside of the ATP binding site and that the linker with the diazine ring does not interfere with binding. ($n=1$) Values within two-fold are considered to be within experimental error.

3.5.4 Photoaffinity labelling experiments with HSP72

To determine the time taken for decomposition of the diazirine ring to the reactive carbene, compound **82** was incubated with methanol under UV light set at 365 nm for six time points between 5 to 90 minutes. Six identical samples were required so that the relative amount of starting material remaining after each time point could be compared by LC-MS. The area under the curve corresponding to the mass of **82** was found to decrease over time and a new mass ion corresponding to a methanol adduct increased over time (Figure 3.12). Analysis was complicated by the fact that both the starting material and the product had overlapping retention times but integration of the starting material peaks after 0 and 45 min shows 36% of the starting material remained after 45 min. By 90 minutes no starting material mass ion was detected.

A



B

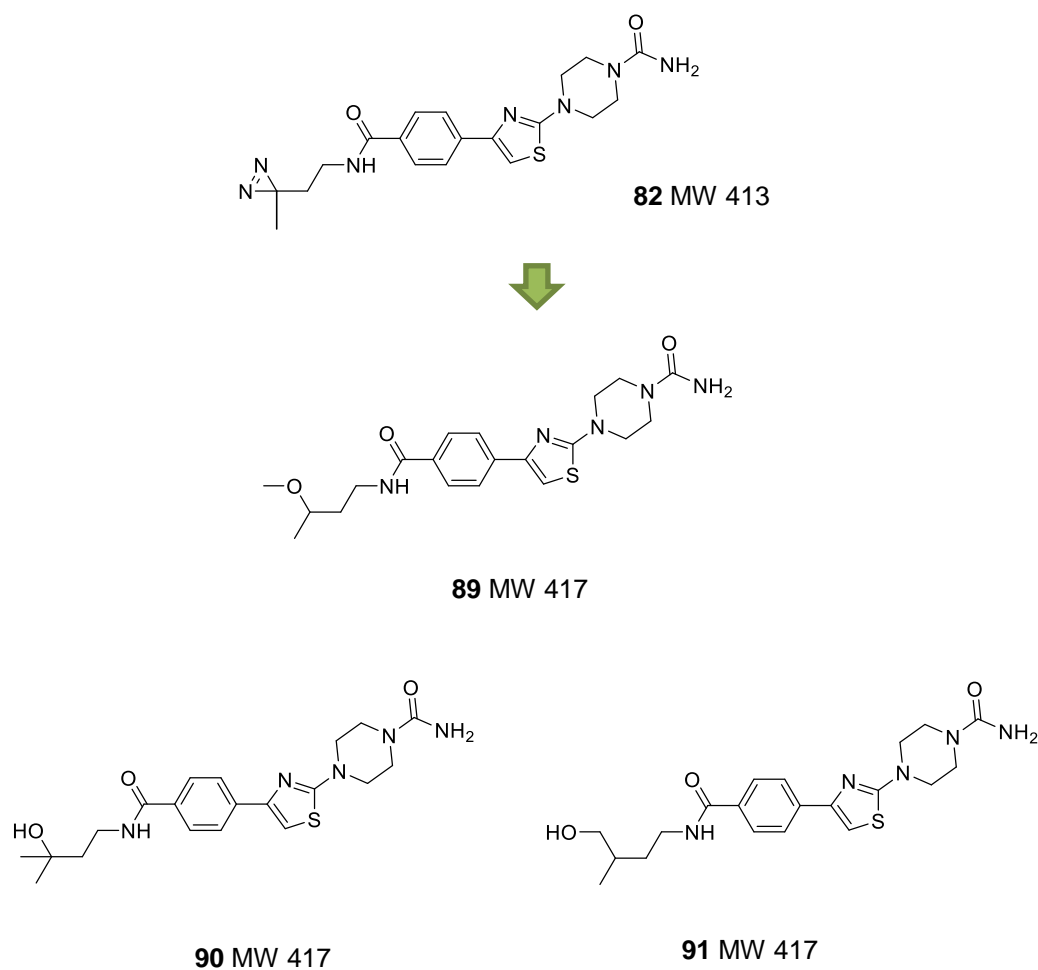
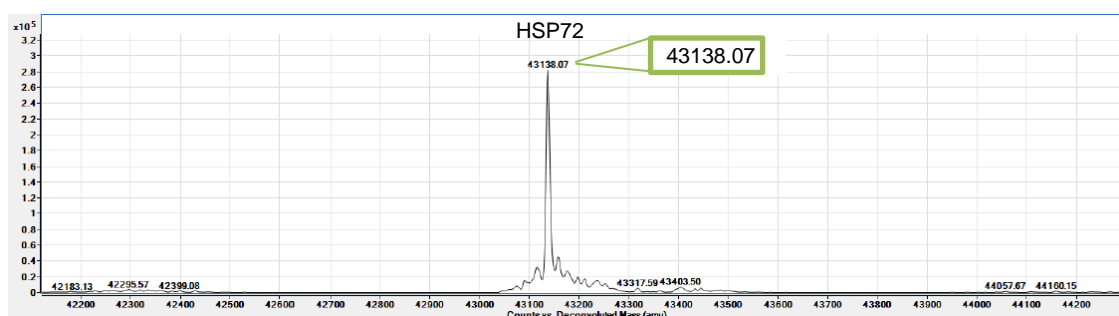


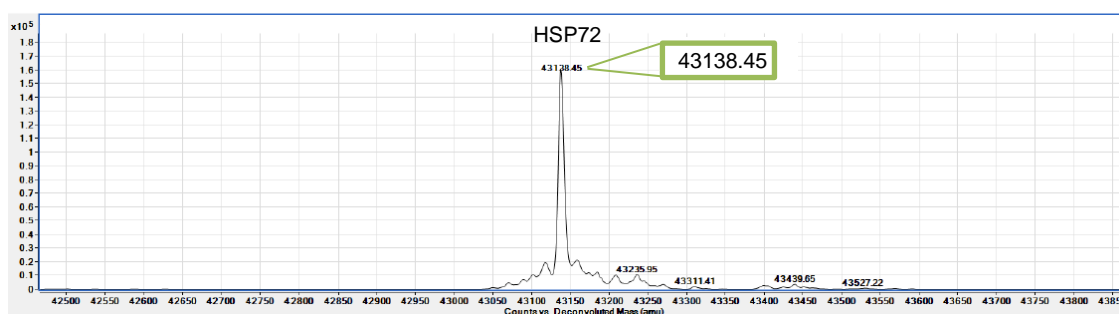
Figure 3.12 – (A) Experimental set-up to measure the decomposition of **82** under UV light over time. Six identical samples of **82** were incubated with methanol at 0°C. After each time point a sample was removed and wrapped in aluminium foil. At the end of the experiment the samples were analysed by LC-MS. (B) Upon exposure to UV light compound **82** decomposed over time and a mass ion for a methanol adduct was observed, which could correspond to three possible adducts 89-91..

The next step was designed to determine whether the protein remains stable under these experimental conditions. It's important that the protein remains folded and intact during the experiment to get an accurate assessment of ligand binding. Electrospray ionisation (ESI) has made efficient ionisation of large proteins possible. Proteins form multiply charged ions during electrospray ionisation and show a charge distribution envelope which can be deconvoluted to give the protein mass.⁹⁵ An LC-MS experiment known as QuickShot, developed at the ICR, was used to detect intact HSP72-NBD before and after irradiation to determine if the protein was affected by the irradiation process. All QuickShot experiments were carried out by Meirion Richards from the Structural Chemistry team at the ICR. Figure 3.13 shows that the protein was not affected by the irradiation process as the deconvoluted spectrum before and after irradiation at 365 nm for one hour showed no significant difference. **82** (1 mM) was then incubated with HSP72-NBD for one hour followed by irradiation at 365 nm for one hour. QuickShot analysis of this sample showed evidence of fragment labelling as the mass of the protein plus the mass of the fragment (43138 + 385). A small amount of the bis labelled protein was also observed (43138 + 2x385).

A



B



C

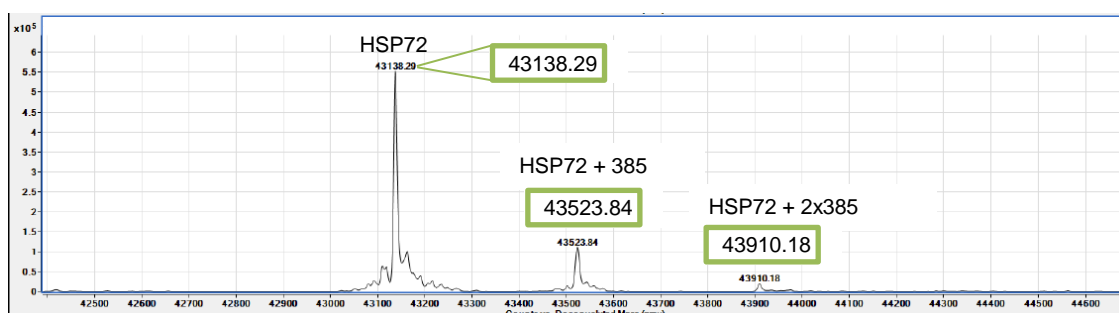


Figure 3.13 - (A) Deconvoluted spectrum of HSP72-NBD. Masses consistent with the average expected molecular weight of the protein were detected in the unmodified protein. (B) Deconvoluted spectrum of HSP72-NBD irradiated at 365 nm for one hour. Masses consistent with the average expected molecular weight of the protein were detected indicating the protein is not damaged by the irradiation process. (C) Deconvoluted spectrum of HSP72-NBD incubated with **82** for one hour followed by irradiation at 365 nm for one hour. Masses consistent with the average expected molecular weight of the unmodified protein, the mono-**82** adduct as well as the bis-**82** adduct were detected.

3.5.5 Sequencing of labelled HSP72

Two samples, HSP72-NBD irradiated with UV light and HSP72-NBD incubated with **82** irradiated with UV light, were submitted for sequencing to FingerPrints Proteomics Facility, School of Life Sciences, The Discovery Centre, University of Dundee.⁹⁶ The objective was to identify the peptide sequences where **82** was covalently bound to HSP72-NBD by comparing the samples with and without fragment **82**.

For a sequencing experiment the protein of interest is first digested with an enzyme such as trypsin to produce short peptide sequences.⁹⁷ Trypsin is a highly specific enzyme that recognises and cleaves next to arginine or lysine amino acids.⁹⁸ The peptides are then ionised and separated according to their different m/z ratios. Each peptide is fragmented into ions and the m/z values of fragment ions are measured. Proteins consist of 20 different types of amino acid each with a different mass (except leucine and isoleucine) so different peptides will produce different spectra. The spectrum of the peptide can therefore be used to determine its sequence. For each MS/MS spectrum, software is used to determine which peptide sequence in a database of protein sequences gives the best match. Each entry in the database is digested, *in silico*, using the known specificity of the enzyme and the masses of the theoretically obtained intact peptides are calculated. If the calculated mass of a peptide matches that of an observed peptide, the masses of the expected fragment ions are calculated and compared with the experimental values.

Not all sequences may be found in a trypsin digest MS experiment. Some fragments will not fly well and may not always be detected. Very good sequence coverage was achieved for the Tr-HSP72 + **82** irradiated with UV light sample (92%; Figure 3.14 A). Good coverage was also achieved for HSP72-NBD irradiated with UV light sample (85%; Figure 3.14 B).

A

```

1  GPLGSMAKAA AIGIDLGTTY SCVGVFQH GK VEIIANDQGN RTTPSYVAFT
51  DTERLIGDAA KNQVALNPQN TVFDAKRLIG RKFQDPVVQS DMKHWPFQVI
101 NDGDKPKVQV SYKGETKAFY PEEISSMVL T KMKEIAEAYL GYPVTNAVIT
151 VPAYFNDSQR QATKDAGVIA GLNVLRIINE PTAAAIAYGL DRTGKGERNV
201 LIFDLGGGTF DVSILTIDDG IFEVKATAGD THLGGEDFDN RLVNHFVEEF
251 KRKHKKDISQ NKRAVRLRT ACERAKRTLS SSTQASLEID SLFEGIDFYT
301 SITRARFEEL CSDLFRSTLE PVEKALRDAK LDKAQIHDLV LVGGSTRIPK
351 VQKLLQDFFN GRDLNKSINP DEAVAYGAAV QAAILIKSTR AAAS

```

B

```

1  GPLGSMAKAA AIGIDLGTTY SCVGVFQH GK VEIIANDQGN RTTPSYVAFT
51  DTERLIGDAA KNQVALNPQN TVFDAKRLIG RKFQDPVVQS DMKHWPFQVI
101 NDGDKPKVQV SYKGETKAFY PEEISSMVL T KMKEIAEAYL GYPVTNAVIT
151 VPAYFNDSQR QATKDAGVIA GLNVLRIINE PTAAAIAYGL DRTGKGERNV
201 LIFDLGGGTF DVSILTIDDG IFEVKATAGD THLGGEDFDN RLVNHFVEEF
251 KRKHKKDISQ NKRAVRLRT ACERAKRTLS SSTQASLEID SLFEGIDFYT
301 SITRARFEEL CSDLFRSTLE PVEKALRDAK LDKAQIHDLV LVGGSTRIPK
351 VQKLLQDFFN GRDLNKSINP DEAVAYGAAV QAAILIKSTR AAAS

```

Figure 3.14 – (A) Sequence coverage of irradiated HSP72-NBD with **82** was 92%. (B) Sequence coverage of irradiated HSP72-NBD was 85%. Matched peptides are shown in red.

Upon exposure to UV light, the diazirine ring of **82** decomposes to a carbene. Addition of this molecule to a peptide would be seen as [mass of peptide + 385]. Trypsin may also break the amide bonds in the molecule. In this case we may see [mass of peptide + 342] or [mass of peptide +71] (Figure 3.15).

Fingerprint Proteomics sent the results of all sequences detected (raw data can be found in the electronic appendix) which I analysed to find sequences that corresponded to the mass of a peptide with **82** covalently attached. By comparing the peptide sequences of the HSP72-NBD alone with the protein incubated with **82**, ten peptide sequences were detected with the mass of the fragment attached, seven of which were non-overlapping sequences. Each of these sequences was coloured in MOE to determine if any were close to the secondary binding site in the X-ray crystal structure (Figure 3.16). However, only one of the sequences has

residues close to the secondary site, suggesting non-selective binding of **82** to the protein in this experiment.

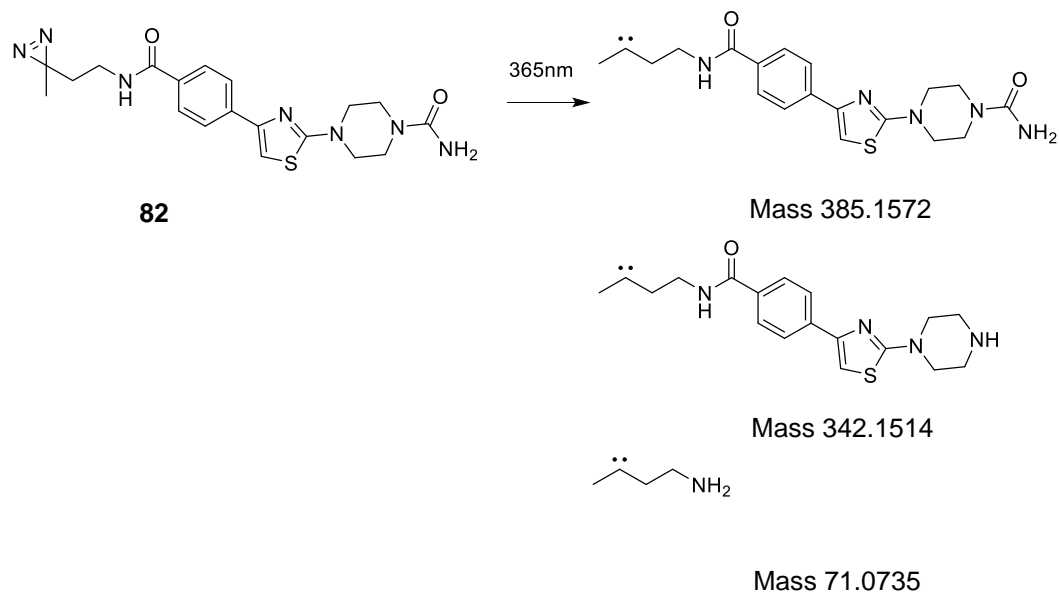
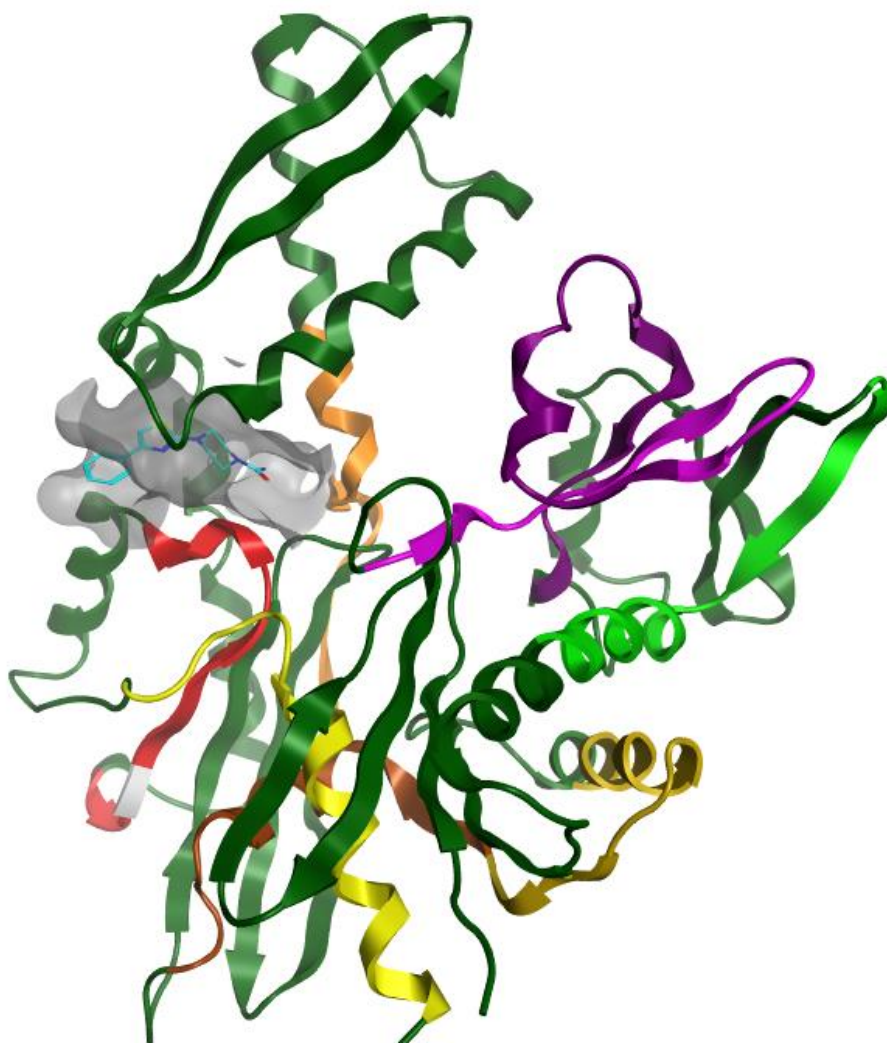


Figure 3.15 – Decomposition of the diazirine ring of **82** forms a carbene with a fragment mass of 385. In the trypsin digest experiment the amide bonds of **82** may also be cleaved. In this case we may see [mass of peptide + 342] or [mass of peptide +71].

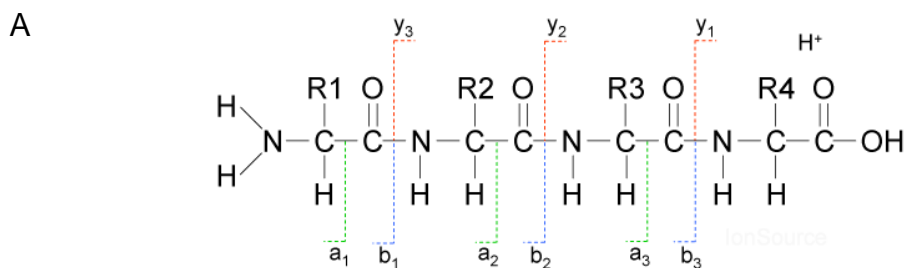


Sequences with [Peptide + 385]		
Sequence	Residues	Colour
1	42-54	Pink
2	55-76	Purple
3	114-131	Bright Green
4	177-192	Brown
5	226-241	Orange
6	334-347	Red
7	367-387	Yellow

Figure 3.16 – Sequences where fragment **82** was detected covalently bound. Fragment **21** (cyan) with the surface of the secondary binding site is highlighted in grey.

The sequence nearest the secondary site (Sequence 6 in red; Figure 3.16) was further analysed to determine which specific amino acid residue was tagged with the fragment. Each sequence has a specific molecular weight detected by MS.

Knowledge of the mass of each amino acid in the sequence means that it is possible to calculate the mass of each theoretical fragment that could be formed in the MS/MS experiment. The most common peptide fragments observed in low energy collisions are a, b and y ions, as shown in Figure 3.17 A. b ions are those that appear to extend from N-terminus, y ions appear to extend from the C-terminus.⁹⁹ a ions may also be formed but they occur at a much lower frequency and abundance in relation to b ions. The b and y daughter ions of this sequence were calculated and compared with the experimental results (Figure 3.17 B and C). By comparing the theoretical and experimental b ions and y ions D333 (white, Figure 15) was identified to be the residue that was covalently linked to the fragment. The b ion for D333 has a theoretical mass of 565 but an experimental mass of 950, equivalent to the mass of the peptide plus 385, which is the mass of the fragment. All other b and y ions found experimentally match with those determined theoretically. This aspartic acid residue is far from the secondary binding site. From this sequencing experiment it is apparent that none of the residues labelled by fragment **82** are near the known secondary binding site identified by fragment-based screening described in Chapter 2.



B

Theoretical Fragment Ions				
#	b	Seq	y	#
1	72.04444	A	1465.81219	14
2	200.10301	Q	1394.77508	13
3	313.18708	I	1266.7165	12
4	450.24599	H	1153.63244	11
5	565.27293	D	1016.57353	10
6	678.35699	L	901.54658	9
7	777.42541	V	788.46252	8
8	890.50947	L	689.39411	7
9	989.57788	V	576.31004	6
10	1046.59994	G	477.24163	5
11	1103.62081	G	420.22017	4
12	1190.65284	S	363.19870	3
13	1291.70052	T	276.16667	2
14	1447.80163	R	175.11900	1

C

Experimental fragment ions				
#	b	Seq	y	#
1	72.0444	A		14
2	200.1030	Q	1779.932	13
3	313.1870	I	1651.874	12
4	450.2459	H	1538.79	11
5	950.4301	D	1401.731	10
6	1063.5142	L	901.5465	9
7	1162.5826	V	788.4625	8
8	1275.6667	L	689.3941	7
9	1374.7351	V	576.3100	6
10	1431.7566	G	477.2416	5
11	1488.7780	G	420.2201	4
12	1575.8100	S	363.1987	3
13	1676.8577	T	276.1666	2
14		R	175.1190	1

Figure 3.17 – (A) The most common peptide fragments observed in low energy collisions are a, b and y ions. **(B)** Calculation of the b and y daughter ions of Sequence 6 was carried out using a fragment ion calculator¹⁰⁰ **(C)** The experimental fragment ions of sequence 6 from the trypsin digest. Comparison of the theoretical and experimental results identified D333 (white; Figure 3.16) as the residue that was covalently linked to the fragment. The remaining calculated values highlighted in green match the experimental values as they are not covalently attached to the fragment.

3.5.6 Conclusions from photoaffinity labelling experiments

Although the photoactivatable fragment **82** was found by QuickShot LC-MS experiments to be bound covalently to the protein, analysis of the sequencing data showed this labelling to be non-specific in this experiment. One of the labelled sequences that was close to the secondary binding site was analysed in more detail and it was found that D333 was the residue labelled by the fragment, a residue that is far from the secondary binding site of **21**.

It's likely that the application of this method for testing the protein-ligand binding of **82** to the cryptic secondary binding site requires significant optimisation. This technique could be more successfully applied with a different photoactivatable analogue of the fragment. Compound **82** placed the diazirine ring towards the solvent exposed region of the protein to avoid any clash of the new group with the protein that would prevent ligand binding. It would be interesting to compare the results of the photoaffinity labelling studies of **82** with different analogues of fragment **21** that placed the photoactivatable group in a more enclosed region of the pocket. Alternatively, increasing the affinity of the ligand for the protein or reducing the concentration of the fragment in the incubation experiments may be more successful.

3.6 Summary of fragment validation

At this point in the project fragment binding had successfully been validated by SPR, WaterLOGSY, CPMG and X-ray crystallography experiments but not by the photoaffinity labelling experiments which would require further optimisation. Although fragment **21** and its more soluble derivatives **58** and **59** were essential in the discovery and subsequent validation of this previously undescribed cryptic secondary binding site they are not ideal for further progression into a lead compound due to their poor ligand efficiency. In order to determine if binding to this secondary site can disrupt the function of HSP70, new fragments would need to be found with the required potency to test in a functional assay.

As discussed in Chapter 1 ligand efficiency, a metric that normalizes compound affinity with respect to molecular size, is useful for comparing fragments and assessing their prospects for further development. Fragment **21** displayed non-saturating binding curves in the SPR so affinity could only be measured accurately with the added solubilising group. The potency of fragments **58** and **59** is quite weak for their size with ligand efficiencies of 0.16 (Figure 3.18). For this reason, collaborations were set up to search for new hit matter by virtual high-throughput screening against the secondary binding site.

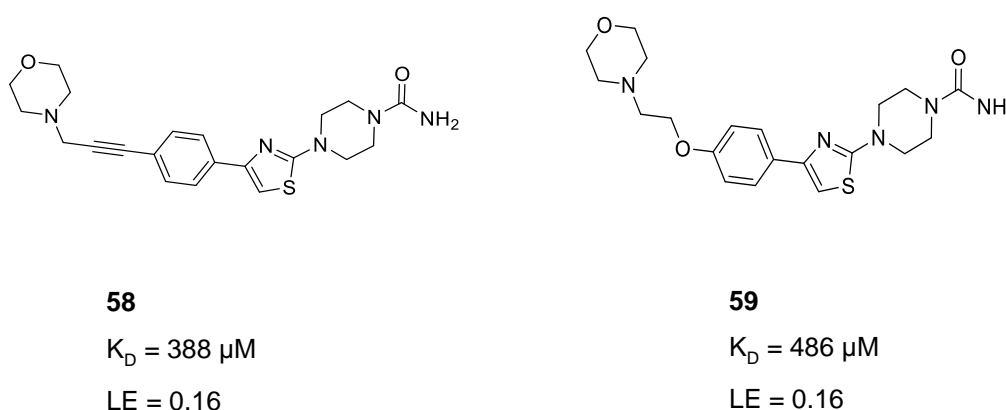


Figure 3.18 – Ligand efficiencies of fragments **58** and **59**

3.7 vHTS screening against the secondary binding site

Virtual high-throughput screening (vHTS) is a computational technique used to assess whether known compounds are likely to bind to a protein target of interest.¹⁰¹ Millions of compounds can be virtually screened to determine their complementarity to the protein pocket in terms of size, shape and potential binding interactions (Figure 3.19). The results from a virtual screen can be used to make experimental screening more efficient by identifying the compounds most likely to be active, giving priority to compounds for testing.

The X-ray crystal structure of the secondary binding site in HSP72 was shared with two separate collaborators with expertise in virtual high-throughput screening – Atomwise, a company that specialises in Artificial Intelligence, and

Johannes Reynisson's group at the University of Auckland, New Zealand. Using their own in-house methods, they screened virtual libraries of compounds against the novel site and applied screening filters to narrow down hits. Although each collaborator used their own methods, common screening techniques include using a variety of scoring functions, prioritising compounds that follow Lipinski's rules with low strain and eliminating groups associated with toxicity and chemical reactivity.

Johannes Reynisson and his PhD students Oi Wei Mak and Raina Chand screened the ChemBridge library (<https://www.chembridge.com>) and the natural product library available from InterBioScreen Ltd (<http://www.ibscreen.com>) against the secondary binding site of HSP72-NBD and recommended 25 virtual hits from each of these libraries for testing by SPR.

Atomwise ran a vHTS with their own library against the secondary binding site of HSP72-NBD. From this screen they recommended 80 compounds for SPR testing. The testing of compounds from these three screens is described in the following sections.

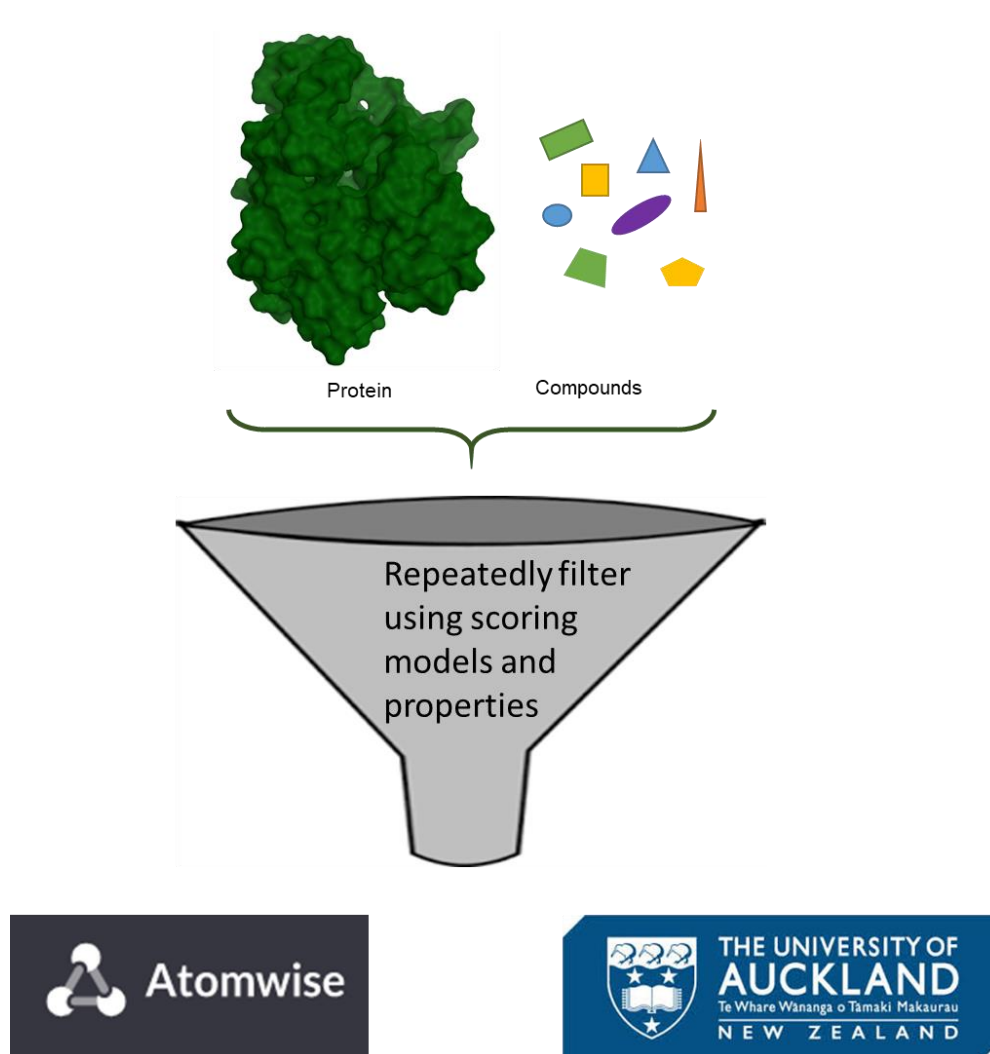


Figure 3.19 – Virtual high-throughput screening was carried out against the secondary binding site in HSP72 by collaborators with expertise in virtual high throughput screening to find new hit matter. The most highly ranked hits were selected for testing by SPR.

3.7.1 Testing of virtual hits by SPR

3.7.1.1 Testing of the vHTS hits from a natural product library

Twenty-five compounds recommended from the virtual high-throughput screen of the natural product library were purchased from InterBioScreen (<http://www.ibscreen.com>). The molecular weight and purity of each compound was assessed by LC-MS analysis (Table 3.2). Compounds shown to have the correct mass and adequate solubility were taken forward to the SPR experiment.

Compound **108** was not soluble in DMSO at 100 mM or even at 25 mM and was therefore not included. The remaining 24 compounds were dissolved in DMSO to a concentration of 100 mM. The first SPR experiment was carried out with these 24 compounds and two control compounds known to bind to HSC70 – adenosine and VER-155008 in eight concentrations. VER-155008 was also run at a single concentration after every two compounds to monitor protein integrity over the course of the experiment. Analysis of the results showed a loss of the VER-155008 control compound binding to the chip over time, most likely due to compound **99** coating the protein and interfering with subsequent compounds from binding (Figure 3.20).

Compound	Supplier ID	MW	Correct mass	UV Purity
93	STOCK1N-01401	280.323	yes (M+H)	100%
94	STOCK1N-02674	295.337	yes (M+H)	100%
95	STOCK1N-03958	284.314	yes (M+H)	100%
96	STOCK1N-04138	279.295	yes (M+H)	100%
97	STOCK1N-04315	360.412	yes (M+H)	100%
98	STOCK1N-04333	324.332	yes (M+H)	92%
99	STOCK1N-04755	310.306	yes (M+H)	100%
100	STOCK1N-06204	296.322	yes (M+H)	100%
101	STOCK1N-06275	472.451	yes (M+H)	100%
102	STOCK1N-07482	537.568	yes (M+H)	100%
103	STOCK1N-07694	312.321	yes (M+H)	100%
104	STOCK1N-08334	352.386	yes (M+H)	100%
105	STOCK1N-09608	317.343	yes (M+H)	100%
106	STOCK1N-09684	338.359	yes (M+H)	100%
107	STOCK1N-10286	287.333	yes (M+H)	100%
108	STOCK1N-10961	339.347	yes (M+H)	100%
109	STOCK1N-11074	326.305	yes (M+H)	100%
110	STOCK1N-11335	300.310	yes (M+H)	95%
111	STOCK1N-18044	306.407	yes (M+H)	21%
112	STOCK1N-24775	301.359	yes (M+H)	100%
113	STOCK1N-24993	301.298	yes (M+H)	100%
114	STOCK1N-25080	315.374	yes (M+H)	100%
115	STOCK1N-26277	301.347	yes (M+H)	100%
116	STOCK1N-26472	330.401	yes (M+H)	100%
117	STOCK1N-27625	282.295	yes (M+H)	100%

Table 3.2 – Compounds recommended from the virtual high-throughput screen of the natural product library were purchased and assessed for purity and correct mass by LC-MS.

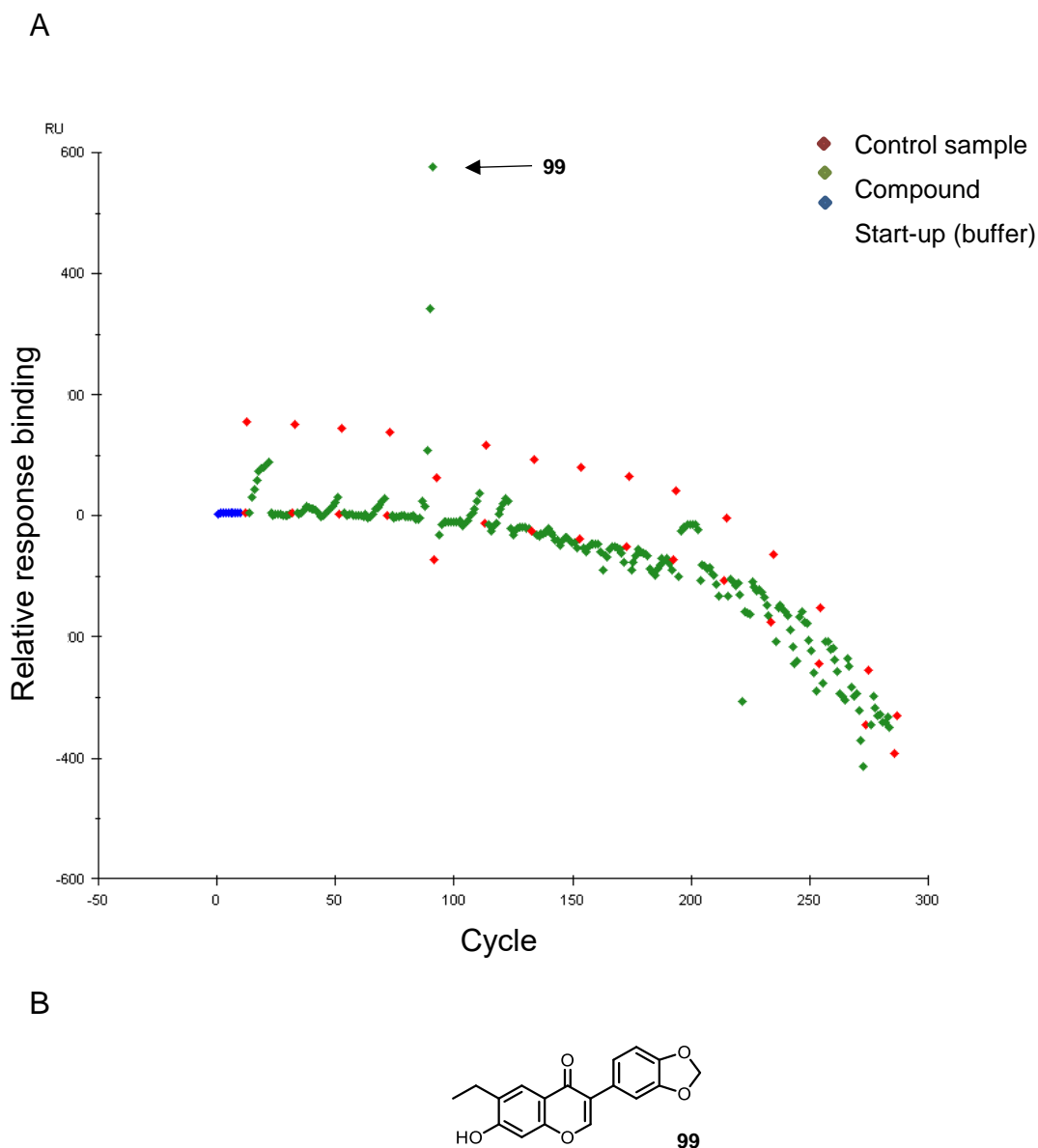


Figure 3.20 – (A) The relative binding response of the control sample VER-155008 at 0.5 μM (red dot) decreases suddenly during the experiment most likely due to compound **99**. This compound was therefore removed from subsequent experiments. (B) Structure of **99**.

The SPR assay was repeated without compound **99**. The control compounds adenosine (at the beginning of the run) and VER-155008 (at the end of the run) gave the expected K_D values and the binding level remained stable across the run (Figure 3.21). Three compounds **94**, **102** and **103** showed binding responses and were repeated ($n = 2$; Table 3.3). Example sensorgrams and binding curves are shown in Figure 3.22. All three have a chromenone structure but so do many

of the inactive compounds so no SAR conclusions could be drawn. **94** and **103** showed very weak binding (response units ~ 10) and should be treated with caution.

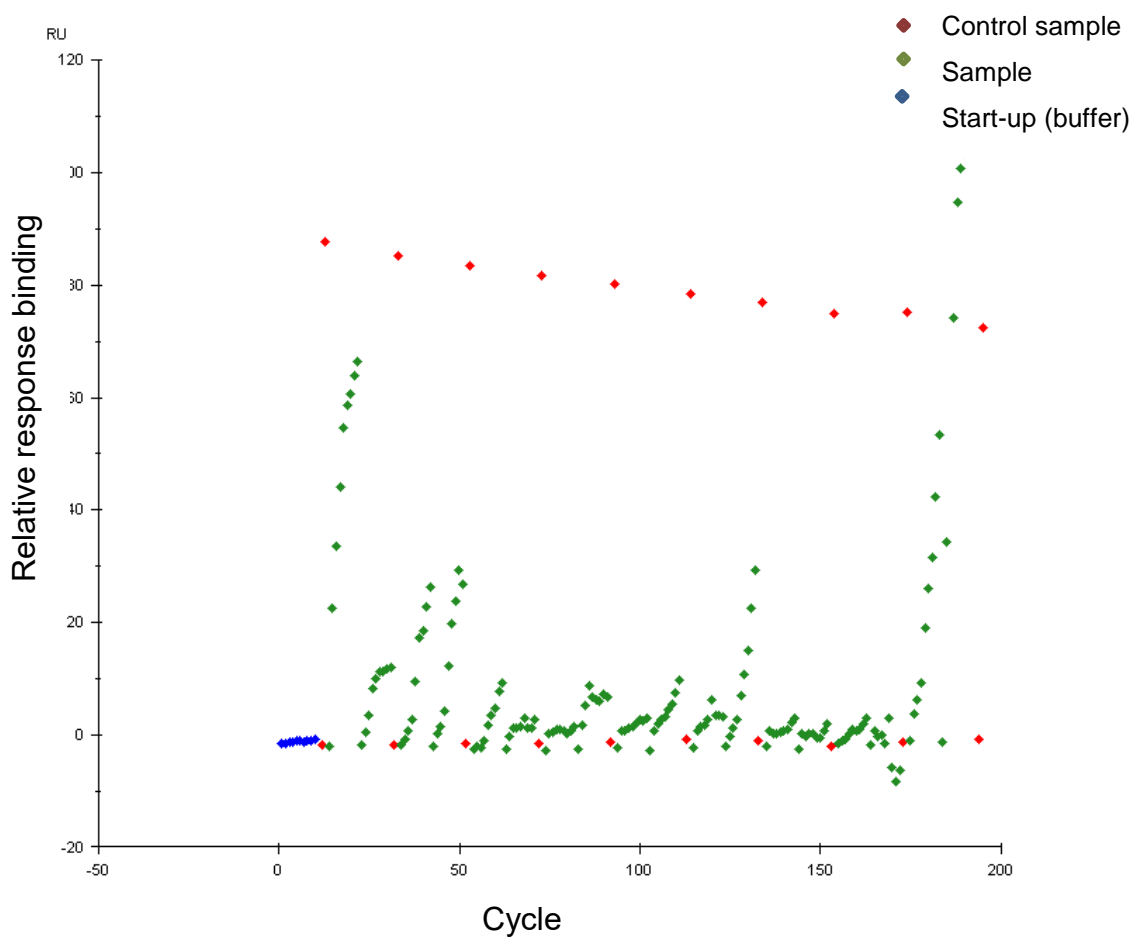


Figure 3.21 – The relative response of the control sample VER-155008 at 0.5 μM remains stable throughout the run.

Compound	Experiment 1		Experiment 2	
	HSC70 WT K _D	HSC70 S275W K _D	HSC70 WT K _D	HSC70 S275W K _D
93	inactive	inactive		
94	26 μ M RU ~10	25 μ M	22 μ M RU ~10	27 μ M
95	no saturation			
96	inactive			
97	No saturation	449 μ M		
98	inactive	inactive		
100	inactive	inactive		
101	no saturation	no saturation		
102	561 μ M	559 μ M	362 μ M	339 μ M
103	242 μ M RU ~10	232 μ M	764 μ M	625 μ M
104	inactive	inactive		
105	inactive	inactive		
106	inactive	inactive		
107	inactive	inactive		
109	inactive	poor solubility		
110	inactive	inactive		
111	no saturation	inactive		
112	inactive	inactive		
113	no saturation	no saturation		
114	inactive	inactive		
115	inactive	inactive		
116	inactive	inactive		
117	inactive	inactive		

Table 3.3 – SPR testing of vHTS hits from natural product library. Compounds are labelled 'inactive' when response units <10 RU or when K_D >1 mM

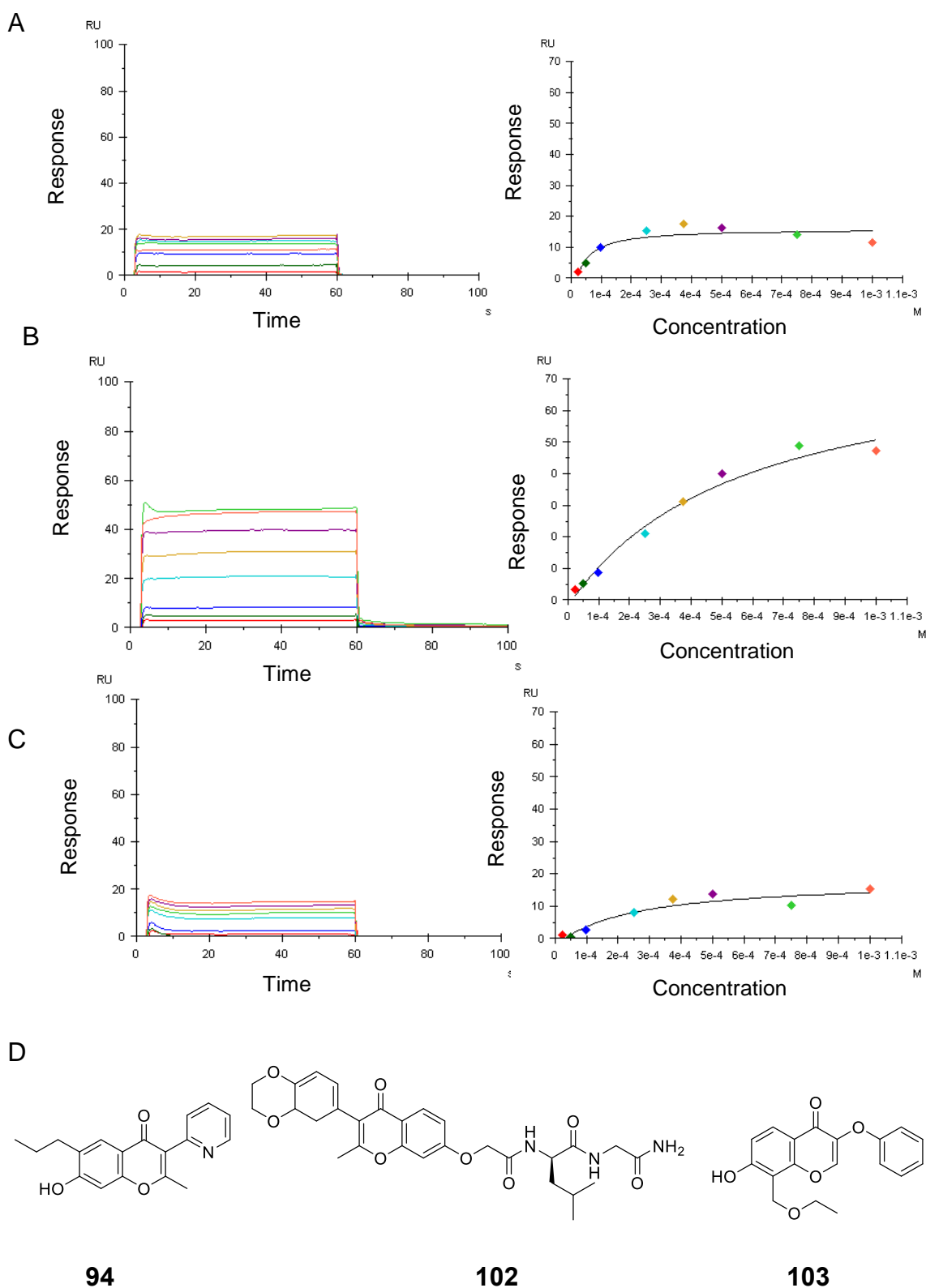


Figure 3.22 – Sensorgrams and binding curves of three compounds from the natural product library that showed binding to HSC70-NBD. (A) **94** (B) **102** and (C) **103** (D) Structures of compounds that show binding to HSC70-NBD.

3.7.1.2 Testing of the vHTS hits from the Chembridge library

Twenty-four compounds recommended from the virtual high-throughput screen with the Chembridge library were purchased from Chembridge (<https://www.hit2lead.com>). The remaining compound N92986533 **137** was unavailable from the supplier. The molecular weight and purity of each compound was assessed by LC-MS analysis (Table 3.4). Compounds shown to have the correct mass and adequate solubility were taken forward to the SPR experiment along with two control compounds, adenosine and VER-155008.

Compound	Supplier ID	MW	Correct mass	UV Purity
118	N10811184	388.5	yes (M+H)	99%
119	N12381023	382.5	yes (M+H)	97%
120	N14729173	368.5	yes (M+H)	94%
121	N18266435	311.4	yes (M+H)	100%
122	N24973712	395.5	yes (M+H)	100%
123	N28875745	379.5	yes (M+H)	97%
124	N28959850	382.5	yes (M+Na)	98%
125	N32668482	381.5	yes (M+H)	100%
126	N37439859	326.4	yes (M+H)	100%
127	N46373143	373.9	yes (M+H)	99%
128	N53636871	371.5	yes (M+H)	95%
129	N56098482	339.4	yes (M+H)	100%
130	N58566643	365.4	yes (M+H)	100%
131	N68644396	296.3	yes (M+H)	100%
132	N75264903	400.4	yes (M+H)	100%
133	N75942182	360.4	yes (M+H)	100%
134	N81245242	326.4	yes (M+H)	100%
135	N84784136	385.5	yes (M+H)	96%
136	N86098553	352.4	yes (M+H)	100%
138	N87909772	350.4	yes (M+H)	98%
139	N92872836	369.5	yes (M+H)	100%
140	N96993224	361.4	yes (M+ Na)	96%
141	N98800514	380.4	yes (M+H)	100%
142	N99354356	380.5	yes (M+H)	97%

Table 3.4 – Compounds from the Chembridge library were assessed for correct mass and UV purity by LC-MS.

Compound	Experiment 1		Experiment 2	
	HSC70 WT K _D	HSC70 S275W K _D	HSC70 WT K _D	HSC70 S275W K _D
118	inactive	inactive		
119	inactive	inactive		
120	261 μ M	288 μ M	526 μ M	481 μ M
121	inactive	inactive		
122	inactive	inactive		
123	Doesn't fully dissociate	Doesn't fully dissociate		
124	inactive	inactive		
125	Poor solubility	Poor solubility		
126	inactive	inactive		
127	inactive	inactive		
128	Inactive	inactive		
129	inactive	inactive		
130	Doesn't fully dissociate	Doesn't fully dissociate		
131	inactive	inactive		
132	896 μ M	753 μ M	> 1mM	> 1mM
133	98 μ M RU ~10	88 μ M RU ~10	236 μ M	263 μ M
134	inactive	inactive		
135	0.3 μ M	0.2 μ M	12 μ M	12 μ M
136	inactive	inactive	Inactive	inactive
138	231 μ M but RU ~10	214 μ M RU ~10	95 μ M RU ~10	104 μ M RU ~10
139	inactive	inactive	Inactive	inactive
140	inactive	inactive	Inactive	inactive
141	104 μ M	97 μ M	79 μ M	74 μ M
142	inactive	inactive	Inactive	inactive

Table 3.5 - SPR testing of vHTS hits from the Chembridge library. Compounds are labelled 'inactive' when response units <10 RU or when K_D >1 mM.

Five fragment hits **120**, **133**, **135**, **138**, **141** showed activity by SPR in n=2 experiments (Table 3.5). The remaining fragments were either inactive or had

non-stoichiometric binding or precipitation that prevented a K_D value from being determined accurately. These five compounds of interest were repurchased for further analysis. The compounds were passed through a plug of silica and analysed by LC-MS and NMR to check for correct structure. For all five of the compounds the LC-MS matched well with the first batch and the $^1\text{H-NMR}$ was consistent with the correct structure.

Batch 1 and Batch 2 were tested in the same SPR experiment for comparison (Expt 3, Table 3.6). **133**, **138** and **141** were active in all experiments and with both batches. Compound **135** was only available in very small quantities which were unfortunately not enough to fully characterise and test. Batch 1 of compound **120** was active in $n=3$ experiments but Batch 2 showed non-stoichiometric binding. These compounds are chemically diverse and could provide interesting scaffolds to improve the potency (Figure 3.23). Attempts to solve the X-ray crystal structures of these compounds with HSP72 are ongoing by the Structural Biology team.

Compound	Batch	Expt 1	Expt 2	Expt 3
120	Batch 1	261 μM	526 μM	430 μM
120	Batch 2			No saturation
133	Batch 1	98 μM	236 μM	354 μM
133	Batch 2			224 μM
135	Batch 1	0.3 μM	12 μM	13 μM
135	Batch 2			Not tested
138	Batch 1	231 μM	95 μM	77 μM
138	Batch 2			383 μM
141	Batch 1	104 μM	79 μM	113 μM
141	Batch 2			177 μM

Table 3.6 - SPR testing of vHTS hits from Chembridge library. Batch 1 has been tested in three independent experiments and all five compounds have been consistently active. Batch 2 has been passed through silica before testing. Three of the four compounds tested showed activity across all experiments and batches.

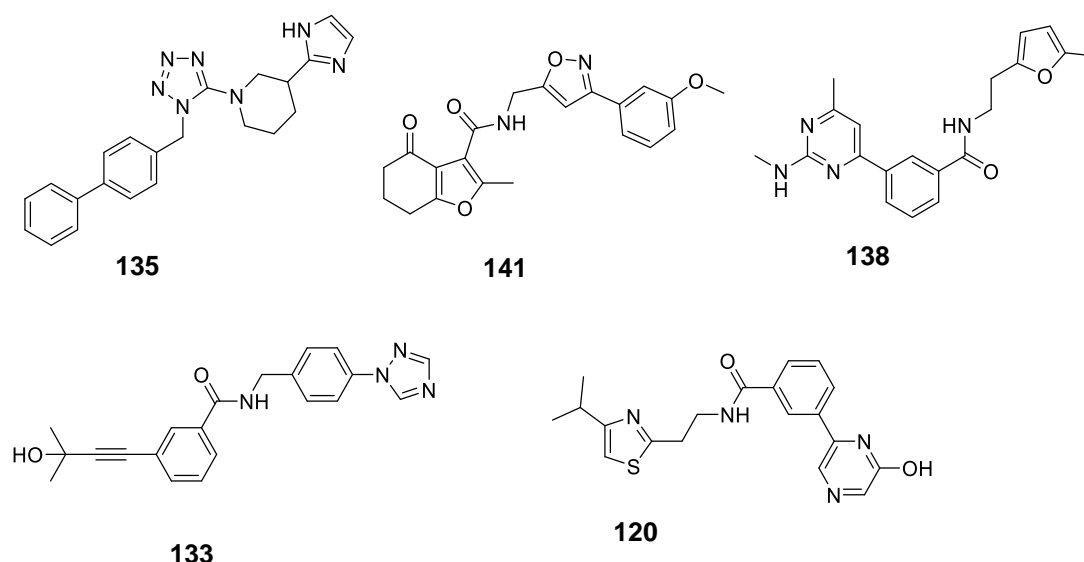


Figure 3.23 – Structures of the compounds from the Chembridge library that showed binding to HSC70-NBD by SPR.

3.7.1.3 Testing of the vHTS hits from the Atomwise library

The 80 hit compounds from the Atomwise virtual high-throughput screen were analysed by LC-MS to ensure the fragments had the correct mass ion and to ascertain sample purity. Compounds were plated using an Echo Liquid Handler to dispense 10 μ L of each sample to a 384 well plate at 1 mM in 100% DMSO. LC-MS analysis was then carried out in a high-throughput fashion by Joe Smith, from the structural chemistry team at the ICR (Figure 3.24). 79 of the compounds displayed a UV purity value of 85% or greater and the correct molecular weight. One compound displayed a UV purity value below 85% and the correct molecular weight (CCT376353; 72% purity).

Purity Category	Samples	Percentage
Purity \geq 95%	67	83.75%
Purity 85-95%	12	15.0%
Purity 50-85%	1	1.25%
Purity <50%	0	0.0%
Incorrect MW	0	0.0%
Total	80	

Figure 3.24 – LC-MS analysis of the 80 compounds from the vHTS Atomwise screen was carried out to ascertain purity and correct mass.

Running all 80 hit compounds in a single SPR experiment with eight-point concentrations is not feasible. Therefore, the compounds were divided into three groups to be run in three identical SPR experiments, each taking approximately 32 hours. Control samples adenosine and VER-155008 were run in eight-point concentrations at the beginning and end respectively for each experiment. VER-155008 and buffer controls were also run at a single concentration after every two compounds to monitor protein integrity throughout the run. Compounds were tested at eight concentrations up to 1 mM. Fifteen compounds that looked potentially interesting from the first experiments were repeated in a second experiment, in eight-point concentrations up to 0.5 mM. The results are summarised in Table 3.7 with example sensorgrams and binding curves in Figure.3.25.

Compound	Experiment 1	Experiment 2
143	insoluble	
144	Non-stoichiometric	
145	Non-stoichiometric	
146	inactive	inactive
147	430 μM	inactive
148	inactive	
149	Non-stoichiometric	
150	Non-stoichiometric	
151	inactive	inactive
152	Non-stoichiometric	
153	Non-stoichiometric	
154	490 μM	202 μM
155	inactive	inactive
156	inactive	
157	inactive	
158	472 μM	397 μM poor sensorgrams
159	Non-stoichiometric	
160	937 μM	
161	inactive	
162	Non-stoichiometric	
163	Poor sensorgrams	
164	inactive	
165	Non-stoichiometric	
166	Non-stoichiometric	
167	Non-stoichiometric	
168	Non-stoichiometric	
169	Non-stoichiometric	
170	Non-stoichiometric	
171	inactive	
172	inactive	
173	inactive	
174	Non-stoichiometric	
175	Non-stoichiometric	
176	inactive	
177	Non-stoichiometric	
178	inactive	
179	inactive	inactive
180	inactive	
181	Non-stoichiometric	
182	poor solubility	
183	767 μM	No saturation
184	inactive	

Compound	Experiment 1	Experiment 2
185	poor solubility	
186	inactive	
187	poor solubility	
188	697 μ M	110 μ M
189	inactive	
190	inactive	
191	Non-stoichiometric	
192	inactive	
193	inactive	
194	inactive	
195	inactive	
196	Non-stoichiometric	
197	Non-stoichiometric	
198	Non-stoichiometric	
199	inactive	
200	Poor solubility	
201	Poor solubility	
202	inactive	
203	inactive	
204	Non-stoichiometric	
205	inactive	
206	Non-stoichiometric	
207	inactive	
208	433 μ M poor shape	Non-stoichiometric
209	200 μ M	247 μ M
210	inactive	
211	inactive	
212	Poor sensorgrams	Poor sensorgrams
213	20 μ M	82 μ M poor solubility
214	inactive	
215	inactive	Inactive
216	Poor solubility	
217	Non-stoichiometric	Non-stoichiometric
218	Non-stoichiometric	
219	Non-stoichiometric	
220	Non-stoichiometric	
221	inactive	
222	inactive	

Table 3.7 – SPR testing of the Atomwise vHTS hits. Compounds are labelled ‘inactive’ when response units <10 RU or when K_D >1 mM.

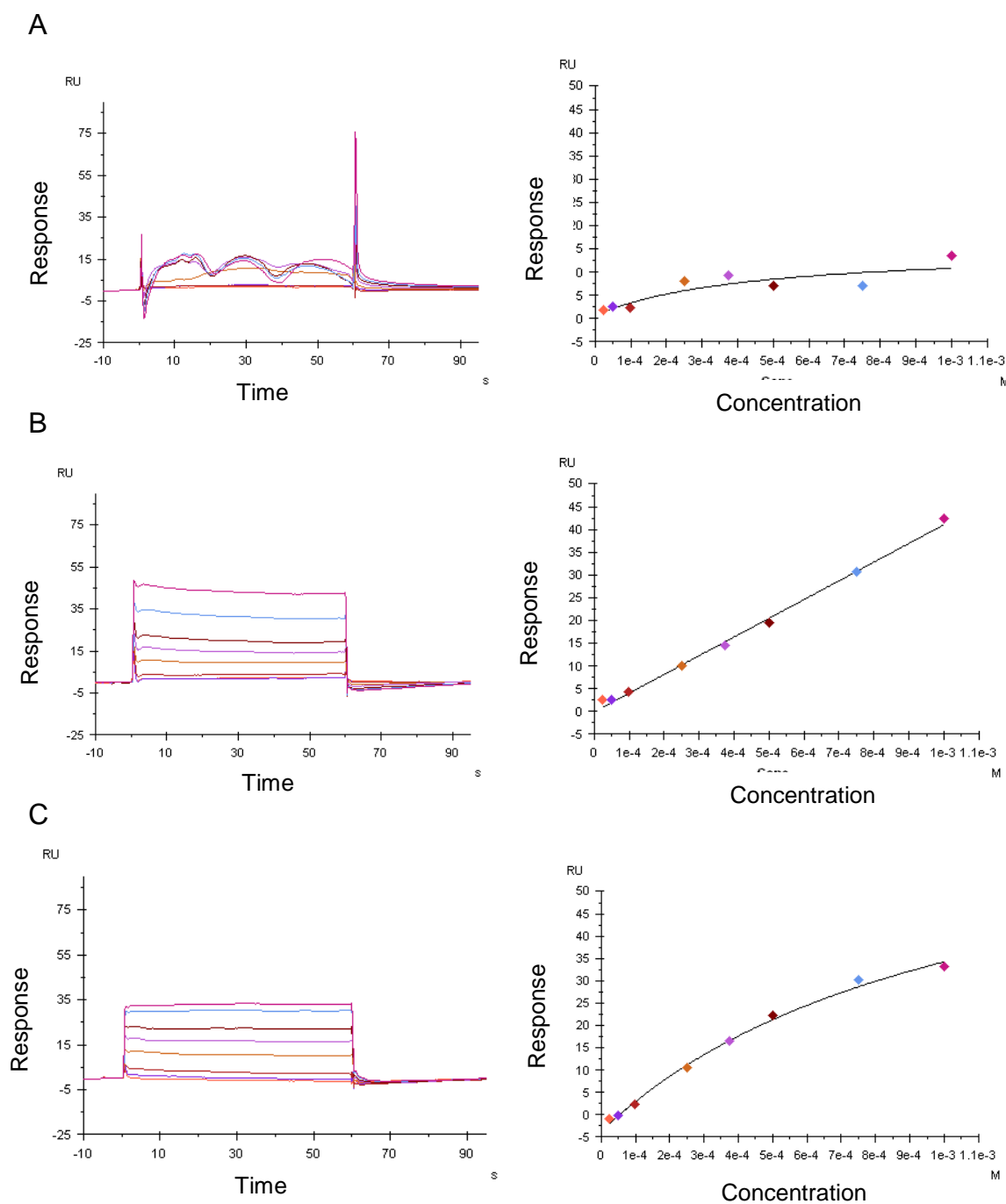


Figure 3.25 - Example sensorgrams and binding curves from SPR testing of the Atomwise vHTS hit compounds. (A) **205** showed poor quality sensorgrams. (B) **217** showed non-stoichiometric binding. (C) **173** was inactive with $K_D > 1\text{mM}$.

Compounds **154**, **188** and **209**, that were active in $n=2$ experiments were then repurchased for further analysis (Figure 3.26). Compound **213** was also active in both experiments but was currently unavailable from the supplier and it had potential issues with poor solubility. Compounds **154**, **188** and **209** were passed through a short column of silica and retested by SPR along with Batch 1 of these

compounds. **154** was consistently active across the different runs and batches. **209** was active in n=2 experiments and across both batches. These compounds were also active against the mutant HSC70 protein S275W indicating that the fragments bind outside of the ATP binding site.

Compound	Batch	Expt 1	Expt 2	Expt 3
154	Batch 1	490 μ M	202 μ M	283 μ M
154	Batch 2			87 μ M
188	Batch 1	697 μ M	110 μ M	208 μ M
188	Batch 2			No saturation
209	Batch 1	200 μ M	247 μ M	No saturation
209	Batch 2			352 μ M

Table 3.8 – SPR testing of Atomwise vHTS hits. Batch 1 of CCT221027, CCT376325 and CCT376346 has been tested in three independent experiments. Batch 2 of CCT221027, CCT376325 and CCT376346 has been repurchased and passed through silica before testing.

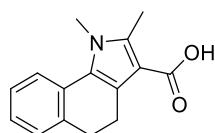
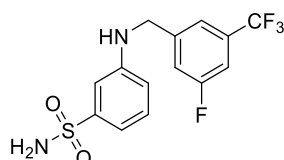
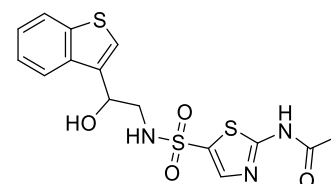
**154****188****209**

Figure 3.26 – Structures of compounds from the Atomwise vHTS that showed binding to HSC70-NBD by SPR.

3.7.2 Conclusions from the vHTS screens and future work

All three vHTS screens suggested compounds that showed binding to HSC70-NBD by SPR. Of the 24 compounds tested from the natural product library, three compounds with a chromenone structure showed binding in two separate experiments in the micromolar range (average 25 μM to 500 μM approximately). Of the 24 compounds tested from the Chembridge library five chemically diverse compounds showed binding responses in two separate experiments in the micromolar range (average 10 μM to 500 μM approximately). Of the 80 compounds from the Atomwise library three chemically diverse compounds tested active in two separate experiments in the micromolar range (average 200 μM to 400 μM approximately). These 11 compounds are of interest to confirm binding by orthogonal methods such as LO-NMR and X-ray crystallography.

Lipinski's rule of five evaluates drug likeness based on the observation that most orally administered drugs are relatively small and moderately lipophilic molecules. The rule of five predicts that poor absorption or permeability is more likely when there are more than 5 H-bond donors, 10 H-bond acceptors, the molecular weight is greater than 500, the TPSA is greater than 140\AA^2 and the cLogP is greater than 5.⁶⁴ Important calculated physicochemical properties of the 11 fragments found to bind to HSP70 are summarised in Table 5.10. With the exception of compound **102** the fragments are all within Lipinski's guidelines with a cLogP range from 1.5-3.7, no more than 5 H-bond donors, no more than 10 H-bond acceptors and the MW is below 500. Small compound size is an advantage because it allows growth to improve potency and other physicochemical properties within drug-like space. These fragments are therefore good starting points for further exploration.

Compound	MW	HBD	HBA	cLogP	TPSA	RB	LE
94	295	1	4	3.7	63	3	0.30
102	539	3	8	1.8	159	10	0.12
103	312	1	5	3.4	69	5	0.20
120	369	1	6	2.9	76	5	0.18
133	360	1	6	2.3	95	5	0.18
135	386	2	6	3.5	88	6	0.24
138	350	2	5	3.7	80	6	0.20
141	380	2	5	1.6	80	4	0.19
154	241	1	2	3.2	42	1	0.26
188	348	2	3	3.1	72	4	0.21
209	397	3	7	1.5	108	6	0.20

Table 5.10 – Properties of the hit compounds from the virtual high-throughput screens, calculated using MOKA.

The 11 fragments bind outside of the ATP binding site, as determined by SPR experiments with the mutant HSC70-NBD S275W. It's possible that these hit fragments bind to a secondary binding site that is not the site occupied by fragment **21**. X-ray crystallography would determine if these hits occupy the same site or a new secondary binding site in the NBD. LO-NMR methods would give confidence that the site is likely to be the same site if the fragments were shown to be ATP competitive like **21** and **58**.

Close analogues of hits that are confirmed by orthogonal methods could be purchased or synthesised for testing. It would be useful to overlay of the predicted or experimentally determined binding modes of fragment hits to determine a pharmacophore which would aid in the understanding of key binding interactions to improve the potency. Fragments with a sub micromolar potency would be suitable to test the effect of inhibition at this new site for its functional relevance, for example with a luciferase refolding assay.¹⁰²

Chapter 2 and 3 have described the identification and validation of a new secondary binding site in HSP70 by multiple orthogonal methods including SPR, WaterLOGSY, CPMG and X-ray crystallography. As discussed in Chapter 1 the development of potent HSP70 inhibitors with good drug-like properties has been hindered by the hydrophilicity and the flexibility of the ATP binding site as well as

its high affinity for ADP and ATP. An alternative approach is to target allosteric binding sites and to incorporate suitable drug-like properties while simultaneously improving potency with fragment-based drug discovery methods. The identification and characterisation of this new secondary binding site and the discovery of multiple fragment hits that bind by SPR may offer a new way to inhibit this important molecular chaperone.

Chapter 4

4 Exploration of the phosphate binding region of HSP70 using structure-based drug design

4.1 Structure-based drug design

Structure-based drug design (SBDD) uses the protein structure, which can be obtained by X-ray crystallography, NMR or homology modelling, for the basis of developing new drug candidates. Once the target for a lead compound has been identified and the structure with a bound ligand is solved, SBDD can be used to observe the binding interactions of a ligand to the protein and to identify modifications that could improve affinity.¹⁰³

SBDD begins with identifying a ligand binding site on the protein. By measuring the distance between the ligand and neighbouring atoms in the protein it is possible to identify important binding interactions between the ligand and the binding site. These interactions can then be optimised and new interactions can be made in regions of the pocket that are not currently occupied by the ligand. By identifying the key binding interactions, it's possible to determine which groups are essential and which groups could be deleted, modified or added so that the new design can occupy the pocket more optimally. The ligand can be removed computationally from the binding site and newly designed analogues can be inserted to assess how well they fit. The compound is then synthesized and tested for activity. If possible, the X-ray crystal structure for the new ligand can be solved to determine if the new ligand has bound as expected and to identify any new interactions, which helps with the subsequent round of design. The process therefore involves iterative cycles of design, synthesis and testing of compounds (Figure 4.1). Both positive and negative hypotheses should be made to challenge the model and any assumptions made. It's important to remember that the binding site may change shape in an unpredictable way to accommodate ligands that would not be expected to fit from the original model and ligands can unexpectedly change binding mode which confounds SAR interpretation.

Solving the X-ray crystal structures of multiple ligands can aid in identifying the pharmacophore. A pharmacophore has been defined by IUPAC as an ensemble of steric, electrostatic and hydrophobic properties which is essential for optimal supramolecular interactions with a biological receptor, to modulate or inhibit a biological effect.¹⁰⁴ A pharmacophore is an abstract concept, not a specific molecule, which describes the common molecular properties of the interaction with a receptor. Identifying a pharmacophore for a target binding site can be useful for the design of novel ligands with diverse chemical structures.

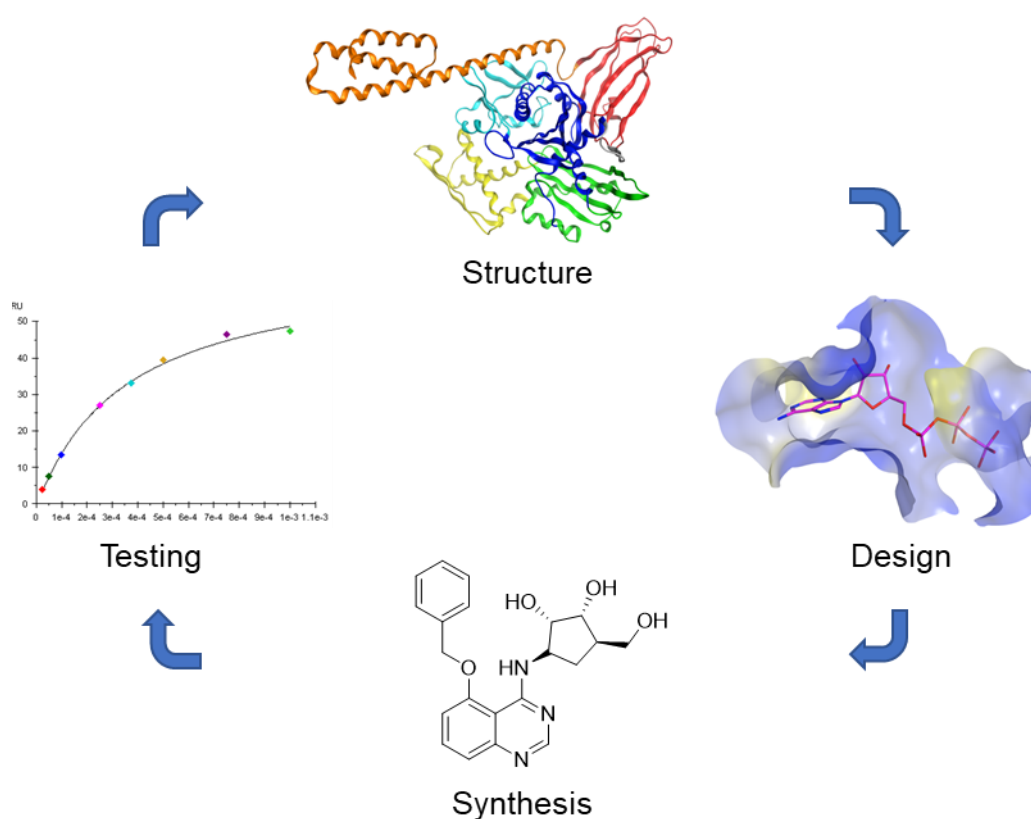


Figure 4.1 - SBDD allows identification of where the ligand is bound in the protein and the key binding interactions and distances between atoms of the ligand and the binding site. Regions that are not occupied by the ligand can be identified which can guide what modifications could be made to improve binding or physicochemical properties. These new designs are then synthesised and tested, which aids the next round of design until a molecule with the desired properties is developed.

4.2 Previous work on quinazoline ATP binding site inhibitors

The fragment screen³¹ discussed in Chapter 2 also identified a quinazoline fragment hit **9**, which binds in the active site of HSP70 (Figure 4.2 A). Removal of the 6-methyl gave a less potent but more ligand efficient fragment **223** which was then modified to improve potency.

In HSP70 the ribose group plays a very important role in nucleoside binding. Both ribose hydroxyls form an extensive network of hydrogen bonds with the protein and these interactions significantly contribute to affinity. 8-Amino adenosine is more than 250 times more potent than 8-amino adenine (8 μ M and 2100 μ M respectively)³¹. With this in mind, the authors noted that the adenine N-9 atom in ATP that provides the link to the ribose ring overlays with the exocyclic 4-amino group of the quinazoline hit **223** (Figure 4.2 B). Synthetic attempts to directly link a ribose ring from this position were unsuccessful but a ribose mimic, cyclopentylaminotriol **224**, could be attached instead. This change gave a seven-fold boost in potency. **10** has a similar affinity for HSP70 as adenosine but with a smaller number of polar atoms making it a more attractive starting point for elaboration. Further improvements in potency were gained by substitution at the 5-position with aromatic rings (**225** and **226**). These quinazoline compounds are the first reported ATP-competitive inhibitors of HSP70 that do not have an adenosine scaffold and so offer the opportunity to develop inhibitors with more drug-like properties.

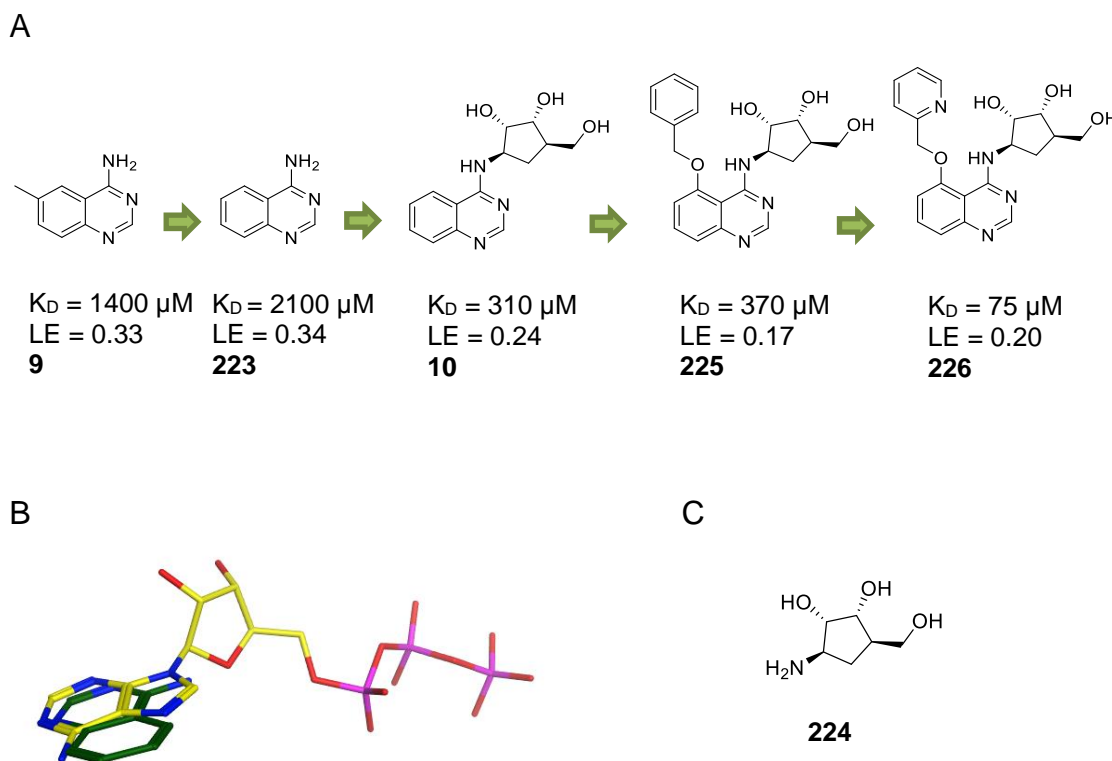


Figure 4.2 – (A) Fragment **9**, discovered from a fragment screen, was developed to improve potency by incorporating a ribose mimic and substitution at the 5 position. Fragment **226** improves the potency almost 20-fold but with a significant drop in ligand efficiency. (B) Overlay of fragment **223** (PDB ID: 5AQP; green) with ATP (PDB ID: 3FZF; yellow) inspired the addition of a ribose mimic to the exocyclic amine of **223**. (C) Cyclopenylaminotriol ribose mimic **224**.

There is currently no X-ray crystal structure of full-length human HSP72 or HSC70. Crystallography efforts were therefore focused on the NBD of these isoforms which has literature precedent.⁴⁹ As discussed in Chapter 1 the ATP binding site changes size and shape depending on whether ADP or ATP is the bound nucleotide. Data from the PDB sample a variety of different conformational states of HSP70. Structures in complex with a nucleotide exchange factor such as BAG1 represent the open conformation of HSP70 and those in the absence of a nucleotide exchange factor represent the closed conformation.³¹ Crystal structures of non-nucleotide inhibitors with HSC70 have only been solved in the presence of a nucleotide exchange factor BAG1 but HSP72 has been solved without a nucleotide exchange factor.

Multiple X-ray crystal structures were solved to assist with understanding the key binding interactions of the quinazoline inhibitors with HSP70. X-ray crystal structures obtained with the quinazoline scaffold have shown a similar binding mode confirming the stability of the scaffold and the suitability for building the fragment into an HSP70 inhibitor (PDB IDs: 5AQO, 5AQP, 5AQQ, 5AQR, 5AQT; 5AQU, 5AQV; ligands shown in Figure 4.3 A). In structural terms the carbocycle **224** does not completely mimic the ribose ring as R272 adopts an extended conformation in the adenosine bound structure but is found in the ‘up’ conformation in the **10** X-ray crystal structure (Figure 4.3 B). Y15 is also found in a different conformation.

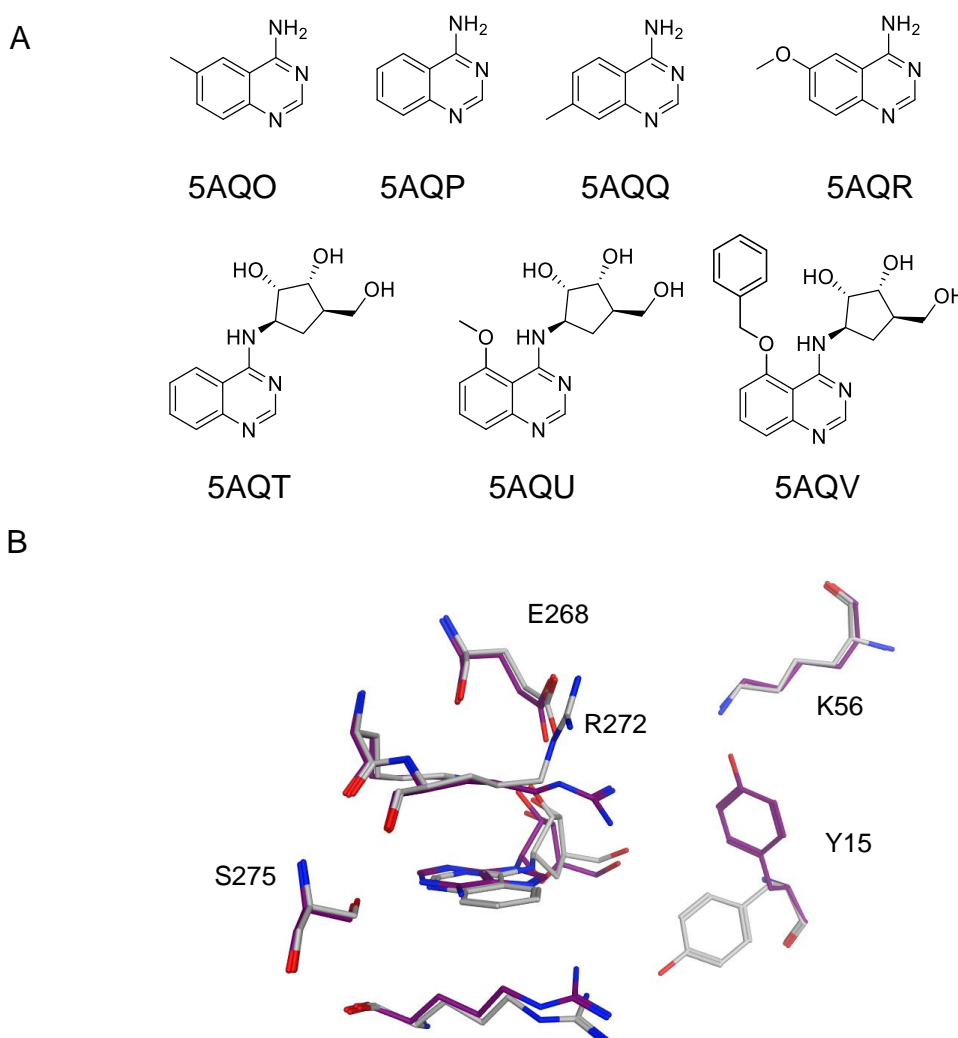


Figure 4.3 – Ligands with solved X-ray crystal structures bound to HSC70-NBD/BAG1 PDB ID: 5AQO, 5AQP, 5AQQ, 5AQR, 5AQT, 5AQU, 5AQV. (B) Overlay of X-ray crystal structures of HSC70-NBD/BAG1 with adenosine (PDB ID 5AQF; purple) and **10** (PDB ID 5AQT; grey). R272 and Y15 have different conformations.

Compounds **10** and **225** were solved with both HSP72 and HSC70/BAG1 to identify key differences in the NBD conformational states in the absence of a nucleotide exchange factor. A comparison of **10** bound to HSC70/BAG1 and HSP72 reveals a shift of 2-3 Å, consistent with the differences in the NBD, while key hydrogen bonds are maintained between the carbocycle and the protein (Figure 4.4).³¹ The side chain R272 changed from 'up' in the HSC70/BAG1 to an extended conformation completing the hydrogen bond network between side chains E268, K56 and Y15 that stabilise the closed conformation. The structure of **10** bound to HSP72-NBD adopts a closed conformation nearly identical to that of ADP bound HSP72-NBD. A salt bridge between E268 and K56 forms when ADP is bound and stabilises the closed conformation.⁵¹

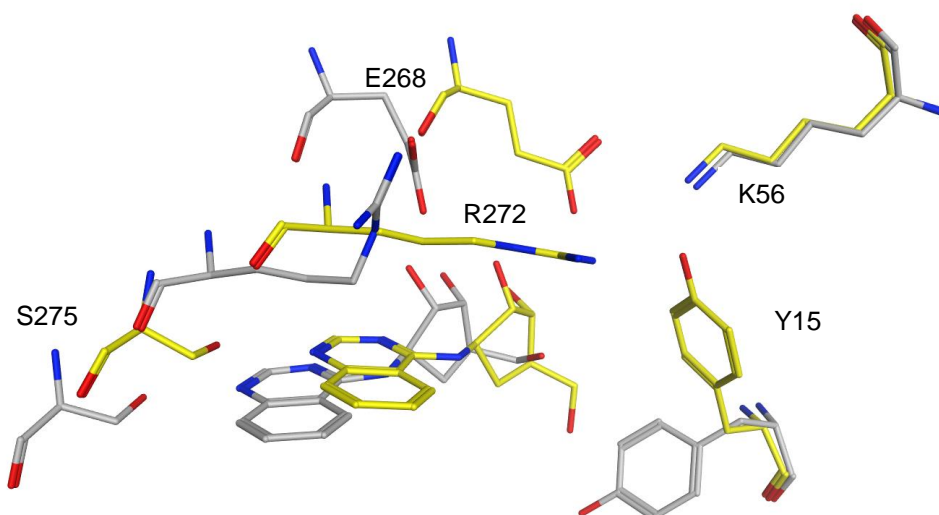


Figure 4.4 – X-ray crystal structures of **10** bound to HSC70-NBD (PDB ID 5AQT; grey) and HSP72-NBD (5AQW; yellow).

The structure of **225** bound to HSP72-NBD adopts an intermediate conformation between the open and closed NBD conformations (Figure 4.5). The ligand shifts as a result of the O-benzyl substituent forming an edge face stacking interaction with Y15 preventing closure of the NBD. R272 also adopts an 'up' conformation similar to the HSC70/BAG1 structure, because an extended conformation would clash with the benzyl group. E268 maintains its salt bridge interaction with R272 but in a conformation that is incompatible with forming a salt bridge with K56.

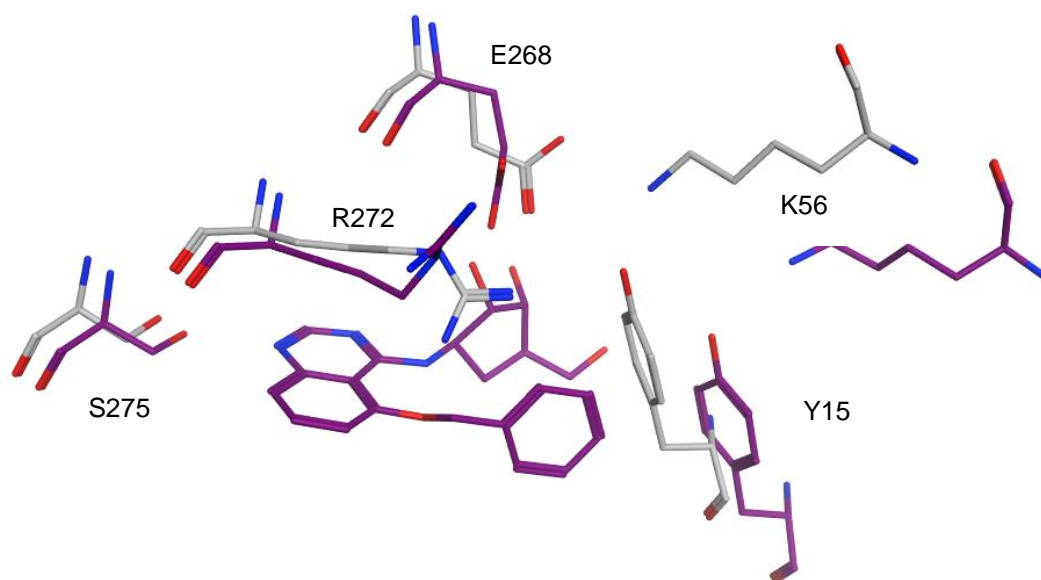
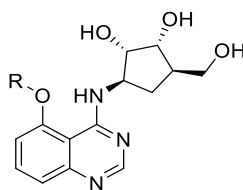


Figure 4.5 – X-ray crystal structure of ADP bound to HSP72-NBD (Grey; PDB ID 3ATU) shows a salt bridge between residues E268 and K56. X-ray crystal structure of **225** bound to HSP72-NBD (Purple; PDB ID 5AQV). The salt bridge between E268 and K56 is no longer present and the binding site is in a more open conformation.

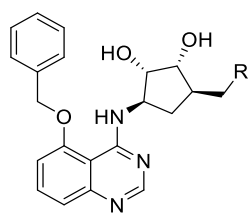
Building on this published work, PhD student Stuart Rankin designed and synthesised a variety of alkyl substituents in the 5 position.¹⁰⁵ Ten analogues of **225** were synthesised which gave ligand efficiencies between 0.18-0.20 (Table 4.1). This exploration at the 5-position did not identify further gains in potency but it did show that many different groups are tolerated here.



	R	SPR K _D	LE		R	SPR K _D	LE
227		1040	0.19	318		290	0.19
228		894	0.18	319		194	0.19
229		335	0.20	320		230	0.18
230		250	0.20	321		172	0.19
231		1450	0.18	322		280	0.19

Table 4.1 - Previous work which modified the substituents at the 5-position of the quinazolinone ring showed that a variety of alkyl substituents are tolerated.¹⁰⁵ SPR K_D is given in μM .

Although the 2-pyridylmethyl analogue **226** showed approximately 4-fold greater binding affinity for HSC70 than the benzyl analogue **225** in the SPR assay, Stuart's work focused on the benzyl analogue because the X-ray crystal structure of **225** bound within the ATP binding site had been solved and it had more tractable physicochemical properties. **226** had poor solubility and although X-ray crystallography was attempted the structure was not solved. Exchanging the primary alcohol **225** for a primary amine **232** or methyl ester **233** resulted in a loss of potency in contrast to the amide **234** which maintained potency. Introduction of a hydroxyacetamide motif in **235** improved the potency three-fold (Table 4.2). This hydroxyacetamide motif, with two hydrogen bond acceptors and a hydrogen bond donor, could potentially be interacting in the phosphate binding region of the ATP binding site, an area yet to be explored by inhibitors. This increase in potency was of interest to understand further.

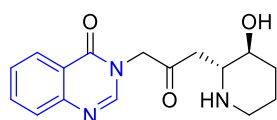


	R	SPR K _D	L.E.
225	OH	290	0.17
232	NH ₂	1200	0.14
233		3000	0.11
234		400	0.15
235		90	0.17

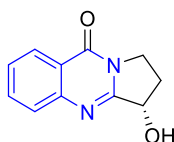
Table 4.2 - Previous work which modified the ribose mimic of **225**. A three-fold increase in potency was achieved with the hydroxyacetamide **235**.¹⁰⁵ SPR K_D is given in μM .

4.3 Quinazolines in medicinal chemistry

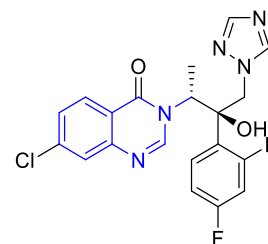
Quinazolines are fused heterocyclic compounds which have generated significant interest because of their medicinal uses including diuretic, hypotensive, anti-cancer, anti-inflammatory, anti-convulsant, anti-allergy, anti-microbial, anti-depressant and anti-hypertensive activity.¹⁰⁶ They are found in almost 200 known natural alkaloids and are a common motif in many clinical candidates and drugs (Figure 4.6).



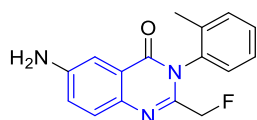
Anti-malarial
Febrifugine



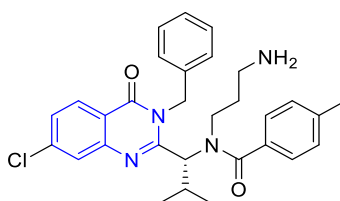
Anti-anaphylactic
Vasiceinone



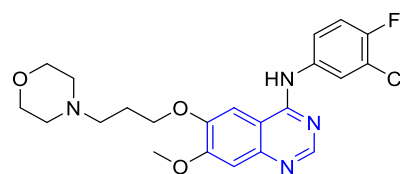
Anti-fungal
Albaconazole



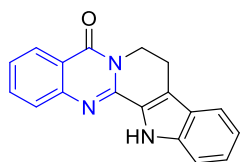
Sedative
Afloqualone



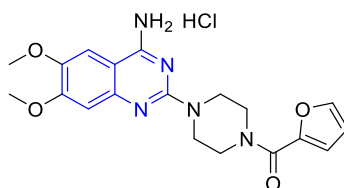
Anti-neoplastic
Ispinesib



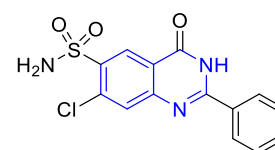
Anti-cancer
Gefitinib



Anti-Inflammatory
Rutaecarpine



Anti-hypertensive
Prazosin chlorohydrate



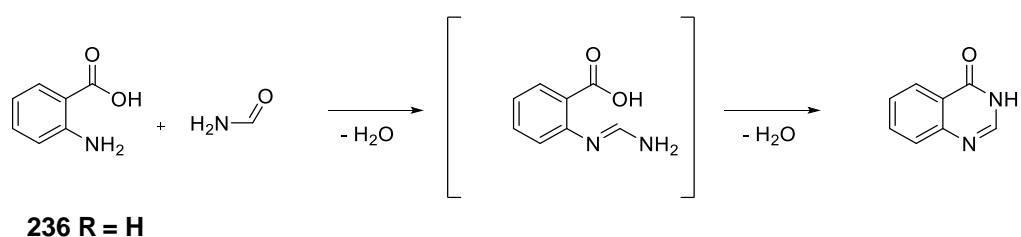
Diuretic
Fenquizone

Figure 4.6 – Quinazolines are a common scaffold in medicinal chemistry and are present in a wide variety of drugs.

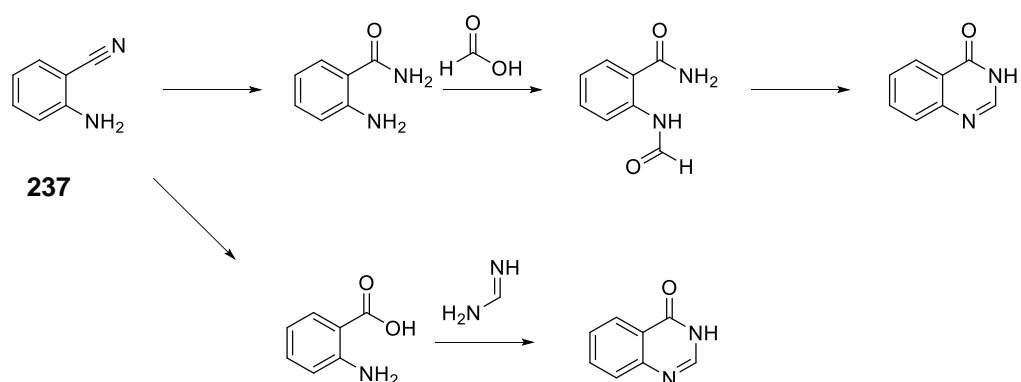
4.4 Quinazolinone synthesis

Given the interest and extensive use of quinazolines in medicinal chemistry it is not surprising that there are many well established methods to synthesise this scaffold. Although there are many synthetic routes only those that do not require the 2-position to be substituted are discussed here as this was a known requirement when the project was started. The Niementowski reaction is the

oldest and most popular method for 4-(3H)-quinazolinone synthesis starting with anthranilic acid **236** (Scheme 4.1).¹⁰⁷ Under the original forcing conditions of high temperatures and long reaction times, the yield has been reported to be variable and complex mixtures can be difficult to separate. Microwave irradiation has been much more successful with better yields and cleaner reactions.¹⁰⁸ Alternative versions of the Niementowski synthesis starting from 2-aminobenzonitrile **237** are shown in Scheme 4.2.



Scheme 4.1 - Niementowski conditions 130°C – 150°C, 6 h average. MW 150°C 20 min average.



Scheme 4.2 - Alternative versions of the Niementowski synthesis.

4.5 Targeting the phosphate binding region

The phosphate group is critical for recognition and binding to phosphatases, enzymes that reverse the action of kinases by removing a phosphate group. In order to target phosphatases, there has therefore been significant interest in

groups that can mimic a phosphate group, known as phosphate isosteres. The challenge in this situation where much of the binding affinity is derived from the phosphate interaction is to make the key interactions of the phosphate group while maintaining membrane permeability. At physiological pH, phosphate groups are always charged and therefore not desirable to incorporate directly into an inhibitor which needs to be cell permeable. These molecules would also be potentially unstable because they could be recognised by phosphatases inside the cell. Prodrugs of phosphates and phosphonates have been designed to mask the negative charge of these groups to allow cell permeability, however, each prodrug must be optimized individually as some masking groups can be more or less readily removed from different types of drugs.¹⁰⁹ Replacing the phosphates when they drive so much of the affinity has been a critical challenge in medicinal chemistry. It is acknowledged that a phosphate group is one of the most difficult groups to mimic when designing biologically active compounds and there is no universal strategy to replace them.¹¹⁰ Phosphate isosteres have recently been reviewed extensively by Elliot *et al.*¹¹¹

Phosphate binding sites are often characterised by flexible glycine rich loops that bind to the phosphates via interactions with the backbone amide NH groups. HSP70 has a flexible glycine rich loop that binds to the phosphates via the amide backbone. It is similar to phosphatases in that much of the binding affinity is derived from the protein phosphate interaction. The phosphates of ADP and ATP play a critical role in the binding of these nucleotides to HSP70. The potency of adenosine, ADP and ATP measured against HSC70-NBD by Jones *et al.*³¹ is shown in Table 4.3. A 500-fold increase in potency was observed for ATP in comparison to adenosine. There are no non-nucleotide inhibitors of HSP70 that have been found to bind in this region of the ATP binding site of HSP70. As mentioned in Section 4.2 the hydroxyacetamide motif of compound **235** could potentially be interacting in the phosphate binding region of HSP70.

Compound	K _D HSC70-NBD	LE
Adenosine	165	0.28
ADP	0.71	0.31
ATP	0.33	0.29

Table 4.3 – The phosphate groups of ADP and ATP significantly improve the potency over adenosine against HSC70-NBD.³¹ SPR K_D is given in μM.

4.6 Design of hydroxyacetamide analogues

As there are no known inhibitors of HSP70 that have been found to bind in the phosphate binding region it was unknown what effect phosphate mimics could have on the binding affinity. Based on the SPR result of **235**, hydroxyacetamide analogues (Figure 4.7) were designed in order to answer three key questions:

- 1) Does the hydroxyacetamide improve potency while maintaining ligand efficiency for other 5-substituted analogues?
- 2) Does the hydroxyacetamide bind in the phosphate binding region?
- 3) Can we improve the potency further by adding substituents at the α hydroxyacetamide position?

Compounds **238**, **239**, **240** and **241** are matched pairs of **10**, **227**, **229** and **226** respectively and were designed to potentially explore the phosphate binding region with the hydroxyacetamide motif. The substituents at the 5-position were chosen to represent groups of different size and ligand efficiency (0.19 - 0.24).

An additional reason for the synthesis of **241** was to attempt to understand the observed difference in potency between **225** and **226** where the pyridine ring improves the potency five-fold over benzyl substituent. Attempts to identify this new interaction or conformation by X-ray crystallography were unsuccessful. Compound **241** may have better properties for X-ray crystallography to answer the question of whether a new interaction is formed and if so could this interaction be further optimised.

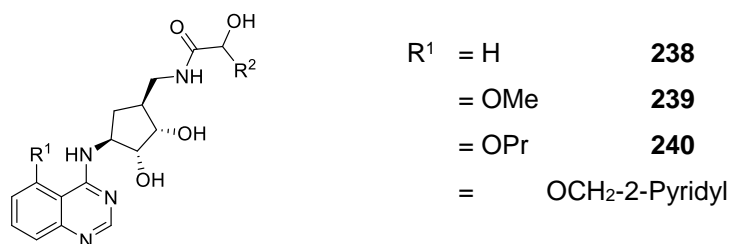
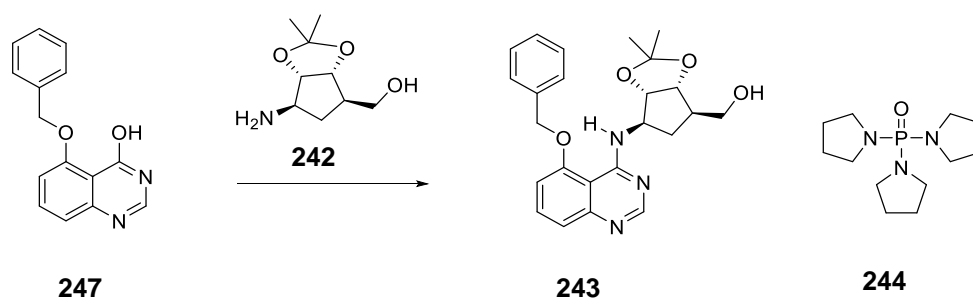


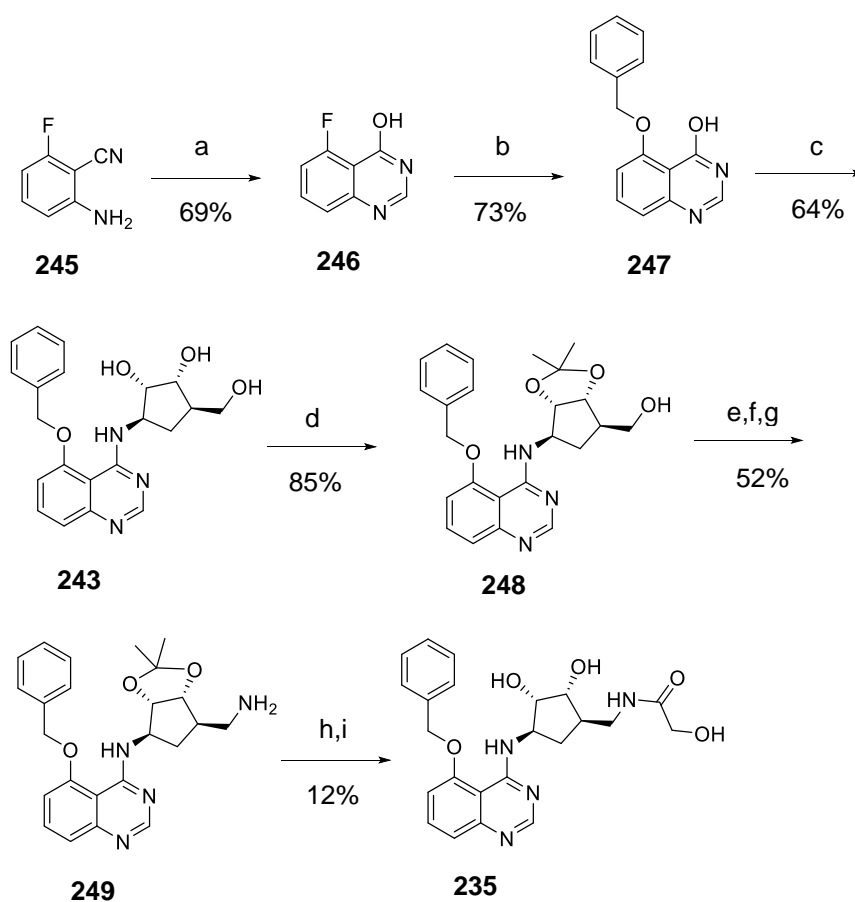
Figure 4.7 - Analogues of **235** were designed to gain a better understanding of the ATP binding site. Once the most ligand efficient R¹ position was determined, exploration at the α position of the hydroxyacetamide (R² substituents) was planned.

4.6.1 Previous work on quinazoline synthesis

Previous work by Stuart Rankin had developed a synthetic route to **235** from the commercially available ribose mimic **224**.¹⁰⁵ This required the addition of substituents to the primary alcohol of the ribose mimic **224** selectively over the two secondary alcohols, which can be achieved with an acetonide protecting group (Scheme 4.3, **242**). It is preferable to couple the acetonide protected ribose mimic to the quinazoline in order to minimise the number of sequential steps. Significant product **243** was formed with the coupling reagent PyBOP but it could not be separated from the HMPA side product **244** in reasonable yields. Other coupling reagents were investigated including HATU, BOPCl and DEPBT but no significant product was observed with these conditions. Therefore, the coupling reaction was carried out with the unprotected ribose mimic. The final route to **235** is shown in Scheme 4.4. This route consists of the following nine steps from **245**: formation of the quinazoline ring **246**, S_NAr at the 5-position **247**, PyBOP coupling of the ribose mimic **243**, diol protection **248**, transformation of the primary alcohol to the primary amine by mesylation, azide displacement and Staudinger reduction **249**, amide bond formation and diol deprotection which gave the desired product **235** in 1.7% overall yield.



Scheme 4.3 – Due to difficulty in separating the phosphoramidite side product **244** from the desired product **243** the protecting group was instead added after the ribose mimic was attached to the quinazolinone (Scheme 4.4).



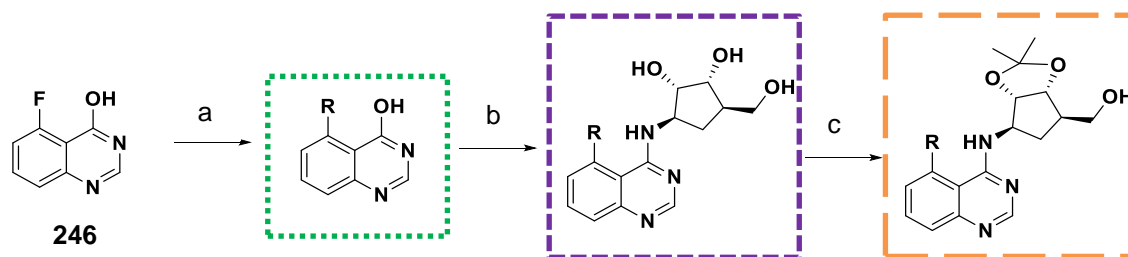
Scheme 4.4 – The previously developed route to **235** was carried out in 9 steps. (a) HCOOH, H₂SO₄, reflux (b) BnOH, NaH, DMSO, 90 °C (c) PyBOP, DBU, MeCN. (d) 2,2-dimethoxypropane, PTSA, MeOH (e) MsCl, NEt₃ CH₂Cl₂ (f) NaN₃, DMF, 0 → 60 °C (g) PPh₃, NH₂OH, THF, 60 °C (h) ethyl glycolate, NEt₃, CHCl₃, 60 °C (i) 1 M HCl, MeCN.

4.6.2 Synthesis of hydroxyacetamides

A modified version of this route was designed to synthesise the desired four hydroxyacetamide analogues **238-241** starting from the commercially available 5-fluoroquinazolin-4-ol (Scheme 4.5). The first S_NAR step was initially attempted with sodium methoxide but after 18 hours no desired product **250** was formed. By changing the reagents to sodium hydride and methanol this reaction proceeded in good yields and these conditions were used for the remaining two alcohols **251** and **252**.

PyBOP coupling was used to install the ribose mimic **224**. These reaction conditions gave good conversion to the desired products **10**, **227**, **229** and **226** by LC-MS but the introduction of three alcohol groups make the products highly polar and difficult to purify. Scale up of this step resulted initially in low yields because low solubility gave poor separation by column chromatography. Isolation by precipitation improved the yields.

The third step required protection of the two secondary alcohols over the primary alcohol which was achieved with PTSA and 2,2-dimethoxypropane. No evidence of formation of the unwanted six membered ring with the primary alcohol was detected by LC-MS.



Reaction	R	Compound	Yield
a	OMe	250	63%
a	OPr	251	85%
a	OCH ₂ Pyridine	252	84%
b	H	10	59%
b	OMe	227	83%
b	OPr	229	73%
b	OCH ₂ Pyridine	226	53%
c	H	253	50%
c	OMe	254	60%
c	OPr	255	67%
c	OCH ₂ Pyridine	256	65%

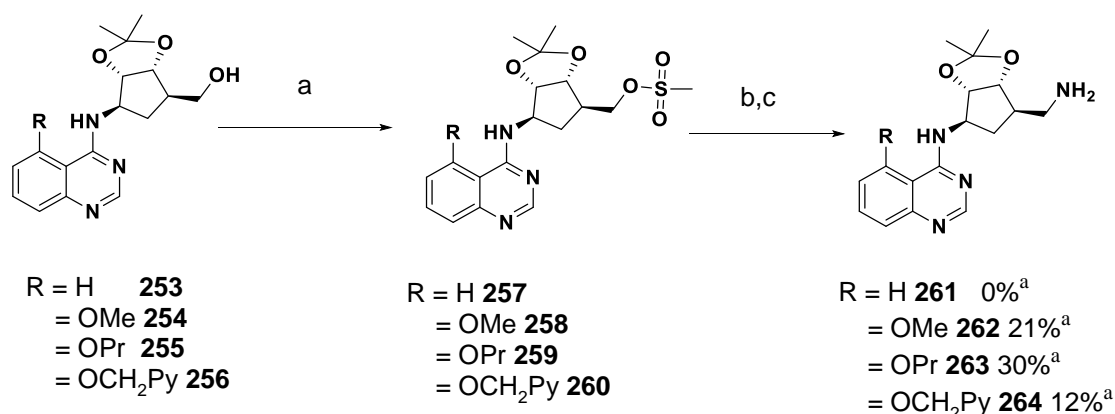
Scheme 4.5 - (a) ROH, NaH (60% in oil), DMSO, 50°C, 24 h (b) **224**, PyBOP, DBU, rt, 24 h (c) 2,2-dimethoxypropane, PTSA, DCM, rt, 2 h.

For the conversion of the hydroxyl group to a primary amine the three-step process was optimised into a two-step process (Scheme 4.6). Mesityl chloride was initially used with success for the methoxy **254** and propoxy **255** analogues but for **256** a chloro by-product **265** was observed which resulted in low overall yields (Scheme 4.7). To avoid this unwanted displacement, mesityl chloride was exchanged for mesityl anhydride which gave full conversion to the desired mesylate. An aqueous work-up was used to isolate the mesylated products **257-260** which were used directly for the next azide displacement step.

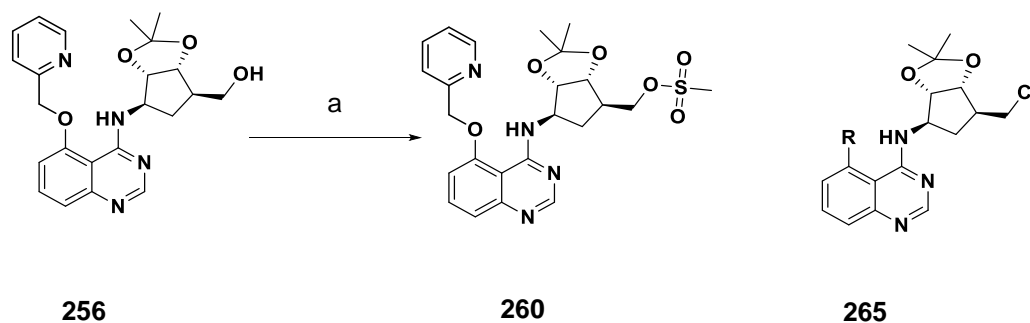
In all three reactions a small amount of an unidentified side product was formed during the azide formation step. Although the mass ion in each case varied it was consistently the mass of the expected product less 43. When the 5-

substituent was methoxy, propoxy or OCH₂pyridyl (**258-260**) this side product was minimal (<20%), however, without substitution at the 5 position this became the major product of the reaction with no desired product isolated for **261**. The identification of this side product and the development of a new synthetic route to overcome this issue is discussed in sections 4.6.3 and 4.6.4.

It was found that once the desired azide was observed by LC-MS, triphenylphosphine could be added directly to the reaction mixture for the Staudinger reduction to form the desired products **262-264**. The products were difficult to isolate cleanly by normal phase conditions. Concerns that the acidic conditions of the reverse phase column chromatography would remove the acid labile protecting group, however, were unfounded. Reverse phase column chromatography gave the desired pure products **262-264**.

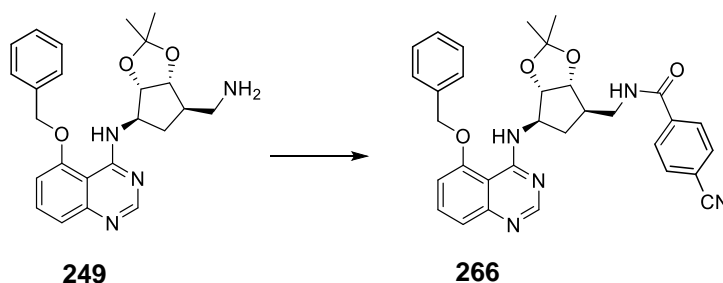


Scheme 4.6 - (a) MsCl or mesyl anhydride TEA, DCM 0 °C -> rt 2.5 h (b) NaN₃ DMF, 0 °C -> 60 °C, 18 h (c) PPh₃, NH₄OH, THF, 60 °C, 3 h. ^a yield over steps a-c.

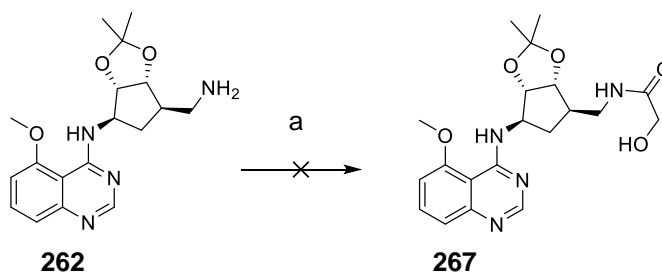


Scheme 4.7 - A side product **265** formed when **256** was treated with mesyl chloride resulting in a lower yield. This problem can be avoided by using mesyl anhydride. (a) MsCl, TEA, DCM 0 °C -> rt 2.5 h.

Multiple strategies were investigated to form the hydroxyacetamide for the penultimate step. There was precedent for the amide coupling with a similar starting material **249** with HATU to form **266** (Scheme 4.8). The amide coupling was attempted with glycolic acid but analysis by LC-MS after 18 hours showed predominantly starting material and no desired product mass ion was observed, suggesting glycolic acid may be the problem for this reaction (Scheme 4.9).

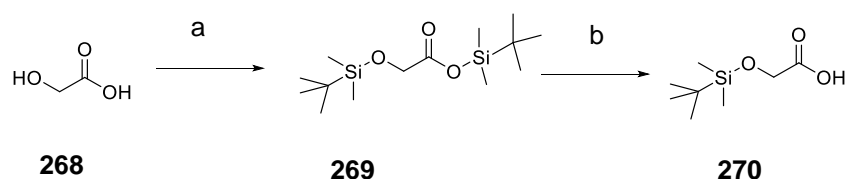


Scheme 4.8 - Precedent for amide coupling with **249**, a similar amine intermediate to **262**. (a) 4-cyanobenzoic acid, HATU, NEt₃, rt, 18 h.



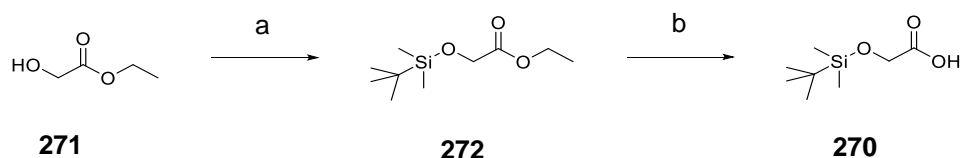
Scheme 4.9 - (a) Glycolic acid, HATU, NEt₃, rt, 18 h.

The amide coupling was therefore investigated with a protected glycolic acid. Synthesis of a protected glycolic acid was first attempted with a silicon protecting group, TBS (Scheme 4.10). Treatment of glycolic acid with TBS-Cl resulted in the expected protection of both the alcohol and carboxylic acid which was isolated by an aqueous workup. However, the selective deprotection of the carboxylic acid with potassium carbonate gave a mixture of products. After column chromatography the desired product was only 50% pure by NMR.



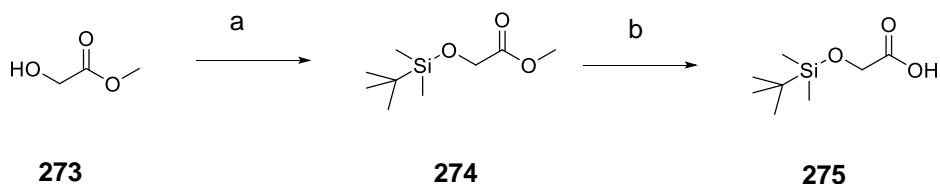
Scheme 4.10 - (a) TBS-Cl Imidazole, DMF, 0 °C → rt, 18 h. (b) K₂CO₃ H₂O, MeOH, THF, 1 h.

Synthesis of the silicon protected glycolic acid was then attempted with ethyl glycolate **271** a following literature procedure¹¹². Treatment with TBS-OTf gave the desired silicon protected ethyl ester **272** (Scheme 4.11). Ester hydrolysis with potassium hydroxide gave impure product after column chromatography.



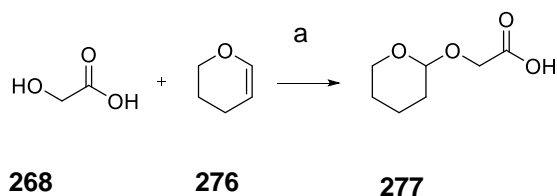
Scheme 4.11 - (a) TBS-OTf NEt₃ DCM, rt, 18 h. (b) KOH, EtOH, rt, 18 h.

The reaction was repeated with the methyl ester **273** to form the desired silicon protected methyl ester intermediate **274** (Scheme 4.12). The methyl ester was hydrolysed with lithium hydroxide. After an aqueous work-up and column chromatography **275** was impure by NMR.



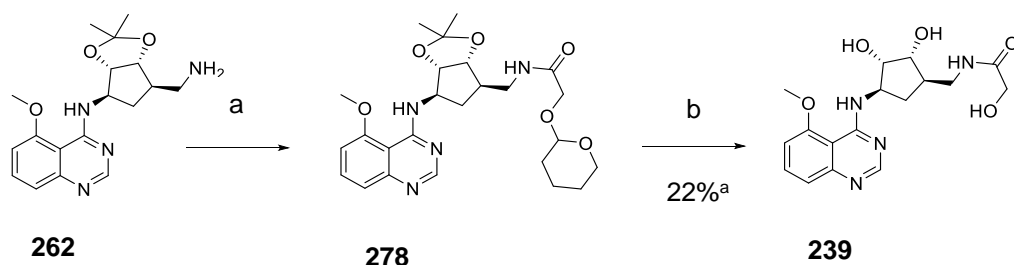
Scheme 4.12 - (a) TBS-OTf, NEt₃, DCM, rt, 18 h (b) LiOH, THF/H₂O, rt, 2 h.

To overcome the issues with the silicon protecting groups which formed multiple products that were difficult to purify, a tetrahydropyran (THP) protecting group was investigated as an alternative method of protection (Scheme 4.13). Glycolic acid **268** was treated with 3,4-dihydropyran **276** using similar conditions to a literature procedure¹¹³ to give the desired product **277** with a 25% yield, similar to that reported (24%). **277** was stored at 4 °C under nitrogen as it is reported to be unstable.



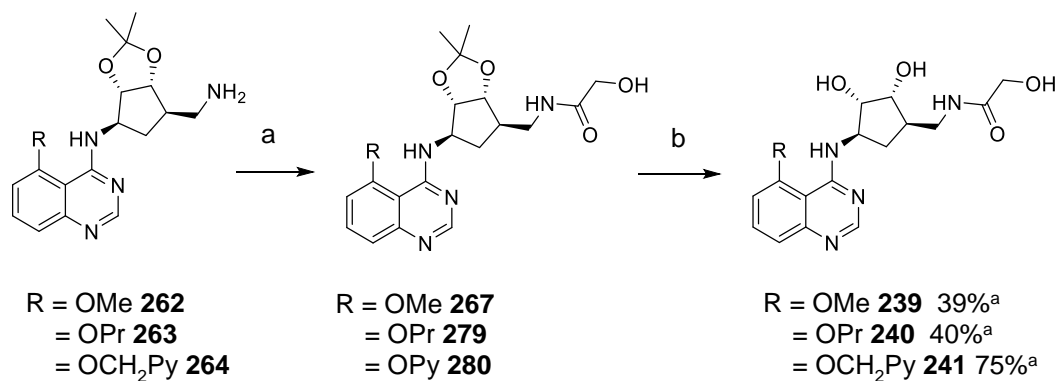
Scheme 4.13 – Protection of glycolic acid with THP (a) HCl, 80 °C, 1 h.

Amide coupling of **277** with the amine intermediate **262** gave the desired product **278** (Scheme 4.14). THP protection results in the formation of two diastereomers which makes the purity difficult to assess by NMR. Deprotection with hydrochloric acid was carried out to simplify the analysis. The desired product **239** was formed but co-eluted with TEA:HCl after column chromatography.



Scheme 4.14 (a) **277**, HATU, TEA MeCN rt 18 h. (b) 4 M HCl in dioxane, MeOH, rt, 3 h. ^a yield calculated over two steps.

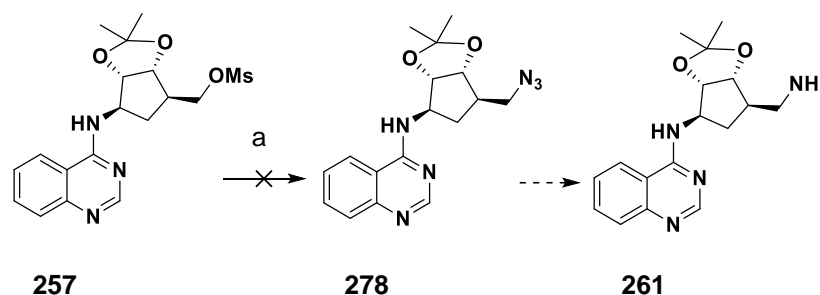
Although it is a very slow reaction, the desired compounds **239**, **240** and **241** were most successfully synthesised by refluxing in ethyl glycolate for 48 h, followed by acetal deprotection in HCl (Scheme 4.15).



Scheme 4.15 - (a) Ethyl glycolate, TEA, CHCl₃, 60 °C, 48 h (b) 4 M HCl in dioxane, MeCN, rt, 2 h. ^a yield calculated over two steps.

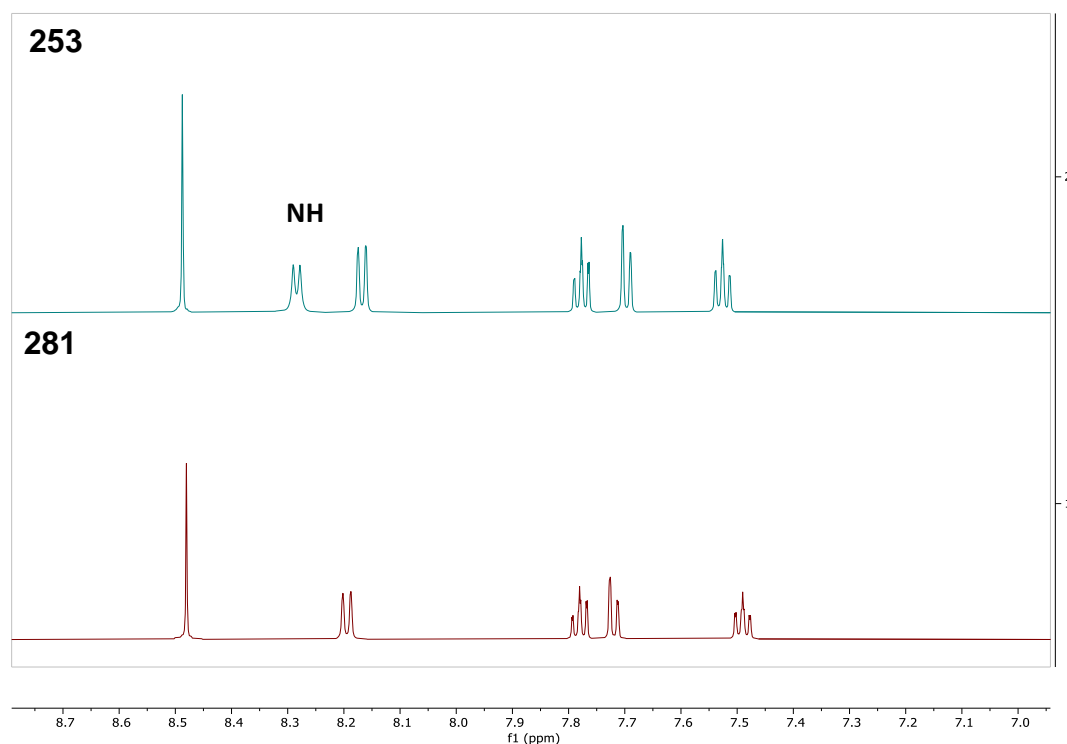
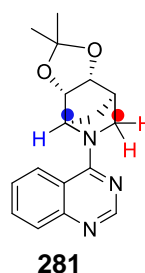
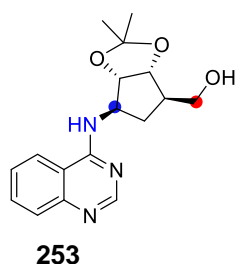
4.6.3 Determination of the major side product by NMR

For the transformation of **257** to **261** none of the desired azide **278** was formed and the major product of the reaction needed to be identified in order to reassess how to make this key intermediate (Scheme 4.16). The major product of this reaction **281** was isolated and characterised by LC-MS and NMR experiments including HSQC, HMBC, COSY, NOESY and DEPT to determine its structure (Figure 4.8).



Scheme 4.16 – (a) NaN₃ DMF, 0°C -> 60°C, 18 h.

In the $^1\text{H-NMR}$ of the starting material **253** the NH is clearly identifiable as a doublet and would be expected also in the desired product but in the $^1\text{H-NMR}$ spectrum of **281** this NH is no longer present. The protons corresponding to the quinazoline ring remain the same for both the starting material and the product. In the aliphatic region a triplet is identifiable as the primary alcohol in the starting material which is not present in the product. The CH_2OH is the most altered signal and is now split into two signals. The CH next to the amine, highlighted with a blue dot, has also moved more downfield in **281**. In the HMBC we can see a clear signal from the carbon in red to the CH in blue (circled), confirming the cyclisation. The mass of **281** observed by LC-MS is 298, consistent with the NMR determined structure.



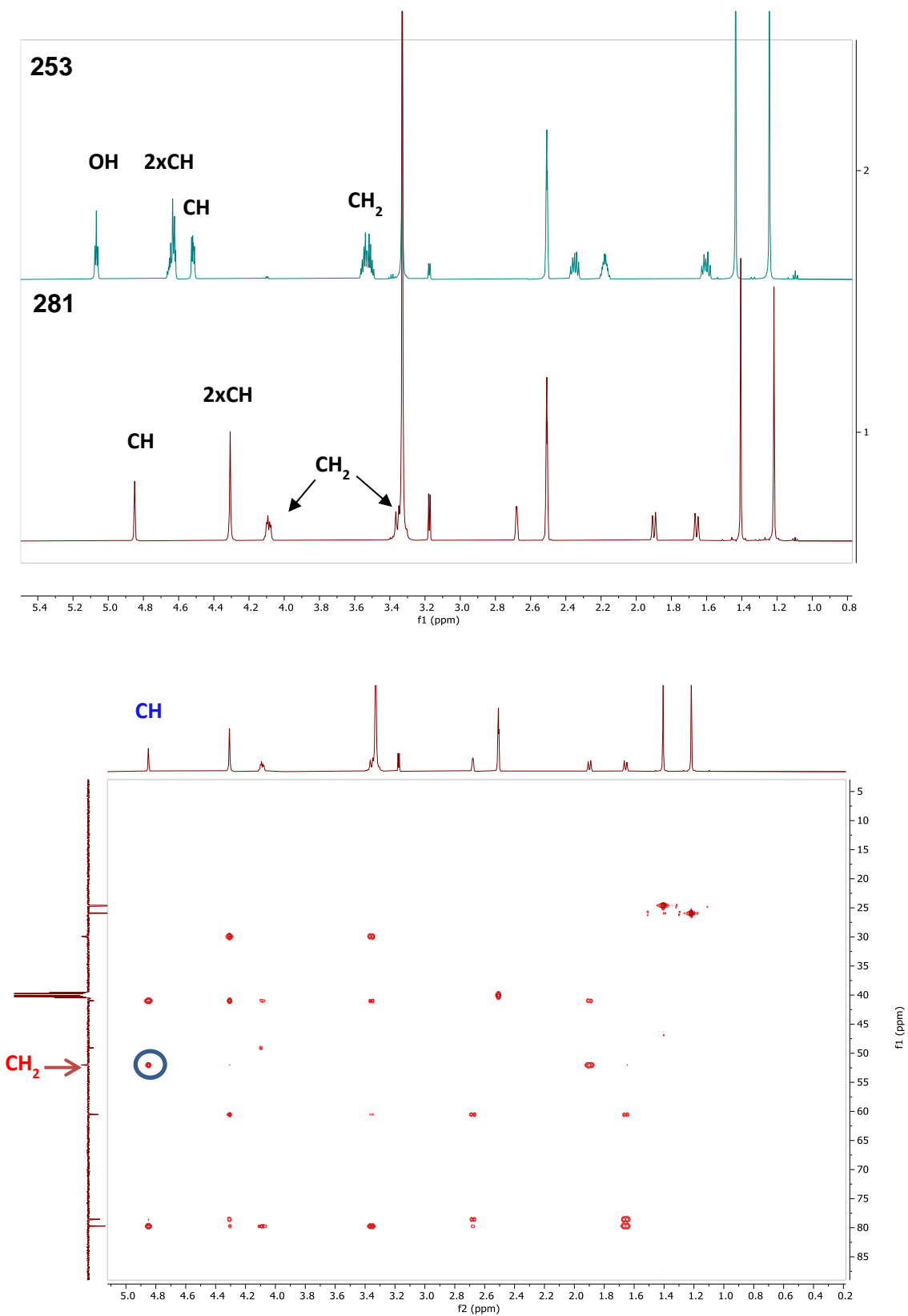
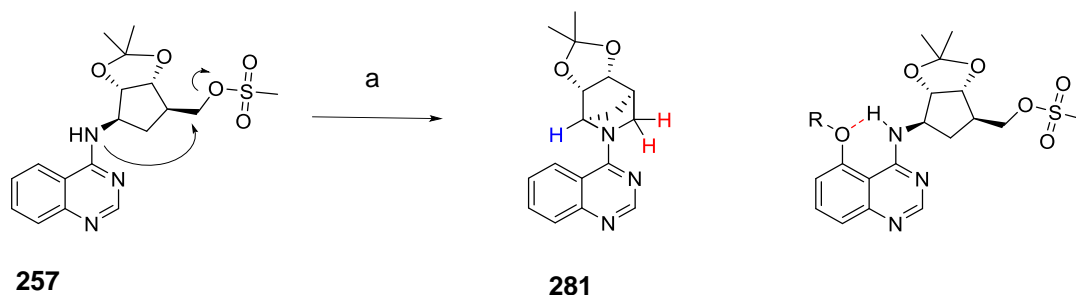


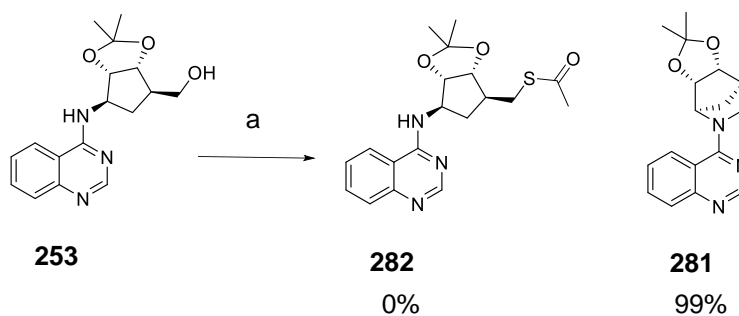
Figure 4.8 – NMR analysis identified the structure of 281.

From this analysis the major product of the reaction has formed a bicycle via intramolecular displacement of the mesylate (Scheme 4.17). This unexpected cyclisation reaction was found to occur to a much lesser extent when the 5 position was substituted with a hydrogen bond acceptor in compounds **258-260** likely due to the effect of hydrogen bonding.



Scheme 4.17 – Internal displacement of the mesylate happens faster than the desired azide formation. This undesired reaction occurs to a much lesser extent if there is a hydrogen bond acceptor in the 5 position (a) NaN_3 DMF, $0\text{ }^\circ\text{C} \rightarrow 60\text{ }^\circ\text{C}$, 18 h.

A paper has since been published by Gill *et al.* which describes the formation of this unexpected product **281** under Mitsunobu conditions instead of the expected product **282** (Scheme 4.18).¹¹⁴ To investigate whether steric compression caused by the acetal protected diol of **253** was the cause or enhanced the rate of cyclisation of **253** to **281**, the authors synthesised two control compounds **283** and **284** without the dihydroxy sugar motif (Figure 4.9). Under Mitsunobu conditions the side product **281** did not form with **283** and **284** which suggested that steric compression from the protected diol played a significant factor in the high yielding formation of **281**.



Scheme 4.18 – Unexpected cyclisation of **253** to **281** has been found to occur under Mitsunobu conditions.¹¹⁴ (a) Thioacetic acid, PPh₃, DTBAD, THF, 0 °C.

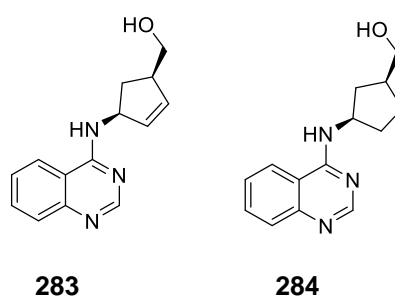
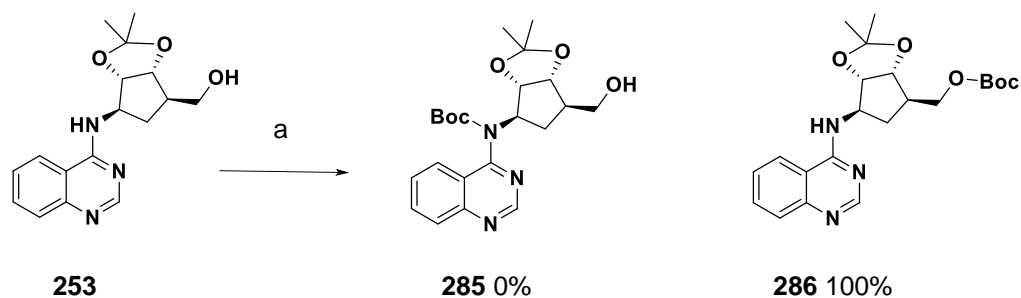


Figure 4.9 – Compounds without the dihydroxy sugar motif synthesised by Gill *et al*¹¹⁴ did not cyclise under Mitsunobu conditions suggesting the protected diol played a significant factor in the high yielding formation of **281**.

4.6.4 Design of an alternative route to hydroxyacetamide **238**

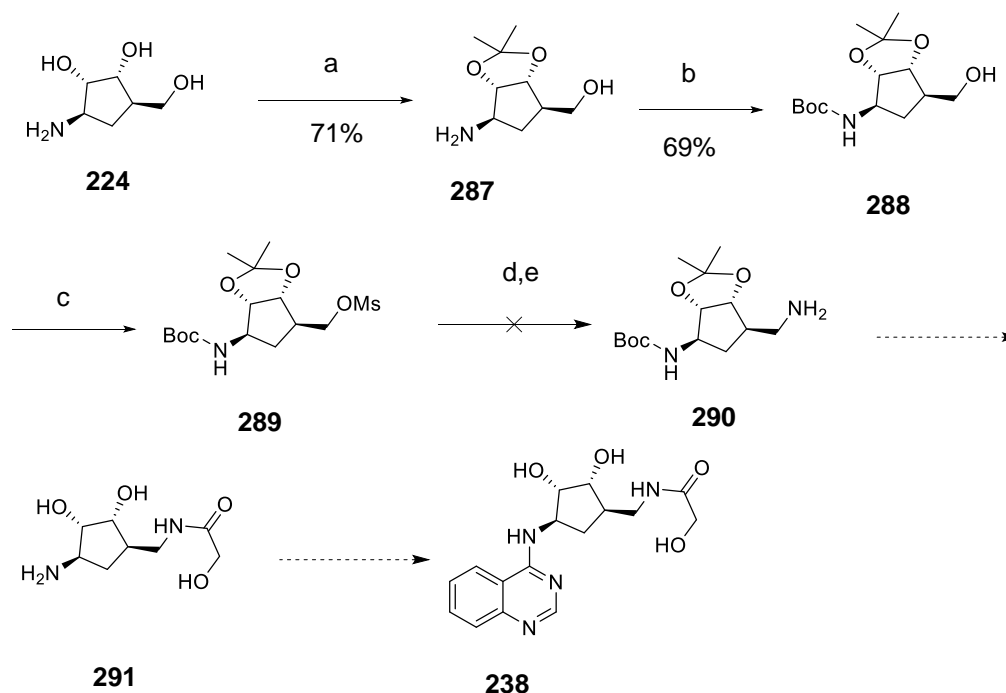
To avoid the intramolecular displacement of the mesylate, Boc protection of **253** was attempted (Scheme 4.19). However, treatment with Boc anhydride gave only the protected alcohol, highlighting that this nitrogen is not very nucleophilic but the specific conformation of this ring encourages cyclisation.



Scheme 4.19 – Attempts to protect the 4-amino group to prevent the unwanted cyclisation to side product **281** resulted in **286** (Boc protection of the alcohol) not **285** (Boc protection of the amine). (a) Boc_2O , DMAP, DCM, rt, 4 h.

A new route was designed to incorporate the quinazoline ring at the last step which would avoid the possibility of unwanted cyclisation (Scheme 4.20). This route was designed to protect the amine of **224** before converting the primary alcohol **287** to the primary amine **290** via mesylation, azide displacement and Staudinger reduction. The three remaining steps to form the desired product **238** would be amide coupling, acid deprotection and attachment of the quinazoline ring with PyBOP using conditions similar to the original route.

The first protection steps of the secondary alcohols and the primary amine worked well on gram scales (Scheme 4.20). During the azide formation step, however, the Boc protecting group did not survive the conditions employed and no desired product was formed. It is possible that using lower temperatures or a different amine protecting group such as phthalimide would overcome this issue although this was not investigated.

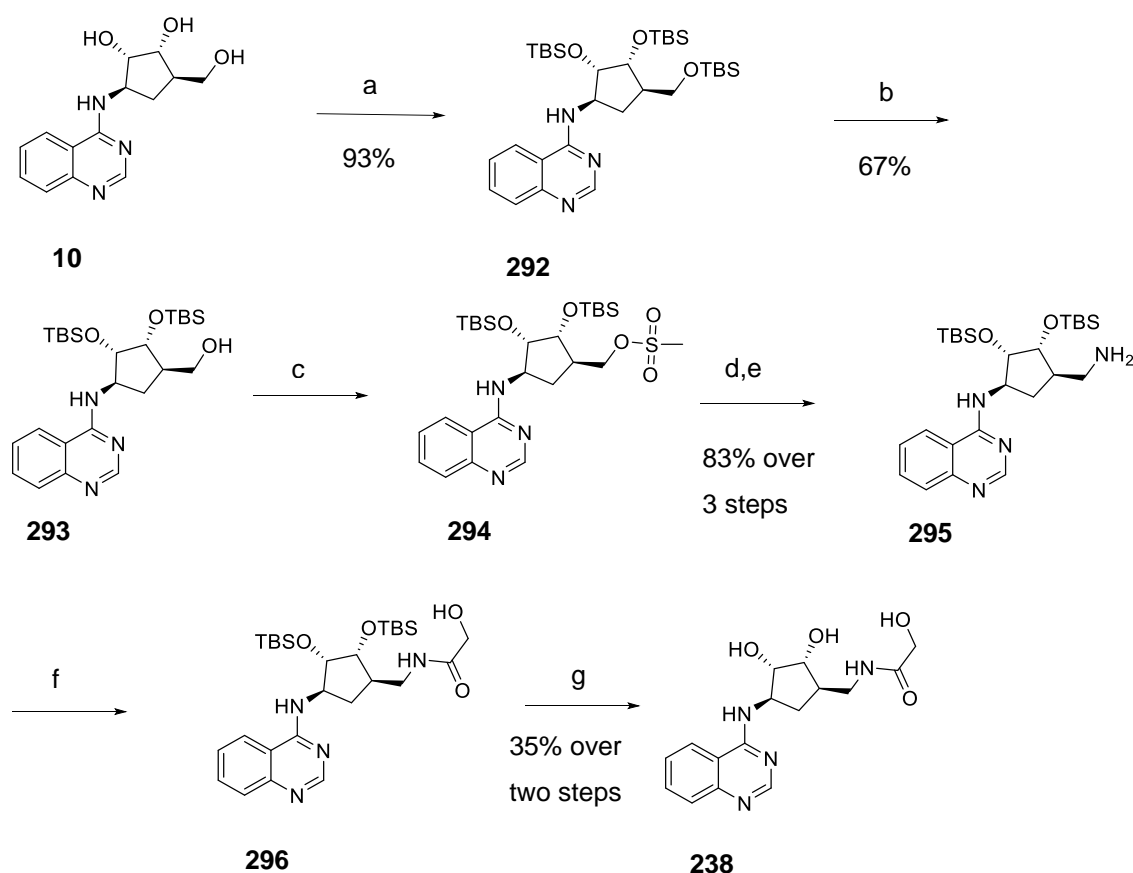


Scheme 4.20 – (a) 2,2-dimethoxypropane, PTSA, DCM, 2 h, rt (b) Boc_2O , DMAP, MeCN, rt, 72 h (c) Mesyl anhydride, TEA, DCM, rt, 2 h (d) NaN_3 , DMF, 60 °C, 18 h (e) PPh_3 , NH_4OH , 60 °C, 3 h.

In parallel, a more flexible protecting group strategy was investigated for the triol **10** with the idea that a less conformationally restricted compound may hinder the undesired cyclisation (Scheme 4.21). TBS protection of triol **10** proceeded in excellent yields, followed by selective deprotection of the primary alcohol by careful optimisation of time and temperature. The conditions to convert the primary alcohol **293** to the primary amine **295** were the same as for the transformation of compounds **254-256**. Using the more flexible TBS protecting groups dramatically reduced the formation of the bicycle **281** and gave 83% yield over the three steps. Changing the protecting group from the conformationally restricted acetal to the more flexible TBS thus improved the yield from 0% to 83%. This transformation is also significantly higher yielding than that achieved for the acetal protected amines **262-264**. The TBS protection had the added benefit of aiding purification as the resulting compounds were much more lipophilic than their acetal protected analogues.

This route was scaled up to form gram quantities of the amine intermediate **295** to enable further exploration of the phosphate binding region.

The final two steps formed the amide bond and removed the protecting groups to yield **238**. Deprotection conditions of the TBS group were achieved with TBAF but this reaction was extremely slow and the product was difficult to isolate cleanly. After a total of 18 equivalents of TBAF and six days no starting material remained.



Scheme 4.21 – (a) Imidazole, DMAP, TBSCl, DMF, 18 h, rt (b) Conc HCl, EtOH, 0 °C, 30 min (c) Mesyl anhydride, TEA, DCM, rt, 2 h (d) NaN₃, DMF, 60 °C, 18 h (e) PPh₃, NH₄OH, 60 °C, 3 h (f) Ethyl glycolate, TEA, CHCl₃, 60 °C, 48 h (g) 1 M TBAF in THF, rt, 6 days.

4.6.5 Testing of hydroxyacetamides by SPR

As discussed in section 4.2 the hydroxyacetamide motif improves the potency of **235** four-fold in comparison with **225**. The four synthesised analogues **238-241** were synthesised to question whether this is the case for other analogues and whether the hydroxyacetamide binds in the phosphate binding region. When the 5-position is unsubstituted the addition of the hydroxyacetamide improves the potency three-fold (**10**; **238**, Table 4.4). The change is most significant in the case of the 5-methoxy where the addition of the hydroxyacetamide improves the potency six-fold (**227**; **239** Table 4.4). However, in the case of the **229** and **226** the addition of the hydroxyacetamide has maintained, not improved, the potency. The X-ray crystal structure of **241** was solved to try to explain this SAR and to determine where the hydroxyacetamide motif is bound.

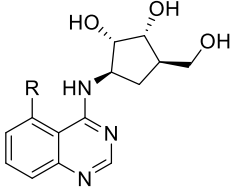
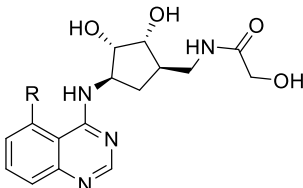
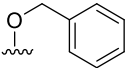
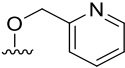
R =			Fold Improvement in Potency
	225 370 μ M 0.17	235 90 μ M 0.17	4
H	10 310 μ M 0.24	238 100 μ M 0.23	3
	227 1040 μ M 0.18	239 166 μ M 0.20	6
	229 335 μ M 0.20	240 322 μ M 0.17	1
	226 75 μ M 0.20	241 50 μ M 0.18	1

Table 4.4 – Testing of hydroxyacetamides **238-241** by SPR in comparison to their previously synthesised matched pairs. Values shown are the SPR K_D in μ M ($n=1$) and the ligand efficiency.

4.6.6 Conformational changes observed by X-ray Crystallography

The X-ray crystal structure of **241** with HSP72-NBD was solved by Marc Cabry at the ICR (Figure 4.10). The hydroxy group makes four new interactions; a direct interaction with G339, a water mediated interaction with T37, a water mediated interaction with D366, and finally with a water molecule that is stabilised by D366, the pyridine nitrogen and the amide nitrogen. The carbonyl group makes three new interactions; with G202, with T14 via a water molecule and with Y15 via a water molecule. Hydroxyl groups are most effective when they form an extended hydrogen bond network.¹¹⁵ Hydrogen bond interactions can reinforce each other through cooperativity where the free energy gain by a network can exceed the sum of the individual components. The quinazoline ring forms an anchoring hydrogen bond to S275 and a hydrogen bond to K271 via a water molecule as observed in the structures of **10** and **225** with HSP72-NBD (PDB IDs 5AQW and 5AQX respectively). R272 is in the up conformation, creating a more open conformation of the binding site. The ligand makes internal hydrogen bonds via a water molecule between the pyridyl nitrogen, the amide nitrogen and the hydroxyl group (Figure 4.10).

The hydroxyacetamide group was observed binding in the phosphate binding region of the protein and overlays well with the first phosphate of ADP (Figure 4.11). This is the first compound that is not ADP or ATP to be observed binding in the phosphate binding region of the protein.

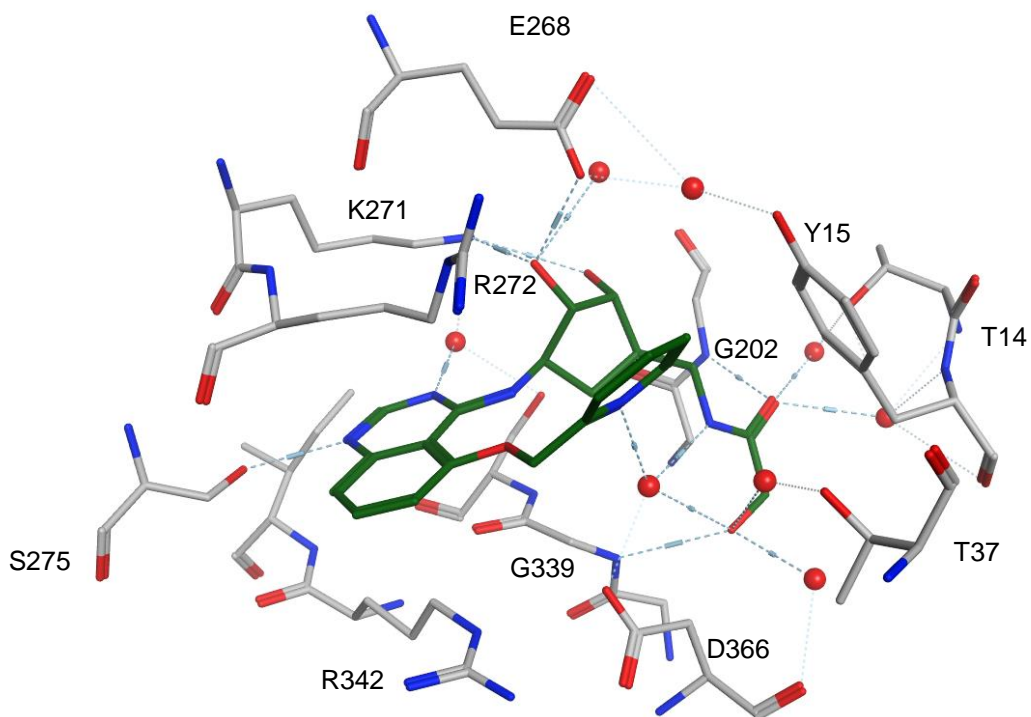


Figure 4.10 – (A) X-ray crystal structure of **241** shows the hydroxyacetamide makes multiple hydrogen bonding interactions with the protein in the phosphate binding region

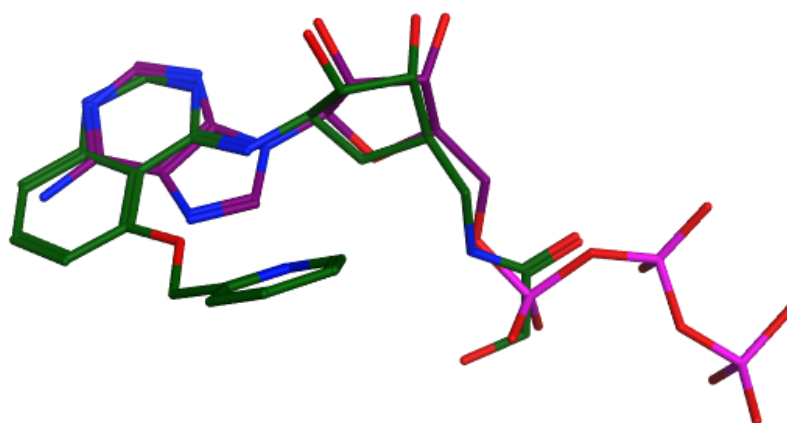


Figure 4.11 – Overlay of the X-ray crystal structures of ATP (PDB ID 3FZF) and **241** shows the hydroxyacetamide motif occupies the same position as the first phosphate group of ATP.

A comparison of the X-ray crystal structures of **10**, **225** and **241** with HSP72-NBD is shown in Figure 4.14. The structure of **241** shows R272 in the 'up' position similar to **225**. The salt bridge between E268 and K56 present in the **10** structure is not present, creating a more open binding pocket than that observed for **10**. The structure of **241** is most similar with that of **225** with key residues S275, K271, R272 and Y15 occupying the same position. Residues E268 and K56 are in a conformation in between that observed for **10** and **225**. The distance between these residues for **10**, **225** and **241** is 3.5 Å, 7.8 Å and 5.4 Å respectively.

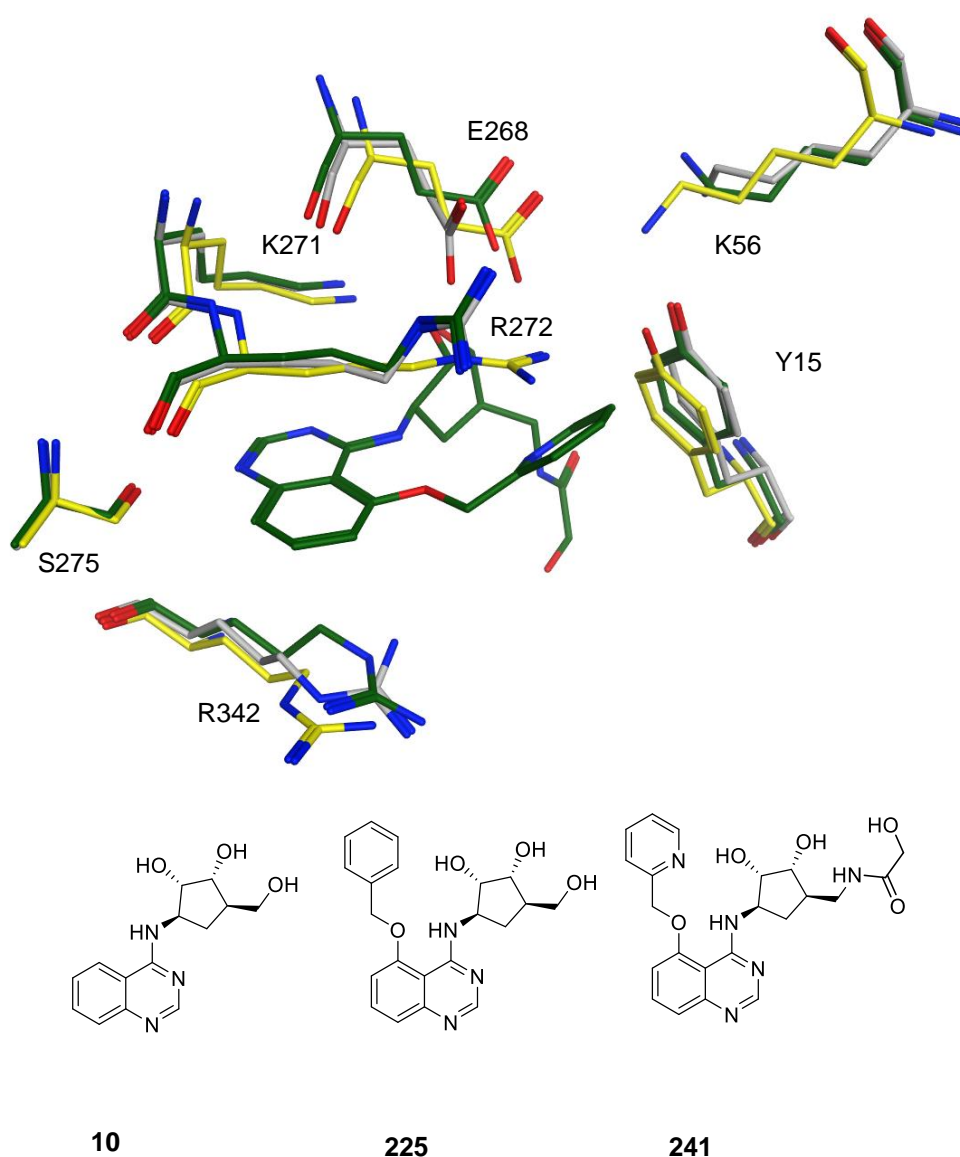


Figure 4.12 – (A) X-ray crystal structures of HSP72-NBD with **10** (5AQW, yellow), **225** (5AQX, grey) and **241** (green). For clarity **10** and **225** ligands are not shown.

As discussed in section 4.6 an additional reason for the synthesis of **241** was to attempt to explain the observed five-fold difference in potency between **225** and **226** and to identify any new interaction which could be targeted. In the X-ray crystal structure of **241** the pyridine ring does not form a new interaction with the protein. It's possible the observed increase in potency between **225** and **226** is instead due to a conformational effect or by the formation of an internal hydrogen bond that decreases the desolvation penalty. This would explain why the SAR differs between compounds **225** and **226** in comparison to compounds **226** and **241**.

Several key questions that arose from SPR testing of **225** have been answered. The hydroxyacetamide does improve the potency of some analogues (**238** and **239**) but not all (**240** and **241**). The hydroxyacetamide makes several new hydrogen bonding interactions with the protein in the phosphate binding region. SPR testing of the hydroxyacetamides **238-241** showed the 5-unsubstituted quinazoline **238** to be the most ligand efficient compound of the series and for this reason the 5-unsubstituted quinazoline was chosen as the basis to explore the phosphate binding region in more depth.

4.7 Library of substituted hydroxyacetamides

4.7.1 Design and conformational analysis

A small library of amides was designed to further explore the phosphate binding region by substitution at the α position of the amide motif of **238**. These compounds included simple substitutions with aliphatic, aromatic, hydrophobic and hydrophilic groups (Appendix 3). Low energy conformations for these molecules were generated and these compounds were then docked into the ATP binding site with the atoms of the quinazoline ring fixed in position, as observed in the X-ray crystal structures **10**, **225** and **241**. Most of the compounds docked well, making interactions with the protein via the carbonyl and NH groups. From the docking results substitution at the α position of the amide with

small aliphatic and aromatic groups appeared to be tolerated, with no clash with the protein predicted for any of the docked compounds. An example is shown in Figure 4.13.

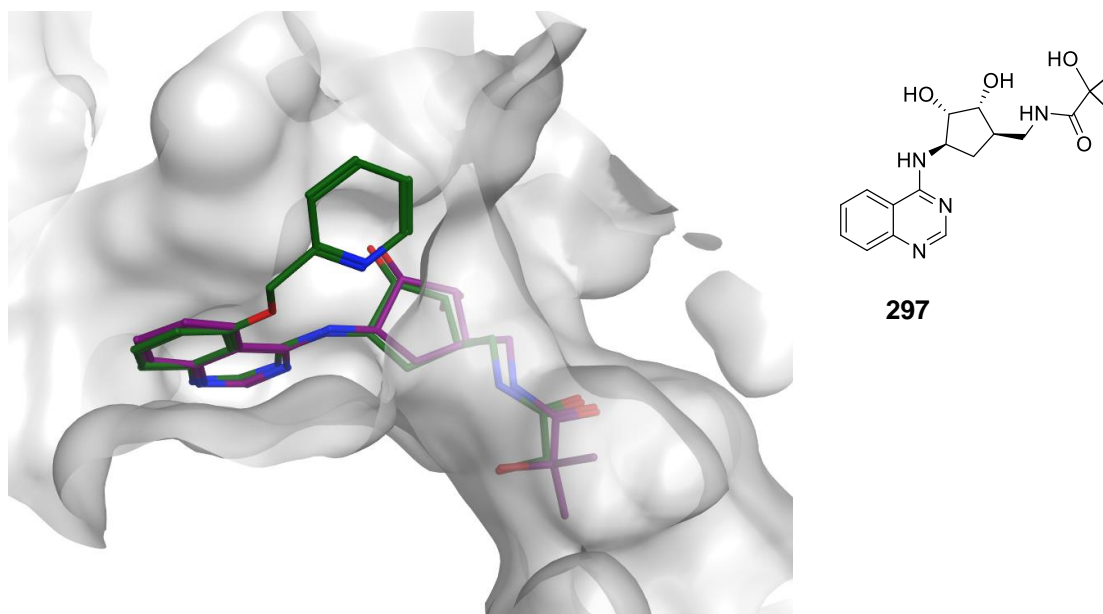


Figure 4.13 – Overlay of the X-ray crystal structure of **241** (green) with the docked design idea **297** (purple).

Comparison of the docked compounds with X-ray crystal structures with a hydroxyacetamide motif in the Cambridge Structural Database (CSD) was carried out to determine the effect of substitution at the α position of the amide. A comparison of compounds from the CSD with the X-ray crystal structure of compound **241** shows that the predicted conformer from the docking studies is not the most common conformation in the database (Figure 4.14). However, when substituted at the α -position of the amide this becomes the most common conformation. From this analysis, compounds with substitution at the α -position should be more likely to be in the active conformation than the unsubstituted matched pair.

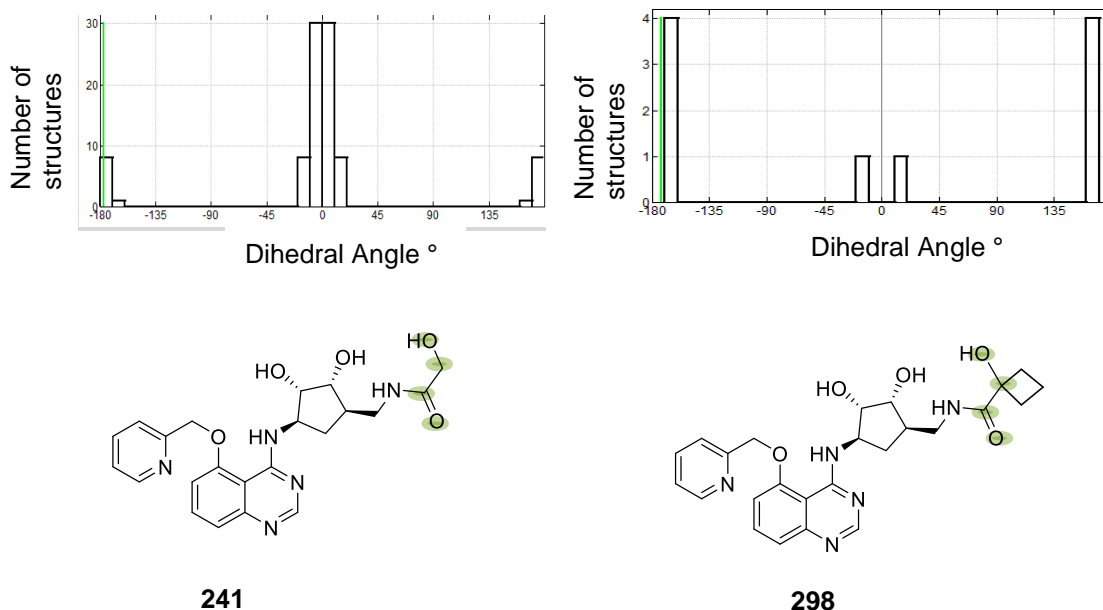


Figure 4.14 – Mogul analysis of **241** and **298**. Comparison of the X-ray crystal structure of compound **241** with compounds from the CSD shows this is not the most common conformation in the database. However, when substituted at the α -position of the amide this becomes the most common conformation suggesting substitution at this position should be conformationally favourable. The conformation of the structure is shown with a green line. The dihedral angle is the angle between two planes, where each plane is defined by three atoms. The query atoms that create the dihedral angle are highlighted in green.

Ten of these docked compounds were selected for synthesis to explore a range of design hypotheses (Figure 4.15). Compounds **297-302** were designed to explore the size of the pocket with aromatic and aliphatic groups. These groups were also predicted to increase the LogD. Lipophilicity is an important parameter in determining the quality of a candidate molecule. It has been suggested that compounds of optimal lipophilicity, with a LogD in the range of 1-3, have increased chances of success in development.¹¹⁶ The calculated LogD pH7.4 of hydroxyacetamide **238** is less than zero. Raising the LogD of the quinazoline series is therefore desirable.

Compounds **303** and **304** added hydrogen bonding groups which may be favourable in such a polar region of the protein. Hydroxyl groups have the

potential to make three interactions simultaneously. Both oxygen lone pairs can act as hydrogen bond acceptors and the acidic hydrogen can act as a hydrogen bond donor. Compound **305** has an electron withdrawing CF_3 group which was designed to make the α hydroxy a better hydrogen bond donor.¹¹⁷ Compound **306** was designed to replace the α hydroxy group with a CF_2H . The C-H bond in this case is designed to mimic the O-H bond as the electronegative fluorines increase the acidity of the adjacent C-H.

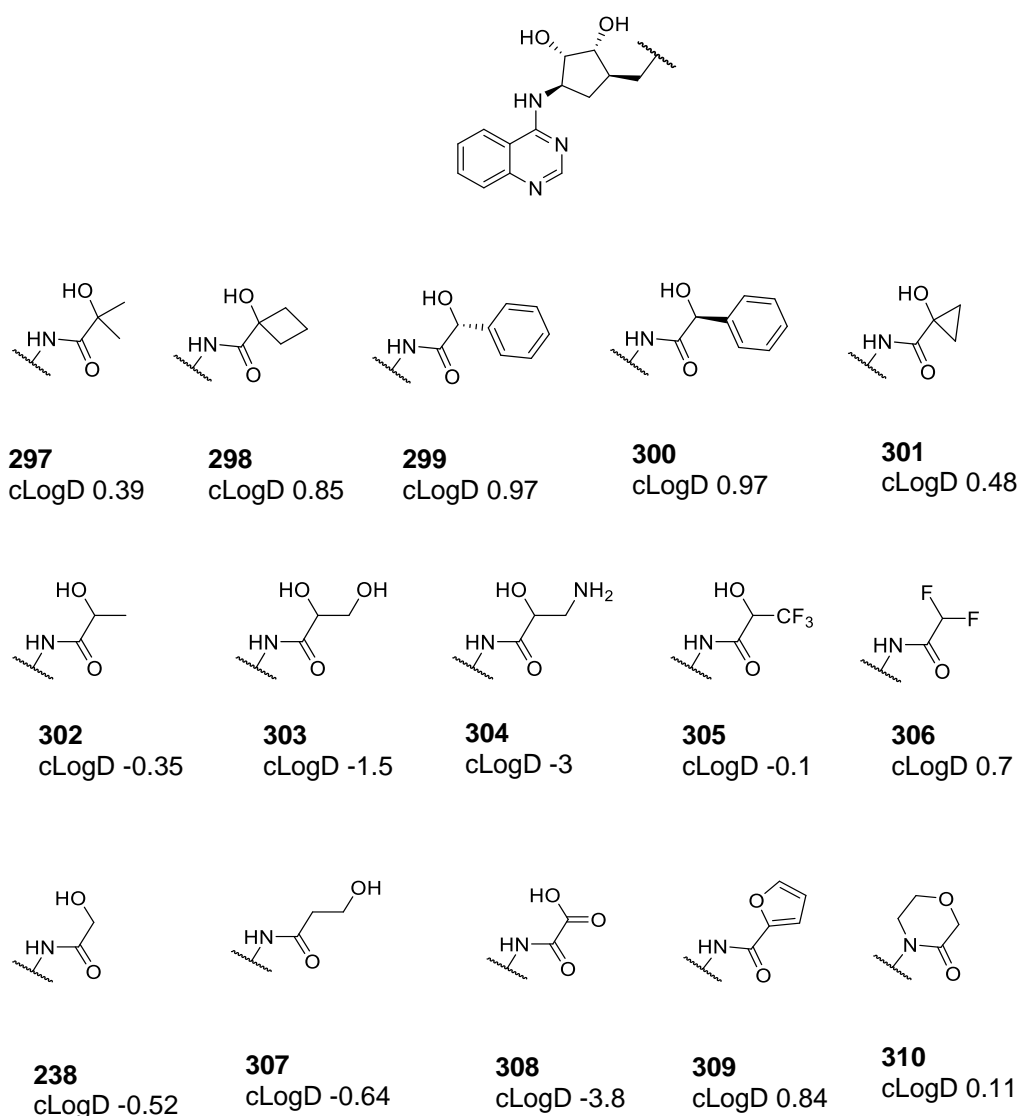


Figure 4.15 – The proposed library of hydroxyacetamides based on compound **238** were designed to explore the phosphate binding region.

Compound **307** extended the hydroxyl group of **238** by one carbon. This strategy is often used in medicinal chemistry to optimise the position of the HBD or HBA or to potentially pick up new interactions with the protein. Compound **308** added a known phosphate mimic.¹¹⁸ Compound **309** incorporates the hydroxyl group into an aromatic ring which removes the hydrogen bond donor.

More flexible ligands often pay a high entropy cost to form the active conformation required for binding.¹¹⁹ Synthesising a conformationally restricted version of the compound can lower this entropy cost by decreasing the number of conformations available to the molecule. Synthesising conformationally restricted molecules can have the benefit of increased affinity, however, it's important that the active conformation is known otherwise restricting the number of conformations available may prevent the conformationally restricted compound from accessing the active conformation. The bound conformation in the X-ray crystal structure was used to design compound **310**, a conformationally restricted analogue of **238** which overlays well with the known bound conformation (Figure 4.16).

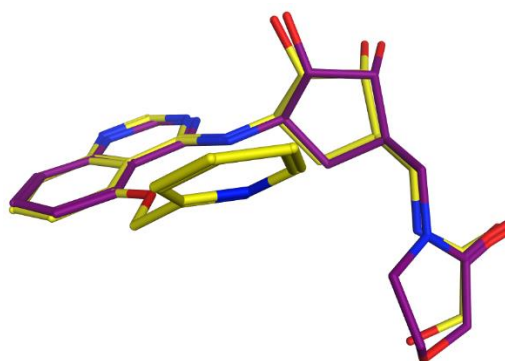
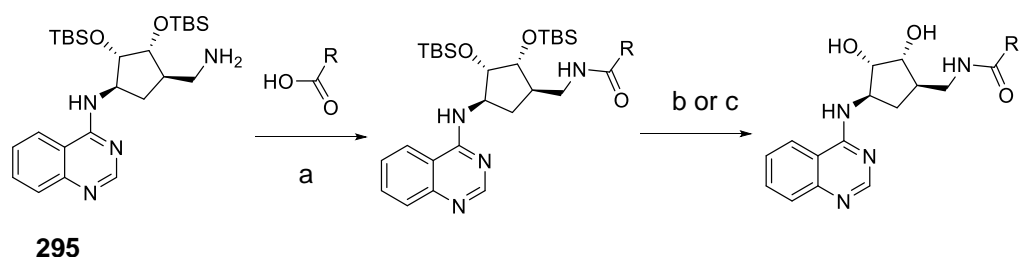


Figure 4.16 - (A) Overlay of X-ray crystal structure of HSP72-NBD with **241** and the proposed ligand **310**. The conformationally restricted molecule overlays well with the bound conformation although it will change the hydrogen bonding ability of the molecule.

4.7.2 Synthesis of compounds to explore the phosphate binding region

Gram scales of intermediate **295** were synthesised using the route described in Scheme 4.21, Section 4.6.4. This intermediate was used to synthesise the fifteen compounds in Figure 4.15. Amides **238-241** were synthesised by refluxing the required amine in ethyl glycolate for two days because previous attempts to form the amide bond with HATU had been unsuccessful. Using (*S*)-mandelic acid, on a test scale, new amide coupling conditions were trialled with DCC and NHS, similar to a literature procedure.¹²⁰ These conditions gave the desired product **300**. A by-product from DCC, 1,3-dicyclohexylurea, which coeluted with the (*S*)-mandelic acid product was removed in the following deprotection step. These conditions were used successfully for the synthesis of the twelve amides in Table 4.5 (Scheme 4.22).

TBS deprotection conditions were initially investigated with TBAF for compounds **297**, **299**, **300** and **307**. The reaction worked well with full conversion by LC-MS, however, after purification by column chromatography a mass ion of 242 corresponding to tetrabutylammonium mass ion was still present. Acidic ion exchange chromatography removed the majority of the impurity but multiple purification steps lead to a lower yield for these compounds. Deprotection with HCl was cleaner and was therefore used for the remaining deprotections.



Scheme 4.22 - Synthesis of amides for exploration of the phosphate binding region (a) DCC, NHS, THF, rt, 2 h (b) Conc HCl, EtOH, rt, 2 h (c) 1 M TBAF, THF, 60 °C, 7 h.

Compound	R	Coupling Yield	Deprotection Yield
297		80%	67% ^b
298		90%	89% ^c
299		88%	40% ^{b,e}
300		63%	39% ^{b,e}
301		87%	91% ^c
302		67%	96% ^c
303		38%	27% ^c
305a		-	69% ^{a, c, d,e}
305b		-	16% ^{a, c, d,e}
306		81%	46% ^c
307		47%	50% ^b
309		45%	88% ^c

Table 4.5 – Synthesis of amides for exploration of the phosphate binding region (Scheme 4.20).

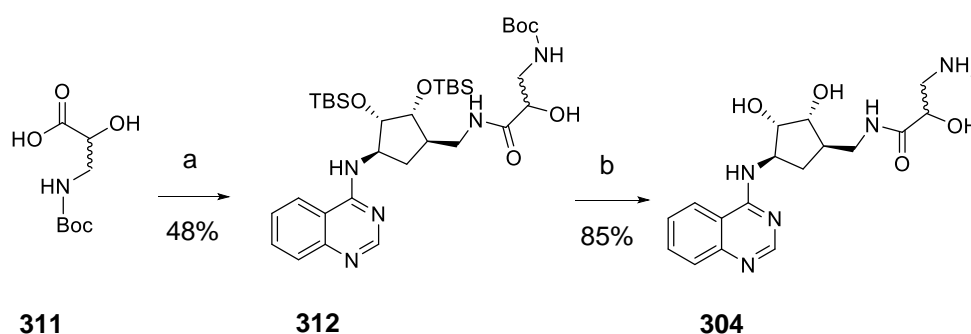
^aYield calculated over two steps. ^bDeprotection with TBAF. ^cDeprotection with HCl.

^dStereochemistry arbitrarily assigned. ^eee >99%

Compound **305**, synthesised from 3,3,3-trifluoro-2-hydroxypropanoic acid, required further purification after column chromatography and was passed through an acidic ion exchange resin. This resulted in partial deprotection of the

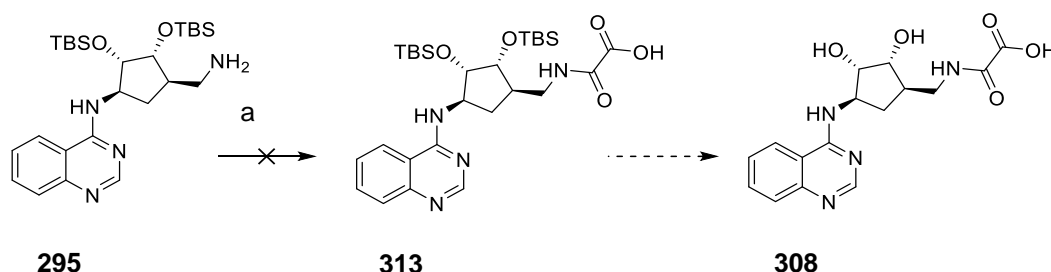
TBS groups and the mixture was taken into the next deprotection step for analysis. Column chromatography gave sufficient separation for both diastereomers **305a** and **305b** to be isolated.

Compound **304** was synthesised as a mixture of diastereomers with Boc protected 3-amino-2-hydroxypropanoic acid **311**. HCl was used to remove both protecting groups. After 24 hours LC-MS analysis showed that the TBS groups had been removed but the Boc protecting group still remained. A further 48 hours with additional HCl gave complete conversion by LC-MS (Scheme 4.23).



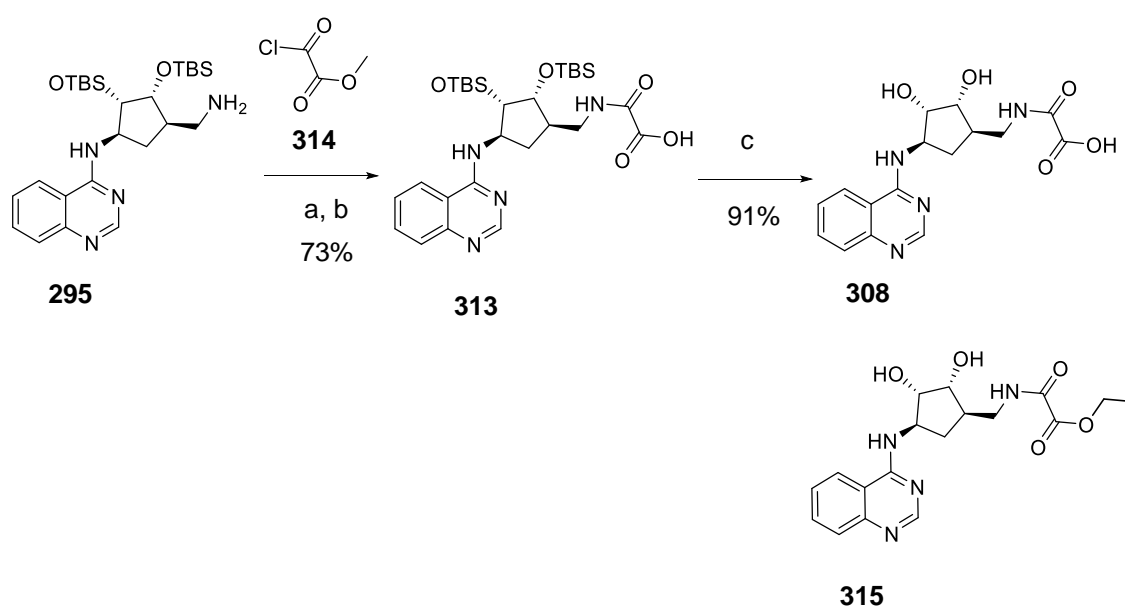
Scheme 4.23 – (a) **295**, DCC, NHS, THF, 1.5 h, rt (b) HCl, EtOH, 48 h, rt.

The synthesis of the phosphate mimic **308** was initially attempted with oxalic acid, DCC and NHS (Scheme 4.24). This reaction was monitored over three days but no product was isolated.



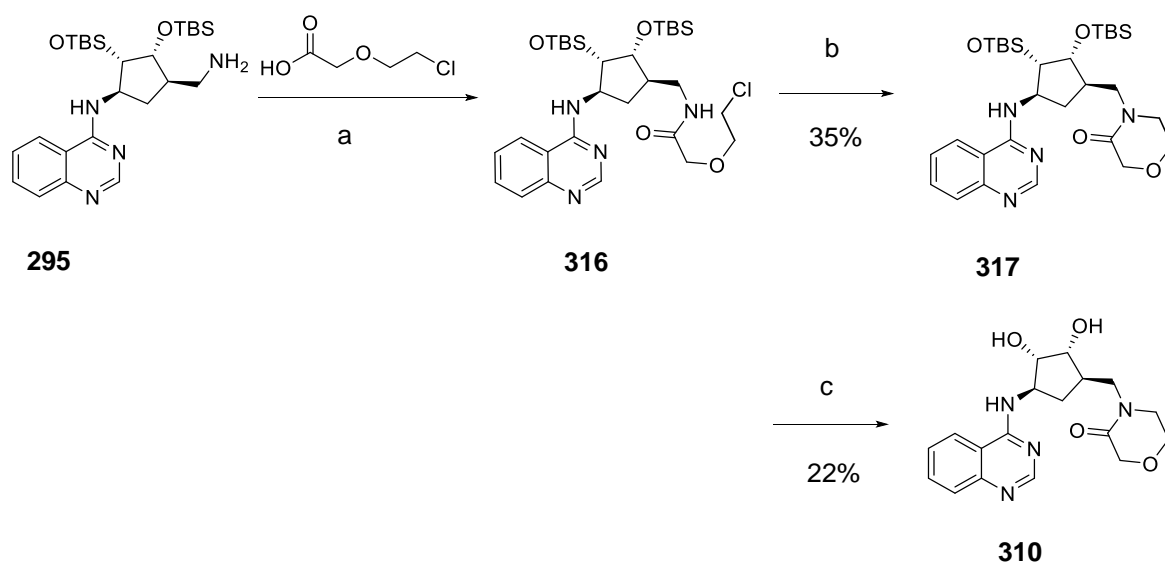
Scheme 4.24 - (a) Oxalic acid, DCC, NHS THF, rt, 72 h.

Following a similar procedure to literature conditions,¹²¹ the reaction was attempted instead with methyl 2-chloro-2-oxoacetate **314** (Scheme 4.25). After an aqueous work-up with DCM, the ester was hydrolysed with lithium hydroxide to the desired intermediate **313**. Deprotection of the TBS groups was first attempted with HCl and EtOH, conditions used for compound **304**. This gave the desired product **308** but also a significant amount of the ethyl ester **315**. Treatment with LiOH converted the ester **315** into the desired final product **308** but this extra step could be avoided by removing the TBS groups with HCl in THF instead of ethanol.



Scheme 4.25 - (a) TEA, DCM, rt, 2 h (b) LiOH, THF, H₂O, 60 °C, 1 h (c) Conc HCl, THF, 18 h.

Synthesis of the conformationally restricted analogue **310** was carried out in three steps. The amide coupling with **295** to form **316** was carried out with EDC, in a similar way to a known literature procedure (Scheme 4.26).¹²² The cyclisation of **316** to **317** was accomplished with potassium carbonate. Compounds **316** and **317** have overlapping retention times and were very difficult to separate by HPLC. To avoid this issue the reaction could be driven to completion by heating at 80°C for 48 hours. Deprotection with HCl gave the desired final product **310**.



Scheme 4.26 (a) EDC, DMAP, MeCN, rt, 18 h (b) K_2CO_3 , MeCN, 80 °C, 48 h (c) Conc HCl, EtOH, rt, 18 h.

4.7.3 SPR testing of new hydroxyacetamide analogues

Fifteen compounds designed to explore the phosphate binding region were tested by SPR against HSC70-NBD (Figure 4.16). The parent compound **238** has a potency of 100 μM . Mono or disubstitution of the hydroxyacetamide at the α position with small alkyl groups decreased the potency significantly (**297-302**). Possible explanations are that the substitution changes the position of the key carbonyl and hydroxy groups. However, conformational analysis suggests this is not the case. An alternative hypothesis is that substitution at this position unfavourably disrupts the water network buried in the polar phosphate binding region (Figure 4.18). Compounds **299** and **300** with phenyl substituents occupy a much larger space than compounds **301** and **302** but are tolerated. Although the potency has decreased approximately 6-fold in comparison to the parent compound **238** they are still capable of binding in the pocket. No preference for either enantiomer was observed.

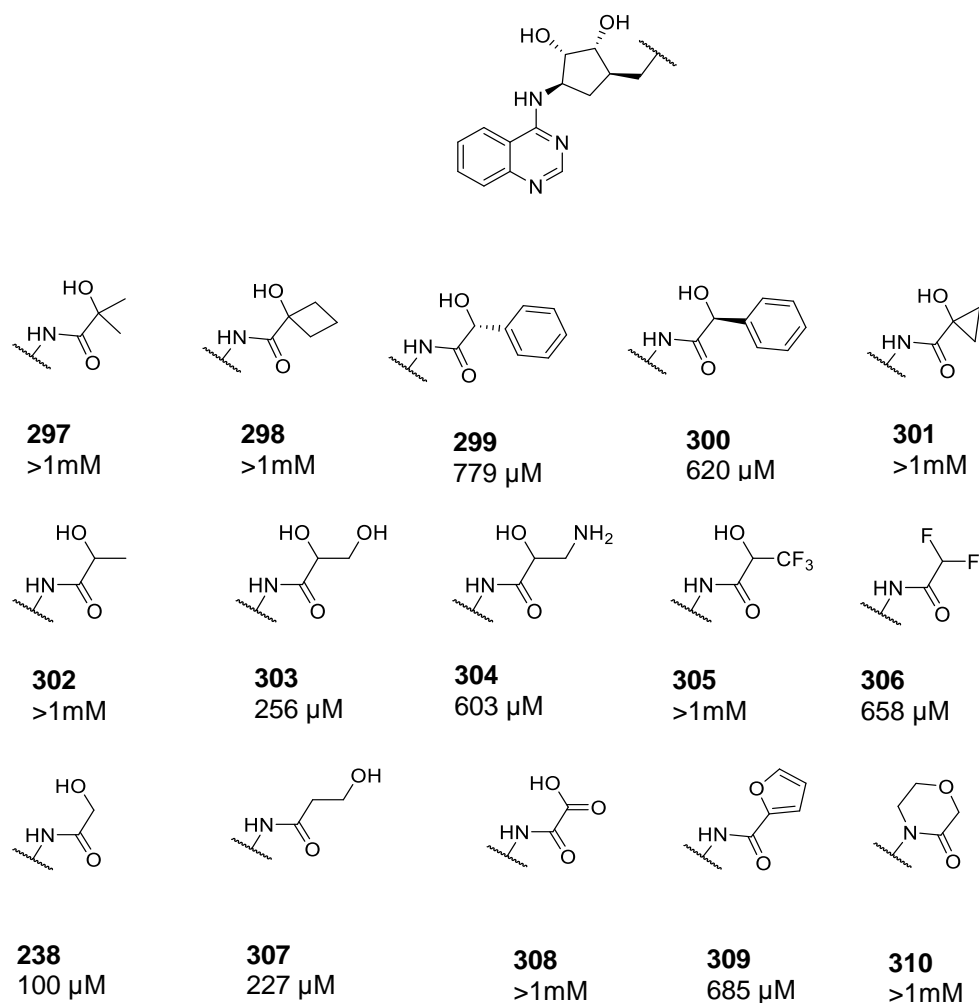


Figure 4.17 – A library of hydroxyacetamides designed to explore the phosphate binding region was tested by SPR. Values shown are the measured SPR K_D .

Extension of the carbon chain by one carbon in compound **307** has decreased potency but within two-fold. This compound may be forming a new interaction with the protein or forming the same interaction as **238** less optimally.

Surprisingly the phosphate mimic **308** has also lost potency. The phosphate binding region is highly polar with a network of bound water molecules. When ATP is bound the phosphates form multiple hydrogen bonding interactions with water and the polar residues of the protein. It's possible that disruption of these ordered networks of water molecules is energetically unfavourable (Figure 4.18).

Cyclisation of the hydroxyacetamide into the active crystal structure conformation **310** also significantly decreased the potency. This cyclisation comes at the expense of two potential hydrogen bond donors. It's possible that the free hydroxyl group of **238** is important as both a hydrogen bond donor and a hydrogen bond acceptor. If the active conformation is already a low energy conformation, then there would be no significant entropic gain in restricting the conformation to the active conformation. Incorporation of the hydroxy group into a furan ring **309**, which also removes the hydrogen bond donor, decreased potency.

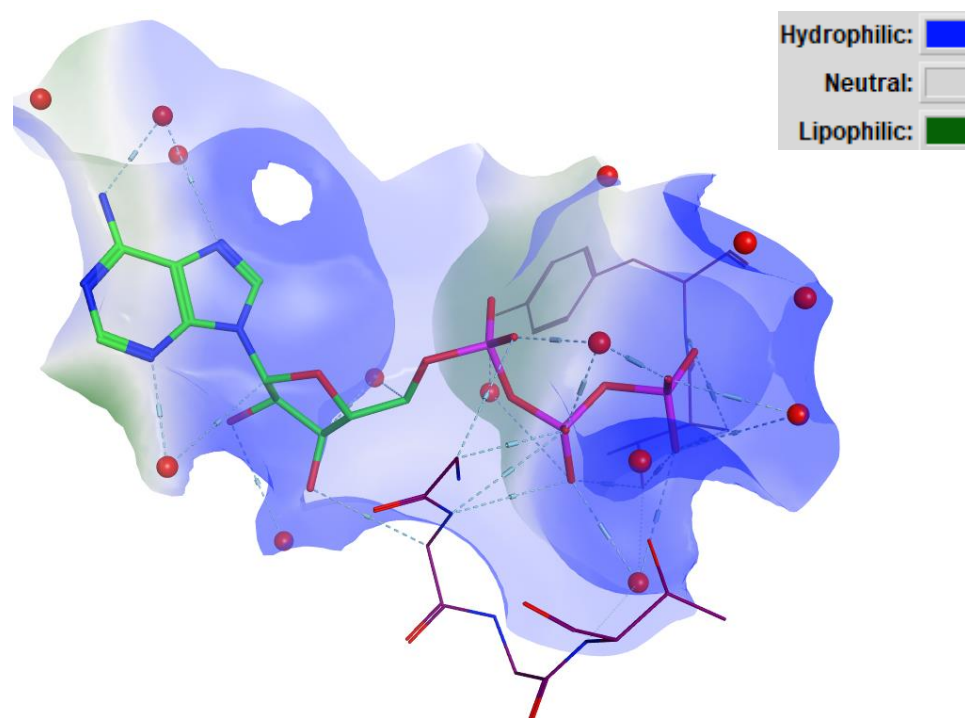


Figure 4.18 – X-ray crystal structure of ATP bound to HSC70-NBD (PDB ID 3FZF). The highly ordered network of molecules may be unfavourable to displace. Compound **238** which occupies the same position as the first phosphate of ATP was tolerated but further substitution with an α carbonyl **308** was not tolerated.

Substitution with small polar groups was tolerated (compounds **303** and **304**). Compound **303** is a combination of compounds **238** and **307** which was designed to add a potential hydrogen bond donor or acceptor in the polar phosphate binding region of the ATP binding site. The SPR sensorgrams for **238**

show binding to be fast on/fast off in contrast to the sensorgrams for **303** which are slower off (Figure 4.19). SPR is a useful technique because it can give a detailed insight into the interactions between a protein and the ligand of interest. Sensorgrams can show binding that is slow on/slow off, fast on/fast off or fast on/slow off. In contrast to slow on rates, fast on rates mean there is very little energy needed to form the interaction. A fast off rate implies that once the interaction is formed it is relatively weak. Fast on/fast off rates have been observed for the majority of the quinazolines studied in this thesis and are typical for weakly potent fragments. Compounds with slower on/off rates can imply the two molecules do not initially encounter each other in a conformation to interact optimally, but a subsequent conformational change can increase the interactions, so the off rate is lowered. The off-rate is especially important, because it informs on how long the compound binds to the ligand or target.

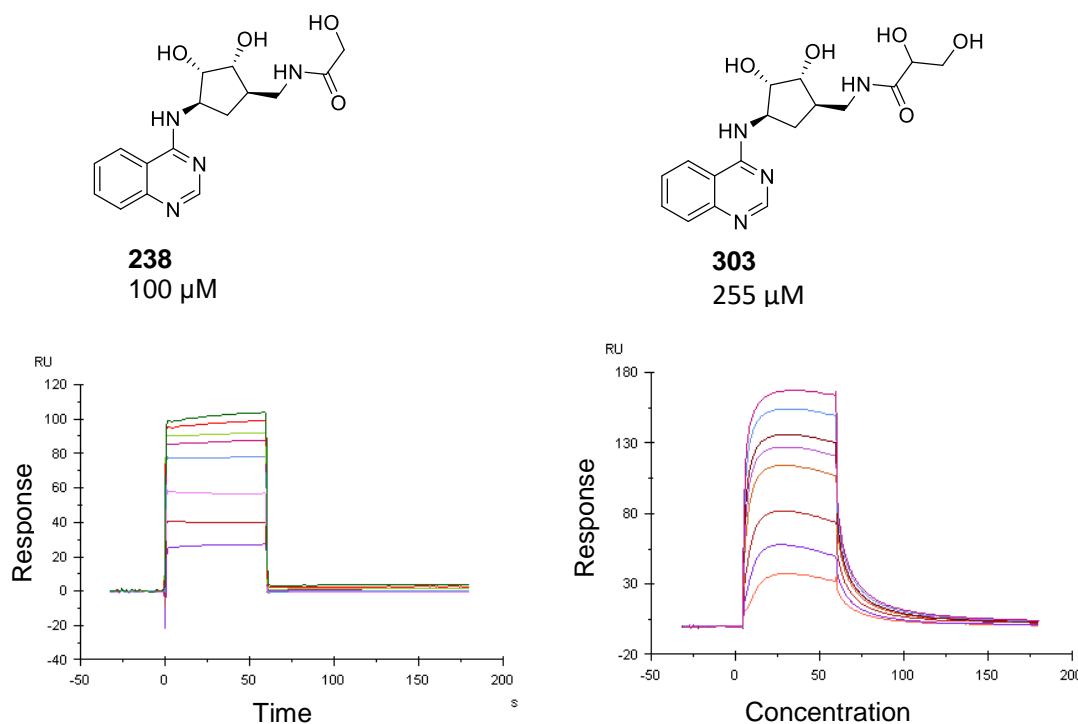


Figure 4.19 – (A) Sensorgrams for compounds **238** and **303**.

The X-ray crystal structure of **303** was solved by Marc Cabry at the ICR to try to explain the observed differences in the SPR experiment between compounds **238** and **303** (Figure 4.20). In this X-ray crystal structure, several new hydrogen

bonds are observed in the phosphate binding region. The carbonyl oxygen forms hydrogen bonds via two water molecules to T14. The α hydroxy group forms hydrogen bonds with D366 directly and via a water molecule. The β hydroxy group forms hydrogen bonds with D366 and G339. The ribose ring forms hydrogen bonds with E268 and R272 in the same way as **238**. R272 remains in the 'up' conformation. K56, Y15 and S275 also remain in similar positions. E268 has moved away from K56 giving the binding site a more open conformation. D366 has flipped its conformation to interact directly with the β hydroxy group via a hydrogen bond. R342 which interacts with D366 in **238** crystal structure has also shifted position and no longer interacts with this residue. The binding of **303** has a significant effect on key residues in the binding site which rearrange to interact with the ligand. This may explain the observed slow-off kinetics in the SPR experiment.

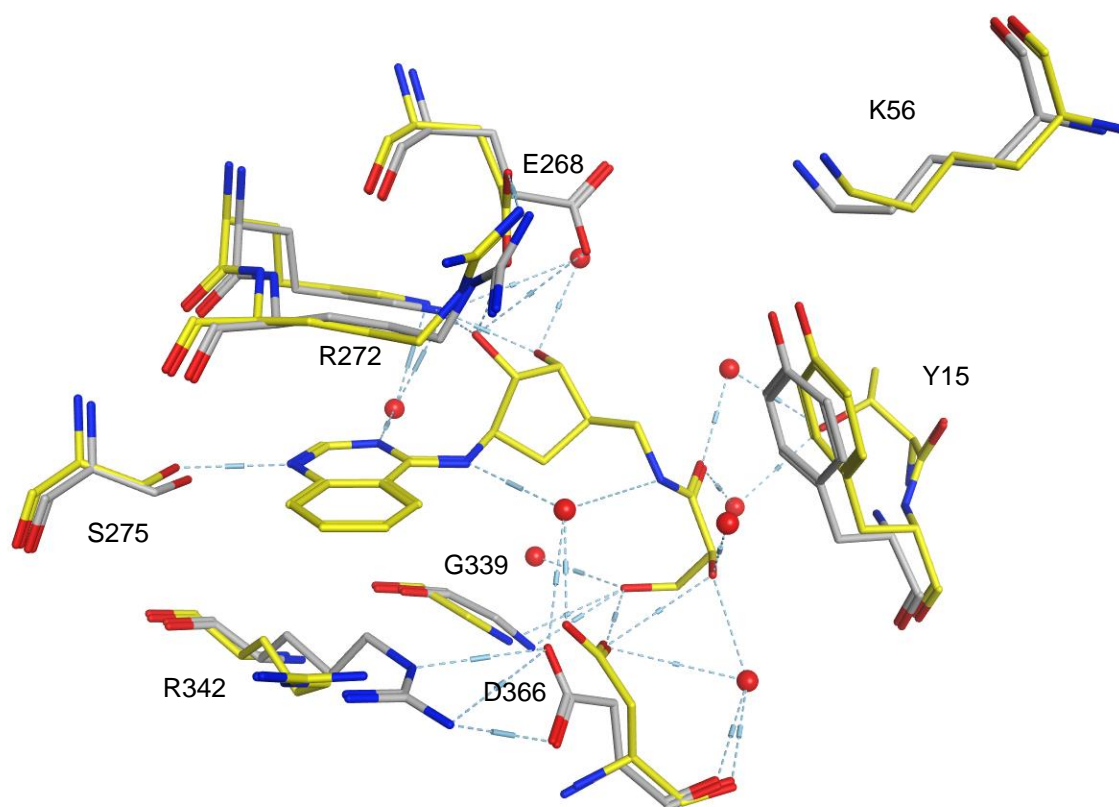


Figure 4.20 – (A) X-ray crystal structures of HSP72-NBD with compound **303** (yellow) and **238** (grey). Ligand **238** and non-bonded solvent are hidden for clarity.

From the X-ray crystal structure of **303** additional hydrogen bonds are observed with the protein but there is no increase in overall affinity in comparison with **238**. Hydroxyl groups can form extended hydrogen bond networks and their contribution to affinity can reach several orders of magnitude.¹¹⁵ However, introducing a hydroxyl group to a ligand to form a new hydrogen bond with the protein does not necessarily mean that the overall binding affinity will increase. While attractive hydrophobic interactions depend on shape complementarity, polar interactions are more complex. Initially both binding partners are surrounded by a network of water molecules, known as a hydration shell. A ligand's hydroxyl group is part of a strong network of hydrogen bonds with water molecules and their removal has a significant energy penalty. Drug-receptor binding relies on the desolvation of both the ligand and the receptor. A spontaneous interaction will only occur when the binding energy exceeds the desolvation energy costs.¹²³

The desolvation energy cost can be offset by the beneficial entropy term which results from the release of water molecules to the bulk solvent and the interaction energy of the new hydrogen bond formed. Cooperative desolvation and intramolecular hydrogen bonds can assist in reducing these desolvation penalties further. Cumulative desolvation penalties for multiple hydroxyl groups can be very difficult to compensate for by ligand protein interactions and usually a hydroxyl group needs to be part of an extended hydrogen bond network to compensate for the desolvation penalty. The maximal interaction energy of a single hydroxyl bond is reported to be 18-21 kJ mol⁻¹.¹¹⁵ Cabani *et al* estimated the free energy required for the transfer of an OH from the aqueous solution to gas phase to be 26 kJ mol⁻¹ of which the enthalpy penalty δH is 36 kJ mol⁻¹ which is reduced by 10 kJ mol⁻¹ from the release of water molecules to bulk solvent.¹²⁴ For the desolvation of vicinal diols the free energy penalty of 17 kJ mol⁻¹ per hydroxyl groups was reported, much lower than that of two hydroxyl groups because of the shared hydration of these neighbouring groups. It has been shown that the strength of an intermolecular hydrogen bond donated by catechol is doubled by a cooperative intramolecular interaction by the second hydroxyl group.¹²⁵ This is indicative of a large positive cooperative effect on forming a

chain of two H bonds compared to a single H bond (Figure 4.21). Compound **303** is a vicinal diol and was designed to increase the potency by potentially forming additional hydrogen bonding interactions in a cooperative manner. However, from SPR testing of **303** the potency has not increased despite the network of hydrogen bonds observed by X-ray crystallography. It's likely the enthalpic gain from the formation of a network of hydrogen bonds is not enough in this instance to compensate for the desolvation penalties required.

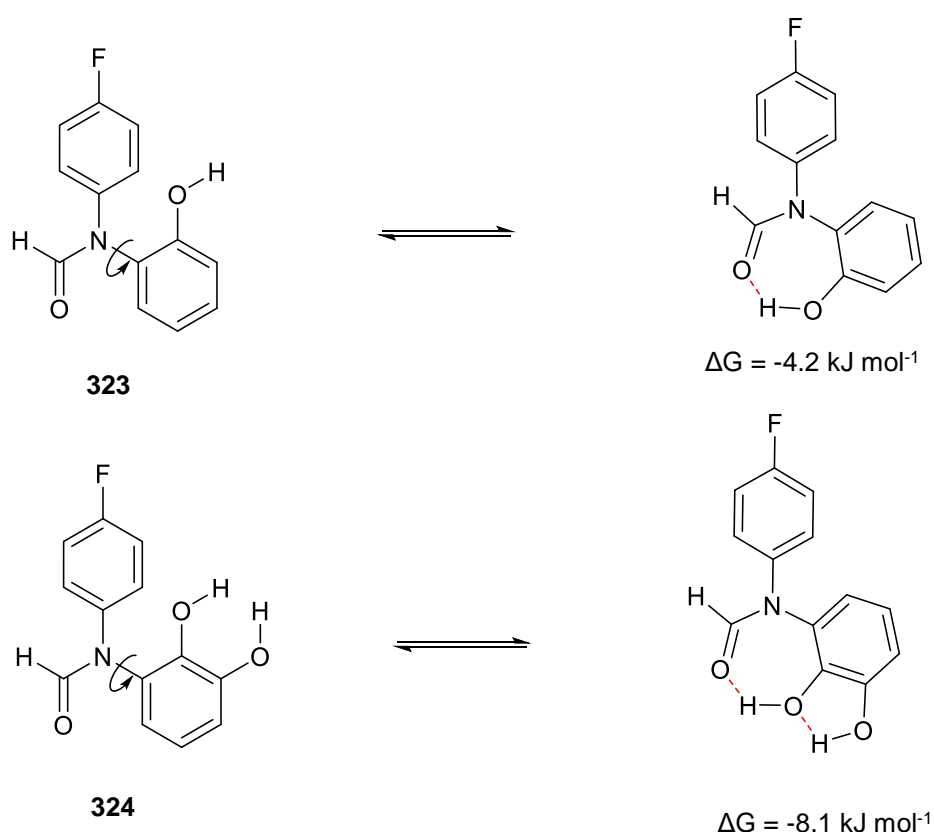


Figure 4.21 – The strength of an intermolecular hydrogen bond donated by catechol **323** is doubled by a cooperative intramolecular interaction by the second hydroxyl group of **324**.¹²⁵

4.8 Conclusions

This chapter has described the exploration of the phosphate binding region of HSP70. A hydroxyacetamide motif was observed by X-ray crystallography to interact with residues in the phosphate binding region via a network of hydrogen bonds and occupies the position of the first phosphate of ADP. This is the first

time a non-nucleotide ligand has been observed to bind to the phosphate binding region of HSP70. Analogues with substituents at the 5 position were synthesised and were found to have variable SAR. This is a highly flexible binding site and the movement of key residues close to the ligands has been demonstrated by X-ray crystallography and the relevance discussed.

The most ligand efficient hydroxyacetamide tested was used to explore the phosphate binding region in more depth by substitution at the α position and through introduction of other potential phospho-mimetic motifs. Addition of substituents at the α position of the hydroxyacetamide has so far not increased affinity, despite a range of different substituents tested. From analysis of the X-ray crystal structure there is space in the binding site for substitution at this position but this region of the pocket is very polar. The release of ordered water molecules from a shallow and solvent exposed binding site can result in a highly beneficial entropy term. However, the release of water molecules from a polar region in the protein can be unfavourable. It is likely that there is a very stable network of water molecules in the phosphate binding region and that displacement or disruption of this network is not favourable.

A second X-ray crystal structure was solved with a ligand substituted at the α position of the hydroxyacetamide. A network of hydrogen bonding interactions in the phosphate binding region was observed with this ligand. Despite the additional hydrogen bonds formed the affinity did not increase. The addition of hydrogen bond donors and acceptors is highly complex due to desolvation energy costs and entropic penalties. The desolvation energy cost can be offset by a beneficial entropy term which results from the release of water molecules to the bulk solvent and the interaction energy of the new hydrogen bond formed, however, this is extremely difficult to predict. Before removing or including hydroxyl in a molecule there are key factors to consider: Is the hydroxyl group making a key interaction or preferably a network of interactions? Is the direction of the hydrogen bond optimal? Is the desolvation cost worth paying? In practice it is much easier to post-rationalise the effect of adding a hydroxyl group to a ligand by measuring the change in affinity for the protein. In the case of

compound **303** the hydroxyl group is making a network of hydrogen bonding interactions and the direction of these hydrogen bonds is within the optimal range, however, ligand-receptor binding relies on the desolvation of both the ligand and the receptor. For compound **303** it's likely that the desolvation penalties are not outweighed by the new bonding interactions and no potency gain was observed. This ligand also alters the conformation of key residues in the binding pocket, altering the shape and forming a more open conformation of the ATP binding pocket.

The phosphate binding region was an interesting novel region of the ATP binding site to explore by growing out from the ribose mimic but it was just one of the many ways the molecule could be developed. The next chapter describes the exploration of other regions of the ATP binding pocket by developing various different parts of the quinazoline hit.

Chapter 5

5 Exploration of the quinazoline fragment hit

5.1 Previous published and unpublished work

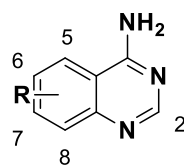
Simple substitution around the amino quinazoline ring of fragment **223** had been previously carried out to determine the effect of methyl and methoxy substituents at the 2, 5, 6, 7 and 8 positions.³¹ Both methyl and methoxy substitutions at the 5, 6, 7 and 8 positions are tolerated (Table 5.1). These positions are the most solvent exposed regions in the X-ray crystal structure. However, introduction of a methyl group at the 2 position is not tolerated. Examination of the X-ray crystal structure shows that substitution at this position would clash with I343 (Figure 5.1 A).

Unsubstituted amino quinazoline **223** is one of the most ligand efficient compounds of the series (0.34). Methyl and methoxy substitutions at the 5, 6, 7 and 8 positions improve potency but at the cost of ligand efficiency with the exception of 7-Me **327** which increases the LE to 0.36 and 5-Me **326** which offers no improvement in either. The 6,7 di-methoxy **333** is equipotent to 7-methoxy **331** and therefore less ligand efficient. Only mono-substitution on the 4 amino group is tolerated.

The N1 of the quinazoline is essential for activity. Sequence conservation of S275 within the HSP70 family and the presence of a hydrogen bond in all available ATP competitive ligand bound HSP70 structures highlights the importance of interacting with this residue. This hypothesis has been tested by comparing the ability of purine nucleotides which can form a hydrogen bond to S275 with pyrimidines which cannot.³¹ Pyrimidine analogues were shown to be completely inactive. Mutation of this key serine residue to an alanine results in significantly weaker binding of adenosine, ADP and ATP.

Extension into the phosphate binding region was discussed in Chapter 4. This chapter will summarize efforts made in replacing the quinazoline core and

exploring substitutions at the 5, 6 and 7 positions in more depth while maintaining those elements known to be essential for activity (Figure 5.1 B).



Compound	R =	SPR K_D (mM)	LE
223	H	2.1	0.34
325	2-Me	no binding	ND
326	5-Me	12	0.22
9	6-Me	1.4	0.33
327	7-Me	0.8	0.36
328	8-Me	2.9	0.29
329	5-OMe	0.83	0.33
330	6-OMe	1	0.32
331	7-OMe	0.85	0.33
332	8-OMe	2	0.29
333	6,7-(OMe) ₂	0.83	0.28

Table 5.1 – Previous published work showed the effect of methyl and methoxy substituents of the amino quinazoline **223** on binding to HSC70-NBD.

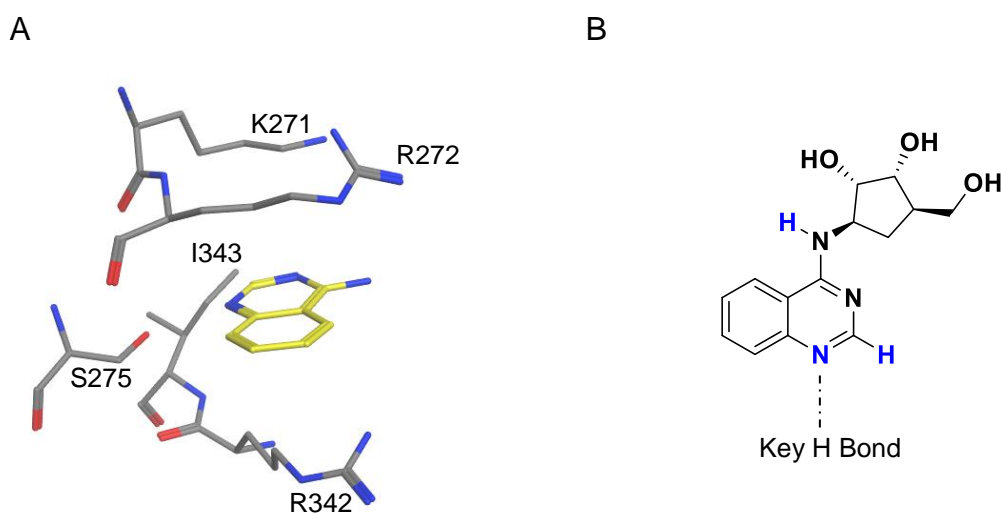


Figure 5.1 – (A) Introduction of a methyl group at the 2-position is not tolerated. Examination of the X-ray crystal structure of **223** with HSC70/Bag1 (PDB ID 5AQP) shows that substitution at this position would clash with I343 (B) Previous work has shown areas of the molecule that are essential for activity (blue).

5.2 Replacement of the quinazoline ring

5.2.1 Design of quinazoline replacements

The quinazoline core of **10** was further investigated to explore the question of whether quinazoline replacements would be tolerated or offer any improvements in potency. The idea of replacing a core is a general strategy used in medicinal chemistry to find an alternative chemical series with different physicochemical properties. Having multiple chemical series for the same target binding site is an advantage, giving more opportunity for success and helping to avoid the attrition of multiple compounds for the same unexpected cause.¹²⁶

To search for the most ligand efficient core the quinazoline ring was replaced with quinoline, cinnoline, pyrimidine and naphthyridine rings. Compound **10** (K_D 310 μ M) with the ribose mimic was used as the parent compound, rather than the fragment **223** (K_D 2100 μ M) because the marked increase in potency with the ribose mimic gives a larger assay window and should allow better comparison between matched pairs. The maximum concentration used in the SPR assay is 1000 μ M because beyond this concentration solubility becomes a limiting factor.

In the X-ray crystal structure of **10** with HSP72-NBD (PDB ID 5AQW), a buried water molecule can be observed forming a hydrogen bonding interaction with K271 and the N3 of the quinazoline ring (Figure 5.2). The importance of the N3 which forms a hydrogen bond to this conserved water molecule was unknown. Quinoline analogues were designed to investigate the effect of removing this hydrogen bond (**334** and **339**) or displacing this conserved water molecule (**335-338**). Changing the quinazoline core in this way is predicted to change both the pKa of the N1 and the LogD (calculated values in Table 5.2). There is literature precedent for the replacement of a quinazoline ring with a 3-cyano quinoline which maintained potency against EGFR, with the cyano substituent mimicking the interaction of the water molecule (Figure 5.3).¹²⁷

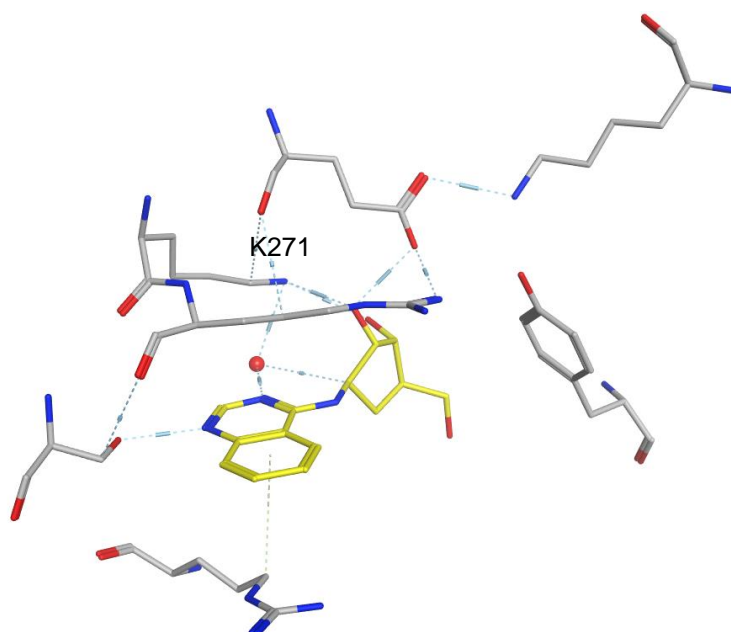


Figure 5.2 - In the X-ray crystal structure of **10** with HSP72-NBD (PDBID 5AQW), the N3 of the quinazoline ring forms a hydrogen bond to a water molecule in the back of pocket which is stabilised by K271.

	334	335	336	337	338	339
LogD7.4	-0.7	-1.2	0.65	0.11	-2.2	-0.3
pKa N1	8.8	8.6	7.3	5.0	9.1	3.5

Table 5.2 – Quinoline and cinnoline replacements of **10** were designed to test whether the interaction with a conserved buried water molecule, highlighted in Figure 5.2, is essential for binding and whether this water molecule could be replaced. LogD and pKa calculations shown were performed with MOKA.

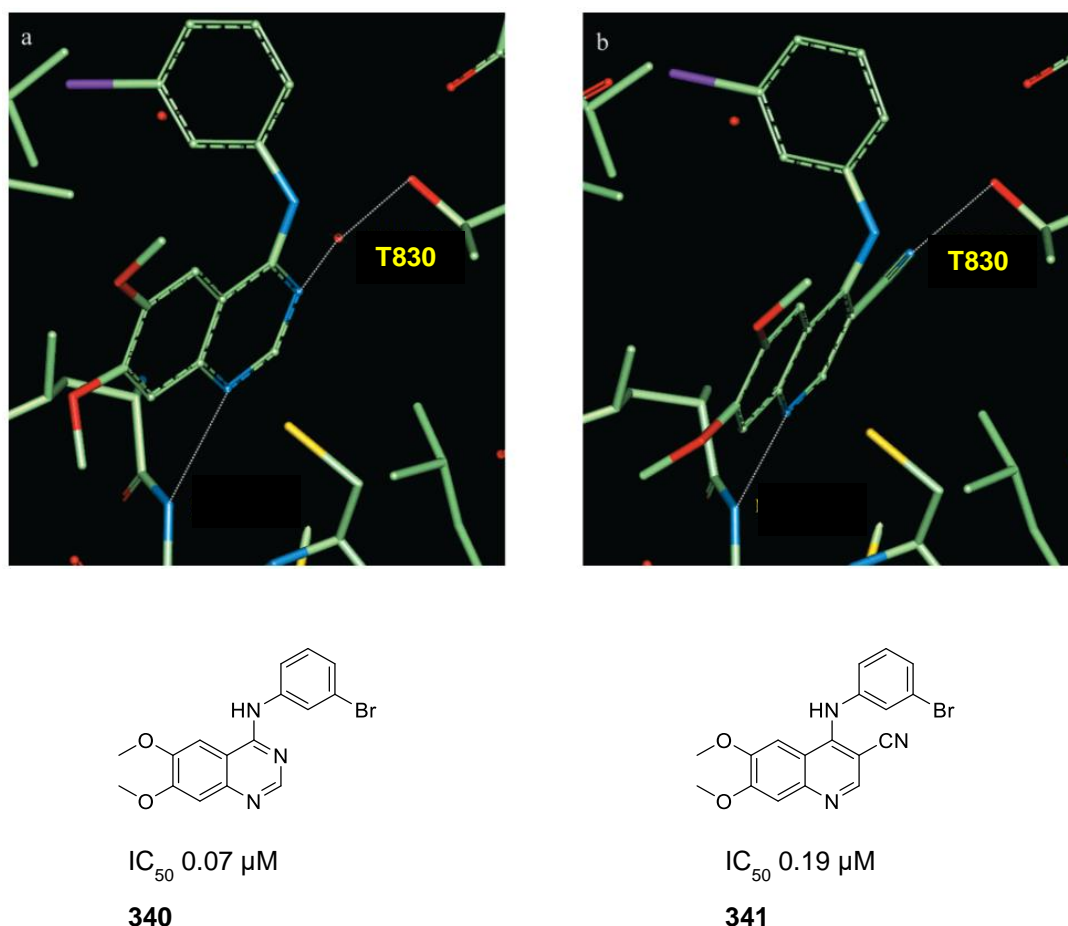
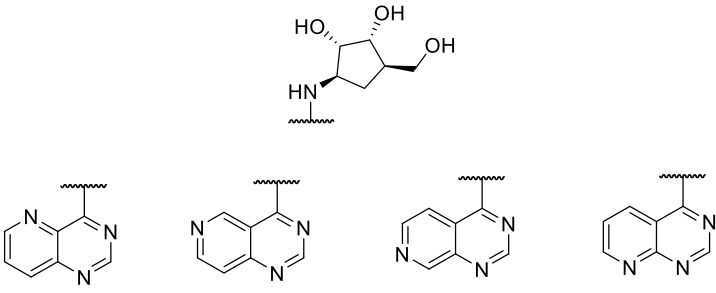


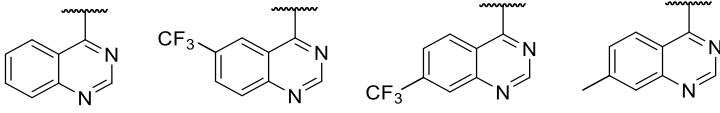
Figure 5.3 - Proposed binding of compounds in the ATP binding site of EGFR based on a homology model.¹²⁷ (a) For quinazoline **340** the N3 atom of the quinazoline ring forms a hydrogen bond with the hydroxyl group of T830 via a water molecule. (b) For 3-cyanoquinoline **341** the 3-cyano group displaces the water molecule that was previously hydrogen-bonded to the N3 atom of the quinazoline and instead makes its own interaction with the hydroxyl group of T830.

A set of naphthyridine analogues was designed to investigate the effect of changing the LogD and the pKa of the N1 of the quinazoline core. The quinazoline **10** makes an anchoring hydrogen bond to S275 via the N1. It's possible that changing the pKa of this nitrogen could affect the potency of these compounds, by changing the strength of the hydrogen bonding interaction with S275. Compounds **342-345** with one extra nitrogen in the ring should make the ring equally electron deficient but depending on the position the effect on the pKa of the N1 is predicted to be different (Table 5.3).

CF₃ groups have been used as bioisosteres of methyl groups.¹²⁸ Matched pairs **347** and **348** were designed to compare the effect of electron donating and electron withdrawing groups on the quinazoline ring. Matched pairs **346** and **347** were designed to help to tease apart potency differences due to LogD or due to changes on the pKa of N1. These compounds are predicted to have the same LogD but a 1.5 log unit difference in pKa. Quinazoline **10** and 6-CF₃ quinazoline **346** are predicted to have the same pKa, however, a log unit difference in LogD is predicted.



	342	343	344	345
LogD7.4	-0.7	-0.9	-0.9	-0.6
pKa N1	4.4	4.3	5.4	5.1



	10	346	347	348
LogD7.4	+0.2	+1.2	+1.2	0.7
pKa N1	5.6	5.6	3.9	6.1

Table 5.3 – Compounds designed to replace the quinazoline core and test the hypothesis that changing the pKa of N1, the LogD or the electronics of the quinazoline ring could affect potency. LogD and PKa calculations shown were performed with MOKA.

A frequently used strategy in medicinal chemistry is to identify a pharmacophore and to simplify the molecule as much as possible to improve the ligand efficiency. The effect of the phenyl ring of the quinazoline was investigated with a series of pyrimidines which are simplified versions of the quinazoline core (Figure 5.4). Designs included the removal of the phenyl ring **349**, reduction of

the phenyl ring **350**, substitution on the pyrimidine ring **351-353** and introduction of a pendant phenyl **354** in place of the fused phenyl of the quinazoline. Thiophene is an aromatic ring that is similar in size to a phenyl ring.¹²⁹ Two thienopyrimidines **355** and **356** were designed as the closest analogues to the original quinazoline **10**.

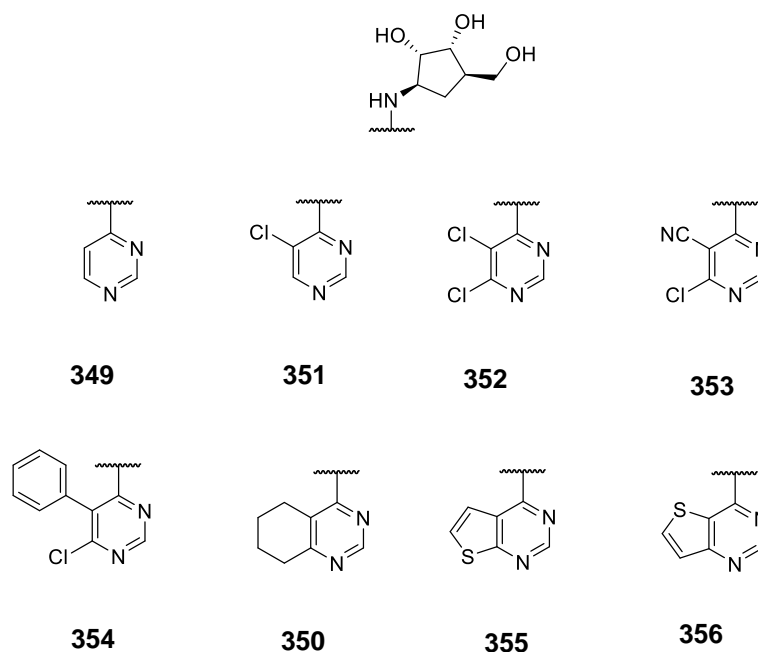


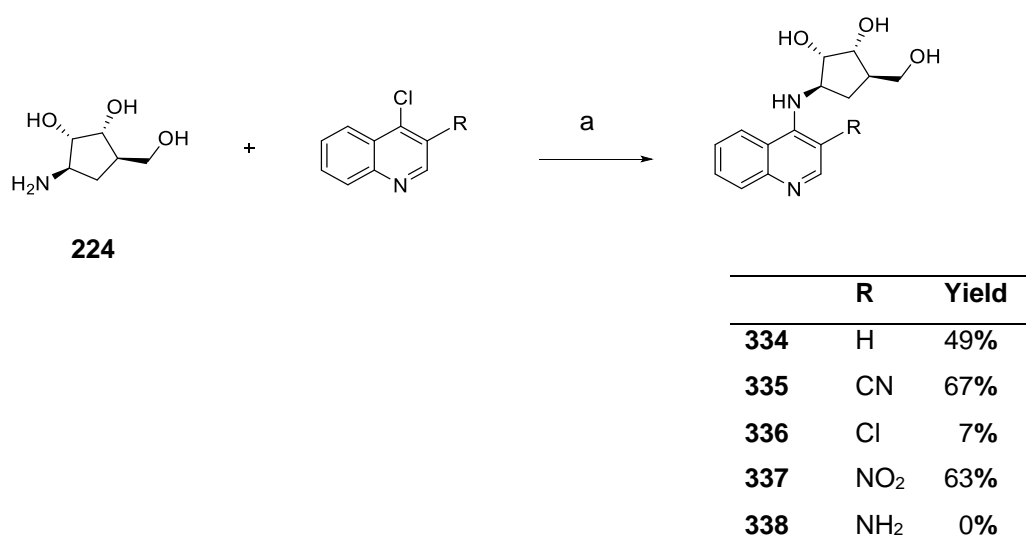
Figure 5.4 – Design of compounds that investigate the effect of the phenyl ring of the quinazoline core.

5.2.2 Synthesis of quinazoline replacements

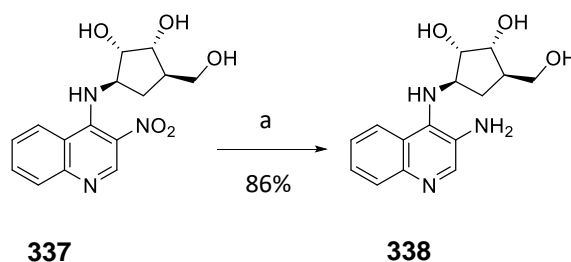
5.2.2.1 Synthesis of quinoline and cinnoline cores

Attaching the carbocycle to the quinazoline core was carried out using pyBOP coupling. For cinnoline or quinoline cores, however, there is no literature precedent for using BOP coupling reagents so S_NAr was investigated instead. A trial reaction with 4-chloro quinoline in the microwave at 120 °C gave just 5% conversion to **334**. Thermally heating the same starting materials at 120 °C for 48 h resulted in almost complete conversion. Compounds **335-337** were also synthesised by S_NAr (Scheme 5.1). In general, the reaction went quickly and cleanly for the 3-cyano **335** and 3-nitro **337** quinolines, as the electron

withdrawing groups encourage the S_NAr . For **336**, the 3-chloro quinoline was slower to react. After heating at 120 °C for 18 hours multiple peaks including the starting material were observed by LC-MS. Attempts to purify by reverse phase and normal phase column chromatography were unsuccessful. The reaction was repeated in NMP, heating in the MW for 3.5 h at 120 °C which gave 50% conversion with a cleaner profile. Purification by normal phase followed by acidic ion exchange chromatography was very low yielding. The 3-amino quinoline **338** was not reactive for enough S_NAr and was instead synthesised via reduction of the 3-nitro quinoline **337** (Scheme 5.2).



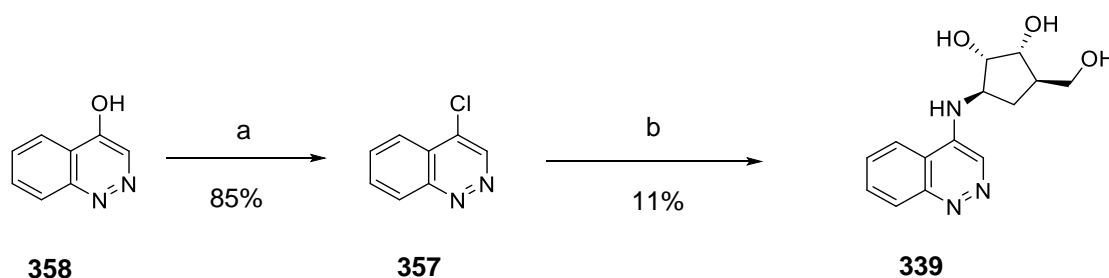
Scheme 5.1 – Synthesis of quinolines as quinazoline replacements (a) DIPEA, DMSO, 120 °C.



Scheme 5.2 – Synthesis of 3-amino quinoline (a) Pd/C, H₂, EtOH, 3 bar, rt, 18 h.

For the cinnoline core the required 4-chloro cinnoline **357** was first synthesised from the 4-hydroxy cinnoline **358** with POCl₃ followed by S_NAr with the ribose

mimic **224** (Scheme 5.3). This coupling step was quite low yielding (7%) and required multiple purification steps (reverse phase column chromatography, acidic ion exchange chromatography and normal phase column chromatography). The reaction was repeated with a different sequence of purification steps (normal phase column chromatography followed by acidic ion exchange chromatography) which gave a similar yield. The second batch of compound **339** had an identical LCMS to the first batch but a different NMR (Figure 5.5). Addition of DCI to the second batch gave an identical NMR to the first, which is likely the HCl salt.



Scheme 5.3 – Synthesis of cinnoline replacements. (a) POCl_3 , 100 °C, 3 h. (b) **224**, DMSO, DIPEA, 120 °C, 48 h.

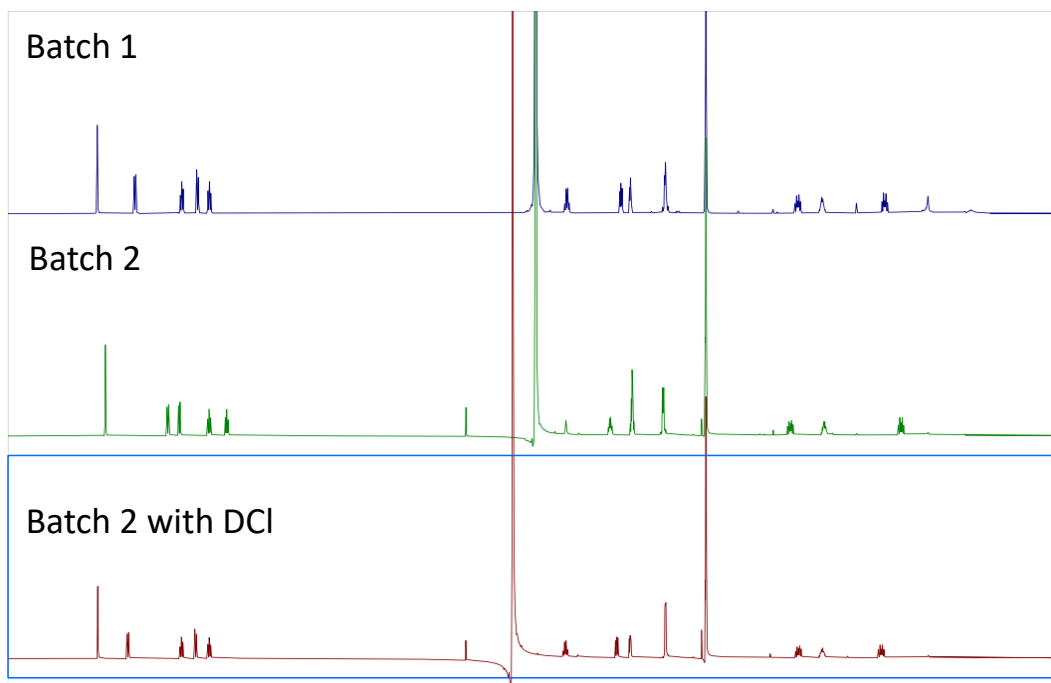
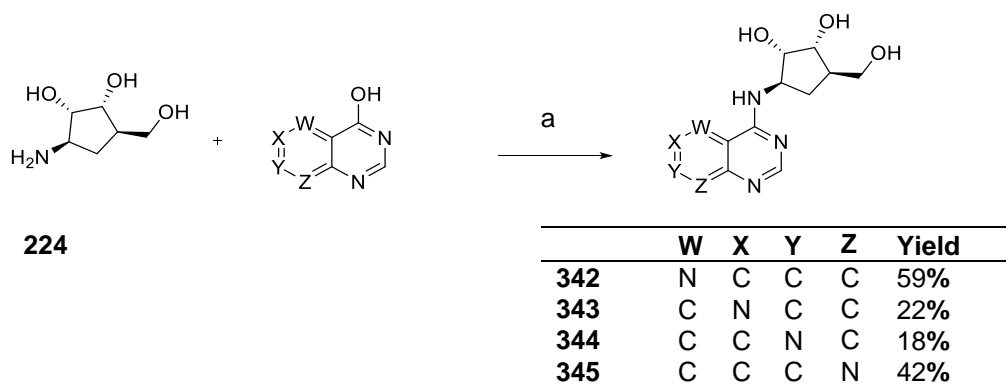


Figure 5.5 – Addition of DCI to batch 2 of compound **339** gave an identical NMR to batch 1.

5.2.2.2 Synthesis of naphthyridines

Four similar reactions were carried out to investigate the effect of introducing an extra nitrogen to the quinazoline core (Scheme 5.4). Synthesis of naphthyridines with the nitrogen in the 5 and 8 positions worked well with the products **342** and **345** isolated cleanly by precipitation. For naphthyridines with the nitrogen in the 6 or 7 positions, however, no precipitate formed. For **344** the product co-eluted with an impurity after column chromatography not present in the crude mixture despite large differences in retention time on the LC-MS. Ion exchange chromatography did not separate the two compounds. Reverse phase column chromatography gave two clean fractions but in a lower overall yield compared to products isolated by precipitation. For the 6-N naphthyridine the reaction was quenched with water, washed with DCM and acidic ion exchange chromatography of the water layer gave the desired product **343**.

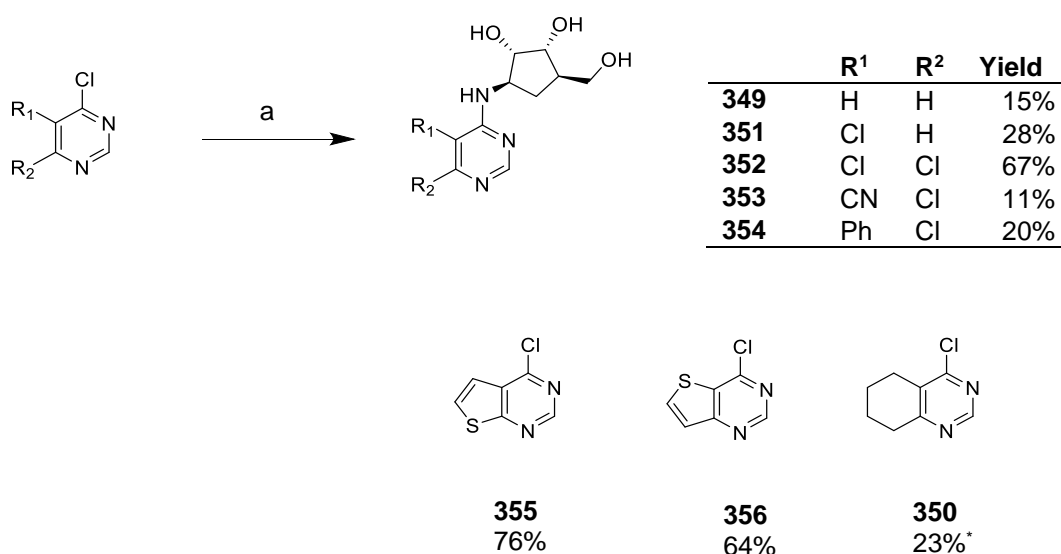


Scheme 5.4 – Synthesis of naphthyridines. (a) DBU, PyBOP, MeCN, rt, 4 h.

5.2.2.3 Synthesis of pyrimidines

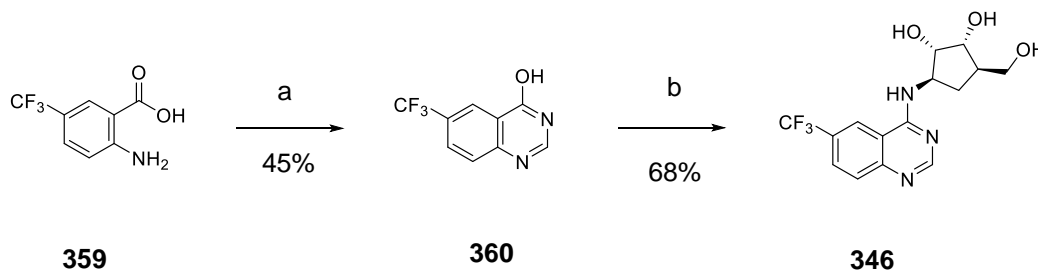
For the unsubstituted pyrimidine **349** synthesis was initially attempted via PyBOP coupling with the 4-hydroxy pyrimidine but after multiple purifications by column chromatography the product, which is highly polar, was not pure. Synthesis by S_NAr using 4-chloro pyrimidine as the starting material and purification with NH_3 in MeOH in DCM followed by anionic ion exchange

chromatography gave a small amount of pure product (Scheme 5.5). The remaining compounds **351-356** were synthesised by S_NAr . Reactions for **351**, **355** and **356** all went to completion and purified well by reverse phase chromatography. The remaining compounds were difficult to purify, requiring multiple purification methods. The reaction for **350** in particular was very slow. Increasing the reaction time from one to five hours gave just 50% conversion by LC-MS. When the temperature was increased to 180 °C multiple peaks were observed after one hour. Heating in the microwave at 120 °C for six hours gave an acceptable yield.



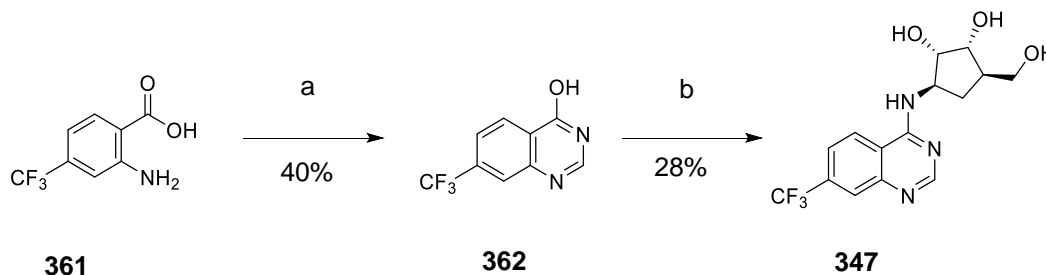
Scheme 5.5 – Synthesis of alternative cores (a) **224**, DIPEA, DMSO, 1 h, 120 °C. *6 h, MW.

Synthesis of 6-CF₃ quinazoline **346** was achieved using a Niementowski reaction with the CF₃ substituted anthranilic acid **359** to form intermediate **360** followed by PyBOP coupling to install the ribose mimic (Scheme 5.6). Acidic ion exchange chromatography was attempted but both the product **346** and the impurities were retained by the column. The product was instead purified by reverse phase column chromatography.



Scheme 5.6 – (a) Formamidine acetate, 2-methoxyethanol, 120 °C, 18 h (b) **224**, DIPEA, PyBOP, DMF, rt, 4 h.

Synthesis of 7- CF_3 quinazoline **347** was achieved using a Niementowski reaction with the CF_3 substituted anthranilic acid **361** to form intermediate **362**, followed by PyBOP coupling (Scheme 5.7). In contrast to **346**, **347** was separated from impurities by acidic ion exchange chromatography which were retained by the column. 6- CF_3 **346** and 7- CF_3 **347** quinazolines are predicted to have the same LogD but a 1.5 log unit difference in pKa. This pKa difference was observed experimentally as only 6- CF_3 **346** was retained with an acidic ion exchange column.



Scheme 5.7 – (a) Formamidine acetate, 2-methoxyethanol, 120 °C, 18 h (b) **224**, DIPEA, PyBOP, DMF, rt, 4 h.

5.2.2.4 SPR testing of quinazoline replacements

Compounds designed to replace the quinazoline ring were tested by SPR (Table 5.4). Replacing the quinazoline ring with a cinnoline **339** or quinoline **334** is not tolerated possibly because of the loss of the hydrogen bond to the conserved water molecule in the back pocket, shown in Figure 5.2. Interestingly this potency can be regained by substitution at the 3 position with a cyano, chloro or nitro substituents (**335-337**). The cyano and nitro groups may be mimicking the conserved water molecule. **335** maintains potency despite a calculated LogD drop of one log unit in comparison to the parent compound **10**. Not all substituted quinolines were able to regain potency as the change to a 3-amino group **338** was not tolerated.

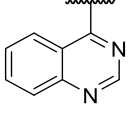
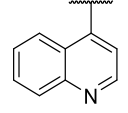
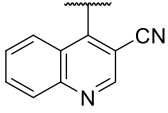
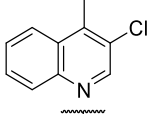
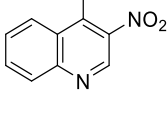
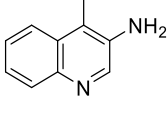
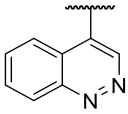
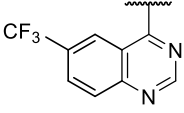
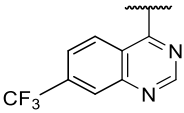
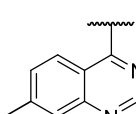
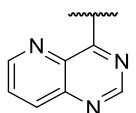
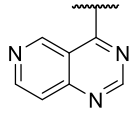
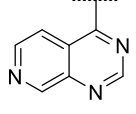
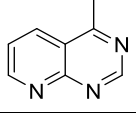
Naphthyridines **342-345** are less potent than the parent compound **10**. All four compounds are predicted to have a lower LogD and are also more electron deficient than **10** which may explain this overall trend. It was hypothesised that the pKa of the N1 and therefore its ability to form the anchoring hydrogen bonding interaction with S275, could vary depending on the position of the nitrogen in the naphthyridine ring. From SPR testing of **342-345** there is no evidence of this as **342**, the compound with the lowest predicted pKa is at least equipotent to **344**, the compound with a predicted pKa of one log unit higher.

6-CF₃ **346** and 7-CF₃ **347** are predicted to have the same LogD, however, the pKa of the N1 is calculated to be more than a log unit lower for the 7-CF₃. 7-CF₃ **347** was inactive. In contrast the potency measured for 6-CF₃ **346** was 410 μM. Theoretically a decrease in the pKa of this nitrogen decreases the basicity and makes it a less effective HBA which may explain the potency difference for these two compounds.

A comparison between the matched pairs 7-CF₃ **347** and 7-Me **348** shows that the EDG is tolerated but the EWG is not. Although a CF₃ is larger than a methyl group it is unlikely that steric clash is the reason for this decrease in potency as much larger groups have since been tolerated at this position (Section 5.5). This

suggests that an electron deficient aromatic ring is not favoured here, which was also observed with the naphthyridines **342-345**. Examination of the X-ray crystal structure shows the residue beneath the ring is an arginine. A stronger interaction is expected between the positively charged, protonated arginine and an electron rich ring rather than an electron deficient ring.

The effect of the phenyl ring of the quinazoline core was investigated with a series of pyrimidines and thienopyrimidines **349-356**. Removal of the phenyl ring **349** or reduction of the phenyl ring **350** was not tolerated. Mono or di-substitution on the pyrimidine ring was not sufficient to regain potency with the analogues tested **351-354**. However, the two thienopyrimidines **355** and **356** which were designed as the closest analogues to the original quinazoline **10** have equipotent or improved potency. Thiophenes have been used as a bioisotere of phenyl groups because they maintain the steric bulk, pi-electron cloud and planar structure of a phenyl ring but are more polar than phenyl groups (log P benzene = 2.15, thiophene = 1.81).¹²⁹ In the investigation of replacements for the quinazoline core the thienopyrimidines **355** and **356** are the most successful analogues tested.

Compound	Structure	LogD7.4	pKa N1	SPR K _D
10		0.2	5.6	310 μ M
334		-0.7	8.8	>1 mM
335		-1.2	8.6	175 μ M
336		0.65	7.3	289 μ M
337		0.11	5	190 μ M
338		-2.2	9.1	>1 mM
339		-0.3	3.5	>1 mM
346		1.2	5.6	410 μ M
347		1.2	3.9	>1 mM
348		0.7	6.1	320 μ M
342		-0.7	4.4	770 μ M
343		-0.9	4.3	>1 mM
344		-0.9	5.4	>1 mM
345		-0.6	5.1	920 μ M

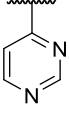
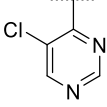
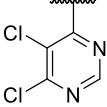
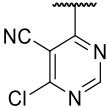
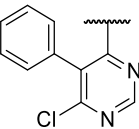
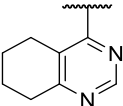
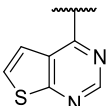
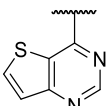
Compound	Structure	LogD7.4	pKa N1	SPR K _D
349		-0.9	5.4	No saturation
351		-0.5	4.5	No saturation
352		0.1	2.2	>1 mM
353		-0.8	0.2	No saturation
354		1.2	2.6	No saturation
350		0.2	6.2	inactive
355		0.5	5.1	150 μM
356		0.2	5.1	210 μM

Table 5.4 – SPR testing of quinazoline replacements (n = 1) with LogD and pKa predictions calculated using MOKA.

5.3 Substitution at the 5 position

5.3.1 Design at the 5 position

As discussed in Chapter 4, the 5-position of the quinazoline ring had been explored more extensively than any other position around the ring. Based on the SPR results of **226** further analogues were designed to potentially make new interactions with nearby water molecules or polar amino acids (**363-366**, Figure 5.6). The regiochemistry of the pyridyl had not been explored. Pyrimidine **363** and pyrazine **364** have an additional hydrogen bond acceptor. A model of **364**

shows the residue T17 is a hydrogen bond donor in close proximity to the pyrazine 4-nitrogen (Figure 5.7 A). In order to move an HBA closer to this T17 residue, substitution at the 4-position was examined. After searching for compounds with an HBA in this position that would be synthetically feasible the 4-methoxy pyridine **366** was chosen to test this hypothesis (Figure 5.7 B). **366** was designed as a potentially more ligand efficient analogue, exchanging a six membered ring for a five membered ring.

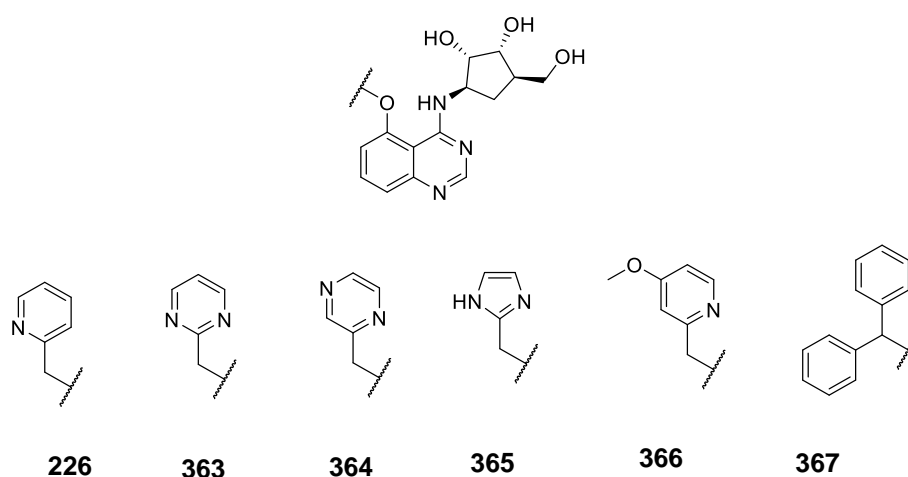


Figure 5.6 – Designs at the 5 position of the quinazoline ring based on **226**.

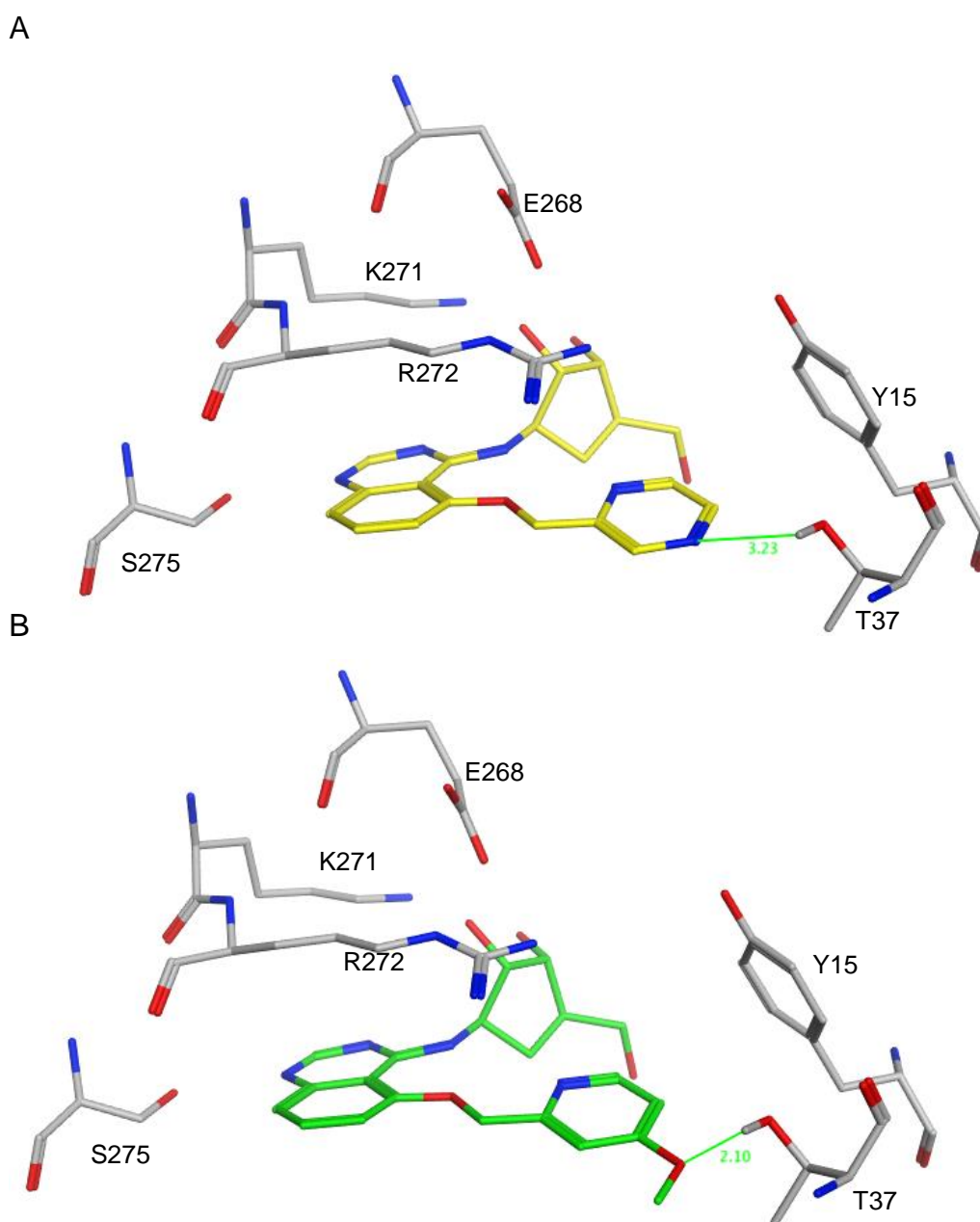


Figure 5.7 – (a) Model of **364** with HSP72-NBD placing an HBA close to T37. (b) Model of **366** with HSP72-NBD placing an HBA close to T37. Distances were measured with MOE.

Compound **367** was designed to explore the pocket size in a similar way to the known HSP70 inhibitor VER-155008 while keeping the 5-O benzyl substituent of **225**. VER-155008 stabilises the open conformation of HSP72.⁴⁹ The new phenyl substituent of **367** is modelled in a similar position as the dichlorophenyl of VER-155008 (Figure 5.8).

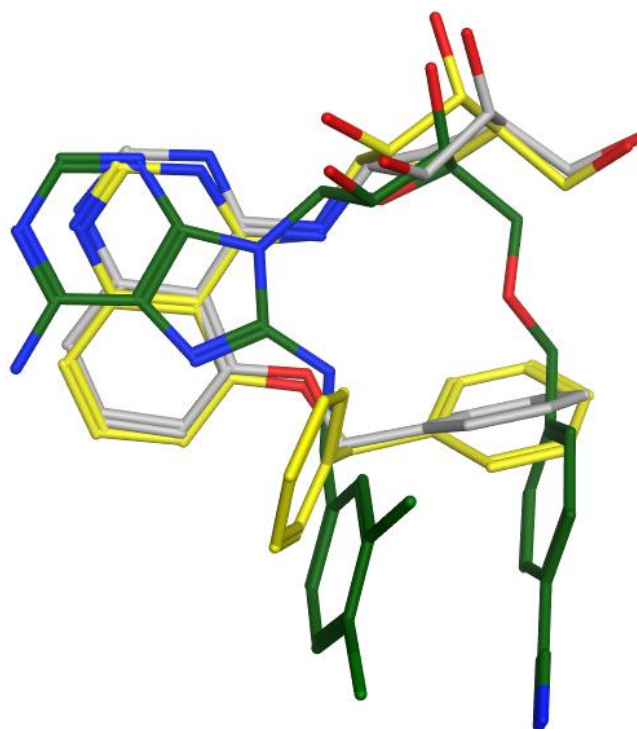
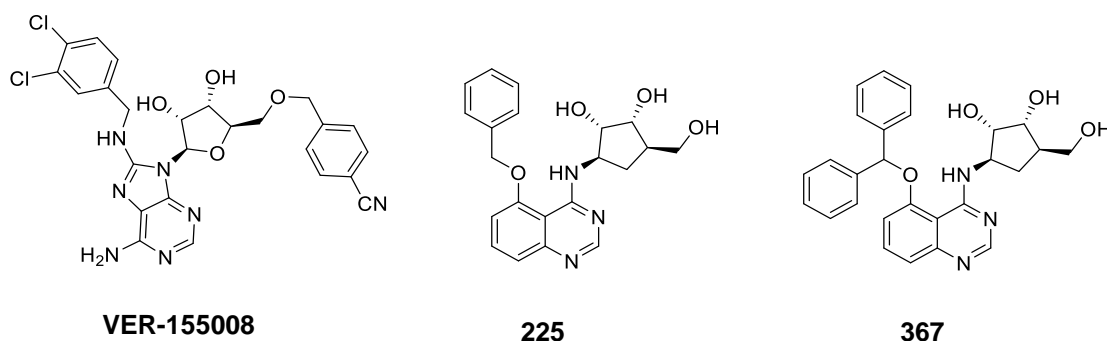
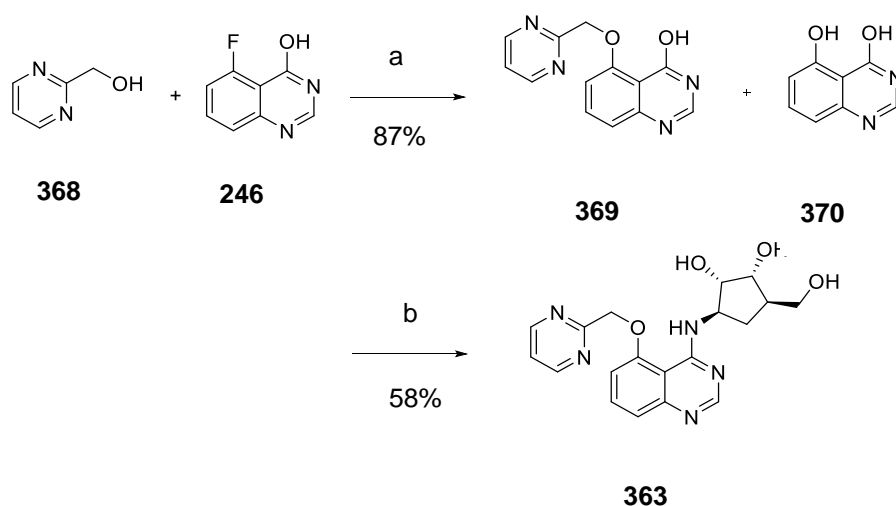


Figure 5.8 – (a) Overlay of X-ray crystal structures of **225** (grey; PDB ID 5AQX) with VER-155008 (green; PDB ID 4IO8) led to the design idea of **367** (yellow, model built from 5AQX and minimised in MOE) which places a second benzyl ring in a similar position as the dichlorophenyl of VER-155008.

5.3.2 Synthesis at the 5 position

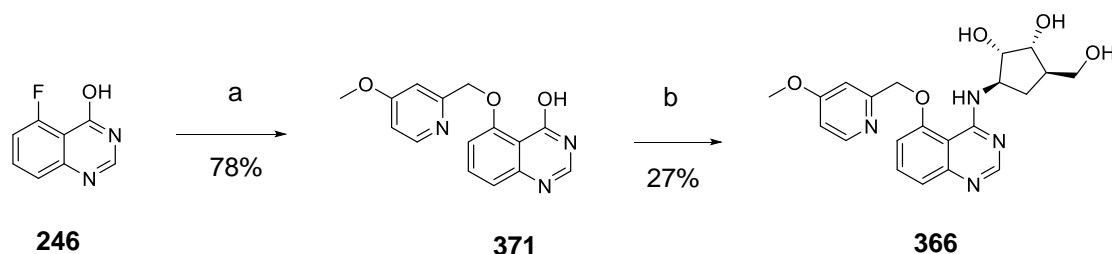
The reaction of pyrimidine methyl alcohol **368** with quinazoline **246** was highly variable, with yields varying from 0% to 87% with the side product quinazoline-4,5-diol **370** often observed (Scheme 5.8). Best results were achieved with a freshly opened bottle of **368**, stored in the freezer. The product was highly water

soluble and remained in the aqueous layer after an aqueous work-up. The most effective purification method was filtration of the precipitate from the DMSO reaction mixture. PyBOP coupling installed the ribose mimic **224** and acidic ion exchange chromatography removed the hydroxy benzotriazole impurity. Further purification by column chromatography gave the desired product **363**.



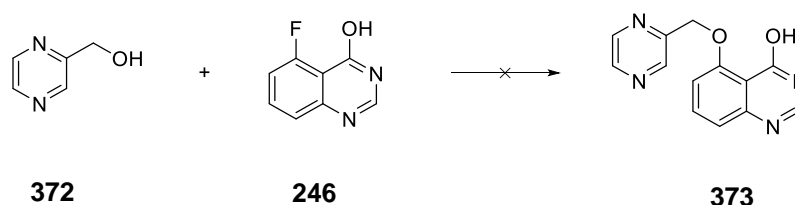
Scheme 5.8 – (a) NaH, DMSO, 50 °C, 24 h (b) **224**, PyBOP, DBU, MeCN, rt, 18 h.

Methoxy pyridine **366** was synthesised and purified in a similar manner to pyrimidine **363** (Scheme 5.9). The S_NAr worked well and the product was precipitated with water. The solvent for the PyBOP coupling was changed from acetonitrile to DMF to dissolve the starting materials. Purification by acidic ion exchange chromatography and two reverse phase columns were necessary, resulting in a lower yield.



Scheme 5.9 – (a) (4-methoxyphenyl)methanol, NaH, DMSO, 50 °C, 6 h (b) PyBOP, DBU, DMF, rt, 5 h.

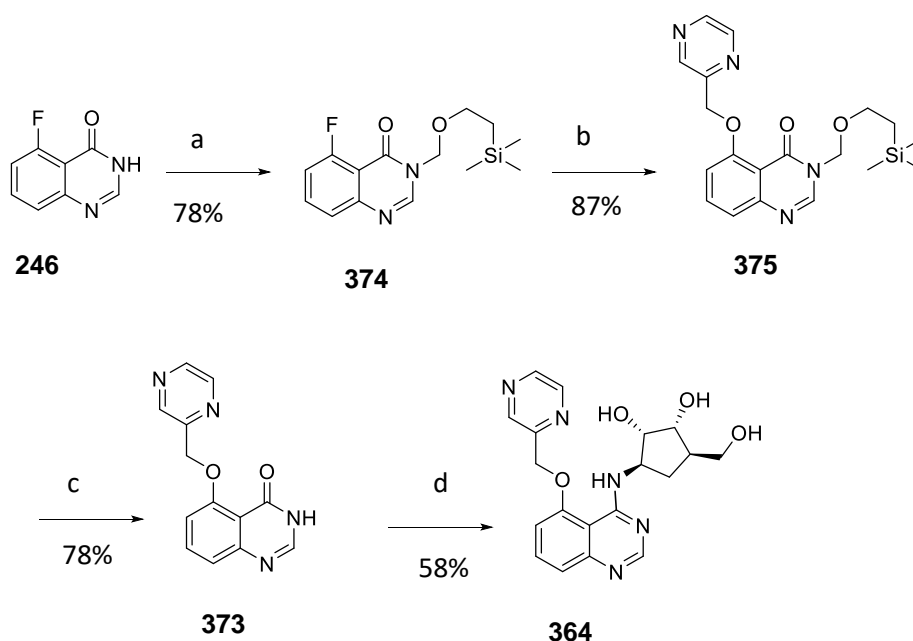
For pyrazine **364** the S_NAr with **246** was attempted following the same procedure as for **369** and **371**, however, no desired mass ion was observed by LC-MS. The experiment was repeated for a range of different bases, solvents, times and temperatures but no desired product was observed for any of the conditions trialled (Table 5.5).



Base	Solvent	Temp.	Time	Result
NaH	DMSO	50 °C	24 h	SM and 370 observed
NaH	DMSO	50 °C	24 h	SM ^a and 370 observed
K ₂ CO ₃	DMF	80 °C	24 h	Only SM observed
K ₂ CO ₃	DMF	120 °C	6 h	Only SM observed
K ₂ CO ₃	DMF	140 °C	18 h	Only SM observed
DIPEA	DMF	90 °C	3 h MW	Only SM observed
DIPEA	DMF	150 °C	3 h MW	Only SM observed
DIPEA	DMF	200 °C	2 h MW	Only SM observed
DIPEA	DMF	240 °C	2 h MW	New peak observed by LC-MS Isolated by chromatography, not desired product.
K ⁺ ^t OBu ⁻	THF	50 °C	24 h	Only SM observed

Table 5.5 – Screen of reaction conditions for the synthesis of **373** from **246**. SM is starting material. ^a**372** was dried with MgSO₄ prior to the reaction.

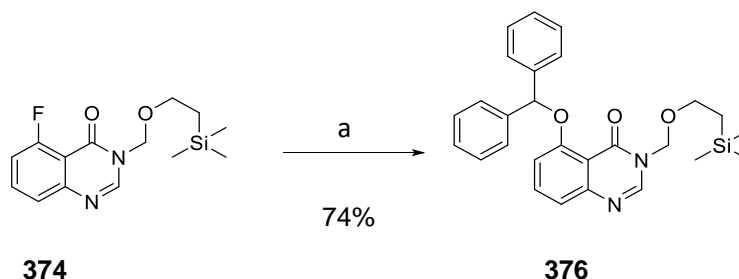
The quinazoline **246** was protected with a SEM group by following a similar literature procedure¹³⁰ in order to increase the susceptibility of the quinazoline ring to nucleophilic attack (Scheme 5.10). After 45 minutes 60% of the desired protected quinazoline **374** was observed by LC-MS. Heating for a further hour gave no increase in product. This reaction was optimised as longer reaction times and higher temperatures gave increasing amounts of a side product. Purification with an aqueous work-up followed by column chromatography gave a good yield of **374**. The S_NAr with **372** proceeded in good yields with the SEM protected quinazoline **374** in contrast to the reaction with the unprotected quinazoline **246**. The product **375** has same retention time as the quinazoline starting material **374** by LC-MS so the reaction was instead followed by TLC. The deprotection of **375** was achieved with TBAF. The ribose mimic was attached by PyBOP coupling and the product **364** was isolated by precipitation.



Scheme 5.10 - (a) SEM-Cl, NaH, DMF, 40 °C, 40 min. (b) **372**, NaH, THF, 40 °C, 5 h (c) TBAF, THF, 60 °C, 18 h (d) PyBOP, DBU, DMF, rt, 18 h.

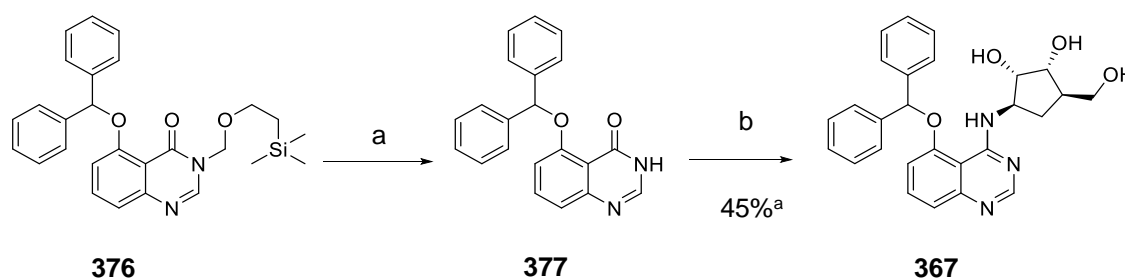
For the diphenyl **367** the S_NAr conditions used for the synthesis of **369** and **371** were attempted but the reaction proceeded very slowly and after two days the reaction mixture was predominantly starting material. S_NAr with the SEM

protected quinazoline **374** was much more successful but the purification required optimisation. The initial yield of 25% isolated by reverse phase column chromatography was increased to 74% using an aqueous work-up followed by normal phase column chromatography (Scheme 5.11).



Scheme 5.11 – (a) Diphenylmethanol, NaH, DMF, rt, 2 h.

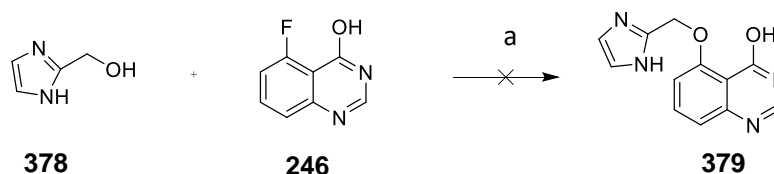
For the removal of the SEM protecting group **376** was treated with HCl in dioxane for one hour but this resulted in the loss of the diphenylmethanol group and no SEM deprotection was observed. Treatment with TBAF gave the desired deprotected product but the TBA impurity observed by NMR was difficult to remove and was therefore removed in the next step. PyBOP coupling gave the desired final product **367** (Scheme 5.12).



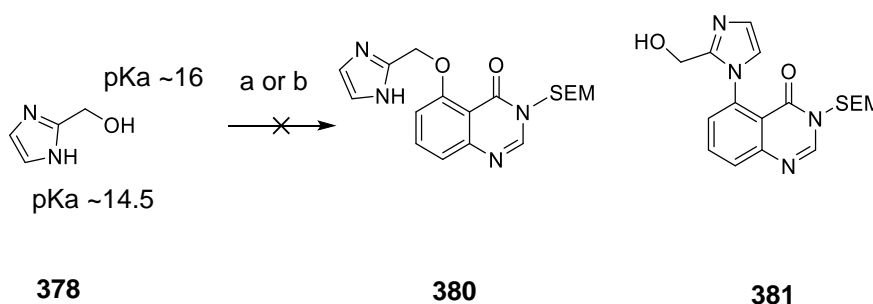
Scheme 5.12 – (a) 1 M TBAF, THF, 60 °C, 18 h (b) **224**, PyBOP, DBU, DMF, rt, 4 h. ^a yield calculated over 2 steps.

For the imidazole **365** the S_NAr conditions used to synthesise **369** and **371** were attempted but no product was observed by LC-MS (Scheme 5.13). S_NAr was then attempted with SEM protected quinazoline **374** and the imidazole methyl alcohol **378**. **378** has two nucleophilic atoms but it should be possible to attack

via the alcohol rather than the imidazole nitrogen if both are deprotonated because theoretically the anion that is formed last reacts first.¹³¹ Two equivalents of sodium hydride were used to first deprotonate the imidazole nitrogen (pKa 14.5) and then the alcohol (pKa ~16) (Scheme 5.14).

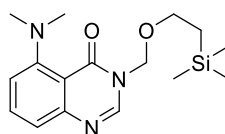


Scheme 5.13 – (a) NaH, DMF, rt, 2 h.

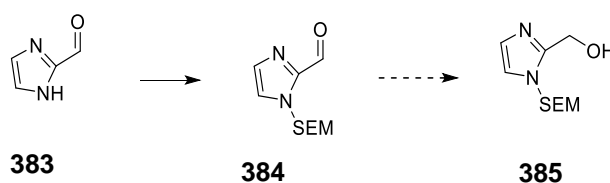


Scheme 5.14 – (a) **374**, NaH, DMF, rt, 24 h (b) **374**, NaH, DMSO, rt, 18 h, 40 °C, 18 h.

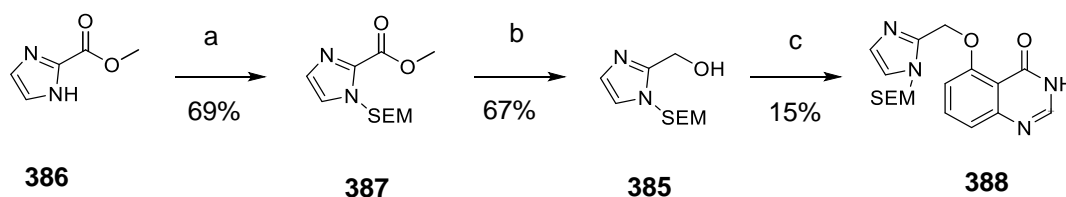
Imidazole methyl alcohol **378** was treated with two equivalents of sodium hydride and added to SEM protected quinazolinone **374**. After 48 hours one new peak was observed by LC-MS but this peak did not correspond to either of the expected products **380** or **381**. This product was isolated by reverse phase column chromatography to determine the major product of the reaction. The mass ion observed by LC-MS corresponds to **382** which could occur from DMF decomposition (Figure 5.9). NMR analysis showed two peaks at 3 ppm in the aliphatic region integrating for six protons, which correspond to the two methyl groups. Therefore, the solvent was changed from DMF to DMSO and the temperature was increased but no desired product formed under these conditions (Scheme 5.14 b).

**382****Figure 5.9** – Side product from Scheme 5.14 a.

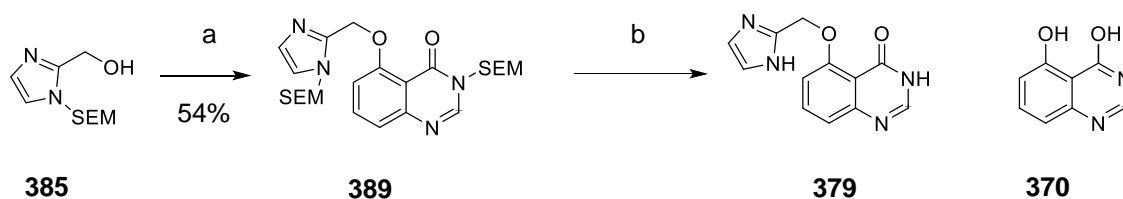
An alternative route was designed to protect the imidazole nitrogen before the S_NAr . (Scheme 5.15). Following a literature procedure¹³⁰ that describes the synthesis of SEM protected alcohol **385**, **383** was treated with SEM-Cl but no desired aldehyde **384** was observed by NMR. NMR analysis of the starting material **383** showed it was impure. The material was purchased from three separate suppliers but was found to be impure in each case and is likely to be unstable.

**Scheme 5.15** – (a) NaH, DMF, rt, 18 h.

The synthesis was therefore attempted with the ester **386**, a more stable alternative to aldehyde **383**. **386** was SEM protected and then reduced with lithium aluminium hydride to the desired alcohol **385** (Scheme 5.16). S_NAr with quinazoline **246** was very slow and after 48 hours 15% product was isolated.

**Scheme 5.16** – (a) NaH, DMF, rt, 1 h. (b) LiAlH₄, THF, rt, 2 h. (c) NaH, **246**, DMSO, 50 °C, 48 h.

S_NAr with SEM protected quinazoline **374** was much faster, with no starting material detected after 1.5 hours (Scheme 5.17). Deprotection with TBAF, which had been used successfully for pyrazine **373** and diphenyl **377** surprisingly formed multiple products, including the loss of the imidazole ring **370**. TBAF is a popular reagent because it is soluble in polar organic solvents and reactions are fast at room temperature. However, as well as being nucleophilic, TBAF is also very basic and is almost impossible to dehydrate entirely. Water in the presence of fluoride generates hydroxide, which may act as a nucleophile forming hydroxy products. TBAT **390** is less nucleophilic and less basic than TBAF and importantly TBAT is not hygroscopic and is available as an anhydrous salt (Figure 5.10).¹³² Deprotection with TBAT was therefore attempted (Scheme 5.17 c). Various conditions were trialed but no conditions were found that removed both SEM protecting groups while leaving the imidazole ring intact.



Scheme 5.17 – (a) **374**, NaH, THF, 40 °C, 1.5 h. (b) TBAF, THF, 60 °C, 18 h

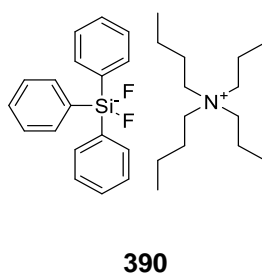


Figure 5.10 - TBAT - Tetrabutylammonium difluorotriphenylsilicate is an alternative to TBAF that is not hygroscopic.

5.3.3 SPR testing of 5 substituted quinazolines

Compounds **363**, **364**, **366** and **367** were tested by SPR (Figure 5.11). Pyrimidine **363**, increases the potency ten-fold over the benzyl analogue **225** and three-fold over the pyridine analogue **226**. Moving this nitrogen around the ring to pyrazine **364** also increases the potency to a similar degree. Methoxy **366** is approximately six-fold less potent than **364** suggesting that this substituent may be too large. Diphenyl **367** loses potency but is still tolerated. It is likely that both rings can be accommodated but this causes a conformational change in the protein that is unfavourable. Compound **391** had previously been synthesised by Alan Jones but not tested by SPR. This compound was tested now as a matched pair to **226**. This saturated analogue is five times less potent than the aromatic analogue suggesting the flat nitrogen containing aromatic rings are best suited here.

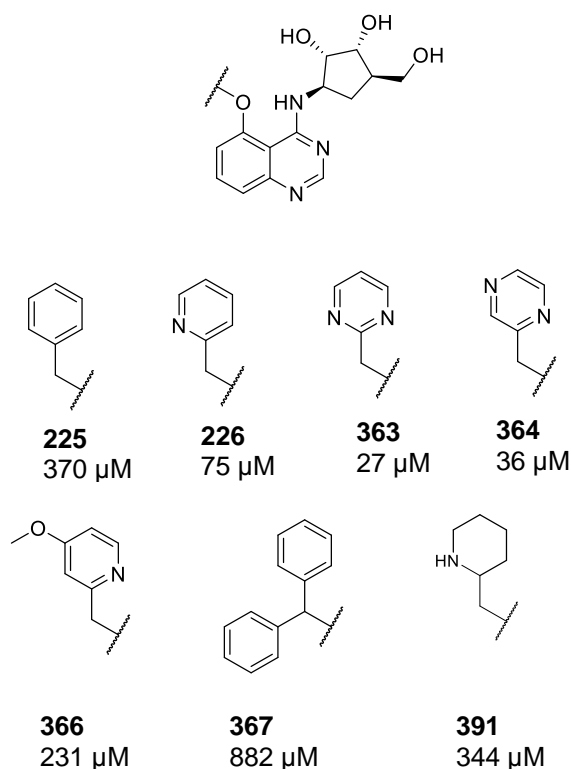


Figure 5.11 – Testing of compounds with substituents at the 5-position. Values shown are measured SPR K_D ($n = 1$).

The X-ray crystal structure of **363** with HSP72-NBD was solved by Marc Cabry at the ICR to try to explain this ten-fold increase in potency over **225** (Figure 5.12 B). No new interactions with the protein are observed. However, the pyrimidine ring of **363** sits differently to the benzene ring of **225** which changes the conformation of the R272 residue above the pocket. R272 is in the ‘up’ conformation for **225** but in the extended conformation for **363**. Unlike the phenyl ring, the pyrimidine ring is in the same plane as the quinazoline ring and this flat conformation binds to a more closed conformation of the ATP binding site. This conformation is more similar to the ADP bound form discussed in Chapter 4 which may explain the increase in potency observed for **363**. The pyrimidine ring is predicted to make internal hydrogen bonds that stabilise the more flat conformation (Figure 5.12 A). This pyrimidine ring also lies directly above D366 potentially forming an anion- π interaction¹³³ which may be another reason why the pyrimidine ring lies flat in contrast to the phenyl ring which is twisted.

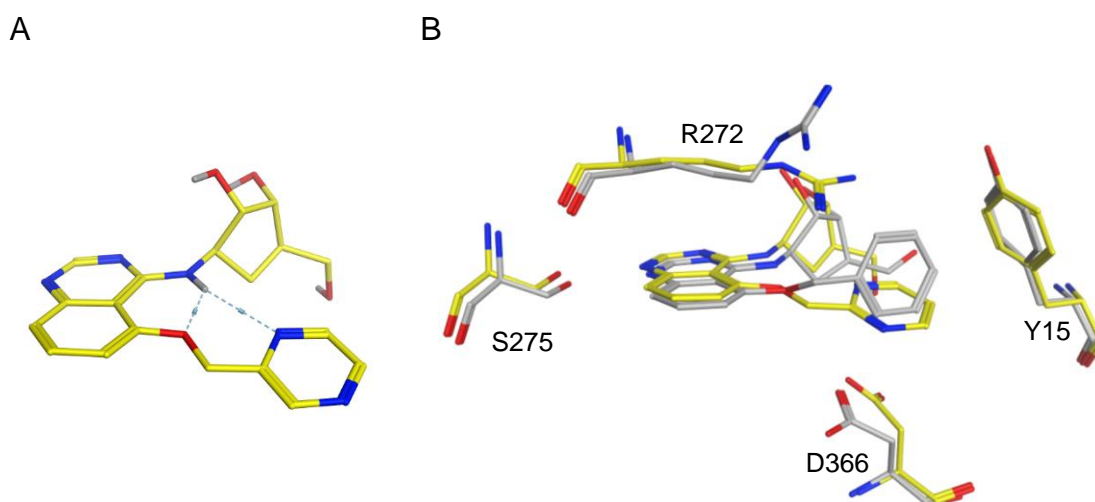


Figure 5.12 – (A) X-ray crystal structure of **363** bound to HSP72-NBD shows internal hydrogen bonds are formed. (B) X-ray crystal structures of **363** (yellow) and **225** (grey) show R272 in different conformations, likely due to the different conformation of the aromatic rings.

5.4 Substitution at the 7 position

5.4.1 Design at the 7 position

As discussed in Chapter 4, the calculated LogD for the quinazoline series was lower than desired. Designs to increase the LogD included the addition of lipophilic groups at positions that would be tolerated. Chapter 4 described alpha substitution of the hydroxyacetamides with hydrophobic groups but this was not tolerated. Substitution at the 7-position with hydrophobic groups, if tolerated, could be a good opportunity to achieve this increase in lipophilicity. The 7-Me **327** was found to be the most ligand efficient quinazoline fragment studied (Table 5.1). A variety of aromatic rings was designed at the 7-position (Figure 5.13).

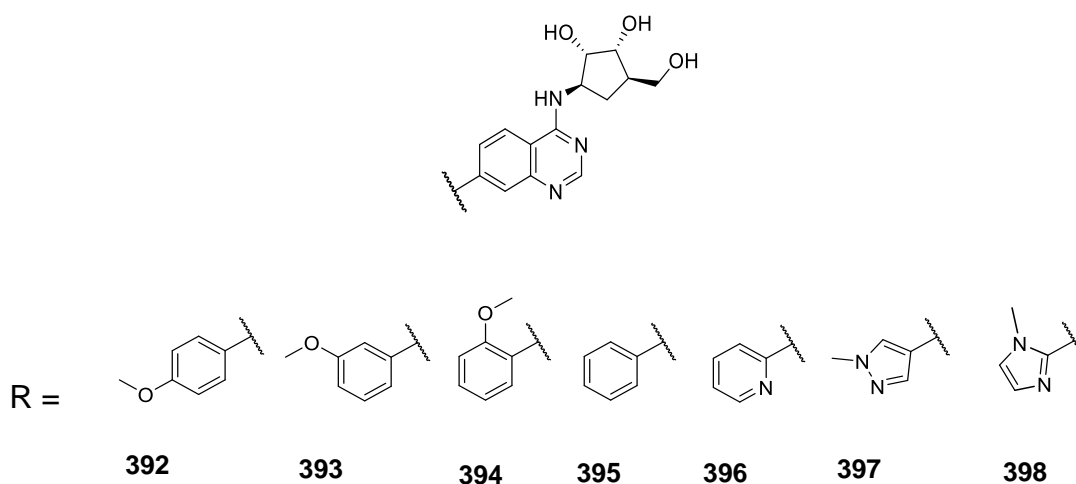


Figure 5.13 – Designs which add aromatic rings to the 7-position to increase lipophilicity.

The five membered ring **397** and the pyridine ring **396** would be expected to lie in the same plane as the quinazoline ring. The phenyl **395** and methoxy phenyls **392-394** would be expected to be in a twisted conformation. The calculated conformational energy profile (CEP) for a biphenyl ring displays an energy minimum at 40° to avoid a steric clash between the ortho hydrogens (Figure 5.14).¹³⁴ The CEP of 2-phenylpyridine displays energy minima at 0° and 180° likely due to a decrease in the steric interaction between the rings because of the elimination of one hydrogen-hydrogen interaction. As a result, the energy

minima are the planar rotamers. The CEP of 2-methylbiphenyl displays a destabilization of the planar conformation relative to biphenyl. As substitution of the ortho positions increases, the energy of the planar conformations increases and the perpendicular conformations become more energetically favourable. For 1-phenylpyrazole the planar rotamer is the lowest energy conformation (Figure 5.14). This is likely a reflection of the loss of one non-bonding hydrogen-hydrogen interaction, analogous to the 2-phenylpyridine.

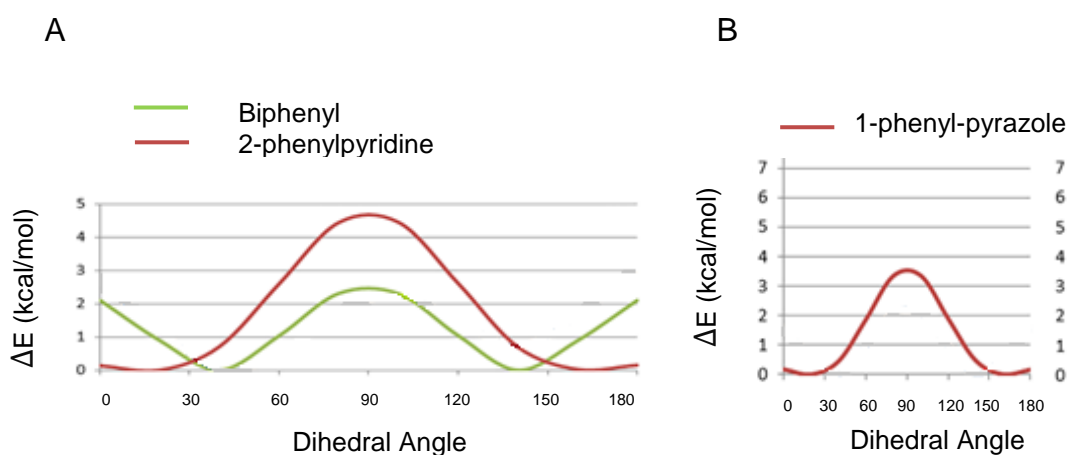


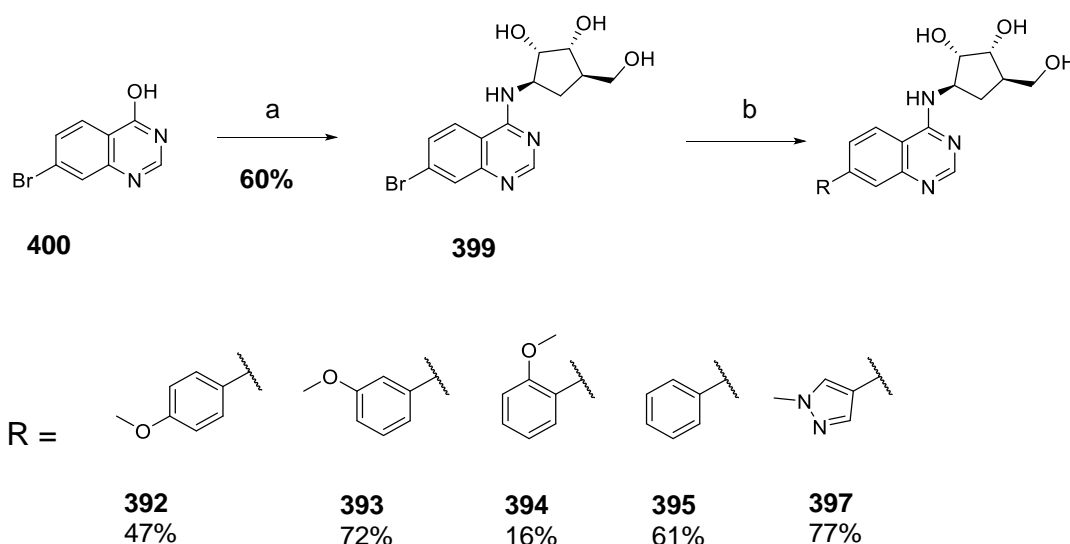
Figure 5.14 – The conformational energy profile calculated by gas phase simulation for (A) biphenyl, 2-phenylpyridine and 2-(2-methylphenyl)pyridine and (B) 1-phenyl-pyrazole. Figure adapted from Schaus *et al.*¹³⁴

5.4.2 Synthesis at the 7 position

Intermediate **399** was synthesised from the commercially available starting material 7-bromo-4-hydroxyquinazoline **400** (Scheme 5.18). This reaction gave good conversion by LC-MS. however, it was difficult to isolate the pure product by column or ion exchange chromatography. As this intermediate was required in large quantities, these conditions were optimised further. On a 300 mg scale the reaction mixture was allowed to cool in the fridge overnight and the resulting precipitate was filtered. NMR analysis showed the precipitate to be impure product. The reaction conditions were then modified. The starting materials were not completely soluble in acetonitrile and the DBU base is highly viscous. Changing the solvent to DMF and THF and the base to DIPEA dissolved the

starting materials completely. The reaction mixture was poured into water and the majority of the impurities were removed by washing with DCM. The product remained in the water layer with just one impurity which was removed by ion exchange chromatography to yield pure product **399** in good yield (60%).

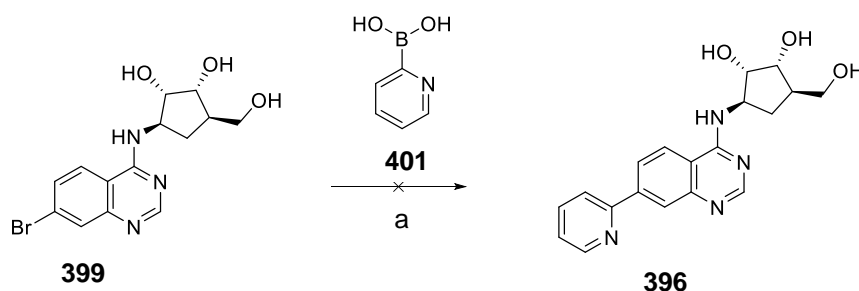
Trial Suzuki coupling reactions were carried out with the ribose mimic in place to determine if the coupling can occur with the unprotected triol **399**. Suzuki couplings with para methoxy phenyl boronic acid gave good conversion by LC-MS to the desired product **392** with Pd(PPh₃)₄. The success of this method meant that the remaining compounds **393-397** could be made in a single step from **400** by Suzuki coupling. In general, the reaction was reliable and proceeded in good yields (Scheme 5.18).



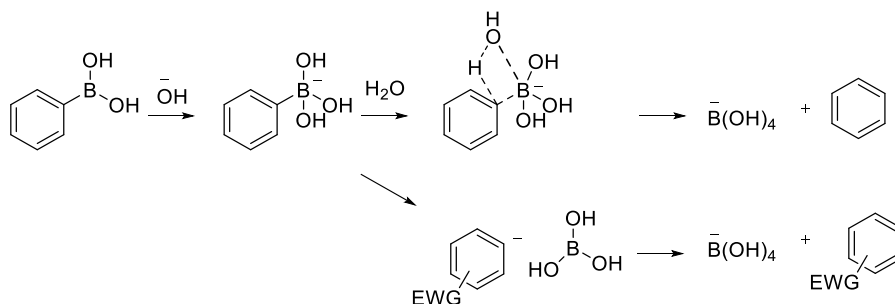
Scheme 5.18 – (a) **224**, PyBOP, DIPEA, DMF, THF, rt, 4 h. (b) R-B(OH)₂, Pd(PPh₃)₄, Na₂CO₃, dioxane, water, 120 °C, 1 h.

Suzuki coupling with **399** and 2-pyridine boronic acid **401** did not yield the desired product **396** (Scheme 5.19). This is a common problem with boronic acids with nitrogen in the 2 position as they can be unstable. 2-Heterocyclic, vinyl, and cyclopropyl boronic acids are known to decompose under air via protodeboronation or oxidation.¹³⁵ In addition, these processes are thought to be accelerated in the presence of heat, base, and/or a Pd catalyst, causing the *in*

situ decomposition of unstable boronic acids to compete with cross-coupling. The mechanism for base catalysed protodeboronation is shown in Scheme 5.20.

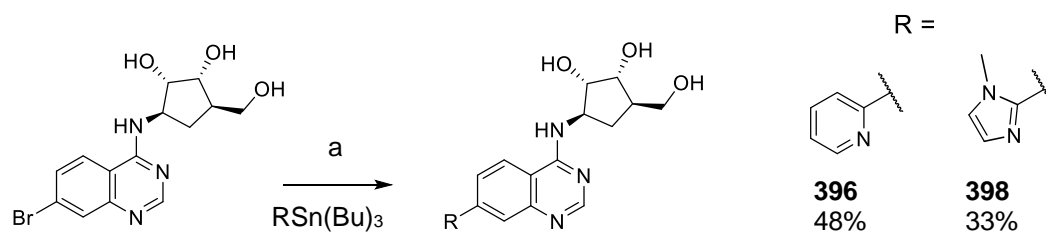


Scheme 5.19 – Suzuki coupling for the 2-pyridine **401** did not yield the desired product **396** most likely due to the instability of **401**.



Scheme 5.20 – Boronic acids with electron withdrawing groups are particularly unstable and can undergo decomposition via protodeboronation.¹³⁶

Compounds **396** and **398** were synthesised by Stille coupling from their respective stannanes (Scheme 5.21). For the methyl imidazole **398** optimisation of conditions was necessary because after multiple purification methods NMR analysis indicated that the methyl imidazole starting material was also present in a 1:1 mixture with the desired product. As it was very difficult to separate the two compounds, the reaction was repeated using less than one equivalent of the stannane to give pure product.



Scheme 5.21 – (a) Pd(Ph₃)₄, LiCl, DMF, MW, 120 °C, 2 h.

5.4.3 SPR testing of 7-substituted quinazolines

Compounds **392-398** and intermediate **399** were tested by SPR and compared to the matched pairs **10** and **348** (Table 5.6). Methyl pyrazole **397**, pyridine **396** and para-methoxy phenyl **392** increase the potency over the parent **398**. Bromo intermediate **399** and phenyl substituted **395** are less potent than **10** despite significant predicted LogD increases. Imidazole **398** is equipotent to **10** and has a similar predicted LogD. Methoxy substitution around the phenyl ring has varying effects with the order of potency para-methoxy phenyl > phenyl > meta-methoxy phenyl > ortho-methoxy phenyl. This sequence could be explained by the para methoxy either making a new interaction or that its electron donating effect is favourable. The ortho methoxy may clash with the protein or twist the phenyl ring into a different, less favourable conformation. Substituents which favour or disfavour the conformation required for binding to the target can have a significant impact on potency.¹³⁷ Biphenyl rings are often slightly twisted due to a clash between the ortho hydrogens. In contrast biaryls with nitrogen in the 2-position are often coplanar to give maximum orbital overlap and better conjugation of the pi systems. Similarly, smaller five membered rings such as **397** usually lie in a flatter conformation than 6, 6 ring systems. **397** and **396** would be expected to lie in the same plane as the quinazoline ring. These compounds are more potent than **395** and **394** which are likely in a twisted conformation.

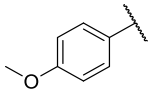
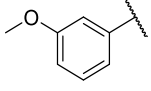
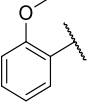
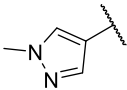
Structure	Compound	LogD	SPR K_D
	10	0.2	310 μM
	348	0.7	320 μM
	392	2.1	197 μM
	393	2.1	591 μM
	394	1.9	847 μM
	395	2.0	429 μM
	396	1.0	215 μM
	397	0.5	124 μM
	398	0.2	301 μM
	399	1.2	543 μM

Table 5.6 – Testing of 7-substituted quinazolines by SPR ($n = 1$).

5.5 Substitution at the 6 position

5.5.1 Design and synthesis at the 6 position

Analysis of the X-ray crystal structure of **10** shows the guanidine of R342 could potentially interact with aromatic rings substituted at the 6-position with a cation- π interaction (Figure 5.15 A). 6-phenyl **402** and 6-methyl pyrazole **403** compounds were designed to test this hypothesis (Figure 5.15 B).

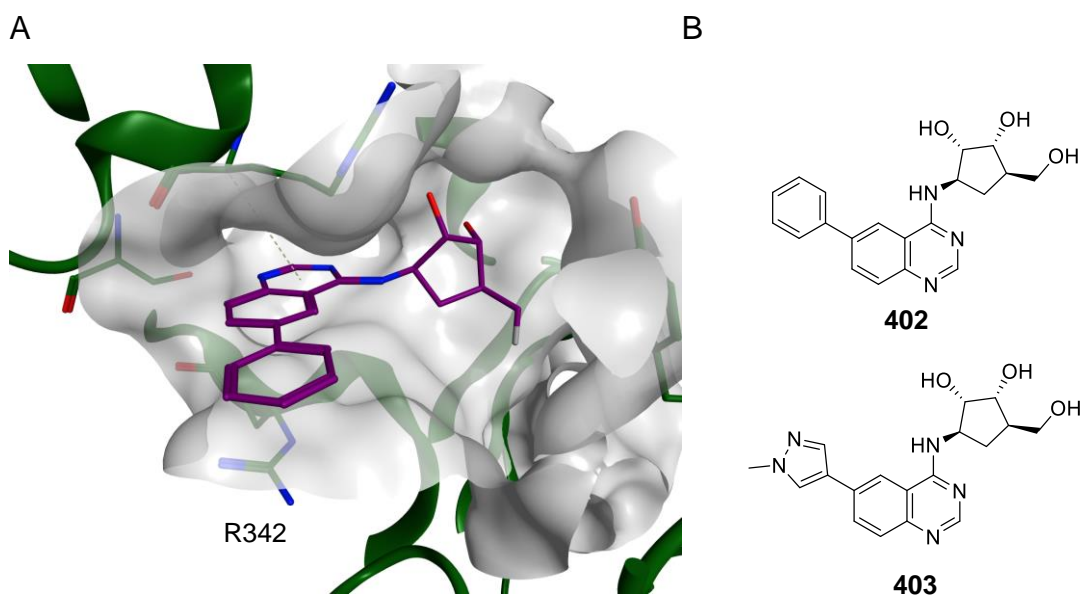
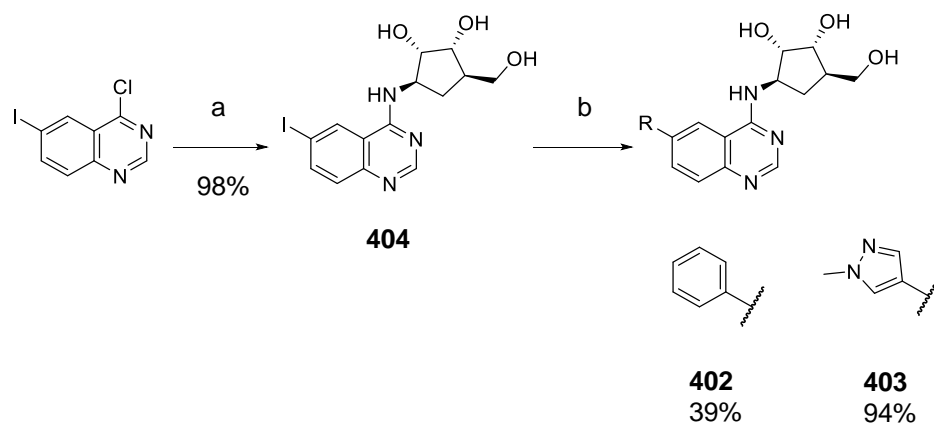


Figure 5.15 - Model built from the X-ray crystal structure of **10** bound to HSP72. (B) 6-phenyl **402** and 6-methyl pyrazole **403** compounds were designed to test the hypothesis that aromatic rings could potentially interact with R342.

In a similar way to the 7-substituted compounds, a route was designed with the ribose mimic in place so that the targets could be made in a single step from one intermediate. S_NAr with the commercially available 6-iodo, 4-chloro quinazoline gave the required intermediate **404** in excellent yields (Scheme 5.22). Purification was much more straightforward than for pyBOP coupling as there are fewer side products formed. Suzuki coupling proceeded well under standard conditions for both targets **402** and **403**.



Scheme 5.22 – (a) DIPEA, DMSO, 120 °C, 3 h. (b) $Pd(Ph_3)_4$, Na_2CO_3 , dioxane, water, 120 °C, 1 h, MW.

5.5.2 SPR testing and X-ray crystallography

The affinity of **402** and **403** for HSP70 was measured by SPR and found to be 55 μM and 60 μM respectively. This is approximately a six-fold increase in affinity in comparison to the parent compound **10**. The X-ray crystal structure was solved for **402** by Marc Cabry at the ICR. This structure shows the phenyl ring directly above the guanidine of R342, forming a cation- π interaction which may explain the increase in observed potency (Figure 5.16). R272 is in the extended conformation and there is no salt bridge between K56 and E268.

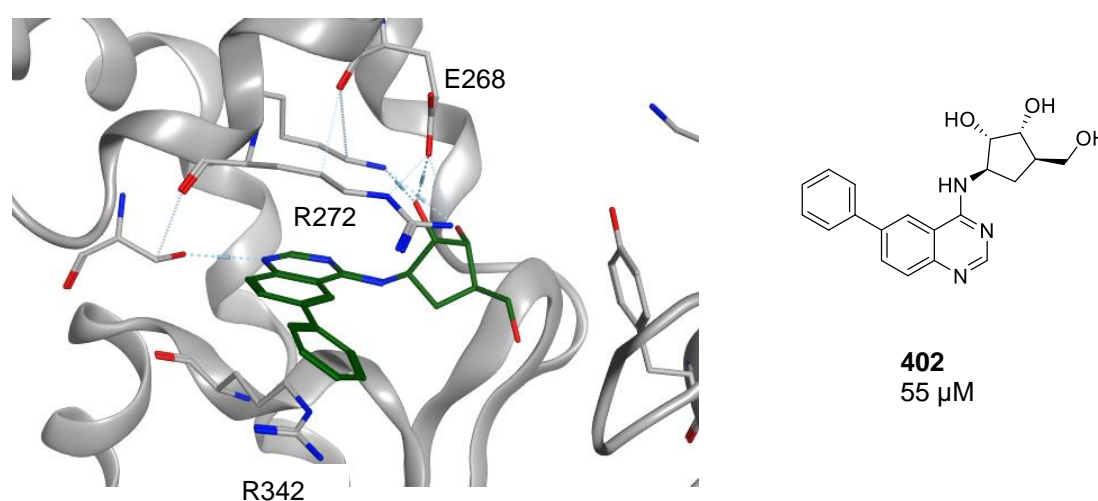


Figure 5.16 – X-ray crystal structure of HSP72-NBD bound with **402** shows the phenyl ring directly above the guanidine of R342, making a cation- π interaction.

The X-ray crystal structures of **403** and **397** were solved by Marc Cabry at the ICR (Figure 5.17) to compare the conformation of the protein for these two matched pairs. These structures show the methyl pyrazole ring of **403** directly above the guanidine of R342, forming a cation- π interaction but for **397** the R342 is observed in two conformations. In order to interact with the methyl pyrazole ring in the 7-position the arginine residue is forced to flip from its previously observed conformation. This may explain the observed increase in potency for **403** over **397**.

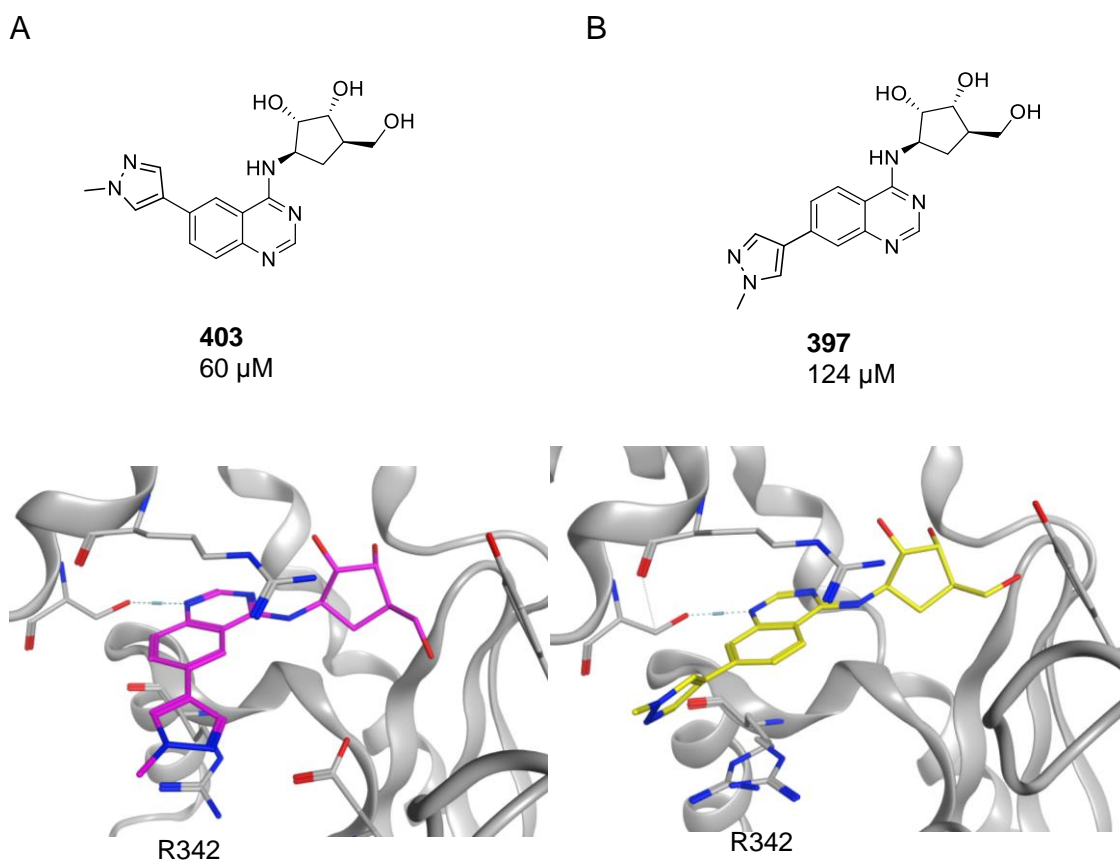


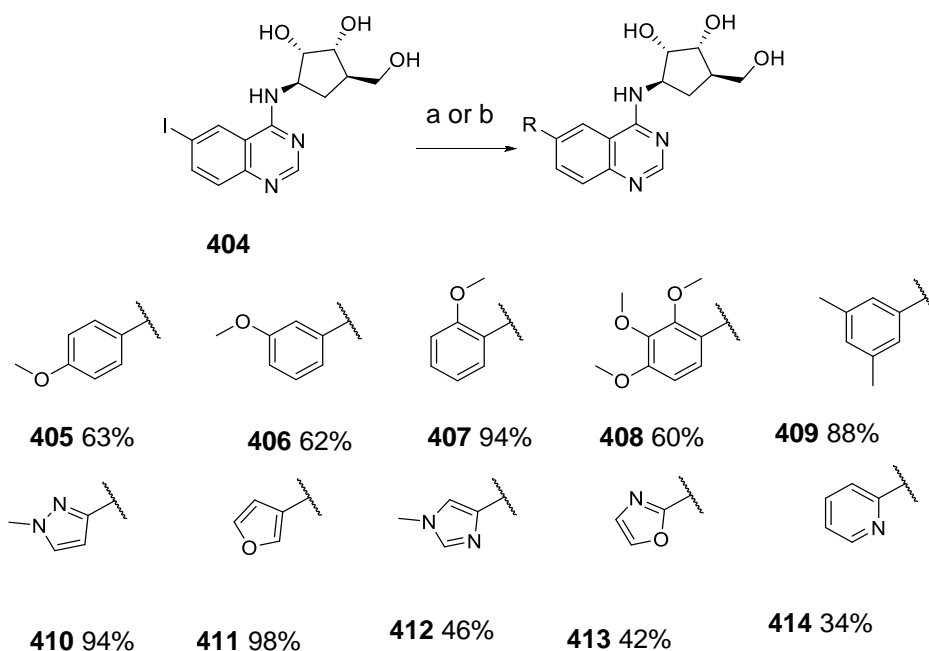
Figure 5.17 – X-ray crystal structures of HSP72-NBD bound with (A) **403** and (B) **397**.

5.5.3 Analogues of the 6-methyl pyrazole and 6-phenyl quinazolines

Based on the SPR results of **402** and **403** ten analogues were designed to investigate the effect of other five and six membered aromatic rings at the 6-position (Scheme 5.23, compounds **405-414**). These designs included increasing the electron density of the phenyl ring with ortho, meta and para methoxy, trimethoxy and 2,4 dimethyl substituents and decreasing the electron density with a pyridine matched pair **405**. Increasing the electron density was hypothesised to be desirable in order to strengthen the interaction with the R342 below the ring. Methyl pyrazole analogues chosen were furan, methyl imidazole, methyl pyrazole and oxazole.

Compounds **405-411** were synthesised from intermediate **404** by Suzuki coupling. Stille coupling was used for the targets with a nitrogen in the two

position, **412-405**, for the reasons described in section 5.4.2. In general, the coupling proceeded in good yields.



Scheme 5.23 – Synthesis of 6-substituted quinazolines (a) DIPEA, DMSO, 120 °C, 3 h. (b) Pd(Ph₃)₄, Na₂CO₃, dioxane, water. Compounds **405-411** were synthesised by Suzuki coupling (conditions a). Compounds **412-414** were synthesised by Stille coupling (conditions b).

Compounds **405-414** were tested by SPR (Table 5.7). In comparison to the parent compounds **402** and **403** none of the replacement aromatic rings improve the potency. *Ortho* and *para* methoxy phenyl both lose potency approximately 12-fold. The trimethoxy phenyl is able to regain some potency and improves affinity three-fold over *ortho* or *para* substituted analogues although it is still much less potent than the parent **402**. Phenyl **402** is five times more potent than pyridine **414**. The phenyl is both more electron rich and has log unit increase in LogD. Moving the nitrogen from the methyl pyrazole **403** to **410** resulted in a significant decrease in potency (13-fold).

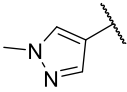
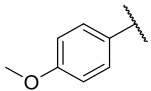
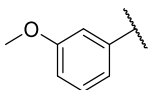
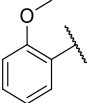
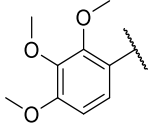
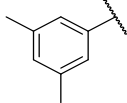
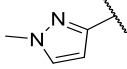
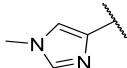
Structure	Compound	LogD	SPR K_D
	402	2.0	55 μM
	403	0.5	60 μM
	405	2.1	660 μM
	406	2.1	precipitated
	407	1.9	696 μM
	408	1.7	230 μM
	409	2.9	Poor sensorgrams
	410	0.4	785 μM
	411	1.1	320 μM
	412	0.4	109 μM
	413	0.5	140 μM Poor solubility
	414	1.0	260 μM
CF ₃		1.2	410 μM
I		1.5	137 μM

Table 5.7 – Testing of 6-substituted quinazolines by SPR (n = 1).

5.5.4 Extension of 6-methyl pyrazole and 6-phenyl quinazolines

Based on the SPR results of **402** and **403**, analogues were designed to further explore the ATP binding site. Figure 5.18 shows a model based on the X-ray crystal structure of **402** which shows that substitution at the meta position of the phenyl ring with aromatic rings should be tolerated. Similarly, a model based on **403** shows that elaboration of the methyl of the methyl pyrazole should occupy a comparable position. Compounds **415-420** were designed to test this hypothesis. Two related compounds **416** and **417** have additional nitrogen atoms as hydrogen bond acceptors may be favourable in this solvent exposed region of the protein.

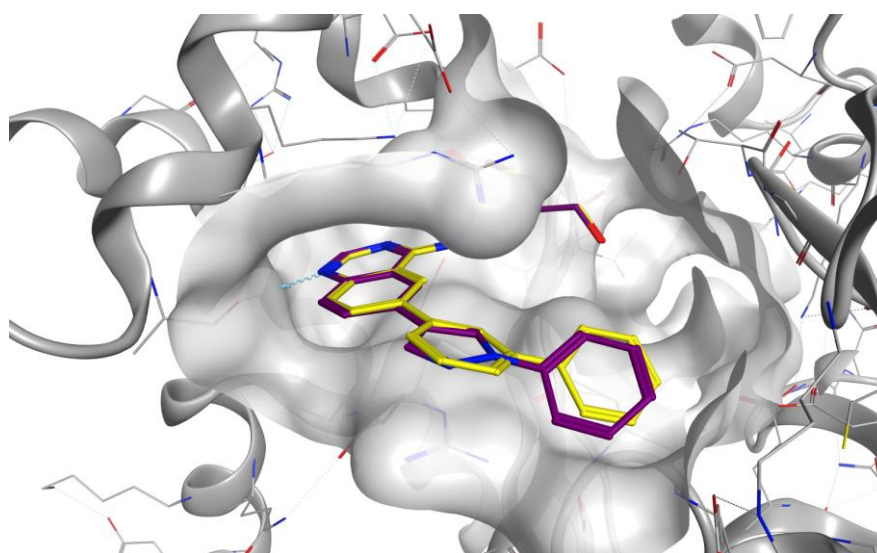
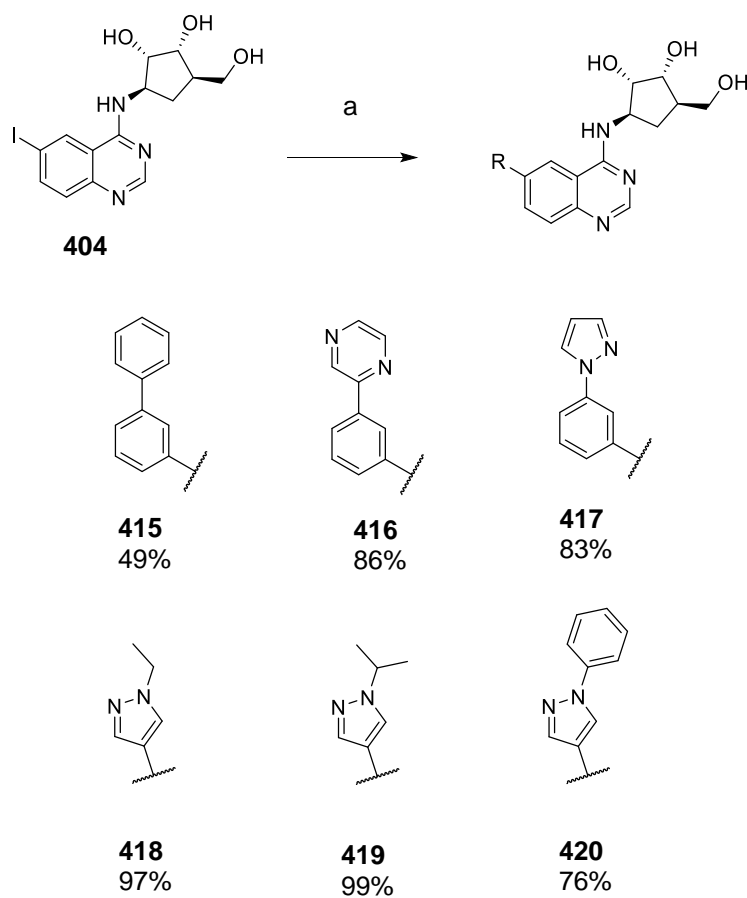


Figure 5.18 - Model of a phenyl substituent extended from 6-methyl pyrazole (purple) or 6-phenyl (yellow) quinazolines.

Compounds **415-420** were synthesised from the intermediate **404** by Suzuki coupling with the appropriate boronic acid in good yields (Scheme 5.24). Purification of the biphenyl **415** required multiple purification steps resulting in a comparatively lower yield. The NMR spectra for pyrazoles **418** and **419** were difficult to interpret as the aromatic peaks were very broad, likely due to slow rotation on the NMR timescale (Figure 5.19). These peaks became much

sharper using a VT experiment which allowed more detailed characterisation (Figure 5.20).



Scheme 5.24 – (a) R-B(OH)₂, Na₂CO₃, Pd(Ph₃)₄, dioxane, water, 120 °C, 1 h.

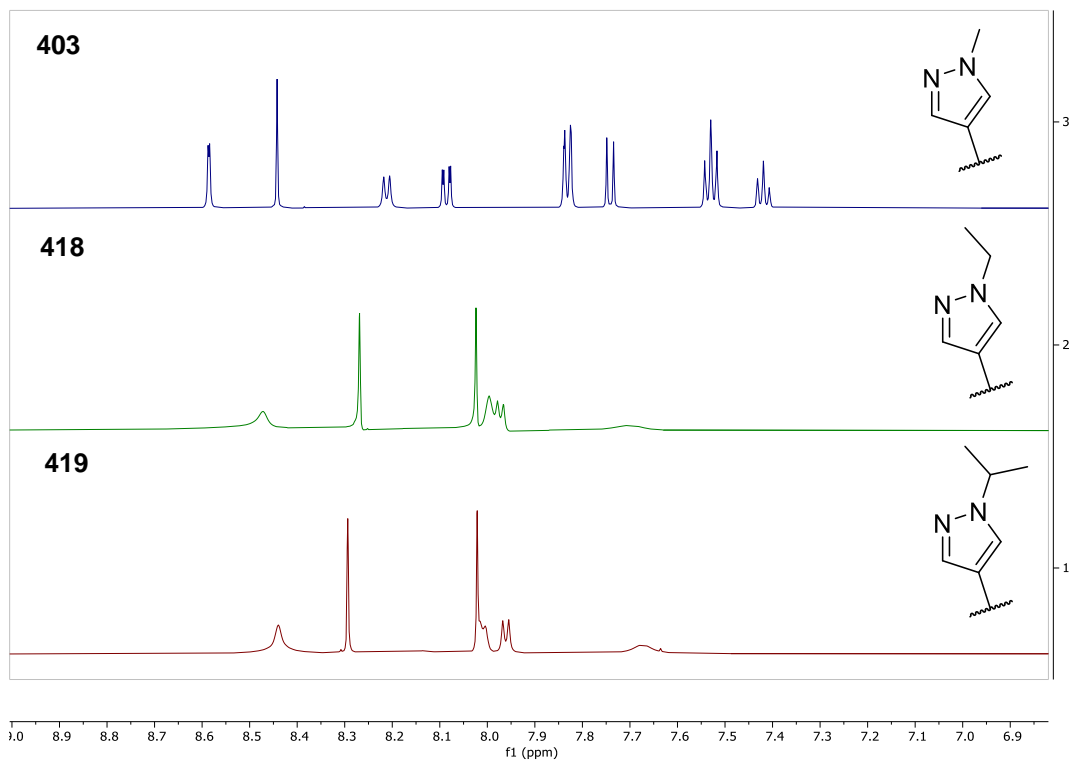
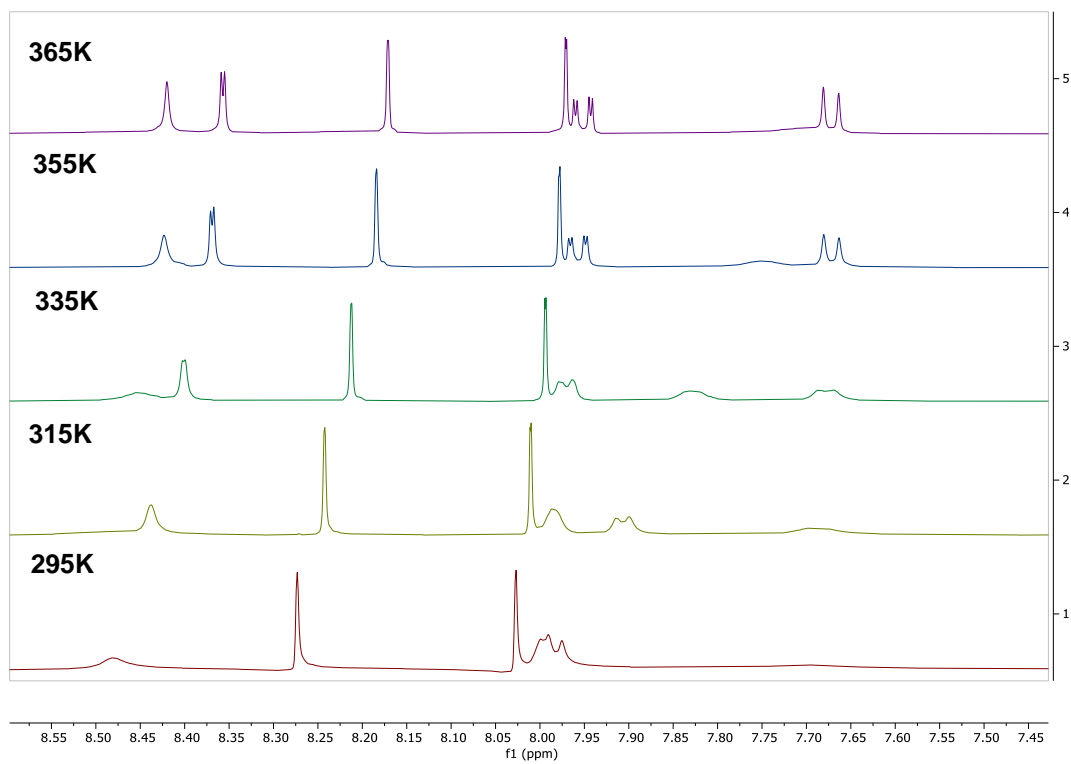


Figure 5.19 – ¹H-NMR spectra of compounds 403, 418, 419.

A



B

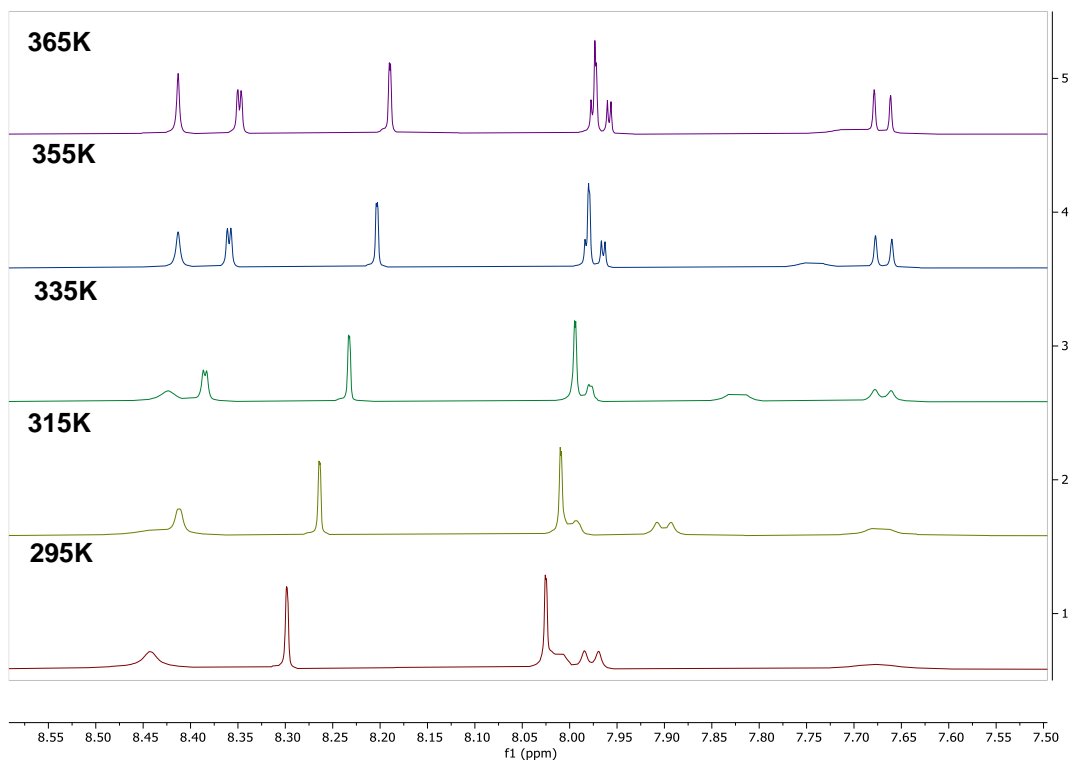


Figure 5.20 – VT experiments with compounds **418** (A) and **419** (B) were used to sharpen the broad ^1H -NMR peaks.

Compounds **415-420** were tested by SPR (Table 5.8). From the X-ray crystal structure of **402**, it was hypothesised that meta substitution from the 6-phenyl ring would place the new aromatic rings in a shallow groove in the pocket. Substitution with aromatic rings at the meta position of **402** with phenyl **415**, pyrazine **416** and imidazole **417** was tolerated with **415** being the most potent of the series. This compound is predicted to have a more twisted conformation than either of the matched pairs **416** and **417** and also a much higher LogD. Only the biphenyl substituent is more potent than the parent compound **402**.

From the X-ray crystal structure of **403**, it was hypothesised that substitution from the 6-pyrazole with aromatic rings would fit in a shallow groove in the pocket, similar to the 6-phenyl **402** but with a slightly different vector. Substitution of ethyl **418**, isopropyl **419** or phenyl **420** is tolerated but offers no increase in

potency over the parent compound **402**. The 6-biphenyl **415** (37 μM) is more potent than the methyl pyrazole matched pair **420** (82 μM). **415** is predicted to have more than 1.5 log unit difference in LogD as well as differences in conformation.

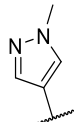
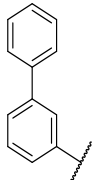
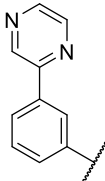
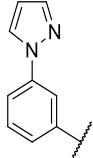
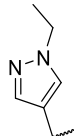
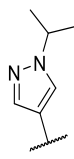
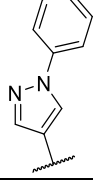
Structure	Compound	LogD	SPR K_D
	402	2.0	55 μM
	403	0.5	60 μM
	415	3.8	37 μM
	416	1.7	115 μM
	417	2.1	148 μM
	418	1.0	70 μM
	419	1.4	100 μM
	420	2.1	82 μM

Table 5.8 – SPR testing of 6-substituted compounds (n = 1).

5.5.5 Novel analogues at the 6 position

Designs suggested by Yann-Vai Le Bihan based on the X-ray crystal structure of **226** included two compounds that could potentially interact with the arginine residues above and below the quinazoline ring. Methyl sulfone **421** has the potential to make hydrogen bonds with both R272 and R342 (Figure 5.21 A). Similarly, the acid **422** has the potential to make a salt bridge and/or a hydrogen bond with either R272 or R342 (Figure 5.21 B).

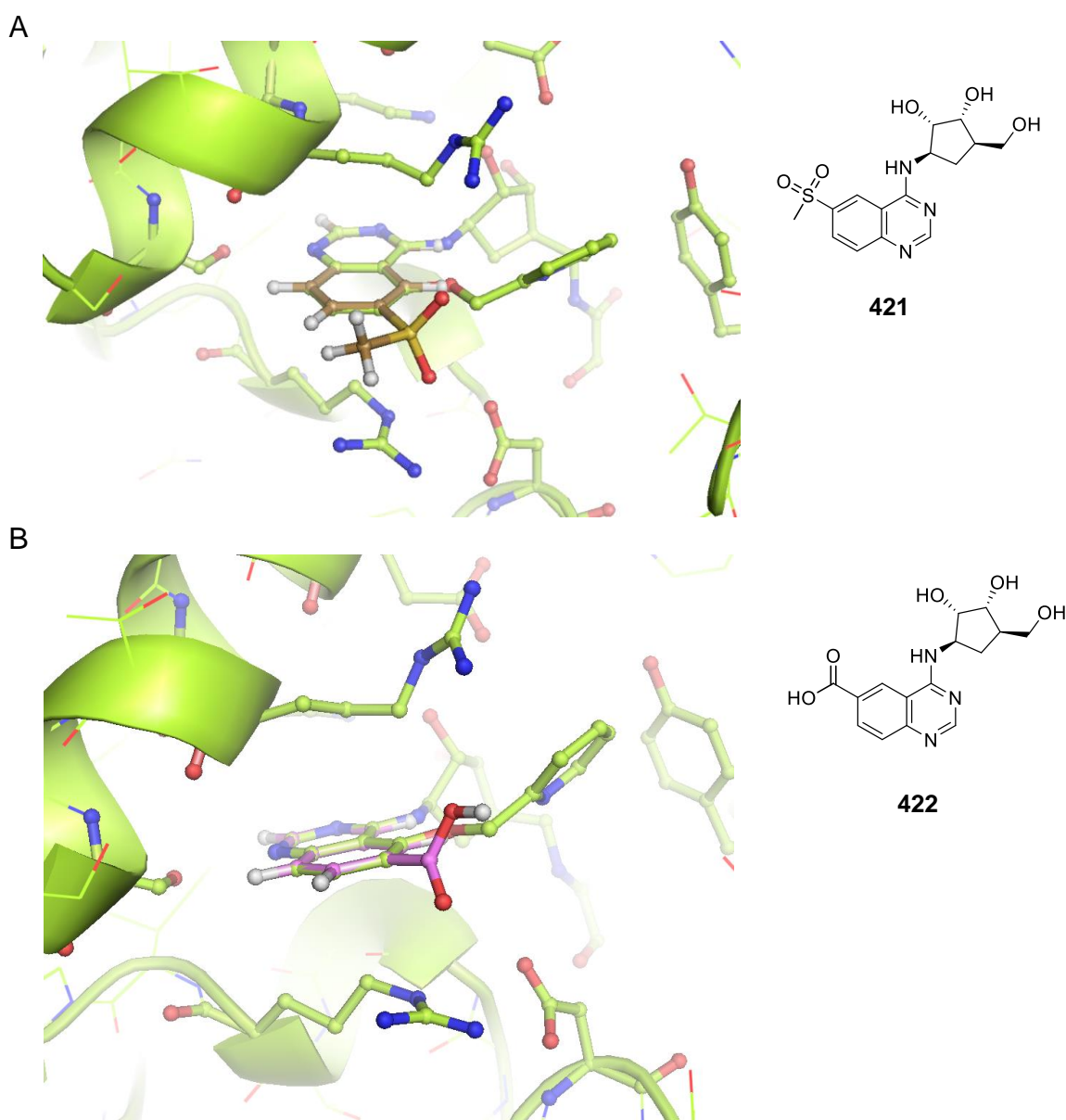
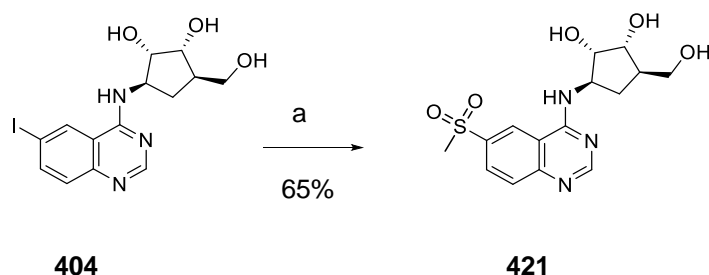


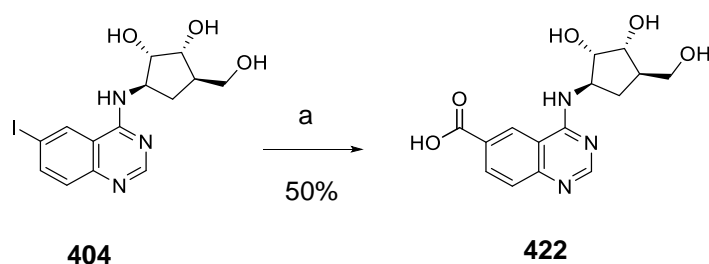
Figure 5.21 – Models of (A) **421** and (B) **422** based on X-ray crystal structure of **226**, designed to interact with R272 and/or R342.

421 was synthesised from the intermediate **404** in a single step with sodium methanesulfinate, similar to literature conditions¹³⁸ but without the reported ionic liquid (Scheme 5.26). The reaction went to completion with no starting material remaining after 24 h. Purification by reverse phase column chromatography gave the desired product.



Scheme 5.26 – (a) Sodium methanesulfinate, CuI, DMSO, 120 °C, 24 h.

422 was synthesised from the intermediate **404** under a balloon of carbon monoxide gas with literature conditions (Scheme 5.25).¹³⁹ A single peak was observed by LC-MS after one hour. The compound was isolated by basic ion exchange chromatography.



Scheme 5.25 – Synthesis of 6-substituted carboxylic acid **422** (a) CO, XantPhos Pd G4, DIPEA, dioxane, water, 60 °C, 1 h.

Compounds **421** and **422** were tested by SPR. For the carboxylic acid **422** the sensorgrams showed that the ligand does not fully dissociate and the compound accumulated over time (Figure 5.22). The methyl sulfone **421** began to show non-specific binding at the two highest concentrations (Figure 5.22). When these

concentrations are excluded the K_D measures 3 μM in contrast to 30 μM with all eight points included. The assay was changed to have the maximum compound concentration of 500 μM instead of 1000 μM . Under these conditions the compound behaves well with no points excluded to calculate the K_D of 58 μM . The sensorgrams for the methyl sulfone **421** are slow on/slow off in contrast to the majority of the quinazolines which are fast on/fast off.

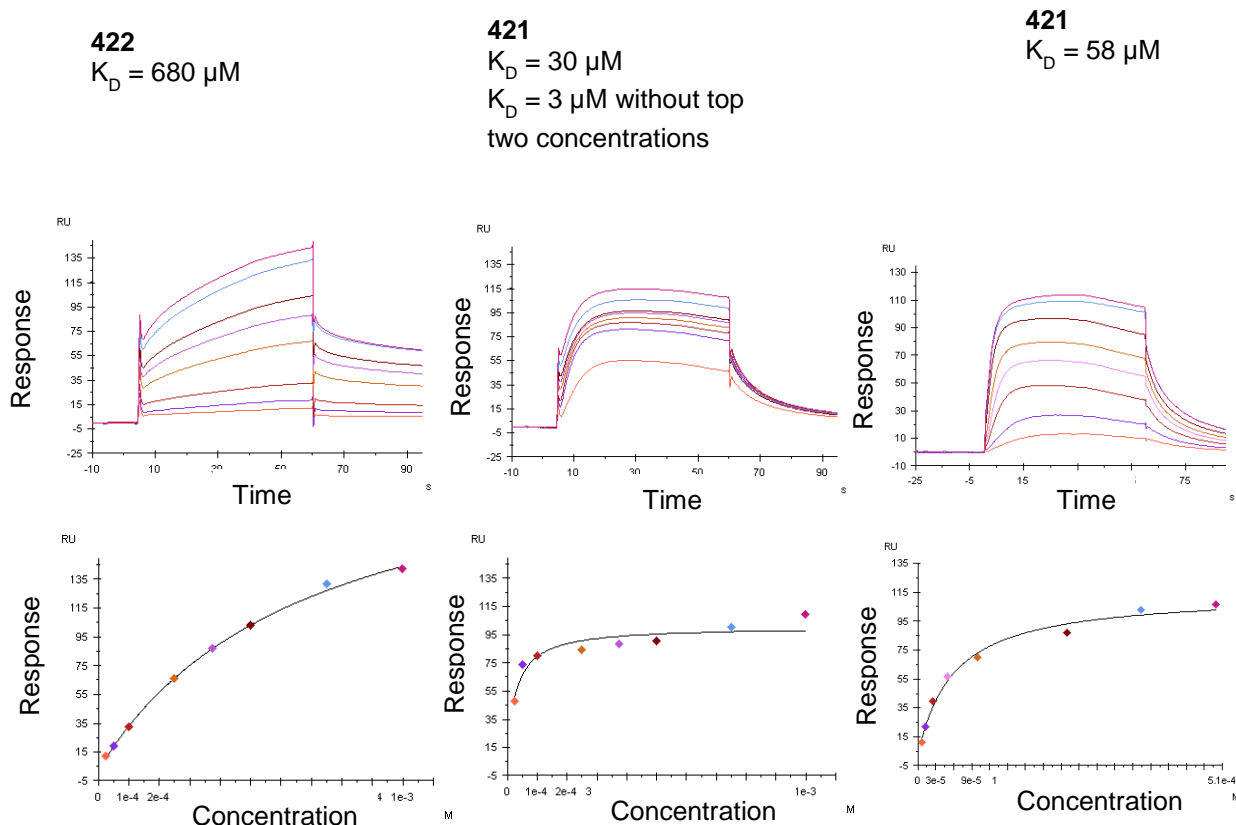


Figure 5.22 – Sensorgrams and binding curves from SPR testing of compounds **422** and **421**.

The X-ray crystal structure of methyl sulfone **421** was solved by Marc Cabry and Yann-Vai Le Bihan at the ICR. R272 is observed in the extended conformation although this residue was not fully resolved. One of the oxygens of the methyl sulfone is pointing towards R342 at a distance of 3.6 \AA , potentially forming a charge dipole interaction.¹⁴⁰

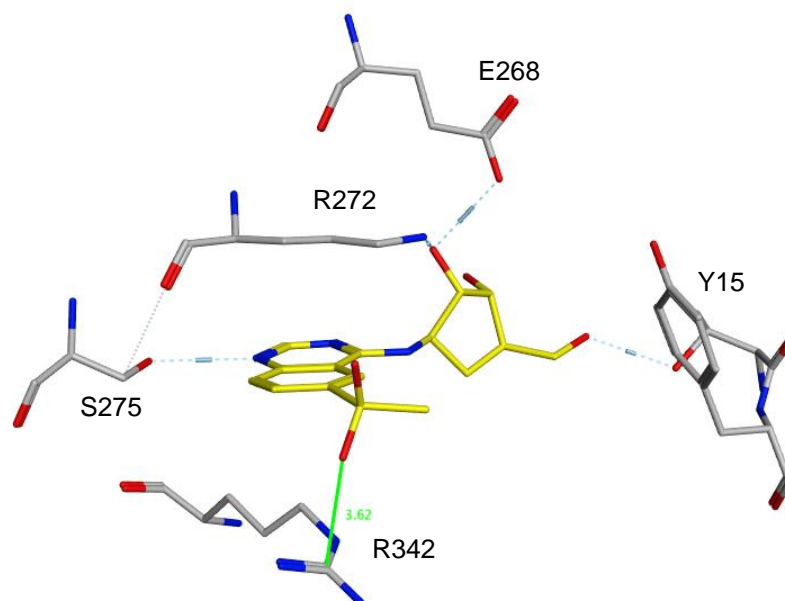


Figure 5.23 – X-ray crystal structure of **421** shows an interaction between the sulfone and R342.

5.5.6 Methyl sulfone analogues

Analogues of the methyl sulfone **421** were designed to explore if substituted sulfones would be tolerated (Figure 5.24).

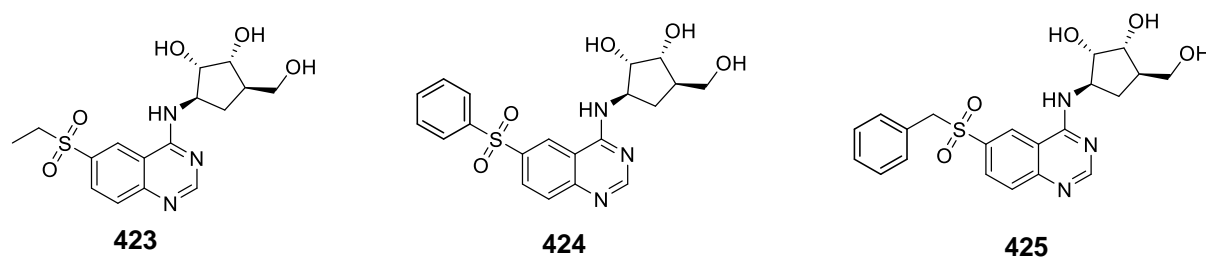
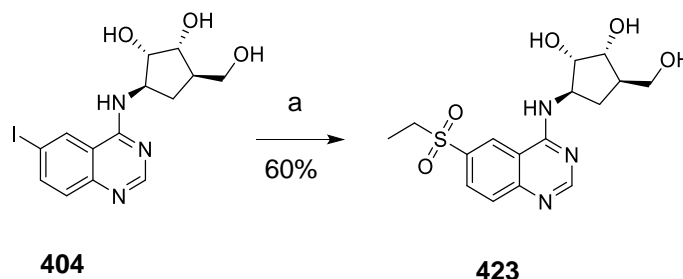


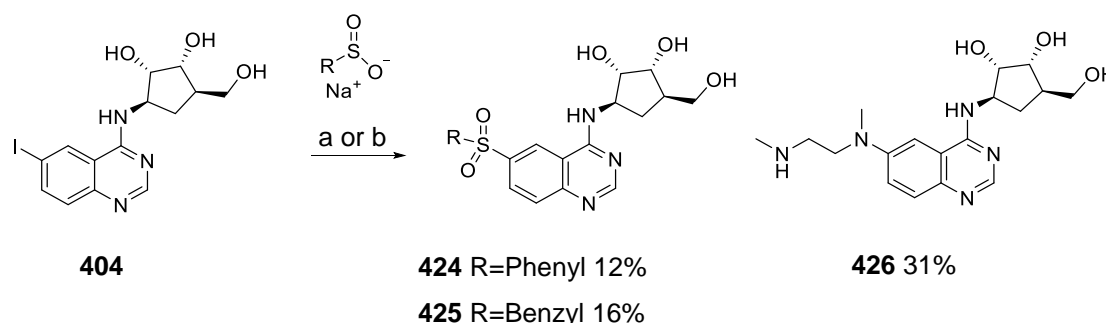
Figure 5.24 – New designs based on methyl sulfone **421**.

Ethyl sulfone **423** was synthesised from the iodo intermediate **404** in a similar way as the methyl sulfone **421** (Scheme 5.27).

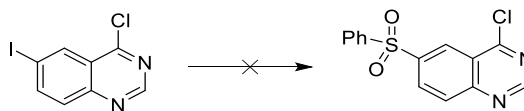


Scheme 5.27 – (a) NaEtSO₂, CuI, DMSO, 120 °C, 24 h.

Using the intermediate **404** reactions were trialed to explore more elaborated sulfone substituents, phenyl **424** and benzyl **425**, but no product was formed under the original conditions (Scheme 5.28 a). Alternative conditions were found after a literature search, with CuBr and DMEDA (Scheme 5.28 b).¹⁴¹ As a trial reaction these new conditions were used with the methyl sulfone and gave the desired mass ion by LC-MS. These new reaction conditions were then attempted for **424** and **425** but the major product of the reaction observed by LC-MS was a mass ion of 362 which corresponded to **426**, the replacement of the iodo substituent with DMEDA. A small but sufficient amount of both desired products **424** and **425** was isolated for testing with these conditions. The side product **426** was also isolated for testing. The reaction was repeated without the ribose mimic in place but no desired product was observed by LC-MS (Scheme 5.29).

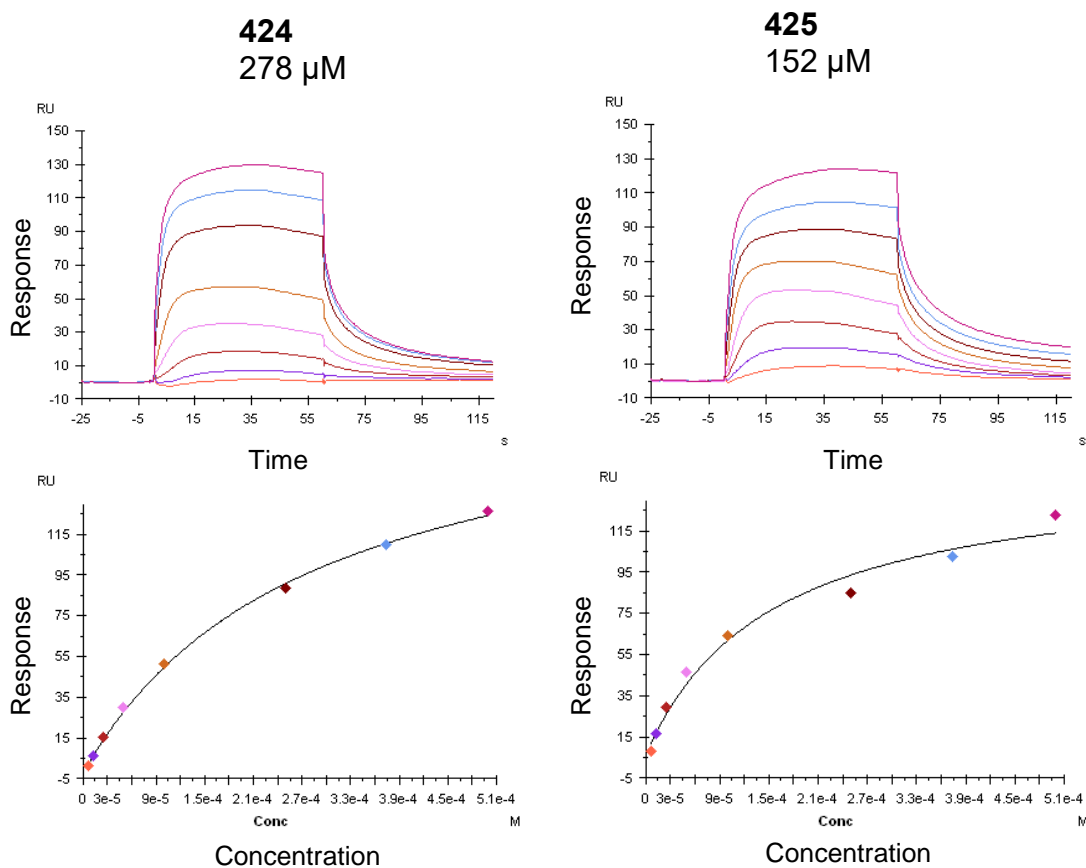


Scheme 5.28 (a) DMSO, CuI, 120 °C, 24 h. (b) CuBr, DMEDA, K₂CO₃, DMSO, 110° C, 2 h.



Scheme 5.29 (a) CuBr, DMEDA, K₂CO₃, DMSO, 110 ° C, 2 h.

Compounds **423-426** were tested by SPR and showed fast on/slow off sensorgrams, as observed for **421**. Although these substitutions were tolerated, none of these compounds were more potent than the parent molecule **421** (Figure 5.25).



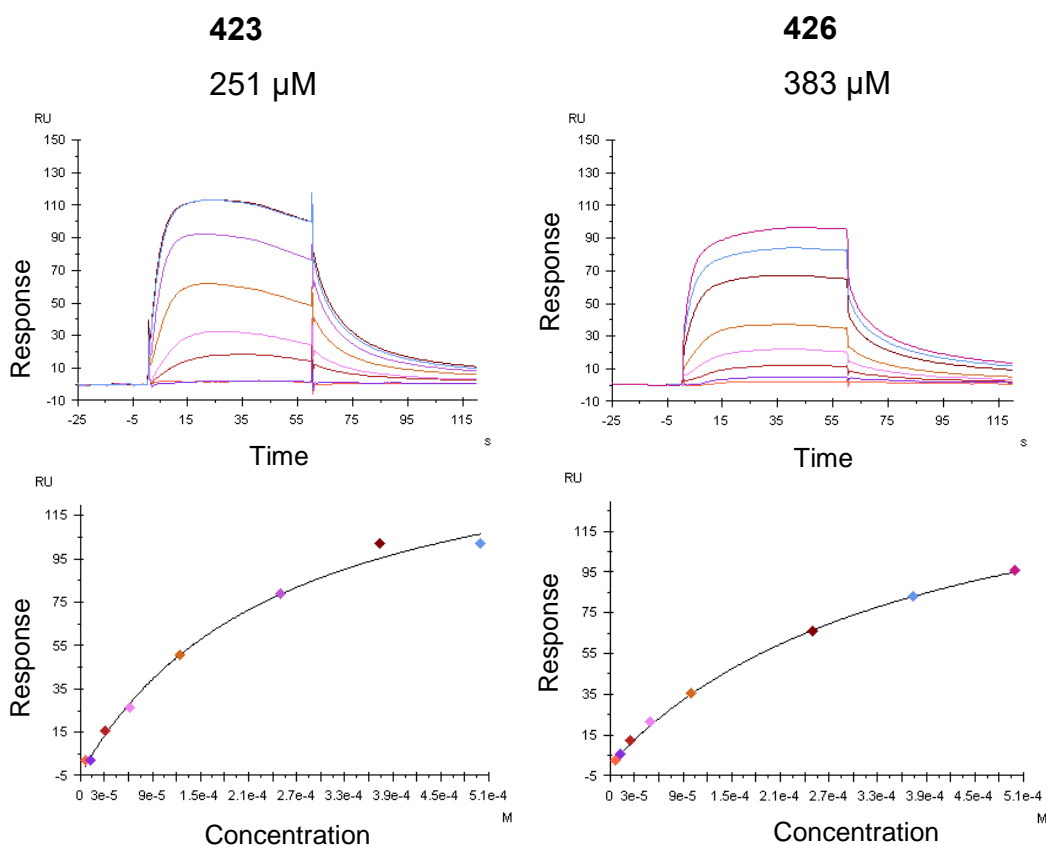


Figure 5.25 – Testing of compounds 423-426 by SPR showed slow on/slow off sensorgrams.

5.6 6-substituted quinazolines with a hydroxyacetamide motif

From analysis of the SPR testing of hydroxyacetamide **226** in Chapter 4, which increased the potency three-fold over the parent compound **10** by binding in the phosphate binding region, two compounds were designed to combine the best 6-substituents, phenyl **402** and methyl sulfone **421** with the hydroxyacetamide motif (Figure 5.26).

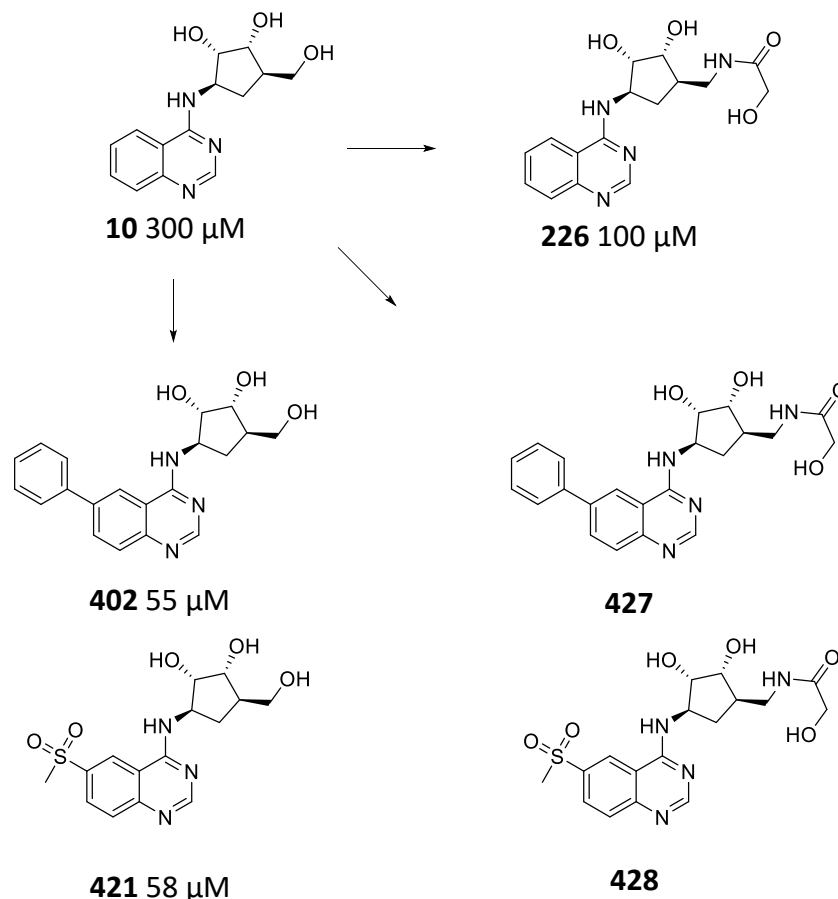
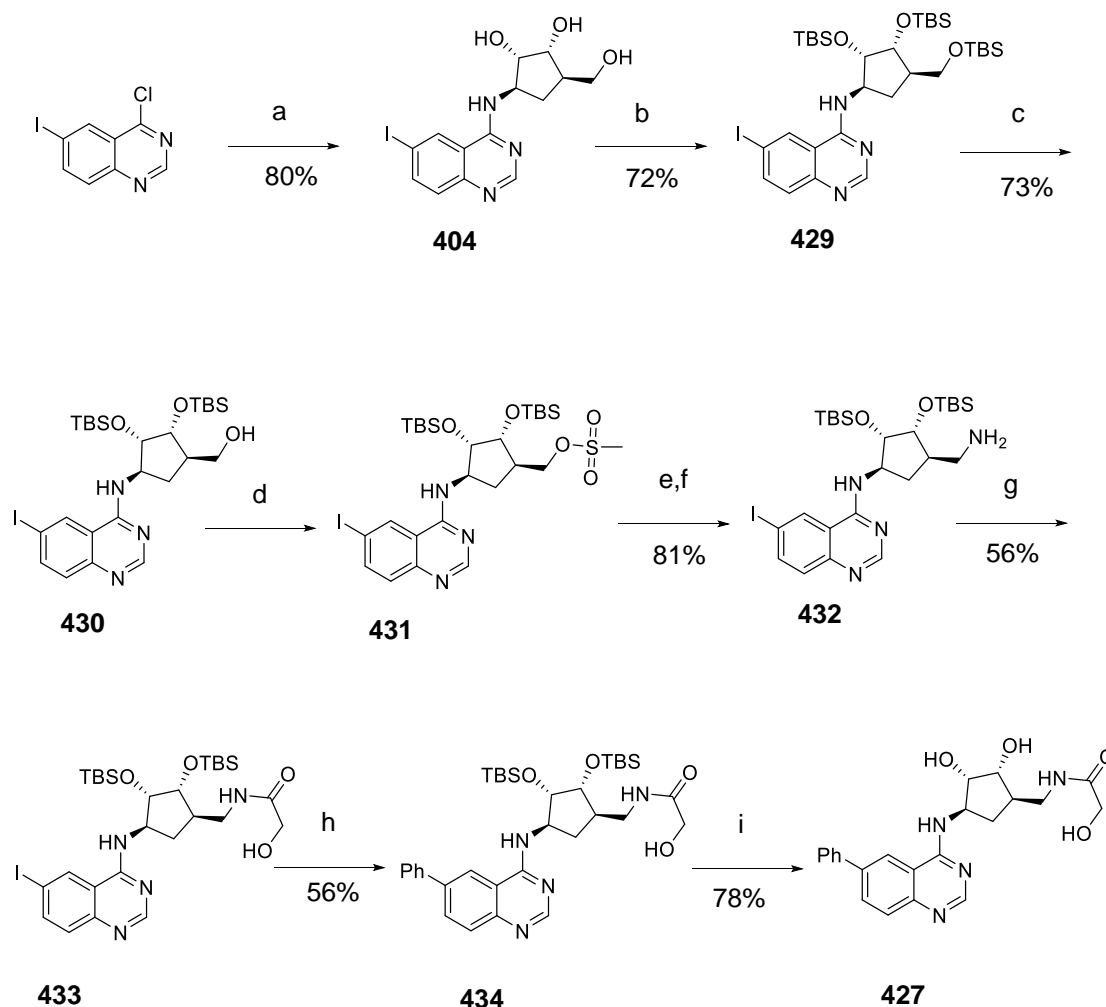


Figure 5.26 – Design of compounds **427** and **428** that combine the most potent 6-substituents with the hydroxyacetamide motif.

An eight-step synthesis, similar to the route to hydroxyacetamide **226**, was designed with a 6-iodo substituent to allow late stage functionalisation at the 6-position (Scheme 5.30). The first $\text{S}_{\text{N}}\text{Ar}$ step was carried out on a two-gram scale and proceeded in good yields. The three hydroxyl groups of the ribose mimic were protected with TBS and the primary alcohol was selectively deprotected with HCl. The mesylation reaction went to completion, followed by azide displacement and Staudinger reduction to yield 81% over the three steps. The amide coupling was first attempted with DCC but the DCC side product **435** co-eluted with the desired product **433** (Figure 5.27). Further purification by acidic ion exchange chromatography removed the DCC impurity but the TBS protecting groups did not fully survive the acidic conditions. The coupling reaction was repeated with EDC, which had a distinct retention time to the product and was removed by reverse phase column chromatography. The

Suzuki coupling went to completion by LC-MS but the product isolated from the reverse phase column was impure and low yielding. The reaction was repeated with less equivalents of sodium carbonate and a fresh bottle of phenyl boronic acid to increase the yield from 20% to 56%. Removal of the TBS protecting groups with HCl gave the final product **427**.



Scheme 5.30 – (a) **224**, DIPEA, DMSO, 120 °C, 1 h (b) Imidazole, DMAP, TBSCl, DMF, rt, 18 h. (c) HCl, EtOH, 0 °C, 1 h. (d) Mesyl anhydride, TEA, DCM, 60 °C, 3 h (e) NaN₃, DMF, 60 °C, 18 h. (f) PPh₃, NH₄OH (g) EDC, NHS, THF, rt, 2.5 h (h) Pd(Ph₃)₄, Na₂CO₃, dioxane, water, 120 °C, 1 h, MW (i) HCl, EtOH, rt, 2 h.

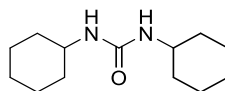
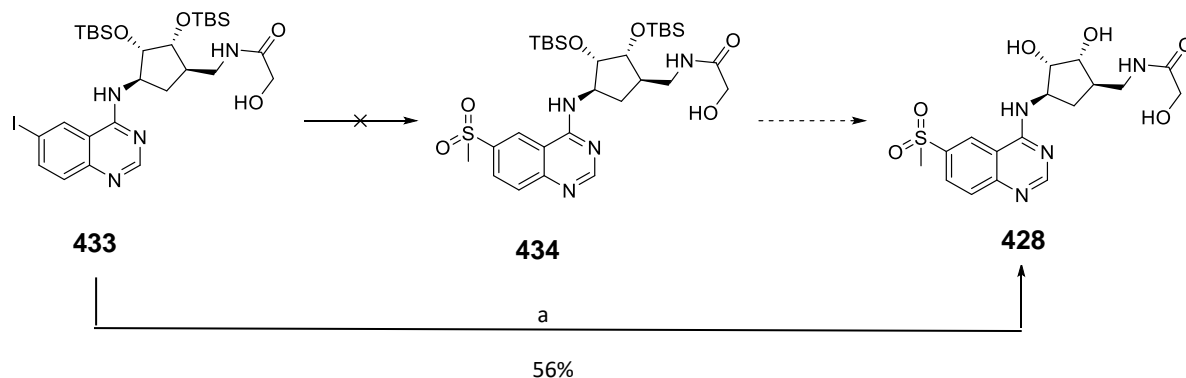
**435**

Figure 5.27 - DCC side product **435** coeluted with the desired product **433**.

Coupling of methyl sulfinic acid with the intermediate **433** surprisingly showed no product mass ion **434** (Scheme 5.31). The observed mass ion 411 instead corresponded to the desired final product **428**. Purification by reverse phase gave the final compound directly. A search of the literature found two reports that describe the use of copper chloride and copper bromide to catalytically deprotect TBS groups.^{142,143} The copper iodide in Scheme 5.31 is able to perform both the desired coupling and the deprotection step in one pot.



Scheme 5.31 – Synthesis of methyl sulfone **428** directly from intermediate **433** (a) sodium methanesulfinate, CuI, DMSO, 120 °C, 24 h.

5.6.1 SPR testing of compounds **427** and **428**

Compounds **427** and **428** were tested by SPR in three individual experiments with consistent results (Table 5.9). Methyl sulfone **428** was 7-fold more potent than phenyl matched pair **427** and like all previously tested sulfones **421**, **423**, **424** and **425**, showed fast on/slow off sensorgrams. The addition of the hydroxyacetamide motif does not increase the potency of either of the 6-substituted quinazolines **402** or **421**.

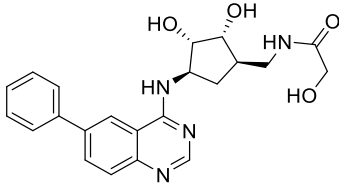
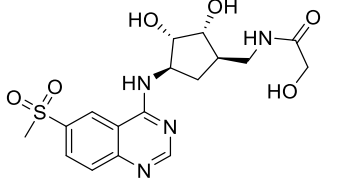
Compound	Structure	Expt 1	Expt 2	Expt 3	Mean \pm SD
427		287	142	201	210 \pm 60
428		37	22	27	29 \pm 6

Table 5.9 – Testing of compounds **427** and **428** by SPR. Values expressed in μ M.

5.7 Conclusions

This chapter has described the replacement of the quinazoline core with naphthyridine, quinoline, cinnoline, pyrimidine and thienopyrimidine cores. Introducing an extra nitrogen in the phenyl ring of the quinazoline in the 5, 6, 7 or 8 positions resulted in a loss of potency. This may be because the new ring is more electron deficient and interacts less favourably with the arginine residue underneath. Cinnoline and quinoline cores changes were not tolerated, most likely because these cores are unable to make a key hydrogen bonding interaction with a conserved water molecule in the ATP binding site. Affinity could be restored with some substituents at the 3 position of the quinoline cores such as cyano, chloro or nitro groups. Thienopyrimidine replacements were at least equipotent with the parent quinazoline and offer the potential for an alternative series with different physicochemical properties. Pyrimidine replacements were not tolerated, highlighting the importance of the benzene ring of the quinazoline.

Substitutions at the 5, 6 and 7 positions of the quinazoline ring were explored. Two substituents at the 5-position, with pyrazine and pyrimidine rings, increased the potency ten-fold. An X-ray crystal structure could explain this observed SAR as the pyrimidine ring lies in the same plane as the quinazoline ring and binds

to a more enclosed conformation of the ATP binding site. Phenyl, methyl pyrazole and methyl sulfone substituents at the 6-position increased potency approximately six-fold. X-ray crystal structures showed the phenyl and methyl pyrazole rings are placed directly above an arginine residue making a cation- π interaction. The methyl sulfone was also observed to interact with this arginine residue. Substitution at the 7-position with a methyl pyrazole increased potency approximately three-fold. This was explained by the X-ray crystal structure in which an arginine residue was observed in two conformations, one of which could make a cation- π interaction with the pyrazole ring. Combining the most potent 6-substituents with the hydroxyacetamide motif did not increase the potency. The observed SAR was often not additive and many residues in the ATP binding site are highly flexible and have been observed in different conformations depending on the ligand bound.

5.8 Thesis conclusion

HSP70s are important molecular chaperones that are highly evolutionarily conserved and play a key role in protein homeostasis. Their ability to recognise damaged proteins to allow them to refold correctly or to facilitate their destruction is fundamental to the survival of both stressed and unstressed cells. HSP70s have been implicated in several neurodegenerative diseases which involve misfolded proteins. In cancer, HSP70s enhance cell growth, suppress senescence and confer chemotherapeutic resistance and its overexpression is often associated with metastasis and a poor prognosis. Dual silencing of both HSC70 and HSP72 isoforms using siRNA has been shown to cause tumour specific apoptosis as well as degradation of HSP90 client proteins. Apoptosis was not induced in non-tumourigenic lines indicating a potential therapeutic window.

HSP70s are highly complex molecular machines that rely on conformational flexibility to carry out their function. As discussed in Chapter 1 the development of potent HSP70 inhibitors with good drug-like properties has been hindered by the flexible nature of the ATP binding site which changes size and shape depending on which ligand is bound. HSP70s have a high affinity for ADP and ATP and therefore require highly potent inhibitors in order to compete effectively. The high polarity of the ATP binding site makes it challenging to design inhibitors that are both potent and have good cellular permeability. Targeting a secondary binding site in HSP70 is an attractive alternative to the ATP binding site to potentially overcome these issues.

Fragments are compounds of less than 300 Da that can provide useful starting points for a drug discovery project as they can be grown to improve potency while monitoring physicochemical properties. Fragment based drug discovery is a well-established method that has been used successfully to find high quality leads for drug development and has been able to tackle difficult targets for which little or no hits have been found by HTS.

Chapters 2 and 3 described the identification and validation of a new secondary binding site in HSP70 by multiple orthogonal methods including SPR, WaterLOGSY, CPMG and X-ray crystallography. The identification and characterisation of this new secondary binding site and the discovery of multiple fragment hits that bind by SPR may offer a new way to inhibit this important molecular chaperone. After validation of the secondary site, three virtual high-throughput screens were run by our collaborators. Out of the 127 fragments hits tested by SPR, 11 were found to bind to HSC70-NBD in at least two separate experiments. These fragment hits also bound to the mutant HSC70-NBD S275W, as expected for fragments that bind outside of the ATP binding site. These fragment hits are all within lead-like space and have the potential to be grown to improve potency.

Chapters 4 and 5 describe the elaboration of a quinazoline fragment hit that binds to the ATP binding site of HSP70. Based on the hit fragment **10**, 78 new quinazoline compounds were designed, synthesised and tested by SPR in order to improve potency and increase our understanding of the ATP binding site of HSP70. A hydroxyacetamide motif was observed by X-ray crystallography to interact with residues in the phosphate binding region via a network of hydrogen bonds and occupies the position of the first phosphate of ADP. This is the first time a non-nucleotide has been observed in the phosphate binding region. Four quinazoline analogues with substituents at the 5 position were synthesised with the hydroxyacetamide motif. The most ligand efficient hydroxyacetamide tested was used to explore the phosphate binding region in more depth by substitution at the α position including potential phospho-mimetic motifs. A new route for the synthesis of the key late stage intermediate was necessary due to an unexpected cyclisation reaction. This cyclised product was identified and by understanding the mechanism of formation, a new route with more flexible protecting groups was successful in delivering gram quantities of the chiral intermediate. Addition of substituents at the α position of the hydroxyacetamide has so far not increased affinity, despite a range of different substituents tested. It is likely that there is a very stable network of water molecules in the phosphate binding region and that displacement or disruption of this network is not

favourable. An X-ray crystal structure was solved with a ligand substituted at the α position of the hydroxyacetamide showing a network of hydrogen bonding interactions in the phosphate binding region to the ligand. This ligand also alters the conformation of key residues in the binding pocket, altering the shape and forming a more open conformation.

A variety of quinazoline replacement cores were investigated including quinoline, cinnoline, naphthyridine, pyrimidine and thienopyrimidine rings. Thienopyrimidines and some 3-substituted quinolines were able to retain potency. Substituents at the 5, 6 and 7 positions were found to increase potency up to ten-fold. Two substituents at the 5-position, with pyrazine and pyrimidine rings, increased the potency ten-fold which could be explained by X-ray crystallography. Phenyl, methyl pyrazole and methyl sulfone substituents at the 6-position increased potency approximately six-fold. Substitution at the 7-position with a methyl pyrazole increased potency approximately three-fold.

5.9 Future Work

5.9.1 Secondary binding site

5.9.1.1 Development of fragment hits

The 11 fragment hits from the virtual high-throughput screens are of interest to confirm binding to HSP70 by orthogonal methods such as LO-NMR or X-ray crystallography if possible. X-ray crystallography would determine if these hits occupy the same site as the original hit fragment **21** or a new secondary binding site in the NBD. LO-NMR methods would give confidence that the site is more likely to be the same site if the fragments are shown to be ATP competitive, similar to compounds **21** and **58**. Close analogues could be purchased or synthesised for testing. It would be useful to overlay the predicted or experimentally determined binding modes of fragment hits to determine a pharmacophore which would aid in the understanding of key binding interactions

to improve the potency. Compounds with sub-micromolar potency would be suitable to test the effect of inhibition at this new site for its functional relevance, for example with a luciferase refolding assay.¹⁰²

5.9.1.2 Analysis of the binding site with molecular dynamics

Targeting a secondary site that is cryptic can be difficult. The nature of a cryptic site means that it is not observable in the absence of a ligand which results in practical challenges. If the conformation required for the ligand to bind occurs very infrequently X-ray crystallography is more challenging as ligand binding will be less frequent. An understanding of the conformation necessary for ligand binding and the nature of this conformation can be helpful in assessing progression of fragment hits in a cryptic site. The nature of the secondary binding site will determine how easy or difficult it may be to develop inhibitors that bind to this cryptic site. In order to better understand whether this is a potentially useful pocket for drug design a collaboration with Alan Jones at the University of Manchester, whose group has expertise in computational analysis, has been set up. This collaboration aims to investigate the movement of the alpha-helix from K271 - S277 which contains the S275 residue that forms the critical hydrogen bond to adenosine and the quinazoline analogues in the ATP pocket. Movement of this helix has been observed in order to form the secondary binding site. (Figure 5.29). This research proposes to use molecular dynamic (MD) simulations of the X-ray crystal structure of HSP72 with the ligand bound in the cryptic pocket, to assess the stability of the complex. MD simulations will also be applied to the apo structure of HSP72 where the ATP-pocket is intact, generated from the ADP-bound form, to see if the cryptic pocket we observe begins to form spontaneously through movement of the helix.

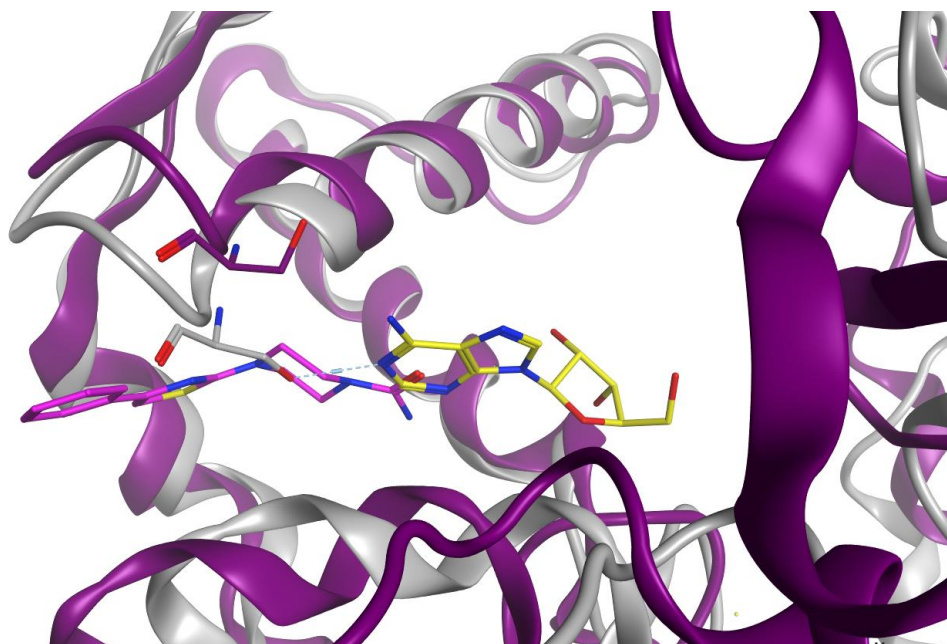


Figure 5.29 - HSP72-NBD with ADP (grey) overlaid with HSP72-NBD with fragment **21** (purple). The alpha helix which contains shifts upwards upon addition of fragment **21**, twisting this key residue out of the ATP binding site.

5.9.2 ATP binding site

5.9.2.1 Synthesis of 5,6 substituted quinazolines

Two of the most potent substituents at the 5-position of the quinazoline ring were found to increase affinity ten-fold (compounds **363** and **364**). The best substituents at the 6-position were found to increase potency six-fold (compounds **402**, **403** and **421**). It may be possible to further increase potency against HSP70 by synthesising compounds that combine the best substituents at the 5 and 6 positions (Figure 5.27).

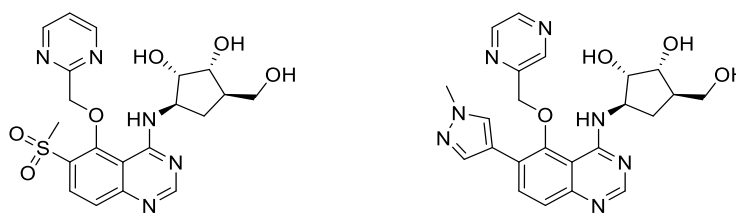


Figure 5.27 – Examples of compounds that combine the best 5 and 6 substituted quinazolines.

5.9.2.2 Analysis of 6-substituted sulfones

The sulfones **421**, **423**, **424**, **425** and **428** showed unexpectedly slower off sensorgrams in contrast to the majority of the tested quinazolines which showed fast off sensorgrams. This potentially interesting difference could be explored further using Isothermal Titration Calorimetry (ITC) which gives information on the thermodynamics of binding. ITC is a quantitative technique that can determine the binding affinity (K_a), enthalpy changes (ΔH) and binding stoichiometry of the interaction between a ligand and the protein. This method therefore allows the entropy and enthalpy to be determined for a given binding event (Equation 5.1).

Equation 5.1
$$\Delta G = \Delta H - T\Delta S = -RT\ln K_a$$

Crystal structures of compounds 6-methyl sulfone **428** and 6-phenyl **402** are remarkably similar yet the SPR experiment shows there is a difference to how these two compounds bind. Comparing these two compounds by ITC may explain this observed difference by giving a better understanding of the entropy and enthalpy of binding in each case.

5.9.2.3 Covalent inhibition

An alternative method to gaining affinity against a protein with a high affinity for ADP/ATP is covalent inhibition.¹⁴⁴ Examination of the X-ray crystal structure,

shows that a cysteine residue C17 is approximately 9 Å away from the hydroxyacetamide of **226**, which has been shown to bind in the phosphate binding region (Figure 5.28). It may be possible to target this cysteine with a suitable electrophile for covalent inhibition. This Cys17 was the original target for compound **7** but these compounds were found to place the electrophile far away from the desired cysteine residue.⁵⁰

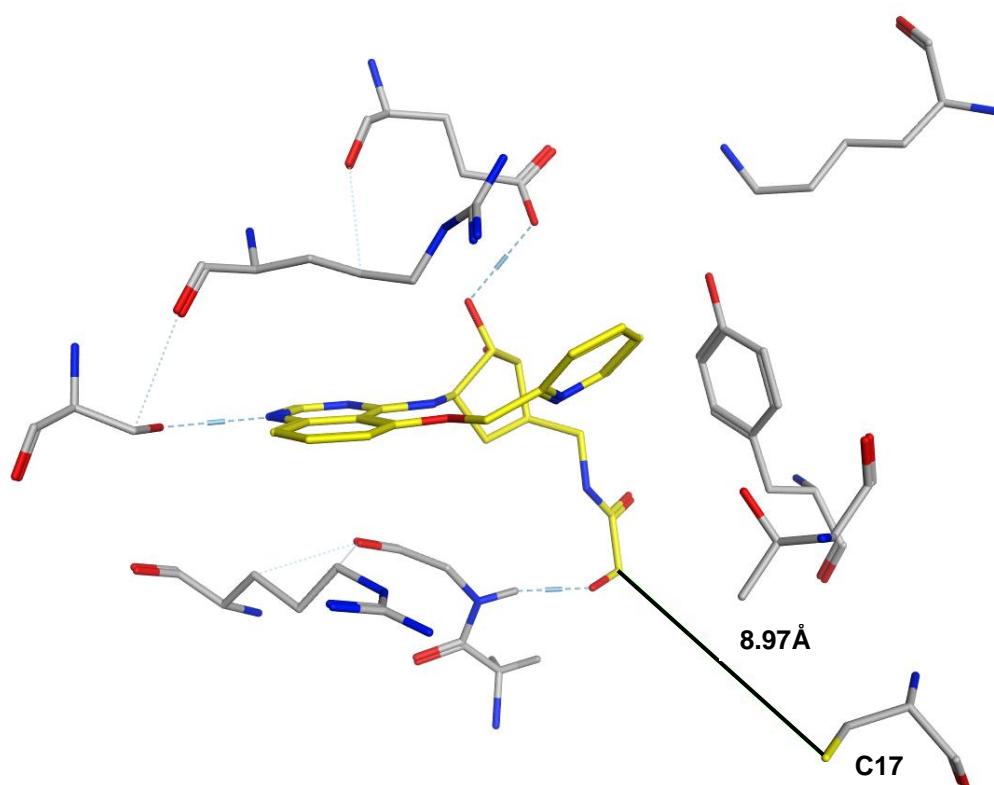


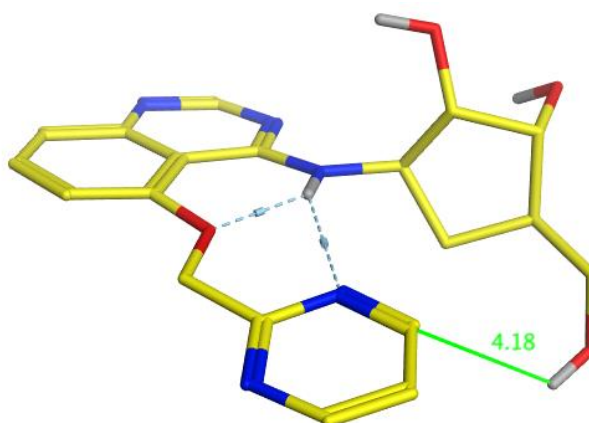
Figure 5.28 – X-ray crystal structure of **226**, highlighting the cysteine residue within 9 Å of the ligand that could potentially be targeted.

5.9.2.4 Macrocyclisation

An alternative method to improve potency can be to decrease the conformational freedom of the molecule by forming a macrocycle which locks the active conformation which can give significant improvements in potency.¹⁴⁵

Macrocyclisation can limit the conformational flexibility of larger molecules, allowing presentation of more chemical groups for favourable interactions with a target without creating an unduly flexible molecule with a prohibitive entropic penalty to binding. A macrocycle, such as compound **436**, could potentially be synthesised based on compounds **363** and **366** (Figure 5.29). Closing the ring may require optimisation but it is an interesting potential strategy to improve potency.

A



B

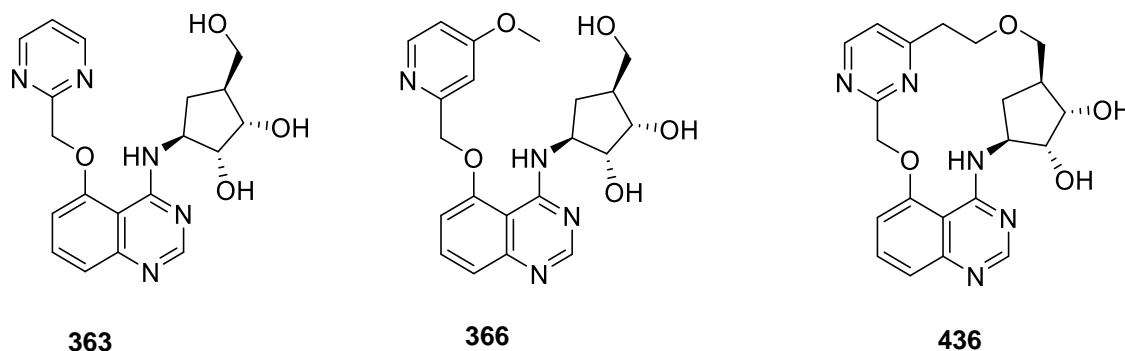


Figure 5.29 – (A) X-ray crystal structure of **363** with HSP72-NBD. (B) Macrocyclisation of known ligands may improve potency. The primary alcohol of the ribose mimic could potentially be linked to the pyrimidine ring to form a macrocycle, for example compound **436**.

6 Experimental

6.1 Synthetic chemistry

6.1.1 General methods

All anhydrous solvents and reagents were obtained from commercial suppliers and used without further purification. All reactions were performed under nitrogen unless otherwise stated. Microwave reactions were performed using a Biotage Initiator Microwave Synthesizer. Column chromatography was performed on a Biotage SP1 purification system using Biotage SNAP KP-Sil cartridges for normal phase and Biotage SNAP Ultra C18 cartridges for reverse-phase chromatography. The mobile phases for reverse phase chromatography contained 0.1% formic acid. Ion exchange chromatography was performed using acidic Isolute Flash SCX-II columns. Analytical thin layer chromatography (TLC) was performed on aluminium sheets pre-coated with silica (60 F₂₅₄, Merck) and visualised by short-wave UV light (254 nm) or potassium permanganate dip. Specific rotations were measured on a Bellingham & Stanley ADP440 polarimeter with a path length of 0.5 dm, using a light emitting diode with interference filter (298 nm). Concentrations (c) are quoted in g/100 mL. Melting points were determined on a Stanford Research Systems EZ-melt apparatus and are uncorrected. Infrared spectra were recorded on a Bruker Alpha-P FT-IR spectrometer. Absorption maxima (ν_{\max}) are quoted in wavenumbers (cm⁻¹). All compounds were >95% purity by HPLC analysis unless otherwise stated.

¹H NMR spectra were recorded on a Bruker AMX500 (500 MHz) or Bruker AMX600 (600 MHz) spectrometers using an internal deuterium lock. Chemical shifts were measured in parts per million (ppm) relative to tetramethylsilane ($\delta = 0$) using the following internal references: CDCl₃ (δ_{H} 7.26), CD₃OD (δ_{H} 3.31) and DMSO-d₆ (δ_{H} 2.50). Signal multiplicities are recorded as singlet (s), doublet (d), triplet (t), quartet (q), multiplet (m), doublet of doublets (dd), doublet of doublet of doublets (ddd), triplet of doublets (td), apparent (app.) or broad (br.) Coupling constants, J , are measured to the nearest 0.1 Hz. ¹³C NMR spectra were

recorded at 126 MHz on Bruker AMX500 spectrometers using an internal deuterium lock. Chemical shifts were measured in parts per million (ppm) relative to tetramethylsilane ($\delta = 0$) using the following internal references: CDCl_3 (δ_c 77.2), CD_3OD (δ_c 49.0) and DMSO-d_6 (δ_c 39.5). 2D NMR spectra were routinely collected for each compound to aid assignment, including COSY, NOESY, HSQC and HMBC spectra. Chemical names and numberings were generated using ChemDraw Professional 19.0 (PerkinElmer Inc.) using IUPAC nomenclature. HRMS analysis was performed using one of the four methods described below:

Method A: Positive mode LC/MS and HRMS analysis was performed on an Agilent 1200 series HPLC and diode array detector coupled to a 6210 time of flight mass spectrometer with dual multimode APCI/ESI source. Analytical separation was carried out at 30 °C on a Merck Chromolith Flash column (RP-18e, 25 x 2 mm) using a flow rate of 0.75 mL/min in a 4 minute gradient elution with detection at 254 nm. The mobile phase was a mixture of methanol (solvent A) and water (solvent B), both containing formic acid at 0.1%. Gradient elution was as follows: 5:95 (A/B) to 100:0 (A/B) over 2.5 min, 100:0 (A/B) for 1 min, and then reversion back to 5:95 (A/B) over 0.1 min, finally 5:95 (A/B) for 0.4 min.

Method B: Positive mode LC/MS and HRMS analysis was performed on a Waters Acquity UPLC and diode array detector coupled to a Waters G2 QToF mass spectrometer fitted with a multimode ESI/APCI source. Analytical separation was carried out at 30 °C on an Agilent Poroshell C18 column (30 x 2.1 mm, 2.6 μ , 100A) using a flow rate of 0.3 mL/min in a 4 minute gradient elution with detection at 254 nm. The mobile phase was a mixture of methanol (solvent A) and water (solvent B), both containing formic acid at 0.1%. Gradient elution was as follows: 10:90 (A/B) to 90:10 (A/B) over 3 min, 90:10 (A/B) for 0.5 min, and then reversion back to 10:90 (A/B) over 0.3 min, finally 10:90 (A/B) for 0.2 min.

Method C: Positive mode LC/MS and HRMS analysis was performed on a Waters Acquity UPLC and diode array detector coupled to a Waters G2 QToF

mass spectrometer fitted with a multimode ESI/APCI source. Analytical separation was carried out at 30 °C on an Agilent Poroshell C18 column (30 x 2.1 mm, 2.6u, 100A) using a flow rate of 0.5 mL/min in a 2 minute gradient elution with detection at 254 nm. The mobile phase was a mixture of methanol (solvent A) and water (solvent B), both containing formic acid at 0.1%. Gradient elution was as follows: 10:90 (A/B) to 90:10 (A/B) over 1.25 min, 90:10 (A/B) for 0.5 min, and then reversion back to 10:90 (A/B) over 0.15 min, finally 10:90 (A/B) for 0.1 min.

Method D: Positive and negative mode LC/MS and HRMS analysis was performed on an Agilent 1260 Infinity II series UPLC and diode array detector coupled to a 6530 Quadrupole time of flight mass spectrometer with Agilent Jet Stream ESI source. Analytical separation was carried out at 40 °C on an Agilent Poroshell C18 column (30 x 2.1 mm, 2.6u, 100A) using a flow rate of 0.4 mL/min in a 4 minute gradient elution with detection at 254, 280 and 214 nm. The mobile phase was a mixture of methanol (solvent A) and water (solvent B), both containing formic acid at 0.1%. Gradient elution was as follows: 10:90 (A/B) to 90:10 (A/B) over 2.5 min, 90:10 (A/B) for 1 min, and then reversion back to 10:90 (A/B) over 0.3 min, finally 10:90 (A/B) for 0.2 min.

The standard quinazoline numbering has been used throughout this thesis and experimental section for all analogues and the ribose mimic has been numbered as shown in Figure 6.1.

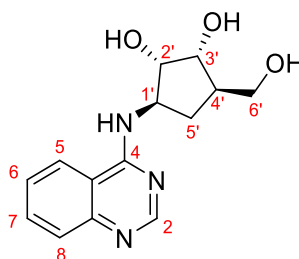
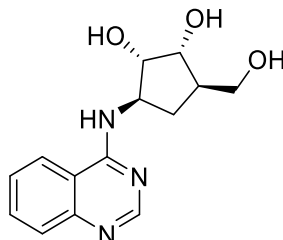
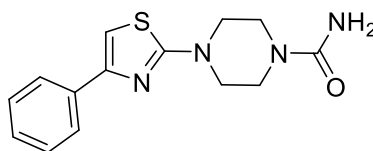


Figure 6.1 – Numbering of quinazoline analogues

6.1.2 Synthesis

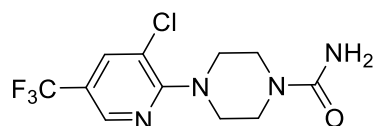
(1*S*,2*R*,3*R*,5*R*)-3-(Hydroxymethyl)-5-(quinazolin-4-ylamino)cyclopentane-1,2-diol (10)

PyBOP (8.11 g, 15.6 mmol) and DBU (5.0 mL, 33.4 mmol) were added to a stirred suspension of 4-hydroxyquinazoline (1.79 g, 12.3 mmol) and (1*R*, 2*S*, 3*R*, 4*R*)-2,3-dihydroxy-4-(hydroxymethanol)-1-aminocyclopentane hydrochloride (2.05 mg, 11.1 mmol) in acetonitrile (55 mL). The solution was stirred at rt for 4 h. The reaction mixture was filtered and washed with Et₂O (10 mL) to afford the title compound (2.58 g, 84%, 9.4 mmol) as a white solid. $[\alpha]^{20}_{\text{D}} +57.8^{\circ}$ ($c=0.5$, MeOH). IR (thin film) $\nu = 3367, 3149, 2907, 2856, 1618, 1586, 1543 \text{ cm}^{-1}$. ¹H NMR (600 MHz, DMSO-*d*₆) δ 8.44 (s, 1H, ArH, H₂), 8.28 (dd, $J = 8.3, 1.3 \text{ Hz}$, 1H, ArH, H₅), 8.05 (d, $J = 7.6 \text{ Hz}$, 1H, ArH, NH), 7.76 (ddd, $J = 8.3, 6.9, 1.4 \text{ Hz}$, 1H, ArH, H₇), 7.67 (dd, $J = 8.4, 1.2 \text{ Hz}$, 1H, ArH, H₈), 7.56 – 7.42 (m, 1H, ArH, H₆), 4.73 (t, $J = 5.1 \text{ Hz}$, 1H, OH), 4.69 (d, $J = 5.7 \text{ Hz}$, 1H, OH), 4.57 (m, 1H, CH, H_{1'}), 4.44 (d, $J = 4.9 \text{ Hz}$, 1H, OH), 3.90 (m, 1H, CH, H_{2'}), 3.78 (m, 1H, CH, H_{3'}), 3.45 (m, 2H, CH₂, H_{6'}), 2.23 (app dt, $J = 13.1, 8.5 \text{ Hz}$, 1H, CH₂, H_{5'}), 2.05 – 1.93 (m, 1H, CH, H_{4'}), 1.23 (app dt, $J = 13.1, 8.3 \text{ Hz}$, 1H, CH₂, H_{5'}) ppm. ¹³C NMR (151 MHz, DMSO-*d*₆) δ 159.9 (C), 155.5 (CH), 149.6 (C), 132.9 (CH), 128.0 (CH), 125.9 (CH), 123.3 (CH), 115.4 (C), 76.2 (CH), 72.6 (CH), 63.4 (CH₂), 56.1 (CH), 45.7 (CH), 30.4 (CH₂) ppm. HRMS (ESI+) calculated for C₁₄H₁₈N₃O₃ 276.1343 found 276.1333; Method A $t_{\text{R}} = 0.27 \text{ min}$; Purity (AUC) $\geq 95\%$.

4-(4-Phenylthiazol-2-yl)piperazine-1-carboxamide (21)

A mixture of piperazine-1-carboxamide hydrochloride (70.4 mg, 0.425 mmol), 2-bromo-4-phenyl-thiazole (68.0 mg, 0.283 mmol), potassium carbonate (117 mg, 0.850 mmol) and DMSO (1.4 mL) was heated at 130 °C in the MW for 7 h. Water (20 mL) was added and the product was extracted with Et₂O (3 x 20 mL), dried with MgSO₄, filtered and concentrated. The remaining oil was purified by column chromatography (Biotage SNAP KP-Sil 10 g eluting with 0-7% MeOH in CH₂Cl₂; 1 CV, gradient over 15 CV, 5 CV). The product was azeotroped with methanol, followed by ethyl acetate and dried to give the title compound as a yellow solid (24.8 mg, 30%, 0.086 mmol). MP 131 °C (decomp.); IR (thin film) ν = 3385, 3214, 2858, 1645, 1599, 1531 cm⁻¹; ¹H NMR (500 MHz, Methanol-*d*₄) δ 7.87 – 7.81 (m, 2H, ArH), 7.44 – 7.33 (m, 2H, ArH), 7.31 – 7.25 (m, 1H, ArH), 7.03 (s, 1H, ArH), 3.63 – 3.52 (m, 8H, piperazine) ppm. ¹³C NMR (126 MHz, Methanol-*d*₄) δ 171.2 (C=O), 159.6 (C), 151.6 (C), 135.0 (C), 128.1 (2 x CH), 127.3 (CH), 125.7 (2 x CH), 101.8 (CH), 42.9 (2 x CH₂), 39.0 (2 x CH₂) ppm. HRMS (ESI+) calculated for C₁₄H₁₇N₄OS 289.1118, found 289.1126; Method A t_R = 2.57 min; Purity (AUC) \geq 95%.

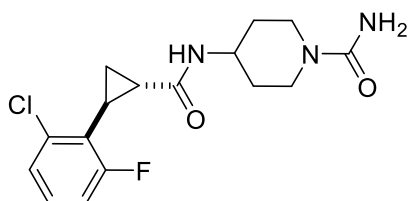
4-[3-Chloro-5-(trifluoromethyl)-2-pyridyl]piperazine-1-carboxamide (22)



To a stirred solution of piperazine-1-carboxamide hydrochloride (59.8 mg, 0.361 mmol) in NMP (0.8 mL) was added 3-chloro-2-fluoro-5-(trifluoromethyl)pyridine (0.040 mL, 0.301 mmol) and DIPEA (0.160 mL, 0.902 mmol). The solution was heated in the MW for 2 h at 100 °C. The reaction mixture was concentrated and purified by column chromatography (Biotage SNAP-Ultra C18 12 g eluting with 30-100% MeOH in water; 1 CV gradient over 10 CV, 6 CV) to give the title compound (67.7 mg, 73%, 0.219 mmol) as a white solid. MP 185 °C (decomp.); IR (thin film) ν = 3196, 2863, 1645, 1597, 1544 cm⁻¹; H NMR (500 MHz, Methanol-*d*₄) δ 8.46 (d, *J* = 2.1 Hz, 1H, ArH), 8.01 (d, *J* = 2.3 Hz, 1H, ArH), 5.50 (s, 2H, NH₂), 3.63-3.47 (m, 8H, piperazine) ppm. ¹³C NMR (126 MHz, Methanol-

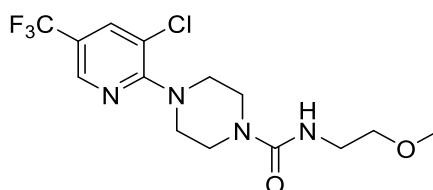
d_4) δ 159.9 (C=O), 159.8 (C), 142.7 (q, J = 4.2 Hz, CH), 135.9 (q, J = 3.4 Hz, CH), 123.4 (q, J = 271 Hz, CF_3), 120.9 (C), 120.0 (q, J = 33.4 Hz, C), 48.1 (2 x CH_2), 43.3 (2 x CH_2) ppm. HRMS (ESI+) calculated for $C_{11}H_{13}ClF_3N_4O$ 309.0724 found 309.0684; Method A t_R = 2.72 min; Purity (AUC) \geq 95%.

4-[[(*trans*)-2-(2-Chloro-6-fluoro-phenyl)cyclopropanecarbonyl]amino]-piperidine-1-carboxamide (23)



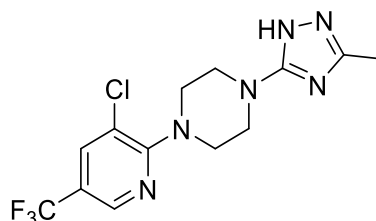
HATU (106.3 mg, 0.280 mmol) and DIPEA (0.160 mL, 0.930 mmol) were added to a solution of *trans*-2-(2-chloro-6-fluoro-phenyl)cyclopropanecarboxylic acid (40.0 mg, 0.186 mmol) in DMF (0.93 mL) at rt and stirred for 15 min. 4-Aminopiperidine-1-carboxamide dihydrochloride (44.3 mg, 0.205 mmol) was added and the solution was stirred for 24 h. Water (20 mL) was added and the product was extracted with ethyl acetate (3 x 15 mL) and dried using $MgSO_4$. The filtrate was concentrated and purified by column chromatography (Biotage SNAP-Ultra C18 12 g eluting with 20-100% MeOH in water; 1 CV gradient over 15 CV, 5 CV) to give the title compound (32.0 mg, 51%, 0.090 mmol) as a white solid. MP 216 °C (decomp.); IR (thin film) ν = 3254, 2925, 1633, 1599, 1561 cm^{-1} ; 1H NMR (500 MHz, Methanol- d_4) δ 7.26 – 7.22 (m, 2H, ArH), 7.06 – 7.00 (m, 1H, ArH), 4.05 – 3.87 (m, 3H, CH_2 , CH), 3.01-2.91 (m, 2H, CH_2), 2.33 (ddd, J = 9.3, 6.8, 4.6 Hz, 1H, CH), 1.98-1.84 (m, 4H, 2 x CH_2), 1.58 – 1.51 (m, 1H, CH_2 , CH_AH_B), 1.48 – 1.33 (m, 3H, CH_2 , CH_2 , CH_AH_B) ppm. ^{13}C NMR (126 MHz, Methanol- d_4) δ 172.7 (C=O), 162.0 (d, J = 248 Hz, CF), 159.8 (C=O) 136.8 (d, J = 5.4 Hz, C), 128.5 (d, J = 9.9 Hz, CH), 125.5 (d, J = 15.0 Hz, C), 125.1 (d, J = 3.6 Hz, CH), 114.2 (d, J = 23.5 Hz, CH), 46.8 (CH), 42.7 (2 x CH_2), 31.3 (2 x CH_2), 23.0 (CH), 18.0 (CH_2), 13.9 (CH) ppm. HRMS (ESI+) calculated for $C_{16}H_{20}ClF_3N_3O_2$ 340.1223 found 340.1193; Method A t_R = 2.46 min; Purity (AUC) \geq 95%.

4-(3-Chloro-5-(trifluoromethyl)pyridin-2-yl)-N-(2-methoxyethyl) piperazine-1-carboxamide (24)



2-Methoxyethanamine (0.040 mL, 0.452 mmol) was added dropwise over 20 min to a solution of CDI (73 mg, 0.452 mmol) dissolved in CH₂Cl₂ (3.1 mL) at 0 °C. After stirring for 20 min the solution was warmed to rt. After 1.5 h, 1-[3-chloro-5-(trifluoromethyl)-2-pyridyl]piperazine (100 mg, 0.376 mmol) was added and the solution was stirred for 18 h. Purification by column chromatography (Biotage SNAP KP-Sil 10 g eluting with 0-10% EtOH in CH₂Cl₂; 1CV, gradient over 10CV, 5CV) gave the title compound (101 mg, 73%, 0.275 mmol) as a white solid. MP 130 °C (decomp.); IR (thin film) ν = 3297, 2891, 2850, 1605, 1543, 1096 cm⁻¹; ¹H NMR (500 MHz, Chloroform-*d*) δ 8.42-8.41 (m, 1H, ArH), 7.80 (d, *J* = 2.1 Hz, 1H, ArH), 3.59 – 3.53 (m, 8H, piperazine), 3.53 – 3.47 (m, 4H, 2 x CH₂), 3.39 (s, 3H, CH₃) ppm; ¹³C NMR (126 MHz, Chloroform-*d*) δ 159.3 (C), 157.7 (C=O), 142.7 (CH), 136.4 (CH), 123.1 (CF₃, q, *J* = 272 Hz), 121.1 (CH), 120.4 (C, q, *J* = 33.8) 71.8 (CH₂), 58.9 (CH₃), 48.3 (2 x CH₂), 43.7 (2 x CH₂), 40.8 (CH₂) ppm; HRMS (ESI+) calculated for C₁₄H₁₉ClF₃N₄O₂ 367.1143, found 367.1142; Method A *t*_R = 2.88 min; Purity (AUC) \geq 95%.

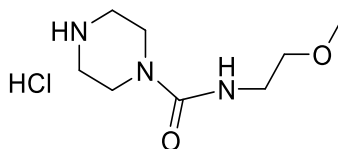
1-(3-Chloro-5-(trifluoromethyl)pyridin-2-yl)-4-(3-methyl-1H-1,2,4-triazol-5-yl) piperazine (25)



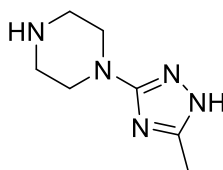
1-Amino-2-methylisothiourea hydroiodide (132 mg, 0.565 mmol) was dissolved in 1:1 IPA (0.47 mL): water (0.47 mL). 1-[3-Chloro-5-(trifluoromethyl)-2-

pyridyl]piperazine (50.0 mg, 0.188 mmol) and triethylamine (0.08 mL, 0.941 mmol) was added and the solution was refluxed for 6 h. The solvent was removed and the resulting solid was dried thoroughly, dissolved in acetic acid (0.95 mL, 16.61 mmol) and heated for 18 h at 130 °C. The solvent was removed. Purification by reverse phase column chromatography (Biotage SNAP-Ultra C18 12 g eluting with 10-100% MeOH in water; 1CV, gradient over 10CV, 6CV) gave the title compound (45.0 mg, 69%, 0.130 mmol) as an orange solid. MP 174 °C (decomp.); IR (thin film) $\nu = 3033, 2912, 2848, 1543, 1114 \text{ cm}^{-1}$; $^1\text{H NMR}$ (500 MHz, Methanol- d_4) δ 8.47 (d, $J = 2.1 \text{ Hz}$, 1H, ArH), 8.01 (d, $J = 2.2 \text{ Hz}$, 1H, ArH), 3.65 – 3.58 (m, 4H, piperazine), 3.51 (dd, $J = 6.4, 3.6 \text{ Hz}$, 4H, piperazine), 2.31 (s, 3H, CH₃) ppm. $^{13}\text{C NMR}$ (126 MHz, Chloroform- d) δ 164.0 (C), 159.6 (C), 159.1 (C), 142.9 (q, $J = 4.2 \text{ Hz}$, CH), 136.0 (q, $J = 4.0 \text{ Hz}$, CH), 123.1 (q, $J = 272 \text{ Hz}$, CF₃), 121.0 (C), 120.4 (q, $J = 34.3 \text{ Hz}$, C), 47.9 (2 x CH₂), 46.5 (2 x CH₂), 15.2 (CH₃) ppm. HRMS (ESI+) calculated for C₁₃H₁₅ClF₃N₆ 347.0993, found 347.0985; Method A $t_{\text{R}} = 2.82 \text{ min}$; Purity (AUC) $\geq 95\%$.

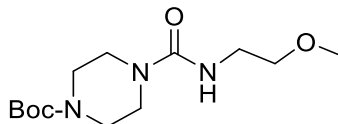
***N*-(2-Methoxyethyl)piperazine-1-carboxamide hydrochloride (30)**



4M HCl in 1,4-dioxane (38 mL, 150 mmol) was added to a stirred solution of *tert*-butyl 4-(2-methoxyethylcarbamoyl)piperazine-1-carboxylate (1.08 g, 3.76 mmol) in methanol (38 mL) and stirred for 4 h at rt. The solvent was removed and the resulting white solid was dried thoroughly to give the title compound (840 mg, 100%, 3.76 mmol) as a white solid. MP 168 °C (decomp.); IR (thin film) $\nu = 3335, 2942, 2731, 2619, 2477, 1695, 1624 \text{ cm}^{-1}$; $^1\text{H NMR}$ (500 MHz, Methanol- d_4) δ 3.69 – 3.64 (m, 4H, piperazine), 3.46 (t, $J = 5.6 \text{ Hz}$, 2H, CH₂), 3.35 (m, 5H, CH₂, CH₃), 3.23 – 3.19 (m, 4H, piperazine) ppm. $^{13}\text{C NMR}$ (126 MHz, Methanol- d_4) δ 159.5 (C=O), 72.6 (CH₂), 59.0 (CH₃), 44.4 (2 x CH₂), 42.1 (2 x CH₂), 41.6 (CH₂) ppm. HRMS (ESI+) calculated for C₈H₁₈N₃O₂ 188.1394, found 188.1402; Method B $t_{\text{R}} = 0.35 \text{ min}$; Purity (AUC) not UV visible.

1-(5-Methyl-1H-1,2,4-triazol-3-yl)piperazine (31)

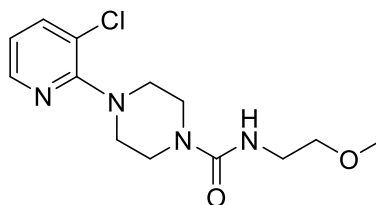
To a stirred solution of 3-bromo-5-methyl-1H-1,2,4-triazole (50.0 mg, 0.309 mmol) in NMP (1.0 mL) was added piperazine (79.8 mg, 0.926 mmol). The resulting solution was heated at 200 °C for 1.5 h in the MW. The reaction mixture was purified by ion exchange chromatography (Biotage SCX, 2 g) and the product was eluted with 2M NH₃ in MeOH. The MeOH layer was concentrated, added dropwise to KPNH column insert and dried in a desiccator. Purification by column chromatography (Biotage NH-Sil 11 g eluting with 0-10% MeOH in CH₂Cl₂; 1 CV, gradient over 10 CV, 5 CV) gave the title compound (28.5 mg, 55%, 0.170 mmol) as a white solid. MP 115 °C (decomp.); IR (thin film) ν = 3305, 2950, 2904, 2847, 1575, 1534 cm⁻¹; ¹H NMR (500 MHz, Methanol-*d*₄) δ 3.37-3.27 (m, 4H, piperazine), 2.96 – 2.86 (m, 4H, piperazine), 2.29 (s, 3H, CH₃) ppm. ¹³C NMR (126 MHz, Methanol-*d*₄) δ 164.5 (C), 156.2 (C), 48.2 (2 x CH₂), 45.7 (2 x CH₂), 12.4 (CH₃) ppm. HRMS (ESI+) calculated for C₇H₁₄N₅ 169.1266, found 169.1270; Method A *t*_R = 0.15 min; Purity (AUC) \geq 95%.

4-(2-Methoxyethylcarbamoyl)piperazine-1-carboxylate (32)

2-Methoxyethanamine (0.56 mL, 6.44 mmol) was added dropwise over 20 min to CDI (1.044 g, 6.44 mmol) dissolved in CH₂Cl₂ (27 mL) at 0 °C. After stirring for 20 min the solution was warmed to rt. After 1.5 h, *tert*-butyl piperazine-1-carboxylate (1.00 g, 5.37 mmol) was added and stirred for 18 h. Purification by column chromatography (Biotage SNAP KP-Sil 100g eluting with 0-10% MeOH

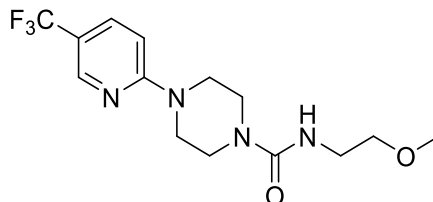
in CH₂Cl₂; 1 CV, gradient over 15 CV, 5 CV) gave the title compound (1.14 g, 74%, 3.96 mmol) as a white solid. MP 94 °C (decomp.); IR (thin film) ν = 3341, 2977, 2862, 1694, 1619, 1540 cm⁻¹; ¹H NMR (500 MHz, Methanol-*d*₄) δ 3.46 – 3.43 (m, 2H, CH₂), 3.42 – 3.35 (m, 8H, piperazine), 3.34 (m, 5H, CH₂, CH₃), 1.47 (s, 9H, CH₃) ppm. ¹³C NMR (126 MHz, Methanol-*d*₄) δ 159.9 (C=O), 156.2 (C=O), 81.4 (C), 72.6 (CH₂), 58.8 (CH₃), 44.5 (4 x CH₂), 41.3 (CH₂), 28.5 (3 x CH₃) ppm. HRMS (ESI+) calculated for C₁₃H₂₆N₃O₄ 288.1918, found 288.1916; Method A *t*_R = 2.47 min; Purity (AUC) not UV visible.

4-(3-Chloro-2-pyridyl)-*N*-(2-methoxyethyl)piperazine-1-carboxamide (39)



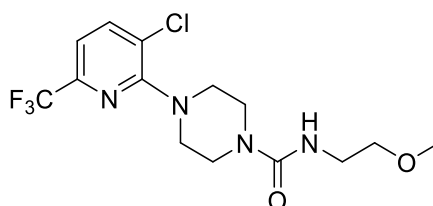
To a stirred solution of *N*-(2-methoxyethyl)piperazine-1-carboxamide hydrochloride (70.0 mg, 0.313 mmol) in ethanol (0.8 mL) was added 2,3-dichloropyridine (35.0 mg, 0.237 mmol) and DIPEA (0.12 mL, 0.710 mmol). The solution was heated in the MW for 8 h at 180°C. The reaction mixture was concentrated and purified by column chromatography (Biotage SNAP KP-Sil 10 g eluting with 0-10% MeOH in CH₂Cl₂; 1 CV, gradient over 10 CV, 5 CV). Fractions with product and coeluted impurity were dissolved in CH₂Cl₂ and loaded onto a pad of silica, washed with 20% MeCN in CH₂Cl₂ to remove the impurity followed by 10% MeOH in CH₂Cl₂ to elute the title compound (10.6 mg, 15%, 0.036 mmol) as a white solid. MP 85 °C (decomp.); IR (thin film) ν = 3356, 2851, 1625, 1577, 1539 cm⁻¹; ¹H NMR (500 MHz, Methanol-*d*₄) δ 8.19 (dd, *J* = 4.8, 1.7 Hz, 1H, ArH), 7.75 (dd, *J* = 7.8, 1.6 Hz, 1H, ArH), 6.99 (dd, *J* = 7.8, 4.8 Hz, 1H, ArH), 3.60 – 3.52 (m, 4H, piperazine), 3.51 – 3.45 (m, 2H, CH₂), 3.39–3.35 (m, 5H, CH₂, CH₃), 3.35 – 3.27 (m, 4H, piperazine) ppm. ¹³C NMR (126 MHz, Methanol-*d*₄) δ 158.8 (C), 158.1 (C=O), 145.6 (CH), 139.0 (CH), 122.9 (C), 118.5 (CH), 71.4 (CH₂), 57.5 (CH₃), 48.7 (2 x CH₂), 43.4 (2 x CH₂), 40.0 (CH₂) ppm. HRMS (ESI+) calculated for C₁₃H₂₀ClN₄O₂ 299.1269, found 299.1276; Method A *t*_R = 2.34 min; Purity (AUC) ≥ 95%.

***N*-(2-Methoxyethyl)-4-[5-(trifluoromethyl)-2-pyridyl]piperazine-1-carboxamide (40)**



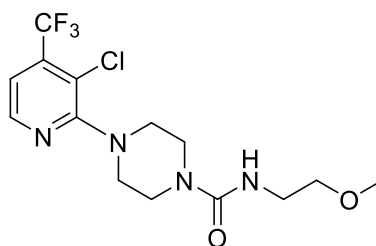
To a stirred solution of *N*-(2-methoxyethyl)piperazine-1-carboxamide hydrochloride (44.3 mg, 0.198 mmol) in ethanol (0.8 mL) was added 2-chloro-5-(trifluoromethyl)pyridine (30.0 mg, 0.165 mmol) and triethylamine (0.070 mL, 0.496 mmol). The resulting solution was heated at 100 °C for 18 h. Purification by column chromatography (Biotage SNAP KP-Sil 10 g eluting with 0-10% MeOH in CH₂Cl₂ 1 CV, gradient over 10 CV, 5 CV) gave the title compound (30.4 mg, 55%, 0.092 mmol) as a white solid. MP 169 °C (decomp.); IR (thin film) ν = 3307, 2923, 2851, 2433, 1607, 1549 cm⁻¹; ¹H NMR (500 MHz, Methanol-*d*₄) δ 8.37-8.34 (m, 1H, ArH), 7.74 (dd, *J* = 9.1, 2.5 Hz, 1H, ArH), 6.89 (d, *J* = 9.2 Hz, 1H, ArH), 3.72 – 3.68 (m, 4H, piperazine), 3.55 – 3.51 (m, 4H, piperazine), 3.46 (t, *J* = 5.7 Hz, 2H, CH₂), 3.39-3.33 (m, 5H, CH₂, CH₃) ppm. ¹³C NMR (126 MHz, Methanol-*d*₄) δ 160.4 (C=O), 158.7 (C), 145.0 (q, *J* = 4.4 Hz, CH), 134.3 (q, *J* = 3.5 Hz, CH), 124.7 (q, *J* = 269 Hz, CF₃), 115.0 (q, *J* = 33.0 Hz, C), 106.1 (CH), 71.4 (CH₂), 57.5 (CH₃), 44.0 (2 x CH₂), 42.8 (2 x CH₂), 40.0 (CH₂) ppm. HRMS (ESI+) calculated for C₁₄H₂₀F₃N₄O₂ 333.1533, found 333.1528.; Method A *t*_R = 2.59 min; Purity (AUC) \geq 95%.

4-[3-Chloro-6-(trifluoromethyl)-2-pyridyl]-*N*-(2-methoxyethyl)piperazine-1-carboxamide (41)



To a stirred solution of *N*-(2-methoxyethyl)piperazine-1-carboxamide hydrochloride (48.5 mg, 0.217 mmol) in ethanol (0.8 mL) was added 2,3-dichloro-6-(trifluoromethyl)pyridine (39.0 mg, 0.181 mmol) and triethylamine (0.080 mL, 0.542 mmol). The resulting solution was heated at 140 °C in the MW for 1.5 h. Purification by column chromatography (Biotage SNAP KP-Sil 10 g eluting with 0-8% MeOH in CH₂Cl₂; 1 CV, gradient over 10 CV, 5 CV) gave the title compound (21.0 mg, 32%, 0.060 mmol) as a clear solid. MP 106 °C (decomp.); IR (thin film) ν = 3370, 2846, 1614, 1542 cm⁻¹; ¹H NMR (500 MHz, Methanol-*d*₄) δ 7.92 (d, *J* = 7.9 Hz, 1H, ArH), 7.32 (d, *J* = 7.9 Hz, 1H, ArH), 3.57 – 3.53 (m, 4H, piperazine), 3.46 (t, *J* = 5.7 Hz, 2H, CH₂), 3.44-3.39 (m, 4H, piperazine), 3.38-3.33 (m, 5H, CH₂,CH₃) ppm. ¹³C NMR (126 MHz, Methanol-*d*₄) δ 160.2 (C=O), 159.3 (C), 145.3 (q, *J* = 34.8 Hz, C), 141.6 (CH), 126.6 (C), 122.7 (q, *J* = 273 Hz, CF₃), 115.7 (q, *J* = 3.4 Hz, CH), 72.8 (CH₂), 58.9 (CH₃), 49.7 (2 x CH₂), 44.6 (2 x CH₂), 41.4 (CH₂) ppm. HRMS (ESI+) calculated for C₁₄H₁₉ClF₃N₄O₂ 367.1143, found 367.1134; Method A *t*_R = 2.83 min; Purity (AUC) \geq 95%.

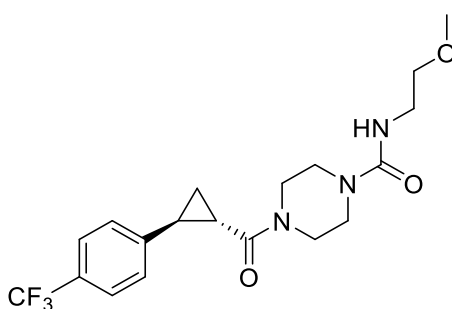
4-[3-Chloro-4-(trifluoromethyl)-2-pyridyl]-*N*-(2-methoxyethyl)piperazine-1-carboxamide (42)



To a stirred solution of *N*-(2-methoxyethyl)piperazine-1-carboxamide hydrochloride (55.9 mg, 0.250 mmol) in ethanol (1.0 mL) was added 2,3-dichloro-4-(trifluoromethyl)pyridine (45.0 mg, 0.208 mmol) and triethylamine (0.090 mL, 0.625 mmol). The resulting solution was heated at 140 °C in the MW for 3.5 h. The reaction mixture was purified by column chromatography (Biotage SNAP KP-Sil 10 g (0-8% MeOH in CH₂Cl₂; 1 CV, gradient over 10 CV, 5 CV) to give the title compound (25.0 mg, 33%, 0.070 mmol) as a white solid. MP 114 °C (decomp.); IR (thin film) ν = 3326, 2850, 1612, 1540 cm⁻¹; ¹H NMR (500 MHz,

Methanol- d_4) δ 8.38 (d, J = 5.1 Hz, 1H, ArH), 7.32 (d, J = 5.1 Hz, 1H, ArH), 3.60 – 3.54 (m, 4H, piperazine), 3.50 – 3.43 (m, 2H, CH₂), 3.39 – 3.33 (m, 9H, piperazine, CH₂, CH₃) ppm. ¹³C NMR (126 MHz, Methanol- d_4) δ 160.0 (C), 158.8 (C=O), 146.5 (CH), 137.6 (q, J = 32.0 Hz, C), 122.1 (q, J = 274 Hz, CF₃), 119.5 (C), 114.7 (q, J = 4.8 Hz, CH), 71.4 (CH₂), 57.5 (CH₃), 49.0 (2 x CH₂), 43.3 (2 x CH₂), 40.0 (CH₂) ppm. HRMS (ESI+) calculated for C₁₄H₁₉ClF₃N₄O₂ 367.1143, found 367.1151; Method A t_R = 2.79 min; Purity (AUC) \geq 95%.

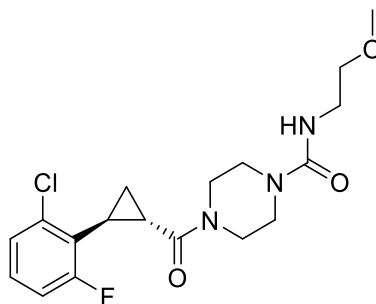
***N*-(2-Methoxyethyl)-4-[(*trans*)-2-[4-(trifluoromethyl)phenyl]cyclopropane-carbonyl] piperazine-1-carboxamide (43)**



HATU (99.1 mg, 0.261 mmol) and DIPEA (0.15 mL, 0.87 mmol) were added to a stirred solution of (*trans*)-2-[4-(trifluoromethyl)phenyl]cyclopropanecarboxylic acid (40.0 mg, 0.174 mmol) in DMF (0.9 mL) at rt for 15 min. *N*-(2-Methoxyethyl)piperazine-1-carboxamide hydrochloride (42.8 mg, 0.191 mmol) was added and the solution was stirred at rt for 48 h. Water (20 mL) was added and the product was extracted with ethyl acetate (3 x 15 mL) and dried using MgSO₄. The crude mixture was purified by reverse phase column chromatography (Biotage SNAP-Ultra C18 12 g eluting with 20-100% MeOH in water; 1 CV gradient over 10 CV, 6 CV) to give the title compound (48 mg, 69%, 0.12 mmol) as a white solid. MP 141 °C (decomp.); IR (thin film) ν = 3412, 2860, 1642, 1615, 1532 cm⁻¹; ¹H NMR (500 MHz, Methanol- d_4) δ 7.67 – 7.49 (m, 2H, ArH), 7.37 (d, J = 8.1 Hz, 2H, ArH), 3.80 – 3.60 (m, 4H, piperazine), 3.50 – 3.38 (m, 6H, CH₂, piperazine), 3.38 - 3.33 (m, 5H, CH₂, CH₃), 2.51 (ddd, J = 9.1, 6.2, 4.2 Hz, 1H, CH), 2.35 (ddd, J = 8.4, 5.4, 4.3 Hz, 1H, CH), 1.63 (ddd, J = 9.0, 5.4, 4.4 Hz, 1H, CH₂, CH_AH_B), 1.42 (ddd, J = 8.5, 6.2, 4.4 Hz, 1H, CH₂, CH_AH_B) ppm. ¹³C NMR (126 MHz, Methanol- d_4) δ 171.1 (C=O), 158.5 (C=O), 145.4 (C), 128.1 (q, J = 32.3 Hz, C), 126.3 (2 x CH), 125.0 (q, J = 3.9 Hz, 2 x CH), 124.4 (q, J =

271 Hz, CF₃), 71.3 (CH₂), 57.5 (CH₃), 45.0 (CH₂), 43.4 (CH₂), 43.1 (CH₂), 41.7 (CH₂), 40.0 (CH₂), 24.7 (CH), 22.9 (CH), 15.8 (CH₂) ppm. HRMS (ESI+) calculated for C₁₉H₂₅F₃N₃O₃ 400.1843, found 400.1825; Method A t_R = 2.75 min; Purity (AUC) ≥ 95%.

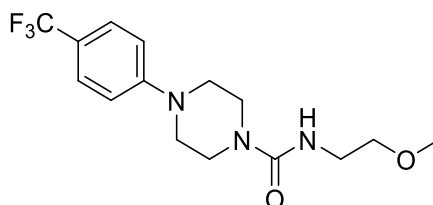
4-[(*trans*)-2-(2-Chloro-6-fluoro-phenyl)cyclopropanecarbonyl]-*N*-(2-methoxyethyl)piperazine-1-carboxamide (44)



HATU (106 mg, 0.280 mmol) and DIPEA (0.160 mL, 0.930 mmol) were added to a solution of (*trans*)-2-(2-chloro-6-fluoro-phenyl)cyclopropanecarboxylic acid (40.0 mg, 0.186 mmol) in DMF (0.9 mL) at rt and stirred for 15 min. *N*-(2-Methoxyethyl)piperazine-1-carboxamide hydrochloride (45.9 mg, 0.205 mmol) was added and the solution was stirred for 72 h. Water (20 mL) was added, the product was extracted with ethyl acetate (3 x 15 mL) and dried with MgSO₄. The filtrate was concentrated, dissolved in DMSO (1 mL) and purified by reverse phase column chromatography (Biotage SNAP-Ultra C18 12 g eluting with 20-100% MeOH in water; 1 CV gradient over 15 CV, 5 CV) to give the title compound (52 mg, 73%, 0.14 mmol) as a pale-yellow oil. IR (thin film) ν = 3365, 2926, 1619, 1538 cm⁻¹; ¹H NMR (500 MHz, Methanol-*d*₄) δ 7.30 – 7.20 (m, 2H, ArH), 7.13 – 6.99 (m, 1H, ArH), 3.88 – 3.38 (m, 10H, CH₂, piperazine), 3.37-3.33 (m, 5H, CH₂, CH₃), 2.41 – 2.27 (m, 2H, CH, CH), 1.69 – 1.58 (m, 1H, CH₂, CH_AH_B), 1.44 (dddd, *J* = 8.2, 6.8, 4.4, 1.3 Hz, 1H, CH₂, CH_AH_B) ppm. ¹³C NMR (126 MHz, Methanol-*d*₄) δ 171.8, (C=O), 162.1 (d, *J* = 248 Hz, CF), 158.6 (C=O), 136.7 (d, *J* = 5.3 Hz, C), 128.7 (d, *J* = 10.0 Hz, CH), 125.4 (d, *J* = 15.0 Hz, C), 125.2 (d, *J* = 3.5 Hz, CH), 114.3 (d, *J* = 23.5 Hz, CH), 71.3 (CH₂), 57.6 (CH₃), 45.2 (CH₂), 43.4 (d, *J* = 40.9 Hz, (CH₂)), 41.8 (CH₂), 40.0 (CH₂), 19.4 (d, *J* = 4.2 Hz, CH), 19.1 (CH), 15.3 (d, *J* = 6.0 Hz, CH₂) ppm. HRMS (ESI+)

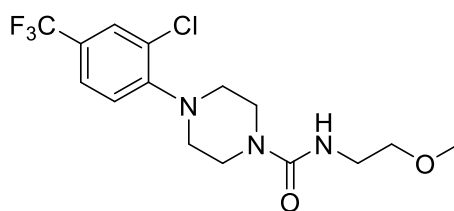
calculated for $C_{18}H_{24}ClFN_3O_3$, 384.1485 found 384.1493; Method A $t_R = 2.65$ min; Purity (AUC) $\geq 95\%$.

***N*-(2-Methoxyethyl)-4-[4-(trifluoromethyl)phenyl]piperazine-1-carboxamide (45)**

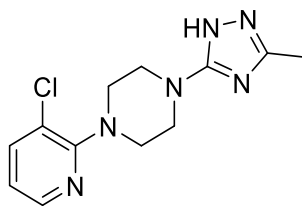


A mixture of *N*-(2-methoxyethyl)piperazine-1-carboxamide hydrochloride (50.0 mg, 0.224 mmol), 1-bromo-4-(trifluoromethyl)benzene (0.030 mL, 0.224 mmol), BINAP (7.0 mg, 0.011 mmol) and Cs_2CO_3 (218 mg, 0.671 mmol) in toluene (2.1 mL) was purged with N_2 . $Pd(OAc)_2$ (2.0 mg, 0.009 mmol) was added and the mixture was refluxed for 18 h. The mixture was passed through a 5g SCX and eluted with 2N $NH_3/MeOH$. The solvent was removed and the remaining solid was purified by column chromatography (Biotage SNAP KP-Sil 10 g eluting with 0-10% MeOH in CH_2Cl_2 ; 1 CV, gradient over 10 CV, 5 CV) to give the title compound (38.5 mg, 52%, 0.116 mmol) as a white solid. MP 167 °C (decomp.); IR (thin film) $\nu = 3293, 2881, 1615, 1543, 1524\text{ cm}^{-1}$; 1H NMR (500 MHz, Methanol- d_4) δ 7.54 – 7.45 (m, 2H, ArH), 7.10 – 7.01 (m, 2H, ArH), 3.62 – 3.53 (m, 4H, piperazine), 3.49 – 3.45 (m, 2H, CH_2), 3.39-3.35 (m, 5H, CH_2, CH_3), 3.34 – 3.30 (m, 4H, piperazine) ppm. ^{13}C NMR (126 MHz, Methanol- d_4) δ 158.6 (C=O), 153.4 (C), 126.0 (2 x CH), 125.0 (q, $J = 250$ Hz, CF_3), 120.1 (q, $J = 32.4$ Hz, C), 114.5 (2 x CH), 71.4 (CH_2), 57.5 (CH_3), 47.4 (2 x CH_2), 43.1 (2 x CH_2), 40.0 (CH_2). HRMS (ESI+) calculated for $C_{15}H_{21}F_3N_3O_2$ 333.1610, found 333.1607; Method A $t_R = 2.75$ min; Purity (AUC) $\geq 95\%$.

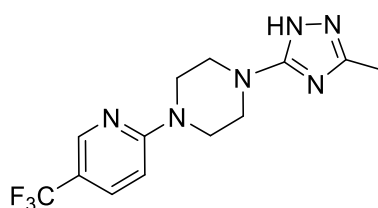
4-[2-Chloro-4-(trifluoromethyl)phenyl]-N-(2-methoxyethyl)piperazine-1-carboxamide (46)



A mixture of *N*-(2-methoxyethyl)piperazine-1-carboxamide hydrochloride (55.0 mg, 0.246 mmol), 1-bromo-2-chloro-4-(trifluoromethyl)benzene (0.040 mL, 0.246 mmol), BINAP (7.7 mg, 0.012 mmol) and Cs₂CO₃ (240.4 mg, 0.738 mmol) in toluene (2.1 mL) was purged with N₂. Pd(OAc)₂ (2.2 mg, 0.010 mmol) was added and the mixture was refluxed for 6 h. The mixture was passed through a SCX column (Biotage, 5 g) with MeOH and the filtrate concentrated *in vacuo*. The remaining solid was purified by column chromatography (Biotage SNAP-Ultra C18 12 g eluting with 10-100% MeOH in water; 1 CV gradient over 10CV, 5 CV) to give the title compound (27.0 mg, 30%, 0.070 mmol) as a beige solid. MP 123.5 °C (decomp.); IR (thin film) ν = 3347, 2887, 2845, 1609, 1540, 1503 cm⁻¹; ¹H NMR (500 MHz, Methanol-*d*₄) δ 7.69 (d, *J* = 2.2 Hz, 1H, ArH), 7.58 (dd, *J* = 8.4, 2.1 Hz, 1H, ArH), 7.28 (d, *J* = 8.5 Hz, 1H, ArH), 3.61 – 3.57 (m, 4H, piperazine), 3.50 – 3.45 (m, 2H, CH₂), 3.40 – 3.35 (m, 5H, CH₂, CH₃), 3.13 – 3.09 (m, 4H, piperazine) ppm. ¹³C NMR (151 MHz, Methanol-*d*₄) δ 158.8 (C=O), 152.3 (C), 127.8 (q, *J* = 197 Hz, C), 127.2 (q, *J* = 3.9 Hz, CH), 125.3 (q, *J* = 33.9 Hz, C), 124.7 (q, *J* = 3.9 Hz, CH), 122.8 (C), 120.8 (CH), 71.4 (CH₂), 57.5 (CH₃), 50.5 (2 x CH₂), 43.6 (2 x CH₂), 40.0 (CH₂) ppm. HRMS (ESI+) calculated for C₁₅H₂₀ClF₃N₃O₂ 366.1191, found 366.1197; Method A *t*_R = 2.96 min; Purity (AUC) \geq 95%.

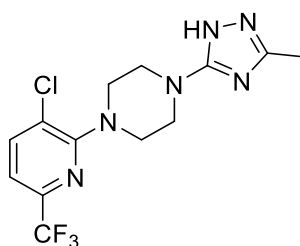
1-(3-Chloro-2-pyridyl)-4-(3-methyl-1*H*-1,2,4-triazol-5-yl)piperazine (47)

To a stirred solution of 1-(3-methyl-1*H*-1,2,4-triazol-5-yl)piperazine dihydrochloride (88.6 mg, 0.369 mmol) in NMP (1.4 mL) was added 2,3-dichloropyridine (42.0 mg, 0.284 mmol) and DIPEA (0.150 mL, 0.851 mmol). The solution was heated in the MW for 4 h at 200 °C. The reaction mixture was concentrated and purified by reverse phase column chromatography (Biotage SNAP-Ultra C18 12 g eluting with 0-80% MeOH in water; 1 CV gradient over 20CV, 5CV). Fractions with product were further purified by column chromatography (Biotage SNAP KP-Sil 10 g eluting with 0-10% MeOH in CH₂Cl₂; 1 CV, gradient over 10CV, 5CV) to give the title compound (11 mg, 14%, 0.04 mmol) as an oil. IR (thin film) $\nu = 3171, 2848, 1578, 1542 \text{ cm}^{-1}$; ¹H NMR (500 MHz, Methanol-*d*₄) δ 8.18 (dd, *J* = 4.8, 1.6 Hz, 1H, ArH), 7.74 (dd, *J* = 7.8, 1.6 Hz, 1H, ArH), 6.98 (dd, *J* = 7.8, 4.8 Hz, 1H, ArH), 3.55-3.46 (m, 4H, piperazine), 3.44-3.38 (m, 4H, piperazine), 2.31 (s, 3H, CH₃) ppm. ¹³C NMR (126 MHz, Methanol-*d*₄) δ 158.2 (C), 145.6 (CH), 139.0 (CH), 122.9 (C), 118.5 (CH), 48.3 (2 x CH₂), 46.5 (2 x CH₂), 11.0 (CH₃) ppm. Triazole quaternary carbons are not visible due to tautomerisation. HRMS (ESI+) calculated for C₁₂H₁₆ClN₆ 279.1119, found 279.1124; Method A *t*_R = 2.15 min; Purity (AUC) \geq 95%.

1-(3-Methyl-1*H*-1,2,4-triazol-5-yl)-4-[5-(trifluoromethyl)-2-pyridyl]piperazine (48)

To a stirred solution of 1-(3-methyl-1*H*-1,2,4-triazol-5-yl)piperazine dihydrochloride (55.6 mg, 0.231 mmol) in ethanol (0.8 mL) was added 2-chloro-5-(trifluoromethyl)pyridine (35.0 mg, 0.193 mmol) and triethylamine (0.080 mL, 0.578 mmol). The resulting solution was heated at 140 °C in the MW for 1.5 h. The reaction mixture was concentrated and purified by column chromatography (Biotage SNAP KP-Sil 10 g eluting with 0-10% MeOH in CH₂Cl₂; 1 CV, gradient over 15 CV, 5 CV). Fractions with product were concentrated and the remaining solid was dissolved in MeOH and washed through a 2 g Biotage Isolute NH₂ column with MeOH to give the title compound (13.4 mg, 22%, 0.043 mmol) as a white solid. MP 237 °C (decomp.); IR (thin film) ν = 3179, 2937, 2852, 1631, 1553 cm⁻¹; ¹H NMR (500 MHz, Methanol-*d*₄) δ 8.37 (d, *J* = 2.7 Hz, 1H, ArH), 7.74 (dd, *J* = 9.1, 2.6 Hz, 1H, ArH), 6.95 (d, *J* = 9.1 Hz, 1H, ArH), 3.85 – 3.72 (m, 4H, piperazine), 3.50 – 3.40 (m, 4H, piperazine), 2.31 (s, 3H, CH₃) ppm. ¹³C NMR (126 MHz, Methanol-*d*₄) δ 160.5 (C), 145.0 (q, *J* = 4.4 Hz, CH), 134.4 (q, *J* = 3.3 Hz, CH), 124.7 (d, *J* = 269 Hz, CF₃), 114.9 (q, *J* = 33.0 Hz, C), 106.2 (CH), 46.2 (2 x CH₂), 43.7 (2 x CH₂), 10.9 (CH₃) ppm. Triazole quaternary carbons are not visible due to tautomerisation. HRMS (ESI+) calculated for C₁₃H₁₆F₃N₆ 313.1383, found 313.1378; Method A *t*_R = 2.52 min; Purity (AUC) \geq 95%.

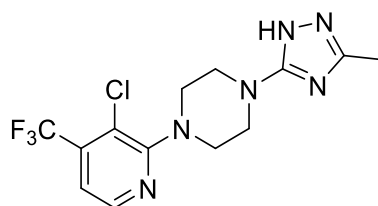
1-[3-Chloro-6-(trifluoromethyl)-2-pyridyl]-4-(3-methyl-1*H*-1,2,4-triazol-5-yl)piperazine (49)



To a stirred solution of 1-(3-methyl-1*H*-1,2,4-triazol-5-yl)piperazine dihydrochloride (53.4 mg, 0.222 mmol) in ethanol (0.8 mL) was added 2,3-dichloro-6-(trifluoromethyl)pyridine (40.0 mg, 0.185 mmol) and triethylamine (0.080 mL, 0.556 mmol). The resulting solution was heated at 140 °C in the MW for 1.5 h. The reaction mixture was concentrated and purified by column chromatography (Biotage SNAP KP-Sil 10 g eluting with 0-8% MeOH in CH₂Cl₂; 1 CV, gradient over 10 CV, 5 CV). Fractions with product were concentrated and

the remaining solid was dissolved in MeOH and washed through a 2 g Biotage Isolute NH₂ column with MeOH to give the title compound (29.0 mg, 45%, 0.080 mmol) as a white solid. MP 139 °C (decomp.); IR (thin film) ν = 3370, 2845, 1614, 1590, 1542 cm⁻¹; ¹H NMR (500 MHz, Methanol-*d*₄) δ 8.39 (d, *J* = 5.0, 1H, ArH), 7.32 (d, *J* = 5.0 Hz, 1H, ArH), 3.56-3.49 (m, 4H, piperazine), 3.50-3.43 (m, 4H, piperazine), 2.30 (s, 3H, CH₃) ppm. ¹³C NMR (126 MHz, Methanol-*d*₄) δ 164.6 (C), 161.5 (C), 156.1 (C), 148.0 (CH), 139.0 (q, *J* = 31.9 Hz, C), 123.5 (q, *J* = 274 Hz, CF₃), 121.0 (C), 116.1 (q, *J* = 4.9 Hz, CH), 50.0 (2 x CH₂), 47.8 (2 x CH₂), 12.4 (CH₃) ppm. HRMS (ESI+) calculated for C₁₃H₁₅ClF₃N₆ 347.0993, found 347.0989; Method A *t*_R = 2.74 min; Purity (AUC) \geq 95%.

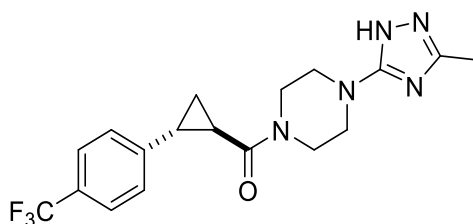
1-[3-Chloro-4-(trifluoromethyl)-2-pyridyl]-4-(3-methyl-1H-1,2,4-triazol-5-yl)piperazine (50)



To a stirred solution of 1-(3-methyl-1H-1,2,4-triazol-5-yl)piperazine dihydrochloride (53.4 mg, 0.222 mmol) in ethanol (0.8 mL) was added 2,3-dichloro-4-(trifluoromethyl)pyridine (40.0 mg, 0.185 mmol) and triethylamine (0.080 mL, 0.556 mmol). The resulting solution was heated at 140 °C in the MW for 1.5 h. The reaction mixture was concentrated and purified by column chromatography (Biotage SNAP KP-Sil 10 g eluting with 0-6% MeOH in CH₂Cl₂; 1 CV, gradient over 10 CV, 5 CV). Fractions with product were concentrated and the remaining solid was dissolved in and washed through a 2 g Biotage Isolute NH₂ column with MeOH to give the title compound (34.0 mg, 53%, 0.100 mmol) as a white solid. MP 140 °C (decomp.); IR (thin film) ν = 2846, 2151, 2012, 1586, 1542 cm⁻¹; ¹H NMR (500 MHz, Methanol-*d*₄) δ 7.93 (d, *J* = 7.9, 1H, ArH), 7.34 (d, *J* = 8.0 Hz, 1H, ArH), 3.60 – 3.44 (m, 8H, piperazine), 2.31 (s, 3H, CH₃) ppm. ¹³C NMR (126 MHz, Methanol-*d*₄) δ 163.1 (C), 158.0 (C), 154.7 (C), 143.9 (q, *J* = 35.1 Hz, C), 140.2 (CH), 125.2 (C), 121.3 (q, *J* = 273 Hz, CF₃), 114.3 (q, *J* =

3.3 Hz, CH), 47.9 (2 x CH₂), 46.3 (2 x CH₂), 11.0 (CH₃) ppm. HRMS (ESI+) calculated for C₁₃H₁₅ClF₃N₆ 347.0993 found 347.0983; Method A t_R = 2.74 min; Purity (AUC) ≥ 95%.

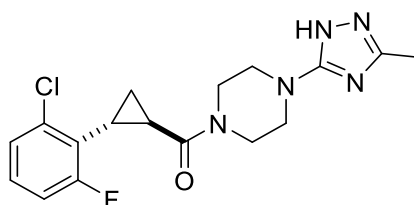
[4-(5-Methyl-1H-1,2,4-triazol-3-yl)piperazin-1-yl]-[(1R,2R)-2-[4-(trifluoromethyl)phenyl]cyclopropyl]methanone (51)



HATU (107 mg, 0.280 mmol) and DIPEA (0.160 mL, 0.934 mmol) were added to a solution of (*trans*)-2-[4-(trifluoromethyl)phenyl] cyclopropanecarboxylic acid (43.0 mg, 0.187 mmol) in DMF (0.9 mL) at rt and stirred for 15 min. 1-(5-Methyl-1H-1,2,4-triazol-3-yl)piperazine dihydrochloride (49.3 mg, 0.206 mmol) was added and the solution was stirred at rt for 18 h. Water (20 mL) was added and the product was extracted with ethyl acetate (3 x 15 mL) and dried using MgSO₄. The crude mixture was concentrated and purified by column chromatography (Biotage SNAP KP-Sil 10 g eluting with 0-20% MeOH in CH₂Cl₂; 1 CV, gradient over 20 CV, 5 CV). Fractions with product were concentrated and purified by reverse phase column chromatography (Biotage SNAP-Ultra C18 12 g eluting with 40-100% MeOH in water; 1 CV gradient over 15 CV, 6 CV) to give the title compound (23.0 mg, 32%, 0.060 mmol) as a white solid. MP 191 °C (decomp.); IR (thin film) ν = 3168, 3079, 2826, 1612, 1536 cm⁻¹; ¹H NMR (500 MHz, Methanol-*d*₄) δ 7.57 (d, *J* = 8.2 Hz, 2H, ArH), 7.36 (d, *J* = 8.1 Hz, 2H, ArH), 3.90 – 3.68 (m, 4H, piperazine), 3.44 – 3.33 (m, 4H, piperazine), 2.50 (ddd, *J* = 9.1, 6.2, 4.2 Hz, 1H, CH), 2.38 (ddd, *J* = 8.5, 5.5, 4.3 Hz, 1H, CH), 2.29 (s, 3H, CH₃), 1.62 (ddd, *J* = 9.5, 5.4, 4.4 Hz, 1H, CH₂, CH_AH_B), 1.41 (ddd, *J* = 8.5, 6.3, 4.4 Hz, 1H, CH₂, CH_AH_B) ppm. ¹³C NMR (126 MHz, Methanol-*d*₄) δ 171.0 (C=O), 145.4 (C), 128.1 (q, *J* = 32.6 Hz, C), 125.4 (2 x CH), 125.0 (q, *J* = 3.8 Hz, 2 x CH), 124.4 (d, *J* = 271 Hz, CF₃), 46.8 (CH₂), 46.2 (CH₂), 44.7 (CH₂), 41.4 (CH₂), 24.7 (CH), 22.9 (CH), 15.8 (CH₂), 10.6 (CH₃) ppm. Triazole quaternary carbons are

not visible due to tautomerisation. HRMS (ESI+) calculated for C₁₈H₂₁ClF₃N₅O 380.1693 found 380.1689; Method A t_R = 2.72 min; Purity (AUC) ≥ 95%.

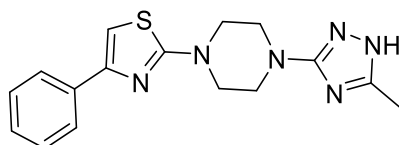
***trans*-[2-(2-Chloro-6-fluorophenyl)cyclopropyl]-[4-(5-methyl-1H-1,2,4-triazol-3-yl)piperazin-1-yl]methanone (52)**



HATU (120 mg, 0.315 mmol) and DIPEA (0.180 mL, 1.049 mmol) were added to a solution of (*trans*)-2-(2-chloro-6-fluoro-phenyl)cyclopropanecarboxylic acid (45.0 mg, 0.210 mmol) in DMF (1.1 mL) at rt and stirred for 15 min. 1-(5-Methyl-1H-1,2,4-triazol-3-yl)piperazine dihydrochloride (55.4 mg, 0.231 mmol) was added and the solution was stirred at rt for 30 h. Water (20 mL) was added, the product was extracted with ethyl acetate (3 x 15 mL) and dried using MgSO₄. The crude mixture was concentrated and purified by reverse phase column chromatography (Biotage SNAP-Ultra C18 12 g eluting with 20-100% MeOH in water; 1 CV gradient over 15 CV, 6 CV). Fractions with product were further purified by column chromatography (Biotage SNAP KP-Sil 10 g eluting with 0-10% MeOH in CH₂Cl₂; 1 CV, gradient over 10 CV, 5 CV) to give the title compound (50.3 mg, 66%, 0.138 mmol) as a white solid. MP 197 °C (decomp.); IR (thin film) ν = 3170, 3072, 2855, 1596, 1532 cm⁻¹; ¹H NMR (500 MHz, Methanol-*d*₄) δ 7.33 – 7.19 (m, 2H, ArH), 7.06 (dd, *J* = 10.6, 6.1 Hz, 1H, ArH), 4.03-3.65 (m, 4H, piperazine), 3.49 – 3.34 (m, 4H, piperazine), 2.44-2.37 (m, 1H, CH), 2.37 – 2.22 (m, 4H, CH, CH₃), 1.72-1.58 (m, 1H, CH₂, CH_AH_B), 1.51 – 1.39 (m, 1H, CH₂, CH_AH_B) ppm. ¹³C NMR (126 MHz, Methanol-*d*₄) δ 171.7 (C=O), 162.1 (d, *J* = 248 Hz, CF), 136.8 (d, *J* = 5.1 Hz, C), 128.7 (d, *J* = 10.0 Hz, CH), 125.4 (d, *J* = 15.1 Hz, C), 125.1 (d, *J* = 3.5 Hz, CH), 114.3 (d, *J* = 23.4 Hz, CH), 44.8 (2 x CH₂), 41.5 (2 x CH₂), 19.3 (CH), 19.0 (CH), 15.2 (CH₂), 10.3 (CH₃) ppm. Triazole quaternary carbons are not visible due to tautomerisation. HRMS

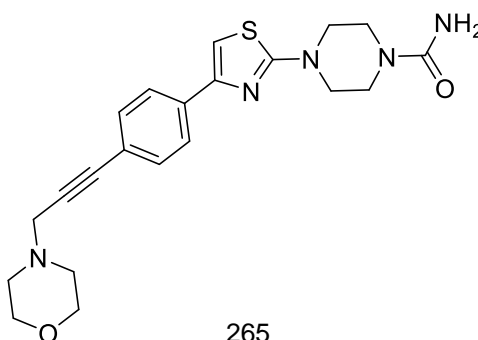
(ESI+) calculated for $C_{17}H_{20}ClFN_5O$ 364.1335, found 364.1345; Method A t_R = 2.56 min; Purity (AUC) \geq 95%.

2-[4-(3-Methyl-1H-1,2,4-triazol-5-yl)piperazin-1-yl]-4-phenylthiazole (55)



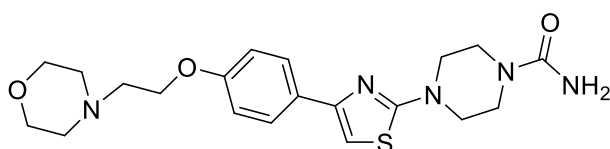
A mixture of 1-(3-methyl-1H-1,2,4-triazol-5-yl)piperazine hydrochloride (63.6 mg, 0.312 mmol), 2-bromo-4-phenylthiazole (50.0 mg, 0.208 mmol) and DMF (0.7 mL) was purged with N_2 and heated at 120 °C for 18 h. Water (20 mL) was added and the product was extracted with Et_2O (3 x 20 mL) and dried with $MgSO_4$. Purification by column chromatography (Biotage SNAP KP-Sil 10 g eluting with 0-10% MeOH in CH_2Cl_2 ; 1 CV, gradient over 10 CV, 5 CV) gave the title compound (16.0 mg, 24%, 0.050 mmol) as an oil; IR (thin film) ν = 3148, 3061, 2915, 2851, 1662, 1531 cm^{-1} ; 1H NMR (500 MHz, Methanol- d_4) δ 7.89 – 7.76 (m, 2H, ArH), 7.44 – 7.31 (m, 2H, ArH), 7.30 – 7.21 (m, 1H, ArH), 7.01 (s, 1H, ArH), 3.68 – 3.59 (m, 4H, piperazine), 3.56 – 3.46 (m, 4H, piperazine), 2.31 (s, 3H, CH_3) ppm. ^{13}C NMR (126 MHz, Methanol- d_4) δ 170.5 (C), 153.1 (C), 149.3 (C), 141.3 (C), 130.0 (CH), 128.8 (2 x CH), 128.3 (C), 126.9 (2 x CH), 103.2 (CH), 48.2 (2 x CH_2), 44.9 (2 x CH_2), 9.5 (CH_3) ppm. HRMS (ESI+) calculated for $C_{16}H_{19}N_6S$ 327.1386, found 327.1388; Method A t_R = 2.75 min; Purity (AUC) \geq 95%.

4-[4-[4-(3-Morpholinoprop-1-ynyl)phenyl]thiazol-2-yl]piperazine-1-carboxamide (58)



Bis(acetonitrile)dichloropalladium(II) (5.1 mg, 0.020 mmol) was added to 4-[4-(4-bromophenyl)thiazol-2-yl]piperazine-1-carboxamide (24.0 mg, 0.065 mmol), SPhos (16.1 mg, 0.039 mmol) and potassium carbonate (36.1 mg, 0.261 mmol). The vial was sealed, evacuated and replaced with N₂ three times. Acetonitrile (0.3 mL) and 4-(prop-2-yn-1-yl)morpholine (0.020 mL, 0.131 mmol) were injected. The orange suspension was stirred at 90 °C for 2 h. The reaction mixture was filtered through Celite, concentrated and purified by column chromatography (Biotage SNAP-Ultra C18 12 g eluted 10-90% MeOH in water; 1 CV gradient over 12 CV, 3 CV) to give the title compound (14.7 mg, 55%, 0.036 mmol) as a brown oil. IR (thin film) ν = 3366, 2924, 2854, 1656, 1601, 1537 cm⁻¹; ¹H NMR (500 MHz, Methanol-*d*₄) δ 8.17 (s, 2H, NH₂), 7.91 – 7.78 (m, 2H, ArH), 7.52 – 7.37 (m, 2H, ArH), 7.11 (s, 1H, ArH), 3.80-3.75 (m, 4H, morpholine), 3.64 (s, 2H, CH₂), 3.62-3.55 (m, 8H, piperazine), 2.80-2.73 (m, 4H, morpholine) ppm. ¹³C NMR (126 MHz, Methanol-*d*₄) δ 163.9 (C=O), 159.6 (C), 150.7 (C), 135.0 (C), 131.4 (2 x CH), 125.6 (2 x CH), 121.5 (C), 103.0 (CH), 85.9 (C), 83.0 (C), 65.9 (2 x CH₂), 51.9 (2 x CH₂), 48.4 (2 x CH₂), 42.9 (2 x CH₂), 39.0 (CH₂) ppm. HRMS (ESI+) calculated for C₂₁H₂₆N₅O₂S 413.1830, found 413.1831; Method A *t*_R = 2.15 min; Purity (AUC) \geq 95%.

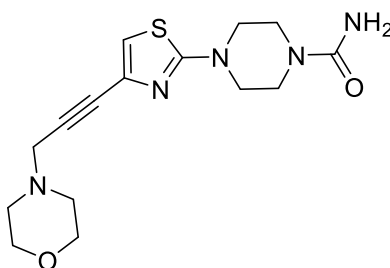
4-(4-(4-(2-morpholinoethoxy)phenyl)thiazol-2-yl)piperazine-1-carboxamide (59)



Tetrakis(triphenylphosphine)palladium(0) (14 mg, 0.01 mmol) and potassium carbonate (50 mg, 0.36 mmol) were added to 4-[2-[4-(4,4,5,5-tetramethyl-1,3,2-dioxaborolan-2-yl)phenoxy]ethyl]morpholine (40 mg, 0.12 mmol) and 4-(4-bromothiazol-2-yl)piperazine-1-carboxamide (35 mg, 0.12 mmol) in acetonitrile (0.3 mL) and water (0.30 mL). The orange solution was heated at 90 °C for 2 h. The reaction mixture was purified by column chromatography (biotage SNAP-Ultra C18 12 g, eluting with 10-100% MeOH in water, 1 CV, gradient over 10

CV, 6 CV) to afford the title compound (10 mg, 20%, 0.02 mmol) as an oil. IR (thin film) $\nu = 3353, 2923, 2856, 1655, 1599, 1540 \text{ cm}^{-1}$. $^1\text{H NMR}$ (600 MHz, Methanol- d_4) δ 8.25 (s, 2H, NH₂), 7.80 (d, $J = 8.8 \text{ Hz}$, 2H, ArH), 7.00 (d, $J = 8.8 \text{ Hz}$, 2H, ArH), 6.90 (s, 1H, ArH), 4.29 (t, $J = 5.2 \text{ Hz}$, 2H, CH₂), 3.84 (t, $J = 4.8 \text{ Hz}$, 4H, morpholine), 3.65 – 3.58 (m, 4H, piperazine), 3.58 – 3.53 (m, 4H, piperazine), 3.18 (t, $J = 5.3 \text{ Hz}$, 2H, CH₂), 2.98 (t, $J = 4.6 \text{ Hz}$, 4H, morpholine) ppm. $^{13}\text{C NMR}$ (151 MHz, Methanol- d_4) δ 171.2 (C), 159.6 (C), 158.0 (C), 151.2 (C), 129.0 (C), 127.1 (2 x CH), 114.2 (2 x CH), 100.3 (C), 65.1 (2 x CH₂, morpholine), 63.6 (CH₂), 56.9 (CH₂), 53.1 (2 x CH₂, morpholine), 47.9 (2 x CH₂, piperazine), 42.9 (2 x CH₂, piperazine) ppm.

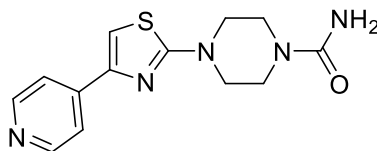
4-[4-(3-Morpholinoprop-1-ynyl)thiazol-2-yl]piperazine-1-carboxamide (60)



Bis(acetonitrile)dichloropalladium(II) (8.0 mg, 0.031 mmol) was added to 4-(4-bromothiazol-2-yl)piperazine-1-carboxamide (30.0 mg, 0.103 mmol), SPhos (25.4 mg, 0.062 mmol) and potassium carbonate (57.0 mg, 0.412 mmol). The vial was sealed, evacuated and replaced with N₂ three times. Acetonitrile (0.5 mL) and 4-(prop-2-yn-1-yl)morpholine (0.030 mL, 0.206 mmol) were added. The orange suspension was stirred at 90 °C for 2 h. The reaction mixture was filtered through Celite, concentrated and purified by column chromatography (Biotage SNAP-Ultra C18 12 g eluting with 0-80% MeOH in water; 1 CV gradient over 1 CV, 3 CV) to give the title compound (9 mg, 26%, 0.027 mmol) as an oil. IR (thin film) $\nu = 3353, 2918, 2855, 1657, 1601, 1533 \text{ cm}^{-1}$; $^1\text{H NMR}$ (500 MHz, Methanol- d_4) δ 8.19 (s, 2H, NH₂), 6.96 (s, 1H, ArH), 3.81-3.70 (m, 4H, morpholine), 3.60 – 3.54 (m, 6H, piperazine, CH₂), 3.52-3.44 (m, 4H, piperazine), 2.76-2.68 (m, 4H, morpholine) ppm. $^{13}\text{C NMR}$ (126 MHz, Methanol- d_4) δ 170.8 (C=O), 159.5 (C), 132.7 (C), 112.6 (CH), 82.0 (C), 80.5 (C), 66.0 (2 x CH₂), 51.9 (2 x CH₂), 46.8 (2 x CH₂), 42.7 (2 x CH₂), 39.0 (CH₂) ppm. HRMS (ESI+) calculated for

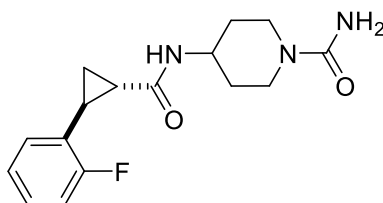
$C_{15}H_{22}N_5O_2S$ 336.1489, found 336.1485; Method A $t_R = 0.88$ min; Purity (AUC) $\geq 95\%$.

4-[4-(4-Pyridyl)thiazol-2-yl]piperazine-1-carboxamide (62)



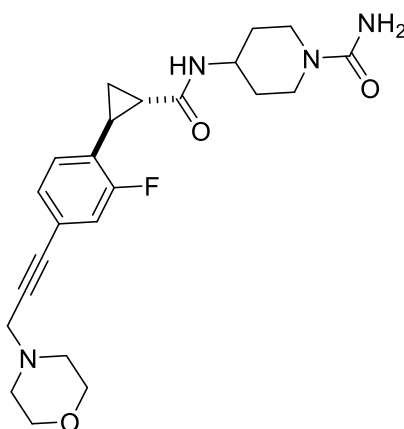
4-Pyridineboronic acid pinacol ester (25.4 mg, 0.124 mmol), palladium (II) acetate (7.0 mg, 0.031 mmol) and potassium phosphate tribasic (65.6 mg, 0.309 mmol) were added to 4-(4-bromothiazol-2-yl)piperazine-1-carboxamide (30.0 mg, 0.103 mmol) in 1,4-dioxane (0.40 mL) and water (0.1 mL). The orange solution was heated at 100°C for 30 min. The solution was filtered through a pad of Celite, concentrated and purified by column chromatography (Biotage SNAP-Ultra C18 12 g eluting with 0-80% MeOH in water; 1 CV gradient over 15 CV, 3 CV). Fractions with product were further purified by reverse phase column chromatography (Biotage SNAP-Ultra C18 12 g (0-80% eluting with MeOH in water; 1 CV gradient over 15 CV, 3 CV). The product was dissolved in 1:1 MeOH/ CH_2Cl_2 (10 mL), loaded onto a 500 mg SCX cartridge and washed with MeOH. The product was eluted with 2N MeOH/ NH_3 and concentrated to give the title compound (9 mg, 30%, 0.031 mmol) as a white solid. MP 204 °C (decomp.); IR (thin film) $\nu = 3358, 3188, 3074, 1675, 1600, 1541$ cm^{-1} ; 1H NMR (500 MHz, Methanol- d_4) δ 8.53 – 8.50 (m, 2H, ArH), 7.90 – 7.86 (m, 2H, ArH), 7.46 (s, 1H, ArH), 3.63 – 3.57 (m, 8H, piperazine) ppm. ^{13}C NMR (126 MHz, Methanol- d_4) δ 171.3 (C=O), 159.6 (C), 148.9 (2 x CH), 148.5 (C), 142.9 (C), 120.5 (2 x CH), 106.9 (CH), 47.9 (2 x CH_2), 42.9 (2 x CH_2) ppm. HRMS (ESI+) calculated for $C_{13}H_{16}N_5OS$ 290.1070 found 290.1069; Method A $t_R = 0.95$ min; Purity (AUC) $\geq 95\%$.

***trans*-4-[[2-(2-Fluorophenyl)cyclopropanecarbonyl]amino]piperidine-1-carboxamide (63)**



HATU (142 mg, 0.375 mmol) and DIPEA (0.20 mL, 1.25 mmol) were added to a solution of *trans*-2-(2-fluorophenyl)cyclopropanecarboxylic acid (45.0 mg, 0.250 mmol) in DMF (1.0 mL) at rt and stirred for 15 min. 4-Aminopiperidine-1-carboxamide dihydrochloride (64.8 mg, 0.300 mmol) was added and the solution was stirred at rt for 72 h. Water (20 mL) was added and the product was extracted with ethyl acetate (3 x 15 mL) and dried using MgSO₄. The crude mixture was purified by reverse phase column chromatography (Biotage SNAP-Ultra C18 12 g eluting with 20-100% MeOH in water; 1 CV gradient over 12 CV, 3 CV) to give the title compound (40.8 mg, 54%, 0.134 mmol) as a white solid. MP 220 °C (decomp.); IR (thin film) ν = 3253, 2940, 1633, 1598, 1545 cm⁻¹; ¹H NMR (500 MHz, Methanol-*d*₄) δ 7.21 (dddd, *J* = 8.2, 7.3, 5.2, 1.9 Hz, 1H, ArH), 7.13 – 6.93 (m, 3H, ArH), 3.98 (d, *J* = 13.8 Hz, 2H, piperidine), 3.95-3.84 (m, 1H, piperidine), 2.96 (dddd, *J* = 13.5, 11.7, 2.9, 1.4 Hz, 2H, piperidine), 2.52 (ddd, *J* = 9.4, 6.4, 4.3 Hz, 1H, CH), 1.95-1.82 (m, 3H, CH, piperidine), 1.49 (ddd, *J* = 9.4, 5.3, 4.3 Hz, 1H, CH₂, CH_AH_B), 1.46 – 1.36 (m, 2H, piperidine), 1.30 (ddd, *J* = 8.3, 6.4, 4.3 Hz, 1H, CH₂, CH_AH_B) ppm. ¹³C NMR (126 MHz, Methanol-*d*₄) δ 172.4 (C=O), 161.7 (d, *J* = 244 Hz, CF), 159.6 (C=O), 127.5 (d, *J* = 7.8 Hz, CH), 127.4 (C), 126.4 (d, *J* = 3.8 Hz, CH), 123.9 (d, *J* = 3.7 Hz, CH), 114.6 (d, *J* = 22.2 Hz, CH), 46.8 (CH), 42.6 (2 x CH₂), 31.3 (2 x CH₂), 23.9 (CH), 17.8 (d, *J* = 5.3 Hz, CH), 13.3 (CH₂) ppm. HRMS (ESI+) calculated for C₁₆H₂₁FN₃O₂ 306.1612, found 306.1607; Method A *t*_R = 2.30 min; Purity (AUC) \geq 95%.

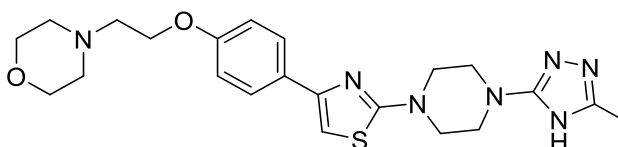
4-[[*(trans)*-2-[2-Fluoro-4-(3-morpholinoprop-1-ynyl)phenyl]cyclopropanecarbonyl]amino]piperidine-1-carboxamide (64)



Bis(acetonitrile)dichloro palladium(II) (5.1 mg, 0.020 mmol) was added to *trans*-4-[2-(4-bromo-2-fluoro-phenyl)cyclopropanecarbonyl]amino] piperidine-1-carboxamide (25.0 mg, 0.065 mmol), SPhos (16.0 mg, 0.039 mmol) and potassium carbonate (36.0 mg, 0.260 mmol). The vial was sealed, evacuated and replaced with N₂ three times. Acetonitrile (0.3 mL) and 4-(prop-2-yn-1-yl)morpholine (0.020 mL, 0.130 mmol) were added. The orange suspension was stirred at 90 °C for 18 h. The reaction mixture was purified by reverse phase column chromatography (Biotage SNAP-Ultra C18 12 g eluting with 20-100% MeOH in water; 1 CV gradient over 12 CV, 3 CV). Fractions with product were combined, concentrated and purified by column chromatography (Biotage SNAP KP-Sil 10 g eluting with 0-10% MeOH in CH₂Cl₂; 1 CV, gradient over 10 CV, 5 CV) to give the title compound (25.0 mg, 0.065 mmol) as an oil. IR (thin film) $\nu = 3298, 2944, 2830, 1656 \text{ cm}^{-1}$; ¹H NMR (500 MHz, Methanol-*d*₄) δ 7.18 (dd, *J* = 8.0, 1.6 Hz, 1H, ArH), 7.13 (dd, *J* = 10.9, 1.7 Hz, 1H, ArH), 7.05-7.00 (m, 1H, ArH), 5.50 (s, 2H, NH₂), 4.03 – 3.84 (m, 3H, piperidine), 3.74 (t, *J* = 4.7 Hz, 4H, morpholine), 3.53 (s, 2H, CH₂), 2.96 (t, *J* = 12.8 Hz, 2H, piperidine), 2.71-2.61 (m, 4H, morpholine), 2.55 – 2.46 (m, 1H, CH), 1.91 (ddd, *J* = 8.4, 5.5, 4.3 Hz, 1H, CH), 1.57-1.23 (m, 6H, piperidine, CH₂) ppm. ¹³C NMR (126 MHz, Methanol-*d*₄) δ 172.1 (C=O), 161.0 (d, *J* = 246 Hz, CF), 159.6 (C=O), 128.6 (C), 127.4 (CH), 126.5 (CH), 122.3 (C), 117.6 (d, *J* = 24.0 Hz, CH), 84.2 (C), 83.9 (C), 66.2 (2 x CH₂), 52.0 (2 x CH₂), 47.0 (CH₂), 46.8 (CH), 42.6 (2 x CH₂), 31.3 (2 x CH₂),

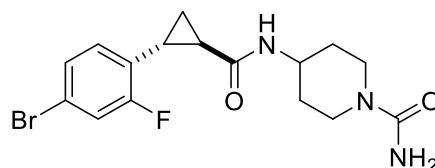
24.2 (CH), 17.7 (CH), 13.5 (CH₂) ppm. HRMS (ESI+) calculated for C₂₃H₃₀FN₄O₃ 429.2296 found 429.2286; Method A t_R = 1.87 min; Purity (AUC) ≥ 95%.

4-(2-(4-(2-(4-(5-methyl-4H-1,2,4-triazol-3-yl)piperazin-1-yl)thiazol-4-yl)phenoxy)ethyl)morpholine (65)

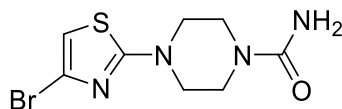


Tetrakis(triphenylphosphine)palladium(0) (47 mg, 0.04 mmol) was added to a stirred solution of 4-bromo-2-[4-(5-methyl-4H-1,2,4-triazol-3-yl)piperazin-1-yl]thiazole (45 mg, 0.14 mmol) in 1,4-dioxane (0.7 mL). The solution was heated at 100 °C for 20 min in the MW. Tributyl-[4-(2-morpholinoethoxy)phenyl]stannane (88 mg, 0.18 mmol) was added and the solution was heated at 70 °C for 18 h, followed by 2 h at 100 °C in the MW. The reaction mixture was concentrated and purified by column chromatography (biotage SNAP-Ultra C18 12 g, eluted with 10-80% MeOH in water, 1 CV, gradient over 10 CV, 6 CV) to afford the title compound (2 mg, 3%) as an oil. IR (thin film) ν = 3408, 2255, 1657 cm⁻¹. ¹H NMR (600 MHz, CDCl₃) δ 7.82 – 7.74 (m, 2H, ArH), 6.96 – 6.89 (m, 2H, ArH), 6.68 (s, 1H, ArH), 4.17 (t, J = 5.7 Hz, 2H, CH₂CH₂O), 3.77 (t, J = 4.7 Hz, 4H, CH₂ morpholine), 3.68 (dd, J = 6.4, 4.0 Hz, 4H, CH₂ piperazine), 3.62 – 3.56 (m, 4H, CH₂ piperazine), 2.85 (t, J = 5.7 Hz, 2H, CH₂CH₂O), 2.66 – 2.60 (m, 4H, CH₂ morpholine), 2.42 (s, 3H, CH₃) ppm. ¹³C NMR (151 MHz, CDCl₃)* δ 128.3 (C), 127.4 (2 x CH), 114.6 (2 x CH), 100.1 (CH), 66.9 (CH₂), 65.7 (2 x CH₂), 57.6 (CH₂), 54.1 (2 x CH₂), 47.9 (2 x CH₂), 46.0 (2 x CH₂), 12.6 (CH₃) ppm. Not all quaternary carbons observed. HRMS (ESI+) calculated for C₂₂H₃₁N₇O₂S 456.2176 found 456.2181; Method A t_R = 2.11 min; Purity (AUC) ≥ 95%.

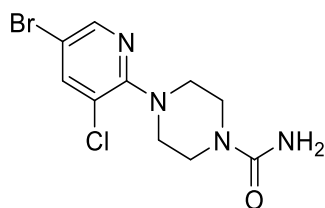
***trans*-4-[[2-(4-Bromo-2-fluoro-phenyl)cyclopropanecarbonyl]amino]piperidine-1-carboxamide (66)**



HATU (154 mg, 0.405 mmol) and DIPEA (0.24 mL, 1.35 mmol) were added to a solution of *trans*-2-(4-bromo-2-fluoro-phenyl)cyclopropanecarboxylic acid (70 mg, 0.270 mmol) in DMF (1.1 mL) at rt and stirred for 15 min. 4-Aminopiperidine-1-carboxamide dihydrochloride (64 mg, 0.297 mmol) was added and the solution was stirred at rt for 72 h. Water (20 mL) was added and the product was extracted with ethyl acetate (3 x 15 mL) and dried with MgSO₄. The mixture was purified by column chromatography (Biotage SNAP-Ultra C18 12 g eluting with 20-100% MeOH in water; 1 CV gradient over 12 CV, 3 CV) to yield the title compound (64 mg, 62%, 0.17 mmol) as a white solid. MP 200 °C (decomp.); IR (thin film) $\nu = 3256, 2910, 2653, 1763, 1634, 1598, 1543 \text{ cm}^{-1}$; ¹H NMR (500 MHz, Methanol-*d*₄) δ 7.35 – 7.22 (m, 2H, ArH), 7.06-6.93 (m, 1H, ArH), 4.05 – 3.93 (m, 2H, piperidine), 3.90 (tt, $J = 10.8, 4.1 \text{ Hz}$, 1H, piperidine), 3.00-2.86 (m, 2H, piperidine), 2.47 (ddd, $J = 9.3, 6.4, 4.3 \text{ Hz}$, 1H, CH), 1.95-1.82 (m, 3H, CH, piperidine), 1.50 (ddd, $J = 9.5, 5.3, 4.4 \text{ Hz}$, 1H, CH₂, CH_AH_B), 1.47 – 1.34 (m, 2H, piperidine), 1.30 (ddd, $J = 8.4, 6.4, 4.4 \text{ Hz}$, 1H, CH₂, CH_AH_B) ppm. ¹³C NMR (126 MHz, Methanol-*d*₄) δ 172.1 (C=O), 161.4 (d, $J = 249 \text{ Hz}$, CF), 159.6 (C=O), 128.0 (d, $J = 4.5 \text{ Hz}$, CH), 127.2 (d, $J = 3.7 \text{ Hz}$, CH), 127.1 (C), 119.4 (d, $J = 9.4 \text{ Hz}$, C), 118.2 (d, $J = 25.5 \text{ Hz}$, CH), 46.8 (CH), 42.6 (2 x CH₂), 31.3 (2 x CH₂), 23.9 (CH), 17.4 (d, $J = 4.7 \text{ Hz}$, CH), 13.2 (CH₂) ppm. HRMS (ESI+) calculated for C₁₆H₂₀BrFN₃O₂ 386.0699, found 386.0694; Method A $t_R = 2.67 \text{ min}$; Purity (AUC) $\geq 95\%$.

4-(4-Bromothiazol-2-yl)piperazine-1-carboxamide (67)

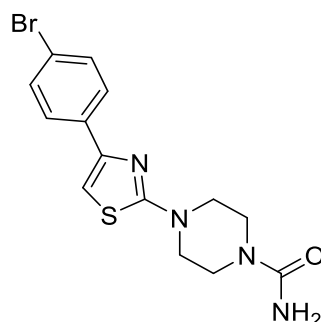
A mixture of piperazine-1-carboxamide hydrochloride (114 mg, 0.687 mmol), 4-bromo-2-chlorothiazole (142 mg, 0.687 mmol) and DIPEA (0.24 mL, 1.37 mmol) in DMSO (1.7 mL) was heated at 100 °C in the MW for 2 h. Purification by column chromatography (Biotage SNAP-Ultra C18 12 g eluting with 10-100% MeOH in water, 1 CV gradient over 12 CV, 3 CV) gave the title compound (83 mg, 42%, 0.285 mmol) as a gold solid. MP 133 °C (decomp.); IR (thin film) ν = 3326, 3208, 2904, 2669, 1972, 1763, 1636, 1593 1540 cm^{-1} ; ^1H NMR (500 MHz, Methanol- d_4) δ 6.68 (s, 1H, ArH), 3.62 – 3.54 (m, 4H, piperazine), 3.54 – 3.43 (m, 4H, piperazine) ppm. ^{13}C NMR (126 MHz, Methanol- d_4) δ 171.1 (C=O), 159.5 (C), 120.8 (C), 104.3 (CH), 47.4 (2 x CH_2), 42.6 (2 x CH_2) ppm. HRMS (ESI+) calculated for $\text{C}_8\text{H}_{12}\text{BrN}_4\text{OS}$ 290.9910, found 290.9908; Method A t_{R} = 2.04 min; Purity (AUC) \geq 95%.

4-(5-Bromo-3-chloro-2-pyridyl)piperazine-1-carboxamide (70)

To a stirred solution of piperazine-1-carboxamide hydrochloride (104 mg, 0.627 mmol) in a microwave vial was added 5-bromo-3-chloro-2-fluoro-pyridine (110 mg, 0.523 mmol) and DIPEA (0.180 mL, 1.046 mmol) in NMP (1.3 mL). The white suspension was heated in the MW at 100 °C for 45 min. The reaction mixture was purified by column chromatography (Biotage SNAP-Ultra C18 12 g eluting with 20-100% MeOH in water; 1 CV gradient over 12 CV, 3 CV) to yield the title compound (49 mg, 30%, 0.155 mmol) as a white solid. MP 176 °C (decomp.); IR (thin film) ν = 3443, 3319, 3185, 2856, 1643, 1589, 1561 cm^{-1} ; ^1H

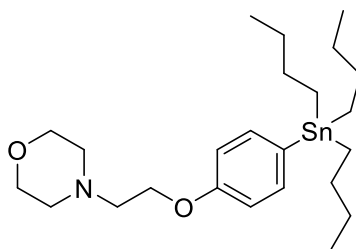
NMR (500 MHz, DMSO- d_6) δ 8.34 (d, J = 2.2 Hz, 1H, ArH), 8.15 (d, J = 2.2 Hz, 1H, ArH), 6.05 (s, 2H, NH₂), 3.45 – 3.37 (m, 4H, piperazine), 3.27 – 3.13 (m, 4H, piperazine) ppm. ¹³C NMR (126 MHz, DMSO- d_6) δ 158.6 (C=O), 157.1 (C), 147.0 (CH), 141.2 (CH), 122.7 (C), 112.0 (C), 49.1 (2 x CH₂), 43.6 (2 x CH₂) ppm. HRMS (ESI+) calculated for C₁₀H₁₃BrClN₄O 320.9934, found 320.9929; Method A t_R = 2.65 min; Purity (AUC) \geq 95%.

4-[4-(4-Bromophenyl)thiazol-2-yl]piperazine-1-carboxamide (71)



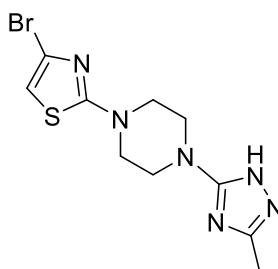
A mixture of piperazine-1-carboxamide hydrochloride (72.4 mg, 0.437 mmol), 4-(4-bromophenyl)-2-chloro-thiazole (80.0 mg, 0.291 mmol), DIPEA (0.100 mL, 0.583 mmol) and DMSO (0.7 mL) was heated in the MW at 100 °C for 7 h. The reaction mixture was purified by column chromatography (Biotage SNAP-Ultra C18 12 g eluting with 30-100% MeOH in water; 1 CV gradient over 15 CV, 3 CV) to give the title compound (25 mg, 23%, 0.067 mmol) as a white solid. MP 151 °C (decomp.); IR (thin film) ν = 3217, 2842, 2121, 2033, 1637, 1587, 1537 cm^{-1} ; ¹H NMR (500 MHz, Methanol- d_4) δ 7.84 – 7.68 (m, 2H, ArH), 7.61 – 7.40 (m, 2H, ArH), 7.09 (s, 1H, ArH), 3.66 – 3.50 (m, 8H, piperazine) ppm. ¹³C NMR (126 MHz, Methanol- d_4) δ 171.2 (C=O), 159.6 (C), 150.3 (C), 134.1 (C), 131.2 (2 x CH), 127.4 (2 x CH), 120.9 (C), 102.5 (CH), 47.9 (2 x CH₂), 42.9 (2 x CH₂) ppm. HRMS (ESI+) calculated for C₁₄H₁₆BrN₄OS 369.0202, found 369.0207; Method A t_R = 2.92 min; Purity (AUC) \geq 95%.

4-(2-(4-(tributylstannyl)phenoxy)ethyl)morpholine (78)



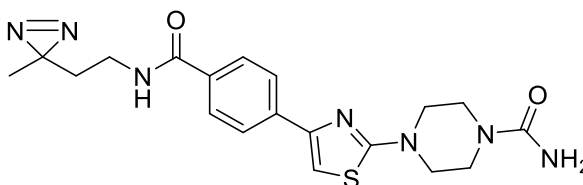
A solution of 4-[2-(4-bromophenoxy)ethyl]morpholine (265 mg, 0.93 mmol) in anhydrous THF (4.6 mL) at $-78\text{ }^{\circ}\text{C}$ was treated dropwise with 1.69 M *n*-BuLi in hexane (0.63 mL, 1.06 mmol) and stirred for 30 min. Tributyltin chloride (0.33 mL, 1.2039 mmol) was added dropwise and the mixture was stirred for 2 h. The reaction was allowed to warm to rt, quenched with water (15 mL) and sat aq NH_4Cl (15 mL), extracted with EtOAc (3 x 25 mL), dried with MgSO_4 and concentrated. The residue was purified by column chromatography (biotage SNAP KP-Sil 25 g (0-100% EtOAc in cyclohexane, 1 CV, gradient over 18 CV, 2 CV) to yield the title product (348 mg, 76%, 0.70 mmol) as a clear oil. IR (thin film) $\nu = 2952, 2894, 1684, 1603, 1563\text{ cm}^{-1}$. ^1H NMR (600 MHz, Chloroform-*d*) δ 7.43 – 7.34 (m, 2H, 2 x ArH), 6.96 – 6.88 (m, 2H, 2 x ArH), 4.13 (t, $J = 5.8$ Hz, 2H, CH_2), 3.76 (t, $J = 4.7$ Hz, 4H, morpholine), 2.83 (t, $J = 5.7$ Hz, 2H, CH_2), 2.64 – 2.57 (m, 4H, morpholine), 1.58 – 1.51 (m, 6H, 3 x CH_3), 1.35 (h, $J = 7.3$ Hz, 6H, 3 x CH_2), 1.07 – 1.02 (m, 6H, 3 x CH_2), 0.90 (t, $J = 7.3$ Hz, 9H, 3 x CH_3) ppm. ^{13}C NMR (151 MHz, Chloroform-*d*) δ 158.8 (C), 137.5 (2 x CH), 132.3 (C), 114.6 (2 x CH), 67.0 (2 x CH_2 , morpholine), 65.5 (CH_2), 57.7 (CH_2), 54.1 (2 x CH_2 morpholine), 29.1 (3 x CH_2), 27.4 (3 x CH_2), 13.7 (3 x CH_3), 9.6 (3 x CH_2) ppm. HRMS (ESI+) calculated for $\text{C}_{24}\text{H}_{44}\text{NO}_2\text{Sn}$ 496.2388 found 496.2395; Method A $t_{\text{R}} = 3.24$ min; Purity (AUC) $\geq 95\%$.

4-Bromo-2-(4-(3-methyl-1H-1,2,4-triazol-5-yl)piperazin-1-yl)thiazole (74)



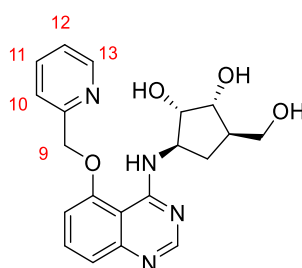
A mixture of 4-bromo-2-chlorothiazole (240 mg, 1.21 mmol), potassium carbonate (771 mg, 5.58 mmol) and DMSO (4 mL) was purged with N₂ and heated at 120 °C for 3 h. Water (40 mL) was added and the product was extracted with EtOAc (3 x 40 mL), dried and concentrated. Purification by column chromatography (biotage SNAP KP-Sil 10 g, eluted with 0-10% MeOH in CH₂Cl₂, 1 CV, gradient over 15 CV, 2 CV) to afford the title product (188 mg, 47%, 0.57 mmol) as a white solid. IR (thin film) $\nu = 3091, 2905, 2849, 1522 \text{ cm}^{-1}$. ¹H NMR (600 MHz, Methanol-*d*₄) δ 6.68 (s, 1H, ArH), 3.58 (dd, *J* = 6.5, 3.9 Hz, 4H, piperazine), 3.50 (dd, *J* = 6.7, 3.7 Hz, 4H, piperazine), 2.33 (s, 3H, CH₃) ppm. ¹³C NMR (151 MHz, Methanol-*d*₄) δ 120.9 (C), 104.3 (CH), 47.0 (2 x CH₂, piperazine), 45.7 (2 x CH₂, piperazine), 11.0 (CH₃, HSQC). Triazole quaternary carbons are not visible due to tautomerization. HRMS (ESI+) calculated for C₁₀H₁₃BrN₆S 329.0184, found 330.9781; Method B t_R = 2.07 min; Purity (AUC) $\geq 95\%$.

4-(4-(4-((2-(3-Methyl-3H-diazirin-3-yl)ethyl)carbamoyl)phenyl)thiazol-2-yl)piperazine-1-carboxamide (82)



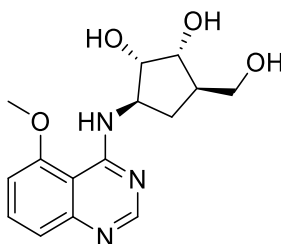
4-Carboxyphenylboronic acid (43 mg, 0.26 mmol), potassium carbonate (71 mg, 0.52 mmol) and tetrakis(triphenylphosphine)palladium(0) (20 mg, 0.02 mmol) and were added to 4-(4-bromothiazol-2-yl)piperazine-1-carboxamide (50 mg, 0.17 mmol) in acetonitrile (0.4 mL) and water (0.4 mL). The orange solution was heated at 100 °C for 45 min. The reaction mixture was loaded directly onto a basic ion exchange column (Isolute-NH₂, 1 g) and washed with acetonitrile. The MeCN layer was concentrated and purified by basic ion exchange chromatography (SCX, 1 g) washing with MeOH, followed by NH₃ in MeOH. The product was 50% pure by LCMS and used directly for the next step. HATU (73 mg, 0.19 mmol) and DIPEA (0.09 mL, 0.51 mmol) were added to 4-[2-(4-carbamoylpiperazin-1-yl)thiazol-4-yl]benzoic acid (43 mg, 0.13 mmol, 50% purity by LCMS) in DMF (0.6 mL). After 2 min 2-(3-methyldiazirin-3-yl)ethylammonium chloride (35 mg, 0.26 mmol) was added and the solution was stirred at room temp for 4 h in the dark covered with aluminium foil. Purification by column chromatography (directly loaded onto biotage SNAP-Ultra C18 12 g, eluted with 20-80% MeOH in water, 1 CV, gradient over 20 CV, 3 CV) to afford the title product (5.3 mg, 20%, 0.01 mmol) as an oil. ¹H NMR (600 MHz, MeOD) δ 8.39 (s, 1H, NH), 7.97 (m, 2H, ArH), 7.85 (dd, J = 8.5, 1.7 Hz, 2H, ArH), 7.21 (s, 1H, ArH), 3.60 (app tt, J = 10.3, 4.2 Hz, 8H, CH₂), 3.39 (d, J = 7.2 Hz, 2H, CH₂), 1.68 (dd, J = 7.8, 6.4 Hz, 2H, CH₂), 1.09 (d, J = 1.5 Hz, 3H, CH₃) ppm. ¹³C NMR (151 MHz, MeOD)* δ 171.1 (C), 168.6 (C), 146.1 (C), 138.3 (C), 134.0 (C), 133.1 (C), 127.2 (CH), 125.6 (CH), 103.8 (CH), 47.9 (4 x CH₂), 42.9 (4 x CH₂), 34.9 (CH₂), 33.7 (CH₂), 29.4 (CH₂), 18.4 (CH₃) ppm. One quaternary carbon not observed. LCMS (ESI+) t_R = 2.63 min, m/z 414 (MeOH adduct).

(1*S*,2*R*,3*R*,5*R*)-3-(Hydroxymethyl)-5-((5-(pyridin-2-ylmethoxy)quinazolin-4-yl)amino)cyclopentane-1,2-diol (226)



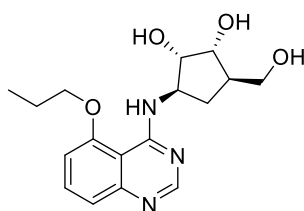
PyBOP (2.55 g, 4.90 mmol) and DBU (1.5 mL, 9.8 mmol) were added to a solution of 5-(2-pyridylmethoxy)quinazolin-4-ol (0.91 g, 3.59 mmol) and (1*R*, 2*S*, 3*R*, 4*R*)-2,3-dihydroxy-4-(hydroxymethyl)-1-aminocyclopentane hydrochloride (0.60 g, 3.27 mmol) in acetonitrile (16 mL) and stirred for 24 h. Water (50 mL) and CH₂Cl₂ (50 mL) were added. The precipitate was filtered and dried to afford the title compound. The filtrate was concentrated to 25 mL. 1:1 CH₂Cl₂ : water was added and the precipitate was allowed to form over 24 h and filtered to afford the title compound (combined yield 681 mg, 49%, 1.60 mmol) as a white solid. IR (thin film) ν = 3303, 2892, 1614, 1574 1531 cm⁻¹. ¹H NMR (600 MHz, DMSO-*d*₆) δ 8.83 (d, *J* = 7.3 Hz, 1H, NH), 8.77 – 8.68 (m, 1H, ArH, H₁₃), 8.37 (s, 1H, ArH, H₂), 7.96 – 7.85 (m, 1H, ArH, H₁₁), 7.72 – 7.59 (m, 1H, ArH, H₇), 7.55 (d, *J* = 7.8 Hz, 1H, ArH, H₁₀), 7.43 (dd, *J* = 7.5, 4.9 Hz, 1H, ArH, H₁₂), 7.26 (d, *J* = 8.2 Hz, 1H, ArH, H₈), 7.11 (d, *J* = 7.9 Hz, 1H, ArH, H₆), 5.51-5.43 (m, 2H, CH₂, H₉), 4.76 (s, 1H, OH), 4.67 (s, 1H, OH), 4.57 (m, 1H, CH, H_{1'}), 4.47 (s, 1H, OH), 3.77 (m, 2H, CH, H_{2'}, H_{3'}), 3.41 (dddd, *J* = 16.0, 10.1, 7.6, 3.5 Hz, 2H, CH₂, H_{6'}), 2.25 (ddd, *J* = 13.1, 8.4 Hz, 1H, CH₂, H_{5'}), 1.99 (dtt, *J* = 8.9, 4.7 Hz, 1H, CH, H_{4'}), 1.19 (ddd, *J* = 13.1, 8.7 Hz, 1H, CH₂, H_{5'}) ppm. ¹³C NMR (151 MHz, DMSO-*d*₆) δ 159.8 (CH), 155.8 (C), 155.7 (C), 155.6 (C), 152.0 (CH), 149.8 (C), 137.6 (CH), 133.1 (CH), 123.8 (CH), 122.3 (CH), 120.5 (CH), 107.5 (CH), 106.8 (C), 77.0 (CH), 72.6 (CH), 71.2 (CH₂), 63.1 (CH₂), 56.1 (CH), 45.7 (CH), 30.7 (CH₂) ppm. HRMS (ESI+) calculated for C₂₀H₂₃N₄O₄ 383.1714, found 383.1713; *t*_R = 1.63 min; Purity (AUC) \geq 95%.

(1*S*,2*R*,3*R*,5*R*)-3-(Hydroxymethyl)-5-((5-methoxyquinazolin-4-yl)amino)cyclopentane-1,2-diol (227)



PyBOP (1.10 mg, 2.11 mmol) and DBU (0.63 mL, 4.22 mmol) were added to a solution of 5-methoxyquinazolin-4-ol (272 mg, 1.55 mmol) and (1*R*, 2*S*, 3*R*, 4*R*)-2,3-dihydroxy-4-(hydroxymethanol)-1-aminocyclopentane hydrochloride (258 mg, 1.41 mmol) in acetonitrile (4.7 mL) and stirred for 18 h. The residue was dissolved in 1:1 CH₂Cl₂: MeOH and filtered through an acidic ion exchange cartridge (SCX, 20 g), eluting with 1:1 1 M NH₃ in MeOH: CH₂Cl₂. The ammonia layer was concentrated and purified by column chromatography (biotage SNAP-Ultra C18 30g, eluted with 0-80% MeOH in water, 1 CV gradient over 15 CV, 3 CV) to yield the title compound (400 mg, 93%, 1.31 mmol) as a clear oil. IR (thin film) $\nu = 3232, 2933 \text{ cm}^{-1}$. ¹H NMR (600 MHz, Methanol-*d*₄) δ 8.45 (s, 1H, H₂), 7.78 (dd, *J* = 8.3 Hz, 1H, ArH, H₇), 7.28 (dd, *J* = 8.4, 0.9 Hz, 1H, ArH, H₈), 7.14 (d, *J* = 8.1 Hz, 1H, ArH, H₆), 4.65 (dt, *J* = 8.0, 6.1 Hz, 1H, CH, H_{1'}), 4.11 (s, 3H, CH₃), 4.03 (app dt, *J* = 16.6, 5.1 Hz, 2H, CH, H_{2'}, H_{3'}), 3.78 – 3.64 (m, 2H, CH₂, H_{6'}), 2.57 (ddd, *J* = 13.6, 9.9, 7.9 Hz, 1H, CH₂, H_{5'}), 2.22 (app ddq, *J* = 9.7, 7.1, 4.8 Hz, 1H, CH, H_{4'}), 1.50 (app dt, *J* = 13.6, 6.8 Hz, 1H, CH₂, H_{5'}) ppm. ¹³C NMR (151 MHz, Methanol-*d*₄) δ 160.1 (C), 157.5 (C), 153.2 (CH), 146.7 (C), 134.4 (CH), 115.7 (CH), 107.0 (CH), 105.5 (C), 77.2 (CH), 73.0 (CH), 62.0 (CH₂), 56.6 (CH), 55.8 (CH₃), 45.0 (CH), 29.4 (CH₂) ppm. HRMS (ESI+) calculated for C₁₅H₂₀N₃O₄ 306.1448, found 306.1463; *t*_R = 0.43 min; Purity (AUC) \geq 95%.

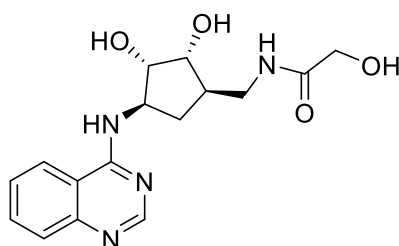
(1*S*,2*R*,3*R*,5*R*)-3-(Hydroxymethyl)-5-(5-propoxyquinazolin-4-yl)amino)cyclopentane-1,2-diol (229)



PyBOP (1.31 mg, 2.51 mmol) and DBU (1.0 mL, 6.71 mmol) were added to a solution of 5-propoxyquinazolin-4-ol (411 mg, 2.01 mmol) and (1*R*, 2*S*, 3*R*, 4*R*)-2,3-dihydroxy-4-(hydroxymethanol)-1-aminocyclopentane hydrochloride (308 mg, 1.68 mmol) in acetonitrile (5.5 mL) and stirred for 6 h. The mixture was concentrated and the residue was dissolved in 1:1 CH₂Cl₂: MeOH, filtered

through an acidic ion exchange cartridge (SCX, 10 g), eluting the product with 2 M NH_3 in MeOH. The NH_3 layer was concentrated and purified by column chromatography (biotage SNAP KP-Sil 10 g, eluted with 0-10% MeOH in CH_2Cl_2 , 1 CV, gradient over 15 CV, 5 CV) to afford the title compound (410 mg, 73%, 1.23 mmol) as a clear oil. IR (thin film) $\nu = 3377, 3250, 2965, 2937, 2879, 1612, 1594, 1582, 1528 \text{ cm}^{-1}$. ^1H NMR (600 MHz, Methanol- d_4) δ 8.37 (s, 1H, ArH, H₂), 7.68 (dd, $J = 8.2 \text{ Hz}$, 1H, ArH, H₇), 7.28 (d, $J = 8.3 \text{ Hz}$, 1H, ArH, H₈), 7.05 (d, $J = 8.1 \text{ Hz}$, 1H, ArH, H₆), 4.53 (td, $J = 8.3, 6.6 \text{ Hz}$, 1H, CH, H_{1'}), 4.24 (t, $J = 6.4 \text{ Hz}$, 2H, CH_2 , $\text{CH}_3\text{CH}_2\text{CH}_2$), 4.00 – 3.90 (m, 2H, CH, H_{2'}, H_{3'}), 3.65 (d, $J = 5.5 \text{ Hz}$, 2H, CH_2 , H_{6'}), 2.58 (app dt, $J = 13.4, 8.6 \text{ Hz}$, 1H, CH_2 , H_{5'}), 2.31 – 2.16 (m, 1H, CH, H_{4'}), 2.02 (h, $J = 7.1 \text{ Hz}$, 2H, CH_2 , $\text{CH}_3\text{CH}_2\text{CH}_2$), 1.47 – 1.24 (m, 1H, CH_2 , H_{5'}), 1.17 (t, $J = 7.4 \text{ Hz}$, 3H, CH_3) ppm. ^{13}C NMR (151 MHz, Methanol- d_4) δ 160.3 (C), 156.5 (C), 154.5 (CH), 150.2 (C), 133.3 (CH), 118.2 (CH), 107.0 (CH), 106.1 (C), 77.7 (CH), 73.0 (CH), 71.2 (CH_2), 62.9 (CH_2), 56.3 (CH), 45.3 (CH), 30.0 (CH_2), 22.0 (CH_2), 9.7 (CH_3) ppm. HRMS (ESI+) calculated for $\text{C}_{17}\text{H}_{24}\text{N}_3\text{O}_4$ 334.1767, found 334.1767; Method B $t_{\text{R}} = 1.18 \text{ min}$; Purity (AUC) $\geq 95\%$.

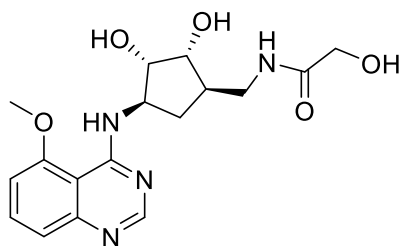
***N*-(((1*R*,2*R*,3*S*,4*R*)-2,3-Dihydroxy-4-(quinazolin-4-ylamino)cyclopentyl)methyl)-2-hydroxyacetamide (238)**



1 M TBAF in THF (0.5 mL, 0.5 mmol) was added to a solution of *N*-[[[(1*R*,2*R*,3*S*,4*R*)-2,3-bis[[*tert*-butyl(dimethyl)silyl]oxy]-4-(quinazolin-4-ylamino)cyclopentyl]methyl]-2-hydroxy-acetamide (89 mg, 0.16 mmol) in THF (0.8 mL) and stirred at rt for 72 h. 1 M TBAF in THF (0.5 mL, 0.5 mmol) was added and the reaction mixture was stirred at rt for a further 24 h. 1 M TBAF in THF (3.0 mL, 3.0 mmol) was added and the reaction mixture was stirred at rt for a further 72 h. The product was purified with an ion exchange column (SCX, 5

g), eluting with 2 M NH₃/MeOH. Further purification by reverse phase column chromatography (biotage 10 g, eluted with 0-100% methanol in water, 2 CV gradient over 15 CV, 2 CV). Fractions with product were combined and passed through an ion exchange column (SCX, 2 g) eluting with 2 M NH₃/MeOH to afford the title product (19 mg, 0.06 mmol, 35%) as a clear oil. $[\alpha]^{20}_D$ -36.0° (c=0.5, MeOH). IR (thin film) ν = 3326, 2926, 1648, 1618, 1587, 1537 cm⁻¹. ¹H NMR (600 MHz, Methanol-*d*₄) δ 8.49 (s, 1H, ArH, H₂), 8.25 (d, *J* = 8.3 Hz, 1H, ArH, H₅), 7.88 – 7.78 (m, 1H, ArH, H₇), 7.73 (d, *J* = 8.4 Hz, 1H, ArH, H₈), 7.57 (dd, *J* = 7.7 Hz, 1H, ArH, H₆), 4.65 (td, *J* = 8.6, 6.5 Hz, 1H, CH, H_{1'}), 4.09 (dd, *J* = 6.1 Hz, 1H, CH, H_{2'}), 4.02 (s, 2H, CH₂, CH₂OH), 3.90 (dd, *J* = 5.5 Hz, 1H, CH, H_{3'}), 3.42 (h, *J* = 6.6, 6.0 Hz, 2H, CH₂, H_{6'}), 2.47 (app dt, *J* = 13.0, 8.2 Hz, 1H, CH₂, H_{5'}), 2.28 (td, *J* = 8.2, 5.6 Hz, 1H, CH, H_{4'}), 1.38 (app dt, *J* = 13.2, 9.2 Hz, 1H, CH₂, H_{5'}) ppm. ¹³C NMR (151 MHz, Methanol-*d*₄) δ 174.0 (C), 160.3 (C), 154.4 (CH), 148.2 (C), 132.9 (CH), 126.2 (CH), 126.1 (CH), 122.3 (CH), 115.0 (C), 76.7 (CH), 74.1 (CH), 61.2 (CH₂), 56.7 (CH), 43.1 (CH), 41.6 (CH₂), 30.4 (CH₂) ppm. HRMS (ESI+) calculated for C₁₆H₂₁N₄O₄ 333.1557 found 333.1552; Method A *t*_R = 0.28 min; Purity (AUC) \geq 95%.

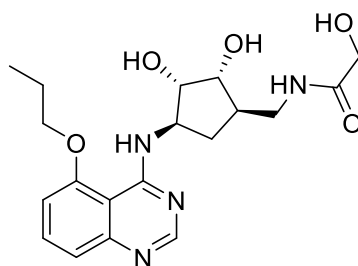
***N*-(((1*R*,2*R*,3*S*,4*R*)-2,3-Dihydroxy-4-((5-methoxyquinazolin-4-yl)amino)cyclopentyl)methyl)-2-hydroxyacetamide (239)**



Ethyl glycolate (0.10 mL, 1.02 mmol) was added to a stirred solution of *N*-[(3*aS*,4*R*,6*R*,6*aR*)-6-(aminomethyl)-2,2-dimethyl-4,5,6,6*a*-tetrahydro-3*aH*-cyclopenta[*d*][1,3]dioxol-4-yl]-5-methoxy-quinazolin-4-amine (35 mg, 0.10 mmol) and TEA (0.03 mL, 0.20 mmol) in CHCl₃ (0.5 mL) and the solution was heated at 60 °C for 48 h. The reaction mixture was concentrated and used directly for next deprotection step. 1 M HCl in 1,4-dioxane (1.0 mL, 1.0 mmol) was added to a solution of *N*-[(3*aS*,4*R*,6*R*,6*aR*)-4-[(5-methoxyquinazolin-4-yl)amino]-2,2-dimethyl-4,5,6,6*a*-tetrahydro-3*aH*-cyclopenta[*d*][1,3]dioxol-6-

yl)methyl]-2-hydroxy-acetamide (41 mg, 0.10 mmol) in MeCN (0.5 mL) and stirred for 2 h. The reaction mixture was poured directly onto an acidic ion exchange cartridge (SCX, 2 g) and washed with MeOH (30 mL). The product was eluted with 1 M NH₃ in MeOH, concentrated and further purified by column chromatography (biotage SNAP-Ultra C18 12 g, eluted with 0-70% MeOH in water, 1 CV gradient over 15 CV, 2 CV) to afford the title compound (14 mg, 39%, 0.04 mmol) as an oil. $[\alpha]_D^{20}$ 20.8° (c=0.5, MeOH). IR (thin film) ν = 3365, 2963, 1613, 1588, 1533 cm⁻¹. ¹H NMR (600 MHz, Methanol-*d*₄) δ 8.37 (s, 1H, ArH, H₂), 7.71 (dd, *J* = 8.2 Hz, 1H, ArH, H₇), 7.30 (d, *J* = 8.2 Hz, 1H, ArH, H₈), 7.08 (d, *J* = 8.2 Hz, 1H, ArH, H₆), 4.49 (td, *J* = 8.4, 6.5 Hz, 1H, CH, H_{1'}), 4.11 (s, 3H, CH₃, O-methoxy), 4.02 (m, 3H, H_{2'}, CH₂OH), 3.89 (t, *J* = 5.5 Hz, 1H, CH, H_{3'}), 3.45 – 3.38 (m, 2H, CH₂, H_{6'}), 2.55 (app dt, *J* = 13.3, 8.2 Hz, 1H, CH₂, H_{5'}), 2.28 (app pd, *J* = 7.8, 5.2 Hz, 1H, CH, H_{4'}), 1.32 (app dt, *J* = 13.4, 8.9 Hz, 1H, CH₂, H_{5'}) ppm. ¹³C NMR (151 MHz, Methanol-*d*₄) δ 174.0 (C), 160.2 (C), 157.2 (C), 154.6 (CH), 150.2 (C), 133.3 (CH), 118.4 (CH), 106.2 (CH), 76.9 (CH), 74.1 (CH), 61.2 (CH₂), 56.6 (CH), 55.7 (CH₃), 43.2 (CH), 41.6 (CH₂), 31.0 (CH₂) ppm. HRMS (ESI+) calculated for C₁₇H₂₃N₄O₅ 363.1663 found 363.1666; Method A *t*_r = 0.55 min; Purity (AUC) \geq 95%.

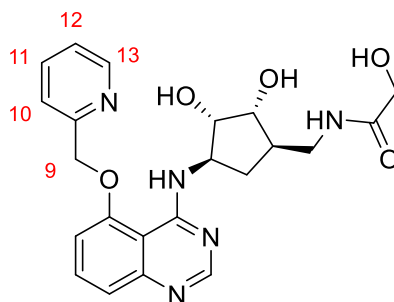
***N*-(((1*R*,2*R*,3*S*,4*R*)-2,3-Dihydroxy-4-((5-propoxyquinazolin-4-yl)amino)cyclopentyl)methyl)-2-hydroxyacetamide (240)**



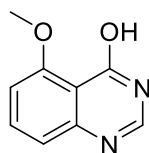
Ethyl glycolate (0.06 mL, 0.62 mmol) was added to a stirred solution of *N*-[[3*aS*,4*R*,6*R*,6*aR*]-6-(aminomethyl)-2,2-dimethyl-4,5,6,6*a*-tetrahydro-3*aH*-cyclopenta[*d*][1,3]dioxol-4-yl]-5-propoxy-quinazolin-4-amine (23 mg, 0.06 mmol) and TEA (0.02 mL, 0.12 mmol) in CHCl₃ (0.6 mL) and the solution heated at 60 °C for 24 h. Ethyl glycolate (0.06 mL, 0.62 mmol) and TEA (0.02 mL, 0.12 mmol)

were added and the solution heated at 60 °C for a further 30 hours. The reaction mixture was concentrated, dried under high vacuum for 18 h and used directly for the next deprotection step. 1 M HCl in 1,4-dioxane (1.2 mL, 1.2 mmol) was added to a solution of *N*-[[(3*a*S,4*R*,6*R*,6*a*R)-2,2-dimethyl-4-[(5-propoxyquinazolin-4-yl)amino]-4,5,6,6*a*-tetrahydro-3*a*H-cyclopenta[*d*][1,3]dioxol-6-yl)methyl]-2-hydroxy-acetamide (26 mg, 0.06 mmol) in MeCN (0.6 mL) and stirred for 2 h. The reaction mixture was concentrated and purified by reverse phase column chromatography (biotage 10 g, eluted with 0-100% MeOH in water, 1 CV, gradient over 15 CV, 2 CV). The product was further purified with an acidic ion exchange column (SCX, 1 g), washing with MeOH and eluting with 2 M NH₃ in MeOH. The NH₃ layer was concentrated to afford the title compound (9 mg, 39%, 0.02 mmol) as a clear oil. $[\alpha]^{20}_{\text{D}} -9.70^{\circ}$ ($c=0.5$, MeOH). IR (thin film) $\nu = 3337, 2966, 1632, 1613, 1586, 1552 \text{ cm}^{-1}$. ¹H NMR (600 MHz, Methanol-*d*₄) δ 8.37 (s, 1H, ArH, H₂), 7.69 (dd, $J = 8.2 \text{ Hz}$, 1H, ArH, H₇), 7.29 (dd, $J = 8.4, 0.9 \text{ Hz}$, 1H, ArH, H₈), 7.06 (dd, $J = 8.2, 1.0 \text{ Hz}$, 1H, ArH, H₆), 4.47 (td, $J = 8.4, 6.5 \text{ Hz}$, 1H, CH, H_{1'}), 4.24 (dd, $J = 6.4 \text{ Hz}$, 2H, CH₂, CH₃CH₂CH₂), 4.00 (s, 2H, CH₂, CH₂OH), 3.96 (dd, $J = 6.5, 5.5 \text{ Hz}$, 1H, CH, H_{2'}), 3.87 (t, $J = 5.5 \text{ Hz}$, 1H, CH, H_{3'}), 3.40 (d, $J = 7.3 \text{ Hz}$, 2H, CH₂, H_{6'}), 2.61 (dt, $J = 13.3, 8.2 \text{ Hz}$, 1H, CH₂, H_{5'}), 2.30 (dq, $J = 12.9, 7.6 \text{ Hz}$, 1H, CH, H_{4'}), 2.03 (app dtd, $J = 13.8, 7.4, 6.4 \text{ Hz}$, 2H, CH₂ CH₃CH₂CH₂), 1.23 (app app dt, $J = 13.3, 9.0 \text{ Hz}$, 1H, CH₂, H_{5'}), 1.18 (t, $J = 7.4 \text{ Hz}$, 3H, CH₃, CH₃CH₂CH₂) ppm. ¹³C NMR (151 MHz, MeOD) δ 174.0 (C), 160.3 (C), 156.5 (C), 154.6 (CH), 150.4 (C), 133.2 (CH), 118.4 (CH), 107.0 (CH), 106.1 (C), 77.2 (CH), 74.1 (CH), 71.2 (CH₂), 61.2 (CH₂), 56.5 (CH), 43.1 (CH), 41.6 (CH₂), 31.4 (CH₂), 22.1 (CH₂), 9.7 (CH₃) ppm. HRMS (ESI+) calculated for C₁₉H₂₇N₄O₅ 391.1981 found 391.1963; Method B $t_{\text{R}} = 1.15 \text{ min}$; Purity (AUC) $\geq 95\%$.

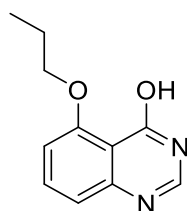
***N*-(((1*R*,2*R*,3*S*,4*R*)-2,3-Dihydroxy-4-((5-(pyridin-2-ylmethoxy)quinazolin-4-yl)amino)cyclopentyl)methyl)-2-hydroxyacetamide (241)**



Ethyl glycolate (0.10 mL, 1.0 mmol) was added to a stirred solution of *N*-[(3*a**S*,4*R*,6*R*,6*a**R*)-6-(aminomethyl)-2,2-dimethyl-4,5,6,6*a*-tetrahydro-3*a*H-cyclopenta[*d*][1,3]dioxol-4-yl]-5-(2-pyridylmethoxy)quinazolin-4-amine (44 mg, 0.10 mmol) and TEA (0.03 mL, 0.21 mmol) in CHCl₃ (0.5 mL) and the solution was heated at 60 °C for 48 h. The reaction mixture was concentrated and dried for 18 h. 1 M aq. HCl (1 mL, 1.0 mmol) and MeCN (0.5 mL) was added and stirred at rt for 2 h. The reaction mixture was poured directly onto an acidic ion exchange cartridge (SCX, 5 g) and washed with MeOH (30 mL). The product was eluted with 2 M NH₃/MeOH and concentrated. The residue was purified by reverse phase column chromatography (biotage SNAP-Ultra C18 12 g, eluted with 0-70% MeOH in water, 1 CV gradient over 15 CV, 2 CV) to afford the title compound (34 mg, 75%, 0.08 mmol) as a white solid. $[\alpha]^{20}_{\text{D}} -23.5^{\circ}$ (*c*=0.5, MeOH). IR (thin film) $\nu = 3307, 2963, 1614, 1580, 1530 \text{ cm}^{-1}$. ¹H NMR (600 MHz, Methanol-*d*₄) δ 8.76 (ddd, *J* = 5.0, 1.3 Hz, 1H, ArH, H₁₃), 8.46 (s, 1H, ArH, H₂), 8.24 (s, 1H, NH), 7.95 (ddd, *J* = 7.7, 1.8 Hz, 1H, ArH, H₁₁), 7.79 (dd, *J* = 8.2 Hz, 1H, ArH, H₇), 7.62 (d, *J* = 7.8 Hz, 1H, ArH, H₁₀), 7.50 (ddd, *J* = 7.7, 4.9, 1.2 Hz, 1H, ArH, H₁₂), 7.33 (d, *J* = 8.3 Hz, 1H, ArH, H₈), 7.26 (d, *J* = 8.0 Hz, 1H, ArH, H₆), 5.49 (d, *J* = 2.1 Hz, 2H, CH₂, H₉), 4.64 (ddd, *J* = 9.3, 7.9, 6.6 Hz, 1H, CH, H_{1'}), 4.00 (m, 3H, CH, CH₂, H_{2'}, CH₂OH), 3.82 (dd, *J* = 5.7 Hz, 1H, CH, H_{3'}), 3.37 – 3.34 (m, 2H, CH₂, H_{6'}), 2.47 (app dt, *J* = 13.3, 8.0 Hz, 1H, CH₂, H_{5'}), 2.31 – 2.21 (m, 1H, CH, H_{4'}), 1.19 (app dt, *J* = 13.2, 9.4 Hz, 1H, CH₂, H_{5'}) ppm. ¹³C NMR (151 MHz, Methanol-*d*₄) δ 174.0 (C), 164.8 (CH), 160.4 (C), 156.1 (C), 154.7 (C), 153.5 (CH), 149.4 (CH), 147.4 (C), 137.6 (CH), 134.2 (CH), 123.8 (CH), 122.4 (CH), 116.7 (CH), 108.1 (CH), 105.9 (C), 76.5 (CH), 73.9 (CH), 71.1 (CH₂), 61.2 (CH₂), 57.0 (CH), 43.1 (CH), 41.7 (CH₂), 31.1 (CH₂) ppm. HRMS (ESI+) calculated for C₂₂H₂₆N₅O₅ 440.1934 found 440.1925; Method B *t*_R = 1.14 min; Purity (AUC) \geq 95%.

5-Methoxyquinazolin-4-ol (250)

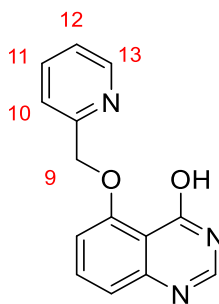
Sodium hydride (60% in oil; 609 mg, 15.23 mmol) was added to DMSO (7 mL). After stirring for 2 min, dry methanol (0.6 mL) was added. After a further 5 min, 5-fluoro-4-hydroxyquinazoline (500 mg, 3.05 mmol) was added and the mixture was stirred at 50 °C for 24 h. The mixture was cooled, water (50 mL) was added and the pH of the mixture was adjusted to 4 with citric acid. The mixture was extracted with EtOAc (4 x 50 mL), dried with MgSO₄, filtered and evaporated under vacuum. The residue was purified by column chromatography (biotage SNAP KP-Sil 10 g, eluted with 0-10% MeOH in CH₂Cl₂, 1 CV, gradient over 10 CV, 5 CV) to yield the title compound (339 mg, 63%, 1.93 mmol) as a white solid. IR (thin film) $\nu = 3074, 2841 \text{ cm}^{-1}$. ¹H NMR (600 MHz, DMSO-*d*₆) δ 11.91 (s, 1H, OH), 7.96 (s, 1H, ArH, H₂), 7.68 (dd, *J* = 8.2, 8.2 Hz, 1H, H₇), 7.17 (dd, *J* = 8.2, 0.9 Hz, 1H, ArH, H₈), 7.01 (dd, *J* = 8.3, 0.9 Hz, 1H, ArH, H₆), 3.85 (s, 3H, CH₃) ppm. ¹³C NMR (151 MHz, DMSO-*d*₆) δ 160.1 (C), 159.3 (C), 151.8 (C), 146.2 (CH), 135.0 (CH), 119.5 (CH), 112.8 (C), 108.8 (CH), 56.4 (CH₃) ppm. HRMS (ESI+) calculated for C₉H₉N₂O₂ 177.0659, found 177.0661; Method A *t*_R = 0.70 min; Purity (AUC) $\geq 95\%$.

5-Propoxyquinazolin-4-ol (251)

Sodium hydride (60% in oil; 1827 mg, 45.7 mmol) was added to stirred DMSO (23 mL). After 2 min, 1-propanol (3.4 mL, 45.7 mmol) was added. After 5 min, 5-fluoro-4-hydroxyquinazoline (1500 mg, 9.14 mmol) was added and the mixture

was stirred at 50 °C for 24 h. The mixture was cooled and water (25 mL) was added. The pH of the mixture was adjusted to 5 with citric acid. The precipitate formed was filtered and dried to yield 496 mg. The remaining product was extracted with EtOAc (4 x 50 mL), followed by CH₂Cl₂ (3 x 30 mL), dried with MgSO₄, filtered and evaporated under vacuum. Purification by column chromatography (biotage SNAP-Ultra C18 30g eluted with 10-90% MeOH in water, 1 CV gradient over 15 CV, 2 CV) afforded the title compound (combined yield 1040 mg, 58%, 5.11 mmol) as a white solid. IR (thin film) ν = 3162, 3024, 2940, 2876 cm⁻¹. ¹H NMR (600 MHz, DMSO-*d*₆) δ 11.83 (s, 1H, OH), 7.94 (s, 1H, H₂), 7.65 (dd, *J* = 8.2 Hz, 1H, H₇), 7.15 (d, *J* = 8.0 Hz, 1H, H₈), 6.99 (d, *J* = 8.2 Hz, 1H, H₆), 4.01 (t, *J* = 6.3 Hz, 2H, CH₃CH₂CH₂), 1.89 – 1.67 (app h, 2H, CH₃CH₂CH₂), 1.04 (t, *J* = 7.4 Hz, 3H, CH₃) ppm. ¹³C NMR (151 MHz, DMSO-*d*₆) δ 159.6 (C), 159.2 (C), 151.8 (C), 146.1 (CH), 134.9 (CH), 119.3 (CH), 113.0 (C), 109.7 (CH), 70.5 (CH₂), 22.5 (CH₂), 11.0 (CH₃) ppm. HRMS (ESI+) calculated for C₁₁H₁₃N₂O₂ 205.0977 found 205.0970; Method B *t*_R = 1.91 min; Purity (AUC) \geq 95%.

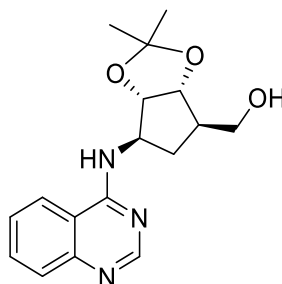
5-(Pyridin-2-ylmethoxy)quinazolin-4-ol (252)



Sodium hydride (60% in oil) (609 mg, 15.23 mmol) was added to stirred DMSO (7.6 mL). After 2 min, 2-(hydroxymethyl)-pyridine (1.5 mL, 15.2 mmol) was added. After 5 min, 5-fluoro-4-hydroxyquinazoline (500 mg, 3.05 mmol) was added and the dark red mixture was heated at 50 °C for 48 h. The mixture was cooled and water (50 mL) was added. The pH of the mixture was adjusted to 4 with citric acid. The precipitate formed was filtered and dried to yield 538 mg desired product. The remaining product was extracted from the water layer with EtOAc (4 x 50 mL), dried with MgSO₄, filtered and evaporated under vacuum.

Purification by column chromatography (biotage SNAP KP-Sil 10 g eluted with 0-10% MeOH in CH₂Cl₂, 1 CV, gradient over 10 CV, 5 CV) to afford the title compound (combined yield 650 mg, 84%, 2.57 mmol) as a white solid. IR (thin film) $\nu = 3172, 3054, 2832 \text{ cm}^{-1}$. ¹H NMR (600 MHz, DMSO-*d*₆) δ 11.95 (s, 1H, OH), 8.58 (ddd, *J* = 4.8, 1.2 Hz, 1H, ArH, H₁₀), 8.08 – 7.96 (m, 2H, ArH, H₂, H₁₃), 7.88 (td, *J* = 7.7, 1.8 Hz, 1H, ArH, H₁₁), 7.69 (dd, *J* = 8.2 Hz, 1H, ArH, H₇), 7.3 (m, 1H, ArH, H₁₂), 7.22 (d, *J* = 8.1 Hz, 1H, ArH, H₈), 7.13 (d, *J* = 8.2 Hz, 1H, ArH, H₆), 5.29 (s, 2H, CH₂, H₉) ppm. ¹³C NMR (151 MHz, DMSO-*d*₆) δ 159.4 (C), 158.5 (C), 157.5 (C), 151.8 (C), 149.2 (CH), 146.4 (CH), 137.4 (CH), 135.1 (CH), 123.1 (CH), 121.6 (CH), 120.0 (CH), 113.1 (C), 110.2 (CH), 71.1 (CH₂) ppm. LCMS (ESI+) *t*_R = 0.72 min, *m/z* 254; HRMS [M+H⁺] calcd for C₁₄H₁₂N₃O₂ 254.0924, found 254.0905.

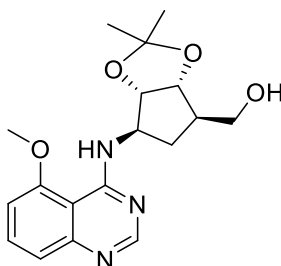
Cyclopenta[d][1,3]dioxol-4-yl)methanol (253)



p-Toluenesulfonic acid monohydrate (414 mg, 2.18 mmol) was added to a suspension of 2,2-dimethoxypropane (2.2 mL, 18.2 mmol) and (1*S*,2*R*,3*R*,5*R*)-3-(hydroxymethyl)-5-(quinazolin-4-ylamino)cyclopentane-1,2-diol (500 mg, 1.82 mmol) in CH₂Cl₂ (5.2 mL). The resulting solution was stirred at rt for 72 h. 2 M NH₃ in MeOH (1 mL) was added and the mixture evaporated under vacuum. The residue was purified by column chromatography (biotage SNAP KP-Sil 100 g, eluted with 4-10% MeOH in CH₂Cl₂, 2 CV, gradient over 16 CV, 2 CV) to afford the title compound (287 mg, 50%, 0.91 mmol) as a white solid. IR (thin film) $\nu = 3260, 3085, 2983, 2935, 1615, 1595, 1540 \text{ cm}^{-1}$. ¹H NMR (600 MHz, DMSO-*d*₆) δ 8.49 (s, 1H, ArH, H₂), 8.28 (d, *J* = 7.2 Hz, 1H, NH), 8.17 (dd, *J* = 8.4, 1.3 Hz, 1H, ArH, H₅), 7.78 (ddd, *J* = 8.3, 6.9, 1.3 Hz, 1H, ArH, H₇), 7.70 (dd, *J* = 8.3, 1.2 Hz, 1H, ArH, H₈), 7.53 (ddd, *J* = 8.2, 6.9, 1.3 Hz, 1H, ArH, H₆), 5.07 (t, *J* = 4.8

Hz, 1H, OH), 4.72 – 4.61 (m, 2H, CH, H₁' , H₂'), 4.52 (dd, *J* = 6.2, 3.7 Hz, 1H, CH, H₃'), 3.53 (m, 2H, CH₂, H₆'), 2.40 – 2.29 (m, 1H, CH₂, H₅'), 2.26 – 2.09 (m, 1H, CH, H₄'), 1.60 (app dt, *J* = 13.0, 7.7 Hz, 1H, CH₂, H₅'), 1.44 (s, 3H, CH₃, acetal), 1.24 (s, 3H, CH₃, acetal) ppm. ¹³C NMR (151 MHz, DMSO-*d*₆) δ 159.3 (C), 155.5 (CH), 149.6 (C), 133.1 (CH), 128.0 (CH), 126.1 (CH), 122.9 (CH), 115.3 (C), 111.3 (C), 85.1 (CH), 82.2 (CH), 62.7 (CH₂), 57.0 (CH), 46.8 (CH), 33.6 (CH₂), 27.7 (CH₃), 25.3 (CH₃) ppm. HRMS (ESI+) calculated for C₁₇H₂₂N₃O₃ 316.1656, found 316.1671; Method A *t*_R = 1.73 min; Purity (AUC) ≥ 95%.

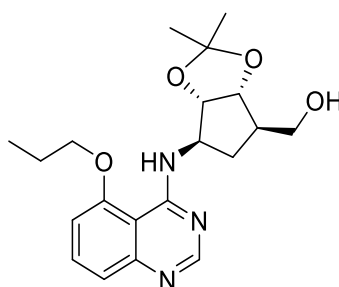
((3*aR*,4*R*,6*R*,6*aS*)-6-((5-Methoxyquinazolin-4-yl)amino)-2,2-dimethyltetrahydro-4*H*-cyclopenta[*d*][1,3]dioxol-4-yl)methanol (254)



p-Toluenesulfonic acid monohydrate (219 mg, 1.15 mmol) was added to a suspension of 2,2-dimethoxypropane (1.2 mL, 9.6 mmol) and (1*S*,2*R*,3*R*,5*R*)-3-(hydroxymethyl)-5-[(5-methoxyquinazolin-4-yl)amino]cyclopentane-1,2-diol (293 mg, 0.95 mmol) in CH₂Cl₂ (4.8 mL). The resulting solution was stirred at rt for 2 h. 2 M NH₃ in MeOH (0.6 mL, 1.2 mmol) was added and the reaction mixture was concentrated. The residue was purified by column chromatography (biotage SNAP KP-Sil 25 g eluted with 2-10% MeOH in CH₂Cl₂, 1 CV, gradient over 18 CV, 5 CV) to afford the title compound (200 mg, 60%, 0.58 mmol) as a white solid. IR (thin film) ν = 3372, 3245, 2984, 2919, 2863, 1614, 1578, 1529 cm⁻¹. ¹H NMR (600 MHz, Chloroform-*d*) δ 8.59 (s, 1H, ArH, H₂), 8.25 (d, *J* = 6.7 Hz, 1H, NH), 7.57 (dd, *J* = 8.2 Hz, 1H, ArH, H₇), 7.38 (dd, *J* = 8.3, 1.0 Hz, 1H, ArH, H₈), 6.80 (dd, *J* = 8.1, 1.0 Hz, 1H, ArH, H₆), 4.70 (app tdd, *J* = 7.4, 5.0, 2.5 Hz, 1H, CH, H₁'), 4.67 – 4.58 (m, 2H, CH, H₂' , H₃'), 4.01 (s, 3H, CH₃, O-methoxy), 3.81 (d, *J* = 5.9 Hz, 2H, CH₂, H₆'), 2.72 – 2.60 (m, 1H, CH₂, H₅'), 2.48 (app dqd, *J* = 8.3, 5.8, 2.5 Hz, 1H, CH, H₄'), 1.76 (app dt, *J* = 13.9, 5.3 Hz, 1H, CH₂, H₅'),

1.56 (s, 3H, CH₃, acetal), 1.35 (s, 3H, CH₃, acetal) ppm. ¹³C NMR (151 MHz, Chloroform-*d*) δ 159.4 (C), 156.6 (C), 155.7 (CH), 151.5 (C), 132.4 (CH), 120.4 (CH), 111.5 (C), 106.9 (C), 105.3 (CH), 86.4 (CH), 83.0 (CH), 64.1 (CH₂), 57.7 (CH), 56.1 (CH₃), 47.3 (CH), 32.6 (CH₂), 27.1 (CH₃), 24.7 (CH₃) ppm. HRMS (ESI+) calculated for C₁₈H₂₃N₃NaO₄ 368.1581, found 368.1573; Method A *t_R* = 1.90 min; Purity (AUC) ≥ 95%.

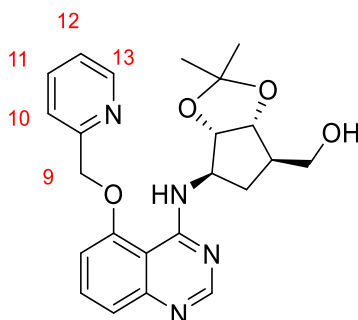
((3*R*,4*R*,6*R*,6*aS*)-2,2-Dimethyl-6-((5-propoxyquinazolin-4-yl)amino)tetrahydro-4*H*-cyclopenta[*d*][1,3]dioxol-4-yl)methanol (255)**



p-Toluenesulfonic acid monohydrate (264 mg, 1.39 mmol) was added to a suspension of 2,2-dimethoxypropane (1.4 mL, 11.5 mmol) and (1*S*,2*R*,3*R*,5*R*)-3-(hydroxymethyl)-5-[(5-propoxyquinazolin-4-yl)amino]cyclopentane-1,2-diol (385 mg, 1.15 mmol) in CH₂Cl₂ (5.8 mL). The resulting solution was stirred at rt for 2 h. 2 M NH₃ in MeOH (0.7 mL, 1.4 mmol) was added and the mixture was concentrated. Purification by column chromatography (biotage SNAP KP-Sil 10 g eluted with 0-10% MeOH in CH₂Cl₂, 1 CV, gradient over 15 CV, 5 CV) afforded the title compound (289 mg, 67%, 0.77 mmol) as a pale-yellow oil. IR (thin film) ν = 3362, 3168, 2925, 1612, 1582, 1542 cm⁻¹. ¹H NMR (500 MHz, DMSO-*d*₆) δ 8.39 (s, 1H, ArH, H₂), 8.26 (d, *J* = 7.1 Hz, 1H, NH), 7.63 (dd, *J* = 8.2 Hz, 1H, ArH, H₇), 7.23 (dd, *J* = 8.4, 1.0 Hz, 1H, ArH, H₈), 7.02 (dd, *J* = 8.2, 1.0 Hz, 1H, ArH, H₆), 4.86 (t, *J* = 4.9 Hz, 1H, OH), 4.57 – 4.43 (m, 3H, CH, H₁' , H₂' , H₃'), 4.25 – 4.14 (m, 2H, CH₂, CH₃CH₂CH₂), 3.54 – 3.41 (m, 2H, CH₂, H₆'), 2.44 (app dt, *J* = 13.5, 7.7 Hz, 1H, CH₂, H₅'), 2.26 – 2.18 (m, 1H, CH, H₄'), 1.89 (tq, *J* = 7.2 Hz, 2H, CH₂, CH₃CH₂CH₂), 1.51 (app dt, *J* = 12.8, 5.9 Hz, 1H, CH₂, H₅'), 1.42 (s, 3H, CH₃, acetal), 1.23 (s, 3H, CH₃, acetal), 1.03 (t, *J* = 7.4 Hz, 3H, CH₃, CH₃CH₂CH₂) ppm. ¹³C NMR (126 MHz, DMSO-*d*₆) δ 159.2 (C), 156.2 (C), 155.6 (CH), 151.9

(C), 133.3 (CH), 120.1 (CH), 110.9 (C), 107.3 (CH), 106.5 (C), 86.3 (CH), 82.7 (CH), 71.1 (CH₂), 62.9 (CH₂), 57.7 (CH), 47.1 (CH), 33.5 (CH₂), 27.6 (CH₃), 25.1 (CH₃), 21.9 (CH₂), 10.8 (CH₃) ppm. HRMS (ESI+) calculated for for C₂₀H₂₈N₃O₄ 374.2074, found 374.2084; Method A t_R = 2.11 min; Purity (AUC) ≥ 95%.

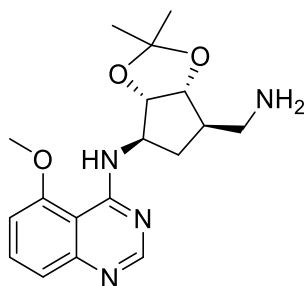
3a*R*,4*R*,6*R*,6a*S*)-2,2-Dimethyl-6-((5-(pyridin-2-ylmethoxy)quinazolin-4-yl)amino)tetrahydro-4H-cyclopenta[d][1,3]dioxol-4-yl)methanol (256)



p-Toluenesulfonic acid monohydrate (155 mg, 0.82 mmol) was added to a suspension of 2,2-dimethoxypropane (0.8 mL, 6.8 mmol) and (1*S*,2*R*,3*R*,5*R*)-3-(hydroxymethyl)-5-[[5-(2-pyridylmethoxy)quinazolin-4-yl]amino]cyclopentane-1,2-diol (260 mg, 0.68 mmol) in CH₂Cl₂ (3.4 mL). The resulting solution was stirred at rt for 2 h. 2 M NH₃ in MeOH (0.4 mL, 0.8 mmol) was added and the reaction mixture was concentrated. The residue was purified by column chromatography (biotage SNAP KP-Sil 25 g, eluted with 2-10% MeOH in CH₂Cl₂, 1 CV, gradient over 18 CV, 5 CV) to afford the title compound (186 mg, 65%, 0.44 mmol) as a white solid. IR (thin film) ν = 3269, 2982, 2927, 2877, 1616, 1576, 1531 cm⁻¹. ¹H NMR (500 MHz, DMSO-*d*₆) δ 8.96 (d, *J* = 7.3 Hz, 1H, NH), 8.80 – 8.61 (ddd, *J* = 5.0, 1.8, 0.9 Hz, 1H, ArH, H₁₃), 8.40 (s, 1H, ArH, H₂), 7.90 (ddd, *J* = 7.6, 7.6, 1.7 Hz, 1H, ArH, H₁₁), 7.66 (t, *J* = 8.2 Hz, 1H, ArH, H₇), 7.54 (dt, *J* = 7.8, 1.0 Hz, 1H, ArH, H₁₀), 7.44 (ddd, *J* = 7.7, 4.9, 1.2 Hz, 1H, ArH, H₁₂), 7.26 (dd, *J* = 8.3, 0.9 Hz, 1H, ArH, H₈), 7.09 (dd, *J* = 8.1, 1.1 Hz, 1H, ArH, H₆), 5.48 (s, 2H, CH₂, H₉), 4.81 (t, *J* = 5.0 Hz, 1H, OH), 4.64 (m, 1H, CH, H_{1'}), 4.58 – 4.47 (m, 2H, CH, H_{2'}, H_{3'}), 3.42 (t, *J* = 5.4 Hz, 2H, CH₂, H_{6'}), 2.34 (app dt, *J* = 13.2, 7.3 Hz, 1H, CH₂, H_{5'}), 2.16 (t, *J* = 6.9 Hz, 1H, CH, H_{4'}), 1.56 (app dt, *J* = 13.2, 8.1 Hz, 1H, CH₂, H_{5'}), 1.43 (s, 3H, CH₃, acetal), 1.24 (s, 3H, CH₃, acetal) ppm. ¹³C NMR (126 MHz, DMSO-*d*₆) δ 159.3 (C), 155.7 (CH), 155.7 (C), 155.6

(C), 151.9 (C), 149.8 (CH), 137.7 (CH), 133.2 (CH), 123.9 (CH), 122.5 (CH), 120.5 (CH), 111.5 (C), 107.7 (CH), 106.7 (C), 85.6 (CH), 82.0 (CH), 71.2 (CH₂), 62.4 (CH₂), 57.4 (CH), 46.7 (CH), 33.7 (CH₂), 27.7 (CH₃), 25.3 (CH₃) ppm. HRMS (ESI+) calculated for calcd for C₂₃H₂₆N₄NaO₄ 445.1846, found 445.1801; Method A t_R = 2.04 min; Purity (AUC) ≥ 95%.

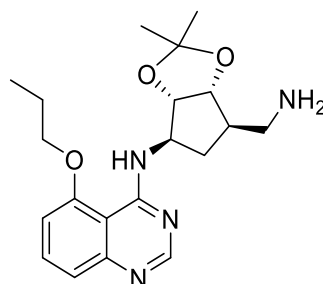
***N*-((3*aS*,4*R*,6*R*,6*aR*)-6-(Aminomethyl)-2,2-dimethyltetrahydro-4H-cyclopenta[*d*][1,3]dioxol-4-yl)-5-methoxyquinazolin-4-amine (262)**



[(3*aS*,4*R*,6*R*,6*aR*)-4-[(5-Methoxyquinazolin-4-yl)amino]-2,2-dimethyl-4,5,6,6*a*-tetrahydro-3*aH*-cyclopenta[*d*][1,3]dioxol-6-yl]methyl methanesulfonate (175 mg, 0.41 mmol) was dissolved in DMF (4.1 mL). Sodium azide (54 mg, 0.83 mmol) was added at 0 °C. The mixture was stirred at 60 °C for 18 h, then cooled and water (40 mL) was added. The mixture was extracted with Et₂O (4 × 20 mL). The organic layers were combined, washed with brine (sat.aq.), dried with Na₂SO₄ and filtered. THF (15 mL) was added and the Et₂O was removed under vacuum. Triphenylphosphine (217 mg, 0.82 mmol) and NH₄OH (28-30% in H₂O, 1.0 mL) were added and the mixture was stirred at 60 °C for 3 h. Water (20 mL) and brine (20 mL) were added and the mixture was extracted with EtOAc (3 × 30 mL). The organic layers were combined, dried with MgSO₄, filtered and evaporated under vacuum. The residue was purified by column chromatography (biotage SNAP KP-Sil 25 g, eluted with 2-20% of 10% NH₃ in MeOH in CH₂Cl₂ to afford the title compound (30 mg, 21%, 0.09 mmol) as a white solid. IR (thin film) ν = 3388, 2932, 1614, 1575, 1523 cm⁻¹. ¹H NMR (600 MHz, DMSO-*d*₆) δ 8.40 (s, 1H, ArH, H₂), 8.30 (d, *J* = 7.0 Hz, 1H, NH), 7.66 (dd, *J* = 8.2 Hz, 1H, ArH, H₇), 7.25 (d, *J* = 7.9 Hz, 1H, ArH, H₈), 7.01 (d, *J* = 7.8 Hz, 1H, ArH, H₆), 4.55 (m, 2H, CH, H₁', H₂'), 4.47 (dd, *J* = 6.2, 2.9 Hz, 1H, CH, H₃'), 4.00 (s, 3H, CH₃, O-

methoxy), 2.79 – 2.60 (m, 2H, CH₂, H_{6'}), 2.37 (app dt, $J = 13.4, 7.4$ Hz, 1H, CH₂, H_{5'}), 2.12 (pd, $J = 6.9, 2.9$ Hz, 1H, CH, H_{4'}), 1.63 (app dt, $J = 13.4, 5.8$ Hz, 1H, CH₂, H_{5'}), 1.42 (s, 3H, CH₃, acetal), 1.24 (s, 3H, CH₃, acetal) ppm. ¹³C NMR (151 MHz, DMSO-*d*₆) δ 159.1 (C), 157.0 (C), 155.6 (CH), 151.9 (C), 133.2 (CH), 120.2 (CH), 110.7 (C), 106.4 (C), 106.4 (CH), 85.9 (CH), 83.4 (CH), 57.4 (CH), 57.0 (CH₃), 47.8 (CH₂), 44.5 (CH), 33.6 (CH₂), 27.5 (CH₃), 25.1 (CH₃) ppm. HRMS (ESI+) calculated for C₁₈H₂₅N₄O₃ 345.1921, found 345.1923; Method A $t_R = 0.017$ min; Purity (AUC) $\geq 95\%$.

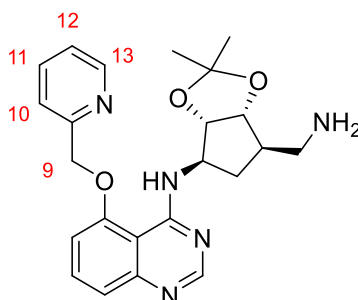
***N*-((3*aS*,4*R*,6*R*,6*aR*)-6-(Aminomethyl)-2,2-dimethyltetrahydro-4H-cyclopenta[*d*][1,3]dioxol-4-yl)-5-propoxyquinazolin-4-amine (263)**



(3*aS*,4*R*,6*R*,6*aR*)-2,2-Dimethyl-4-[(5-propoxyquinazolin-4-yl)amino]-4,5,6,6*a*-tetrahydro-3*aH*-cyclopenta[*d*][1,3]dioxol-6-yl]methyl methanesulfonate (314 mg, 0.70 mmol) was dissolved in DMF and sodium azide (90 mg, 1.39 mmol) was added at 0 °C. The mixture was stirred at 60 °C for 18 h. Water (20 mL) was added and the mixture was extracted with Et₂O (3 × 20 mL). The organic layers were combined, dried with MgSO₄ and filtered. THF (15 mL) was added and the Et₂O was removed under vacuum. NH₄OH (28-30% in H₂O, 1.0 mL) and triphenylphosphine (365 mg, 1.39 mmol) were added. The mixture was stirred at 60 °C for 18 h. Water (20 mL) and brine (20 mL) were added and the mixture was extracted with EtOAc (3 × 30 mL). The organic layers were combined, dried with MgSO₄, filtered and evaporated under vacuum. The residue was purified by column chromatography (biotage SNAP KP-Sil 25 g, eluted with 2-15% of 10% NH₃ in MeOH in CH₂Cl₂ to afford the title compound (78 mg, 30%, 0.21 mmol) as an oil. IR (thin film) $\nu = 3387, 1648$ cm⁻¹. ¹H NMR (600 MHz, DMSO-*d*₆) δ 8.41 (s, 1H, ArH, H₂), 8.18 (d, $J = 6.6$ Hz, 1H, NH), 7.65 (dd, $J = 8.2, 1.4$ Hz, 1H, ArH, H₇), 7.25 (d, $J = 8.2$ Hz, 1H, ArH, H₈), 7.04 (d, $J = 8.1$ Hz, 1H, ArH, H₆), 4.55 – 4.41 (m, 3H, CH, H_{1'}, H_{2'}, H_{3'}), 4.27 – 4.15 (m, 2H, CH₂, CH₃CH₂CH₂),

2.65 (qdd, $J = 10.6, 7.0, 3.5$ Hz, 2H, CH₂, H_{6'}), 2.44 (app dt, $J = 13.7, 7.1$ Hz, 1H, CH₂, H_{5'}), 2.09 (td, $J = 7.2, 2.6$ Hz, 1H, CH, H_{4'}), 1.91 (app h, $J = 7.1$ Hz, 2H, CH₂, CH₃CH₂CH₂), 1.56 – 1.45 (m, 1H, CH₂, H_{5'}), 1.43 (s, 3H, CH₃, acetal), 1.25 (s, 3H, CH₃, acetal), 1.05 (t, $J = 7.4$ Hz, 3H, CH₃, CH₃CH₂CH₂) ppm. ¹³C NMR (151 MHz, DMSO-*d*₆) δ 159.4 (C), 156.1 (C), 155.6 (CH), 151.9 (C), 133.3 (CH), 120.2 (CH), 111.3 (C), 107.4 (CH), 106.5 (C), 85.8 (CH), 83.0 (CH), 71.3 (CH₂), 57.6 (CH), 47.5 (CH), 44.8 (CH₂), 34.4 (CH₂), 27.6 (CH₃), 25.2 (CH₃), 22.1 (CH₂), 10.9 (CH₃) ppm. HRMS (ESI+) calculated for C₂₀H₂₉N₄O₃ 373.2234 found 373.2235; Method A $t_R = 1.82$ min; Purity (AUC) $\geq 95\%$.

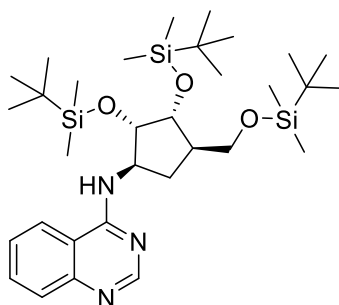
***N*-((3*aS*,4*R*,6*R*,6*aR*)-6-(Aminomethyl)-2,2-dimethyltetrahydro-4H-cyclopenta[*d*][1,3]dioxol-4-yl)-5-(pyridin-2-ylmethoxy)quinazolin-4-amine (264)**



Sodium azide (92 mg, 1.41 mmol) was added at 0 °C to a solution of [(3*aS*,4*R*,6*R*,6*aR*)-2,2-dimethyl-4-[[5-(2-pyridylmethoxy)quinazolin-4-yl]amino]-4,5,6,6*a*-tetrahydro-3*aH*-cyclopenta[*d*][1,3]dioxol-6-yl]methyl methanesulfonate (236 mg, 0.47 mmol) in DMF (2.4 mL). The mixture was stirred at 60 °C for 18 h. Triphenylphosphine (247 mg, 0.94 mmol) was added and the mixture was stirred at 60 °C for 4 h. When the reaction mixture was cool, water (10 mL) and brine (10 mL) were added and the mixture was extracted with CH₂Cl₂ (3 × 20 mL). The organic layers were combined, dried with MgSO₄ and filtered. Purification by reverse phase column chromatography (biotage SNAP-Ultra C18 30g, eluted with 10-70% MeOH in water, 5 CV gradient over 15 CV, 2 CV) afforded the title compound as a white solid. IR (thin film) $\nu = 3307, 2963, 1614, 1580, 1530$ cm⁻¹. ¹H NMR (600 MHz, Methanol-*d*₄) δ 8.75 – 8.72 (m, 1H, ArH, H₁₃), 8.40 (s, 1H, ArH, H₂), 7.96 (td, $J = 7.7, 1.8$ Hz, 1H, ArH, H₁₁), 7.77 (t, $J =$

8.2 Hz, 1H, ArH, H₇), 7.63 (d, $J = 7.8$ Hz, 1H, ArH, H₁₀), 7.51 – 7.48 (m, 1H, ArH, H₁₂), 7.36 (d, $J = 8.2$ Hz, 1H, ArH, H₈), 7.22 (d, $J = 8.0$ Hz, 1H, ArH, H₆), 5.50 (d, $J = 3.3$ Hz, 2H, CH₂, H₉), 4.75 – 4.66 (m, 2H, CH, H_{1'}, H_{2'}), 4.56 (q, $J = 6.5$ Hz, 1H, CH, H_{3'}), 3.22 – 2.96 (m, 2H, CH₂, H_{6'}), 2.73 – 2.64 (m, 1H, CH₂, H_{5'}), 2.45 – 2.35 (m, 1H, CH, H_{4'}), 1.68 – 1.59 (m, 1H, CH₂, H_{5'}), 1.56 (s, 3H, CH₃, acetal), 1.35 (s, 3H, CH₃, acetal) ppm. ¹³C NMR (151 MHz, Methanol-*d*₄) δ 159.8 (C), 155.8 (C), 155.0 (C), 154.3 (CH), 149.4 (C), 149.2 (CH), 137.6 (CH), 133.7 (CH), 123.5 (CH), 122.4 (CH), 118.2 (CH), 113.6 (C), 107.7 (CH), 106.3 (C), 84.8 (CH), 82.3 (CH), 71.0 (CH₂), 57.2 (CH), 42.8 (CH), 41.9 (CH₂) 34.4 (CH₂), 26.2 (CH₃), 24.0 (CH₃) ppm. HRMS (ESI+) calculated for C₂₃H₂₈N₅O₃ 422.2187 found 422.2194; Method A $t_R = 1.71$ min; Purity (AUC) $\geq 95\%$.

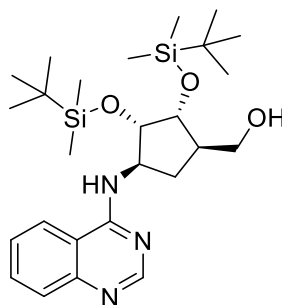
***N*-((1*R*,2*S*,3*R*,4*R*)-2,3-Bis((*tert*-butyldimethylsilyloxy)-4-(((*tert*-butyldimethylsilyloxy)methyl)cyclopentyl)quinazolin-4-amine (292)**



To a solution of (1*S*,2*R*,3*R*,5*R*)-3-(hydroxymethyl)-5-(quinazolin-4-ylamino)cyclopentane-1,2-diol (50 mg, 0.18 mmol) in DMF (1.8 mL) was added imidazole (123 mg, 1.82 mmol), DMAP (2 mg, 0.02 mmol) and *tert*-butyldimethylsilyl chloride (192 mg, 1.27 mmol). The mixture was stirred at rt for 18 h. The reaction was quenched with water (15 mL) and extracted with EtOAc (3 x 20 mL). The combined organic layers were dried with MgSO₄, filtered and concentrated *in vacuo*. The residue was purified by column chromatography (biotage SNAP KP-Sil 10 g, eluted with 0-50% EtOAc in Cyclohexane, 2 CV, gradient over 10 CV, 2 CV) to yield the title compound (104 mg, 93%, 0.17 mmol) as a viscous oil. IR (thin film) $\nu = 2928, 2854, 1674, 1619, 1580, 1527$ cm⁻¹. ¹H NMR (600 MHz, Chloroform-*d*) δ 8.67 (s, 1H, ArH, H₅), 7.86 (dd, $J = 8.5, 1.2$ Hz, 1H, ArH, H₇), 7.75 (ddd, $J = 8.3, 7.0, 1.3$ Hz, 1H, ArH, H₈), 7.65 (dd, $J = 8.3, 1.4$ Hz, 1H, ArH, H₆), 7.46 (ddd, $J = 8.2, 6.9, 1.2$ Hz, 1H, ArH), 5.73 (d, $J = 6.9$ Hz,

1H, NH), 4.53 (dp, $J = 10.5, 3.5$ Hz, 1H, CH, H_{1'}), 4.09 (dd, $J = 6.9, 3.5$ Hz, 1H, CH, H_{2'}), 4.01 (t, $J = 3.6$ Hz, 1H, CH, H_{3'}), 3.75 (m, 2H, CH₂, H_{6'}), 2.66 – 2.56 (m, 1H, CH, H_{5'}), 2.29 (m, 1H, CH₂, H_{4'}), 1.48 – 1.42 (m, 1H, H_{5'}), 1.01 (s, 9H, CH₃, ^tBu), 0.94 (s, 9H, CH₃, ^tBu), 0.91 (s, 9H, CH₃, ^tBu), 0.26 (s, 3H, CH₃, Si-CH₃), 0.19 (s, 3H, CH₃, Si-CH₃), 0.18 (s, 3H, CH₃, Si-CH₃), 0.14 (s, 3H, CH₃, Si-CH₃), 0.06 (s, 3H, CH₃, Si-CH₃), 0.04 (s, 3H, CH₃, Si-CH₃) ppm. ¹³C NMR (151 MHz, Chloroform-*d*) δ 158.7 (C), 155.6 (CH), 149.5 (C), 132.4 (CH), 128.6 (CH), 125.7 (CH), 120.4 (CH), 114.8 (C), 78.1 (CH), 74.2 (CH), 62.7 (CH₂), 55.4 (CH), 44.2 (CH), 29.2 (CH₂), 26.2 (3 x CH₃), 26.0 (3xCH₃), 25.9 (3xCH₃), 25.7 (3 x C), -4.1 (CH₃), -4.2 (CH₃), -4.5 (CH₃), -4.7 (CH₃), -4.9 (CH₃), -5.3 (CH₃) ppm. HRMS (ESI+) calculated for C₃₂H₆₀N₃O₃Si₃ 618.3937, found 618.3925 $t_R = 3.52$ min; Purity (AUC) $\geq 95\%$.

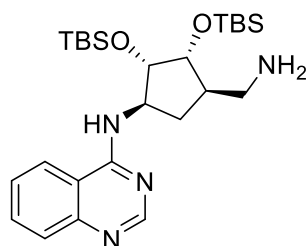
((1*R*,2*R*,3*S*,4*R*)-2,3-Bis((*tert*-butyldimethylsilyl)oxy)-4-(quinazolin-4-ylamino)cyclopentyl)methanol (293)



To a solution of *N*-[(1*R*,2*S*,3*R*,4*R*)-2,3-bis[[*tert*-butyl(dimethyl)silyl]oxy]-4-[[*tert*-butyl(dimethyl) silyl]oxymethyl]cyclopentyl]quinazolin-4-amine (93 mg, 0.15 mmol) in EtOH (6.5 mL) at 0 °C was added a solution of 1% conc HCl in EtOH (0.02 mL, 0.45 in 2 mL EtOH). The reaction was stirred at 0 °C for 4 h. The reaction was quenched with sat aq. NaHCO₃ (20 mL) and extracted with EtOAc (4 x 15 mL). The combined organic layers were dried with MgSO₄, filtered and concentrated. The residue was purified by column chromatography (biotage SNAP KP-Sil 10 g, eluted with 0-50% EtOAc in cyclohexane, 1 CV, gradient over 15 CV, 2 CV) to afford the title compound (56 mg, 75%, 0.11 mmol) as a white solid. IR (thin film) $\nu = 3137, 2928, 2856, 1619, 1583, 1541$ cm⁻¹. ¹H NMR (600 MHz, Chloroform-*d*) δ 8.64 (s, 1H, ArH, H₂), 7.84 (d, $J = 8.3$ Hz, 1H, ArH, H₅), 7.72 (dd, $J = 7.7$ Hz, 1H, ArH, H₇), 7.66 (d, $J = 8.2$ Hz, 1H, ArH, H₈), 7.43 (dd, J

= 7.6 Hz, 1H, ArH, H₆), 6.82 (d, J = 7.0 Hz, 1H, NH), 4.46 (m, 1H, CH, H₁'), 4.24 (m, 1H, CH, H₂'), 4.11 (m, 1H, CH, H₃'), 3.95 (dd, J = 9.6, 2.3 Hz, 1H, CH₂, H₆'), 3.85 (dd, J = 9.6, 3.0 Hz, 1H, CH₂, H₆'), 2.71 (ddd, J = 13.9, 11.9, 7.3 Hz, 1H, CH₂, H₅'), 2.50 (s, 1H, OH), 2.33 (m, 1H, CH, H₄'), 1.60 (m, 1H, CH₂, H₅'), 0.96 (s, 9H, CH₃, ^tBu), 0.91 (s, 9H, CH₃, ^tBu), 0.27 (s, 3H, CH₃, ^tBu), 0.14 (s, 3H, CH₃, Si-CH₃), 0.06 (s, 3H, CH₃, Si-CH₃), 0.03 (s, 3H, CH₃, Si-CH₃) ppm. ¹³C NMR (151 MHz, Chloroform-*d*) δ 158.3 (C), 155.6 (CH), 149.5 (C), 132.3 (CH), 128.4 (CH), 125.8 (CH), 120.7 (CH), 115.2 (C), 77.6 (CH), 74.5 (CH), 62.5 (CH₂), 56.1 (CH), 44.0 (CH), 29.8 (CH₂), 26.9 (C), 25.9 (6 x CH₃), 18.1 (C), -4.1 (CH₃), -4.3 (CH₃), -4.6 (CH₃), -4.8 (CH₃) ppm. HRMS (ESI+) calculated for C₂₆H₄₆N₃NaO₃Si₂ 526.2892 found 526.2892; Method A t_R = 3.15 min; Purity (AUC) \geq 95%.

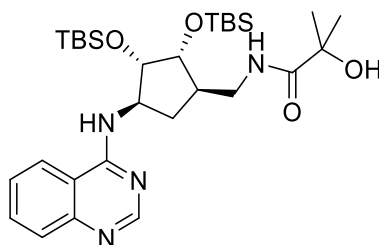
***N*-((1*R*,2*S*,3*R*,4*R*)-4-(Aminomethyl)-2,3-bis((*tert*-butyldimethylsilyl)oxy)cyclopentyl)quinazolin-4-amine (295)**



[(1*R*,2*R*,3*S*,4*R*)-2,3-Bis[[*tert*-butyl(dimethyl)silyl]oxy]-4-(quinazolin-4-ylamino)cyclopentyl]methyl methanesulfonate (993 mg, 1.71 mmol) was dissolved in DMF (8.5 mL) and sodium azide (222 mg, 3.41 mmol) was added at 0 °C. The mixture was stirred at 60 °C for 18 h. Triphenylphosphine (895 mg, 3.41 mmol) and NH₃ (28-30% in H₂O, 3 mL) were added and the mixture was heated at 60 °C for 3 h. The reaction mixture was allowed to cool. Water (80 mL) and brine (10 mL) were added and the mixture was extracted with Et₂O (4 x 50 mL). The organic layers were combined, dried with MgSO₄, filtered and evaporated under vacuum. The residue was purified by column chromatography (biotage SNAP KP-Sil 25 g, eluted with 5-15% 10% NH₃ in MeOH in CH₂Cl₂, 1 CV, gradient over 12 CV, 5 CV) to afford the title compound (673 mg, 78%, 1.34 mmol) as a yellow solid. $[\alpha]_D^{20}$ -4.16° (c=0.5, MeOH). IR (thin film) ν = 2928, 2855, 1619, 1579, 1530 cm⁻¹. ¹H NMR (600 MHz, Methanol-

d_4) δ 8.47 (s, 1H, ArH, H₂), 8.20 (dd, J = 8.4, 1.4 Hz, 1H, ArH, H₅), 7.81 (ddd, J = 8.3, 6.9, 1.3 Hz, 1H, ArH, H₇), 7.73 (dd, J = 8.4, 1.3 Hz, 1H, ArH, H₈), 7.56 (ddd, J = 8.3, 6.9, 1.3 Hz, 1H, ArH, H₆), 4.74 (ddd, J = 9.3, 6.2, 4.7 Hz, 1H, CH, H_{1'}), 4.14 (dd, J = 4.3 Hz, 1H, CH, H_{2'}), 3.94 (dd, J = 6.1, 3.9 Hz, 1H, CH, H_{3'}), 2.97 (dd, J = 12.5, 5.3 Hz, 1H, CH₂, H_{6'}), 2.74 (dd, J = 12.5, 8.4 Hz, 1H, CH₂, H_{6'}), 2.55 (app dt, J = 13.9, 9.3 Hz, 1H, CH₂, H_{5'}), 2.33 – 2.21 (m, 1H, CH, H_{4'}), 1.49 – 1.38 (m, 1H, CH₂, H_{5'}), 0.96 (s, 9H, CH₃, ^tBu), 0.87 (s, 9H, CH₃, ^tBu), 0.15 (s, 3H, CH₃, Si-CH₃), 0.14 (s, 3H, CH₃, Si-CH₃), 0.11 (d, J = 1.3 Hz, 6H, CH₃, Si-CH₃) ppm. ¹³C NMR (151 MHz, Methanol- d_4) δ 159.8 (C), 154.6 (CH), 148.4 (C), 132.7 (CH), 126.3 (CH), 126.0 (CH), 122.1 (CH), 115.0 (C), 78.0 (CH), 76.4 (CH), 55.5 (CH), 44.4 (CH), 44.1 (CH₂), 30.0 (CH₂), 25.1 (3 x CH₃), 17.6 (C), 17.6 (C), 25.0 (3 x CH₃), -5.3 (CH₃), -5.4 (CH₃), -5.6 (CH₃), -5.8 (CH₃) ppm. HRMS (ESI+) calculated for C₂₆H₄₇N₄O₂Si₂ 503.3232 found 503.3250; Method A t_R = 2.80 min; Purity (AUC) \geq 95%.

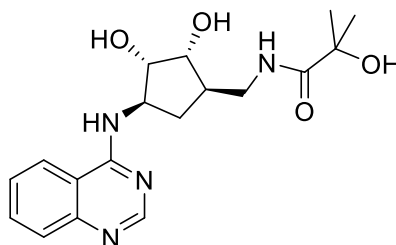
***N*-(((1*R*,2*R*,3*S*,4*R*)-2,3-bis((*tert*-butyldimethylsilyl)oxy)-4-(quinazolin-4-ylamino)cyclopentyl)methyl)-2-hydroxy-2-methylpropanamide (297a)**



1 M *N,N*-Dicyclohexylcarbodiimide in CH₂Cl₂ (0.15 mL, 0.15 mmol) was added dropwise at 0 °C to a stirred solution of *N*-[(1*R*,2*S*,3*R*,4*R*)-4-(aminomethyl)-2,3-bis[[*tert*-butyl(dimethyl)silyl]oxy]cyclopentyl]quinazolin-4-amine (67 mg, 0.13 mmol), 2-hydroxyisobutyric acid (15 mg, 0.15 mmol) and *N*-hydroxysuccinimide (17 mg, 0.15 mmol) in THF (0.7 mL). The solution was allowed to warm to rt and stirred for 2.5 h. The reaction mixture was concentrated and purified by column chromatography (biotage SNAP KP-Sil 10 g, eluted with 0-100% EtOAc in cyclohexane, 1 CV, gradient over 20 CV, 5 CV) to afford the title compound (63 mg, 80%, 0.1070 mmol) as a clear oil. IR (thin film) ν = 3324, 2929, 2856, 1620, 1583, 1532 cm⁻¹. ¹H NMR (600 MHz, Chloroform-*d*) δ 8.66 (s, 1H, ArH, H₂), 7.93

(dd, $J = 8.3, 1.4$ Hz, 1H, ArH, H₈), 7.86 (dd, $J = 8.4, 1.2$ Hz, 1H, ArH, H₅), 7.75 (ddd, $J = 8.3, 6.9, 1.3$ Hz, 1H, ArH, H₆), 7.50 (ddd, $J = 8.3, 6.9, 1.2$ Hz, 1H, ArH, H₇), 7.05 (dd, $J = 7.8, 4.8$ Hz, 1H, NH), 6.19 (d, $J = 6.2$ Hz, 1H, NH), 4.52 (dtd, $J = 8.8, 6.0, 5.2, 3.0$ Hz, 1H, CH, H_{1'}), 4.21 (t, $J = 4.0$ Hz, 1H, CH, H_{2'}), 3.85 (dd, $J = 5.7, 3.7$ Hz, 1H, CH, H_{3'}), 3.44 (dddd, $J = 99.6, 11.1, 8.0, 6.4$ Hz, 2H, CH₂, H_{6'}), 2.63 (app dt, $J = 14.4, 9.3$ Hz, 1H, CH₂, H_{5'}), 2.33 (ddt, $J = 15.7, 9.8, 5.9$ Hz, 1H, CH, H_{4'}), 1.52 (s, 3H, CH₃, gem), 1.49 (s, 3H, CH₃, gem), 1.18 – 1.05 (m, 1H, CH₂, H_{5'}), 0.92 (s, 18H, CH₃), 0.20 (s, 3H, CH₃), 0.12 (s, 3H, CH₃), 0.09 (s, 3H, CH₃), 0.07 (s, 3H, CH₃) ppm. ¹³C NMR (151 MHz, Chloroform-*d*) δ 177.0 (C), 159.3 (C), 155.3 (CH), 149.3 (C), 132.5 (CH), 128.3 (CH), 126.0 (CH), 121.1 (CH), 115.0 (C), 78.1 (CH), 77.0 (CH) 73.9 (C), 56.0 (CH), 43.2 (CH), 42.3 (CH₂), 33.9 (2 x C), 30.8 (CH₂), 28.3 (CH₃), 28.1 (CH₃), 26.0 (3 x CH₃), 26.0 (3 x CH₃), -4.1 (CH₃), -4.2 (CH₃), -4.5 (CH₃), -4.7 (CH₃) ppm. HRMS (ESI+) calculated for C₃₀H₅₂N₄NaO₄Si₂ 611.3419; Method A $t_R = 3.10$ min; Purity (AUC) $\geq 95\%$.

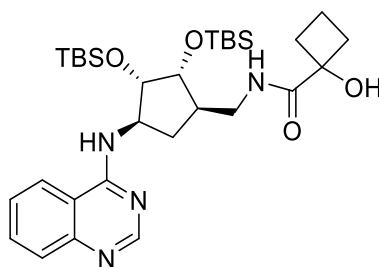
***N*-(((1*R*,2*R*,3*S*,4*R*)-2,3-Dihydroxy-4-(quinazolin-4-ylamino)cyclopentyl)methyl)-2-hydroxy-2-methylpropanamide (297)**



1 M TBAF in THF (0.3 mL, 0.28 mmol) was added dropwise to a solution of *N*-[[[(1*R*,2*R*,3*S*,4*R*)-2,3-bis[[*tert*-butyl(dimethyl)silyl]oxy]-4-(quinazolin-4-ylamino)cyclopentyl]methyl]-2-hydroxy-2-methyl-propanamide (42 mg, 0.07 mmol) in MeOH (0.4 mL). The solution was stirred for 36 h at 60 °C. The reaction mixture was concentrated and purified by column chromatography (biotage SNAP-Ultra C18 12 g, eluted with 0-40% MeOH in water, 4 CV gradient over 15 CV, 2 CV). The crude product was passed through an acidic ion exchange cartridge (SCX, 2 g) with MeOH, followed by 2 M NH₃/MeOH to afford the title product (15 mg, 58%, 0.04 mmol) as an oil. $[\alpha]^{20}_D +117.7^\circ$ ($c=0.5$, MeOH). IR (thin film) $\nu = 3333, 2949, 2836, 1647$ cm⁻¹. ¹H NMR (600 MHz, Methanol-*d*₄) δ 8.55 (s, 1H, ArH, H₂), 8.31 (d, $J = 8.3$ Hz, 1H, ArH, H₅), 7.88 (dd, $J = 7.6$ Hz, 1H,

ArH, H₇), 7.74 (d, *J* = 8.3 Hz, 1H, ArH, H₈), 7.63 (dd, *J* = 7.7 Hz, 1H, ArH, H₆), 4.74 (td, *J* = 8.7, 6.8 Hz, 1H, CH, H_{1'}), 4.12 (t, *J* = 6.2 Hz, 1H, CH, H_{2'}), 3.89 (t, *J* = 5.4 Hz, 1H, CH, H_{3'}), 3.36 (dd, *J* = 7.5, 5.3 Hz, 2H, CH₂, H_{6'}), 2.45 (app dt, *J* = 13.5, 8.3 Hz, 1H, CH₂, H_{5'}), 2.27 (td, *J* = 8.2, 5.6 Hz, 1H, CH, H_{4'}), 1.39 – 1.35 (m, 7H, CH₃, CH₂, gem dimethyl, H_{5'}) ppm. ¹³C NMR (151 MHz, Methanol-*d*₄) δ 178.6 (C), 160.7 (C), 153.3 (CH), 145.1 (C), 133.8 (CH), 126.8 (CH), 124.1 (CH), 122.7 (CH), 114.5 (C), 76.4 (CH), 73.9 (CH), 72.4 (C), 56.9 (CH), 43.2 (CH), 41.8 (CH₂), 30.2 (CH₂), 26.5 (CH₃) 26.5 (CH₃) ppm. HRMS (ESI+) calculated for C₁₈H₂₅N₄O₄ 361.1870, found 361.1867; Method A t_R = 0.68 min; Purity (AUC) ≥ 95%.

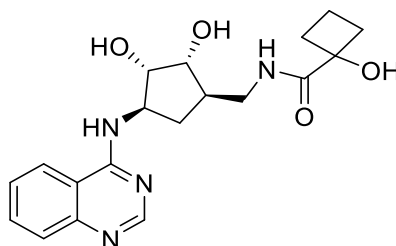
***N*-(((1*R*,2*R*,3*S*,4*R*)-2,3-Bis((*tert*-butyldimethylsilyl)oxy)-4-(quinazolin-4-ylamino)cyclopentyl)methyl)-1-hydroxycyclobutane-1-carboxamide (298a)**



N,N'-Dicyclohexylcarbodiimide (32 mg, 0.15 mmol) was added to a solution of *N*-[(1*R*,2*S*,3*R*,4*R*)-4-(aminomethyl)-2,3-bis[[*tert*-butyl(dimethyl)silyl]oxy]cyclopentyl]quinazolin-4-amine (70 mg, 0.14 mmol), 1-hydroxycyclobutane-1-carboxylic acid (18 mg, 0.15 mmol) and *N*-hydroxysuccinimide (18 mg, 0.15 mmol) in THF (0.7 mL) at 0 °C. The solution was allowed to warm to rt and stirred for 2.5 h. The reaction mixture was concentrated and purified by column chromatography (biotage SNAP KP-Sil 10 g, eluted with 50-100% EtOAc in cyclohexane), 1 CV, gradient over 18 CV, 5 CV) to afford the title compound (25 mg, 30%, 0.04 mmol) as an oil. IR (thin film) ν = 3322, 2929, 2855, 1647, 1620, 1582, 1530 cm⁻¹. ¹H NMR (500 MHz, Chloroform-*d*) δ 8.62 (s, 1H, ArH, H₂), 7.95 (dd, *J* = 8.3, 1.3 Hz, 1H, ArH, H₅), 7.82 (dd, *J* = 8.4, 1.2 Hz, 1H, ArH, H₈), 7.72 (ddd, *J* = 8.3, 6.9, 1.3 Hz, 1H, ArH, H₇), 7.47 (ddd, *J* = 8.3, 7.0, 1.2 Hz, 1H, ArH, H₆), 6.95 (dd, *J* = 7.6, 4.9 Hz, 1H,

NH), 6.27 (d, $J = 6.4$ Hz, 1H, NH), 4.52 (ddt, $J = 8.8, 6.3, 4.3$ Hz, 1H, H_{1'}), 4.18 (t, $J = 4.0$ Hz, 1H, H_{2'}), 3.83 (dd, $J = 5.5, 3.8$ Hz, 1H, H_{3'}), 3.54 – 3.27 (m, 2H, CH₂, H_{6'}), 2.75-2.53 (m, 2H, CH₂, cyclobutane), 2.29 (tq, $J = 10.6, 5.7$ Hz, 1H, H_{4'}), 2.23 – 2.11 (m, 2H, CH₂, cyclobutane), 1.92 (m, 3H, CH₂, CH₂, cyclobutane, H_{5'}), 1.14-1.08 (m, 1H, H_{5'}), 0.89 (s, 18H, CH₃), 0.16 (s, 3H, CH₃), 0.09 (s, 3H, CH₃), 0.05 (s, 3H, CH₃), 0.04 (s, 3H, CH₃) ppm. ¹³C NMR (151 MHz, Chloroform-*d*) δ 176.0 (C), 159.3 (C), 155.3 (CH), 149.4 (C), 132.5 (CH), 128.2 (CH), 125.9 (CH), 121.2 (CH), 115.1 (C), 78.3 (CH), 77.0 (CH), 75.8 (C), 55.9 (CH), 43.1 (CH), 42.0 (CH₂), 35.9 (CH₂), 35.7 (CH₂), 34.0 (CH₂), 25.9 (6 x CH₃), 18.1 (C), 18.1 (C), 13.3 (CH₂), -4.1 (CH₃), -4.2 (CH₃), -4.51 (CH₃), -4.7 (CH₃) ppm. HRMS (ESI+) calculated for C₃₁H₅₂N₄NaO₄Si₂ 623.3419 found 623.3410; Method A $t_R = 3.11$ min; Purity (AUC) $\geq 95\%$.

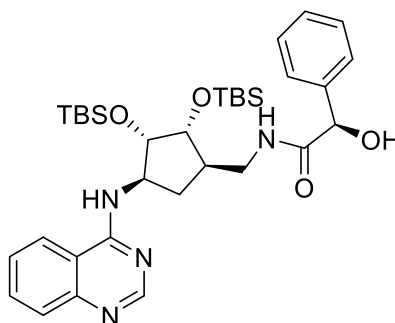
***N*-(((1*R*,2*R*,3*S*,4*R*)-2,3-Dihydroxy-4-(quinazolin-4-ylamino)cyclopentyl)methyl)-1-hydroxycyclobutane-1-carboxamide (298)**



HCl (36% w/v in water, 0.1 mL, 0.34 mmol) was added to *N*-[[[(1*R*,2*R*,3*S*,4*R*)-2,3-bis[[*tert*-butyl(dimethyl)silyl]oxy]-4-(quinazolin-4-ylamino)cyclopentyl]methyl]-1-hydroxy-cyclobutanecarboxamide (68 mg, 0.11 mmol) in EtOH (2.3 mL) and the reaction was stirred at rt for 2 h. The reaction mixture was concentrated and purified by column chromatography (biotage SNAP-Ultra C18 12 g, eluted with 0-50% MeOH in water, 1 CV, gradient over 12 CV, 6 CV) to afford the title compound (38 mg, 89%, 0.10 mmol) as an oil. $[\alpha]_D^{20} -18.0^\circ$ ($c=0.5$, MeOH). IR (thin film) $\nu = 3330, 1639$ cm⁻¹. ¹H NMR (600 MHz, Methanol-*d*₄) δ 8.54 (s, 1H, ArH, H₂), 8.32, 8.31 (d, $J = 8.4$ Hz, 1H, ArH, H₅), 7.94 (t, $J = 6.0$ Hz, 1H, NH), 7.87 (dd, $J = 7.7$ Hz, 1H, ArH, H₇), 7.73 (d, $J = 8.3$ Hz, 1H, ArH, H₈), 7.62 (dd, $J = 8.0$ Hz, 1H, ArH, H₆), 4.73 (td, $J = 8.7, 6.7$ Hz, 1H, CH, H_{1'}), 4.12 (dd, $J = 6.2$ Hz, 1H, CH, H_{2'}), 3.90 (dd, $J = 5.4$ Hz, 1H, CH, H_{3'}), 3.38 (dp, $J = 13.0, 6.2$ Hz, 2H, CH₂, H_{6'}), 2.60 – 2.50 (m, 2H, CH₂,

cyclobutane), 2.44 (app dt, $J = 13.4, 8.2$ Hz, 1H, CH₂, H_{5'}), 2.34 – 2.22 (m, 1H, CH, H_{4'}), 2.15 (ddd, $J = 12.8, 9.9, 8.0$ Hz, 2H, CH₂, cyclobutane), 1.92 (pd, $J = 7.1, 5.8, 2.4$ Hz, 3H, CH₂, cyclobutane), 1.39 (app dt, $J = 13.4, 9.1$ Hz, 1H, CH₂, H_{5'}) ppm. ¹³C NMR (151 MHz, Methanol-*d*₄) δ 177.2 (C), 160.6 (C), 153.3 (CH), 145.2 (C), 133.8 (CH), 126.8 (CH), 124.2 (CH), 122.7 (CH), 114.5 (C), 76.5 (CH), 75.0 (C), 73.9 (CH), 56.9 (CH), 43.2 (CH), 41.7 (CH₂), 34.4 (CH₂), 34.4 (CH₂), 30.2 (CH₂), 12.7 (CH₂) ppm. HRMS (ESI+) calculated for C₁₉H₂₅N₄O₄ 373.187, found 373.1876; Method A $t_R = 1.27$ min; Purity (AUC) $\geq 95\%$.

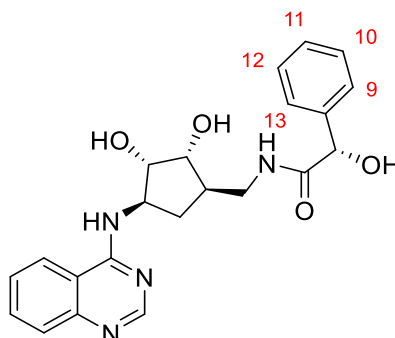
(*R*)-*N*-(((1*R*,2*R*,3*S*,4*R*)-2,3-Bis((*tert*-butyldimethylsilyl)oxy)-4-(quinazolin-4-ylamino)cyclopentyl)methyl)-2-hydroxy-2-phenylacetamide (299a)



1 M *N,N*-Dicyclohexylcarbodiimide in CH₂Cl₂ (0.1 mL, 0.1 mmol) was added dropwise at 0 °C to a stirred solution of *N*-[(1*R*,2*S*,3*R*,4*R*)-4-(aminomethyl)-2,3-bis[[*tert*-butyl(dimethyl)silyl]oxy]cyclopentyl]quinazolin-4-amine (61 mg, 0.12 mmol), (2*R*)-2-hydroxy-2-phenyl-acetic acid (20 mg, 0.13 mmol) and *N*-hydroxysuccinimide (15 mg, 0.13 mmol) in THF (0.6 mL). The solution was warmed to rt and stirred for 2.5 h. The reaction mixture was concentrated and purified by column chromatography (biotage SNAP KP-Sil 10 g, eluted with 0-100% EtOAc in cyclohexane, 1 CV, gradient over 20 CV, 5 CV) to yield the title compound (68 mg, 89%, 0.10 mmol) as an oil. IR (thin film) $\nu = 3323, 2927, 2850, 1655, 1623, 1577, 1531$ cm⁻¹. ¹H NMR (600 MHz, Chloroform-*d*) δ 8.61 (s, 1H, ArH, H₂), 7.83 (dd, $J = 8.4, 1.2$ Hz, 1H, ArH, H₅), 7.81 (dd, $J = 8.4, 1.3$ Hz, 1H, ArH, H₈), 7.74 (ddd, $J = 8.3, 6.9, 1.3$ Hz, 1H, ArH, H₇), 7.48 (ddd, $J = 8.2, 6.9, 1.3$ Hz, 1H, ArH, H₆), 7.45 – 7.40 (m, 2H, ArH, H₉, H₁₃), 7.36 – 7.29 (m, 3H, ArH, H₁₀, H₁₁, H₁₂), 6.69 (t, $J = 6.3$ Hz, 1H, NH), 5.96 (d, $J = 6.1$ Hz, 1H, NH),

5.14 (s, 1H, CH, *CHOH*), 4.43 (ddd, $J = 8.8, 6.1, 4.3$ Hz, 1H, CH, H_1'), 4.17 (dd, $J = 3.9$ Hz, 1H, CH, H_2'), 3.80 (dd, $J = 6.1, 3.7$ Hz, 1H, CH, H_3'), 3.56 – 3.36 (m, 2H, CH_2 , H_6'), 2.56 (dt, $J = 14.3, 9.3$ Hz, 1H, CH_2 , H_5'), 2.33 (tq, $J = 9.6, 6.1$ Hz, 1H, CH, H_4'), 1.30 – 1.21 (m, 1H, CH_2 , H_5'), 0.91 (s, 18H, CH_3), 0.20 (s, 3H, CH_3), 0.11 (s, 3H, CH_3), 0.04 (s, 6H, CH_3) ppm. ^{13}C NMR (151 MHz, Chloroform-*d*) δ 172.8 (C), 159.1 (C), 155.3 (CH), 149.4 (C), 139.4 (C), 132.5 (CH), 128.9 (2 x CH), 128.8 (CH), 128.4 (CH), 126.7 (2 x CH), 126.0 (CH), 120.9 (CH), 115.0 (C), 77.9 (CH), 76.9 (CH), 74.5 (CH), 55.9 (CH), 42.9 (CH), 42.4 (CH_2), 30.8 (CH_2), 26.0 (6 x CH_3), 18.1 (C), 18.1 (C), -4.1 (CH_3), -4.2 (CH_3), -4.6 (CH_3), -4.7 (CH_3) ppm. HRMS (ESI+) calculated for $C_{34}H_{53}N_4O_4Si_2$ 638.3624, found 638.3635; Method A $t_R = 3.14$ min; Purity (AUC) $\geq 95\%$.

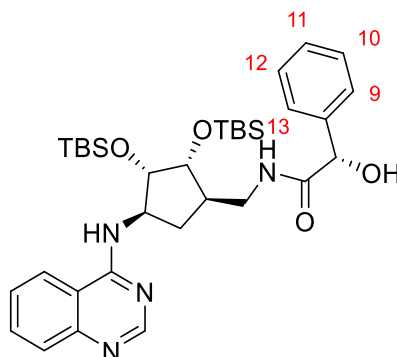
(*R*)-*N*-(((1*R*,2*R*,3*S*,4*R*)-2,3-Dihydroxy-4-(quinazolin-4-ylamino)cyclopentyl)methyl)-2-hydroxy-2-phenylacetamide (299)



1 M TBAF in THF (0.6 mL, 0.6 mmol) was added dropwise to a solution of (2*S*)-*N*-[[[(1*R*,2*R*,3*S*,4*R*)-2,3-bis[[*tert*-butyl(dimethyl)silyl]oxy]-4-(quinazolin-4-ylamino)cyclopentyl]methyl]-2-hydroxy-2-phenyl-acetamide (40 mg, 0.06 mmol) in THF (0.4 mL). The solution was stirred for 7 h at 50 °C. The reaction mixture was cooled, water (15 mL) was added and washed with EtOAc (3 x 15 mL). The water layer was concentrated. CH_2Cl_2 / MeOH (50mL) was added and the remaining solid was filtered. The filtrate was purified by column chromatography (biotage SNAP KP-Sil 10 g, eluting with 0-15% NH_3 /MeOH in CH_2Cl_2 , 1 CV, gradient over 10 CV, 5 CV). The product was dissolved in MeOH and passed through SCX (2 g) washed with MeOH followed by NH_3 in MeOH to afford the title compound (10.1 mg, 40%, 0.0247 mmol). $[\alpha]^{20}_D -9.70^\circ$ ($c=0.5$, MeOH). 1H NMR (600 MHz, Methanol-*d*₄) δ 8.47 (s, 1H, ArH, H_2), 8.21 (dd, $J =$

8.4, 1.4 Hz, 1H, ArH, H₅), 7.81 (ddd, $J = 8.3, 6.9, 1.3$ Hz, 1H, ArH, H₇), 7.73 (dd, $J = 8.4, 1.2$ Hz, 1H, ArH, H₈), 7.55 (ddd, $J = 8.3, 6.9, 1.3$ Hz, 1H, ArH, H₆), 7.50 – 7.46 (m, 2H, ArH, H₉, H₁₃), 7.33 (dd, $J = 8.4, 6.8$ Hz, 2H, ArH, H₁₀, H₁₂), 7.29 – 7.24 (m, 1H, ArH, H₁₁), 5.05 (s, 1H, CH, *CHOH*), 4.59 (td, $J = 8.6, 6.3$ Hz, 1H, CH, H_{1'}), 4.06 (t, $J = 6.0$ Hz, 1H, CH, H_{2'}), 3.88 (t, $J = 5.5$ Hz, 1H, CH, H_{3'}), 3.40 (dd, $J = 7.4, 3.5$ Hz, 2H, CH₂, H_{6'}), 2.41 (app dt, $J = 13.3, 8.2$ Hz, 1H, CH₂, H_{5'}), 2.28 (pd, $J = 7.8, 5.5$ Hz, 1H, CH, H_{4'}), 1.32 (app dt, $J = 13.3, 9.0$ Hz, 1H, CH₂, H_{5'}) ppm. ¹³C NMR (151 MHz, Methanol-*d*₄) δ 174.4 (C), 160.3 (C), 154.4 (CH), 148.2 (C), 140.4 (C), 132.9 (CH), 128.0 (2 x CH), 127.7 (CH), 126.6 (2 x CH), 126.3 (CH), 126.1 (CH), 122.3 (CH), 115.0 (C), 76.7 (CH), 74.2 (CH), 74.1 (CH), 56.7 (CH), 43.2 (CH), 41.7 (CH₂), 30.4 (CH₂) ppm. HRMS (ESI+) calculated for C₂₂H₂₅N₄O₄ 409.187 found 409.1875; Method A $t_R = 1.52$ min; Purity (AUC) $\geq 95\%$.

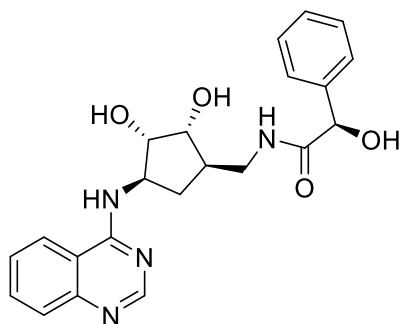
(S)-N-(((1R,2R,3S,4R)-2,3-Bis((*tert*-butyldimethylsilyl)oxy)-4-(quinazolin-4-ylamino)cyclopentyl)methyl)-2-hydroxy-2-phenylacetamide (300a)



1 M *N,N'*-dicyclohexylcarbodiimide in CH₂Cl₂ (0.05 mL, 0.05 mmol) was added dropwise at 0 °C to a stirred solution of *N*-[(1*R*,2*S*,3*R*,4*R*)-4-(aminomethyl)-2,3-bis[[*tert*-butyl(dimethyl)silyl]oxy]cyclopentyl]quinazolin-4-amine (25 mg, 0.05 mmol), (*S*)-(+)-mandelic acid (8 mg, 0.06 mmol) and *N*-hydroxysuccinimide (6 mg, 0.06 mmol) in THF (0.25 mL). The solution was warmed to rt and stirred for 2.5 h. The reaction mixture was concentrated and purified by column chromatography (biotage SNAP KP-Sil 10 g, eluted with 0-100% EtOAc in Cyclohexane, 1 CV, gradient over 20 CV, 5 CV). to yield the title compound (26 mg, 82%, 0.04 mmol) as a clear oil. IR (thin film) $\nu = 3322, 2927, 2850, 1622,$

1576, 1532 cm^{-1} . ^1H NMR (500 MHz, Chloroform-*d*) δ 8.56 (s, 1H, ArH, H₂), 7.84 (dd, $J = 8.5, 1.3$ Hz, 1H, ArH, H₅), 7.79 (dd, $J = 8.3, 1.2$ Hz, 1H, ArH, H₈), 7.71 (ddd, $J = 8.3, 6.9, 1.3$ Hz, 1H, ArH, H₇), 7.45 (app ddd, $J = 8.3, 2.8, 1.5$ Hz, 3H, ArH, H₆, H₉, H₁₃), 7.40 – 7.33 (m, 3H, ArH, H₁₀, H₁₁, H₁₂), 6.75 (dd, $J = 7.9, 4.7$ Hz, 1H, NH), 6.14 (d, $J = 6.3$ Hz, 1H, NH), 5.14 (s, 1H, CH, *CHOH*), 4.47 (ddt, $J = 9.0, 6.3, 4.5$ Hz, 1H, CH, H_{1'}), 4.16 (dd, $J = 4.0$ Hz, 1H, CH, H_{2'}), 3.79 (dd, $J = 5.7, 3.7$ Hz, 1H, CH, H_{3'}), 3.52 (ddd, $J = 13.6, 9.6, 7.9$ Hz, 1H, CH₂, H_{6'}), 3.35 (ddd, $J = 13.5, 6.3, 4.7$ Hz, 1H, CH₂, H_{6'}), 2.53 (dd, $J = 14.3, 9.3$ Hz, 1H, CH₂, H_{5'}), 2.27 (dddd, $J = 9.6, 6.1$ Hz, 1H, H_{4'}), 1.32 – 1.21 (m, 1H, CH₂, H_{5'}), 0.91 (s, 9H, CH₃), 0.89 (s, 9H, CH₃), 0.17 (s, 3H, CH₃), 0.08 (s, 3H, CH₃), 0.05 (s, 3H, CH₃), 0.03 (s, 3H, CH₃) ppm. ^{13}C NMR (126 MHz, Chloroform-*d*) δ 173.1 (C), 159.3 (C), 155.2 (CH), 149.1 (C), 139.5 (C), 132.5 (CH), 128.8 (2 x CH), 128.6 (CH), 128.1 (CH), 126.7 (2 x CH), 126.1 (CH), 121.0 (C), 115.0 (CH), 78.0 (CH), 77.0 (CH), 74.1 (CH), 56.0 (CH), 43.0 (CH), 42.6 (CH₂), 30.8 (CH₂), 25.9 (3 x CH₃), 25.9 (3 x CH₃), 18.1 (2 x C), -4.2 (CH₃), -4.2 (CH₃), -4.6 (CH₃), -4.7 (CH₃) ppm. HRMS (ESI+) calculated for C₃₄H₅₃N₄O₄Si₂ 638.3624, found 638.3634; Method A $t_{\text{R}} = 3.16$ min; Purity (AUC) $\geq 95\%$.

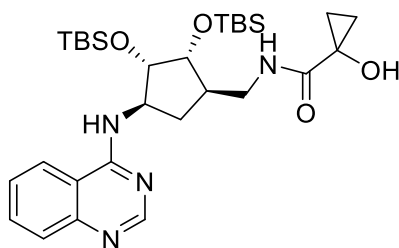
(S)-N-(((1*R*,2*R*,3*S*,4*R*)-2,3-Dihydroxy-4-(quinazolin-4-ylamino)cyclopentyl)methyl)-2-hydroxy-2-phenylacetamide (300)



1 M TBAF in THF (0.7 mL, 0.7 mmol) was added dropwise to a solution of (2*R*)-*N*-[[[(1*R*,2*R*,3*S*,4*R*)-2,3-bis[[*tert*-butyl(dimethyl)silyl]oxy]-4-(quinazolin-4-ylamino)cyclopentyl]methyl]-2-hydroxy-2-phenyl-acetamide (48.0 mg, 0.07 mmol) in THF (0.4 mL). The solution was stirred for 8 h at 50 °C. The reaction mixture was cooled. Water (15 mL) was added and washed with EtOAc (3 x 15

mL). The water layer was concentrated, dissolved in CH₂Cl₂/MeOH and purified by column chromatography (dry loaded onto biotage SNAP KP-Sil 10 g, eluted with 0-10% 10% NH₃ in MeOH in CH₂Cl₂, 1 CV, gradient over 10 CV, 5 CV). The product was further purified by acidic ion exchange chromatography (SCX, 2 g), washed with MeOH and eluted with 2 M NH₃ in MeOH to afford the title compound (12 mg, 39%, 0.029 mmol) as an oil. $[\alpha]^{20}_{\text{D}} -117.7^{\circ}$ (c=0.5, MeOH). ¹H NMR (600 MHz, Methanol-*d*₄) δ 8.47 (s, 1H, ArH, H₂), 8.27 – 8.19 (m, 1H, ArH, H₅), 7.81 (ddd, *J* = 8.4, 7.0, 1.4 Hz, 1H, ArH, H₇), 7.73 (d, *J* = 8.4 Hz, 1H, ArH, H₈), 7.55 (ddd, *J* = 8.3, 6.9, 1.3 Hz, 1H, ArH, H₆), 7.48 (d, *J* = 7.4 Hz, 2H, ArH, H₉, H₁₃), 7.33 (dd, *J* = 8.3, 6.8 Hz, 2H, ArH, H₁₀, H₁₂), 7.28 (td, *J* = 7.1, 6.6, 1.5 Hz, 1H, ArH H₉, H₁₁), 5.05 (s, 1H, CH, *CHOH*), 4.61 (td, *J* = 8.6, 6.5 Hz, 1H, CH, H_{1'}), 4.07 (t, *J* = 6.0 Hz, 1H, CH, H_{2'}), 3.87 (t, *J* = 5.5 Hz, 1H, CH, H_{3'}), 3.39 (d, *J* = 7.4 Hz, 2H, CH₂, H_{6'}), 2.45 (app dt, *J* = 13.4, 8.3 Hz, 1H, CH₂, H_{5'}), 2.34 – 2.24 (m, 1H, CH, H_{4'}), 1.38 – 1.30 (m, 1H, CH₂, H_{5'}) ppm. ¹³C NMR (151 MHz, Methanol-*d*₄) δ 174.4 (C), 160.3 (C), 154.4 (CH), 148.3 (C), 140.4 (C), 132.9 (CH), 128.0 (2 x CH), 127.7 (CH), 126.6 (2 x CH), 126.3 (CH), 126.1 (CH), 122.3 (CH), 115.0 (C), 76.7 (CH), 74.2 (CH), 74.1 (CH), 56.6 (CH), 43.1 (CH), 41.8 (CH₂), 30.5 (CH₂) ppm. HRMS (ESI+) calculated for C₂₂H₂₅N₄O₄ 409.1870 found 409.1870; Method A *t*_R = 1.64 min; Purity (AUC) ≥ 95%.

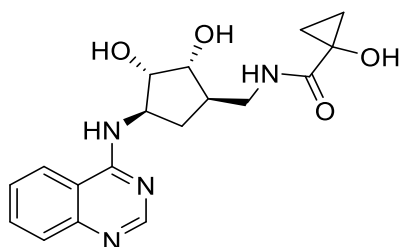
***N*-(((1*R*,2*R*,3*S*,4*R*)-2,3-Bis((*tert*-butyldimethylsilyl)oxy)-4-(quinazolin-4-ylamino)cyclopentyl)methyl)-1-hydroxycyclopropane-1-carboxamide (301a)**



N,N-Dicyclohexylcarbodiimide (29 mg, 0.14 mmol) was added at 0 °C to a stirred solution of *N*-[(1*R*,2*S*,3*R*,4*R*)-4-(aminomethyl)-2,3-bis[[*tert*-butyl(dimethyl)silyl]oxy]cyclopentyl]quinazolin-4-amine (65 mg, 0.13 mmol), 1-hydroxy-1-cyclopropanecarboxylic acid (15 mg, 0.14 mmol) and *N*-hydroxysuccinimide (16.4 mg, 0.14 mmol) in THF (0.7 mL). The solution was

allowed to warm to rt and stirred for 2.5 h. The reaction mixture was concentrated, and purified by column chromatography (biotage SNAP KP-Sil 10 g, eluted with 0-100% EtOAc in cyclohexane, 1 CV, gradient over 20 CV, 5 CV) to yield the title compound (43 mg, 56%, 0.07 mmol) as a clear oil. IR (thin film) $\nu = 3425, 3322, 2929, 2854, 1650, 1621, 1582, 1529 \text{ cm}^{-1}$. ^1H NMR (600 MHz, Chloroform-*d*) δ 8.60 (s, 1H, ArH, H₂), 7.85 (dd, $J = 8.3, 1.3 \text{ Hz}$, 1H, ArH, H₅), 7.80 (dd, $J = 8.4, 1.2 \text{ Hz}$, 1H, ArH, H₈), 7.71 (ddd, $J = 8.3, 6.9, 1.3 \text{ Hz}$, 1H, ArH, H₇), 7.44 (ddd, $J = 8.2, 6.9, 1.3 \text{ Hz}$, 1H, ArH, H₆), 7.18 (dd, $J = 7.6, 5.0 \text{ Hz}$, 1H, NH), 6.19 (d, $J = 6.3 \text{ Hz}$, 1H, NH), 4.49 (ddt, $J = 9.1, 6.1, 4.5 \text{ Hz}$, 1H, CH, H_{1'}), 4.16 (t, $J = 4.1 \text{ Hz}$, 1H, CH, H_{2'}), 3.83 (dd, $J = 5.5, 3.7 \text{ Hz}$, 1H, CH, H_{3'}), 3.57 – 3.33 (m, 2H, CH₂, H_{6'}), 2.58 (app dt, $J = 14.3, 9.4 \text{ Hz}$, 1H, CH₂, H_{5'}), 2.30 (ddt, $J = 15.5, 9.6, 5.7 \text{ Hz}$, 1H, CH, H_{4'}), 1.45 – 1.21 (m, 3H, CH₂, H_{5'}, cyclopropane), 1.13 – 1.03 (m, 1H, CH₂, cyclopropane), 0.89 (s, 18H, CH₃), 0.16 (s, 3H, CH₃), 0.09 (s, 3H, CH₃), 0.06 (s, 3H, CH₃), 0.04 (s, 3H, CH₃) ppm. ^{13}C NMR (151 MHz, Chloroform-*d*) δ 174.8 (C), 159.3 (C), 155.2 (CH), 149.1 (C), 132.5 (CH), 128.1 (CH), 126.0 (CH), 121.1 (CH), 115.0 (C), 78.1 (CH), 76.9 (CH), 56.1 (C), 56.0 (CH), 43.2 (CH), 42.6 (CH₂), 30.9 (CH₂), 26.0 (6 x CH₃), 18.1 (2 x C), 17.0 (2 x CH₂ cyclopropane), -4.1 (CH₃), -4.2 (CH₃), -4.5 (CH₃), -4.7 (CH₃) ppm. HRMS (ESI+) calculated for C₃₀H₅₁N₄O₄ Si₂ 588.3467 found 588.3466; Method A $t_{\text{R}} = 3.10 \text{ min}$; Purity (AUC) $\geq 95\%$.

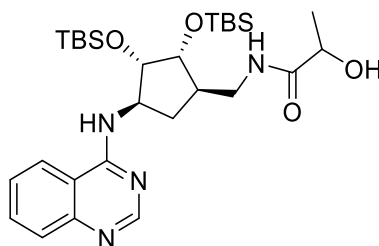
***N*-(((1*R*,2*R*,3*S*,4*R*)-2,3-Dihydroxy-4-(quinazolin-4-ylamino)cyclopentyl)methyl)-1-hydroxycyclopropane-1-carboxamide (301)**



Conc aq. HCl (0.10 mL, 0.29 mmol) was added to *N*-[[[(1*R*,2*R*,3*S*,4*R*)-2,3-bis[[*tert*-butyl(dimethyl)silyl]oxy]-4-(quinazolin-4-ylamino)cyclopentyl]methyl]-1-hydroxy-cyclopropanecarboxamide (57 mg, 0.09 mmol) in EtOH (1.9 mL) and the reaction was stirred at rt for 2 h. The reaction mixture was concentrated and

purified by column chromatography (biotage SNAP-Ultra C18 12 g, eluted with 0-50% MeOH in water, 2 CV gradient over 15 CV, 2 CV) to afford the title compound (32 mg, 91%, 0.08 mmol) as a clear oil. $[\alpha]^{20}_{\text{D}} -8.31^{\circ}$ ($c=0.5$, MeOH). IR (thin film) $\nu = 3335, 2963, 1618, 1586, 1536 \text{ cm}^{-1}$. $^1\text{H NMR}$ (600 MHz, Methanol- d_4) δ 8.58 (s, 1H, ArH, H₂), 8.33 (dd, $J = 8.4, 1.3 \text{ Hz}$, 1H, ArH, H₅), 7.90 (ddd, $J = 8.4, 7.1, 1.4 \text{ Hz}$, 1H, ArH, H₇), 7.75 (d, $J = 8.4 \text{ Hz}$, 1H, ArH, H₈), 7.65 (ddd, $J = 8.4, 7.2, 1.4 \text{ Hz}$, 1H, ArH, H₆), 4.78 (td, $J = 8.8, 6.8 \text{ Hz}$, 1H, CH, H_{1'}), 4.17 – 4.09 (m, 1H, CH, H_{2'}), 3.92 (t, $J = 5.4 \text{ Hz}$, 1H, CH, H_{3'}), 3.44 – 3.35 (m, 2H, CH₂, H_{6'}), 2.47 (app dt, $J = 13.3, 8.3 \text{ Hz}$, 1H, CH₂, H_{5'}), 2.29 (td, $J = 8.1, 5.2 \text{ Hz}$, 1H, CH, H_{4'}), 1.40 (app dt, $J = 13.4, 9.1 \text{ Hz}$, 1H, CH₂, H_{5'}), 1.22 (q, $J = 4.2 \text{ Hz}$, 2H, CH₂, cyclopropane), 1.04 – 0.94 (m, 2H, CH₂, cyclopropane) ppm. $^{13}\text{C NMR}$ (151 MHz, Methanol- d_4) δ 176.1 (C), 160.8 (C), 153.0 (CH), 144.3 (C), 134.0 (CH), 127.0 (CH), 123.5 (CH), 122.8 (CH), 114.3 (C), 76.4 (CH), 73.9 (CH), 57.0 (CH), 54.3 (C), 43.3 (CH), 42.2 (CH₂), 30.2 (CH₂), 15.3 (2 x CH₂) ppm. HRMS (ESI+) calculated for $\text{C}_{18}\text{H}_{23}\text{N}_4\text{O}_4$ 359.1719 found 359.1708; Method B $t_{\text{R}} = 0.94 \text{ min}$; Purity (AUC) $\geq 95\%$.

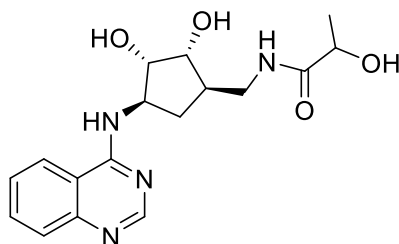
***N*-(((1*R*,2*R*,3*S*,4*R*)-2,3-Bis((*tert*-butyldimethylsilyl)oxy)-4-(quinazolin-4-ylamino)cyclopentyl)methyl)-2-hydroxypropanamide (302a)**



N-Hydroxysuccinimide (23 mg, 0.20 mmol) was added to a stirred solution of *N*-[[*(1R,2S,3R,4R)*-4-(aminomethyl)-2,3-bis[[*tert*-butyl(dimethyl)silyl]oxy]cyclopentyl]quinazolin-4-amine (83 mg, 0.17 mmol), *N,N*-dicyclohexylcarbodiimide (40 mg, 0.20 mmol) and *D/L*-lactic acid (0.01 mL, 0.20 mmol) in THF (0.83 mL). The solution was stirred at rt for 18 h. The reaction mixture was concentrated, dissolved in CH_2Cl_2 (2 mL with 0.1 mL methanol) and purified by column chromatography (biotage SNAP KP-Sil 25 g eluted with 0-100% EtOAc in cyclohexane, 5 CV, gradient over 30 CV, 5 CV). Fractions with

product were combined, concentrated and passed through an acidic ion exchange cartridge (SCX, 2 g) with MeOH, followed by 3.5 M NH₃ in MeOH to afford the title compound (63 mg, 0.11 mmol, 66%) as an oil. IR (thin film) ν = 3321, 2952, 2929, 2857, 1652, 1619, 1583, 1531 cm⁻¹. ¹H NMR (600 MHz, Chloroform-*d*) δ 8.65 (s, 1H, ArH, H₂), 7.86 (m, 2H, ArH, H₅, H₇), 7.78 – 7.71 (m, 1H, ArH, H₈), 7.53 – 7.46 (m, 1H, ArH, H₆), 6.89 – 6.83 (m, 1H, NH), 6.07 (d, *J* = 6.2 Hz, 1H, NH), 4.55 – 4.47 (m, 1H, CH, H_{1'}), 4.32 (q, *J* = 6.9 Hz, 1H, CH, CHOH), 4.21 (dd, *J* = 4.0 Hz, 1H, CH, H_{2'}), 3.89 – 3.82 (m, 1H, CH, H_{3'}), 3.56 (dt, *J* = 13.6, 8.6 Hz, 1H, CH₂, H_{6'}), 3.37 (dt, *J* = 13.4, 5.6 Hz, 1H, CH₂, H_{6'}), 2.64 (app dt, *J* = 14.3, 9.3 Hz, 1H, CH₂, H_{5'}), 2.34 (dt, *J* = 9.7, 4.7, 3.4 Hz, 1H, CH, H_{4'}), 1.51 (d, *J* = 6.9 Hz, 3H, CH₃), 1.34 (ddd, *J* = 14.0, 5.3 Hz, 1H, CH₂, H_{5'}), 0.96 – 0.88 (m, 18H, 6 x CH₃), 0.21 (s, 3H, CH₃), 0.13 (s, 3H, CH₃), 0.09 (s, 3H, CH₃), 0.07 (s, 3H, CH₃) ppm. ¹³C NMR (151 MHz, Chloroform-*d*) δ 174.9 (C), 159.2 (C), 155.2 (CH), 149.3 (C), 132.6 (CH), 128.3 (CH), 126.1 (CH), 120.9 (CH), 115.0 (C), 78.0 (CH), 77.0 (CH), 68.5 (CH), 56.1 (CH), 43.0 (CH), 42.4 (CH₂), 31.0 (CH₂), 25.9 (6 x CH₃), 21.4 (CH₃), 18.1 (C), -4.1 (CH₃), -4.2 (CH₃), -4.5 (CH₃), -4.6 (CH₃) ppm. HRMS (ESI+) calculated for C₂₉H₅₁N₄O₄Si₂ 575.3443 found 575.3436; Method A *t*_R = 3.13 min; Purity (AUC) \geq 95%.

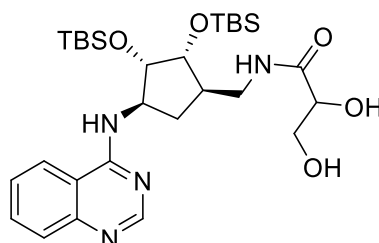
***N*-(((1*R*,2*R*,3*S*,4*R*)-2,3-Dihydroxy-4-(quinazolin-4-ylamino)cyclopentyl)methyl)-2-hydroxypropanamide (302)**



Conc aq. HCl (0.10 mL, 0.26 mmol) was added to *N*-[[[(1*R*,2*R*,3*S*,4*R*)-2,3-bis[[*tert*-butyl(dimethyl)silyl]oxy]-4-(quinazolin-4-ylamino)cyclopentyl]methyl]-2-hydroxy-propanamide (50 mg, 0.09 mmol) in EtOH (2.0 mL) and the reaction was stirred at rt for 2 h. The reaction mixture was concentrated and purified by column chromatography (biotage SNAP-Ultra C18 12 g, eluted with 0-50% MeOH in water, 2 CV, gradient over 15 CV, 2 CV) to afford the title compound

(29 mg, 96%, 0.084 mmol) as an oil. IR (thin film) $\nu = 3285, 2973, 1636, 1617, 1584, 1536 \text{ cm}^{-1}$. $^1\text{H NMR}$ (600 MHz, Methanol- d_4) δ 8.56 (s, 1H, ArH, H₂), 8.31 (dd, $J = 8.4, 1.3 \text{ Hz}$, 1H, ArH, H₅), 7.88 (ddd, $J = 8.4, 7.0, 1.3 \text{ Hz}$, 1H, ArH, H₇), 7.74 (d, $J = 8.3 \text{ Hz}$, 1H, ArH, H₈), 7.64 (ddd, $J = 8.3, 7.0, 1.2 \text{ Hz}$, 1H, ArH, H₆), 4.74 (td, $J = 8.8, 6.8 \text{ Hz}$, 1H, CH, H_{1'}), 4.16 (q, $J = 6.8 \text{ Hz}$, 1H, CH, CHOH), 4.13 – 4.09 (m, 1H, CH, H_{2'}), 3.89 (dd, $J = 5.4 \text{ Hz}$, 1H, CH, H_{3'}), 3.38 (dd, $J = 7.5, 4.2 \text{ Hz}$, 2H, CH₂, H_{6'}), 2.46 (app. dt, $J = 13.3, 8.3 \text{ Hz}$, 1H, CH₂, H_{5'}), 2.27 (pd, $J = 7.8, 5.1 \text{ Hz}$, 1H, CH, H_{4'}), 1.42 – 1.34 (m, 4H, CH₂, CH₃, H_{5'}) ppm. $^{13}\text{C NMR}$ (151 MHz, Methanol- d_4) δ 176.7 (C), 160.7 (C), 153.3 (CH), 145.1 (C), 133.8 (CH), 126.8 (CH), 124.1 (CH), 122.7 (CH), 114.5 (C), 76.4 (CH), 73.9 (CH), 67.7 (CH), 56.9 (CH), 43.2 (CH), 41.6 (CH₂), 30.3 (CH₂), 19.9 (CH₃) ppm. HRMS (ESI+) calculated for C₁₇H₂₃N₄O₄ 347.1714 found 347.1710; Method A $t_R = 0.41 \text{ min}$; Purity >95%

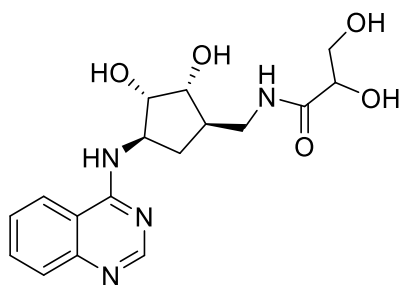
***N*-(((1*R*,2*R*,3*S*,4*R*)-2,3-Bis((*tert*-butyldimethylsilyl)oxy)-4-(quinazolin-4-ylamino)cyclopentyl)methyl)-2,3-dihydroxypropanamide (303a)**



N-Hydroxysuccinimide (21 mg, 0.18 mmol) was added to a stirred solution of *N*-[[*(1R,2S,3R,4R)*]-4-(aminomethyl)-2,3-bis[[*tert*-butyl(dimethyl)silyl]oxy]cyclopentyl]quinazolin-4-amine (76 mg, 0.15 mmol), 1 M *N,N*-dicyclohexylcarbodiimide in CH₂Cl₂ (0.2 mL, 0.18 mmol) and *D/L*-glyceric acid (20% in water, ca. 2 mol/L, 0.08 mL, 0.15 mmol) in THF (0.8 mL). The solution was allowed to warm to rt and stirred for 18 h. The reaction mixture was concentrated and purified by column chromatography (biotage SNAP KP-Sil 25 g, eluted with 1-8% MeOH in CH₂Cl₂, 5 CV, gradient over 18 CV, 5 CV) to afford the title compound (34 mg, 38%, 0.06 mmol) as a clear oil. IR (thin film) $\nu = 3334, 2954, 2930, 2857, 1653, 1619, 1584, 1533 \text{ cm}^{-1}$. $^1\text{H NMR}$ (600 MHz, Chloroform-

d) δ 8.63 (app. d, $J = 2.7$ Hz, 1H, ArH, H₂), 7.88 (dd, $J = 8.6$ Hz, 1H, ArH, H₅), 7.82 (dd, $J = 8.2, 3.2$ Hz, 1H, ArH, H₃), 7.72 (dd, $J = 7.7$ Hz, 1H, ArH, H₇), 7.47 (app. ddt, $J = 8.9, 6.4, 1.8$ Hz, 1H, ArH, H₆), 7.03 (app. dt, $J = 35.6, 6.5$ Hz, 1H, NH), 6.10 (app. dd, $J = 26.0, 6.1$ Hz, 1H, NH), 4.46 (tq, $J = 9.1, 4.4$ Hz, 1H, CHOH), 4.28 (dt, $J = 9.7, 4.7$ Hz, 1H, CH₂OH), 4.17 (dt, $J = 10.3, 3.8$ Hz, 1H, H₂'), 4.02 (dd, $J = 11.0, 4.5$ Hz, 1H, H₁'), 3.96 – 3.93 (m, 1H, CH₂OH), 3.83 (ddd, $J = 10.5, 6.3, 3.7$ Hz, 1H, H₃'), 3.55 – 3.44 (m, 2H, CH₂, H₆'), 2.59 (dt, $J = 14.4, 9.5$ Hz, 1H, CH₂, H₅'), 2.37 (tdt, $J = 12.1, 9.2, 6.5$ Hz, 1H, CH, H₄'), 1.35 (ddt, $J = 14.0, 7.0, 3.4$ Hz, 1H, CH₂, H₅'), 0.94 – 0.90 (m, 18H, CH₃), 0.21 (s, 3H, CH₃), 0.12 (s, 3H, CH₃), 0.09 (s, 3H, CH₃), 0.07 – 0.05 (m, 3H, CH₃) ppm.

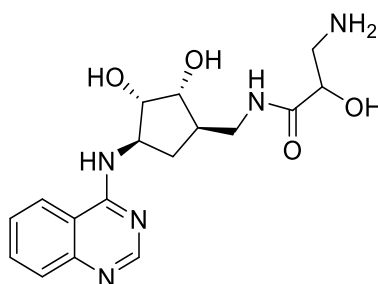
***N*-(((1*R*,2*R*,3*S*,4*R*)-2,3-Dihydroxy-4-(quinazolin-4-ylamino)cyclopentyl)methyl)-2,3-dihydroxypropanamide (303)**



Conc aq. HCl (0.10 mL, 0.15 mmol) was added to *N*-[[[(1*R*,2*R*,3*S*,4*R*)-2,3-bis[[*tert*-butyl(dimethyl)silyl]oxy]-4-(quinazolin-4-ylamino)cyclopentyl]methyl]-2,3-dihydroxy-propanamide (30 mg, 0.05 mmol) in EtOH (1 mL) and the reaction was stirred at rt for 2 h. The reaction mixture was concentrated and purified by column chromatography (biotage SNAP-Ultra C18 12 g, eluted with 0-10% MeOH in water, 5 CV gradient over 12 CV, 2 CV) to afford the title compound (5 mg, 27%, 0.01 mmol) as an oil. IR (thin film) $\nu = 3279, 1632, 1614, 1591, 1544$ cm⁻¹. ¹H NMR (600 MHz, Methanol-*d*₄) δ 8.77 (s, 1H, ArH, H₂), 8.52 (dt, $J = 8.4, 1.4$ Hz, 1H, ArH, H₅), 8.07 (ddd, $J = 8.4, 7.2, 1.2$ Hz, 1H, ArH, H₇), 7.83 (dd, $J = 8.0$ Hz, 1H, ArH, H₆), 7.80 (d, $J = 8.4$ Hz, 1H, ArH, H₈), 5.02 (q, $J = 8.4$ Hz, 1H, CH, H₁'), 4.19 (dd, $J = 7.4, 5.5$ Hz, 1H, CH, H₂'), 4.11 (dd, $J = 5.0, 2.9$ Hz, 1H, CH, CHOH), 3.92 (dt, $J = 7.2, 5.0$ Hz, 1H, CH, H₃'), 3.85 – 3.73 (m, 2H, CH₂, CH₂OH), 3.44 (td, $J = 12.7, 7.3$ Hz, 2H, CH₂, H₆'), 2.43 (dt, $J = 13.4, 8.4$ Hz, 1H,

CH₂, H_{5'}), 2.28 (dq, $J = 12.4, 7.7$ Hz, 1H, CH, H_{4'}), 1.51 – 1.37 (m, 1H, CH₂, H_{5'}) ppm. ¹³C NMR (151 MHz, Methanol-*d*₄) δ 174.0 (C), 161.6 (C), 150.5 (CH), 137.4 (C), 136.0 (CH), 128.7 (CH), 123.8 (CH), 118.7 (CH), 113.1 (C), 75.8 (CH), 73.4 (CH), 72.8 (CH), 64.0 (CH₂), 57.4 (CH), 43.4 (CH), 41.4 (CH₂), 29.7 (CH₂) ppm. HRMS (ESI+) calculated for C₁₇H₂₃N₄O₅ 363.1668 found 363.1660; Method B $t_R = 0.42$ min; Purity (AUC) $\geq 95\%$.

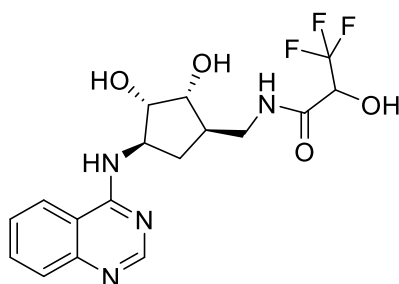
3-Amino-*N*-(((1*R*,2*R*,3*S*,4*R*)-2,3-dihydroxy-4-(quinazolin-4-ylamino)cyclopentyl)methyl)-2-hydroxypropanamide (304)



Conc aq. HCl (0.80 mL, 0.83 mmol) was added to *tert*-butyl *N*-[3-[[*(1R,2R,3S,4R)*-2,3-bis[[*tert*-butyl(dimethyl)silyl]oxy]-4-(quinazolin-4-ylamino)cyclopentyl]methylamino]-2-hydroxy-3-oxo-propyl]carbamate (57 mg, 0.08 mmol) in EtOH (0.8 mL) and the reaction was stirred at rt for 24 h. 4 M HCl in 1,4-dioxane (0.60 mL, 2.48 mmol) was added and the solution was stirred at rt for a further 48 h. The reaction mixture was concentrated and purified by column chromatography (biotage SNAP-Ultra C18 12 g, eluted with 0-50% MeOH in water, 1 CV, gradient over 12 CV, 6 CV). Fractions with product were further purified by acidic ion exchange chromatography (SCX, 2 g), eluting with 3.5 M NH₃ in MeOH to yield the title product (26 mg, 85%, 0.07 mmol) as an orange oil. IR (thin film) $\nu = 3292, 2921, 2454, 1635, 1618, 1582, 1532$ cm⁻¹. ¹H NMR (600 MHz, Methanol-*d*₄) δ 8.47 (s, 1H, ArH, H₂), 8.24 (d, $J = 8.3$ Hz, 1H, ArH, H₅), 7.81 (ddd, $J = 8.3, 6.9, 1.4$ Hz, 1H, ArH, H₇), 7.73 (d, $J = 8.2$ Hz, 1H, ArH, H₈), 7.56 (ddd, $J = 8.3, 6.9, 1.3$ Hz, 1H, ArH, H₆), 4.62 (tdd, $J = 9.0, 6.6, 2.9$ Hz, 1H, CH, H_{1'}), 4.11 – 4.04 (m, 2H, CH, CHOH, H_{2'}), 3.90 (dt, $J = 7.8, 5.7$ Hz, 1H, CH, H_{3'}), 3.44 – 3.35 (m, 2H, CH₂, H_{6'}), 2.84 (ddd, $J = 13.2, 7.8, 6.5$ Hz, 2H, CH₂, CH₂NH₂), 2.46 (dtd, $J = 13.2, 8.1, 1.6$ Hz, 1H, CH₂, H_{5'}), 2.33 – 2.22 (m, 1H, CH, H_{4'}), 1.41 – 1.31 (m, 1H, CH₂, H_{5'}) ppm. ¹³C NMR (151 MHz, Methanol-

d_4) δ 174.3 (C), 160.3 (C), 154.4 (CH), 148.3 (C), 132.9 (CH), 126.3 (CH), 126.1 (CH), 122.3 (CH), 115.0 (C), 76.6 (CH), 74.4 (CH), 72.3 (CH), 56.7 (CH), 44.9 (CH₂), 43.2 (CH), 41.8 (CH₂), 30.5 (CH₂) ppm. HRMS (ESI+) calculated for for C₁₇H₂₄N₅O₄ 362.1823, found 362.1833; Method A t_R = 0.22 min; Purity >95%.

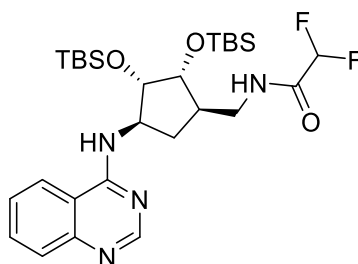
***N*-(((1*R*,2*R*,3*S*,4*R*)-2,3-Dihydroxy-4-(quinazolin-4-ylamino)cyclopentyl)methyl)-3,3,3-trifluoro-2-hydroxypropanamide (305)**



N-Hydroxysuccinimide (23 mg, 0.20 mmol) was added to a stirred solution of *N*-[[*(1R,2S,3R,4R)*-4-(aminomethyl)-2,3-bis[[*tert*-butyl(dimethyl)silyl]oxy]cyclopentyl]quinazolin-4-amine (83 mg, 0.17 mmol), 1 M *N,N*-dicyclohexylcarbodiimide (0.03 mL, 0.20 mmol) and 3,3,3-trifluoro-2-hydroxypropanoic acid (0.02 mL, 0.20 mmol) in THF (0.8 mL). The solution was stirred at rt for 4 h. The reaction mixture was concentrated and purified by column chromatography (biotage SNAP KP-Sil 10 g eluted with 0-5% MeOH in CH₂Cl₂, 1 CV, gradient over 10 CV, 5CV). Fractions with product were concentrated and passed through an acidic ion exchange column (SCX, 1 g) with MeOH followed by 3.5 M NH₃ in MeOH. EtOH (2 mL) and conc HCl (0.10 mL, 0.50 mmol) was added and the reaction was stirred at rt for 2 h. The reaction mixture was concentrated and purified by column chromatography (biotage SNAP-Ultra C18 12 g eluted with 0-40% MeOH in water, 3 CV, gradient over 18 CV, 5 CV) to yield the title product as two separate diastereomers (46. mg, 69%, 0.11 mmol, diastereomer 1; 11 mg 0.30 mmol 16% diastereomer 2) as oils. Diastereomer 1: ¹H NMR (600 MHz, Methanol-*d*₄) δ 8.64 (s, 1H, ArH, H₂), 8.38 (ddd, *J* = 8.4, 3.7, 1.2 Hz, 1H, ArH, H₅), 7.96 (ddd, *J* = 8.4, 7.1, 1.3 Hz, 1H, ArH, H₇), 7.75 (d, *J* = 8.3 Hz, 1H, ArH, H₈), 7.71 (ddd, *J* = 8.3, 7.2, 1.2 Hz, 1H, ArH, H₆), 4.83 (m, 1H, CH, H_{1'}), 4.51 – 4.44 (m, 1H, CH, CHOH), 4.14 (dd, *J* =

7.0, 5.5 Hz, 1H, CH, H_{2'}), 3.91 – 3.85 (m, 1H, CH, H_{3'}), 3.40 (dd, $J = 7.7, 2.9$ Hz, 2H, CH₂, H_{6'}), 2.48 – 2.40 (m, 1H, CH₂, H_{5'}), 2.33 – 2.24 (m, 1H, CH, H_{4'}), 1.38 (dq, $J = 13.3, 9.5$ Hz, 1H, CH₂, H_{5'}) ppm. ¹³C NMR (151 MHz, Methanol-*d*₄) δ 167.1 (C, HMBC), 161.2 (C, HMBC), 153.0 (CH), 144.6 (C, HMBC), 135.8 (CH), 128.6 (CH), 124.1 (CH), 122.7 (CH), 114.0 (C, HMBC), 77.0 (CH), 74.6 (CH), 70.0 (q, $J = 30.3$ Hz, CH), 58.1 (CH), 43.9 (CH), 42.8 (CH₂), 31.1 (CH₂) ppm. HRMS (ESI+) calculated for C₁₇H₂₀F₃N₄O₄ 401.1436, found 401.1423; Method B $t_R = 1.01$ min; Purity >95%. Diastereomer 2: ¹H NMR (600 MHz, Methanol-*d*₄) δ 8.54 (s, 1H, ArH, H₂), 8.30 (dd, $J = 8.4, 1.3$ Hz, 1H, ArH, H₅), 7.87 (ddd, $J = 8.4, 7.0, 1.3$ Hz, 1H, ArH, H₇), 7.73 (d, $J = 8.3$ Hz, 1H, ArH, H₈), 7.62 (ddd, $J = 8.3, 7.0, 1.2$ Hz, 1H, H₆), 4.72 (td, $J = 8.7, 6.7$ Hz, 1H, H_{1'}), 4.48 (q, $J = 7.5$ Hz, 1H, CHOH), 4.14 – 4.04 (m, 1H, CH, H_{2'}), 3.86 (t, $J = 5.5$ Hz, 1H, CH, H_{3'}), 3.41 (d, $J = 7.5$ Hz, 2H, CH₂, H_{6'}), 2.43 (app. dt, $J = 13.4, 8.3$ Hz, 1H, CH₂, H_{5'}), 2.33 – 2.22 (m, 1H, CH, H_{4'}), 1.38 (app. dt, $J = 13.4, 9.2$ Hz, 1H, CH₂, H_{5'}) ppm. ¹³C NMR (151 MHz, Methanol-*d*₄) δ 167.2 (C, HMBC), 160.8 (C, HMBC), 153.2 (CH), 145.0 (C, HMBC), 133.8 (CH), 126.9 (CH), 124.0 (CH), 122.7 (CH), 114.5 (C, HMBC), 76.4 (CH), 73.8 (CH), 70.1 (q, $J = 30.3$ Hz, CH), 56.9 (CH), 43.1 (CH), 41.8 (CH₂), 30.2 (CH₂) ppm. HRMS (ESI+) calculated for C₁₇H₂₀F₃N₄O₄ 401.1436, found 401.1425; Method B $t_R = 1.09$ min; Purity >95%.

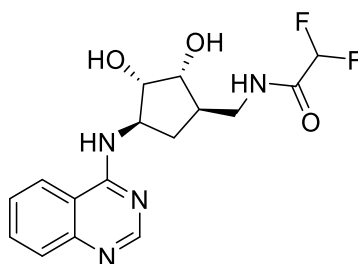
***N*-(((1*R*,2*R*,3*S*,4*R*)-2,3-Bis((*tert*-butyldimethylsilyl)oxy)-4-(quinazolin-4-ylamino)cyclopentyl)methyl)-2,2-difluoroacetamide (306a)**



Difluoroacetic acid (0.01 mL, 0.15 mmol) was added to a stirred solution of 1 M *N,N'*-dicyclohexylcarbodiimide in CH₂Cl₂ (0.15 mL, 0.15 mmol), *N*-hydroxysuccinimide (18 mg, 0.15 mmol) and *N*-[(1*R*,2*S*,3*R*,4*R*)-4-(aminomethyl)-2,3-bis[[*tert*-butyl(dimethyl)silyl]oxy]cyclopentyl]quinazolin-4-

amine (70 mg, 0.14 mmol) in THF (0.75 mL). The solution was allowed to warm to rt and stirred for 3 h. The reaction mixture was concentrated and purified by column chromatography (biotage SNAP KP-Sil 25 g, eluted with 20-100% EtOAc in cyclohexane, 3 CV, gradient over 18 CV, 5 CV) to afford the title compound (64 mg, 80%, 0.11 mmol) as a clear oil. IR (thin film) $\nu = 2931, 2858, 1704, 1651, 1615 \text{ cm}^{-1}$. $^1\text{H NMR}$ (600 MHz, Chloroform-*d*) δ 8.50 (s, 1H, ArH, H₂), 8.25 (d, $J = 8.3 \text{ Hz}$, 1H, ArH, H₅), 7.73 (d, $J = 8.3 \text{ Hz}$, 1H, ArH, H₈), 7.63 (dd, $J = 7.5 \text{ Hz}$, 1H, ArH, H₇), 7.46 (dd, $J = 7.7 \text{ Hz}$, 1H, ArH, H₆), 6.12 – 5.76 (m, 1H, CHF₂), 4.82 (d, $J = 8.0 \text{ Hz}$, 1H, CH, H_{1'}), 4.08 (dd, $J = 5.7, 3.8 \text{ Hz}$, 1H, H_{2'}), 3.87 (t, $J = 4.3 \text{ Hz}$, 1H, H_{3'}), 3.49 (s, 2H, H_{6'}), 2.49 (app. dt, $J = 13.9, 9.4 \text{ Hz}$, 1H, H_{5'}), 2.40 (tq, $J = 9.9, 5.7 \text{ Hz}$, 1H, H_{4'}), 1.68 (app. dt, $J = 13.4, 6.5 \text{ Hz}$, 1H, H_{5'}), 0.92 (s, 9H, CH₃), 0.77 (s, 9H, CH₃), 0.10 (s, 3H, CH₃), 0.06 (s, 3H, CH₃), 0.02 (s, 3H, CH₃) ppm. $^{13}\text{C NMR}$ (151 MHz, Chloroform-*d*) δ 163.6 (C, HMBC), 160.3 (C), 150.9 (CH), 139.2 (C, HMBC), 135.2 (CH), 128.3 (CH), 123.5 (CH), 120.9 (CH), 112.6 (C), 109.7 (d, $J = 283 \text{ Hz}$, CHF₂), 77.9 (CH), 76.2 (CH), 56.7 (CH), 42.7 (CH₂) 42.7 (CH), 29.7 (CH₂) 25.7 (3 x CH₃), 25.5 (3 x CH₃), 18.1 (C), 17.9 (C), -4.3 (CH₃), -4.5 (CH₃), -4.6 (CH₃), -4.7 (CH₃) ppm. HRMS (ESI+) calculated for C₂₈H₄₇F₂N₄O₃Si₂ 581.3149, found 581.3148; Method A $t_{\text{R}} = 3.14 \text{ min}$; Purity (AUC) $\geq 95\%$.

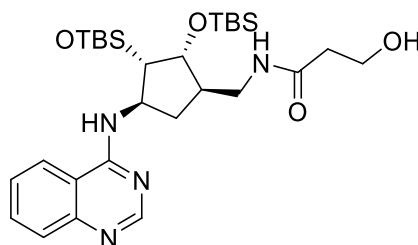
(((1*R*,2*R*,3*S*,4*R*)-2,3-Dihydroxy-4-(quinazolin-4-ylamino)cyclopentyl)methyl)-2,2-difluoroacetamide (306)



1 M aq. HCl (0.80 mL, 0.86 mmol) was added to *N*-[[(1*R*,2*R*,3*S*,4*R*)-2,3-bis[[*tert*-butyl(dimethyl)silyl]oxy]-4-(quinazolin-4-ylamino)cyclopentyl]methyl]-2,2-difluoro-acetamide (50 mg, 0.09 mmol) in EtOH (1.6 mL) and stirred at rt for 5 h. The reaction mixture was concentrated and purified by column

chromatography (biotage SNAP-Ultra C18 12 g, eluted with 0-50% MeOH in water, 3 CV, gradient over 18 CV, 2 CV) to afford the title compound (14 mg, 46%, 0.04 mmol) as an oil. IR (thin film) $\nu = \text{cm}^{-1}$. ^1H NMR (600 MHz, Methanol- d_4) δ 8.77 (s, 1H, ArH, H₂), 8.50 (dd, $J = 8.4, 0.6$ Hz, 1H, ArH, H₅), 8.13 – 8.05 (m, 1H, ArH, H₇), 7.84 (ddd, $J = 8.4, 7.2, 1.1$ Hz, 1H, ArH, H₆), 7.80 (dd, $J = 8.4, 0.8$ Hz, 1H, ArH, H₈), 6.08 (t, $J = 54.0$ Hz, 1H, CHF₂), 5.02 (dt, $J = 9.7, 8.0$ Hz, 1H, CH, H_{1'}), 4.20 (dd, $J = 7.6, 5.6$ Hz, 1H, CH, H_{2'}), 3.91 (dd, $J = 5.6, 4.5$ Hz, 1H, CH, H_{3'}), 3.50 – 3.38 (m, 2H, CH₂, H_{6'}), 2.45 (app. dt, $J = 13.2, 8.3$ Hz, 1H, CH₂, H_{5'}), 2.30 (pd, $J = 7.9, 4.5$ Hz, 1H, CH, H_{4'}), 1.45 – 1.36 (m, 1H, CH₂, H_{5'}) ppm. ^{13}C NMR (151 MHz, Methanol- d_4) δ 164.5 (C), 161.7 (C), 150.5 (CH), 137.5 (C), 136.1 (CH), 128.7 (CH), 123.8 (CH), 118.8 (CH), 113.1 (C), 109.5 (t, $J = 248$ Hz, CF₂), 75.6 (CH), 73.2 (CH), 57.4 (CH), 43.1 (CH), 41.8 (CH₂), 29.8 (CH₂) ppm. HRMS (ESI+) calculated for C₁₆H₁₉N₄O₃F₂ 353.1425, found 353.1422; Method C $t_{\text{R}} = 0.61$ min; Purity (AUC) $\geq 95\%$.

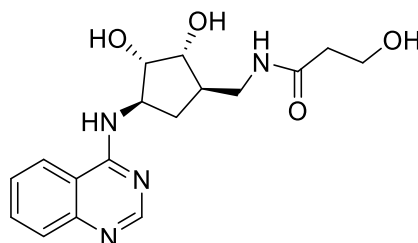
***N*-(((1*R*,2*R*,3*S*,4*R*)-2,3-Bis((*tert*-butyldimethylsilyl)oxy)-4-(quinazolin-4-ylamino)cyclopentyl)methyl)-3-hydroxypropanamide (307a)**



N,N-dicyclohexylcarbodiimide (34 mg, 0.16 mmol) was added at 0 °C to a solution of *N*-[(1*R*,2*S*,3*R*,4*R*)-4-(aminomethyl)-2,3-bis[[*tert*-butyl(dimethyl)silyl]oxy]cyclopentyl]quinazolin-4-amine (75 mg, 0.15 mmol), 3-hydroxypropanoic acid 30% in water (0.05 mL, 0.16 mmol) and *N*-hydroxysuccinimide (19 mg, 0.16 mmol) in THF (0.75 mL). The solution was warmed to rt and stirred for 2.5 h. The reaction mixture was concentrated and purified by column chromatography (biotage SNAP KP-Sil 10 g (50-100% EtOAc in cyclohexane, 1 CV, gradient over 18 CV, 5 CV) to afford the title compound (40 mg, 47%, 0.07 mmol) as a clear oil. IR (thin film) $\nu = 3302, 2928, 2887, 2856, 1703, 1647, 1619, 1581, 1530$ cm⁻¹. ^1H NMR (600 MHz, Chloroform- d) δ 8.62

(s, 1H, ArH, H₂), 7.93 (dd, $J = 8.4, 1.3$ Hz, 1H, ArH, H₅), 7.86 (dd, $J = 8.4, 1.2$ Hz, 1H, ArH, H₈), 7.73 (ddd, $J = 8.3, 7.0, 1.3$ Hz, 1H, ArH, H₇), 7.48 (ddd, $J = 8.2, 6.9, 1.2$ Hz, 1H, ArH, H₆), 6.48 – 6.36 (m, 1H, NH), 4.50 (h, $J = 4.4$ Hz, 1H, CH, H_{1'}), 4.19 (t, $J = 3.9$ Hz, 1H, CH, H_{2'}), 3.99 – 3.91 (m, 2H, CH₂, CH₂CH₂OH), 3.84 (dd, $J = 6.0, 3.7$ Hz, 1H, CH, H_{3'}), 3.58 (ddd, $J = 13.6, 8.7, 7.4$ Hz, 1H, CH₂, CH₂CH₂OH), 3.34 (ddd, $J = 13.6, 6.2, 4.6$ Hz, 1H, CH₂, H_{6'}), 2.59 (app dt, $J = 14.3, 9.4$ Hz, 1H, CH₂, H_{5'}), 2.51 (t, $J = 5.4$ Hz, 2H, CH₂, CH₂CH₂OH), 2.33 (tq, $J = 9.2, 6.2$ Hz, 1H, CH, H_{4'}), 1.48 – 1.37 (m, 1H, CH₂, H_{5'}), 0.92 (s, 9H, CH₃), 0.90 (s, 9H, CH₃), 0.19 (s, 3H, CH₃), 0.11 (s, 3H, CH₃), 0.08 (s, 3H, CH₃), 0.06 (s, 3H, CH₃) ppm. ¹³C NMR (151 MHz, Chloroform-*d*) δ 173.1 (C), 159.4 (C), 154.8 (CH), 148.1 (C), 132.9 (CH), 127.4 (CH), 126.3 (CH), 121.2 (CH), 114.7 (C), 77.9 (CH), 77.2 (CH), 58.5 (CH₂), 56.2 (CH), 42.7 (CH), 42.5 (CH₂), 38.3 (CH₂), 30.4 (CH₂), 25.5 (6 X CH₃), 18.1 (C), 18.1 (C) -4.1 (CH₃), -4.2 (CH₃), -4.5 (CH₃), -4.7 (CH₃) ppm. HRMS (ESI+) calculated for C₂₉H₅₀N₄NaO₄Si₂ 597.3263 found 597.3263; Method A t_R = 3.00 min; Purity (AUC) \geq 95%.

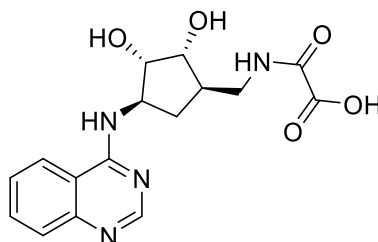
***N*-(((1*R*,2*R*,3*S*,4*R*)-2,3-Dihydroxy-4-(quinazolin-4-ylamino)cyclopentyl)methyl)-3-hydroxypropanamide (307)**



1M TBAF in THF (0.3 mL, 0.31 mmol) was added dropwise to a solution of *N*-(((1*R*,2*R*,3*S*,4*R*)-2,3-bis[[*tert*-butyl(dimethyl)silyl]oxy]-4-(quinazolin-4-ylamino)cyclopentyl)methyl]-3-hydroxy-propanamide (30 mg, 0.05 mmol) in THF (0.5 mL). The solution was stirred for 5 h at 60 °C. The reaction mixture was concentrated and purified by column chromatography (biotage SNAP-Ultra C18 12 g, eluted with 0-30% MeOH in water, 5 CV gradient over 15 CV, 2 CV). Fractions with product were combined and passed through an acidic ion exchange cartridge (SCX, 2 g) with MeOH and the product was eluted with 2 M NH₃/MeOH to afford the title compound (9 mg, 50%, 0.03 mmol) as an oil. $[\alpha]^{20}_D$

-18.0° (c=0.5, MeOH). IR (thin film) ν = 3279, 2962, 1586 cm^{-1} . ^1H NMR (600 MHz, Methanol- d_4) δ 8.50 (s, 1H, ArH, H₂), 8.29 – 8.25 (m, 1H, ArH, H₅), 7.83 (ddd, J = 8.4, 7.0, 1.3 Hz, 1H, ArH, H₇), 7.73 (d, J = 8.3 Hz, 1H, ArH, H₈), 7.58 (ddd, J = 8.3, 7.0, 1.2 Hz, 1H, ArH, H₆), 4.69 (td, J = 8.7, 6.8 Hz, 1H, CH, H_{1'}), 4.09 (t, J = 6.2 Hz, 1H, CH, H_{2'}), 3.88 (t, J = 5.4 Hz, 1H, CH, H_{3'}), 3.85 (t, J = 6.2 Hz, 2H, CH₂, CH₂CH₂OH), 3.43 – 3.29 (m, 2H, CH₂, H_{6'}), 2.45 (m, Hz, 3H, CH₂, CH₂, CH₂CH₂OH, H_{5'}), 2.29 – 2.20 (m, 1H, CH, H_{4'}), 1.37 (app dt, J = 13.3, 9.1 Hz, 1H, CH₂, H_{5'}) ppm. ^{13}C NMR (151 MHz, Methanol- d_4) δ 173.1 (C), 160.5 (C), 153.9 (CH), 146.9 (C), 133.3 (CH), 126.4 (CH), 125.3 (CH), 122.5 (CH), 114.8 (C), 76.5 (CH), 73.7 (CH), 58.1 (CH₂), 56.7 (CH), 43.3 (CH), 41.9 (CH₂), 38.8 (CH₂), 30.4 (CH₂) ppm. HRMS (ESI+) calculated for C₁₇H₂₃N₄O₄ 347.1714, found 347.1717; Method A t_R = 0.35 min; Purity (AUC) \geq 95%.

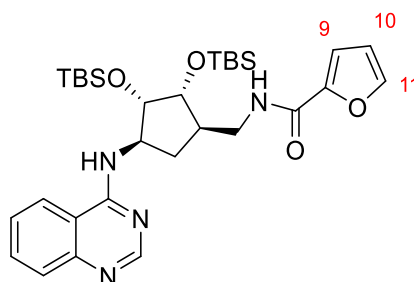
2-((((1*R*,2*R*,3*S*,4*R*)-2,3-Dihydroxy-4-(quinazolin-4-ylamino)cyclopentyl)methyl)amino)-2-oxoacetic acid (308)



Conc aq. HCl (0.10 mL, 0.3 mmol) was added to 2-[[[(1*R*,2*R*,3*S*,4*R*)-2,3-bis[[*tert*-butyl(dimethyl)silyl]oxy]-4-(quinazolin-4-ylamino)cyclopentyl]methylamino]-2-oxo-acetic acid (54 mg, 0.09 mmol) in THF (2 mL) and the reaction was stirred at rt for 30 min. The reaction mixture was concentrated and purified by column chromatography (biotage SNAP-Ultra C18 12 g, eluted with 0-100% MeCN in water, 2 CV, gradient over 15 CV, 2 CV) to afford the title compound (30 mg, 91%, 0.086 mmol). IR (thin film) ν = 3379, 2132, 1648, 1587 cm^{-1} . ^1H NMR (600 MHz, Deuterium Oxide) δ 8.40 (s, 1H, ArH, H₂), 8.06 (d, J = 8.3 Hz, 1H, ArH, H₅), 7.76 – 7.71 (m, 1H, ArH, H₇), 7.51 – 7.46 (m, 2H, ArH, H₆, H₈), 4.59 (dt, J = 9.8, 7.8 Hz, 1H, CH, H_{1'}), 3.99 (dd, J = 7.5, 5.8 Hz, 1H, CH, H_{2'}), 3.70 (t, J = 5.5 Hz, 1H, CH, H_{3'}), 3.24 – 3.11 (m, 2H, CH₂, H_{6'}), 2.16 (app dt, J = 13.3, 8.2 Hz, 1H, CH₂, H_{5'}), 2.04 (h, J = 7.7 Hz, 1H, CH, H_{4'}), 1.21 (app dt, J = 13.2, 9.6 Hz,

1H, CH₂, H_{5'}) ppm. ¹³C NMR (126 MHz, DMSO-*d*₆) δ 162.9 (C), 160.0 (C), 157.5 (C), 155.2 (CH), 148.5 (C), 133.2 (CH), 127.2 (CH), 126.1 (CH), 123.5 (CH), 115.2 (C), 75.9 (CH), 73.6 (CH), 56.2 (CH), 42.9 (CH), 42.8 (CH₂), 31.4 (CH₂) ppm. HRMS (ESI+) calculated for calcd for C₁₆H₁₉N₄O₅ 347.1350 found 347.1348; t_R = 0.33 min; Purity (AUC) ≥ 95%.

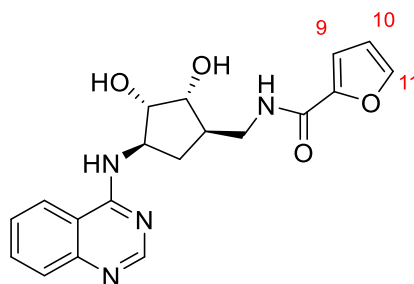
***N*-(((1*R*,2*R*,3*S*,4*R*)-2,3-Bis((*tert*-butyldimethylsilyl)oxy)-4-(quinazolin-4-ylamino)cyclopentyl)methyl)furan-2-carboxamide (309a)**



N,N'-Dicyclohexylcarbodiimide (37 mg, 0.18 mmol) was added at 0 °C to a solution of *N*-[(1*R*,2*S*,3*R*,4*R*)-4-(aminomethyl)-2,3-bis[[*tert*-butyl(dimethyl)silyl]oxy]cyclopentyl]quinazolin-4-amine (83 mg, 0.17 mmol), furan-2-carboxylic acid (20 mg, 0.18 mmol) and *N*-hydroxysuccinimide (21 mg, 0.18 mmol) in THF (0.8 mL). The solution was warmed to rt and stirred for 2.5 h. The reaction mixture was concentrated and purified by column chromatography (biotage SNAP KP-Sil 25 g, eluted with 30-100% EtOAc in cyclohexane, 1 CV, gradient over 18 CV, 5 CV) to afford the title compound (44 mg, 45%, 0.07 mmol) as an oil. IR (thin film) ν = 3306, 2928, 2855, 140, 1580, 1529 cm⁻¹. ¹H NMR (600 MHz, Chloroform-*d*) δ 8.67 (s, 1H, ArH, H₂), 7.86 (d, *J* = 8.3 Hz, 1H, ArH, H₅), 7.83 (d, *J* = 8.3 Hz, 1H, ArH, H₈) 7.75 (ddd, *J* = 8.3, 7.0, 1.3 Hz, 1H, ArH, H₇), 7.49 (ddd, *J* = 8.3, 7.0, 1.3 Hz, 1H, ArH, H₆), 7.47 – 7.46 (m, 1H, ArH, H₁₁), 7.16 (dd, *J* = 3.5, 0.8 Hz, 1H, ArH, H₉), 6.72 (dd, *J* = 7.6, 4.7 Hz, 1H, NH), 6.54 (dd, *J* = 3.5, 1.7 Hz, 1H, ArH, H₁₀), 6.05 (d, *J* = 6.0 Hz, 1H, NH), 4.47 (ddt, *J* = 8.7, 6.1, 4.3 Hz, 1H, CH, H_{1'}), 4.24 (t, *J* = 3.8 Hz, 1H, CH, H_{2'}), 3.92 (dd, *J* = 6.2, 3.7 Hz, 1H, CH, H_{3'}), 3.73 (ddd, *J* = 13.7, 10.4, 7.8 Hz, 1H, CH₂, H_{6'}), 3.57 – 3.47 (m, 1H, CH₂, H_{6'}), 2.68 (app dt, *J* = 14.4, 9.4 Hz, 1H, CH₂, H_{5'}), 2.43 (ddt, *J* = 15.5, 9.1, 6.1 Hz, 1H, CH, H_{4'}), 1.50 (ddd, *J* = 14.4, 6.1, 4.4 Hz, 1H, CH₂,

H_{5'}), 0.93 (s, 9H, CH₃), 0.92 (s, 9H, CH₃), 0.21 (s, 3H, CH₃), 0.13 (s, 3H, CH₃), 0.08 (s, 3H, CH₃), 0.07 (s, 3H, CH₃) ppm. ¹³C NMR (151 MHz, Chloroform-*d*) δ 159.1 (C), 159.1 (C), 155.3 (CH), 149.5 (C), 147.7 (C), 144.1 (CH), 132.5 (CH), 128.5 (CH), 126.0 (CH), 120.8 (CH), 115.0 (C), 114.6 (CH), 112.3 (CH), 77.8 (CH), 77.2 (CH), 56.2 (CH), 42.9 (CH), 42.4 (CH₂), 30.9 (CH₂), 26.0 (6 x CH₃), 18.1 (C), 17.9 (C), -4.1 (CH₃), -4.2 (CH₃), -4.5 (CH₃), -4.7 (CH₃) ppm. HRMS (ESI+) calculated for C₃₁H₄₉N₄O₄Si₂ 597.3287 found 597.3284. Method A t_R = 3.13 min; Purity (AUC) ≥ 95%.

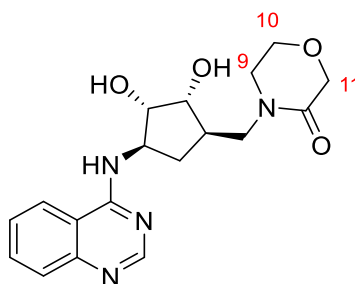
***N*-(((1*R*,2*R*,3*S*,4*R*)-2,3-Dihydroxy-4-(quinazolin-4-ylamino)cyclopentyl)methyl)furan-2-carboxamide (309)**



Conc aq. HCl (0.1 mL) in EtOH (2.0 mL) was added to *N*-[[[(1*R*,2*R*,3*S*,4*R*)-2,3-bis[[*tert*-butyl(dimethyl)silyl]oxy]-4-(quinazolin-4-ylamino)cyclopentyl]methyl]furan-2-carboxamide (37 mg, 0.06 mmol) and the reaction was stirred at rt for 3 h. The reaction mixture was concentrated and purified by column chromatography (biotage SNAP-Ultra C18 12 g, eluted with 0-50% MeOH in water, 1 CV gradient over 12 CV, 6 CV) to afford the title compound (20 mg, 88%, 0.05 mmol) as a clear oil. [α]²⁰_D -13.8° (c=0.5, MeOH). IR (thin film) ν = 3320, 2928, 2581, 2777, 1698, 1614 cm⁻¹. ¹H NMR (600 MHz, Methanol-*d*₄) δ 8.50 (s, 1H, ArH, H₂), 8.26 (d, *J* = 8.4 Hz, 1H, ArH, H₅), 7.83 (dd, *J* = 7.6 Hz, 1H, ArH, H₇), 7.72 (d, *J* = 8.3 Hz, 1H, ArH, H₈), 7.67 (m, 1H, ArH, H₁₁), 7.58 (dd, *J* = 7.6 Hz, 1H, ArH, H₆), 7.13 (d, *J* = 3.5 Hz, 1H, ArH, H₉), 6.59 (dd, *J* = 3.5, 1.8 Hz, 1H, ArH, H₁₀), 4.70 (td, *J* = 8.2 Hz, 1H, CH, H_{1'}), 4.13 (dd, *J* = 6.3 Hz, 1H, CH, H_{2'}), 3.96 (dd, *J* = 5.2 Hz, 1H, CH, H_{3'}), 3.52 (d, *J* = 7.3 Hz, 2H, CH₂, H_{6'}), 2.49 (app dt, *J* = 13.6, 8.2 Hz, 1H, CH₂, H_{5'}), 2.42 – 2.30 (m, 1H, CH, H_{4'}), 1.44 (app dt, *J* = 13.9, 9.2 Hz, 1H, CH₂, H_{5'}) ppm. ¹³C NMR (151 MHz,

Methanol- d_4) δ 160.5 (C), 159.7 (C), 153.8 (CH), 147.6 (C), 146.6 (C), 144.9 (CH), 133.3 (CH), 126.5 (CH), 125.1 (CH), 122.5 (CH), 114.7 (C), 113.9 (CH), 111.6 (CH), 76.5 (CH), 73.8 (CH), 56.8 (CH), 43.4 (CH), 41.7 (CH₂), 30.4 (CH₂) ppm. HRMS (ESI+) calculated for C₁₉H₂₁N₄O₄ 369.1557, found 369.1556. Method A t_R = 1.63 min; Purity (AUC) \geq 95%.

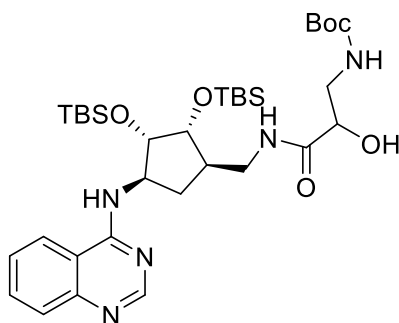
4-(((1*R*,2*R*,3*S*,4*R*)-2,3-Dihydroxy-4-(quinazolin-4-ylamino)cyclopentyl)methyl)morpholin-3-one (310)



Conc aq. HCl (0.10 mL, 0.19 mmol) was added to 4-[[[(1*R*,2*R*,3*S*,4*R*)-2,3-bis[[*tert*-butyl(dimethyl)silyl]oxy]-4-(quinazolin-4-ylamino)cyclopentyl]methyl]morpholin-3-one (30 mg, 0.05 mmol) in EtOH (2.0 mL) and stirred at rt for 5 h. The reaction mixture was concentrated and purified by reverse phase column chromatography (biotage SNAP-Ultra C18 12 g, eluted with 0-50% MeOH in water, 1 CV gradient over 12 CV, 6 CV) to afford the title compound (4 mg, 22%, 0.01 mmol) as an oil. $[\alpha]^{20}_D$ -98.3° ($c=0.5$, MeOH). IR (thin film) ν = 2963, 2013 cm^{-1} . ¹H NMR (600 MHz, Methanol- d_4) δ 8.59 (s, 1H, ArH, H₂), 8.35 (d, J = 8.3 Hz, 1H, ArH, H₅), 7.92 (ddd, J = 8.4, 7.0, 1.3 Hz, 1H, ArH, H₇), 7.76 (d, J = 8.3 Hz, 1H, ArH, H₈), 7.67 (ddd, J = 8.3, 7.0, 1.2 Hz, 1H, ArH, H₆), 4.79 (td, J = 7.8 Hz, 1H, CH, H_{1'}), 4.17 (s, 2H, CH₂, H₁₁), 4.15 (d, J = 6.2 Hz, 1H, CH, H_{2'}), 3.96 – 3.92 (m, 2H, CH₂, H₁₀), 3.91 (t, J = 5.2 Hz, 1H, CH, H_{3'}), 3.66 – 3.54 (m, 2H, CH₂, H₉), 3.52 (q, J = 4.7 Hz, 2H, CH₂, H_{6'}), 2.51 – 2.39 (m, 2H, CH, CH₂, H_{4'}, H_{5'}), 1.46 – 1.37 (m, 1H, CH₂, H_{5'}) ppm. ¹³C NMR (151 MHz, Methanol- d_4) δ 168.4 (C), 160.8 (C), 152.9 (CH), 143.9 (C), 134.2 (CH), 127.1 (CH), 123.3 (CH), 122.9 (CH), 114.3 (C), 76.2 (CH), 73.7 (CH), 67.2 (CH₂), 63.4 (CH₂), 57.0 (CH), 48.8 (CH₂), 46.0 (CH₂), 40.9 (CH), 30.3 (CH₂) ppm.

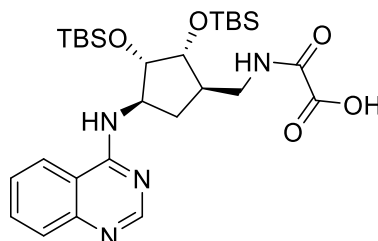
HRMS (ESI+) calculated for C₁₈H₂₃N₄O₄ 359.1714 found 359.1716; Method A t_R = 0.24 min; Purity (AUC) ≥ 95%.

Tert-butyl (3-((((1*R*,2*R*,3*S*,4*R*)-2,3-bis((*tert*-butyldimethylsilyl)oxy)-4-(quinazolin-4-ylamino)cyclopentyl)methyl)amino)-2-hydroxy-3-oxopropyl)carbamate (312)



1 M *N,N*-Dicyclohexylcarbodiimide in CH₂Cl₂ (0.19 mL, 0.19 mmol) was added at 0 °C to a solution of *N*-[(1*R*,2*S*,3*R*,4*R*)-4-(aminomethyl)-2,3-bis[[*tert*-butyl(dimethyl)silyl]oxy]cyclopentyl]quinazolin-4-amine (86 mg, 0.17 mmol), 3-amino-*N*-*boc*-2-hydroxy-propionic acid (39 mg, 0.19 mmol) and *N*-hydroxysuccinimide (22 mg, 0.19 mmol) in THF (0.75 mL). The solution was warmed to rt and stirred for 1.5 h. The reaction mixture was concentrated, dissolved in CH₂Cl₂ (1 mL) and purified by column chromatography (biotage SNAP KP-Sil 25 g, eluted with 20-100% EtOAc in cyclohexane, 3 CV, gradient over 18 CV, 5 CV) to yield the title product (57 mg, 48%, 0.08 mmol) as a clear oil. IR (thin film) ν = 3324, 2928, 2853, 1621, 1580, 1529 cm⁻¹. ¹H NMR (600 MHz, Methanol-*d*₄) δ 8.46 (s, 1H, ArH, H₂), 8.22 (dt, *J* = 8.4, 2.0 Hz, 1H, ArH, H₅), 7.81 (ddd, *J* = 8.3, 7.0, 1.3 Hz, 1H, ArH, H₇), 7.73 (dd, *J* = 8.4, 1.2 Hz, 1H, ArH, H₈), 7.57 (ddd, *J* = 8.3, 7.0, 1.2 Hz, 1H, ArH, H₆), 4.25 – 4.19 (m, 1H, CH), 4.16 – 4.09 (m, 3H, CH, CH₂), 3.94 (q, *J* = 3.9 Hz, 1H, CH), 2.50 (app. dt, *J* = 14.1, 9.6 Hz, 1H, CH), 2.37 – 2.31 (m, 1H, CH₂), 1.40 (s, 9H, CH₃), 0.97 (s, 9H, CH₃), 0.83 (s, 9H, CH₃), 0.16 (d, *J* = 1.9 Hz, 3H, CH₃), 0.12 (s, 3H, CH₃), 0.10 (s, 3H, CH₃), 0.09 (s, 3H, CH₃) ppm. HRMS (ESI+) calculated for for C₃₄H₆₀N₅O₆Si₂ 690.4082, found 690.4064; Method B t_R = 3.20 min; Purity (AUC) >95%.

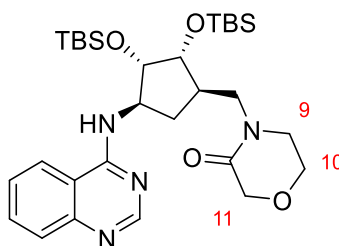
2-((((1*R*,2*R*,3*S*,4*R*)-2,3-Bis((*tert*-butyldimethylsilyl)oxy)-4-(quinazolin-4-ylamino)cyclopentyl)methyl)amino)-2-oxoacetic acid (313)



To a solution of *N*-[(1*R*,2*S*,3*R*,4*R*)-4-(aminomethyl)-2,3-bis[[*tert*-butyl(dimethyl)silyl]oxy]cyclopentyl]quinazolin-4-amine (80 mg, 0.16 mmol) in CH₂Cl₂ (0.4 mL) was added triethylamine (0.03 mL, 0.19 mmol) and the reaction mixture was cooled to 0°C. Methyl 2-chloro-2-oxoacetate (0.02 mL, 0.19 mmol) was added slowly at 0°C and the reaction was warmed to rt and stirred for 2 h. The reaction mixture was quenched with water (10 mL) and extracted with CH₂Cl₂ (3 x 15 mL). The combined extracts were washed with water (10 mL), dried with Na₂SO₄ and concentrated. The residue was dissolved in THF (2.5 mL) and H₂O (2.50 mL) and lithium hydroxide (53 mg, 1.27 mmol) was added. The reaction mixture was stirred at 60°C for 2 h. The reaction mixture was poured into water (10 mL) and acidified to pH 1 with aq. HCl. The resulting precipitate was filtered to afford the title compound (47 mg, 50%, 0.08 mmol) as a yellow solid. IR (thin film) ν = 2928, 2855, 1611, 1580, 1521 cm⁻¹. ¹H NMR (600 MHz, Methanol-*d*₄) δ 8.72 (s, 1H, ArH, H₂), 8.40 (d, *J* = 8.4 Hz, 1H, ArH, H₅), 8.00 (ddd, *J* = 8.4, 7.1, 1.3 Hz, 1H, ArH, H₇), 7.81 (d, *J* = 8.3 Hz, 1H, ArH, H₈), 7.77 (ddd, *J* = 8.4, 7.1, 1.2 Hz, 1H, ArH, H₆), 5.20 (q, *J* = 8.4 Hz, 1H, CH, H_{1'}), 4.26 (dd, *J* = 8.1, 3.8 Hz, 1H, CH, H_{2'}), 4.00 (dd, *J* = 4.0, 2.3 Hz, 1H, CH, H_{3'}), 3.38 (d, *J* = 7.5 Hz, 2H, CH₂, H_{6'}), 2.45 (app dt, *J* = 14.0, 9.6 Hz, 1H, CH₂, H_{5'}), 2.34 (dtd, *J* = 9.8, 6.3, 5.5, 2.2 Hz, 1H, CH, H_{4'}), 1.50 (ddd, *J* = 13.8, 8.2, 5.6 Hz, 1H, CH₂, H_{5'}), 0.96 (s, 9H, CH₃), 0.77 (s, 9H, CH₃), 0.16 (s, 3H, CH₃), 0.12 (s, 3H, CH₃), 0.09 (s, 3H, CH₃), 0.00 (s, 3H, CH₃) ppm. ³C NMR (151 MHz, Methanol-*d*₄) δ 164.7 (C), 164.6 (C), 161.2 (C), 151.6 (CH), 140.4 (C, HMBC), 135.2 (CH), 128.1 (CH), 123.2 (CH), 120.9 (CH), 113.6 (C), 77.4 (CH), 75.6 (CH), 56.1 (CH), 43.6 (CH),

42.1 (CH₂), 28.5 (CH₂), 25.1 (3 x CH₃), 24.9 (3 x CH₃), 17.6 (C), 17.4 (C), -5.4 (CH₃), -5.5 (CH₃), -5.6 (CH₃), -5.8 (CH₃) ppm. HRMS (ESI+) calculated for C₂₈H₄₆N₄NaO₅Si₂ 597.2899 found 597.2900; t_R = 3.24 min; Method A Purity (AUC) ≥ 95%

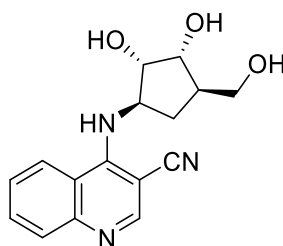
4-(((1*R*,2*R*,3*S*,4*R*)-2,3-Bis((*tert*-butyldimethylsilyl)oxy)-4-(quinazolin-4-ylamino)cyclopentyl)methyl)morpholin-3-one (317)



K₂CO₃ (66 mg, 0.48 mmol) was added to a stirred solution of *N*-[[(1*R*,2*R*,3*S*,4*R*)-2,3-bis[[*tert*-butyl(dimethyl)silyl]oxy]-4-(quinazolin-4-ylamino)cyclopentyl]methyl]-2-(2-chloroethoxy)acetamide (123 mg, 0.20 mmol) in MeCN (1 mL). The solution was heated at 80°C for 96 h. The reaction mixture was concentrated and purified by biotage SNAP-Ultra C18 12 g, eluted with 15-100% MeOH in water, 1 CV gradient over 18 CV, 6 CV) to yield the title compound (41 mg, 35%, 0.070 mmol) as a clear oil. IR (thin film) ν = 3368, 2947, 1647 cm⁻¹. ¹H NMR (600 MHz, Chloroform-*d*) δ 8.66 (s, 1H, ArH, H₂), 8.08 (dd, *J* = 8.4, 1.3 Hz, 1H, ArH, H₅), 7.90 (dd, *J* = 8.5, 1.2 Hz, 1H, ArH, H₈), 7.75 (ddd, *J* = 8.4, 7.0, 1.3 Hz, 1H, ArH, H₇), 7.52 (ddd, *J* = 8.3, 7.0, 1.3 Hz, 1H, ArH, H₆), 6.96 (d, *J* = 6.2 Hz, 1H, NH), 4.54 (dq, *J* = 8.1, 3.9 Hz, 1H, CH, H_{1'}), 4.30 (t, *J* = 3.8 Hz, 1H, CH, H_{2'}), 4.28 – 4.18 (m, 2H, CH₂, H₁₁), 4.13 – 4.04 (m, 1H, CH₂, H₉), 3.99 – 3.90 (m, 2H, CH₂, H₁₀), 3.89 – 3.86 (m, 1H, CH, H₃), 3.51 – 3.34 (m, 2H, CH₂, H_{6'}), 3.09 (dd, *J* = 13.7, 6.5 Hz, 1H, CH₂, H₉), 2.57 (ddd, *J* = 14.3, 9.9, 8.4 Hz, 1H, CH₂, H_{5'}), 2.48 – 2.38 (m, 1H, CH, H_{4'}), 1.35 (app dt, *J* = 14.3, 3.7 Hz, 1H, CH₂, H_{5'}), 0.90 (s, 18H, CH₃), 0.17 (s, 3H, CH₃), 0.10 (s, 3H, CH₃), 0.05 (s, 6H, CH₃) ppm. ¹³C NMR (151 MHz, Chloroform-*d*) δ 168.0 (C), 159.7 (C), 154.2 (CH), 146.9 (C), 133.1 (CH), 126.6 (CH), 126.3 (CH), 121.6 (CH), 114.6 (C), 78.1 (CH), 77.7 (CH), 67.9 (CH₂), 63.7 (CH₂), 56.8 (CH), 49.5 (CH₂), 45.9 (CH₂), 40.8 (CH), 29.9 (CH₂), 25.9 (3 x CH₃), 25.9 (3 x CH₃), 18.0 (C), 18.0 (C),

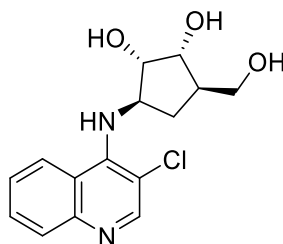
-4.1 (CH₃), -4.3 (CH₃), -4.6 (CH₃), -4.8 (CH₃) ppm. HRMS (ESI+) calculated for C₃₀H₅₁N₄O₄Si₂ 587.3443 found 587.3460; Method A t_R = 3.10 min; Purity (AUC) ≥ 95%.

4-(((1*R*,2*S*,3*R*,4*R*)-2,3-Dihydroxy-4-(hydroxymethyl)cyclopentyl)amino)quinoline-3-carbonitrile (335)



DIPEA (0.06 mL, 0.36 mmol) was added to (1*R*, 2*S*, 3*R*, 4*R*)-2,3-dihydroxy-4-(hydroxymethyl)-1-aminocyclopentane hydrochloride (30 mg, 0.16 mmol) and 4-chloroquinoline-3-carbonitrile (37 mg, 0.20 mmol) in DMSO (0.91 mL). The suspension was heated in the MW for 1 h at 120 °C. Purification by reverse phase column chromatography (biotage SNAP-Ultra C18 12 g, eluted with 0-40% MeOH in water, 1 CV, gradient over 10 CV, 6 CV) to afford the title compound (33 mg, 67%, 0.11 mmol) as a white solid. m.p. 225 °C. IR (thin film) $\nu = 3464, 3383, 3122, 2898, 2212, 1617, 1594, 1572, 1544 \text{ cm}^{-1}$. ¹H NMR (600 MHz, DMSO-*d*₆) δ 8.49 (s, 1H, H₂), 8.43 (dd, *J* = 8.6, 1.3 Hz, 1H, H₅), 7.83 (dd, *J* = 8.4, 1.4 Hz, 1H, H₈), 7.82 – 7.75 (m, 1H, H₇), 7.57 (ddd, *J* = 8.4, 6.8, 1.4 Hz, 1H, H₆), 4.82 (t, *J* = 5.0 Hz, 1H, OH), 4.78 (d, *J* = 6.4 Hz, 1H, OH), 4.63 (q, *J* = 7.8 Hz, 1H, CH, H₁'), 4.57 (d, *J* = 4.4 Hz, 1H, OH), 4.07 (hept, *J* = 4.8 Hz, 1H, CH, H₂'), 3.81 (q, *J* = 4.3 Hz, 1H, CH, H₃'), 3.45 (app.dh, *J* = 21.1, 5.2 Hz, 2H, CH₂, H₆'), 2.37 (ddd, *J* = 13.1, 9.1, 7.7 Hz, 1H, CH₂, H₅'), 2.00 (dddd, *J* = 11.1, 9.5, 4.7, 2.0 Hz, 1H, CH, H₄'), 1.34 (app. dt, *J* = 13.1, 7.9 Hz, 1H, CH₂, H₅') ppm. ¹³C NMR (151 MHz, DMSO-*d*₆) δ 153.9 (CH), 152.8 (C), 148.4 (C), 132.1 (CH), 129.8 (CH), 126.3 (CH), 122.9 (CH), 120.3 (C), 118.6 (CN), 82.7 (C), 76.7 (CH), 72.2 (CH), 63.1 (CH₂), 59.8 (CH), 45.7 (CH), 32.3 (CH₂) ppm. HRMS (ESI+) calculated for C₁₆H₁₇N₃NaO₃ 323.1192, found 323.1206; Method A t_R = 0.45 min; Purity (AUC) ≥ 95%.

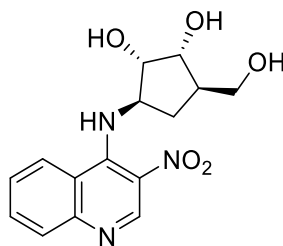
(1*R*,2*S*,3*R*,5*R*)-3-((3-Chloroquinolin-4-yl)amino)-5-(hydroxymethyl)cyclopentane-1,2-diol (336)



DIPEA (0.09 mL, 0.54 mmol) was added to (1*R*, 2*S*, 3*R*, 4*R*)-2,3-dihydroxy-4-(hydroxymethyl)-1-aminocyclopentane hydrochloride (45 mg, 0.25 mmol) and 3,4-dichloroquinoline (58 mg, 0.29 mmol) in NMP (1.2 mL).

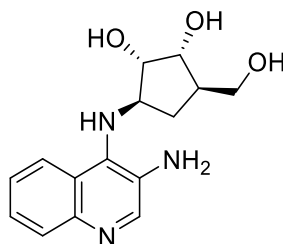
The suspension was heated in the MW for 3.5 h at 120 °C. Purification by column chromatography (biotage SNAP KP-Sil 10 g, eluted with 0-10% 10% NH₃ in MeOH in CH₂Cl₂, 1 CV, gradient over 20 CV, 5 CV) followed by acidic ion exchange chromatography (SCX, 1 g) washing with MeOH followed by 2.5 M NH₃ in MeOH to elute the title product (5 mg, 7%, 0.02 mmol) as a beige solid. IR (thin film) ν = 3366, 2925, 1671, 1574, 1544 cm⁻¹. ¹H NMR (600 MHz, Methanol-*d*₄) δ 8.46 (s, 1H, ArH, H₂), 8.33 (dd, *J* = 8.6, 1.3 Hz, 1H, ArH, H₅), 7.88 (dd, *J* = 8.5, 1.3 Hz, 1H, ArH, H₈), 7.70 (ddd, *J* = 8.4, 6.8, 1.3 Hz, 1H, ArH, H₇), 7.55 (ddd, *J* = 8.4, 6.8, 1.3 Hz, 1H, ArH, H₆), 4.59 (td, *J* = 7.0, 5.4 Hz, 1H, CH, H_{1'}), 4.05 (t, *J* = 5.0 Hz, 1H, CH, H_{2'}), 4.02 (t, *J* = 5.2 Hz, 1H, CH, H_{3'}), 3.69 (qd, *J* = 10.6, 4.8 Hz, 2H, CH₂, H_{6'}), 2.51 (ddd, *J* = 13.7, 9.8, 7.5 Hz, 1H, CH₂, H_{5'}), 2.14 (ddq, *J* = 9.8, 7.3, 5.0 Hz, 1H, CH, H_{4'}), 1.52 (app. dt, *J* = 13.8, 7.0 Hz, 1H, CH₂, H_{5'}) ppm. ¹³C NMR (151 MHz, Methanol-*d*₄) δ 149.6 (CH), 148.2 (C), 147.4 (C), 129.3 (CH), 128.1 (CH), 125.4 (CH), 122.8 (CH), 121.2 (C), 111.8 (C, HMBC), 78.2 (CH), 72.8 (CH), 62.4 (CH₂), 61.5 (CH), 44.8 (CH), 31.6 (CH₂) ppm. HRMS (ESI+) calculated for C₁₅H₁₈ClN₂O₃ 309.1000 found 309.1002; Method D *t*_R = 1.09 min, Purity (AUC) \geq 95%.

(1*S*,2*R*,3*R*,5*R*)-3-(Hydroxymethyl)-5-((3-nitroquinolin-4-yl)amino)cyclopentane-1,2-diol (337)

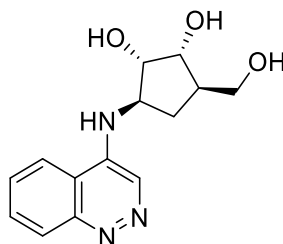


DIPEA (0.10 mL, 0.66 mmol) was added to (1*R*, 2*S*, 3*R*, 4*R*)-2,3-dihydroxy-4-(hydroxymethanol)-1-aminocyclopentane hydrochloride (55 mg, 0.30 mmol) and 4-chloro-3-nitroquinoline (75 mg, 0.36 mmol) in DMSO (1.5 mL). The suspension was heated in the MW for 1 h at 120 °C. Purification by reverse phase column chromatography (biotage SNAP-Ultra C18 12 g, eluted with 0-40% MeOH in water, 1 CV, gradient over 10 CV, 6 CV) followed by acidic ion exchange chromatography (SCX, 2 g) washed with CH₂Cl₂ followed by 2 M NH₃ in MeOH to afford the title compound (60 mg, 63%, 0.19 mmol) as a yellow solid. m.p. 184 °C. IR (thin film) ν = 3312, 3041, 2889, 1650, 1611, 1587, 1524 cm⁻¹. ¹H NMR (600 MHz, DMSO-*d*₆) δ 9.12 (s, 1H, ArH, H₂), 8.52 (dd, *J* = 8.5, 1.3 Hz, 1H, ArH, H₅), 7.91 (dd, *J* = 8.3, 1.4 Hz, 1H, ArH, H₈), 7.85 (ddd, *J* = 8.2, 6.8, 1.3 Hz, 1H, ArH, H₇), 7.62 (ddd, *J* = 8.4, 6.8, 1.5 Hz, 1H, ArH, H₆), 5.04 (d, *J* = 6.2 Hz, 1H, OH), 4.73 (t, *J* = 5.1 Hz, 1H, OH), 4.59 (d, *J* = 4.4 Hz, 1H, OH), 4.28 (p, *J* = 8.1 Hz, 1H, CH, H₁'), 3.88 (dt, *J* = 7.3, 5.3 Hz, 1H, CH, H₂'), 3.74 (q, *J* = 3.9 Hz, 1H, CH, H₃'), 3.43 (td, *J* = 5.1, 2.9 Hz, 2H, CH₂, H₆'), 2.42 (ddd, *J* = 13.4, 9.2, 7.8 Hz, 1H, CH₂, H₅'), 1.98 (dddd, *J* = 11.3, 8.9, 7.4, 4.4 Hz, 1H, CH, H₄'), 1.45 (ddd, *J* = 13.3, 8.7, 7.6 Hz, 1H, CH₂, H₅') ppm. ¹³C NMR (151 MHz, DMSO-*d*₆) δ 150.4 (C), 149.7 (C), 147.1 (CH), 133.1 (CH), 130.0 (CH), 126.9 (CH), 126.7 (C), 126.3 (CH), 119.7 (C), 78.9 (CH), 72.6 (CH), 63.6 (CH), 63.1 (CH₂), 45.4 (CH), 31.0 (CH₂) ppm. HRMS (ESI+) calculated for C₁₅H₁₈N₃O₅ 320.1241, found 320.1252; Method A *t*_R = 0.48 min; Purity (AUC) \geq 95%.

(1*R*,2*S*,3*R*,5*R*)-3-((3-Aminoquinolin-4-yl)amino)-5-(hydroxymethyl)cyclopentane-1,2-diol (338)

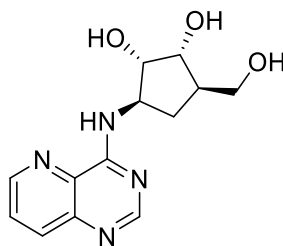


(1*S*,2*R*,3*R*,5*R*)-3-(Hydroxymethyl)-5-[(3-nitro-4-quinoly)amino]cyclopentane-1,2-diol (20 mg, 0.06 mmol) and palladium on carbon 10% (7 mg, 0.06 mmol) were added to a 25 mL RBF and the flask was flushed with nitrogen. EtOH (1.2 mL) was added and the reaction was put under an atmosphere of hydrogen at 3 bar for 18 hours stirring at rt. The reaction mixture was filtered through celite, concentrated and purified by acidic ion exchange chromatography (SCX, 2 g), washing with MeOH followed by 2.5 M NH₃ in MeOH to elute the title compound (16 mg, 86%, 0.05 mmol) as a yellow oil. IR (thin film) ν = 3230, 2929, 1575, 1433, 1341 cm⁻¹. ¹H NMR (600 MHz, Methanol-*d*₄) δ 8.33 (dd, *J* = 8.7, 1.2 Hz, 1H, ArH, H₅), 8.24 (s, 1H, ArH, H₂), 7.79 (dd, *J* = 8.5, 1.2 Hz, 1H, ArH, H₈), 7.65 (ddd, *J* = 8.3, 6.7, 1.2 Hz, 1H, ArH, H₇), 7.55 (ddd, *J* = 8.4, 6.8, 1.3 Hz, 1H, ArH, H₆), 4.60 (q, *J* = 7.7 Hz, 1H, CH, H_{1'}), 4.00 (dd, *J* = 5.4, 4.1 Hz, 1H, CH, H_{2'}), 3.96 (dd, *J* = 7.2, 5.3 Hz, 1H, CH, H_{3'}), 3.69 – 3.64 (m, 2H, CH₂, H_{6'}), 2.36 (ddd, *J* = 13.3, 9.2, 7.7 Hz, 1H, CH₂, H_{5'}), 2.13 (dddd, *J* = 13.5, 9.4, 5.4, 3.9 Hz, 1H, CH, H_{4'}), 1.61 – 1.48 (m, 1H, CH₂, H_{5'}) ppm. ¹³C NMR (151 MHz, Methanol-*d*₄) δ 167.9, 142.9 (C, HMBC), 138.0 (C), 128.7 (CH), 125.6 (CH), 122.5 (CH), 122.4 (CH), 120.1 (C), 119.7 (C), 77.4 (CH), 72.6 (CH), 63.0 (CH₂), 59.9 (CH), 45.0 (CH), 31.1 (CH₂) ppm. HRMS (ESI+) calculated for C₁₅H₂₀N₃O₃ 290.1499, found 290.1502; Method D *t*_R = 0.85 min, Purity (AUC) \geq 95%.

(1*R*,2*S*,3*R*,5*R*)-3-(Cinnolin-4-ylamino)-5-(hydroxymethyl)cyclopentane-1,2-diol (339)

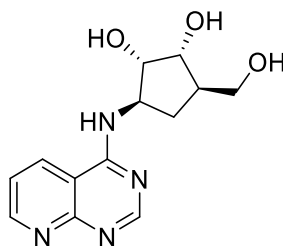
DIPEA (0.07 mL, 0.41 mmol) was added to (1*R*, 2*S*, 3*R*, 4*R*)-2,3-dihydroxy-4-(hydroxymethanol)-1-aminocyclopentane hydrochloride (30 mg, 0.16 mmol) and 4-chlorocinnoline (40 mg, 0.25 mmol) in DMSO (0.82 mL). The suspension was heated at 120 °C for 48 h. The reaction mixture was concentrated and purified by column chromatography (biotage SNAP KP-Sil 10 g, eluted with 0-10% 10% NH₃ in MeOH in CH₂Cl₂, 1 CV, gradient over 18 CV, 5 CV). Fractions with product were concentrated and passed through an acidic ion exchange column (SCX, 1 g) with MeOH and the product was eluted with 2.5 M NH₃ in MeOH to afford the title compound (5 mg, 11%, 0.02 mmol) as a brown oil. IR (thin film) ν = 3138, 3045, 1627, 1590 cm⁻¹. ¹H NMR (600 MHz, Methanol-*d*₄) δ 8.79 (s, 1H, ArH, H₃), 8.22 (d, *J* = 8.5 Hz, 1H, ArH, H₅), 8.12 (d, *J* = 8.5 Hz, 1H, ArH, H₈), 7.85 (ddd, *J* = 8.4, 6.8, 1.2 Hz, 1H, ArH, H₇), 7.69 (ddd, *J* = 8.3, 6.8, 1.2 Hz, 1H, ArH, H₆), 4.20 (td, *J* = 7.6, 4.6 Hz, 1H, CH, H_{2'}), 4.00 (m, 2H, CH, H_{3'}), 3.74 – 3.68 (m, 2H, CH₂, H_{6'}), 2.56 (ddd, *J* = 13.5, 9.2, 7.8 Hz, 1H, CH₂, H_{5'}), 2.25 (tdd, *J* = 11.2, 7.5, 5.6 Hz, 1H, CH, H_{4'}), 1.55 (ddd, *J* = 13.5, 7.7 Hz, 1H, CH₂, H_{5'}) ppm. ¹³C NMR (151 MHz, Methanol-*d*₄) δ 147.8 (C, HMBC), 142.5 (C), 130.9 (CH), 128.4 (CH), 128.1 (CH), 126.5 (CH), 120.5 (CH), 115.8 (C), 76.7 (CH), 73.0 (CH), 62.6 (CH₂), 57.6 (CH), 44.9 (CH), 29.6 (CH₂) ppm. HRMS (ESI+) calculated for C₁₄H₁₈N₃O₃ 276.1348, found 276.1350; Method B *t*_R = 0.87 min; Purity (AUC) \geq 95%.

(1*S*,2*R*,3*R*,5*R*)-3-(hydroxymethyl)-5-(pyrido[3,2-*d*]pyrimidin-4-ylamino)cyclopentane-1,2-diol (342)



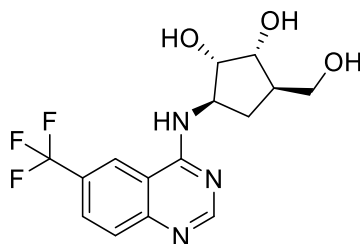
PyBOP (139 mg, 0.27 mmol) and DBU (0.09 mL, 0.57 mmol) were added to a stirred suspension of pyrido[3,2-*d*]pyrimidin-4(3*H*)-one (34 mg, 0.23 mmol) and (1*R*, 2*S*, 3*R*, 4*R*)-2,3-dihydroxy-4-(hydroxymethanol)-1-aminocyclopentane hydrochloride (35 mg, 0.19 mmol) in acetonitrile (1.0 mL). The suspension was stirred at rt for 4 h. The precipitate was filtered and washed with Et₂O to afford the title product (31 mg, 59%, 0.11 mmol) as a white solid. ¹H NMR (600 MHz, DMSO) δ 8.79 (dd, *J* = 4.2, 1.6 Hz, 1H, ArH, H₆), 8.48 (s, 1H, ArH, H₂), 8.32 (d, *J* = 8.3 Hz, 1H, NH), 8.10 (dd, *J* = 8.4, 1.6 Hz, 1H, ArH, H₈), 7.82 (dd, *J* = 8.4, 4.2 Hz, 1H, H₇), 4.70 (t, *J* = 5.1 Hz, 1H, OH), 4.68 (d, *J* = 5.7 Hz, 1H, OH), 4.54 (app. p, *J* = 7.9 Hz, 1H, H_{1'}), 4.43 (d, *J* = 4.8 Hz, 1H, OH), 3.94 (dt, *J* = 6.9, 5.4 Hz, 1H, CH, H_{2'}), 3.79 (q, *J* = 4.7 Hz, 1H, CH, H_{3'}), 3.43 (app. dh, *J* = 21.2, 5.4 Hz, 2H, CH₂, H_{6'}), 2.24 (dt, *J* = 13.1, 8.6 Hz, 1H, CH₂, H_{5'}), 2.02 – 1.93 (m, 1H, CH, H_{4'}), 1.28 (dt, *J* = 13.2, 7.8 Hz, 1H, CH₂, H_{5'}) ppm. ¹³C NMR (151 MHz, DMSO) δ 159.9 (C), 156.4 (CH), 148.8 (CH), 144.5 (C), 135.8 (CH), 132.1 (C), 128.6 (CH), 76.2 (CH), 72.7 (CH), 63.2 (CH₂), 55.6 (CH), 45.6 (CH), 30.2 (CH₂) ppm. HRMS (ESI+) calculated for C₁₃H₁₇N₄O₃ 277.1295 found 277.1308; Method A *t_R* = 0.19 min; Purity (AUC) ≥ 95%.

(1*S*,2*R*,3*R*,5*R*)-3-(Hydroxymethyl)-5-(pyrido[2,3-*d*]pyrimidin-4-ylamino)cyclopentane-1,2-diol (345)



PyBOP (270 mg, 0.52 mmol) and DBU (0.2 mL, 1.1 mmol) were added to a stirred suspension of pyrido[2,3-d]pyrimidin-4-ol (65 mg, 0.44 mmol) and (1*R*, 2*S*, 3*R*, 4*R*)-2,3-dihydroxy-4-(hydroxymethyl)-1-aminocyclopentane hydrochloride (68 mg, 0.37 mmol) in acetonitrile (1.9 mL) under an N₂ atmosphere. The solution was stirred at rt for 4 h. The resulting precipitate was filtered, washed with Et₂O and dried thoroughly to afford the title compound (43 mg, 42%, 0.16 mmol) as a white solid. IR (thin film) $\nu = 3297, 2906, 2865, 2455, 1582, 1542, 1528 \text{ cm}^{-1}$. ¹H NMR (600 MHz, DMSO-*d*₆) δ 8.97 (dd, *J* = 4.4, 1.8 Hz, 1H, ArH, H₅), 8.75 (dd, *J* = 8.2, 1.9 Hz, 1H, ArH, H₇), 8.57 (s, 1H, ArH, H₂), 8.38 (d, *J* = 7.6 Hz, 1H, NH), 7.53 (dd, *J* = 8.2, 4.3 Hz, 1H, ArH, H₆), 4.70 (m, 2H, OH), 4.57 (td, *J* = 8.0 Hz, 1H, CH, H_{1'}), 4.47 (d, *J* = 4.7 Hz, 1H, OH), 3.88 (dt, *J* = 8.0, 4.2 Hz, 1H, CH, H_{2'}), 3.76 (q, *J* = 4.2 Hz, 1H, CH, H_{3'}), 3.49 – 3.38 (m, 2H, CH₂, H_{6'}), 2.21 (app. dt, *J* = 13.1, 8.4 Hz, 1H, CH₂, H_{5'}), 1.98 (ddt, *J* = 13.3, 8.5, 4.7 Hz, 1H, CH, H_{4'}), 1.21 (app. dt, *J* = 13.1, 8.6 Hz, 1H, CH₂, H_{5'}) ppm. ¹³C NMR (151 MHz, DMSO-*d*₆) δ 161.3 (C), 158.8 (CH), 158.7 (C), 156.0 (CH), 133.1 (CH), 121.5 (CH), 110.1 (C), 76.1 (CH), 72.5 (CH), 63.4 (CH₂), 56.5 (CH), 45.7 (CH), 30.2 (CH₂) ppm. HRMS (ESI+) calculated for C₁₃H₁₇N₄O₃ 277.1295 found 277.1293; Method A *t*_R = 0.17 min; Purity (AUC) \geq 95%.

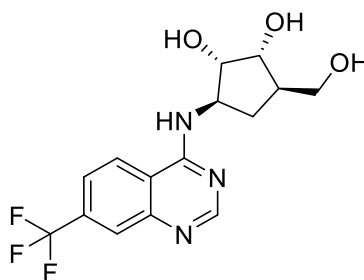
(1*S*,2*R*,3*R*,5*R*)-3-(Hydroxymethyl)-5-((6-(trifluoromethyl)quinazolin-4-yl)amino)cyclopentane-1,2-diol (346)



PyBOP (87 mg, 0.17 mmol) and DIPEA (0.06 mL, 0.36 mmol) were added to a stirred suspension of 6-(trifluoromethyl)quinazolin-4-ol (26 mg, 0.12 mmol) and (1*R*, 2*S*, 3*R*, 4*R*)-2,3-dihydroxy-4-(hydroxymethyl)-1-aminocyclopentane hydrochloride (22 mg, 0.12 mmol) in DMF (1.2 mL). The solution was stirred at rt for 4 h. Water (15 mL) was added and washed with CH₂Cl₂ (2 x 20 mL). The water layer was concentrated and purified by acidic ion exchange chromatography (SCX, 2 g). The product was eluted with 3.5 M NH₃ in MeOH

and concentrated to afford the title compound (28 mg, 68%, 0.08 mmol) as a yellow oil. $[\alpha]_D^{23} -18.01^\circ$ ($c=0.5$, MeOH). IR (thin film) $\nu = 3280, 1633, 1591, 1542$ cm^{-1} . ^1H NMR (600 MHz, Methanol- d_4) δ 8.70 – 8.67 (m, 1H, ArH, H₅), 8.58 (s, 1H, ArH, H₂), 8.04 (dd, $J = 8.7, 1.9$ Hz, 1H, ArH, H₇), 7.86 (d, $J = 8.7$ Hz, 1H, ArH, H₈), 4.76 (td, $J = 8.3, 6.9$ Hz, 1H, CH, H_{1'}), 4.05 (dd, $J = 6.9, 5.4$ Hz, 1H, CH, H_{2'}), 3.98 (dd, $J = 5.0$ Hz, 1H, CH, H_{3'}), 3.66 (dd, $J = 5.6, 1.3$ Hz, 2H, CH₂, H_{6'}), 2.47 (ddd, $J = 13.3, 8.5$ Hz, 1H, CH₂, H_{5'}), 2.21 (ddt, $J = 14.1, 8.6, 5.4$ Hz, 1H, CH, H_{4'}), 1.45 (ddd, $J = 13.4, 8.4$ Hz, 1H, CH₂, H_{5'}) ppm. ^{13}C NMR (151 MHz, Methanol- d_4) δ 160.6 (C), 156.1 (CH), 149.1 (C), 128.9 (q, $J = 3.3$ Hz, CH), 127.7 (q, $J = 32.8$ Hz, C), 126.8 (CH), 123.9 (q, $J = 268$ Hz, CF₃), 121.0 (q, $J = 4.4$ Hz, CH), 114.4 (C), 76.4 (CH), 72.7 (CH), 63.1 (CH₂), 56.5 (CH), 45.2 (CH), 29.1 (CH₂) ppm. HRMS (ESI+) calculated for C₁₅H₁₇F₃N₃O₃ 344.1217, found 344.1205; Method A $t_R = 0.92$ min; Purity (AUC) $\geq 95\%$.

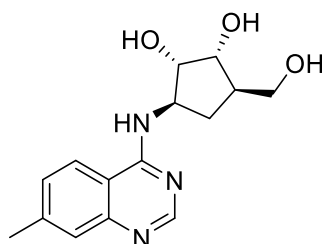
(1*S*,2*R*,3*R*,5*R*)-3-(Hydroxymethyl)-5-((7-(trifluoromethyl)quinazolin-4yl)amino)cyclopentane-1,2-diol (347)



PyBOP (99 mg, 0.19 mmol) and DIPEA (0.07 mL, 0.40 mmol) were added to a stirred suspension of 7-(trifluoromethyl)quinazolin-4-ol (30 mg, 0.14 mmol) and (1*R*, 2*S*, 3*R*, 4*R*)-2,3-dihydroxy-4-(hydroxymethanol)-1-aminocyclopentane hydrochloride (25 mg, 0.13 mmol) in DMF (1.4 mL). The solution was stirred at rt for 4 h. The reaction mixture was quenched with water (25 mL), washed with CH₂Cl₂ (3 x 15 mL) and concentrated. The product was dissolved in MeOH and passed through an acidic ion exchange cartridge (SCX, 1 g) with MeOH followed by 3.5 M NH₃ in MeOH. Purification by column chromatography (biotage SNAP-Ultra C18 12 g, eluted with 0-100% MeOH in water, 3 CV, gradient over 18 CV, 6 CV) and a second acidic ion exchange column (SCX, 1 g) afforded the title compound (13 mg, 28%, 0.04 mmol) as an oil. IR (thin film)

$\nu = 3260, 1585, 1544, 1500 \text{ cm}^{-1}$. $^1\text{H NMR}$ (600 MHz, Methanol- d_4) δ 8.54 (s, 1H, ArH, H₂), 8.35 (d, $J = 8.6$ Hz, 1H, ArH, H₅), 7.97 (d, $J = 1.9$ Hz, 1H, ArH, H₈), 7.74 (dd, $J = 8.7, 1.8$ Hz, 1H, ArH, H₆), 4.69 (td, $J = 8.0, 6.4$ Hz, 1H, CH, H_{1'}), 4.03 (dd, $J = 6.5, 5.3$ Hz, 1H, CH, H_{2'}), 3.98 (dd, $J = 5.1$ Hz, 1H, CH, H_{3'}), 3.67 (d, $J = 5.4$ Hz, 2H, CH₂, H_{6'}), 2.48 (ddd, $J = 13.3, 9.2, 7.8$ Hz, 1H, CH₂, H_{5'}), 2.20 (ddq, $J = 10.2, 8.3, 5.2$ Hz, 1H, CH, H_{4'}), 1.45 (app. dt, $J = 13.4, 8.1$ Hz, 1H, CH₂, H_{5'}) ppm. $^{13}\text{C NMR}$ (151 MHz, Methanol- d_4) δ 159.9 (C), 156.0 (CH), 148.1 (C), 134.1 (q, $J = 32.8$ Hz, C), 124.1 (CH), 123.7 (q, $J = 4.2$ Hz, CH), 123.6 (q, $J = 272$ Hz, CF₃), 121.4 (q, $J = 3.3$ Hz, CH), 117.1 (C), 76.5 (CH), 72.8 (CH), 63.0 (CH₂), 56.4 (CH), 45.2 (CH), 29.3 (CH₂) ppm. HRMS (ESI+) calculated for C₁₅H₁₇F₃N₃O₃ 344.1217, found 344.1207; Method A $t_R = 0.83$ min; Purity (AUC) $\geq 95\%$.

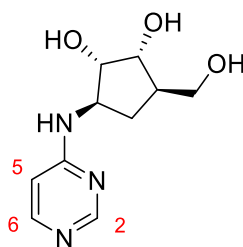
(1*S*,2*R*,3*R*,5*R*)-3-(Hydroxymethyl)-5-((7-methylquinazolin-4-yl)amino)cyclopentane-1,2-diol (348)



PyBOP (198 mg, 0.38 mmol) and DBU (0.12 mL, 0.82 mmol) were added to a stirred suspension of 7-methylquinazolin-4-ol (52 mg, 0.33 mmol) and (1*R*, 2*S*, 3*R*, 4*R*)-2,3-dihydroxy-4-(hydroxymethanol)-1-aminocyclopentane hydrochloride (50 mg, 0.27 mmol) in acetonitrile (1.4 mL). The solution was stirred at rt for 4 h. The reaction mixture was concentrated and purified by column chromatography (biotage SNAP KP-Sil 10 g, eluted with 0-10% NH₃/MeOH in CH₂Cl₂, 1 CV, gradient over 10 CV, 5 CV). Fractions with product were further purified by reverse phase column chromatography (biotage SNAP-Ultra C18 12 g, eluted with 0-50% MeOH in water, 5 CV, gradient over 15 CV, 2 CV), followed by an acidic ion exchange column (SCX, 1 g) eluting with 2 M NH₃ in MeOH to afford the title compound (14mg, 18%, 0.05 mmol). IR (thin film) $\nu = 3271, 2931, 1586 \text{ cm}^{-1}$. $^1\text{H NMR}$ (600 MHz, Methanol- d_4) δ 8.54 (s, 1H, ArH, H₂),

8.13 (d, $J = 8.4$ Hz, 1H, ArH, H₅), 7.53 (s, 1H, ArH, H₈), 7.49 (dd, $J = 8.6, 1.6$ Hz, 1H, ArH, H₆), 4.78 (q, $J = 7.7$ Hz, 1H, CH, H_{1'}), 4.05 (dd, $J = 6.0$ Hz, 1H, CH, H_{2'}), 4.01 (dd, $J = 5.0$ Hz, 1H, CH, H_{3'}), 3.69 (d, $J = 5.3$ Hz, 2H, CH₂, H_{6'}), 2.56 (s, 3H, CH₃), 2.47 (app. dt, $J = 13.6, 8.6$ Hz, 1H, CH₂, H_{5'}), 2.22 (td, $J = 8.5, 4.4$ Hz, 1H, CH, H_{4'}), 1.49 (app. dt, $J = 13.6, 8.1$ Hz, 1H, CH₂, H_{5'}) ppm. ¹³C NMR (151 MHz, Methanol-*d*₄) δ 160.4 (C), 152.8 (CH), 145.7 (C), 144.0 (C), 128.8 (CH), 122.5 (CH), 122.4 (CH), 112.0 (C), 76.5 (CH), 72.7 (CH), 62.9 (CH₂), 56.6 (CH), 45.3 (CH), 29.2 (CH₂), 20.5 (CH₃) ppm. HRMS (ESI+) calculated for C₁₅H₂₀N₃O₃ 290.1505 found 290.1510; Method B t_R = 1.10 min; Purity (AUC) \geq 95%.

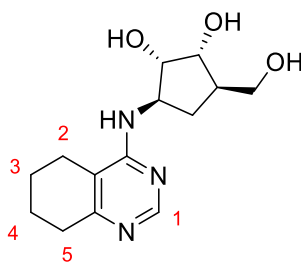
(1*S*,2*R*,3*R*,5*R*)-3-(Hydroxymethyl)-5-(pyrimidin-4-ylamino)cyclopentane-1,2-diol (349)



DIPEA (0.13 mL, 0.73 mmol) was added to (1*R*, 2*S*, 3*R*, 4*R*)-2,3-dihydroxy-4-(hydroxymethanol)-1-aminocyclopentane hydrochloride (42 mg, 0.23 mmol) and 4-chloropyrimidine hydrochloride (41 mg, 0.27 mmol) in DMSO (1 mL). The suspension was heated in the MW for 1 h at 120 °C. The reaction mixture was passed through an acidic ion exchange column (SCX, 2 g) with MeOH and the product was eluted with 2 M NH₃ in MeOH. Purification by column chromatography (biotage SNAP KP-Sil 10 g, eluted with 0-10% 20% NH₃ in MeOH in CH₂Cl₂, 1 CV, gradient over 10 CV, 5 CV) to yield the title product as a clear oil. IR (thin film) $\nu = 3256, 2925, 1650, 1600, 1509$ cm⁻¹. ¹H NMR (600 MHz, Methanol-*d*₄) δ 8.43 (s, 1H, ArH, H₂), 8.02 (br. s, 1H, ArH), 6.60 (br. s, 1H, ArH), 4.46 – 4.18 (br. s, 1H, CH), 3.89 (t, $J = 5.1$ Hz, 1H, CH), 3.83 (dd, $J = 6.7, 5.4$ Hz, 1H, CH, H_{3'}), 3.62 (qd, $J = 10.8, 5.8$ Hz, 2H, CH₂, H_{6'}), 2.38 (app. dt, $J = 13.3, 8.5$ Hz, 1H, CH₂, H_{5'}), 2.16 (ddt, $J = 14.4, 8.7, 5.5$ Hz, 1H, CH, H_{4'}), 1.36 – 1.19 (m, 1H, CH₂, H_{5'}) ppm. ¹³C NMR (151 MHz, Methanol-*d*₄) δ 162.5 (C), 156.4 (CH), 151.5 (CH), 106.7 (CH), 77.0 (CH), 72.8 (CH), 63.1 (CH₂), 55.9 (CH,

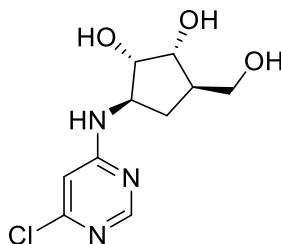
HMBC), 45.1 (CH), 29.6 (CH₂) ppm. HRMS (ESI+) calculated for C₁₀H₁₅N₃O₃ 226.1186 found 226.1184; Method D t_R = 0.22 min; Purity (AUC) ≥ 95%.

(1*S*,2*R*,3*R*,5*R*)-3-(Hydroxymethyl)-5-((5,6,7,8-tetrahydroquinazolin-4-yl)amino)cyclopentane-1,2-diol (350)



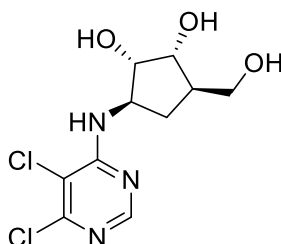
DIPEA (0.07 mL, 0.42 mmol) was added to (1*R*, 2*S*, 3*R*, 4*R*)-2,3-dihydroxy-4-(hydroxymethyl)-1-aminocyclopentane hydrochloride (35 mg, 0.19 mmol) and 4-chloro-5,6,7,8-tetrahydroquinazoline (39 mg, 0.23 mmol) in DMSO (1 mL). The suspension was heated in the MW for 6 h at 120 °C. Purification by reverse phase column chromatography (biotage SNAP-Ultra C18 12 g, eluted with 0-100% MeOH in water, 6 CV, gradient over 18 CV, 2 CV) followed by acidic ion exchange chromatography (SCX, 1 g) washed with MeOH and the product eluted with 2 M NH₃ in MeOH followed by column chromatography (biotage SNAP KP-Sil 10 g, eluted with 0-20% 10% NH₃ in MeOH in CH₂Cl₂, 1 CV, gradient over 18 CV, 5 CV) to afford the title compound (12 mg, 0.04 mmol, 23%) as a clear oil. IR (thin film) ν = 3298, 2932, 1643, 1592, 1511 cm⁻¹. ¹H NMR (600 MHz, Methanol-*d*₄) δ 8.22 (s, 1H, ArH, H₂), 4.43 (td, *J* = 7.4, 5.8 Hz, 1H, CH, H₁'), 3.98 (t, *J* = 5.2 Hz, 1H, CH, H₂'), 3.89 (t, *J* = 5.5 Hz, 1H, CH, H₃'), 3.65 (app.h, *J* = 5.3 Hz, 2H, CH₂, H₆'), 2.66 (t, *J* = 5.9 Hz, 2H, CH₂, H₂ or H₅), 2.44 (ddd, *J* = 13.3, 9.5, 7.6 Hz, 1H, CH₂, H₅'), 2.40 – 2.35 (m, 2H, CH₂, H₂ or H₅), 2.16 (dtd, *J* = 9.6, 4.9, 2.3 Hz, 1H, CH, H₄'), 1.89 – 1.81 (m, 4H, CH₂, H₃, H₄), 1.38 (app. dt, *J* = 13.4, 7.3 Hz, 1H, CH₂, H₅') ppm. ¹³C NMR (151 MHz, Methanol-*d*₄) δ 160.5 (C), 159.6 (C), 153.8 (CH), 112.7 (C), 76.9 (CH), 72.9 (CH), 62.6 (CH₂), 56.0 (CH), 45.1 (CH), 30.5 (CH₂), 29.8 (CH₂), 21.7 (CH₂), 21.7 (CH₂), 21.6 (CH₂) ppm. HRMS (ESI+) calculated for C₁₄H₂₁N₃O₃ 280.1656 found 280.1657; Method D t_R = 0.79 min, Purity (AUC) ≥ 95%.

(1*R*,2*S*,3*R*,5*R*)-3-((6-Chloropyrimidin-4-yl)amino)-5-(hydroxymethyl)cyclopentane-1,2-diol (351)



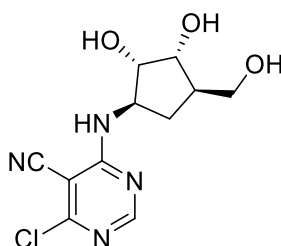
DIPEA (0.08 mL, 0.44 mmol) was added to (1*R*, 2*S*, 3*R*, 4*R*)-2,3-dihydroxy-4-(hydroxymethyl)-1-aminocyclopentane hydrochloride (35 mg, 0.19 mmol) and 4,5-dichloropyrimidine (37 mg, 0.25 mmol) in DMSO (0.64 mL). The reaction mixture was heated at 120 °C in the MW for 1 h. Purification by reverse phase column chromatography (biotage SNAP-Ultra C18 12 g, eluted with 0-20% MeOH in water, 6 CV, gradient over 10 CV, 3 CV) followed by acidic ion exchange chromatography (SCX, 1 g). The product was washed with MeOH and eluted with 2.5 M NH₃ in MeOH to afford the title compound (14 mg, 28%, 0.05 mmol) as an orange solid. m.p. 149 °C. $[\alpha]_D^{23}$ -6.93° (c=0.5, MeOH). IR (thin film) ν = 3318, 3128, 2885 2529, 2467, 2430, 2260, 1584, 1538 cm⁻¹. ¹H NMR (600 MHz, Methanol-*d*₄) δ 8.37 (s, 1H, ArH, H₂), 8.15 (s, 1H, ArH, H₄), 4.52 (td, *J* = 7.4, 5.8 Hz, 1H, CH, H_{1'}), 3.99 (t, *J* = 5.1 Hz, 1H, CH, H_{2'}), 3.94 (t, *J* = 5.5 Hz, 1H, CH, H_{3'}), 3.70 – 3.62 (m, 2H, CH₂, H_{6'}), 2.44 (ddd, *J* = 13.4, 9.6, 7.7 Hz, 1H, CH₂, H_{5'}), 2.15 (ddq, *J* = 9.9, 7.3, 5.0 Hz, 1H, CH, H_{4'}), 1.43 – 1.34 (m, 1H, CH₂, H_{5'}) ppm. ¹³C NMR (151 MHz, Methanol-*d*₄) δ 157.9 (C), 155.5 (CH), 151.2 (CH), 114.3 (C), 76.4 (CH), 72.8 (CH), 62.6 (CH₂), 55.8 (CH), 45.0 (CH), 29.5 (CH₂) ppm. HRMS (ESI+) calculated for C₁₀H₁₅ClN₃O₃ 260.0802 found 260.0801; Method C *t*_R = 0.32 min; Purity (AUC) \geq 95%.

(1*R*,2*S*,3*R*,5*R*)-3-((5,6-Dichloropyrimidin-4-yl)amino)-5-(hydroxymethyl)cyclopentane-1,2-diol (352)



DIPEA (0.10 mL, 0.50 mmol) was added to (1*R*, 2*S*, 3*R*, 4*R*)-2,3-dihydroxy-4-(hydroxymethyl)-1-aminocyclopentane hydrochloride (40 mg, 0.22 mmol) and 4,5,6-trichloropyrimidine (60 mg, 0.33 mmol) in DMSO (0.7 mL). The reaction was heated at 120 °C in the MW for 1 h. Purification by reverse phase column chromatography (biotage SNAP-Ultra C18 12 g, eluted with 0-80% MeOH in water, 3 CV, gradient over 18 CV, 3 CV) to afford the title compound (43 mg, 67%, 0.15 mmol) as a white solid. m.p. 194 °C. $[\alpha]_{\text{D}}^{23}$ ° (c=0.5, MeOH). IR (thin film) $\nu = 3374, 3272, 2920, 2871, 1579, 1554, 1501 \text{ cm}^{-1}$. ^1H NMR (600 MHz, DMSO- d_6) δ 8.25 (s, 1H, ArH, H₂), 7.60 (d, $J = 8.1 \text{ Hz}$, 1H, NH), 4.82 (d, $J = 6.0 \text{ Hz}$, 1H, OH), 4.62 (d, $J = 5.7 \text{ Hz}$, 1H, OH), 4.46 – 4.41 (m, 1H, OH), 4.39 (q, $J = 7.7 \text{ Hz}$, 1H, CH, H_{1'}), 3.83 (q, $J = 4.9 \text{ Hz}$, 1H, CH, H_{2'}), 3.75 (q, $J = 4.0 \text{ Hz}$, 1H, CH, H_{3'}), 3.45 – 3.37 (m, 2H, CH₂, H_{6'}), 2.15 (app. dt, $J = 13.0, 8.6 \text{ Hz}$, 1H, CH₂, H_{5'}), 1.93 (dp, $J = 9.8, 5.2 \text{ Hz}$, 1H, CH, H_{4'}), 1.21 (app. dt, $J = 14.0, 7.6 \text{ Hz}$, 1H, CH₂, H_{5'}) ppm. ^{13}C NMR (151 MHz, DMSO- d_6) δ 159.1 (C), 155.7 (CH), 154.8 (C), 110.1 (C), 75.8 (CH), 72.5 (CH), 63.0 (CH₂), 56.7 (CH), 45.4 (CH), 30.1 (CH₂) ppm. HRMS (ESI+) calculated for C₁₀H₁₄Cl₂N₃O₃ 294.0412, found 294.0410; Method B $t_{\text{R}} = 1.54 \text{ min}$; Purity (AUC) $\geq 95\%$.

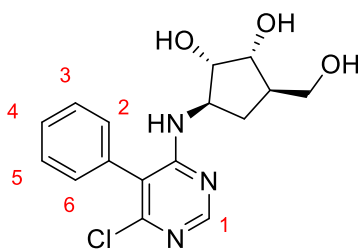
4-Chloro-6-(((1*R*,2*S*,3*R*,4*R*)-2,3-dihydroxy-4-(hydroxymethyl)cyclopentyl)amino)pyrimidine-5-carbonitrile (353)



DIPEA (0.08 mL, 0.44 mmol) was added to (1*R*, 2*S*, 3*R*, 4*R*)-2,3-dihydroxy-4-(hydroxymethyl)-1-aminocyclopentane hydrochloride (35 mg, 0.19 mmol) and 4,6-dichloropyrimidine-5-carbonitrile (43 mg, 0.25 mmol) in DMSO (0.6 mL). The reaction mixture was heated at 120 °C in the MW for 1 h. Purification by reverse phase column chromatography (biotage SNAP-Ultra C18 12 g, eluted with 0-80% MeOH in water, 3 CV, gradient over 10 CV, 6 CV) to afford the title

compound (6 mg, 11%, 0.02 mmol) as an orange oil. IR (thin film) $\nu = 3375, 2934, 2870, 2203, 1574 \text{ cm}^{-1}$. $^1\text{H NMR}$ (600 MHz, Methanol- d_4) δ 8.42 (s, 1H, Ar, H₂), 4.62 (td, $J = 7.5, 5.9 \text{ Hz}$, 1H, CH, H_{1'}), 4.00 – 3.92 (m, 2H, CH, H_{2'}, H_{3'}), 3.69 – 3.56 (m, 2H, CH₂, H_{6'}), 2.40 (ddd, $J = 13.4, 9.6, 7.7 \text{ Hz}$, 1H, CH₂, H_{5'}), 2.16 – 2.10 (m, 1H, CH, H_{4'}), 1.43 – 1.34 (m, 1H, CH₂, H_{5'}) ppm. $^{13}\text{C NMR}$ (151 MHz, Methanol- d_4) δ 162.2 (C), 161.8 (C), 159.2 (CH), 112.2 (C), 76.1 (CH), 72.7 (CH), 62.6 (CH₂), 56.5 (CH), 45.0 (CH), 29.2 (CH₂) ppm. HRMS (ESI+) calculated for C₁₁H₁₄ClN₄O₃ 285.0754, found 285.0744; Method B $t_{\text{R}} = 1.36 \text{ min}$; Purity (AUC) $\geq 95\%$.

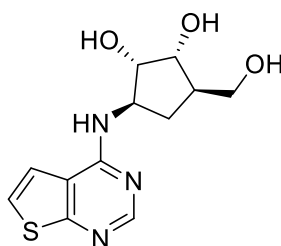
(1*R*,2*S*,3*R*,5*R*)-3-((6-Chloro-5-phenylpyrimidin-4-yl)amino)-5-(hydroxymethyl)cyclopentane-1,2-diol (354)



DIPEA (0.08 mL, 0.45 mmol) was added to (1*R*, 2*S*, 3*R*, 4*R*)-2,3-dihydroxy-4-(hydroxymethanol)-1-aminocyclopentane hydrochloride (33 mg, 0.18 mmol) and 4,6-dichloro-5-phenylpyrimidine (61 mg, 0.27 mmol) in DMSO (0.7 mL). The reaction mixture was heated at 120 °C in the MW for 1 h. Purification by reverse phase column chromatography (biotage SNAP-Ultra C18 12 g, eluted with 0-80% MeOH in water, 3 CV, gradient over 18 CV, 3 CV) followed by acidic ion exchange chromatography (SCX, 1 g). Further purification by column chromatography (biotage SNAP KP-Sil 10 g, eluted with 0-10% 10% NH₃ in MeOH in CH₂Cl₂, 1 CV, gradient over 10 CV, 5 CV) to afford the title compound (12 mg, 20%, 0.036 mmol) as a clear oil. IR (thin film) $\nu = 3306, 2926, 1563, 1502 \text{ cm}^{-1}$. $^1\text{H NMR}$ (600 MHz, Methanol- d_4) δ 8.30 (s, 1H, ArH, H₂), 7.57 – 7.52 (m, 2H, ArH, H₃, H₅), 7.51 – 7.46 (m, 1H, ArH, H₄), 7.34 – 7.26 (m, 2H, ArH, H₂, H₆), 4.42 (dt, $J = 7.7, 6.1 \text{ Hz}$, 1H, CH, H_{1'}), 3.84 (t, $J = 5.1 \text{ Hz}$, 1H, CH, H_{2'}), 3.78 (t, $J = 5.2 \text{ Hz}$, 1H, CH, H_{3'}), 3.53 – 3.44 (m, 2H, CH₂, H_{6'}), 2.38 (ddd, $J = 13.5, 9.9, 7.7 \text{ Hz}$, 1H, CH₂, H_{5'}), 2.06 (ddq, $J = 9.8, 6.9, 4.8 \text{ Hz}$, 1H, CH, H_{4'}), 1.17

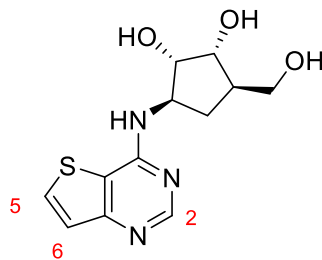
(app. dt, $J = 13.4, 6.7$ Hz, 1H, CH₂, H_{5'}) ppm. ¹³C NMR (151 MHz, Methanol-*d*₄) δ 161.4 (C), 156.3 (CH), 155.7 (C), 132.0 (C), 129.5 (2 x CH), 129.2 (2 x CH), 128.8 (CH), 117.0 (C), 76.5 (CH), 72.8 (CH), 62.1 (CH₂), 56.3 (CH), 44.7 (CH), 29.4 (CH₂) ppm. HRMS (ESI+) calculated for C₁₆H₁₈ClN₃NaO₃ 358.0929, found 358.0945; Method A t_R 2.22 = min; Purity (AUC) \geq 95%.

(1*S*,2*R*,3*R*,5*R*)-3-(Hydroxymethyl)-5-(thieno[2,3-*d*]pyrimidin-4-ylamino)cyclopentane-1,2-diol (355)



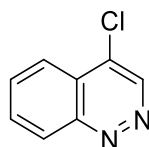
DIPEA (0.08 mL, 0.48 mmol) was added to (1*R*, 2*S*, 3*R*, 4*R*)-2,3-dihydroxy-4-(hydroxymethanol)-1-aminocyclopentane hydrochloride (38 mg, 0.21 mmol) and 4-chlorothieno[2,3-*d*]pyrimidine (53 mg, 0.31 mmol) in DMSO (0.7 mL). The reaction mixture was heated at 120 °C in the MW for 1 h. Purification by reverse phase column chromatography (biotage SNAP-Ultra C18 12 g, eluted with 0-40% MeOH in water, 3 CV, gradient over 10 CV, 6 CV) followed by acidic ion exchange column (SCX, 1 g) washing with MeOH followed by 2.5 M NH₃ in MeOH to afford the title compound (44 mg, 76%, 0.16 mmol) as a pale green solid. m.p. 192 °C. $[\alpha]^{23}_D$ -54.0° (c=0.5, MeOH). IR (thin film) $\nu = 3318, 3105, 2924, 2854, 1594, 1541, 1510$ cm⁻¹. ¹H NMR (600 MHz, DMSO-*d*₆) δ 8.32 (s, 1H, ArH, H₂), 7.81 (d, $J = 7.6$ Hz, 1H, NH), 7.65 (d, $J = 6.0$ Hz, 1H, ArH), 7.55 (d, $J = 5.9$ Hz, 1H, ArH), 4.66 (m, 2H, OH), 4.53 – 4.46 (m, 1H, CH, H_{1'}), 4.45 (d, $J = 4.8$ Hz, 1H, OH), 3.81 (dt, $J = 7.4, 5.4$ Hz, 1H, CH, H_{2'}), 3.74 (q, $J = 4.6$ Hz, 1H, CH, H_{3'}), 3.43 (m, 2H, CH₂, H_{6'}), 2.19 (ddd, $J = 13.0, 8.4$ Hz, 1H, CH₂, H_{5'}), 1.96 (dddd, $J = 14.5, 8.6, 5.9, 4.4$ Hz, 1H, CH, H_{4'}), 1.18 (ddd, $J = 13.1, 8.7$ Hz, 1H, CH₂, H_{5'}) ppm. ¹³C NMR (151 MHz, DMSO-*d*₆) δ 166.0 (C), 157.5 (C), 154.2 (CH), 122.8 (CH), 120.0 (CH), 116.5 (C), 76.4 (CH), 72.5 (CH), 63.4 (CH₂), 55.8 (CH), 45.7 (CH), 30.5 (CH₂) ppm. HRMS (ESI+) calculated for C₁₂H₁₆N₃O₃S 282.0912 found 282.0915; Method C $t_R = 0.59$ min; Purity (AUC) \geq 95%.

(1*S*,2*R*,3*R*,5*R*)-3-(Hydroxymethyl)-5-(thieno[3,2-*d*]pyrimidin-4-ylamino)cyclopentane-1,2-diol (356)



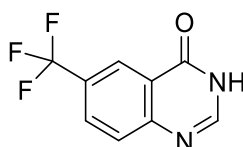
DIPEA (0.08 mL, 0.44 mmol) was added to (1*R*, 2*S*, 3*R*, 4*R*)-2,3-dihydroxy-4-(hydroxymethanol)-1-aminocyclopentane hydrochloride (35 mg, 0.19 mmol) and 4-chlorothieno[3,2-*d*]pyrimidine (49 mg, 0.29 mmol) in DMSO (0.6 mL). The reaction mixture was heated at 120 °C in the MW for 1 h. Purification by reverse phase column chromatography (biotage SNAP-Ultra C18 12 g, eluted with 0-10% MeOH in water, 6 CV gradient over 10 CV, 3 CV) followed by an acidic ion exchange column (SCX, 1 g), washing with MeOH, followed by 2.5 M NH₃ in MeOH to afford the title compound (35 mg, 64%, 0.12 mmol) as a white solid. m.p. 192 °C. $[\alpha]^{23}_{\text{D}} -33.2^{\circ}$ ($c=0.5$, MeOH). IR (thin film) $\nu = 3364, 3285, 3107, 2907, 1597, 1542, 1514 \text{ cm}^{-1}$. ¹H NMR (600 MHz, DMSO-*d*₆) δ 8.41 (s, 1H, ArH, H₂), 8.09 (d, $J = 5.4 \text{ Hz}$, 1H, ArH, H₆), 7.75 (d, $J = 7.7 \text{ Hz}$, 1H, NH), 7.36 (d, $J = 5.4 \text{ Hz}$, 1H, ArH, H₅), 4.71 – 4.60 (m, 2H, OH), 4.51 (app. t, $J = 7.9 \text{ Hz}$, 1H, CH, H_{1'}), 4.42 (d, $J = 4.8 \text{ Hz}$, 1H, OH), 3.83 (dt, $J = 7.2, 5.0 \text{ Hz}$, 1H, CH, H_{2'}), 3.74 (q, $J = 4.7 \text{ Hz}$, 1H, CH, H_{3'}), 3.42 (m, 2H, CH₂, H_{6'}), 2.20 (app. dt, $J = 13.1, 8.5 \text{ Hz}$, 1H, CH₂, H_{5'}), 1.96 (tt, $J = 8.3, 3.4 \text{ Hz}$, 1H, CH, H_{4'}), 1.19 (ddd, $J = 13.1, 8.5 \text{ Hz}$, 1H, CH₂, H_{5'}) ppm. ¹³C NMR (151 MHz, DMSO-*d*₆) δ 159.7 (C), 157.4 (C), 154.9 (CH), 133.3 (CH), 124.8 (CH), 115.1 (C), 76.2 (CH), 72.6 (CH), 63.5 (CH₂), 55.8 (CH), 45.6 (CH), 30.6 (CH₂) ppm. HRMS (ESI+) calculated for C₁₂H₁₆N₃O₃S 282.0912, found 282.0911; Method C $t_{\text{R}} = 0.44 \text{ min}$; Purity (AUC) $\geq 95\%$.

4-Chlorocinnoline (357)

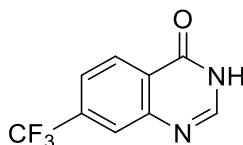


A suspension of 4-hydroxycinnoline (115 mg, 0.79 mmol) in POCl₃ (1.8 mL, 18.89 mmol) was heated at 100 °C for 3 h. After cooling, the mixture was concentrated, adjusted to pH 6 with aqueous ammonia and extracted with ethyl acetate. The combined organic layers were washed with water and brine, dried, filtered and concentrated to yield the title product (110 mg, 0.67 mmol, 85%) as a sticky black solid. IR (thin film) ν = 2711, 1622, 1560 cm⁻¹. ¹H NMR (600 MHz, Chloroform-*d*) δ 9.39 (s, 1H, ArH, H₃), 8.63 (d, *J* = 8.5 Hz, 1H, ArH, H₅), 8.24 (dd, *J* = 8.4, 1.3 Hz, 1H, ArH, H₈), 8.01 – 7.95 (m, 1H, ArH, H₇), 7.95 – 7.90 (m, 1H, ArH, H₆) ppm. ¹³C NMR (151 MHz, Chloroform-*d*) δ 150.8 (C), 144.3 (CH), 135.2 (C), 132.4 (CH), 131.8 (CH), 130.0 (CH), 125.0 (C), 123.0 (CH) ppm. LCMS Method A *t*_R = 1.24 min; Purity (AUC) \geq 95%.

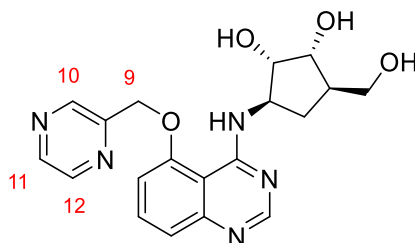
6-(Trifluoromethyl)quinazolin-4-ol (360)



2-Amino-5-(trifluoromethyl)benzoic acid (106 mg, 0.52 mmol) and formamidine acetate (108 mg, 1.03 mmol) were added to 2-methoxyethanol (2 mL, 0.5 mmol). The resulting solution was heated at 120 °C for 18 h. The reaction mixture was passed through an acidic ion exchange cartridge (SCX, 2 g) with MeOH. The product was eluted with 3.5 M NH₃ in MeOH. The NH₃ layer was concentrated and purified by column chromatography (biotage SNAP KP-Sil 10 g, eluted with 0-100% EtOAc in cyclohexane, 5 CV, gradient over 18 CV, 2 CV) to afford the title compound (42 mg, 38%, 0.20 mmol) as a white solid. IR (thin film) ν = 3378, 2926, 2855, 1729, 1697, 1618 cm⁻¹. ¹H NMR (600 MHz, DMSO-*d*₆) δ (12.6, 1H, NH), 8.37 (d, *J* = 2.3 Hz, 1H, ArH, H₂), 8.26 (s, 1H, ArH, H₅), 8.12 (dd, *J* = 8.6, 2.3 Hz, 1H, ArH, H₇), 7.87 (d, *J* = 8.5 Hz, 1H, ArH, H₈) ppm. ¹³C NMR (151 MHz, DMSO-*d*₆) δ 160.7 (C), 151.7 (C), 148.4 (CH), 130.79 (q, *J* = 3.4 Hz, CH), 129.2 (CH), 127.1 (q, *J* = 32.6 Hz, C_{fz}), 124.3 (q, *J* = 272 Hz, C), 123.7 (q, *J* = 4.2 Hz, CH), 123.2 (C) ppm. HRMS (ESI⁺) calculated for C₉H₆F₃N₂O 215.0432 found 215.0428; Method C *t*_R = 1.12 min; Purity (AUC) \geq 95%.

7-(Trifluoromethyl)quinazolin-4-ol (362)

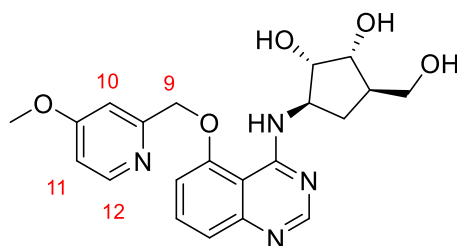
2-Amino-4-trifluoromethylbenzoic acid (103 mg, 0.50 mmol) and formamidine acetate (105 mg, 1.00 mmol) were added to 2-methoxyethanol (2 mL, 0.5 mmol). The resulting solution was heated at 120 °C for 18 h. The reaction mixture was passed through an acidic ion exchange cartridge (SCX, 2 g) and the product was eluted with MeOH. The MeOH layer was concentrated, triturated with water, filtered and washed with Et₂O to afford the title compound (43 mg, 40%, 0.20 mmol) as a white solid. IR (thin film) ν = 3071, 2662, 1702, 1607, 1567 cm⁻¹. ¹H NMR (600 MHz, DMSO-*d*₆) δ 12.57 (s, 1H, NH), 8.33 (d, *J* = 8.3 Hz, 1H, ArH, H₅), 8.23 (d, *J* = 3.5 Hz, 1H, ArH, H₂), 8.00 (s, 1H, ArH, H₈), 7.83 (dd, *J* = 8.4, 1.8 Hz, 1H, ArH, H₆) ppm. ¹³C NMR (151 MHz, DMSO-*d*₆) δ 160.5 (C), 149.3 (C), 147.6 (CH), 134.5 (q, *J* = 32.1 Hz, C), 128.2 (CH), 124 (q, *J* = 274 Hz, CF₃), 126.0 (C), 124.9 (q, *J* = 4.1 Hz, CH), 123.0 (q, *J* = 3.4 Hz, CH) ppm. HRMS (ESI+) calculated for C₉H₆F₃N₂O 215.0427, found 215.0437; Method A *t*_R = 2.29 min; Purity (AUC) \geq 95%.

(1*S*,2*R*,3*R*,5*R*)-3-(Hydroxymethyl)-5-((5-(pyrazin-2-ylmethoxy)quinazolin-4-yl)amino)cyclopentane-1,2-diol (363)

PyBOP (170 mg, 0.33 mmol) and DBU (0.10 mL, 0.9 mmol) were added to 5-(pyrazin-2-ylmethoxy)quinazolin-4-ol (61 mg, 0.24 mmol) and (1*R*, 2*S*, 3*R*, 4*R*)-2,3-dihydroxy-4-(hydroxymethyl)-1-aminocyclopentane hydrochloride (40 mg, 0.22 mmol) in DMF (1.1 mL) and stirred for 18 h. The resulting precipitate

was filtered and washed with Et₂O to yield the title compound (49 mg, 58%, 0.13 mmol) as a white solid. $[\alpha]^{20}_{\text{D}} -22.2^{\circ}$ ($c=0.5$, DMSO). IR (thin film) $\nu = 3324, 2878, 1649, 1614, 1579, 1568, 1531 \text{ cm}^{-1}$. ¹H NMR (600 MHz, DMSO-*d*₆) δ 8.84 (d, $J = 1.5 \text{ Hz}$, 1H, ArH, H₁₀), 8.78 (dd, $J = 2.6, 1.5 \text{ Hz}$, 1H, ArH, H₁₁), 8.70 (d, $J = 2.5 \text{ Hz}$, 1H, ArH, H₁₂), 8.68 (d, $J = 7.3 \text{ Hz}$, 1H, NH), 8.38 (s, 1H, ArH, H₂), 7.69 (dd, $J = 8.1 \text{ Hz}$, 1H, ArH, H₇), 7.28 (d, $J = 8.2 \text{ Hz}$, 1H, ArH, H₈), 7.13 (d, $J = 7.9 \text{ Hz}$, 1H, ArH, H₆), 5.64 – 5.50 (m, 2H, CH₂, H₉), 4.74 (d, $J = 5.0 \text{ Hz}$, 1H, OH), 4.67 (t, $J = 5.1 \text{ Hz}$, 1H, OH), 4.55 (ddt, $J = 7.8 \text{ Hz}$, 1H, CH, H_{1'}), 4.48 (d, $J = 4.1 \text{ Hz}$, 1H, OH), 3.79 – 3.73 (m, 2H, H_{2'}, H_{3'}), 3.42 (dd, $J = 14.3, 5.3 \text{ Hz}$, 2H, CH₂, H_{6'}), 2.26 (app dt, $J = 13.1, 8.4 \text{ Hz}$, 1H, CH₂, H_{5'}), 1.99 (dt, $J = 8.8, 3.7 \text{ Hz}$, 1H, CH, H_{4'}), 1.18 (app dt, $J = 13.1, 8.5 \text{ Hz}$, 1H, CH₂, H_{5'}) ppm. ¹³C NMR (151 MHz, DMSO-*d*₆) δ 159.8 (C), 155.8 (CH), 155.5 (C), 152.0 (C), 151.4 (C), 144.9 (CH), 144.7 (CH), 144.2 (CH), 133.2 (CH), 120.8 (CH), 107.5 (CH), 106.7 (C), 77.1 (CH), 72.7 (CH), 69.1 (CH₂), 63.1 (CH₂), 56.1 (CH), 45.6 (CH), 30.6 (CH₂) ppm. HRMS (ESI+) calculated for C₁₉H₂₂N₅O₄ 384.1666 found 384.1671; Method A $t_{\text{R}} = 1.59 \text{ min}$; Purity (AUC) $\geq 95\%$.

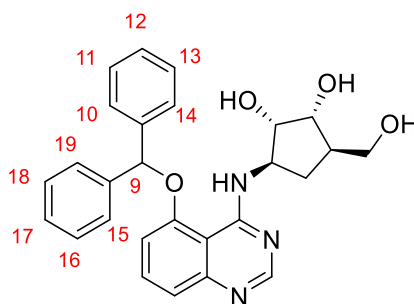
(1*S*,2*R*,3*R*,5*R*)-3-(Hydroxymethyl)-5-((5-((4-methoxy-2-pyridyl)methoxy)quinazolin-4-yl)amino)cyclopentane-1,2-diol (366)



PyBOP (149 mg, 0.29 mmol) and DBU (0.10 mL, 0.8 mmol) were added to 5-[(4-methoxy-2-pyridyl)methoxy]quinazolin-4-ol (54 mg, 0.19 mmol) and (1*R*, 2*S*, 3*R*, 4*R*)-2,3-dihydroxy-4-(hydroxymethanol)-1-aminocyclopentane hydrochloride (35 mg, 0.19 mmol) in DMF (1.0 mL) and stirred for 5 h. The reaction mixture was loaded directly onto an acidic ion exchange cartridge (SCX, 5 g) and washed with water:methanol 1:1 (80 mL). The product was eluted with a mixture of 2 M NH₃/MeOH in water (80 mL). Purification of the ammonia layer by column chromatography (biotage SNAP-Ultra C18 12 g, eluted with 0-80%

MeOH in water, 1 CV gradient over 12 CV, 2 CV) to afford the title compound (21 mg, 27%, 0.05 mmol) as a brown oil. $[\alpha]^{20}_{\text{D}} -2.77^{\circ}$ ($c=0.5$, MeOH). IR (thin film) $\nu = 3257, 2916, 1581, 1531 \text{ cm}^{-1}$. $^1\text{H NMR}$ (600 MHz, Methanol- d_4) δ 8.54 (d, $J = 5.8$ Hz, 1H, ArH, H₁₂), 8.46 (s, 1H, ArH, H₂), 7.79 (dd, $J = 8.3$ Hz, 1H, ArH, H₇), 7.33 (d, $J = 8.4$ Hz, 1H, ArH, H₈), 7.23 (d, $J = 8.1$ Hz, 1H, ArH, H₆), 7.18 (d, $J = 2.5$ Hz, 1H, ArH, H₁₀), 7.04 (dd, $J = 5.8, 2.5$ Hz, 1H, ArH, H₁₁), 5.42 (s, 2H, CH₂, H₉), 4.72 (m, 1H, CH, H_{1'}), 3.94 (s, 3H, CH₃), 3.94 – 3.92 (m, 2H, CH, H_{2'}, H_{3'}), 3.66 – 3.55 (m, 2H, CH₂, H_{6'}), 2.43 (ddd, $J = 13.3, 8.4$ Hz, 1H, CH₂, H_{5'}), 2.23 – 2.15 (m, 1H, CH, H_{4'}), 1.35 (ddd, $J = 13.3, 8.8$ Hz, 1H, CH₂, H_{5'}) ppm. $^{13}\text{C NMR}$ (151 MHz Methanol- d_4) δ 168.9 (C), 161.9 (C), 158.1 (C), 157.6 (C), 155.8 (CH), 152.3 (CH), 150.8 (C), 135.2 (CH), 119.6 (CH), 111.1 (CH), 110.5 (CH), 109.3 (CH), 107.8 (C), 78.9 (CH), 74.5 (CH), 72.7 (CH₂), 64.7 (CH₂), 58.3 (CH), 56.5 (CH₃), 47.0 (CH), 31.5 (CH₂) ppm. HRMS (ESI+) calculated for C₂₁H₂₅N₄O₅ 413.1819, found 413.1807; Method A $t_{\text{R}} = 1.42$ min; Purity (AUC) $\geq 95\%$.

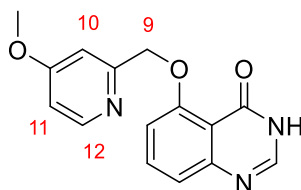
(1*R*,2*S*,3*R*,5*R*)-3-((5-(Benzhydryloxy)quinazolin-4-yl)amino)-5-(hydroxymethyl)cyclopentane-1,2-diol (367)



PyBOP (191 mg, 0.37 mmol) and DBU (0.15 mL, 0.98 mmol) were added to 5-benzhydryloxyquinazolin-4-ol (88 mg, 0.27 mmol) and (1*R*, 2*S*, 3*R*, 4*R*)-2,3-dihydroxy-4-(hydroxymethanol)-1-aminocyclopentane hydrochloride (45 mg, 0.25 mmol) in DMF (1.2 mL) and stirred for 4 h. Purification by column chromatography (biotage SNAP KP-Sil 25 g, eluted with 0-10% 10% NH₃ in MeOH in CH₂Cl₂, 1 CV, gradient over 15 CV, 5 CV) to yield the title compound (51 mg, 45%, 0.11 mmol) as an oil. $[\alpha]^{20}_{\text{D}} +8.31^{\circ}$ ($c=0.5$, MeOH). IR (thin film) ν

= 3380, 2924, 1613, 1584, 1535 cm^{-1} . ^1H NMR (600 MHz, Methanol- d_4) δ 8.36 (s, 1H, ArH, H₂), 7.55 – 7.48 (m, 5H, H₇, H₁₅, H₁₉, H₁₀, H₁₄), 7.45 (t, J = 7.6 Hz, 4H, ArH, H₁₁, H₁₃, H₁₆, H₁₈), 7.41 – 7.35 (m, 2H, ArH, H₁₂, H₁₇), 7.26 (dd, J = 8.4, 0.9 Hz, 1H, ArH, H₈), 6.93 (d, J = 8.1 Hz, 1H, ArH, H₆), 6.69 (s, 1H, CH, H₉), 4.52 (dt, J = 9.5, 7.8 Hz, 1H, CH, H₁'), 3.72 (dd, J = 5.5, 4.3 Hz, 1H, CH, H₂'), 3.49 (dd, J = 7.5, 5.5 Hz, 1H, CH, H₃'), 3.48 – 3.37 (m, 2H, CH₂, H₆'), 2.31 (app dt, J = 13.2, 8.4 Hz, 1H, CH₂, H₅'), 2.16 – 2.04 (m, 1H, CH, H₄'), 0.80 (app dt, J = 13.2, 9.1 Hz, 1H, CH₂, H₅') ppm. ^{13}C NMR (151 MHz, Methanol- d_4) δ 160.5 (C), 155.2 (C), 154.1 (CH), 149.1 (C), 139.5 (C), 139.3 (C), 133.3 (CH), 128.8 (2 x CH), 128.8 (2 x CH), 128.4 (CH), 128.3 (CH), 127.1 (2 x CH), 126.9 (2 x CH), 117.9 (CH), 109.9 (CH), 106.3 (C), 83.9 (CH), 77.3 (CH), 72.7 (CH), 63.5 (CH₂), 56.2 (CH), 45.3 (CH), 30.0 (CH₂) ppm. HRMS (ESI+) calculated for C₂₇H₂₈N₃O₄ 458.2074, found 458.2077; Method A t_R = 2.28 min; Purity (AUC) \geq 95%

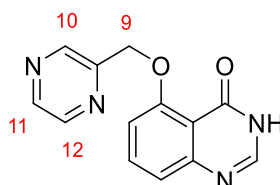
5-((4-Methoxypyridin-2-yl)methoxy)quinazolin-4-ol (371)



Sodium hydride (60% in oil, 61 mg, 1.52 mmol) was added to DMSO (1.5 mL, 0.2 M). After 2 min, (4-methoxy-2-pyridyl)methanol (127 mg, 0.91 mmol) was added. After 5 min, 5-fluoro-4-hydroxyquinazoline (50 mg, 0.30 mmol) was added and the dark red mixture was heated at 50 °C for 6 h. Sat aq. NH₄Cl (20 mL) was added and the precipitate in the water layer was filtered and dried to yield the title compound (68 mg, 78%) as a white solid. IR (thin film) ν = 3352, 3074, 2949, 2879, 1674, 1621, 1600, 1570 cm^{-1} . ^1H NMR (600 MHz, DMSO) δ 12.04 (s, 1H, NH), 8.37 (d, J = 5.7 Hz, 1H, H₂), 8.01 (d, J = 2.6 Hz, 1H, H₁₂), 7.83 (d, J = 2.6 Hz, 1H, H₁₀), 7.71 (t, J = 8.2 Hz, 1H, H₇), 7.25 – 7.21 (m, 1H, H₈), 7.17 – 7.12 (m, 1H, H₆), 6.90 (dd, J = 5.7, 2.6 Hz, 1H, ArH, H₁₁), 5.23 (s, 2H, CH₂, H₉), 3.90 (s, 3H, CH₃) ppm. ^{13}C NMR (151 MHz, DMSO) δ 166.6 (C), 159.6 (C), 159.5 (C), 158.4 (C), 151.8 (C), 150.5 (CH), 146.3 (CH), 135.1 (CH), 120.0 (CH), 113.1 (C), 110.0 (CH), 109.5 (CH), 107.4 (CH), 70.7 (CH₂), 55.7 (CH₃) ppm. HRMS

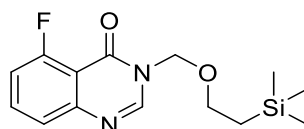
(ESI+) calculated for C₁₅H₁₄N₃O₃ 284.1035, found 284.1037; Method B t_R = 1.27 min; Purity (AUC) ≥ 95%.

5-(Pyrazin-2-ylmethoxy)quinazolin-4-ol (373)



1 M TBAF in THF (1.8 mL, 1.8 mmol) was added dropwise to a solution of 5-(pyrazin-2-ylmethoxy)-3-(2-trimethylsilyloxyethyl)quinazolin-4-one (200 mg, 0.52 mmol) in THF (2.6 mL). The solution was stirred for 18 h at 60 °C. Water (20 mL) was added and the flask was cooled in the fridge for 1 h. The resulting precipitate was filtered to yield the title compound (103 mg, 78%, 0.41 mmol) as a white solid. IR (thin film) ν = 3085, 2902, 1675, 1604, 1584, 1567 cm⁻¹. ¹H NMR (600 MHz, DMSO-*d*₆) δ 12.01 (d, *J* = 3.6 Hz, 1H, NH), 9.29 (d, *J* = 1.4 Hz, 1H, ArH, H₁₀), 8.67 – 8.64 (m, 2H, ArH, H₁₁, H₁₂), 8.02 (d, *J* = 3.7 Hz, 1H, ArH, H₂), 7.72 (dd, *J* = 8.2 Hz, 1H, ArH, H₇), 7.26 (d, *J* = 8.0 Hz, 1H, ArH, H₈), 7.19 (d, *J* = 8.2 Hz, 1H, ArH, H₆), 5.40 (d, *J* = 12.1 Hz, 2H, CH₂, H₉) ppm. ¹³C NMR (151 MHz, DMSO-*d*₆) δ 159.5 (C), 158.3 (C), 153.0 (C), 151.9 (C), 146.4 (CH), 144.4 (CH), 144.2 (CH), 143.9 (CH), 135.1 (CH), 120.4 (CH), 113.2 (C), 110.3 (CH), 69.7 (CH₂) ppm. HRMS (ESI+) calculated for C₁₃H₁₁N₄O₂ 255.0877, found 255.0883; Method A t_R = 1.90 min; Purity (AUC) ≥ 95%.

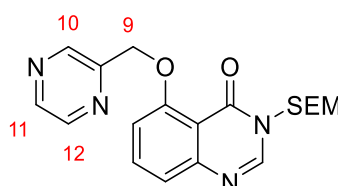
5-Fluoro-3-((2-(trimethylsilyl)ethoxy)methyl)quinazolin-4(3H)-one (374)



Sodium hydride (60% in oil, 227 mg, 5.67 mmol) was added to 5-fluoro-4-hydroxyquinazolinone (620 mg, 3.78 mmol) in DMF (10.8 mL). After 10 min, SEM-

Cl (0.7 mL, 3.85 mmol) was added dropwise and the solution was stirred at 40 °C for 30 min. The reaction mixture was poured into water (100 mL) and extracted with Et₂O (4 x 30 mL), dried with MgSO₄, concentrated and purified by column chromatography (biotage SNAP KP-Sil 25 g (0-80% EtOAc in cyclohexane, 1 CV, gradient over 18 CV, 2 CV) to yield the title compound (862 mg, 78%, 2.93 mmol) as a clear oil. IR (thin film) ν = 2953, 1688, 1618, 1560 cm⁻¹. ¹H NMR (600 MHz, Chloroform-*d*) δ 8.15 (s, 1H, ArH, H₂), 7.73 (m, 1H, ArH, H₇), 7.54 (m, 1H, ArH, H₈), 7.19 (m, 1H, ArH, H₆), 5.44 (s, 2H, CH₂, NCH₂O), 3.76 – 3.68 (m, 2H, CH₂, CH₂CH₂Si(CH₃)₃), 1.05 – 0.96 (m, 2H, CH₂, CH₂CH₂Si(CH₃)₃), 0.02 (s, 9H, CH₃, CH₂CH₂Si-(CH₃)₃) ppm. ¹³C NMR (151 MHz, Chloroform-*d*) δ 161.5 (d, *J* = 267 Hz, C), 158.2 (d, *J* = 4.1 Hz, C), 150.1 (C), 146.8 (CH), 135.0 (d, *J* = 10.4 Hz, CH), 123.6 (d, *J* = 4.2 Hz, CH), 114.2 (d, *J* = 20.9 Hz, CH), 111.7 (d, *J* = 5.7 Hz, C), 74.3 (CH₂), 67.7 (CH₂), 18.1 (CH₂), -1.4 (3 x CH₃) ppm. HRMS (ESI+) calculated for C₁₄H₂₀FN₂O₂Si 295.1273 found 295.1271; Method A *t*_R = 2.91 min; Purity (AUC) \geq 95%.

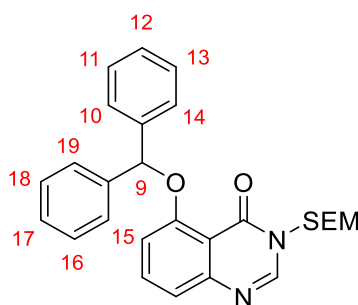
4-Hydroxy-5-(pyrazin-2-ylmethoxy)-3-((2-(trimethylsilyl)ethoxy)methyl)quinazolin-3-ium (375)



Sodium hydride (60% in oil, 109 mg, 2.72 mmol) was added to a stirred solution of 2-pyrazinylmethanol (224 mg, 2.04 mmol) in THF (3.4 mL). 5-Fluoro-3-(2-trimethylsilylethoxymethyl)quinazolin-4-one (200 mg, 0.68 mmol) was added and the solution was stirred at 40 °C for 8 h. The reaction mixture was concentrated and purified by column chromatography (biotage SNAP KP-Sil 10 g (0-10% EtOH in CH₂Cl₂, 1 CV, gradient over 15 CV, 5 CV) to afford the title compound (227 mg, 87%, 0.59 mmol). IR (thin film) ν = 2951, 2894, 1697, 1603, 1566 cm⁻¹. ¹H NMR (500 MHz, Chloroform-*d*) δ 9.33 (app dt, *J* = 1.5, 0.7 Hz, 1H, ArH, H₁₀), 8.59 – 8.56 (m, 2H, ArH, H₁₁, H₁₂), 8.15 (s, 1H, ArH, H₂), 7.69 (dd, *J*

= 8.2 Hz, 1H, ArH, H₇), 7.37 (dd, J = 8.1, 1.0 Hz, 1H, ArH, H₈), 7.02 (dd, J = 8.3, 1.0 Hz, 1H, ArH, H₆), 5.44 (s, 2H, CH₂, NCH₂O), 5.42 (s, 2H, CH₂, H₉), 3.81 – 3.66 (m, 2H, CH₂, CH₂CH₂Si(CH₃)₃), 1.07 – 0.89 (m, 2H, CH₂, CH₂CH₂Si(CH₃)₃), 0.02 (s, 9H, CH₃) ppm. ¹³C NMR (151 MHz, Chloroform-*d*) δ 159.1 (C), 158.5 (C), 152.3 (C), 150.8 (C), 146.8 (CH), 144.1 (CH), 144.0 (CH), 143.5 (CH), 134.9 (CH), 120.9 (CH), 112.4 (C), 110.2 (CH), 74.4 (CH₂), 70.0 (CH₂), 67.5 (CH₂), 18.1 (CH₂), -1.4 (3 x CH₃) ppm. HRMS (ESI+) calculated for C₁₉H₂₄N₄NaO₃Si 407.1510, found 407.1515; Method A t_R = 2.92 min; Purity (AUC) ≥ 95%.

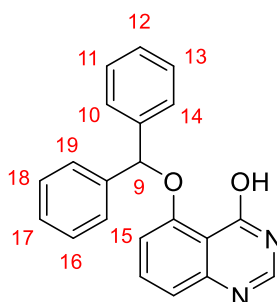
5-(Benzhydryloxy)-3-((2-(trimethylsilyl)ethoxy)methyl)quinazolin-4(3H)-one (376)



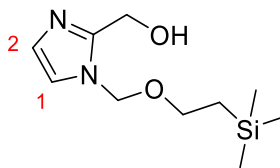
Sodium hydride (60% in oil, 68 mg, 1.70 mmol) was added to a stirred solution of diphenyl methanol (250 mg, 1.36 mmol) in DMF (3.4 mL). After 10 min 5-fluoro-3-((2-(trimethylsilyl)ethoxymethyl)quinazolin-4-one (200 mg, 0.68 mmol) was added dropwise and the solution was stirred at rt for 1.5 h. Water (30 mL) and brine (5 mL) were added and the product was extracted with Et₂O (3 x 35 mL), dried with MgSO₄ and concentrated. Purification by column chromatography (biotage SNAP KP-Sil 10 g (0-50% EtOAc in cyclohexane, 2 CV, gradient over 15 CV, 2 CV) to afford the title compound (232 mg, 74%, 0.51 mmol) as a pale-yellow solid. IR (thin film) ν = 2951, 1682, 1602, 1562 cm⁻¹. ¹H NMR (600 MHz, Chloroform-*d*) δ 8.12 (s, 1H, ArH, H₂), 7.68 (d, J = 7.3 Hz, 4H, ArH, H₁₀, H₁₄, H₁₅, H₁₉), 7.50 (dd, J = 8.2 Hz, 1H, ArH, H₇), 7.36 (dd, J = 7.8 Hz, 4H, ArH, H₁₁, H₁₃, H₁₆, H₁₈), 7.28 – 7.20 (m, 3H, ArH, H₈, H₁₂, H₁₇), 6.94 (d, J = 8.2 Hz, 1H, ArH, H₆), 6.44 (s, 1H, CH, H₉), 5.47 (s, 2H, CH₃, NCH₂O), 3.80 – 3.73 (m, 2H, CH₂, CH₂CH₂Si(CH₃)₃), 1.07 – 1.00 (m, 2H, CH₂, CH₂CH₂Si(CH₃)₃), 0.05 (s, 9H, CH₃, CH₂CH₂Si(CH₃)₃) ppm. ¹³C NMR (151 MHz, Chloroform-*d*) δ

159.1 (C), 158.1 (C), 150.6 (C), 146.5 (CH), 141.3 (2 x C), 134.5 (CH), 128.7 (4 x CH), 127.7 (2 x CH), 126.5 (4 x CH), 119.9 (CH), 112.8 (C), 111.9 (CH), 82.4 (CH), 74.4 (CH₂), 67.3 (CH₂), 18.0 (CH₂), -1.3 (3 x CH₃) ppm. HRMS (ESI+) calculated for C₂₇H₃₁N₂O₃Si 459.2098 found 459.2086; Method A t_R = 3.36 min; Purity (AUC) ≥ 95%.

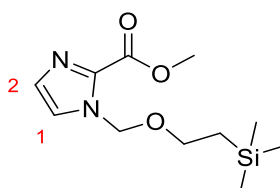
5-(Benzhydryloxy)quinazolin-4-ol (377)



1M TBAF in THF (1.0 mL, 1.0 mmol) was added dropwise to a solution of 5-benzhydryloxy-3-(2-trimethylsilylethoxymethyl)quinazolin-4-one (135 mg, 0.29 mmol) in THF (2.0 mL). The solution was stirred for 18 h at 60 °C. Water (15 mL) and brine (5 mL) were added and the product was extracted with EtOAc (3 x 20 mL). The combined extracts were washed with water (10 mL), dried with MgSO₄ and concentrated to yield the title compound (97 mg, 100%, 0.29 mmol). IR (thin film) ν = 3027, 2954, 2903, 1670, 1619, 1603, 1555 cm⁻¹. ¹H NMR (600 MHz, Chloroform-*d*) δ 11.13 (s, 1H, NH), 7.97 (s, 1H, ArH, H₂), 7.72 – 7.67 (m, 4H, ArH, H₁₀, H₁₄, H₁₅, H₁₉), 7.53 (dd, *J* = 8.2 Hz, 1H, ArH, H₇), 7.37 (dd, *J* = 7.7 Hz, 4H, H₁₆, H₁₈, H₁₁, H₁₃), 7.31 – 7.24 (m, 3H, ArH, H₈, H₁₂, H₁₇), 6.94 – 6.89 (m, 1H, ArH, H₆), 6.43 (s, 1H, CH, H₉) ppm. ¹³C NMR (151 MHz, Chloroform-*d*) δ 160.9 (C), 157.9 (C), 151.4 (C), 143.9 (CH), 141.3 (2 x C), 134.8 (CH), 128.7 (4 x CH), 127.8 (2 x CH), 126.5 (4 x CH), 120.1 (CH), 113.6 (C), 112.2 (CH), 82.8 (CH) ppm. HRMS (ESI+) calculated for C₂₁H₁₇N₂O₂ 329.1285 found 329.1288; Method A t_R = 2.82 min; Purity (AUC) ≥ 95%.

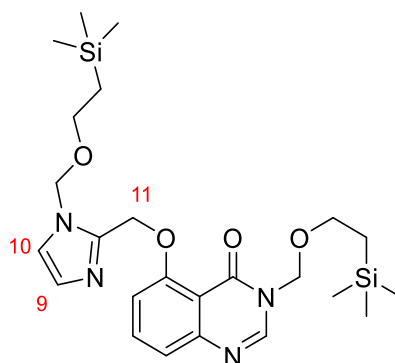
(1-((2-(Trimethylsilyl)ethoxy)methyl)-1H-imidazol-2-yl)methanol (385)

1 M LiAlH₄ in THF (12.4 mL, 12.4 mmol) was added dropwise to a stirred solution of methyl 1-(2-trimethylsilylethoxymethyl)imidazole-2-carboxylate (1.06 g, 4.13 mmol) in THF (6.9 mL) at 0 °C. The solution was allowed to warm to rt and stirred for 1.5 h. The reaction was quenched with Et₂O (10 mL) and water (0.5 mL), carefully added dropwise. After gas evolution subsided, 1 M aq. NaOH (1 mL) was added and stirred for 30 min, followed by water (1.5 mL). The resulting precipitate was filtered through a celite funnel and washed with THF. The filtrate was concentrated, dissolved in CH₂Cl₂ and purified by column chromatography (biotage SNAP KP-Sil 50 g, eluted with 0-10% MeOH in CH₂Cl₂, 1 CV, gradient over 10 CV, 5 CV) to afford the title compound (633 mg, 67%, 2.77 mmol) as a white solid. IR (thin film) $\nu = 3117, 2953, 2828 \text{ cm}^{-1}$. ¹H NMR (600 MHz, Chloroform-*d*) δ 6.98 (d, $J = 1.4 \text{ Hz}$, 1H, ArH, H₁), 6.94 (d, $J = 1.4 \text{ Hz}$, 1H, ArH, H₂), 5.35 (s, 2H, CH₂, NCH₂O), 4.72 (s, 2H, CH₂, CH₂OH), 3.55 – 3.48 (m, 2H, CH₂, CH₂CH₂Si(CH₃)₃), 0.94 – 0.86 (m, 2H, CH₂, CH₂CH₂Si(CH₃)₃), -0.02 (s, 9H, CH₃) ppm. ¹³C NMR (151 MHz, Chloroform-*d*) δ 148.0 (C), 127.3 (CH), 120.6 (CH), 75.1 (CH₂), 66.5 (CH₂), 56.5 (CH₂), 17.8 (CH₂), -1.4 (3 x CH₃) ppm. HRMS (ESI+) calculated for C₁₀H₂₁N₂O₂Si 229.1367, found 229.1356; Method A; Not uv visible.

Methyl 1-((2-(trimethylsilyl)ethoxy)methyl)-1H-imidazole-2-carboxylate (387)

Methyl 1H-imidazole-2-carboxylate (1.50 g, 11.9 mmol) was added portionwise to a stirred solution of sodium hydride (60% in oil, 523 mg, 13.1 mmol) in DMF (30 mL). The solution was stirred at rt for 15 min. 2-(Trimethylsilyl)ethoxymethylchloride (2.3 mL, 13.1 mmol) was added dropwise and the solution was stirred at rt for 1 h. Water (300 mL) was added and the product was extracted with Et₂O (3 x 90 mL). The organic layers were combined and washed with H₂O (50 mL), dried and concentrated. Purification by column chromatography (biotage SNAP KP-Sil 50 g, eluted with 0-80% EtOAc in cyclohexane, 4 CV, gradient over 18 CV, 2 CV) to afford the title compound (2.10 g, 69%, 8.2 mmol) as a clear oil. IR (thin film) $\nu = 2954, 1718 \text{ cm}^{-1}$. ¹H NMR (600 MHz, Chloroform-*d*) δ 7.30 (d, *J* = 1.1 Hz, 1H, ArH, H₁), 7.22 (d, *J* = 1.1 Hz, 1H, ArH, H₂), 5.82 (s, 2H, CH₂, NCH₂O), 3.97 (s, 3H, CH₃, O-CH₃), 3.63 – 3.55 (m, 2H, CH₂, CH₂CH₂Si(CH₃)₃), 0.97 – 0.92 (m, 2H, CH₂, CH₂CH₂Si(CH₃)₃), 0.00 (s, 9H, CH₃, Si-CH₃) ppm. ¹³C NMR (151 MHz, Chloroform-*d*) δ 159.6 (C), 136.2 (C), 130.0 (CH), 124.4 (CH), 76.9 (CH₂), 66.9 (CH₂), 52.4 (CH₃), 17.8 (CH₂), -1.5 (3 x CH₃) ppm. HRMS (ESI+) calculated for C₁₁H₂₁N₂O₃Si 257.1316, found 257.1320; Method A *t*_R = 2.76 min; Purity (AUC) \geq 95%.

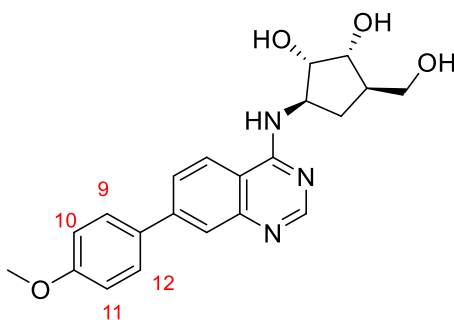
3-((2-(Trimethylsilyl)ethoxy)methyl)-5-((1-((2-(trimethylsilyl)ethoxy)methyl)-1H-imidazol-2-yl)methoxy)quinazolin-4(3H)-one (389)



Sodium hydride (60% in oil, 108 mg, 2.72 mmol) was added to a stirred solution of [1-(2-trimethylsilylethoxymethyl)imidazol-2-yl]methanol (465 mg, 2.04 mmol) in THF (3.4 mL). 5-Fluoro-3-(2-trimethylsilylethoxymethyl)quinazolin-4-one (200 mg, 0.68 mmol) was added and the solution was stirred at 40 °C for 1.5 h.

The reaction mixture was concentrated, dissolved in CH₂Cl₂ (1.5 mL) and purified by column chromatography (biotage SNAP KP-Sil 10 g, eluted with 0-80% EtOAc in cyclohexane, 1 CV, gradient over 18 CV, 2 CV) to afford the title compound (184 mg, 54%, 0.37 mmol) as a clear oil. IR (thin film) ν = 3293, 2953, 1683, 1605, 1563 cm⁻¹. ¹H NMR (600 MHz, Chloroform-*d*) δ 8.11 (s, 1H, CH, H₂), 7.67 (dd, *J* = 8.2 Hz, 1H, CH, H₇), 7.33 (dd, *J* = 8.1, 1.0 Hz, 1H, CH, H₈), 7.25 (dd, *J* = 8.4, 0.9 Hz, 1H, CH, H₆), 7.06 (d, *J* = 1.3 Hz, 1H, ArH, H₉), 7.04 (d, *J* = 1.4 Hz, 1H, ArH, H₁₀), 5.64 (s, 2H, CH₂, NCH₂O), 5.43 (s, 2H, CH₂, H₁₁), 5.39 (s, 2H, CH₂, NCH₂O), 3.72 – 3.65 (m, 2H, CH₂, CH₂CH₂Si(CH₃)₃), 3.52 – 3.46 (m, 2H, CH₂, CH₂CH₂Si(CH₃)₃), 1.00 – 0.96 (m, 2H, CH₂, CH₂CH₂Si(CH₃)₃), 0.90 – 0.84 (m, 2H, CH₂, CH₂CH₂Si(CH₃)₃), 0.02 (s, 9H, CH₃), -0.06 (s, 9H, CH₃) ppm. ¹³C NMR (151 MHz, Chloroform-*d*) δ 159.1 (C), 158.5 (C), 150.6 (C), 146.4 (CH), 142.9 (C), 135.0 (CH), 127.8 (CH), 121.6 (CH), 120.7 (CH), 112.3 (C), 111.2 (CH), 75.7 (CH₂), 74.4 (CH₂), 67.4 (CH₂), 66.3 (CH₂), 64.0 (CH₂), 18.1 (CH₂), 17.9 (CH₂), -1.4 (3 x CH₃), -1.5 (3 x CH₃) ppm. HRMS (ESI+) calculated for C₂₄H₃₉N₄O₄Si₂ 503.2504, found 503.2523; Method A *t*_R = 3.08 min; Purity (AUC) \geq 95%.

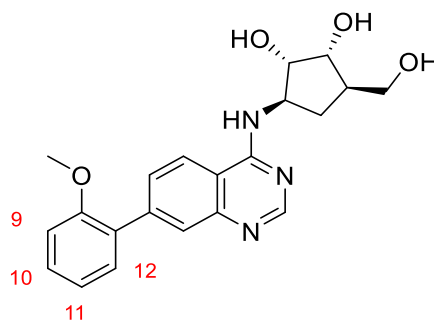
(1*S*,2*R*,3*R*,5*R*)-3-(Hydroxymethyl)-5-((7-(4-methoxyphenyl)quinazolin-4-yl)amino)cyclopentane-1,2-diol (392)



4-Methoxyphenyl boronic acid (38 mg, 0.25 mmol) was added to a solution of (1*R*,2*S*,3*R*,5*R*)-3-[(7-bromoquinazolin-4-yl)amino]-5-(hydroxymethyl)cyclopentane-1,2-diol (44 mg, 0.12 mmol), sodium carbonate (40 mg, 0.37 mmol) and tetrakis(triphenylphosphine)palladium(0) (7 mg, 0.01 mmol) in water (0.6 mL) and 1,4-dioxane (0.6 mL). The solution was heated at 120 °C in the MW for 1 h. Water (15 mL) was added and washed with CH₂Cl₂ (3

an acidic ion exchange column (SCX, 1 g) with MeOH and eluted with 3.5 M NH₃ in MeOH to afford the title compound (31 mg, 72%, 0.08 mmol) as an oil. IR (thin film) $\nu = 3312, 2938, 1620, 1589, 1536 \text{ cm}^{-1}$. ¹H NMR (600 MHz, Methanol-*d*₄) δ 8.47 (s, 1H, ArH, H₂), 8.19 (d, $J = 8.6 \text{ Hz}$, 1H, ArH, H₅), 7.88 (d, $J = 1.9 \text{ Hz}$, 1H, ArH, H₈), 7.79 (dd, $J = 8.6, 1.9 \text{ Hz}$, 1H, ArH, H₆), 7.42 (dd, $J = 7.9 \text{ Hz}$, 1H, ArH, H₁₁), 7.31 (ddd, $J = 7.8, 1.1 \text{ Hz}$, 1H, ArH, H₁₂), 7.26 (dd, $J = 2.1 \text{ Hz}$, 1H, ArH, H₉), 7.01 (ddd, $J = 8.2, 2.6, 0.9 \text{ Hz}$, 1H, ArH, H₁₀), 4.67 (td, $J = 7.9, 6.0 \text{ Hz}$, 1H, CH, H_{1'}), 4.08 – 4.00 (m, 2H, CH, H_{2'}, H_{3'}), 3.89 (s, 3H, CH₃), 3.71 (d, $J = 5.3 \text{ Hz}$, 2H, CH₂, H_{6'}), 2.51 (ddd, $J = 13.3, 9.2, 7.8 \text{ Hz}$, 1H, CH₂, H_{5'}), 2.23 (ddq, $J = 10.0, 8.0, 5.1 \text{ Hz}$, 1H, CH, H_{4'}), 1.49 (app. dt, $J = 13.3, 8.0 \text{ Hz}$, 1H, CH₂, H_{5'}) ppm. ¹³C NMR (151 MHz, Methanol-*d*₄) δ 160.4 (C), 159.9 (C), 154.9 (CH), 148.6 (C), 145.7 (C), 140.7 (C), 129.8 (CH), 125.2 (CH), 123.7 (CH), 122.7 (CH), 119.3 (CH), 114.0 (C), 113.6 (CH), 112.6 (CH), 76.8 (CH), 72.9 (CH), 63.0 (CH₂), 56.4 (CH), 54.4 (CH₃), 45.3 (CH), 29.4 (CH₂) ppm. HRMS (ESI+) calculated for C₂₁H₂₄N₃O₄ 382.1761 found 382.1744; Method A $t_R = 2.07 \text{ min}$; Purity (AUC) $\geq 95\%$.

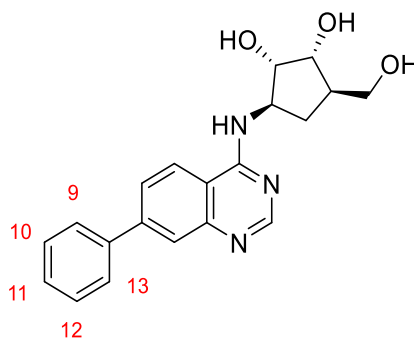
(1*S*,2*R*,3*R*,5*R*)-3-(Hydroxymethyl)-5-((7-(2-methoxyphenyl)quinazolin-4-yl)amino)cyclopentane-1,2-diol (394)



(2-methoxyphenyl)boronic acid (34 mg, 0.23 mmol) was added to a solution of (1*R*,2*S*,3*R*,5*R*)-3-[(7-bromoquinazolin-4-yl)amino]-5-(hydroxymethyl)cyclopentane-1,2-diol (40 mg, 0.11 mmol), sodium carbonate (36 mg, 0.34 mmol) and tetrakis(triphenylphosphine)palladium(0) 7 mg, 0.01 mmol) in water (0.6 mL) and 1,4-dioxane (0.6 mL). The solution was heated at 120 °C in the MW for 1 h. Water (15 mL) was added and washed with CH₂Cl₂

(15 mL). The water layer was concentrated and purified by column chromatography (biotage SNAP-Ultra C18 12 g, eluted with 5-100% MeOH in water, 2 CV gradient over 18 CV, 2 CV) to afford the title compound (7 mg, 16%, 0.02 mmol) as a white solid. IR (thin film) $\nu = 3221, 2931, 1636, 1581 \text{ cm}^{-1}$. ^1H NMR (600 MHz, Methanol- d_4) δ 8.59 (s, 1H, ArH, H₂), 8.24 (d, $J = 8.6 \text{ Hz}$, 1H, ArH, H₆), 7.88 (d, $J = 1.8 \text{ Hz}$, 1H, ArH, H₈), 7.81 (dd, $J = 8.6, 1.5 \text{ Hz}$, 1H, ArH H₇), 7.44 (dddd, $J = 7.7, 1.7 \text{ Hz}$, 2H, ArH, H₁₀, H₁₂), 7.17 (d, $J = 8.2 \text{ Hz}$, 1H, ArH, H₉), 7.11 (ddd, $J = 7.4, 1.1 \text{ Hz}$, 1H, ArH, H₁₁), 4.82 (td, $J = 8.0, 6.5 \text{ Hz}$, 1H, CH, H_{1'}), 4.09 (dd, $J = 6.7, 5.3 \text{ Hz}$, 1H, CH, H_{2'}), 4.03 (dd, $J = 4.9 \text{ Hz}$, 1H, CH, H_{3'}), 3.87 (s, 3H, CH₃), 3.70 (d, $J = 5.4 \text{ Hz}$, 2H, CH₂, H_{6'}), 2.50 (ddd, $J = 13.3, 9.2, 7.9 \text{ Hz}$, 1H, CH₂, H_{5'}), 2.30 – 2.18 (m, 1H, CH, H_{4'}), 1.52 (app. dt, $J = 13.3, 8.0 \text{ Hz}$, 1H, CH₂, H_{5'}) ppm. ^{13}C NMR (151 MHz, Methanol- d_4) δ 160.4 (C), 156.6 (C), 153.0 (CH), 145.1 (C), 143.9 (C), 130.3 (CH), 130.0 (CH), 128.9 (CH), 128.2 (C), 123.4 (CH), 122.0 (CH), 120.8 (CH), 112.7 (C), 111.4 (CH), 76.5 (CH), 72.8 (CH), 62.9 (CH₂), 56.7 (CH), 54.7 (CH₃), 45.3 (CH), 29.2 (CH₂) ppm. HRMS (ESI+) calculated for C₂₁H₂₃N₃O₄ 382.1767 found 382.1765; Method B $t_{\text{R}} = 1.88 \text{ min}$; Purity (AUC) $\geq 95\%$.

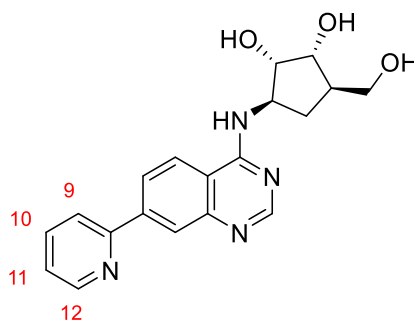
(1*S*,2*R*,3*R*,5*R*)-3-(Hydroxymethyl)-5-((7-phenylquinazolin-4-yl)amino)cyclopentane-1,2-diol (395)



Phenylboronic acid (30 mg, 0.25 mmol) was added to a solution of (1*R*,2*S*,3*R*,5*R*)-3-[(7-bromoquinazolin-4-yl)amino]-5-(hydroxymethyl)cyclopentane-1,2-diol (44 mg, 0.12 mmol), sodium carbonate (40 mg, 0.37 mmol) and tetrakis(triphenylphosphine)palladium(0) (7 mg, 0.01 mmol) in water (0.6 mL) and 1,4-dioxane (0.6 mL). The solution was heated at

120 °C in the MW for 1 h. The reaction mixture was concentrated and purified by column chromatography (biotage SNAP-Ultra C18 12 g, eluted with 5-100% MeOH in water, 2 CV, gradient over 18 CV, 2 CV). The product was further purified by acidic ion exchange chromatography (SCX, 2 g) with MeOH. The product was eluted with 3.5 M NH₃ in MeOH to afford the title compound (27 mg, 0.08, 62% mmol) as an oil. $[\alpha]^{23}_{\text{D}} -69.2^{\circ}$ (c=0.5, MeOH). IR (thin film) $\nu = 3310, 2927, 1622, 1587, 1570, 1536 \text{ cm}^{-1}$. ¹H NMR (600 MHz, Methanol-*d*₄) δ 8.47 (s, 1H, ArH, H₂), 8.20 (d, *J* = 8.6 Hz, 1H, ArH, H₅), 7.90 (d, *J* = 1.8 Hz, 1H, ArH, H₈), 7.80 (dd, *J* = 8.6, 1.9 Hz, 1H, ArH, H₆), 7.77 – 7.72 (m, 2H, ArH, H₉, H₁₃), 7.52 (dd, *J* = 7.7 Hz, 2H, ArH, H₁₀, H₁₂), 7.46 – 7.41 (m, 1H, ArH, H₁₁), 4.67 (td, *J* = 7.9, 6.1 Hz, 1H, CH, H_{1'}), 4.08 – 4.01 (m, 2H, CH, H_{2'}, H_{3'}), 3.71 (d, *J* = 5.3 Hz, 2H, CH₂, H_{6'}), 2.51 (ddd, *J* = 13.3, 9.2, 7.8 Hz, 1H, CH₂, H_{5'}), 2.24 (ddq, *J* = 10.0, 8.0, 5.1 Hz, 1H, CH, H_{4'}), 1.50 (app. dt, *J* = 13.3, 8.0 Hz, 1H, CH₂, H_{5'}) ppm. ¹³C NMR (151 MHz, Methanol-*d*₄) δ 160 (C), 154.9 (CH), 148.7 (C), 145.8 (C), 139.3 (C), 128.8 (2 x CH), 128.2 (CH), 127.0 (2 x CH), 125.2 (CH), 123.7 (CH), 122.8 (CH), 113.9 (C), 76.8 (CH), 72.9 (CH), 63.0 (CH₂), 56.4 (CH), 45.3 (CH), 29.4 (CH₂) ppm. HRMS (ESI+) calculated for C₂₀H₂₂N₃O₃ 352.1656 found 352.1639; Method A *t*_R = 1.99 min; Purity (AUC) \geq 95%.

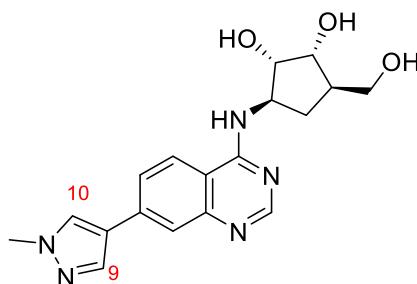
(1*S*,2*R*,3*R*,5*R*)-3-(Hydroxymethyl)-5-((7-(pyridin-2-yl)quinazolin-4-yl)amino)cyclopentane-1,2-diol (396)



2-Tri-*N*-butylstannylpyridine (0.08 mL, 0.24 mmol) was added to a solution of (1*R*,2*S*,3*R*,5*R*)-3-[(7-bromoquinazolin-4-yl)amino]-5-(hydroxymethyl)cyclopentane-1,2-diol (43 mg, 0.12 mmol), tetrakis(triphenylphosphine)palladium(0) (14 mg, 0.01 mmol) and LiCl (26 mg, 0.61 mmol) in DMF (0.6 mL). The solution was heated at 120 °C in the MW for 2 h. The reaction mixture was

passed through an acidic ion exchange column (SCX, 1 g) with MeOH and eluted with 3.5 M NH₃ in MeOH. Purification by column chromatography (biotage SNAP-Ultra C18 12 g, eluted with 10-80% MeOH in water, 1 CV, gradient over 18 CV, 6 CV). Fractions with product were combined and passed through an acidic ion exchange column (SCX, 2 g) with MeOH and eluted with 3.5 M NH₃ in MeOH to afford the title compound (21 mg, 48%, 0.06 mmol) as an oil. IR (thin film) $\nu = 3275, 2155, 1623, 1584, 1538 \text{ cm}^{-1}$. ¹H NMR (600 MHz, Methanol-*d*₄) δ 8.71 (ddd, $J = 4.9, 1.7, 0.9 \text{ Hz}$, 1H, ArH, H₁₂), 8.50 (s, 1H, ArH, H₂), 8.27 – 8.26 (m, 1H, ArH, H₅), 8.25 (s, 1H, ArH, H₈), 8.15 (dd, $J = 8.6, 1.8 \text{ Hz}$, 1H, ArH, H₆), 8.03 (app. dt, $J = 8.0, 1.1 \text{ Hz}$, 1H ArH, H₉), 7.97 (td, $J = 7.7, 1.8 \text{ Hz}$, 1H, ArH, H₁₀), 7.46 (ddd, $J = 7.4, 4.9, 1.2 \text{ Hz}$, 1H, ArH, H₁₁), 4.69 (td, $J = 7.9, 6.1 \text{ Hz}$, 1H, CH, H_{1'}), 4.11 – 3.99 (m, 2H, CH, H_{2'}, H_{3'}), 3.71 (d, $J = 5.3 \text{ Hz}$, 2H, CH₂, H_{6'}), 2.52 (ddd, $J = 13.3, 9.2, 7.8 \text{ Hz}$, 1H, CH₂, H_{5'}), 2.24 (dtd, $J = 9.3, 4.9, 2.8 \text{ Hz}$, 1H, CH, H_{4'}), 1.50 (app. dt, $J = 13.3, 7.9 \text{ Hz}$, 1H, CH₂, H_{5'}) ppm. ¹³C NMR (151 MHz, Methanol-*d*₄) δ 160.0 (C), 155.7 (C), 155.1 (CH), 149.4 (CH), 148.6 (C), 143.5 (C), 137.6 (CH), 124.7 (CH), 124.4 (CH), 123.3 (CH), 122.8 (CH), 121.6 (CH), 115.1 (C), 76.7 (CH), 72.9 (CH), 63.0 (CH₂), 56.4 (CH), 45.3 (CH), 29.4 (CH₂) ppm. HRMS (ESI+) calculated for C₁₉H₂₁N₄O₃ 353.1608, found 353.1621; Method A $t_R = 1.68 \text{ min}$; Purity (AUC) $\geq 95\%$.

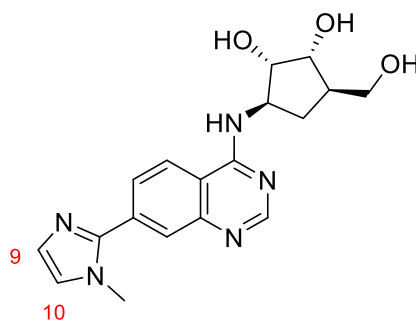
(1*S*,2*R*,3*R*,5*R*)-3-(Hydroxymethyl)-5-((7-(1-methyl-1H-pyrazol-4-yl)quinazolin-4-yl)amino)cyclopentane-1,2-diol (397)



1-Methyl-1H-pyrazole-4-boronic acid (31 mg, 0.25 mmol) was added to a solution of (1*R*,2*S*,3*R*,5*R*)-3-[(7-bromoquinazolin-4-yl)amino]-5-(hydroxymethyl)cyclopentane-1,2-diol (44 mg, 0.12 mmol), sodium carbonate (40 mg, 0.37 mmol) and tetrakis(triphenylphosphine)palladium(0) (7 mg, 0.01

mmol) in water (0.6 mL) and 1,4-dioxane (0.6 mL). The solution was heated at 120 °C in the MW for 1 h. The reaction mixture was concentrated and purified by column chromatography (biotage SNAP-Ultra C18 12 g, eluted with 5-100% MeOH in water, 2 CV, gradient over 18 CV, 2 CV). The product was passed through an acidic ion exchange column (SCX, 1 g) with MeOH and eluted with 3.5 M NH₃ in MeOH to afford the title compound (34 mg, 77%, 0.10 mmol) as an off-white solid. m.p. 211 °C. IR (thin film) ν = 3294, 2501, 1638 cm⁻¹. ¹H NMR (600 MHz, Methanol-*d*₄) δ 8.44 (s, 1H, ArH, H₂), 8.18 (s, 1H, ArH, H₉), 8.14 (d, *J* = 8.6 Hz, 1H, ArH, H₅), 8.00 (s, 1H, ArH, H₁₀), 7.82 (d, *J* = 1.8 Hz, 1H, ArH, H₈), 7.76 (dd, *J* = 8.7, 1.8 Hz, 1H, ArH, H₆), 4.65 (td, *J* = 7.9, 5.8 Hz, 1H, CH, H_{1'}), 4.07 – 4.00 (m, 2H, CH, H_{2'}, H_{3'}), 3.98 (s, 3H, CH₃), 3.70 (d, *J* = 5.4 Hz, 2H, CH₂, H_{6'}), 2.50 (ddd, *J* = 13.4, 9.2, 7.8 Hz, 1H, CH₂, H_{5'}), 2.27 – 2.18 (m, 1H, CH, H_{4'}), 1.48 (app. dt, *J* = 13.4, 8.0 Hz, 1H, CH₂, H_{5'}) ppm. ¹³C NMR (151 MHz, Methanol-*d*₄) δ 159.8 (C), 154.8 (CH), 148.9 (C), 137.6 (C), 136.6 (CH), 128.9 (CH), 123.9 (CH), 122.9 (CH), 121.7 (C), 121.0 (CH), 113.2 (C), 76.8 (CH), 72.9 (CH), 63.0 (CH₂), 56.3 (CH), 45.3 (CH), 37.7 (CH₃), 29.4 (CH₂) ppm. HRMS (ESI+) calculated for C₁₈H₂₂N₅O₃ 356.1717 found 356.1700; Method A *t*_R = 1.76 min; Purity (AUC) \geq 95%.

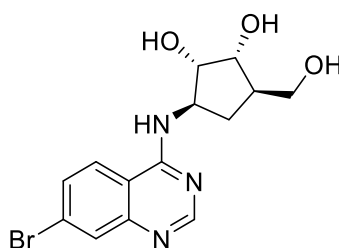
(1*S*,2*R*,3*R*,5*R*)-3-(Hydroxymethyl)-5-((7-(1-methyl-1*H*-imidazol-2-yl)quinazolin-4-yl)amino)cyclopentane-1,2-diol (398)



1-Methyl-2-(tri-*n*-butylstannyl)imidazole (0.03 mL, 0.10 mmol) was added to a solution of (1*R*,2*S*,3*R*,5*R*)-3-[(7-bromoquinazolin-4-yl)amino]-5-(hydroxymethyl)cyclopentane-1,2-diol (40 mg, 0.11 mmol), tetrakis(triphenylphosphine)palladium(0) (13 mg, 0.01 mmol) and LiCl (24 mg, 0.56 mmol) in DMF (0.6 mL).

The solution was heated at 120 °C in the MW for 2 h. Purification by column chromatography (biotage SNAP-Ultra C18 12 g, eluted with 0-20% MeOH in water, 5 CV, gradient over 10 CV, 6 CV) followed by an acidic ion exchange column (SCX, 2 g) washing with MeOH followed by 2 M NH₃ in MeOH eluting the title product (12 mg, 33%, 0.03 mmol) as a white solid. m.p. 151 °C. $[\alpha]^{23}_{\text{D}} +4.16^{\circ}$ (c=0.5, MeOH). IR (thin film) $\nu = 3301, 3114, 2917, 1682, 1586, 1542, 1505 \text{ cm}^{-1}$. ¹H NMR (600 MHz, Methanol-*d*₄) δ 8.50 (s, 1H, ArH, H₂), 8.24 (d, *J* = 8.6 Hz, 1H, ArH, H₅), 7.81 (dd, *J* = 8.0, 1.5 Hz, 2H, ArH, H₉, H₁₀), 7.68 (dd, *J* = 8.6, 1.8 Hz, 1H, ArH, H₆), 7.28 (d, *J* = 1.2 Hz, 1H, ArH, H₈), 4.69 (td, *J* = 7.9, 6.2 Hz, 1H, CH, H_{1'}), 4.06 – 4.00 (m, 2H, CH, H_{2'}, H_{3'}), 3.86 (s, 3H, CH₃), 3.70 (d, *J* = 5.4 Hz, 2H, CH₂, H_{6'}), 2.51 (ddd, *J* = 13.3, 9.2, 7.8 Hz, 1H, CH₂, H_{5'}), 2.23 (dtd, *J* = 9.3, 4.9, 3.0 Hz, 1H, CH, H_{4'}), 1.49 (app. dt, *J* = 13.3, 8.0 Hz, 1H, CH₂, H_{5'}) ppm. ¹³C NMR (151 MHz, Methanol-*d*₄) δ 159.9 (C), 155.3 (CH), 148.5 (C), 140.4 (CH), 134.3 (C), 132.3 (C), 127.9 (CH), 125.9 (CH), 124.6 (CH), 123.0 (CH), 114.1 (C), 76.7 (CH), 72.8 (CH), 63.0 (CH₂), 56.4 (CH), 45.2 (CH), 32.1 (CH₃), 29.4 (CH₂) ppm. HRMS (ESI+) calculated for C₁₈H₂₂N₅O₃ 356.1723 found 356.1722; Method C *t*_R = 0.27 min; Purity (AUC) \geq 95%.

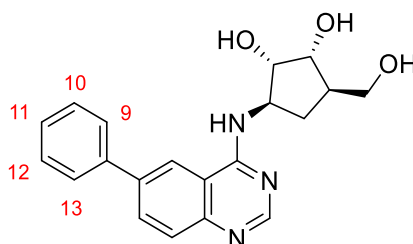
(1*R*,2*S*,3*R*,5*R*)-3-((7-Bromoquinazolin-4-yl)amino)-5-(hydroxymethyl)cyclopentane-1,2-diol (399)



DIPEA (0.7 mL, 4.0 mmol) and (1*R*, 2*S*, 3*R*, 4*R*)-2,3-dihydroxy-4-(hydroxymethyl)-1-aminocyclopentane hydrochloride (294 mg, 1.6 mmol) were added to a suspension of 7-bromoquinazolin-4-ol (432 mg, 1.92 mmol) and PyBOP (1166 mg, 2.24 mmol) in THF (2.5 mL) and DMF (5.0 mL) and stirred for 18 h. Water (50 mL) was added and washed with CH₂Cl₂ (3 x 40 mL). The water layer was concentrated and passed through an acidic ion exchange cartridge (SCX, 5 g) and washed with MeOH. The product was eluted with 3.5

M NH₃ in MeOH and concentrated to afford the title compound (338 mg, 60%, 0.95 mmol) as a beige foam. $[\alpha]^{23}_{\text{D}} -6.93^{\circ}$ ($c=0.5$, MeOH). IR (thin film) $\nu = 3237, 2916, 1711, 1584, 1538 \text{ cm}^{-1}$. ¹H NMR (600 MHz, DMSO-*d*₆) δ 8.45 (s, 1H, ArH, H₂), 8.27 (d, $J = 8.9$ Hz, 1H, ArH, H₅), 8.22 (d, $J = 7.6$ Hz, 1H, NH), 7.87 (d, $J = 2.0$ Hz, 1H, ArH, H₈), 7.69 (dd, $J = 8.8, 2.1$ Hz, 1H, ArH, H₆), 4.71 – 4.64 (m, 2H, 2 x OH), 4.57 (p, $J = 8.0$ Hz, 1H, CH, H_{1'}), 4.45 (d, $J = 4.8$ Hz, 1H, OH), 3.88 (dt, $J = 7.4, 5.6$ Hz, 1H, CH, H_{2'}), 3.76 (q, $J = 4.8$ Hz, 1H, CH, H_{3'}), 3.43 (app. dh, $J = 21.7, 5.5$ Hz, 2H, CH₂, H_{6'}), 2.21 (ddd, $J = 13.1, 8.5$ Hz, 1H, CH₂, H_{5'}), 2.04 – 1.92 (m, 1H, CH, H_{4'}), 1.21 (ddd, $J = 13.1, 8.6$ Hz, 1H, CH₂, H_{5'}) ppm. ¹³C NMR (151 MHz, DMSO-*d*₆) δ 159.9 (C), 156.7 (CH), 150.9 (C), 129.9 (CH), 128.9 (CH), 126.4 (C), 125.6 (CH), 114.3 (C), 76.1 (CH), 72.5 (CH), 63.4 (CH₂), 56.2 (CH), 45.7 (CH), 30.2 (CH₂) ppm. HRMS (ESI+) calculated for C₁₄H₁₇BrN₃O₃ 354.0448 found 354.0443; Method A $t_{\text{R}} = 0.62$ min; Purity (AUC) $\geq 95\%$.

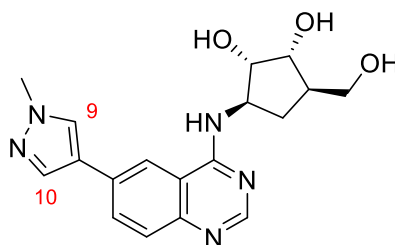
(1*S*,2*R*,3*R*,5*R*)-3-(Hydroxymethyl)-5-((6-phenylquinazolin-4-yl)amino)cyclopentane-1,2-diol (402)



Phenylboronic acid (27 mg, 0.22 mmol) was added to a solution of (1*S*,2*R*,3*R*,5*R*)-3-(hydroxymethyl)-5-[(6-iodoquinazolin-4-yl)amino]cyclopentane-1,2-diol (44 mg, 0.11 mmol), sodium carbonate (35 mg, 0.33 mmol) and tetrakis(triphenylphosphine)palladium(0) (10 mg, 0.01 mmol) in water (0.6 mL) and 1,4-dioxane (0.6 mL). The solution was heated at 120 °C in the MW for 1 h. The reaction mixture was concentrated and purified by column chromatography (biotage SNAP-Ultra C18 12 g, eluted with 5-85% MeOH in water, 2 CV, gradient over 18 CV, 2CV). Fractions with product were concentrated, dissolved in CH₂Cl₂ and passed through an acidic ion exchange column (SCX, 1 g) with 1:1 CH₂Cl₂: MeOH followed by 2.5 M NH₃ in CH₂Cl₂: MeOH 1:1 to afford the title compound (24 mg, 62%, 0.07 mmol) as a beige solid. M.p. 106 °C. $[\alpha]^{23}_{\text{D}} +69.3^{\circ}$ ($c=0.5$, MeOH). IR (thin film) $\nu = 3666, 3195,$

2928, 1624, 1584, 1534 cm^{-1} . ^1H NMR (600 MHz, $\text{DMSO-}d_6$) δ 8.59 (d, $J = 2.0$ Hz, 1H, ArH, H₅), 8.44 (s, 1H, ArH, H₂), 8.21 (d, $J = 7.5$ Hz, 1H, NH), 8.09 (dd, $J = 8.6, 2.0$ Hz, 1H, Ar, H₇), 7.87 – 7.81 (m, 2H, ArH, H₉, H₁₃), 7.74 (d, $J = 8.6$ Hz, 1H, ArH, H₈), 7.56 – 7.49 (m, 2H, ArH, H₁₀, H₁₂), 7.45 – 7.39 (m, 1H, ArH, H₁₁), 4.75 – 4.67 (m, 2H, OH), 4.62 (tdd, $J = 9.2, 7.7$ Hz, 1H, CH, H_{1'}), 4.46 (d, $J = 4.7$ Hz, 1H, OH), 3.92 (dd, $J = 7.5, 5.5$ Hz, 1H, CH, H_{2'}), 3.78 (dd, $J = 4.7$ Hz, 1H, CH, H_{3'}), 3.44 (dq, $J = 13.8, 5.2$ Hz, 2H, CH₂, H_{6'}), 2.23 (ddd, $J = 13.0, 8.4$ Hz, 1H, CH₂, H_{5'}), 1.98 (dddd, $J = 14.5, 8.6, 5.9, 4.4$ Hz, 1H, CH, H_{4'}), 1.24 (ddd, $J = 13.0, 8.8$ Hz, 1H, CH, H_{5'}) ppm. ^{13}C NMR (151 MHz, $\text{DMSO-}d_6$) δ 160.1 (C), 155.6 (CH), 149.0 (C), 139.8 (C), 137.7 (C), 131.6 (CH), 129.5 (2 x CH), 128.5 (CH), 128.2 (CH), 127.5 (2 x CH), 120.8 (CH), 115.6 (C), 76.2 (CH), 72.5 (CH), 63.4 (CH₂), 56.3 (CH), 45.7 (CH), 30.3 (CH₂) ppm. HRMS (ESI+) calculated for $\text{C}_{20}\text{H}_{22}\text{N}_3\text{O}_3$ 352.1661, found 352.1659; Method C $t_R = 0.92$ min; Purity (AUC) $\geq 95\%$.

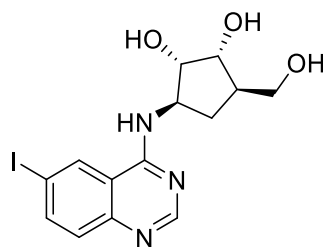
(1S,2R,3R,5R)-3-(Hydroxymethyl)-5-((6-(1-methyl-1H-pyrazol-4-yl)quinazolin-4-yl)amino)cyclopentane-1,2-diol (403)



1-Methyl-1H-pyrazole-4-boronic acid (28 mg, 0.22 mmol) was added to a solution of (1S,2R,3R,5R)-3-(hydroxymethyl)-5-[(6-iodoquinazolin-4-yl)amino]cyclopentane-1,2-diol (44 mg, 0.11 mmol), sodium carbonate (35 mg, 0.33 mmol) and tetrakis(triphenylphosphine)palladium(0) (6.3 mg, 0.01 mmol) in water (0.6 mL) and 1,4-dioxane (0.6 mL). The solution was heated at 120 °C in the MW for 1 h. The reaction mixture was concentrated and purified by column chromatography (biotage SNAP-Ultra C18 12 g, eluted with 5-85% MeOH in water, 2 CV, gradient over 18 CV, 2 CV) to afford the title compound (37 mg, 95%, 0.10 mmol) as a beige solid. m.p. 188 °C. $[\alpha]_D^{23} -34.2^\circ$ ($c=0.5$, MeOH). IR (thin film) $\nu = 3098, 2909, 2784, 1645, 1581$ cm^{-1} . ^1H NMR (600 MHz, Methanol-

d_4) δ 8.50 (s, 1H, ArH, H₂), 8.43 (d, J = 1.9 Hz, 1H, ArH, H₅), 8.12 (s, 1H, ArH, H₁₀), 8.08 (dd, J = 8.6, 1.9 Hz, 1H, ArH, H₇), 8.01 (d, J = 0.8 Hz, 1H, ArH, H₉), 7.72 (d, J = 8.6 Hz, 1H, ArH, H₈), 4.79 (td, J = 8.1, 6.7 Hz, 1H, CH, H_{1'}), 4.09 (dd, J = 6.8, 5.3 Hz, 1H, CH, H_{2'}), 4.03 (dd, J = 5.0 Hz, 1H, CH, H_{3'}), 3.99 (s, 3H, CH₃), 3.71 (d, J = 5.4 Hz, 2H, CH₂, H_{6'}), 2.51 (ddd, J = 13.4, 9.2, 7.8 Hz, 1H, CH₂, H_{5'}), 2.24 (ddq, J = 9.9, 8.0, 5.2 Hz, 1H, CH, H_{4'}), 1.52 (app. dt, J = 13.3, 8.2 Hz, 1H, CH₂, H_{5'}) ppm. ¹³C NMR (151 MHz, Methanol- d_4) δ 160.3 (C), 152.5 (CH), 143.3 (C), 136.4 (CH), 131.9 (C), 131.5 (CH), 128.4 (CH), 124.5 (CH), 121.8 (C), 117.6 (CH), 114.8 (C), 76.6 (CH), 72.8 (CH), 63.0 (CH₂), 56.7 (CH), 45.3 (CH), 37.8 (CH₃), 29.2 (CH₂) ppm. HRMS (ESI+) calculated for C₁₈H₂₂N₅O₃ 356.1723, found 356.1717; Method C t_R = 0.73 min; Purity (AUC) \geq 95%.

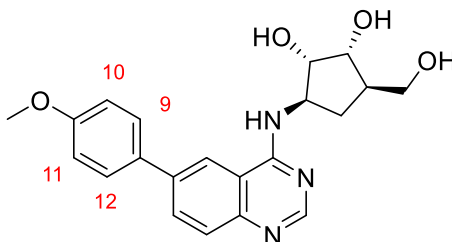
(1*S*,2*R*,3*R*,5*R*)-3-(Hydroxymethyl)-5-((6-iodoquinazolin-4-yl)amino)cyclopentane-1,2-diol (404)



DIPEA (0.2 mL, 1.2 mmol) was added to (1*R*, 2*S*, 3*R*, 4*R*)-2,3-dihydroxy-4-(hydroxymethyl)-1-aminocyclopentane hydrochloride (100 mg, 0.54 mmol) and 4-chloro-6-iodoquinazoline (190 mg, 0.65 mmol) in DMSO (1.8 mL) and the solution was heated at 120 °C for 3 h. Purification by reverse phase column chromatography (biotage SNAP-Ultra C18 12 g, eluted with 0-40% MeOH in water, 5 CV gradient over 18 CV, 6 CV) afforded the title compound (215 mg, 98%, 0.54 mmol) as a white solid. m.p. 210 °C. $[\alpha]^{23}_D$ -29.1° (c=0.5, MeOH). IR (thin film) ν = 3258, 2930, 1578, 1533 cm⁻¹. ¹H NMR (600 MHz, Methanol- d_4) δ 8.66 (d, J = 1.9 Hz, 1H, CH, H₅), 8.52 (s, 1H, ArH, H₂), 8.11 (dd, J = 8.7, 1.8 Hz, 1H, ArH, H₇), 7.49 (d, J = 8.8 Hz, 1H, ArH, H₈), 4.72 (td, J = 8.2, 6.7 Hz, 1H, CH, H_{1'}), 4.04 (dd, J = 6.7, 5.4 Hz, 1H, CH, H_{2'}), 3.98 (dd, J = 5.0 Hz, 1H, CH, H_{3'}), 3.68 (dd, J = 5.5, 1.1 Hz, 2H, CH₂, H_{6'}), 2.47 (ddd, J = 13.4, 9.1, 8.0 Hz, 1H, CH₂, H_{5'}), 2.21 (ddt, J = 14.1, 8.6, 5.3 Hz, 1H, CH, H_{4'}), 1.45 (ddd, J = 13.4, 8.3 Hz, 1H, CH₂, H_{5'}) ppm. ¹³C NMR (151 MHz, Methanol- d_4) δ

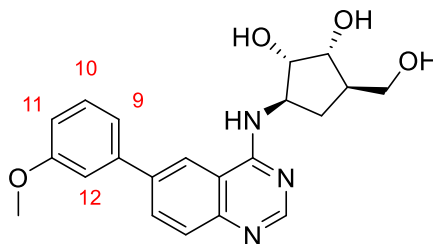
159.1 (C), 154.4 (CH), 146.0 (C), 142.0 (CH), 131.6 (CH), 127.0 (CH), 116.5 (C), 90.1 (C), 76.5 (CH), 72.7 (CH), 63.0 (CH₂), 56.5 (CH), 45.3 (CH), 29.2 (CH₂) ppm. HRMS (ESI+) calculated for C₁₄H₁₇N₃O₃ 402.0315 found 402.0315; Method C *t_R* = 0.71 min; Purity (AUC) ≥ 95%.

(1*S*,2*R*,3*R*,5*R*)-3-(Hydroxymethyl)-5-((6-(4-methoxyphenyl)quinazolin-4-yl)amino)cyclopentane-1,2-diol (405)



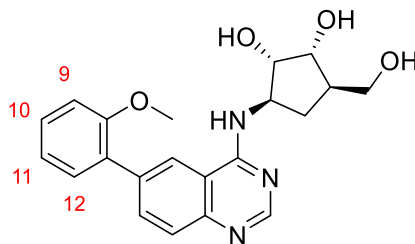
4-Methoxyphenyl boronic acid (32 mg, 0.21 mmol) was added to a solution of (1*S*,2*R*,3*R*,5*R*)-3-(hydroxymethyl)-5-[(6-iodoquinazolin-4-yl)amino]cyclopentane-1,2-diol (42 mg, 0.10 mmol), sodium carbonate (33 mg, 0.31 mmol) and tetrakis(triphenylphosphine)palladium(0) (6 mg, 0.01 mmol) in water (0.6 mL) and 1,4-dioxane (0.6 mL). The solution was heated at 120 °C in the MW for 1 h. The reaction mixture was purified by column chromatography (biotage SNAP-Ultra C18 12 g, eluted with 0-80% MeOH in water, 2 CV, gradient over 18 CV, 2 CV) to yield the title compound (25 mg, 63%, 0.07 mmol) as a white solid. m.p. 111 °C. [α]_D²³ -15.2° (c=0.5, MeOH). IR (thin film) ν = 3255, 2930, 1575 cm⁻¹. ¹H NMR (600 MHz, Methanol-*d*₄) δ 8.53 (s, 1H, ArH, H₂), 8.46 (d, *J* = 2.0 Hz, 1H, ArH, H₅), 8.14 (dd, *J* = 8.7, 2.0 Hz, 1H, ArH, H₇), 7.78 (d, *J* = 8.7 Hz, 1H, ArH, H₈), 7.76 – 7.73 (m, 2H, ArH, H₉, H₁₂), 7.11 – 7.06 (m, 2H, ArH, H₁₀', H₁₁'), 4.80 (td, *J* = 8.1, 6.6 Hz, 1H, CH, H₁'), 4.09 (dd, *J* = 6.7, 5.3 Hz, 1H, CH, H₂'), 4.02 (t, *J* = 5.0 Hz, 1H, CH, H₃'), 3.88 (s, 3H, CH₃), 3.70 (d, *J* = 5.5 Hz, 2H, CH₂, H₆'), 2.50 (ddd, *J* = 13.4, 9.1, 7.9 Hz, 1H, CH₂, H₅'), 2.28 – 2.19 (m, 1H, CH, H₄'), 1.51 (app. dt, *J* = 13.4, 8.2 Hz, 1H, CH₂, H₅') ppm. ¹³C NMR (151 MHz, Methanol-*d*₄) δ 160.5 (C), 160.0 (C), 152.9 (CH), 143.9 (C), 139.8 (C), 132.5 (CH), 131.6 (C), 128.0 (2 x CH), 124.6 (CH), 119.4 (CH), 114.8 (C), 114.2 (2 x CH), 76.6 (CH), 72.8 (CH), 63.0 (CH₂), 56.6 (CH), 54.4 (CH₃), 45.3 (CH), 29.2 (CH₂) ppm. HRMS (ESI+) calculated for C₂₁H₂₄N₃O₄ 382.1761, found 382.1770; Method A *t_R* = 2.13 min; Purity (AUC) ≥ 95%.

(1*S*,2*R*,3*R*,5*R*)-3-(Hydroxymethyl)-5-((6-(3-methoxyphenyl)quinazolin-4-yl)amino)cyclopentane-1,2-diol (406)



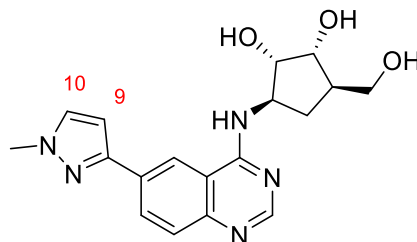
3-Methoxyphenolboronic acid (33 mg, 0.22 mmol) was added to a solution of (1*S*,2*R*,3*R*,5*R*)-3-(hydroxymethyl)-5-[(6-iodoquinazolin-4-yl)amino]cyclopentane-1,2-diol (44 mg, 0.11 mmol), sodium carbonate (35 mg, 0.33 mmol) and tetrakis(triphenylphosphine)palladium(0) (6 mg, 0.01 mmol) in water (0.4 mL) and 1,4-dioxane (0.4 mL). The solution was heated at 120 °C in the MW for 1 h. The reaction mixture was concentrated and purified by column chromatography (biotage SNAP-Ultra C18 12 g, eluted with 0-80% MeOH in water, 2 CV, gradient over 18 CV, 2 CV) Further purification was carried out with an acidic ion exchange column (SCX, 1 g), washing with MeOH, followed by 2.5 M NH₃ in MeOH to afford the title compound (26 mg, 62%, 0.07 mmol) as a white solid. m.p. 214 °C. IR (thin film) ν = 3305, 3001, 2893, 2744, 1608, 1584, 1536, 1514 cm⁻¹. ¹H NMR (600 MHz, DMSO-*d*₆) δ 8.58 (d, *J* = 2.1 Hz, 1H, ArH, H₅), 8.45 (s, 1H, ArH, H₂), 8.22 (d, *J* = 7.5 Hz, 1H, NH), 8.10 (dd, *J* = 8.6, 2.0 Hz, 1H, ArH, H₈), 7.74 (d, *J* = 8.6 Hz, 1H, ArH, H₉), 7.46 (dd, *J* = 7.9 Hz, 1H, ArH, H₁₀), 7.41 (dd, *J* = 7.7, 1.2 Hz, 1H, ArH, H₇), 7.37 (dd, *J* = 2.1 Hz, 1H, ArH, H₁₂), 7.01 (ddd, *J* = 8.1, 2.6, 1.0 Hz, 1H, ArH, H₁₁), 4.73 (d, *J* = 5.9 Hz, 1H, OH), 4.70 (t, *J* = 5.1 Hz, 1H, OH), 4.62 (m, 1H, CH, H_{1'}), 4.47 (d, *J* = 4.7 Hz, 1H, OH), 3.93 (ddd, *J* = 7.6, 5.6 Hz, 1H, CH, H_{2'}), 3.87 (s, 3H, CH₃), 3.79 (m, 1H, CH, H_{3'}), 3.51 – 3.40 (m, 2H, CH₂, H_{6'}), 2.24 (ddd, *J* = 13.0, 8.4 Hz, 1H, CH₂, H_{5'}), 1.99 (dddd, *J* = 14.5, 8.6, 5.9, 4.4 Hz, 1H, CH, H_{4'}), 1.25 (ddd, *J* = 13.0, 8.8 Hz, 1H, CH₂, H_{5'}) ppm. ¹³C NMR (151 MHz, DMSO-*d*₆) δ 160.3 (C), 160.1 (C), 155.6 (CH), 149.1 (C), 141.2 (C), 137.5 (C), 131.7 (CH), 130.6 (CH), 128.5 (CH), 120.9 (CH), 119.9 (CH), 115.6 (C), 113.4 (CH), 113.3 (CH), 76.2 (CH), 72.5 (CH), 63.4 (CH₂), 56.3 (CH), 55.7 (CH₃), 45.8 (CH), 30.3 (CH₂) ppm. HRMS (ESI+) calculated for C₂₁H₂₄N₃O₄ 382.1761 found 382.1774; Method A *t*_R = 2.11 min; Purity (AUC) \geq 95%.

(1*S*,2*R*,3*R*,5*R*)-3-(Hydroxymethyl)-5-((6-(2-methoxyphenyl)quinazolin-4-yl)amino)cyclopentane-1,2-diol (407)



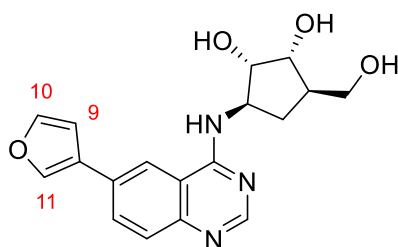
2-Methoxyphenyl)boronic acid (31 mg, 0.20 mmol) was added to a solution of (1*S*,2*R*,3*R*,5*R*)-3-(hydroxymethyl)-5-[(6-iodoquinazolin-4-yl)amino]cyclopentane-1,2-diol (41 mg, 0.10 mmol), sodium carbonate (32 mg, 0.31 mmol) and tetrakis(triphenylphosphine)palladium(0) (6 mg, 0.01 mmol) in water (0.34 mL) and 1,4-dioxane (0.34 mL). The solution was heated at 120 °C in the MW for 1 h. The reaction mixture was concentrated and purified by column chromatography (biotage SNAP-Ultra C18 12 g (0-80%) MeOH in water, 2 CV, gradient over 18 CV, 2 CV) to afford the title compound (37 mg, 95%, 0.10 mmol) as a clear oil. IR (thin film) $\nu = 3276, 2968, 1583, 1536 \text{ cm}^{-1}$. $^1\text{H NMR}$ (600 MHz, Methanol- d_4) δ 8.53 (s, 1H, ArH, H₂), 8.31 (d, $J = 1.8 \text{ Hz}$, 1H, ArH, H₅), 8.03 (dd, $J = 8.6, 1.9 \text{ Hz}$, ArH, 1H, H₇), 7.73 (d, $J = 8.6 \text{ Hz}$, 1H, ArH, H₈), 7.46 – 7.38 (m, 2H, ArH, H₁₀, H₁₂), 7.14 (dd, $J = 8.4, 1.0 \text{ Hz}$, 1H, ArH, H₉), 7.09 (td, $J = 7.5, 1.1 \text{ Hz}$, 1H, ArH, H₁₁), 4.76 (td, $J = 8.0, 6.5 \text{ Hz}$, 1H, H_{1'}), 4.05 (dd, $J = 6.5, 5.3 \text{ Hz}$, 1H, H_{2'}), 4.00 (t, $J = 5.0 \text{ Hz}$, 1H, H_{3'}), 3.85 (s, 3H), 3.67 (d, $J = 5.4 \text{ Hz}$, 2H, H_{6'}), 2.49 (ddd, $J = 13.4, 9.2, 7.9 \text{ Hz}$, 1H, H_{5'}), 2.22 (ddq, $J = 10.1, 8.1, 5.2 \text{ Hz}$, 1H, H_{4'}), 1.48 (app. dt, $J = 13.4, 8.1 \text{ Hz}$, 1H, H_{5'}) ppm. $^{13}\text{C NMR}$ (151 MHz, Methanol- d_4) δ 160.4 (C), 156.6 (C), 153.3 (CH), 144.8 (C), 138.0 (C), 135.6 (CH), 130.6 (CH), 129.3 (CH), 129.0 (C), 123.8 (CH), 122.5 (CH), 120.7 (CH), 114.4 (C), 111.2 (CH), 76.6 (CH), 72.8 (CH), 62.9 (CH₂), 56.5 (CH), 54.7 (CH), 29.2 (CH₂) ppm. HRMS (ESI+) calculated for C₂₁H₂₄N₃O₄ 382.1761, found 382.1773; Method A $t_R = 2.03 \text{ min}$; Purity (AUC) $\geq 95\%$.

(1*S*,2*R*,3*R*,5*R*)-3-(Hydroxymethyl)-5-((6-(1-methyl-1*H*-pyrazol-3-yl)quinazolin-4-yl)amino)cyclopentane-1,2-diol (410)



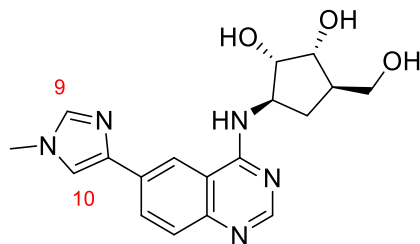
(1*S*,2*R*,3*R*,5*R*)-3-(Hydroxymethyl)-5-[(6-iodoquinazolin-4-yl)amino]cyclopentane-1,2-diol (40 mg, 0.10 mmol) was added to a solution of 1-methyl-3-(4,4,5,5-tetramethyl-1,3,2-dioxaborolan-2-yl)-1*H*-pyrazole (41.5 mg, 0.20 mmol), sodium carbonate (32 mg, 0.30 mmol) and tetrakis(triphenylphosphine)palladium(0) (6 mg, 0.01 mmol) in water (0.6 mL) and 1,4-dioxane (0.6 mL). The solution was heated at 120 °C in the MW for 1 h. The reaction mixture was concentrated and purified by column chromatography (biotage SNAP-Ultra C18 12 g, eluted with 0-80% MeOH in water, 2 CV, gradient over 18 CV, 2 CV) to yield the title product (38 mg, 95%, 0.0947 mmol) as a white solid. $[\alpha]^{23}_{\text{D}} -29.1^{\circ}$ ($c=0.5$, MeOH). IR (thin film) $\nu = 3125, 2916, 1574, 1506 \text{ cm}^{-1}$. ^1H NMR (600 MHz, DMSO- d_6) δ 8.61 (d, $J = 1.9$ Hz, 1H, ArH, H₅), 8.41 (s, 1H, ArH, H₂), 8.20 (dd, $J = 8.6, 1.8$ Hz, 1H, ArH, H₇), 7.81 (d, $J = 2.2$ Hz, 1H, ArH, H₁₀), 7.68 (d, $J = 8.6$ Hz, 1H, ArH, H₈), 6.84 (d, $J = 2.3$ Hz, 1H, ArH, H₉), 4.65 – 4.58 (m, 1H, CH, H₁'), 3.94 (d, $J = 5.6$ Hz, 1H, CH, H₂'), 3.93 (s, 3H, CH₃), 3.79 (dd, $J = 5.3, 4.1$ Hz, 1H, CH, H₃'), 3.45 (qd, $J = 10.5, 5.9$ Hz, 2H, CH₂, H₆'), 2.23 (app. dt, $J = 13.0, 8.4$ Hz, 1H, CH₂, H₅'), 1.99 (ddq, $J = 8.6, 6.6, 2.9, 2.2$ Hz, 1H, CH, H₄'), 1.25 (app. dt, $J = 13.0, 8.8$ Hz, 1H, CH₂, H₅') ppm. ^{13}C NMR (151 MHz, DMSO- d_6) δ 160.0 (C), 155.2 (CH), 150.0 (C), 149.0 (C), 133.1 (CH), 131.2 (C), 130.2 (CH), 128.3 (CH), 118.9 (CH), 115.6 (C), 103.5 (CH), 76.1 (CH), 72.5 (CH), 63.5 (CH₂), 56.2 (CH), 45.7 (CH), 39.2 (CH₃), 30.3 (CH₂) ppm. HRMS (ESI+) calculated for C₁₈H₂₂N₅O₃ 356.1722 found 356.1720; Method B $t_{\text{R}} = 1.23$ min; Purity (AUC) $\geq 95\%$.

(1*R*,2*S*,3*R*,5*R*)-3-((6-(Furan-3-yl)quinazolin-4-yl)amino)-5-(hydroxymethyl)cyclopentane-1,2-diol (411)



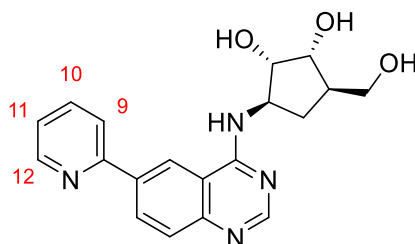
3-Furanylboric acid (22 mg, 0.20 mmol) was added to a solution of (1*S*,2*R*,3*R*,5*R*)-3-(hydroxymethyl)-5-[(6-iodoquinazolin-4-yl)amino]cyclopentane-1,2-diol (40 mg, 0.10 mmol), sodium carbonate (32 mg, 0.30 mmol) and tetrakis(triphenylphosphine)palladium(0) (6 mg, 0.01 mmol) in water (0.4 mL) and 1,4-dioxane (0.4 mL). The solution was heated at 120 °C in the MW for 1 h. The reaction mixture was concentrated and purified by column chromatography (biotage SNAP-Ultra C18 12 g, eluted with 0-80% MeOH in water, 2 CV, gradient over 18 CV, 2 CV) to afford the title compound (34 mg, 98%, 0.01 mmol) as a white solid. m.p. 112 °C. $[\alpha]^{23}_{\text{D}} -34.6^{\circ}$ ($c=0.5$, MeOH). IR (thin film) $\nu = 3119, 2873, 1644, 1568 \text{ cm}^{-1}$. $^1\text{H NMR}$ (600 MHz, DMSO- d_6) δ 8.44 (d, $J = 1.9 \text{ Hz}$, 1H, ArH, H₅), 8.42 (s, 1H, ArH, H₂), 8.30 (dd, $J = 1.5, 0.9 \text{ Hz}$, 1H, ArH, H₁₁), 8.05 – 8.02 (m, 2H, ArH, NH, H₇), 7.84 (t, $J = 1.7 \text{ Hz}$, 1H, ArH, H₁₀), 7.68 (d, $J = 8.6 \text{ Hz}$, 1H, ArH, H₈), 7.12 (dd, $J = 1.9, 0.9 \text{ Hz}$, 1H, ArH, H₉), 4.64 – 4.53 (m, 1H, CH, H_{1'}), 3.92 (dd, $J = 7.6, 5.4 \text{ Hz}$, 1H, CH, H_{2'}), 3.80 (dd, $J = 5.4, 4.1 \text{ Hz}$, 1H, CH, H_{3'}), 3.51 – 3.42 (m, 2H, CH₂, H_{6'}), 2.29 – 2.21 (m, 1H, CH₂, H_{5'}), 2.04 – 1.94 (m, 1H, CH, H_{4'}), 1.25 (app. dt, $J = 13.0, 8.7 \text{ Hz}$, 1H, CH₂, H_{5'}) ppm. $^{13}\text{C NMR}$ (151 MHz, DMSO- d_6) δ 159.8 (C), 155.2 (CH), 148.7 (C), 145.0 (CH), 140.3 (CH), 130.8 (CH), 129.7 (C), 128.5 (CH), 125.9 (C), 119.0 (CH), 115.6 (C), 109.3 (CH), 76.2 (CH), 72.5 (CH), 63.3 (CH₂), 56.3 (CH), 45.7 (CH), 30.3 (CH₂) ppm. HRMS (ESI+) calculated for C₁₈H₂₀N₃O₄ 342.1454 found 342.1455; Method B $t_{\text{R}} = 1.55 \text{ min}$; Purity (AUC) $\geq 95\%$.

(1*S*,2*R*,3*R*,5*R*)-3-(Hydroxymethyl)-5-((6-(1-methyl-1*H*-imidazol-4-yl)quinazolin-4-yl)amino)cyclopentane-1,2-diol (412)



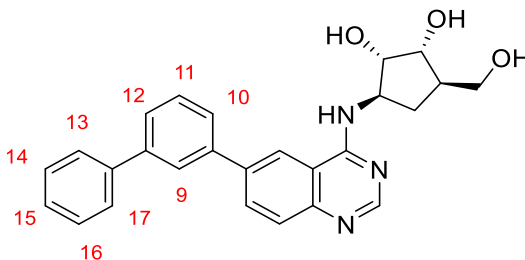
N-Methyl-4-(tributylstannyl)imidazole (0.03 mL, 0.10 mmol) was added to a solution of (1*S*,2*R*,3*R*,5*R*)-3-(hydroxymethyl)-5-[(6-iodoquinazolin-4-yl)amino]cyclopentane-1,2-diol (39 mg, 0.10 mmol), tetrakis(triphenylphosphine) palladium(0) (11 mg, 0.01 mmol) and LiCl (21 mg, 0.49 mmol) in DMF (0.6 mL). The solution was heated at 120 °C in the MW for 1 h. The reaction mixture was purified by column chromatography (biotage SNAP-Ultra C18 12 g, eluted with 10-80% MeOH in water, 1 CV, gradient over 18 CV, 6 CV) followed by normal phase column chromatography (biotage SNAP KP-Sil 10 g, eluted with 0-10% 10% NH₃ in MeOH in CH₂Cl₂, 1 CV, gradient over 10 CV, 5 CV). Further purification by acidic ion exchange chromatography (SCX, 1 g) to afford the title compound (16 mg, 46%, 0.05 mmol) as a white solid. m.p. 157 °C. IR (thin film) $\nu = 3272, 1590, 1563, 1540 \text{ cm}^{-1}$. ¹H NMR (600 MHz, DMSO-*d*₆) δ 8.59 (d, *J* = 1.8 Hz, 1H, ArH, H₅), 8.38 (s, 1H, ArH, H₂), 8.13 (m, 2H, ArH, NH, H₇), 7.72 (d, *J* = 1.3 Hz, 1H, ArH, H₉), 7.70 (d, *J* = 1.3 Hz, 1H, ArH, H₁₀), 7.64 (d, *J* = 8.6 Hz, 1H, ArH, H₈'), 4.73 – 4.68 (m, 1H, OH), 4.65 – 4.55 (m, 1H, CH, H₁'), 4.43 (d, *J* = 4.7 Hz, 1H, OH), 4.10 (q, *J* = 5.2 Hz, 1H, OH), 3.95 (dt, *J* = 7.5, 5.5 Hz, 1H, CH, H₂'), 3.79 (q, *J* = 4.7 Hz, 1H, CH, H₃'), 3.74 (s, 3H, CH₃), 3.45 (app. dh, *J* = 21.6, 5.5 Hz, 2H, CH₂, H₆'), 2.23 (app. dt, *J* = 13.0, 8.4 Hz, 1H, CH₂, H₅'), 1.99 (tdd, *J* = 8.0, 4.1, 1.6 Hz, 1H, CH, H₄'), 1.24 (app. dt, *J* = 13.0, 8.7 Hz, 1H, CH₂, H₅') ppm. ¹³C NMR (151 MHz, DMSO-*d*₆) δ 159.9 (C), 154.7 (CH), 148.4 (C), 140.7 (C), 139.2 (CH), 132.5 (C), 129.8 (CH), 128.0 (CH), 118.0 (CH), 117.4 (CH), 115.7 (C), 76.1 (CH), 72.6 (CH), 63.5 (CH₂), 56.2 (CH), 45.7 (CH), 33.6 (CH₃), 30.4 (CH₂) ppm. HRMS (ESI+) calculated for C₁₈H₂₂N₅O₃ 356.1717, found 356.1722; Method A *t*_R = 0.35 min; Purity (AUC) \geq 95%.

(1*S*,2*R*,3*R*,5*R*)-3-(Hydroxymethyl)-5-((6-(pyridin-2-yl)quinazolin-4-yl)amino)cyclopentane-1,2-diol (414)



2-Tri-*N*-butylstannylpyridine (0.06 mL, 0.20 mmol) was added to a solution of (1*S*,2*R*,3*R*,5*R*)-3-(hydroxymethyl)-5-[(6-iodoquinazolin-4-yl)amino]cyclopentane-1,2-diol (40 mg, 0.10 mmol), tetrakis(triphenylphosphine) palladium(0) (12 mg, 0.01 mmol) and LiCl (21 mg, 0.50 mmol) in DMF (0.6 mL). The solution was heated at 120 °C in the MW for 1 h. Purification by column chromatography (biotage SNAP-Ultra C18 12 g, eluted with 10-80% MeOH in water, 1 CV, gradient over 18 CV, 6 CV) to afford the title compound (12 mg, 34%, 0.03 mmol) as a yellow oil. $[\alpha]^{23}_{\text{D}} -69.2^{\circ}$ ($c=0.5$, MeOH). IR (thin film) $\nu = 3239, 1623, 1586, 1537 \text{ cm}^{-1}$. $^1\text{H NMR}$ (600 MHz, Methanol- d_4) δ 8.86 (d, $J = 1.9 \text{ Hz}$, 1H, ArH, H₅), 8.72 (ddd, $J = 4.8, 1.8, 0.9 \text{ Hz}$, 1H, ArH, H₁₂), 8.55 (s, 1H, ArH, H₂), 8.51 (dd, $J = 8.7, 1.9 \text{ Hz}$, 1H, ArH, H₇), 8.07 (dt, $J = 8.1, 1.1 \text{ Hz}$, 1H, ArH, H₁₀), 7.98 (td, $J = 7.7, 1.8 \text{ Hz}$, 1H, ArH, H₁₁), 7.84 (d, $J = 8.7 \text{ Hz}$, 1H, ArH, H₈), 7.44 (ddd, $J = 7.5, 4.8, 1.1 \text{ Hz}$, 1H, ArH, H₁₂), 4.79 (td, $J = 8.1, 6.6 \text{ Hz}$, 1H, CH, H_{1'}), 4.10 (dd, $J = 6.7, 5.3 \text{ Hz}$, 1H, CH, H_{2'}), 4.03 (t, $J = 5.0 \text{ Hz}$, 1H, CH, H_{3'}), 3.70 (d, $J = 5.5 \text{ Hz}$, 2H, CH₂, H_{6'}), 2.52 (ddd, $J = 13.4, 9.1, 7.9 \text{ Hz}$, 1H, CH₂, H_{5'}), 2.24 (ddt, $J = 13.9, 8.4, 5.3 \text{ Hz}$, 1H, CH, H_{4'}), 1.52 (app. dt, $J = 13.4, 8.2 \text{ Hz}$, 1H, CH₂, H_{5'}) ppm. $^{13}\text{C NMR}$ (151 MHz, Methanol- d_4) δ 160.6 (C), 155.8 (C), 154.1 (CH), 149.3 (CH), 146.4 (C), 137.6 (C), 137.6 (CH), 132.0 (CH), 125.3 (CH), 122.9 (CH), 121.2 (CH), 121.0 (CH), 114.7 (C), 76.6 (CH), 72.8 (CH), 63.0 (CH₂), 56.6 (CH), 45.3 (CH), 29.3 (CH₂) ppm. HRMS (ESI+) calculated for C₁₉H₂₀N₄NaO₃ 375.1428, found 375.1433; Method A $t_{\text{R}} = 1.64 \text{ min}$; Purity (AUC) $\geq 95\%$.

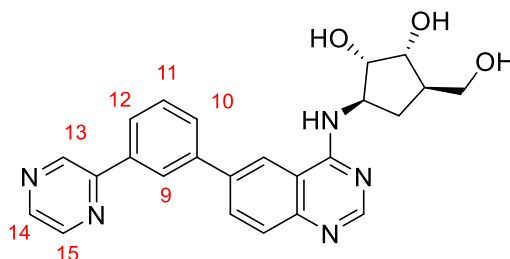
(1*R*,2*S*,3*R*,5*R*)-3-((6-([1,1'-Biphenyl]-3-yl)quinazolin-4-yl)amino)-5-(hydroxymethyl)cyclopentane-1,2-diol (415)



Biphenyl-3-boronic acid (50 mg, 0.25 mmol) was added to a solution of (1*S*,2*R*,3*R*,5*R*)-3-(hydroxymethyl)-5-[(6-iodoquinazolin-4-yl)amino]cyclopentane-1,2-diol (50 mg, 0.12 mmol), sodium carbonate (40 mg, 0.37 mmol) and tetrakis(triphenylphosphine)palladium(0) (12 mg, 0.01 mmol) in water (0.3 mL) and 1,4-dioxane (0.3 mL). The solution was heated at 120 °C in the MW for 1 h. The reaction mixture was concentrated and purified by column chromatography (biotage SNAP-Ultra C18 12 g, eluted with 5-85% MeOH in water, 2 CV, gradient over 18 CV, 2 CV followed by 10 CV of 1:10:100 NH₃:MeOH:CH₂Cl) to yield the title product (26 mg, 49%, 0.06 mmol) as a white solid. $[\alpha]_{\text{D}}^{23}$ -47.09° (c=0.5, MeOH). IR (thin film) ν = 3249, 2925, 1583, 1532 cm⁻¹. ¹H NMR (600 MHz, DMSO-*d*₆) δ 8.66 (d, *J* = 2.2 Hz, 1H, ArH, H₅), 8.46 (s, 1H, ArH, H₂), 8.23 (d, *J* = 7.5 Hz, 1H, NH), 8.20 (dd, *J* = 8.6, 2.0 Hz, 1H, ArH, H₇), 8.05 (t, *J* = 1.8 Hz, 1H, ArH, H₉), 7.83 (dt, *J* = 7.7, 1.5 Hz, 1H, ArH, H₁₀), 7.82 – 7.79 (m, 2H, ArH, H₁₃, H₁₇), 7.78 (d, *J* = 8.6 Hz, 1H, ArH, H₄), 7.71 (dt, *J* = 7.7, 1.4 Hz, 1H, ArH, H₁₂), 7.64 (t, *J* = 7.7 Hz, 1H, ArH, H₃₀), 7.53 (t, *J* = 7.7 Hz, 2H, ArH, H₁₄, H₁₆), 7.45 – 7.39 (m, 1H, ArH, H₁₁), 4.73 (d, *J* = 5.9 Hz, 1H, OH), 4.69 (t, *J* = 5.1 Hz, 1H, OH), 4.63 (dq, *J* = 9.3, 7.7 Hz, 1H, CH, H_{1'}), 4.47 (d, *J* = 4.7 Hz, 1H, OH), 3.93 (ddd, *J* = 7.7, 5.4 Hz, 1H, CH, H_{2'}), 3.78 (dd, *J* = 4.6 Hz, 1H, CH, H_{3'}), 3.45 (dtd, *J* = 14.6, 10.6, 5.3 Hz, 2H, CH₂, H_{6'}), 2.23 (app. dt, *J* = 13.0, 8.4 Hz, 1H, CH₂, H_{5'}), 2.03 – 1.95 (m, 1H, CH, H_{4'}), 1.25 (app. dt, *J* = 13.0, 8.9 Hz, 1H, CH₂, H_{5'}) ppm. ¹³C NMR (151 MHz, DMSO-*d*₆) δ 160.2 (C), 155.6 (CH), 149.2 (C), 141.6 (C), 140.7 (C), 140.6 (C), 137.8 (C), 132.0 (CH), 130.1 (CH), 129.5 (2 x CH), 128.6 (CH), 128.2 (CH), 127.5 (2 x CH), 126.7 (CH), 126.6 (CH), 126.0 (CH), 121.1 (CH), 115.6 (C), 76.1 (CH), 72.5 (CH), 63.4 (CH₂), 56.3 (CH), 45.8

(CH), 30.2 (CH₂) ppm. HRMS (ESI+) calculated for C₂₆H₂₆N₃O₃ 428.1969, found 428.1985; Method D t_R = 2.39 min, Purity (AUC) ≥ 95%.

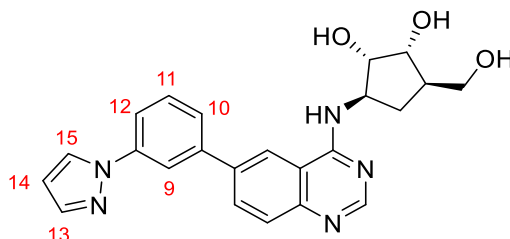
(1*S*,2*R*,3*R*,5*R*)-3-(Hydroxymethyl)-5-((6-(3-(pyrazin-2-yl)phenyl)quinazolin-4-yl)amino)cyclopentane-1,2-diol (416)



(3-Pyrazin-2-ylphenyl)boronic acid (50 mg, 0.25 mmol) was added to a solution of (1*S*,2*R*,3*R*,5*R*)-3-(hydroxymethyl)-5-[(6-iodoquinazolin-4-yl)amino]cyclopentane-1,2-diol (50 mg, 0.12 mmol), sodium carbonate (40 mg, 0.37 mmol) and tetrakis(triphenylphosphine)palladium(0) (11 mg, 0.01 mmol) in water (0.3 mL) and 1,4-dioxane (0.3 mL). The solution was heated at 120 °C in the MW for 1 h. Purification by column chromatography (biotage SNAP-Ultra C18 12 g, eluted with 5-50% MeOH in water, 1CV gradient over 20CV, 6CV) to yield the title product (46 mg, 86%, 0.1071 mmol) as a white solid. [α]²³_D -8.31° (c=0.5, MeOH). m.p. 172 °C. IR (thin film) ν = 3217, 2921, 1574, 1519 cm⁻¹. ¹H NMR (600 MHz, DMSO-*d*₆) δ 9.43 (s, 1H, ArH, H₁₃), 8.80 (t, *J* = 2.0 Hz, 1H, ArH, H₁₄), 8.70 (s, 1H, ArH, H₂), 8.68 (d, *J* = 2.5 Hz, 1H, ArH, H₁₅), 8.52 (d, *J* = 1.9 Hz, 1H, ArH, H₉), 8.25 (d, *J* = 7.5 Hz, 1H, ArH, H₈), 8.23 – 8.21 (m, 1H, ArH, H₇), 8.20 (dt, *J* = 7.8, 1.3 Hz, 1H, ArH, H₁₂), 7.98 (dt, *J* = 7.7, 1.3 Hz, 1H, ArH, H₁₀), 7.80 (br s, 1H, ArH, H₅), 7.72 (t, *J* = 7.7 Hz, 1H, ArH, H₁₁), 4.68 – 4.59 (m, 1H, CH, H₁'), 3.93 (m, 1H, CH, H₂'), 3.81 – 3.76 (m, 1H, CH, H₃'), 3.45 (app. qd, *J* = 10.5, 5.8 Hz, 2H, CH₂, H₆'), 2.24 (app. dt, *J* = 13.0, 8.3 Hz, 1H, CH₂, H₅'), 1.99 (app. tt, *J* = 8.7, 3.6 Hz, 1H, CH, H₄'), 1.26 (app. dt, *J* = 13.0, 8.9 Hz, 1H, CH₂, H₅') ppm. ¹³C NMR (151 MHz, DMSO-*d*₆) δ 160.2 (C), 155.7 (C), 151.9 (C), 149.3 (HMBC,C), 144.8 (CH), 144.2 (CH), 142.9 (CH), 140.7 (C), 137.4 (C), 137.2 (C), 131.9 (CH), 130.2 (CH), 129.2 (CH), 128.7 (CH), 126.6 (CH), 125.8 (CH), 121.2 (CH), 76.2 (CH), 72.5 (CH), 63.4 (CH₂), 56.3 (CH), 45.8 (CH), 30.3 (CH₂) ppm.

HRMS (ESI+) calculated for C₂₄H₂₄N₅O₃ 430.1879, found 430.1866; Method B
 t_R = 1.75 min, Purity (AUC) ≥ 95%.

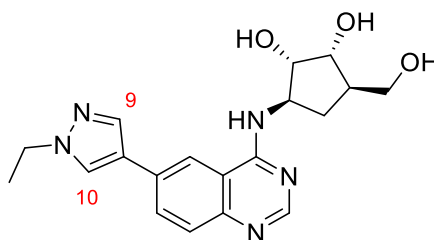
(1S,2R,3S,5S)-3-((6-(3-(1H-pyrazol-1-yl)phenyl)quinazolin-4-yl)amino)-5-(hydroxymethyl)cyclopentane-1,2-diol (417)



[3-(1H-Pyrazol-1-yl)phenyl]boronic acid (47 mg, 0.25 mmol) was added to a solution of (1S,2R,3R,5R)-3-(hydroxymethyl)-5-[(6-iodoquinazolin-4-yl)amino]cyclopentane-1,2-diol (50 mg, 0.12 mmol), sodium carbonate (40 mg, 0.37 mmol) and tetrakis(triphenylphosphine)palladium(0) (12 mg, 0.01 mmol) in water (0.60 mL) and 1,4-dioxane (0.60 mL). The solution was heated at 120 °C in the MW for 1 h. Purification by column chromatography (biotage SNAP-Ultra C18 12 g, eluted with 5-60% MeOH in water, 1 CV, gradient over 30 CV, 2 CV) to yield the title product (43 mg, 83%, 0.10 mmol) as a white solid. m.p. 182 °C. [α]_D²³ -51.2° (c=0.5, MeOH). IR (thin film) ν = 2913, 1649, 1581 cm⁻¹. ¹H NMR (600 MHz, DMSO-*d*₆) δ 8.68 (d, *J* = 2.0 Hz, 1H, ArH, H₁₃), 8.67 (d, *J* = 2.5 Hz, 1H, ArH, H₅), 8.47 (s, 1H, ArH, H₂), 8.27 (d, *J* = 7.5 Hz, 1H, NH), 8.23 (dd, *J* = 2.0 Hz, 1H, ArH, H₉), 8.19 (dd, *J* = 8.6, 2.0 Hz, 1H, ArH, H₇), 7.90 (ddd, *J* = 8.1, 2.3, 1.0 Hz, 1H, ArH, H₁₂), 7.81 (d, *J* = 1.7 Hz, 1H, ArH, H₁₅), 7.79 (d, *J* = 8.6 Hz, 1H, ArH, H₈), 7.78 – 7.76 (m, 1H, ArH, H₁₀), 7.66 (dd, *J* = 7.9 Hz, 1H, ArH, H₁₁), 6.61 (dd, *J* = 2.1 Hz, 1H, ArH, H₁₄), 4.64 (app. dq, *J* = 9.3, 7.7 Hz, 1H, CH, H_{1'}), 3.94 – 3.92 (m, 1H, CH, H_{2'}), 3.78 (dd, *J* = 5.4, 4.1 Hz, 1H, CH, H_{3'}), 3.45 (app. qd, *J* = 10.5, 5.9 Hz, 2H, CH₂, H_{6'}), 2.24 (app. dt, *J* = 13.0, 8.4 Hz, 1H, CH₂, H_{5'}), 1.99 (app. dddd, *J* = 14.6, 8.7, 5.9, 4.3 Hz, 1H, CH, H_{4'}), 1.26 (app. dt, *J* = 13.1, 8.9 Hz, 1H, CH₂, H_{5'}) ppm. ¹³C NMR (151 MHz, DMSO-*d*₆) δ 160.2 (C), 155.8 (CH), 149.3 (C), 141.6 (CH), 141.3 (C), 140.9 (C), 137.1 (C), 131.9 (CH), 130.7 (CH), 128.6 (CH), 128.6 (CH), 125.4 (CH), 121.3 (CH), 118.3 (CH), 117.5 (CH), 115.6 (C), 108.5 (CH), 76.2 (CH), 72.5 (CH), 63.4 (CH₂), 56.3 (CH), 45.8 (CH),

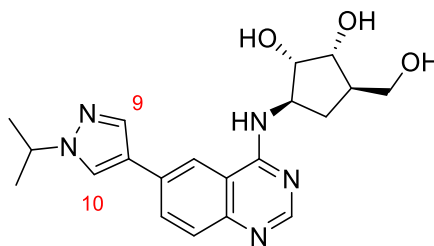
30.3 (CH₂) ppm. HRMS (ESI+) calculated for C₂₃H₂₃N₅O₃ 418.1879, found 418.1892; Method B t_R = 1.78 min, Purity (AUC) ≥ 95%.

(1R,2S,3R,5R)-3-((6-(1-ethyl-1H-pyrazol-4-yl)quinazolin-4-yl)amino)-5-(hydroxymethyl)cyclopentane-1,2-diol (418)



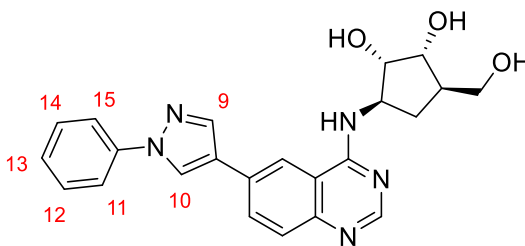
(1-Ethylpyrazol-4-yl)boronic acid (31 mg, 0.22 mmol) was added to a solution of (1S,2R,3R,5R)-3-(hydroxymethyl)-5-[(6-iodoquinazolin-4-yl)amino]cyclopentane-1,2-diol (44 mg, 0.11 mmol), sodium carbonate (35 mg, 0.33 mmol) and tetrakis(triphenylphosphine)palladium(0) (10 mg, 0.01 mmol) in water (0.6 mL) and 1,4-dioxane (0.6 mL). The solution was heated at 120 °C in the MW for 1 h. Purification by column chromatography (biotage SNAP-Ultra C18 12 g, eluted with 5-70% MeOH in water, 3CV, gradient over 18 CV, 6 CV) to yield the title product (39 mg, 97%, 0.11 mmol) as a white solid. m.p. 168 °C. $[\alpha]^{23}_{\text{D}} -40.2^{\circ}$ (c=0.5, MeOH). IR (thin film) $\nu = 2785, 1688, 1645, 1561 \text{ cm}^{-1}$. ¹H NMR (500 MHz, DMSO-*d*₆, 365 K) δ 8.42 (s, 1H, ArH, H₂), 8.36 (d, *J* = 1.9 Hz, 1H, ArH, H₅), 8.17 (d, *J* = 0.8 Hz, 1H, ArH, H₉), 7.97 (d, *J* = 0.8 Hz, 1H, ArH, H₁₀), 7.95 (dd, *J* = 8.6, 1.9 Hz, 1H, H₇), 7.67 (d, *J* = 8.6 Hz, 1H, ArH, H₈), 4.58 (q, *J* = 7.7 Hz, 1H CH, H_{1'}), 4.22 (q, *J* = 7.3 Hz, 2H, CH₂, CH₂CH₃), 3.99 (dd, *J* = 6.7, 5.5 Hz, 1H, CH, H_{2'}), 3.88 (t, *J* = 5.2 Hz, 1H CH, H_{3'}), 3.55 (qd, *J* = 10.5, 5.6 Hz, 2H, CH₂, H_{6'}), 2.33 (app. dt, *J* = 13.0, 8.3 Hz, 1H, CH₂, H_{5'}), 2.07 (ddt, *J* = 14.1, 8.6, 5.4 Hz, 1H CH, H_{4'}), 1.48 (t, *J* = 7.3 Hz, 3H, CH₃, CH₂CH₃), 1.38 (app. dt, *J* = 13.1, 8.5 Hz, 1H, CH₂, H_{5'}) ppm. ¹³C NMR (151 MHz, DMSO-*d*₆) δ 159.7 (C), 136.7 (CH), 130.6 (C), 130.6 (CH), 127.1 (CH), 121.7 (C), 117.9 (CH), 76.3 (CH), 72.5 (CH), 63.3 (CH₂), 56.3 (CH), 47.0 (CH₂), 45.7 (CH), 30.4 (CH₂), 15.9 (CH₃) ppm. Not all quaternary carbons observed due to slow rotation on NMR time scale. HRMS (ESI+) calculated for C₁₉H₂₄N₅O₃ 370.1879 found 370.1872; Method C t_R = 0.72 min, Purity (AUC) ≥ 95%.

(1S,2R,3R,5R)-3-(hydroxymethyl)-5-((6-(1-isopropyl-1H-pyrazol-4-yl)quinazolin-4-yl)amino)cyclopentane-1,2-diol (419)



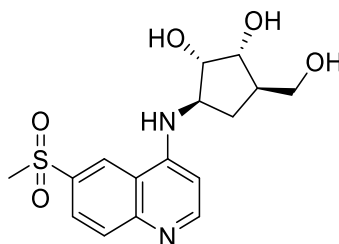
(1-Isopropylpyrazol-4-yl)boronic acid (30 mg, 0.19 mmol) was added to a solution of (1S,2R,3R,5R)-3-(hydroxymethyl)-5-[(6-iodoquinazolin-4-yl)amino]cyclopentane-1,2-diol (39 mg, 0.10 mmol), sodium carbonate (31 mg, 0.29 mmol) and tetrakis(triphenylphosphine)palladium(0) (9 mg, 0.01 mmol) in water (0.6 mL) and 1,4-dioxane (0.6 mL). The solution was heated at 120 °C in the MW for 1 h. Purification by column chromatography (biotage SNAP-Ultra C18 12 g, eluted with 2-70% MeOH in water, 3 CV, gradient over 18 CV, 6 CV) to yield the title product (37 mg, 99%, 0.10 mmol) as a white solid. m.p. 169 °C. $[\alpha]^{23}_{\text{D}} +33.2^{\circ}$ (c=0.5, MeOH). IR (thin film) $\nu = 3344, 2925, 1568 \text{ cm}^{-1}$. $^1\text{H NMR}$ (500 MHz, DMSO- d_6 , 365 K) δ 8.41 (s, 1H, ArH, H₂), 8.35 (d, $J = 1.9 \text{ Hz}$, 1H, H₅), 8.19 (s, 1H, ArH, H₉), 8.01 – 7.94 (m, 2H, ArH, H₁₀, H₇), 7.67 (d, $J = 8.6 \text{ Hz}$, 1H, ArH, H₈), 4.62 – 4.53 (m, 2H, CH, H_{1'}, CH₃CHCH₃), 3.99 (dd, $J = 6.7, 5.6 \text{ Hz}$, 1H, H_{2'}), 3.88 (t, $J = 5.2 \text{ Hz}$, 1H, H_{3'}), 3.55 (qd, $J = 10.5, 5.6 \text{ Hz}$, 2H, CH₂, H_{6'}), 2.33 (app. dt, $J = 13.0, 8.3 \text{ Hz}$, 1H, CH₂, H_{5'}), 2.07 (ddt, $J = 14.1, 8.6, 5.4 \text{ Hz}$, 1H, CH, H_{4'}), 1.52 (d, $J = 6.6 \text{ Hz}$, 6H, CH₃, CH₃CHCH₃), 1.41 – 1.34 (m, 1H, CH₂, H_{5'}) ppm. $^{13}\text{C NMR}$ (151 MHz, DMSO) δ 159.7 (C), 136.4 (CH), 130.7 (C), 130.7 (CH), 128.7 (CH, HSQC), 125.5 (CH), 121.4 (C), 117.8 (CH), 76.3 (CH), 72.5 (CH), 63.3 (CH₂), 56.3 (CH), 53.7 (CH), 45.7 (CH), 30.4 (CH₂), 23.2 (2 x CH₃) ppm. Not all quaternary carbons observed due to slow rotation on NMR time scale. HRMS (ESI+) calculated for C₂₀H₂₆N₅O₃ 384.2036, found 384.2021; Method B $t_{\text{R}} = 1.52 \text{ min}$, Purity (AUC) $\geq 95\%$.

(1S,2R,3R,5R)-3-(hydroxymethyl)-5-((6-(1-phenyl-1H-pyrazol-4-yl)quinazolin-4-yl)amino)cyclopentane-1,2-diol (420)



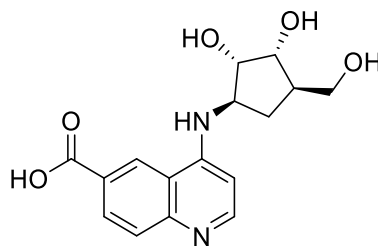
(1-Phenyl-1H-pyrazol-4-yl)boronic acid (37 mg, 0.20 mmol) was added to a solution of (1S,2R,3R,5R)-3-(hydroxymethyl)-5-[(6-iodoquinazolin-4-yl)amino]cyclopentane-1,2-diol (40 mg, 0.10 mmol), sodium carbonate (32 mg, 0.30 mmol) and tetrakis(triphenylphosphine)palladium(0) (9 mg, 0.01 mmol) in water (0.6 mL) and 1,4-dioxane (0.6 mL). The solution was heated at 120 °C in the MW for 1 h. Purification by column chromatography (biotage SNAP-Ultra C18 12 g, eluted with 5-60% MeOH in water, 1 CV, gradient over 30 CV, 2 CV) to yield the title product (32 mg, 76%, 0.08 mmol) as a white solid. m.p. 160 °C. $[\alpha]_D^{23}$ -31.9° (c=0.5, MeOH). IR (thin film) ν = 3209, 2912, 1623, 1574 cm^{-1} . ^1H NMR (600 MHz, $\text{DMSO}-d_6$) δ 9.06 (s, 1H, ArH, H₂), 8.57 (d, J = 1.9 Hz, 1H, ArH, H₅), 8.43 (s, 1H, ArH, H₉), 8.35 (s, 1H, ArH, H₁₀), 8.14 (dd, J = 8.6, 1.9 Hz, 1H, ArH, H₇), 8.03 (d, J = 7.4 Hz, 1H, NH), 7.95 – 7.90 (m, 2H, ArH, H₁₁, H₁₅), 7.72 (d, J = 8.6 Hz, 1H, ArH, H₈), 7.59 – 7.53 (m, 2H, ArH, H₁₂, H₁₄), 7.39 – 7.34 (m, 1H, ArH, H₁₃), 4.65 – 4.56 (m, 1H, CH, H_{1'}), 3.94 (dd, J = 7.6, 5.3 Hz, 1H, CH, H_{2'}), 3.82 (dd, J = 5.3, 4.1 Hz, 1H, CH, H_{3'}), 3.52 – 3.44 (m, 2H, CH₂, H_{6'}), 2.27 (app. dt, J = 13.0, 8.4 Hz, 1H, CH₂, H_{5'}), 2.04 – 1.97 (m, 1H, CH, H_{4'}), 1.27 (app. dt, J = 13.1, 8.7 Hz, 1H, CH₂, H_{5'}) ppm. ^{13}C NMR (151 MHz, $\text{DMSO}-d_6$) δ 159.8 (C), 155.1 (CH), 148.5 (C), 140.0 (C), 139.3 (CH), 130.9 (CH), 130.1 (2 x CH), 129.6 (C), 128.6 (CH), 127.0 (CH), 125.4 (CH), 124.2 (C), 118.8 (2 x CH), 118.6 (CH), 115.7 (C), 76.3 (CH), 72.5 (CH), 63.3 (CH₂), 56.3 (CH), 45.7 (CH), 30.4 (CH₂) ppm. HRMS (ESI+) calculated for $\text{C}_{23}\text{H}_{24}\text{N}_5\text{O}_3$ 418.1879 found 418.1857; Method B t_R = 1.86 min, Purity > 90%

(1*S*,2*R*,3*R*,5*R*)-3-(Hydroxymethyl)-5-((6-(methylsulfonyl)quinolin-4-yl)amino)cyclopentane-1,2-diol (421)



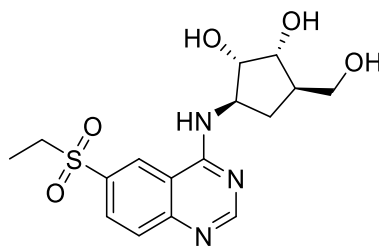
Copper iodide (8 mg, 0.04 mmol) and sodium methanesulfinate (45 mg, 0.44 mmol) were added to a stirred solution of (1*S*,2*R*,3*R*,5*R*)-3-(hydroxymethyl)-5-[(6-iodoquinazolin-4-yl)amino]cyclopentane-1,2-diol (35 mg, 0.09 mmol) in DMSO. The reaction mixture was heated for 24 h at 120 °C. Purification by column chromatography (biotage SNAP KP-Sil 10 g, eluted with 0-10% 10% NH₃ in MeOH in CH₂Cl₂, 1 CV, gradient over 10 CV, 5 CV) to afford the title compound (20 mg, 65%, 0.06 mmol) as a yellow oil. IR (thin film) $\nu = 3353, 1615, 1587, 1540 \text{ cm}^{-1}$. ¹H NMR (600 MHz, DMSO-*d*₆) δ 9.03 (d, *J* = 2.1 Hz, 1H, ArH, H₅), 8.70 (d, *J* = 7.6 Hz, 1H, NH), 8.62 (s, 1H, ArH, H₂), 8.22 – 8.17 (m, 1H, ArH, H₇), 7.87 (s, 1H, ArH, H₈), 4.70 – 4.60 (m, 3H, 2 x OH, CH, H₁'), 4.48 (d, *J* = 4.5 Hz, 1H, OH), 3.94 (dt, *J* = 8.4, 4.9 Hz, 1H, CH, H₂'), 3.77 (q, *J* = 3.9 Hz, 1H, CH, H₃'), 3.43 (dp, *J* = 15.8, 5.4 Hz, 2H, CH₂, H₆'), 3.30 (s, 3H, CH₃), 2.19 (app. dt, *J* = 13.0, 8.4 Hz, 1H, CH₂, H₅'), 1.98 (ttt, *J* = 9.3, 6.0, 3.7 Hz, 1H, CH, H₄'), 1.22 (app. dt, *J* = 12.9, 8.9 Hz, 1H, CH₂, H₅') ppm. ¹³C NMR (151 MHz, DMSO-*d*₆) δ 160.5 (C), 158.0 (CH), 152.5 (C), 137.6 (C), 130.0 (CH), 129.3 (CH), 124.5 (CH), 114.8 (C), 75.9 (CH), 72.4 (CH), 63.5 (CH₂), 56.3 (CH), 45.7 (CH), 44.2 (CH₃), 30.0 (CH₂) ppm. HRMS (ESI+) calculated for C₁₅H₂₀N₃O₅S 354.1118, found 354.1131; Method A *t*_R = 0.25 min, Purity (AUC) $\geq 95\%$.

4-(((1*R*,2*S*,3*R*,4*R*)-2,3-Dihydroxy-4-(hydroxymethyl)cyclopentyl)amino)quinoline-6-carboxylic acid (422)



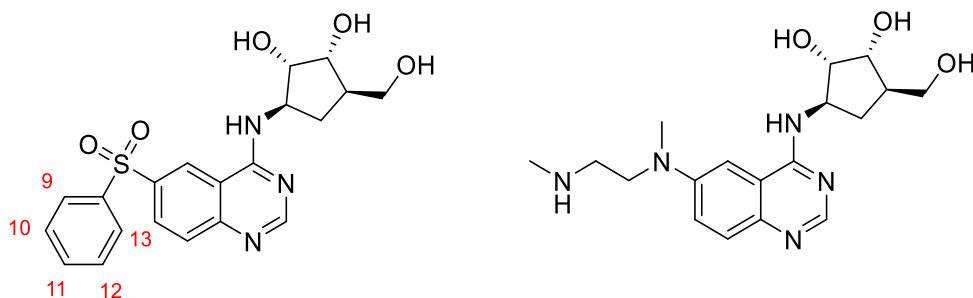
(1*S*,2*R*,3*R*,5*R*)-3-(Hydroxymethyl)-5-[(6-iodoquinazolin-4-yl)amino]cyclopentane-1,2-diol (50 mg, 0.12 mmol) and methanesulfonato[4,5-Bis(diphenylphosphino)-9,9-dimethylxanthene](2'-methylamino-1,1'-biphenyl-2-yl)palladium(II) (6 mg, 0.01 mmol) were dissolved in 1,4-dioxane (0.3 mL) and water (0.3 mL). The MW vial was evacuated and filled with carbon monoxide from a balloon. DIPEA (0.10 mL, 0.37 mmol) was added and the reaction was heated at 60 °C for 1 h. The reaction mixture was directly loaded onto an ion exchange cartridge (Flash-NH₂ 2 g) and flushed with acetonitrile. The product was eluted with formic acid in acetonitrile to yield the title product (20 mg, 50%, 0.06 mmol) as a clear oil. IR (thin film) $\nu = 3281, 1634 \text{ cm}^{-1}$. ¹H NMR (600 MHz, DMSO-*d*₆) δ 9.25 (d, $J = 1.8 \text{ Hz}$, 1H, ArH, H₅), 8.88 (s, 1H, ArH, H₂), 8.42 (dd, $J = 8.7, 1.8 \text{ Hz}$, 1H, ArH, H₇), 7.99 (d, $J = 8.6 \text{ Hz}$, 1H, ArH, H₈), 4.84 (q, $J = 8.9 \text{ Hz}$, 1H, CH, H_{1'}), 4.06 – 3.98 (m, 1H, CH, H_{2'}), 3.76 (dd, $J = 5.2, 3.2 \text{ Hz}$, 1H, CH, H_{3'}), 3.37 (qd, $J = 10.7, 6.3 \text{ Hz}$, 2H, CH₂, H_{6'}), 2.09 (app. dt, $J = 13.1, 8.6 \text{ Hz}$, 1H, CH₂, H_{5'}), 1.97 (ttt, $J = 9.0, 6.2, 3.0 \text{ Hz}$, 1H, CH, H_{4'}), 1.41 – 1.29 (m, 1H, CH₂, H_{5'}) ppm. ¹³C NMR (151 MHz, DMSO) δ 166.3 (C), 161.4 (C), 152.0 (CH), 140.4 (C), 136.0 (CH), 130.7 (C), 127.2 (CH), 120.0 (CH), 113.1 (C), 75.5 (CH), 72.3 (CH), 63.3 (CH₂), 57.7 (CH), 45.6 (CH), 29.1 (CH₂) ppm. HRMS (ESI+) calculated for C₁₅H₁₇N₃O₅ 320.1241 found 320.1241; Method D $t_R = 0.64 \text{ min}$; Purity = 90%.

(1*R*,2*S*,3*R*,5*R*)-3-((6-(ethylsulfonyl)quinazolin-4-yl)amino)-5-(hydroxymethyl)cyclopentane-1,2-diol (423)



Copper iodide (7 mg, 0.04 mmol) and sodium ethylsulfinate (43 mg, 0.37 mmol) were added to a stirred solution of (1*S*,2*R*,3*R*,5*R*)-3-(hydroxymethyl)-5-[(6-iodoquinazolin-4-yl)amino]cyclopentane-1,2-diol (30 mg, 0.07 mmol) in DMSO (0.3 mL). The reaction mixture was heated for 18 h at 120 °C. Purification by column chromatography (biotage SNAP-Ultra C18 10 g, 1-40% MeOH in water, 5 CV, gradient over 20 CV, 6 CV) to yield the title product (17 mg, 60%, 0.05 mmol) as a yellow oil. IR (thin film) $\nu = 3289, 2899, 1615, 1588, 1541 \text{ cm}^{-1}$. ^1H NMR (600 MHz, DMSO- d_6) δ 8.99 (d, $J = 2.0$ Hz, 1H, ArH, H₅), 8.70 (d, $J = 7.6$ Hz, 1H, NH), 8.58 (s, 1H, ArH, H₂), 8.13 (dd, $J = 8.6, 2.0$ Hz, 1H, ArH, H₇), 7.86 (d, $J = 8.7$ Hz, 1H, ArH, H₈), 4.65 (dq, $J = 9.7, 7.9$ Hz, 1H, CH, H_{1'}), 3.94 (dd, $J = 8.0, 5.4$ Hz, 1H, CH, H_{2'}), 3.76 (dd, $J = 5.4, 3.7$ Hz, 1H, CH, H_{3'}), 3.43 (tt, $J = 10.5, 5.3$ Hz, 2H, CH₂, H_{6'}), 3.37 (q, $J = 7.4$ Hz, 2H, CH₂, CH₂CH₃), 2.19 (app. dt, $J = 12.9, 8.4$ Hz, 1H, CH₂, H_{5'}), 1.98 (dddd, $J = 14.7, 8.6, 6.0, 3.7$ Hz, 1H, CH, H_{4'}), 1.28 – 1.17 (m, 1H, CH₂, H_{5'}), 1.15 (t, $J = 7.4$ Hz, 3H, CH₃, CH₂CH₃) ppm. ^{13}C NMR (151 MHz, DMSO- d_6) δ 160.5 (C), 158.2 (CH), 152.4 (C, HMBC), 135.2 (C), 130.6 (CH), 129.3 (CH), 125.5 (CH), 115.1 (C, HMBC), 75.9 (CH), 72.4 (CH), 63.5 (CH₂), 56.3 (CH), 49.9 (CH₂), 45.7 (CH), 29.9 (CH₂), 7.7 (CH₃) ppm. HRMS (ESI+) calculated for C₁₆H₂₁N₃O₅S 368.1280, found 368.1264; Method B $t_{\text{R}} = 0.79$ min, Purity (AUC) $\geq 95\%$.

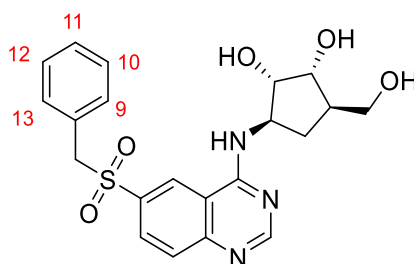
(1*S*,2*R*,3*R*,5*R*)-3-(Hydroxymethyl)-5-((6-(phenylsulfonyl)quinazolin-4-yl)amino)cyclopentane-1,2-diol (424) and (1*S*,2*R*,3*R*,5*R*)-3-(hydroxymethyl)-5-((6-(methyl(2-(methylamino)ethyl)amino)quinazolin-4-yl)amino)cyclopentane-1,2-diol (426)



Copper bromide (3 mg, 0.02 mmol) was added to benzenesulfinic acid sodium salt (24 mg, 0.14 mmol), (1*S*,2*R*,3*R*,5*R*)-3-(hydroxymethyl)-5-[(6-iodoquinazolin-4-yl)amino]cyclopentane-1,2-diol (48 mg, 0.12 mmol), dimethylethylenediamine (0.01 mL, 0.05 mmol) and potassium carbonate (33 mg, 0.24 mmol) in DMSO (0.4 mL). The reaction mixture was heated for 3 h at 110 °C. Purification by reverse phase column chromatography (biotage SNAP-Ultra C18 12 g, eluted with 10-100% MeOH in water, 1 CV, gradient over 10 CV, 6 CV) to afford the title compounds as oils. **424** (6 mg, 12%, 0.01 mmol). IR (thin film) $\nu = 3291, 2924, 1613, 1584, 1537 \text{ cm}^{-1}$. $^1\text{H NMR}$ (600 MHz, Methanol- d_4) δ 9.02 (d, $J = 1.9 \text{ Hz}$, 1H, ArH, H₂), 8.57 (br s, 1H, ArH, H₅), 8.22 (dd, $J = 8.6, 2.0 \text{ Hz}$, 1H, ArH, H₇), 8.08 – 8.05 (m, 2H, ArH, H₉, H₁₃), 7.83 (d, $J = 8.8 \text{ Hz}$, 1H, ArH, H₈), 7.70 – 7.65 (m, 1H, ArH, H₁₁), 7.64 – 7.59 (m, 2H, ArH, H₁₀, H₁₂), 4.76 (q, $J = 8.0 \text{ Hz}$, 1H, CH, H_{1'}), 4.09 (dd, $J = 7.0, 5.4 \text{ Hz}$, 1H, CH, H_{2'}), 4.00 (d, $J = 5.1 \text{ Hz}$, 1H, CH, H_{3'}), 3.73 – 3.65 (m, 2H, CH₂, H_{6'}), 2.48 (app. dt, $J = 13.3, 8.5 \text{ Hz}$, 1H, CH₂, H_{5'}), 2.22 (ddt, $J = 14.1, 8.6, 5.4 \text{ Hz}$, 1H, CH, H_{4'}), 1.47 (app. dt, $J = 13.3, 8.5 \text{ Hz}$, 1H, CH₂, H_{5'}) ppm. $^{13}\text{C NMR}$ (151 MHz, Methanol- d_4) δ 160.6 (C), 141.4 (C), 138.7 (C), 133.4 (CH), 130.3 (CH), 129.3 (2 x CH), 127.5 (2 x CH), 124.1 (CH), 76.4 (CH), 72.7 (CH), 63.2 (CH₂), 56.4 (CH), 45.2 (CH), 29.1 (CH₂) ppm. Not all quaternary carbons observed. HRMS (ESI+) calculated for C₂₀H₂₁N₃O₅S 416.1274680, found 416.1278672; Method D $t_{\text{R}} = 1.48 \text{ min}$; Purity >95%. **426** (14 mg, 31%, 0.04 mmol). IR (thin film) $\nu = 3318, 1588, 1536 \text{ cm}^{-1}$. $^1\text{H NMR}$ (600 MHz, Methanol- d_4) δ 8.43 (s, 1H, ArH, H₅), 7.68 (d, $J = 9.1 \text{ Hz}$, 1H,

ArH, H₂), 7.58 – 7.53 (m, 1H, ArH, H₈), 7.42 (s, 1H, ArH, H₇), 4.76 (app. p, $J = 8.3$ Hz, 1H, CH, H_{1'}), 4.11 (dd, $J = 7.3, 5.5$ Hz, 1H, CH, H_{2'}), 4.01 (app. t, $J = 4.9$ Hz, 1H, CH, H_{3'}), 3.81 (t, $J = 6.6$ Hz, 1H, CH₂), 3.69 (dd, $J = 5.4, 2.4$ Hz, 2H, CH₂), 3.32 (d, $J = 3.8$ Hz, 2H, CH₂, H_{6'}), 3.15 (s, 3H, CH₃), 2.78 (d, $J = 4.0$ Hz, 3H, CH₃), 2.49 (ddd, $J = 13.3, 9.1, 7.8$ Hz, 1H, CH₂, H_{5'}), 2.23 (ddt, $J = 13.6, 8.7, 4.7$ Hz, 1H, CH, H_{4'}), 1.52 (dtd, $J = 16.4, 8.2, 3.1$ Hz, 1H, CH₂, H_{5'}) ppm. ¹³C NMR (151 MHz, Methanol-*d*₄) δ 159.5 (C), 150.0 (CH, HSQC), 148.4 (C), 125.2 (CH), 122.0 (CH), 102.0 (CH), 76.5 (CH), 72.7 (CH), 63.0 (CH₂), 56.8 (CH), 49.0 (CH₂), 46.1 (CH₂), 45.3 (CH), 37.9 (CH₃), 32.6 (CH₃), 29.2 (CH₂) ppm. Not all quaternary carbons observed. HRMS (ESI+) calculated for C₁₈H₂₇N₅O₃ 362.2192, found 362.2143; Method D t_R = 0.32 min; Purity >95%.

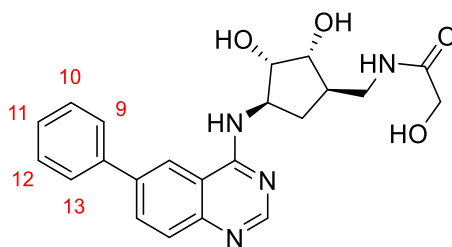
(1*R*,2*S*,3*R*,5*R*)-3-((6-(Benzylsulfonyl)quinazolin-4-yl)amino)-5-(hydroxymethyl)cyclopentane-1,2-diol (425)



Dimethylethylenediamine (0.01 mL, 0.07 mmol) was added to a solution of potassium carbonate (24 mg, 0.17 mmol), copper bromide (1 mg, 0.01 mmol), (1*S*,2*R*,3*R*,5*R*)-3-(hydroxymethyl)-5-[(6-iodoquinazolin-4-yl)amino]cyclopentane-1,2-diol (35 mg, 0.09 mmol) and phenylmethanesulfinic acid (17 mg, 0.10 mmol) in DMSO (0.4 mL). The reaction mixture was heated for 2 h at 110 °C. Purification by column chromatography (biotage SNAP-Ultra C18 12 g, eluted with 0-100% MeOH in water, 1 CV, gradient over 20 CV, 6 CV) to yield the title product (6 mg, 16%, 0.014 mmol) as a yellow oil. IR (thin film) $\nu = 3272, 1613, 1582, 1533$ cm⁻¹. ¹H NMR (600 MHz, Methanol-*d*₄) δ 7.97 (s, 1H, ArH), 7.84 (s, 1H, ArH), 7.45 – 7.42 (m, 1H, ArH), 7.36 – 7.30 (m, 1H, ArH), 7.29 – 7.24 (m, 2H, ArH, H₁₀, H₁₂), 7.18 – 7.14 (m, 2H, ArH, H₉, H₁₃), 4.76

(q, $J = 7.8$ Hz, 1H, CH, H_{1'}), 4.61 (s, 2H, CH₂, CH₂ benzyl), 4.06 (d, $J = 8.0$ Hz, 1H, CH, H_{2'}), 3.98 (t, $J = 5.0$ Hz, 1H, CH, H_{3'}), 3.72 – 3.64 (m, 2H, CH₂, H_{6'}), 2.46 (app. dt, $J = 13.3, 8.5$ Hz, 1H, CH₂, H_{5'}), 2.22 (ddt, $J = 14.0, 8.4, 5.3$ Hz, 1H, CH, H_{4'}), 1.44 (app. dt, $J = 13.4, 8.3$ Hz, 1H, CH₂, H_{5'}) ppm. ¹³C NMR (151 MHz, MeOD) δ 160.5 (C), 135.7 (C), 131.3 (CH), 130.8 (2 x CH), 130.2 (CH), 128.5 (CH), 128.4 (CH), 128.3 (C), 128.2 (2 x CH), 125.5 (CH), 76.3 (CH), 72.7 (CH), 63.1 (CH₂), 61.7 (CH₂), 56.5 (CH), 45.2 (CH), 29.1 (CH₂). Not all quaternary carbons observed due to slow rotation on NMR timescale. HRMS (ESI+) calculated for C₂₁H₂₃N₃O₅S 430.1431 found 430.1441; Method D $t_R = 1.44$ min, Purity (AUC) $\geq 95\%$.

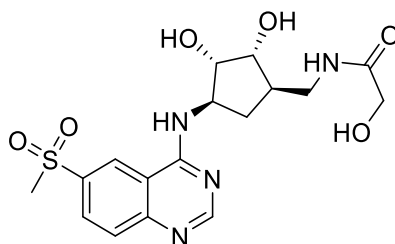
***N*-(((1*R*,2*R*,3*S*,4*R*)-2,3-Dihydroxy-4-((6-phenylquinazolin-4-yl)amino)cyclopentyl)methyl)-2-hydroxyacetamide (427)**



conc HCl (0.05 mL, 0.11 mmol) was added to *N*-(((1*R*,2*R*,3*S*,4*R*)-2,3-bis[[*tert*-butyl(dimethyl)silyl]oxy]-4-[(6-phenylquinazolin-4-yl)amino]cyclopentyl)methyl)-2-hydroxyacetamide (22 mg, 0.03 mmol) in EtOH (0.7 mL) and the reaction was stirred at rt for 2 h. The reaction mixture was concentrated and purified by column chromatography (biotage SNAP-Ultra C18 12 g, eluted with 0-50% MeOH in water, 2 CV gradient over 15 CV, 2 CV) to yield the title compound (11 mg, 78%, 0.03 mmol) as a white solid. IR (thin film) $\nu = 3245, 1636, 1583, 1536$ cm⁻¹. ¹H NMR (600 MHz, Methanol-*d*₄) δ 8.63 (s, 1H, ArH, H₅), 8.58 (s, 1H, ArH, H₂), 8.23 – 8.17 (m, 1H, ArH, H₇), 7.87 – 7.78 (m, 3H, H₈, H₁₀, H₁₂), 7.54 (t, $J = 7.7$ Hz, 2H, ArH, H₉, H₁₃), 7.47 – 7.42 (m, 1H, ArH, H₁), 4.77 (td, $J = 8.6, 6.6$ Hz, 1H, CH, H_{1'}), 4.14 (dd, $J = 6.7, 5.6$ Hz, 1H, CH, H_{2'}), 4.02 (s, 2H, CH₂, CH₂OH), 3.91 (t, $J = 5.3$ Hz, 1H, CH, H_{3'}), 3.48 – 3.37 (m, 2H, CH₂, H_{6'}), 2.49 (app. dt, $J = 13.3, 8.3$ Hz, 1H, CH₂, H_{5'}), 2.29 (pd, $J = 7.8, 5.1$ Hz, 1H, CH, H_{4'}), 1.42 (app. dt, $J = 13.3, 9.0$ Hz, 1H, CH₂, H_{5'}) ppm. ¹³C NMR (151 MHz, Methanol-*d*₄) δ

174.1 (C), 160.7 (C), 153.2 (CH), 145.1 (C, HSQC), 140.0 (C), 139.4 (C), 132.7 (CH), 128.7 (2 x CH), 127.8 (CH), 127.0 (2 x CH), 124.8 (CH), 120.5 (CH), 109.1 (C), 76.5 (CH), 74.0 (CH), 61.2 (CH₂), 56.9 (CH), 43.2 (CH), 41.6 (CH₂), 30.3 (CH₂) ppm. HRMS (ESI+) calculated for C₂₂H₂₅N₄O₄ 409.1876, found 409.1864; Method C t_R = 0.89 min; Purity (AUC) ≥ 95%.

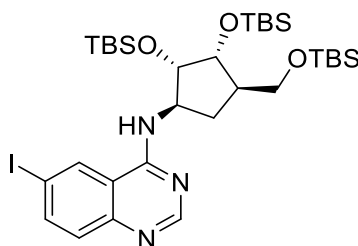
***N*-(((1*R*,2*R*,3*S*,4*R*)-2,3-Dihydroxy-4-((6-(methylsulfonyl)quinazolin-4-yl)amino)cyclopentyl)methyl)-2-hydroxyacetamide (428)**



Copper iodide (7 mg, 0.04 mmol) and sodium methanesulfinate (36 mg, 0.36 mmol) were added to a stirred solution of *N*-[[[(1*R*,2*R*,3*S*,4*R*)-2,3-bis[[*tert*-butyl(dimethyl)silyl]oxy]-4-[(6-iodoquinazolin-4-yl)amino]cyclopentyl)methyl]-2-hydroxy-acetamide (50 mg, 0.07 mmol) in DMSO (0.7 mL). The reaction mixture was heated for 24 h at 120 °C. Purification by column chromatography (biotage SNAP-Ultra C18 12 g, eluted with 10-100% MeOH in water, 1 CV gradient over 10 CV, 6 CV) to yield the title product (17 mg, 58%, 0.04 mmol) as a yellow solid. IR (thin film) ν = 3292, 2918, 1645, 1614, 1589, 1539 cm⁻¹. ¹H NMR (600 MHz, Methanol-*d*₄) δ 9.00 (d, *J* = 2.0 Hz, 1H, ArH, H₅), 8.63 (br s, 1H, ArH, H₂), 8.28 (dd, *J* = 8.2, 2.1 Hz, 1H, ArH, H₇), 7.92 (d, *J* = 8.8 Hz, 1H, ArH, H₈), 4.73 (td, *J* = 8.7, 6.6 Hz, 1H, CH, H_{1'}), 4.15 – 4.08 (m, 1H, CH, H_{2'}), 4.02 (s, 2H, CH₂, CH₂OH), 3.90 (t, *J* = 5.5 Hz, 1H, CH, H_{3'}), 3.44 – 3.37 (m, 2H, CH₂, H_{6'}), 3.23 (s, 3H, CH₃), 2.48 (app. dt, *J* = 13.3, 8.3 Hz, 1H, CH₂, H_{5'}), 2.28 (dq, *J* = 13.0, 7.7 Hz, 1H, CH, H_{4'}), 1.38 (app. dt, *J* = 13.4, 9.1 Hz, 1H, CH₂, H_{5'}) ppm. ¹³C NMR (151 MHz, Methanol-*d*₄) δ 174.7 (C, HMBC), 157.4 (CH, HSQC), 137.9 (C), 130.0 (CH), 127.9 (CH, HSCQ) 124.1 (CH), 76.3 (CH), 74.0 (CH), 61.2 (CH₂), 56.6 (CH), 43.0 (CH), 43.0 (CH₃), 41.6 (CH₂), 30.3 (CH₂) ppm. Not all quaternary carbons observed due to slow rotation on NMR timescale. HRMS (ESI+)

calculated for $C_{17}H_{23}N_4O_6S$ 411.1338, found 411.1332; Method B $t_R = 0.77$ min; Purity (AUC) $\geq 95\%$.

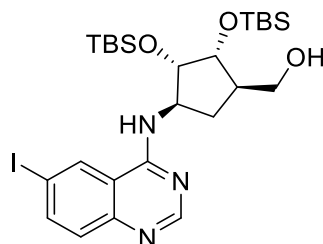
***N*-((1*R*,2*S*,3*R*,4*R*)-2,3-Bis((*tert*-butyldimethylsilyl)oxy)-4-(((*tert*-butyldimethylsilyl)oxy)methyl)cyclopentyl)-6-iodoquinazolin-4-amine (429)**



To a solution of (1*S*,2*R*,3*R*,5*R*)-3-(hydroxymethyl)-5-[(6-iodoquinazolin-4-yl)amino]cyclopentane-1,2-diol (650 mg, 1.62 mmol) in DMF (5.4 mL) was added imidazole (1100 mg, 16.20 mmol) and DMAP (20 mg, 0.16 mmol) followed by TBDMSCl (1465 mg, 9.72 mmol) and the mixture was stirred at rt for 18 h. The reaction was quenched by the addition of water (60 mL) and extracted with EtOAc (3 x 50 mL). The combined organic layers were dried with $MgSO_4$, filtered and concentrated under vacuum. The residue was purified by column chromatography (biotage SNAP KP-Sil 50 g, eluted with 0-50% EtOAc in cyclohexane, 2 CV, gradient over 20 CV, 2 CV) to afford the title product (864 mg, 72%, 1.16 mmol) as a foam. IR (thin film) $\nu = 2952, 2928, 2885, 2856, 1572, 1522$ cm^{-1} . 1H NMR (600 MHz, $DMSO-d_6$) δ 8.63 (d, $J = 1.9$ Hz, 1H, ArH, H₅), 8.45 (s, 1H, ArH, H₂), 8.02 (dd, $J = 8.7, 1.9$ Hz, 1H, ArH, H₇), 7.97 (d, $J = 8.4$ Hz, 1H, NH), 7.45 (d, $J = 8.7$ Hz, 1H, ArH, H₈), 4.79 (p, $J = 8.3$ Hz, 1H, CH, H_{1'}), 4.10 (dd, $J = 7.7, 4.0$ Hz, 1H, CH, H_{2'}), 3.97 (t, $J = 3.4$ Hz, 1H, CH, H_{3'}), 3.61 – 3.55 (m, 2H, CH₂, H_{6'}), 2.22 (dt, $J = 13.5, 9.4$ Hz, 1H, CH₂, H_{5'}), 2.13 – 2.07 (m, 1H, CH, H_{4'}), 1.23 (ddd, $J = 13.8, 8.1, 6.0$ Hz, 1H, CH₂, H_{5'}), 0.91 (s, 9H, CH₃), 0.89 (s, 9H, CH₃), 0.85 (s, 9H, CH₃), 0.10 (s, 3H, CH₃), 0.07 (d, $J = 1.7$ Hz, 6H, CH₃), 0.07 (s, 3H, CH₃), 0.00 (s, 3H, CH₃), -0.06 (s, 3H, CH₃) ppm. ^{13}C NMR (151 MHz, $DMSO-d_6$) δ 158.7 (C), 155.8 (CH), 148.7 (C), 141.3 (CH), 131.7 (CH), 130.0 (CH), 117.2 (C), 90.7 (CH₂), 77.2 (CH), 74.6 (CH), 65.2 (CH₂), 54.6 (CH), 45.3 (CH), 28.8 (CH₂), 26.3 (3 x CH₃), 26.3 (3 x CH₃), 26.2 (3 x CH₃), 18.5 (C), 18.3

(C), 18.2 (C), -3.9 (CH₃), -4.0 (CH₃), -4.2 (CH₃), -4.2 (CH₃), -4.9 (CH₃), -5.0 (CH₃) ppm.

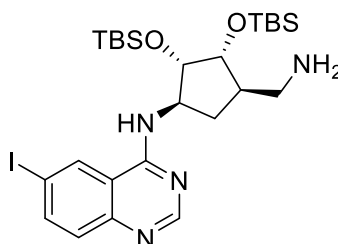
((1R,2R,3S,4R)-2,3-bis((*tert*-butyldimethylsilyl)oxy)-4-((6-iodoquinazolin-4-yl)amino)cyclopentyl)methanol (430)



To a solution of *N*-[(1*R*,2*S*,3*R*,4*R*)-2,3-bis[[*tert*-butyl(dimethyl)silyl]oxy]-4-[[*tert*-butyl(dimethyl)silyl]oxymethyl]cyclopentyl]-6-iodo-quinazolin-4-amine (850 mg, 1.14 mmol) in EtOH (6 mL) in an ice bath was added dropwise over 30 min a solution conc HCl (0.2 mL, 3.43 mmol) in EtOH (6 mL). The reaction was stirred at 0°C for 1 h. The reaction was quenched with sat NaHCO₃ (15 mL), water (15 mL) was added and the product was extracted with Et₂O (3 x 35 mL). The combined organic layers were dried with MgSO₄, filtered and concentrated. Purification by column chromatography (biotage SNAP KP-Sil 50g eluted with 0-50% EtOAc in cyclohexane, 3 CV, gradient over 15 CV, 2 CV) to yield the title product (528 mg, 73%, 0.84 mmol) as a white foam. IR (thin film) ν = 2927, 2855, 1606, 1576, 1536 cm⁻¹. ¹H NMR (600 MHz, Methanol-*d*₄) δ 8.56 (d, *J* = 1.9 Hz, 1H, ArH, H₅), 8.47 (s, 1H, ArH, H₂), 8.07 (dd, *J* = 8.8, 1.9 Hz, 1H, ArH, H₇), 7.48 (d, *J* = 8.7 Hz, 1H, ArH, H₈), 4.77 (dt, *J* = 8.9, 5.5 Hz, 1H, CH, H₁'), 4.12 – 4.05 (m, 2H, 2 CH, H₂', H₃'), 3.69 (h, *J* = 5.2 Hz, 2H, CH₂, H₆'), 2.48 (ddd, *J* = 13.9, 10.2, 8.8 Hz, 1H, CH₂, H₅'), 2.30 – 2.18 (m, 1H, CH, H₄'), 1.51 – 1.44 (m, 2H, CH₂, H₅'), 0.96 (s, 9H, CH₃), 0.86 (s, 9H, CH₃), 0.15 (s, 3H, CH₃), 0.13 (s, 3H, CH₃), 0.11 (s, 3H, CH₃), 0.11 (s, 3H, CH₃) ppm. ¹³C NMR (151 MHz, Methanol-*d*₄) δ 158.4 (C), 155.2 (CH), 147.7 (C), 141.5 (CH), 131.2 (CH), 128.2 (CH), 116.8 (C), 89.6 (C), 78.0 (CH), 74.7 (CH), 62.6 (CH₂), 55.2 (CH), 44.8 (CH), 28.6 (CH₂), 25.1 (3 x CH₃), 25.1 (3 x CH₃), 17.6 (C), 17.6 (C), -5.4 (CH₃), -5.5 (CH₃), -5.5 (CH₃), -5.8 (CH₃) ppm. HRMS (ESI+) calculated for

C₂₆H₄₄IN₃O₃Si₂ 630.2044, found 630.0779; Method B ext mass range t_R = 3.77 min; Purity (AUC) ≥ 95%.

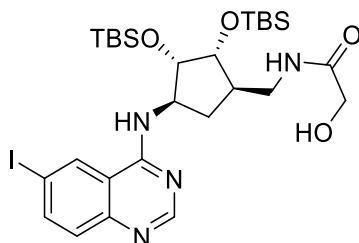
***N*-((1*R*,2*S*,3*R*,4*R*)-4-(Aminomethyl)-2,3-bis((*tert*-butyldimethylsilyl)oxy)cyclopentyl)-6-iodoquinazolin-4-amine (432)**



Methanesulfonic anhydride (415 mg, 2.38 mmol) was added to a stirred solution of [(1*R*,2*R*,3*S*,4*R*)-2,3-bis[[*tert*-butyl(dimethyl)silyl]oxy]-4-[(6-iodoquinazolin-4-yl)amino]cyclopentyl]methanol (500 mg, 0.79 mmol) and triethylamine (0.6 mL, 3.97 mmol) in CH₂Cl₂ (5 mL) at 0 °C. The clear solution was stirred at rt for 2 h. Water (20 mL) and brine (sat. aq., 5 mL) were added. The product was extracted with EtOAc (3 × 30 mL). The organic layers were combined, dried with MgSO₄, filtered and evaporated under vacuum. The product (562 mg, 0.79 mmol) was dissolved in DMF and sodium azide (103 mg, 1.6 mmol) was added at 0 °C. The mixture was stirred at 60 °C for 18 h. Triphenylphosphine (417 mg, 1.59 mmol) and NH₄OH (28-30% in H₂O, 1.5 mL) were added and the mixture was heated at 60 °C for 3 h. The reaction mixture was allowed to cool. Water (80 mL) and brine (10 mL) were added and the mixture was extracted with Et₂O (4 × 40 mL). The organic layers were combined, dried with MgSO₄, filtered and evaporated under vacuum. The residue was purified by column chromatography (biotage SNAP KP-Sil 50 g, eluted with 0-15% MeOH in CH₂Cl₂, 1 CV, gradient over 18 CV, 5 CV) to afford the title product (403 mg, 81%, 0.64 mmol) as a yellow oil. IR (thin film) ν = 2928, 2856, 1607, 1574, 1529 cm⁻¹. ¹H NMR (600 MHz, Methanol-*d*₄) δ 8.66 (d, *J* = 1.8 Hz, 1H, ArH, H₅), 8.49 (s, 1H, ArH, H₂), 8.08 (dd, *J* = 8.8, 1.9 Hz, 1H, ArH, H₇), 7.50 (d, *J* = 8.8 Hz, 1H, ArH, H₈), 4.75 – 4.69 (m, 1H, CH, H_{1'}), 4.11 (t, *J* = 4.1 Hz, 1H, CH, H_{2'}), 3.92 (dd, *J* = 6.7, 3.9 Hz, 1H, CH, H_{3'}), 3.00 (dd, *J* = 12.5, 5.1 Hz, 1H, CH₂, H_{6'}), 2.76 (dd, *J* = 12.5, 8.9 Hz, 1H, CH₂, H_{6'}), 2.56 (app. dt, *J* = 13.9, 9.3 Hz, 1H, CH₂,

H_{5'}), 2.31 (tt, $J = 8.6, 6.6$ Hz, 1H, CH, H_{4'}), 1.41 (ddd, $J = 13.8, 7.8, 6.0$ Hz, 1H, CH₂, H_{5'}), 0.97 (s, 9H, CH₃), 0.89 (s, 9H, CH₃), 0.16 (s, 6H, 2 x CH₃), 0.12 (s, 6H, 2 x CH₃) ppm. ¹³C NMR (151 MHz, Methanol-*d*₄) δ 158.4 (C), 155.1 (CH), 147.7 (C), 141.5 (CH), 131.4 (CH), 128.2 (CH), 116.7 (C), 89.7 (C), 78.0 (CH), 76.4 (CH), 55.5 (CH), 44.0 (CH₂), 43.8 (CH), 30.0 (CH₂), 25.1 (3 x CH₃), 25.1 (3 x CH₃), 17.6 (C), 17.6 (C), -5.3 (CH₃), -5.4 (CH₃), -5.6 (CH₃), -5.9 (CH₃) ppm. HRMS (ESI+) calculated for C₂₆H₄₆N₄O₂Si₂l 629.2204, found 629.2203; Method C $t_R = 1.57$ min; Purity >95%.

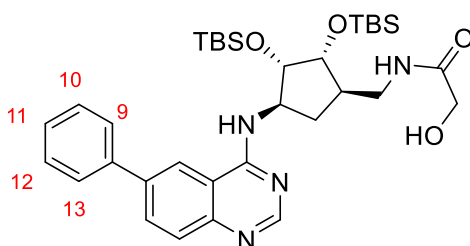
***N*-(((1*R*,2*R*,3*S*,4*R*)-2,3-Bis((*tert*-butyldimethylsilyl)oxy)-4-((6-iodoquinazolin-4-yl)amino)cyclopentyl)methyl)-2-hydroxyacetamide (433)**



N-(3-Dimethylaminopropyl)-*N'*-ethylcarbodiimide hydrochloride (148 mg, 0.77 mmol) was added to a stirred solution of *N*-[(1*R*,2*S*,3*R*,4*R*)-4-(aminomethyl)-2,3-bis[[*tert*-butyl(dimethyl)silyl]oxy]cyclopentyl]-6-iodo-quinazolin-4-amine (440 mg, 0.70 mmol), 2-hydroxyacetic acid (70 mg, 0.91 mmol) and *N*-hydroxysuccinimide (89 mg, 0.77 mmol) in THF (3.5 mL). The solution was stirred at rt for 18 h. The reaction mixture was concentrated and purified by column chromatography (biotage SNAP KP-Sil 25 g, eluted with 0-100% EtOAc in cyclohexane, 1 CV, gradient over 40 CV, 5 CV) followed by reverse phase column chromatography (biotage SNAP-Ultra C18 12 g, eluted with 0-100% MeOH in water, 1 CV gradient over 20 CV, 6 CV) to afford the title compound (270 mg, 56%, 0.39 mmol) as an off white solid. IR (thin film) $\nu = 3265, 2928, 2855, 1650, 1607, 1575, 1530$ cm⁻¹. ¹H NMR (600 MHz, Methanol-*d*₄) δ 8.68 (d, $J = 1.9$ Hz, 1H, ArH, H₆), 8.50 (s, 1H, ArH, H₂), 8.10 (dd, $J = 8.8, 1.9$ Hz, 1H, ArH, H₇), 7.49 (d, $J = 8.8$ Hz, 1H, ArH, H₈), 4.92 (dt, $J = 9.6, 7.2$ Hz, 1H, CH, H_{1'}), 4.22 (dd, $J = 7.0, 3.9$ Hz, 1H, CH, H_{2'}), 4.02 (s, 2H, CH₂, CH₂OH), 3.96 (t, $J = 3.7$ Hz, 1H, CH, H_{3'}), 3.44 (ddd, $J = 13.4, 8.1, 5.4$ Hz, 1H, CH₂, H_{6'}), 3.30 (m,

1H, CH₂, H₆'), 2.54 – 2.41 (m, 1H, CH₂, H₅'), 2.35 – 2.25 (m, 1H, CH, H₄'), 1.36 (ddd, *J* = 13.6, 7.4, 6.0 Hz, 1H, CH₂, H₅'), 0.97 (d, *J* = 1.7 Hz, 9H, CH₃), 0.81 (s, 9H, CH₃), 0.15 (s, 3H, CH₃), 0.12 (s, 3H, CH₃), 0.10 (s, 3H, CH₃), 0.06 (s, 3H, CH₃) ppm. ¹³C NMR (151 MHz, Methanol-*d*₄) δ 174.0 (C), 158.9 (C), 154.8 (CH), 146.8 (C), 141.8 (CH), 131.5 (CH), 127.6 (CH), 116.6 (C), 89.8 (C), 77.6 (CH), 76.0 (CH), 61.2 (CH₂), 55.2 (CH), 43.2 (CH), 42.0 (CH₂), 29.5 (CH₂), 25.1 (3 x CH₃), 25.0 (3 x CH₃), 17.6 (C), 17.5 (C), -5.4 (CH₃), -5.4 (CH₃), -5.7 (CH₃), -5.7 (CH₃) ppm. HRMS (ESI+) calculated for C₂₈H₄₇N₄O₄Si₂ 687.2259, found 687.0936; Method B *t*_R = 3.57 min; Purity (AUC) > 95%.

***N*-(((1*R*,2*R*,3*S*,4*R*)-2,3-Bis((*tert*-butyldimethylsilyloxy)-4-((6-phenylquinazolin-4-yl)amino)cyclopentyl)methyl)-2-hydroxyacetamide (434)**



Sodium carbonate (15 mg, 0.15 mmol) was added to a solution of tetrakis(triphenylphosphine)palladium(0) (8 mg, 0.01 mmol), *N*-[[[(1*S*,2*S*,3*R*,4*S*)-2,3-bis[[*tert*-butyl(dimethyl)silyloxy]-4-[(6-iodoquinazolin-4-yl)amino]cyclopentyl]methyl]-2-hydroxy-acetamide (50 mg, 0.07 mmol) and phenylboronic acid (18 mg, 0.15 mmol) in water (0.4 mL) and 1,4-dioxane (0.4 mL). The solution was heated at 120 °C in the MW for 1 h. The reaction mixture was concentrated and purified by column chromatography (biotage SNAP-Ultra C18 12 g, eluted with 10-100% MeOH in water, 1 CV, gradient over 20 CV, 6 CV) to yield the title product (26 mg, 56%, 0.04 mmol) as a fine white powder. IR (thin film) ν = 3291, 2928, 2855, 1582, 1532 cm⁻¹. ¹H NMR (600 MHz, Methanol-*d*₄) δ 8.62 (br. s, 1H, ArH, H₅), 8.19 (s, 1H, ArH, H₂), 7.88 (br. s, 1H, ArH, H₇), 7.85 – 7.78 (m, 2H, ArH, H₁₀, H₁₂), 7.54 (t, *J* = 7.8 Hz, 2H, ArH, H₉, H₁₃), 7.45 (td, *J* = 7.3, 1.3 Hz, 1H, ArH, H₁₁), 5.05 (dt, *J* = 9.4, 7.6 Hz, 1H, CH, H₁'), 4.28 (dd, *J* = 7.5, 3.9 Hz, 1H, CH, H₂'), 4.03 (s, 2H, CH₂, CH₂OH), 3.98 (t,

$J = 3.5$ Hz, 1H, CH, H_{3'}), 3.48-3.25 (m, 2H, CH₂, H_{6'}), 2.51 (app. dt, $J = 13.9$, 9.6 Hz, 1H, CH₂, H_{5'}), 2.33 (q, $J = 8.7$ Hz, 1H, CH, H_{4'}), 1.42 (ddd, $J = 13.5$, 7.6, 5.6 Hz, 1H, CH₂, H_{2'}, H_{5'}), 0.98 (s, 9H, CH₃), 0.80 (s, 9H, CH₃), 0.16 (s, 3H, CH₃), 0.13 (s, 3H, CH₃), 0.11 (s, 3H, CH₃), 0.06 (s, 3H, CH₃) ppm. ¹³C NMR (151 MHz, Methanol-*d*₄) δ 174.7 (C, HMBC), 140.0 (C), 139.5 (C), 132.6 (CH), 128.8 (2 x CH), 127.8 (CH), 126.9 (2 x CH), 120.4 (CH, HSQC), 77.5 (CH), 75.8 (CH), 61.2 (CH₂), 55.4 (CH), 43.4 (CH), 41.9 (CH₂), 29.3 (CH₂), 25.1 (3 x CH₃), 25.0 (3 x CH₃), 17.6 (C), 17.5 (C), -5.4 (CH₃), -5.4 (CH₃), -5.7 (CH₃), -5.7 (CH₃) ppm. Not all quaternary carbons observed due to slow rotation on NMR timescale. HRMS (ESI+) calculated for C₃₄H₅₂N₄O₄Si₂ 637.3605 found 637.3602; Method B $t_R = 3.23$ min; Purity (AUC) $\geq 95\%$.

6.2 Biological Evaluation

6.2.1 Ligand Observed NMR experiments

To confirm binding of hit compounds to HSP72-NBD a series of CPMG and WaterLOGSY experiments were performed. Compounds were assayed at 200 μM in the presence or absence of 10 μM HSP72-NBD. 200 μM ATP was also included in competition experiments. The total assay volume was 200 μL and the experiments were performed in 1.7 mm NMR tubes. The buffer was 25 mM Tris pH7.5, 50 mM NaCl, 10% D_2O and 100 μM of DTT in deionised water. NMR experiments were conducted at a ^1H frequency of 600 MHz using a Bruker Avance 600 spectrometer (Bruker, Bilerica, USA) equipped with a 1.7 mm TXI probe. All data were acquired and processed using MNova. The Relaxation edited ^1H -NMR spectrum was acquired at 295 K using the CPMG sequence with a spin-lock time of 600 ms. The water signal was suppressed using pre-saturation during relaxation delay (2 s) and by using the Watergate sequence subsequent to the CPMG sequence. For each spectrum 64 transients were acquired.

6.2.2 Photoaffinity Labelling Experiments

4 μM of HSP72-NBD in a buffer of 25 mM Tris and 50 mM NaCl in deionised water was placed in a MS vial at 0 $^\circ\text{C}$ under UV light set at 365 nm at distance of 4 cm for 1 h. 1 mM of compound **82** with a maximum DMSO concentration of 5% was incubated with 4 μM HSP72-NBD in buffer for one hour, followed by irradiation under UV light set at 365 nm at distance of 4 cm at 0 $^\circ\text{C}$ for 1 h. Samples were covered with aluminium foil and analysed by QuickShot MS. A sample with protein and a sample with protein incubated with compound **82** was sent to Fingerprint Proteomics Facility, The Discovery Centre, School of Life Sciences, University of Dundee, DD1 5EH for sequencing.

6.2.3 QuickShot analysis of HSP72-NBD

LC-MS CHROMASOLV solvents, formic acid, or alternative eluent modifiers were purchased from Merck Life Science unless otherwise stated. 0.2 μ L injections (8 step custom injection program with water, methanol and acetonitrile washes) of the sample was made onto a Security Guard C8 column cartridge (4 x 3 mm, AJO-4290, Phenomenex, Torrence, USA). The sample was refrigerated at 4°C in a G1367B auto-sampler with G1330B thermostat module prior to injection.

QuickShot chromatographic separation at 60 °C was carried out using a 1200 Series HPLC (Agilent, Santa Clara, USA) over a 1 minute gradient elution (Protein010713QuickShot.m). Sample was loaded onto the column cartridge using a G1312A binary pump dispensing a gradient from 95:5 to 10:90 water and acetonitrile (both modified with 0.1% formic acid) at a flow rate of 3 mL/min. Between 0.3 and 0.6 minutes a ten port column selection valve (G1316A column module) was used to reverse eluent flow through the column cartridge. During this stage, a second binary pump (G1312B SL) was used to elute protein off the cartridge using a gradient from 60:40 to 10:90 water and acetonitrile (both modified with 0.1% formic acid) at a flow rate of 0.5 mL/min. The post column eluent flow was infused into a 6520 Series qToF mass spectrometer (G6520A) fitted with a dual ESI ionisation source (Agilent, Santa Clara, USA).

LC eluent and nebulising gas was introduced into the grounded nebuliser with spray direction orthogonal to the capillary axis. The aerosol was dried by heated gas (10 L/min of nitrogen at 350 °C, 50 psi), producing ions by ESI. Ions entered the transfer capillary along which a potential difference of 4kV was applied. The fragmentor voltage was set at 190V and skimmer at 65V. The signal was optimised by AutoTune.m. Profile mass spectrometry data was acquired in positive ionisation mode over a scan range of m/z 650-2000 (scan rate 1.0) with reference mass correction at m/z 922.009798 hexakis(1H,1H,3H-perfluoropropoxy)phosphazene.

Raw data was processed using Agilent MassHunter Qualitative Analysis B.06.00 and MagTran 1.02.

6.2.4 SPR experiments

6.2.4.1 Protein immobilization

All surface plasmon resonance (SPR) experiments were carried out on a Biacore T100 enhanced to T200 sensitivity (GE Healthcare) and amine coupling chemistry was used to immobilise the proteins on a research grade CM5 sensor chip. The running buffer was phosphate buffered saline (10 mM NaHPO₄-NaH₂PO₄, pH 7.4, 2.7 mM KCl, 137 mM NaCl) and the chip's surface was activated for 10 min using a 1:1 mixture of 100 mM *N*-hydroxysuccinimide and 400 mM 1-ethyl-3-(3-dimethylaminopropyl)-carbodiimide. Wild Type-HSC70-NBD and the S275W mutant proteins were injected for 10 min at a concentration of 2 μM in a 10 mM sodium acetate buffer pH 5.0 with 100 μM ADP as protection for the active site lysines. Finally, the surface was blocked via an injection of 1 M ethanolamine pH 8.5 for 7 min. The flow rate was maintained at 10 μL/min for all the above procedures. On average, ~12,000 response units (RU) of the wild type and the mutant proteins were immobilised on the chip. Flow cell one was left unmodified as the reference surface. Following protein immobilisation, the running buffer was changed to phosphate buffered saline containing 0.05% Tween20 (v/v) and 5% DMSO.

6.2.4.2 Determination of Binding Constants (K_D) for Compounds

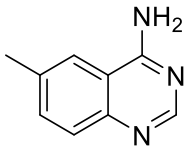
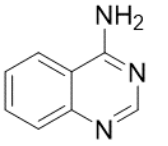
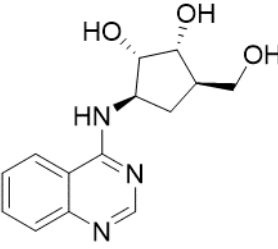
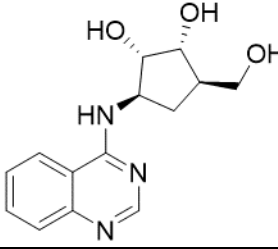
All liquid handling was carried out using an ECHO 550 acoustic liquid dispenser (Labcyte, Dublin, Ireland) and compounds were added to 384-well polypropylene V-bottomed plates (Greiner, Stonehouse, UK), which were used as sample plates for the SPR experiments. Fresh 100 mM DMSO stocks of each compound were prepared and used to generate an eight-point concentration response range from 25 μM to 1000 μM or from 6.25 μM to 500 μM. For adenosine, the concentration range was 50 μM to 2000 μM, from a 200 mM stock in DMSO and for VER155008, a stock solution of 0.25 mM in DMSO was prepared with a concentration range of 0.0625 μM to 2.5 μM. The buffer mix

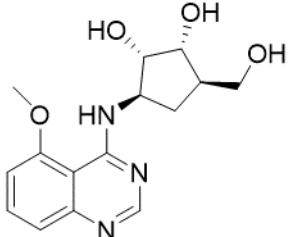
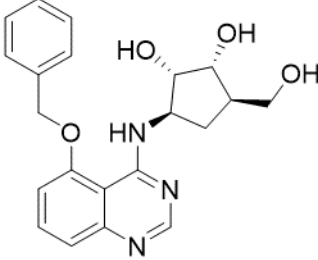
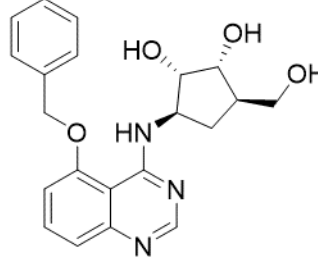
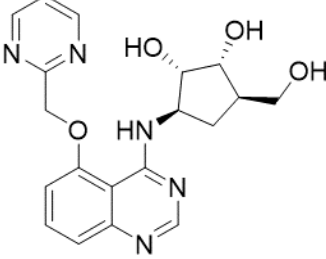
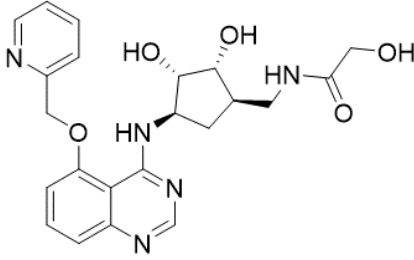
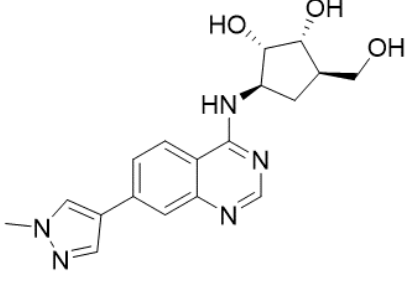
was made compatible with the Biacore running buffer and the experiments were performed at a flow rate of 30 $\mu\text{L}/\text{min}$, a sample injection time of 60 s, and a dissociation time of 200 s. The CM5 surface was not regenerated between sample injections.

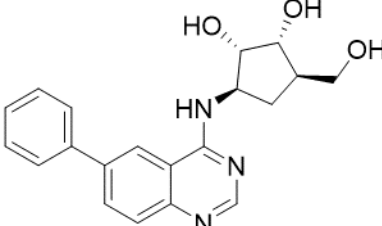
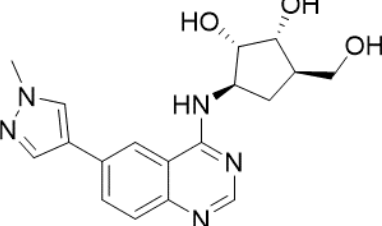
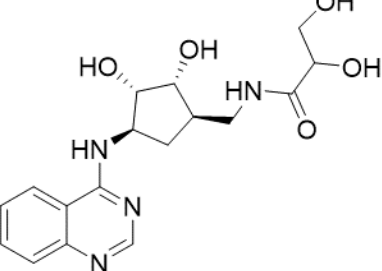
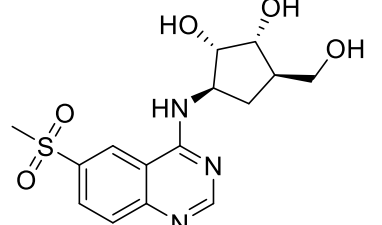
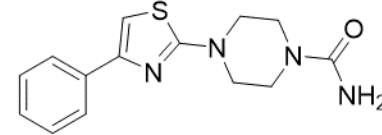
Binding constants (K_D) were calculated from the DMSO corrected and background normalised binding curves generated from the sensorgrams under equilibrium conditions using the 1:1 binding model in the Biacore software version 2 (GE Life Sciences, Amersham, UK).

7 Appendix

7.1 List of relevant X-ray crystal structures of HSP70

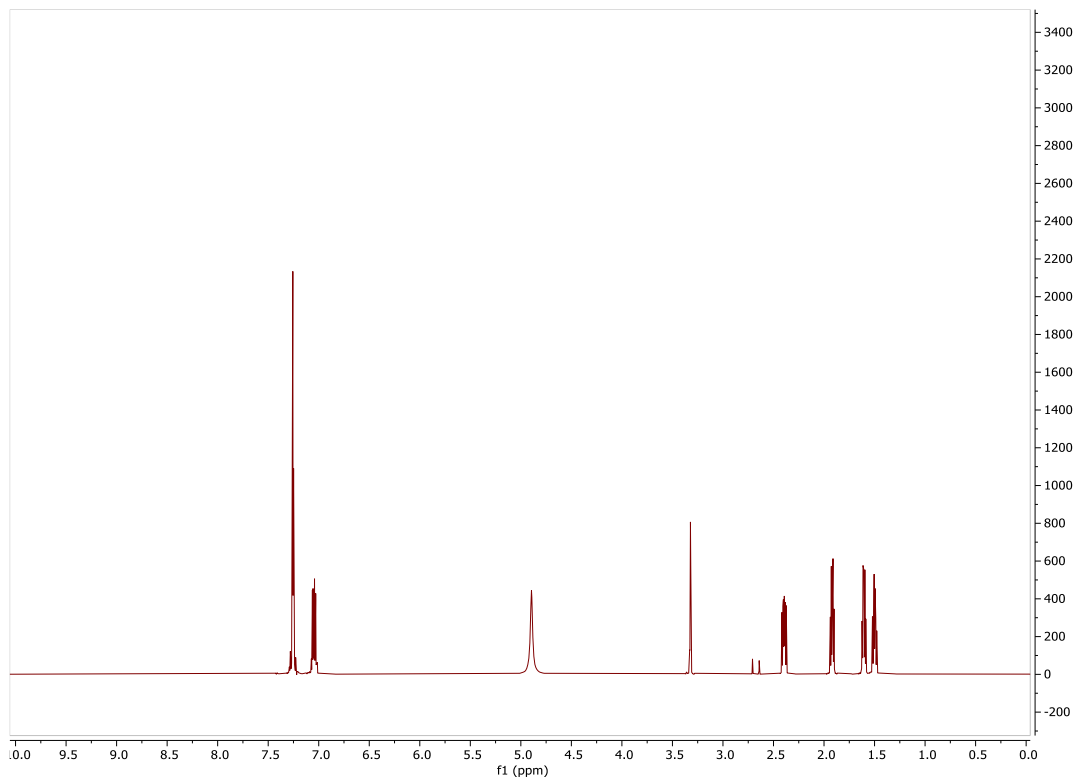
Name	Resolution	Ligand	Protein
3FZF	2.2	ATP	HSC70 NBD Bag1
4H5T	1.9	ADP	HSC70 NBD
3ATU	1.65	ADP	HSP72 NBD
5AQF	1.88	Adenosine	HSC70 NBD Bag1
5AQY	1.56	Adenosine	HSP72 NBD
5AQL	1.69	-	HSC70 NBD Bag1 S275W Mutant
5AQO, 9	2.12		HSC70 NBD Bag1
5AQP, 223	2.08		HSC70 NBD Bag1
5AQT, 10	1.9		HSC70 NBD Bag1
5AQW, 10	1.53		HSP72 NBD

Name	Resolution	Ligand	Protein
5AQU, 227	1.92		HSC70 NBD Bag1
5AQV, 225	1.75		HSC70 NBD Bag1
5AQX, 225	2.12		HSP72 NBD
CCT369825 363	1.63		HSP72 NBD
CCT370001 241	1.98		HSP72 NBD
CCT374436 397	1.50		HSP72 NBD

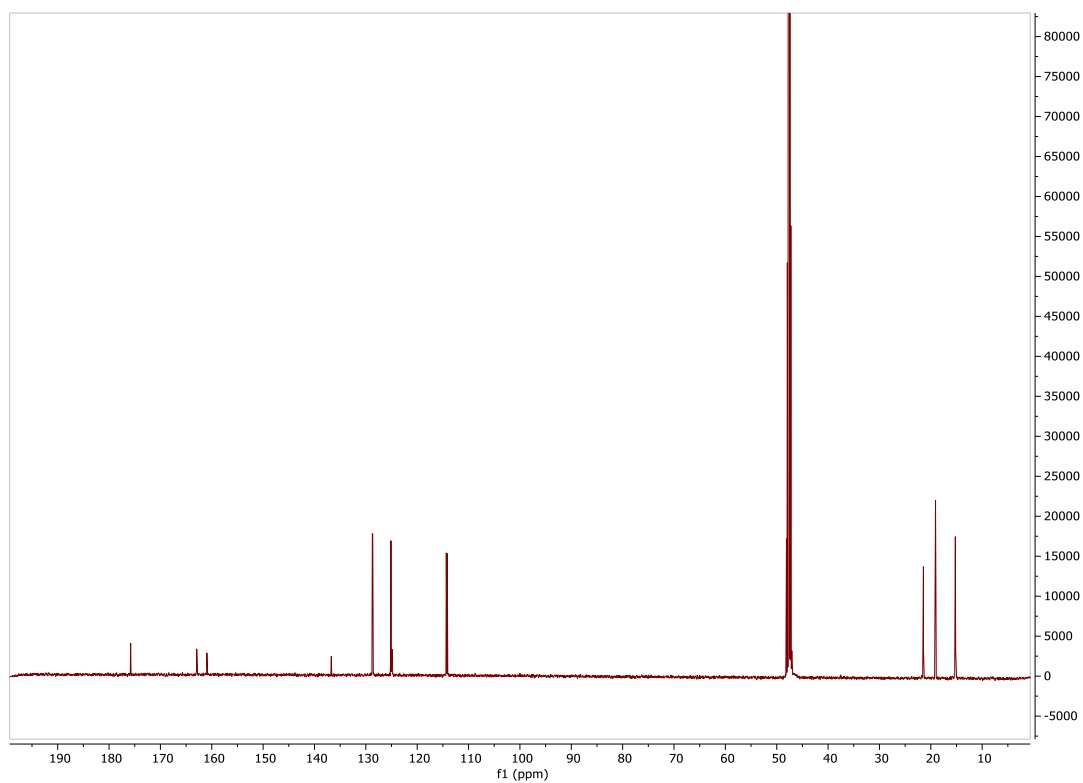
Name	Resolution	Ligand	Protein
CCT374761 402	1.41		HSP72 NBD
CCT374803 403	1.40		HSP72 NBD
CCT374833 303	1.32		HSP72 NBD
CCT375144 421	1.55		HSP72 NBD
CCT240677 21	1.49		HSP72 NBD

7.2 NMR of compound 57 to aid in the determination of stereochemistry

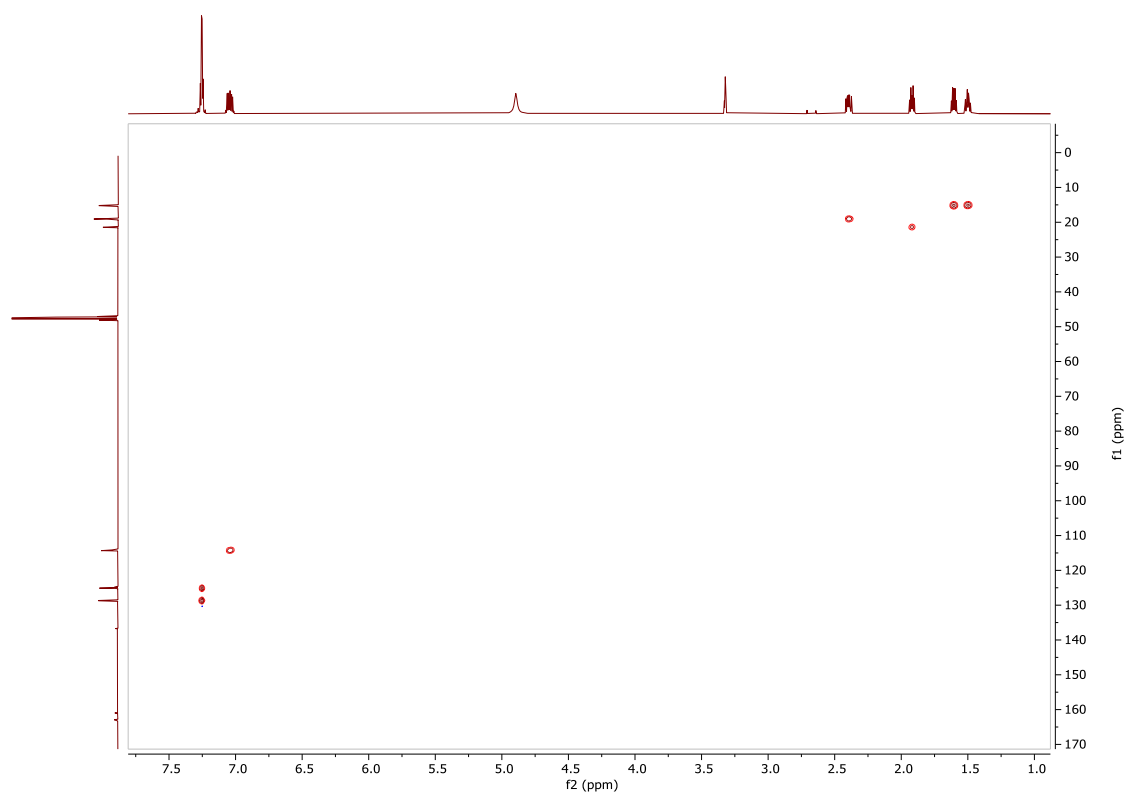
$^1\text{H-NMR}$



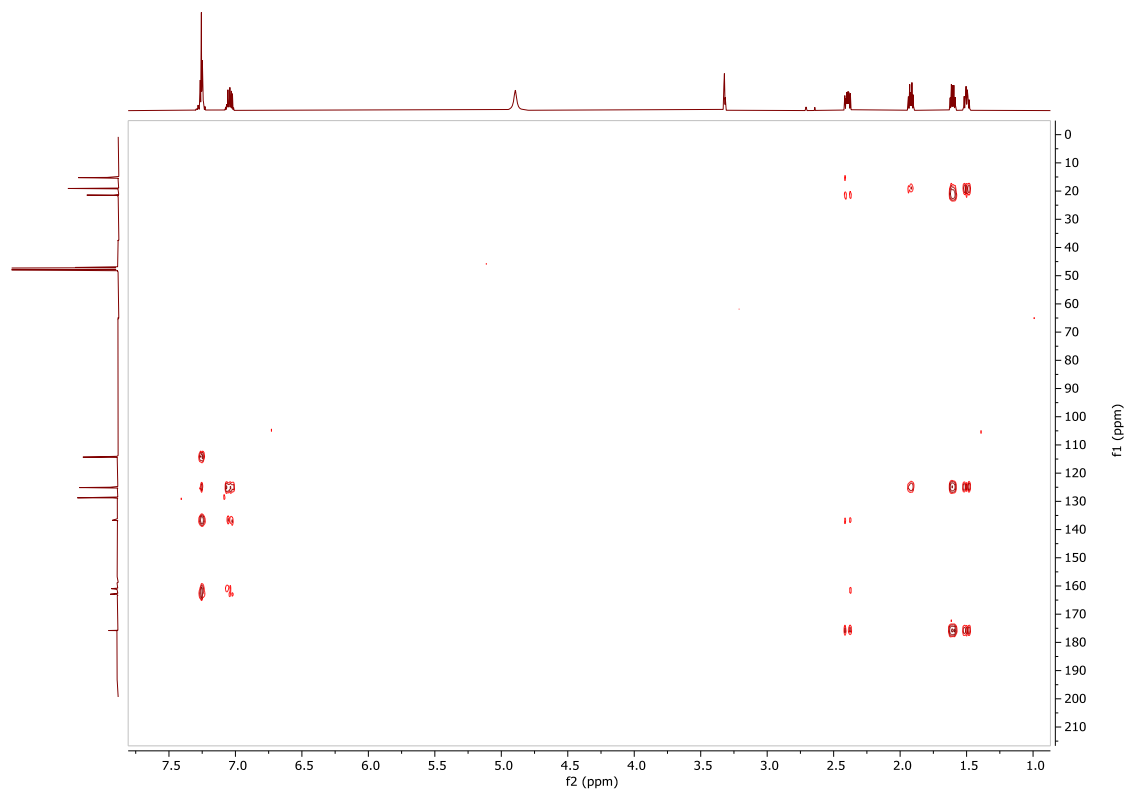
$^{13}\text{C-NMR}$



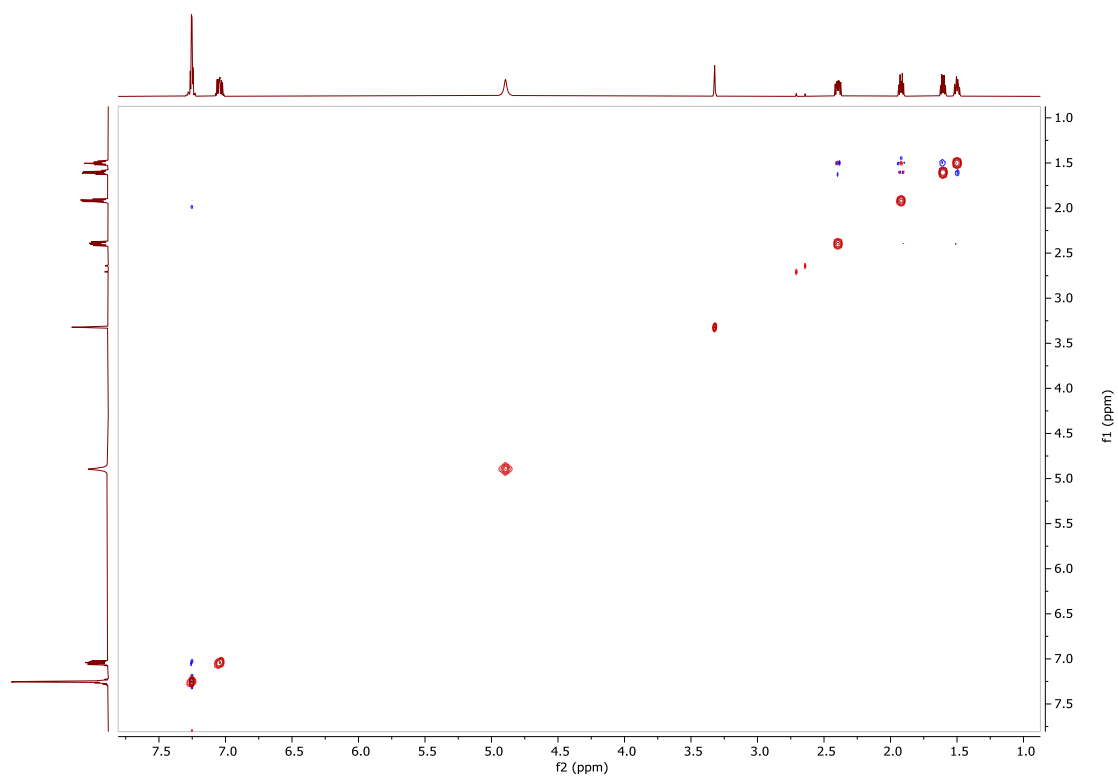
HSQC



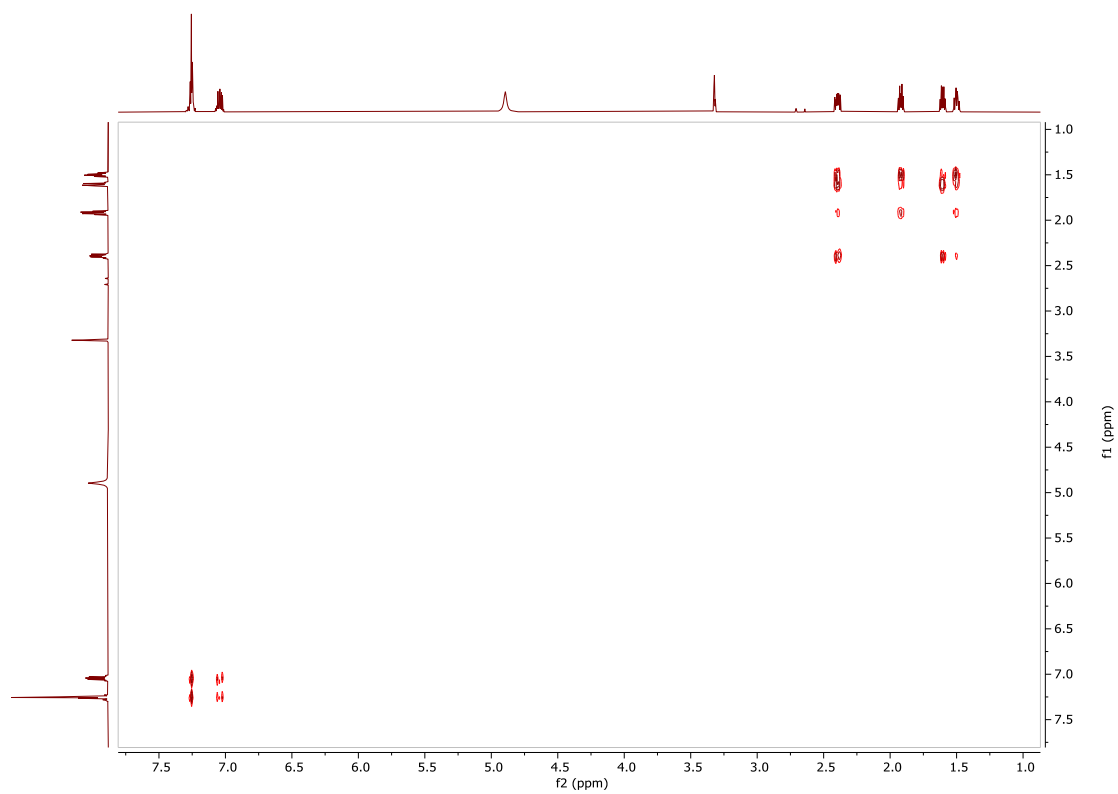
HMBC



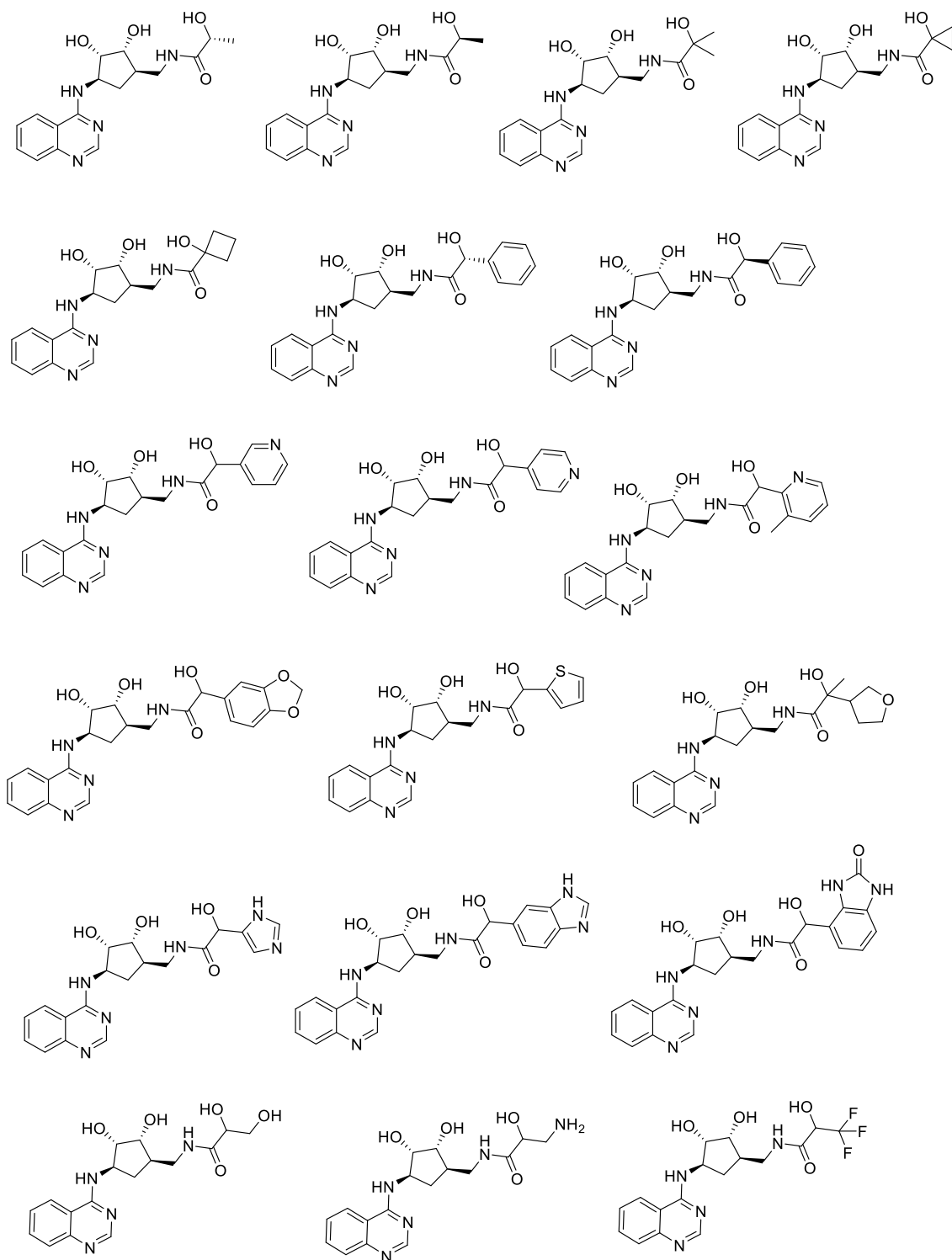
NOESY

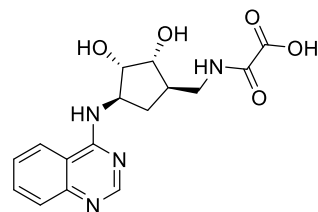
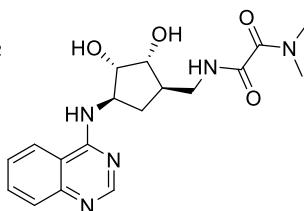
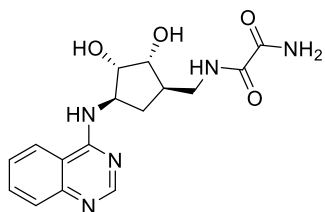
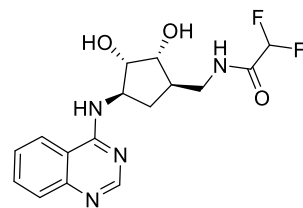
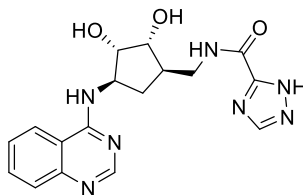
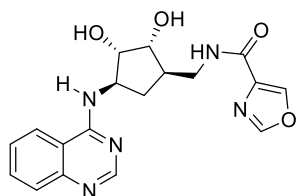
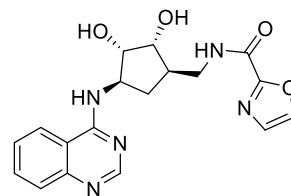
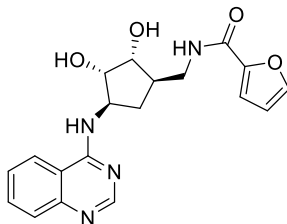
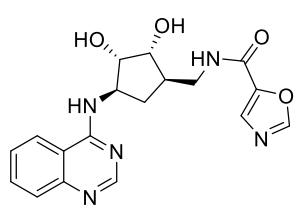


COSY



7.3 Docked compounds from Chapter 4, Section 4.7.1





References

8 References

- (1) Our world in data <https://ourworldindata.org/grapher/number-of-people-with-cancer-by-age> (accessed Nov 29, 2019).
- (2) Ahmad, A. S.; Ormiston-Smith, N.; Sasieni, P. D. Trends in the Lifetime Risk of Developing Cancer in Great Britain: Comparison of Risk for Those Born from 1930 to 1960. *Br. J. Cancer* **2015**, *112* (5), 943–947. <https://doi.org/10.1038/bjc.2014.606>.
- (3) Our world in data <https://ourworldindata.org/grapher/number-of-people-with-cancer> (accessed Nov 29, 2019).
- (4) The International Agency for Research on Cancer (IARC) report, W. Latest Global Cancer Data: Cancer Burden Rises to 18.1 Million New Cases and 9.6 Million Cancer Deaths in 2018. *Int. Agency Res. Cancer* **2018**, No. September, 13–15.
- (5) Tarver, T. American Cancer Society. Cancer Facts and Figures 2014. *J. Consum. Health Internet* **2012**, *16*, 366–367.
- (6) Biemar, F.; Foti, M. Global Progress against Cancer-Challenges and Opportunities. *Cancer Biol. Med.* **2013**, *10* (4), 183–186. <https://doi.org/10.7497/j.issn.2095-3941.2013.04.001>.
- (7) Cancer Research UK <https://www.cancerresearchuk.org/what-is-cancer/how-cancer-starts/types-of-cancer> (accessed Jun 7, 2020).
- (8) Hanahan, D.; Weinberg, R. A. *The Hallmarks of Cancer Review Evolve Progressively from Normalcy via a Series of Pre*; 2000; Vol. 100.
- (9) Hanahan, D.; Weinberg, R. A. Hallmarks of Cancer: The next Generation. *Cell*. March 4, 2011, pp 646–674. <https://doi.org/10.1016/j.cell.2011.02.013>.
- (10) Papavramidou, N.; Papavramidis, T.; Demetriou, T. Ancient Greek and Greco-Roman Methods in Modern Surgical Treatment of Cancer. *Annals of Surgical Oncology*. Springer March 2010, pp 665–667. <https://doi.org/10.1245/s10434-009-0886-6>.
- (11) Papac, R. J. *Origins of Cancer Therapy*; 2001; Vol. 74.
- (12) DeVita, V. T.; Chu, E. A History of Cancer Chemotherapy. *Cancer Research*. American Association for Cancer Research November 1,

- 2008, pp 8643–8653. <https://doi.org/10.1158/0008-5472.CAN-07-6611>.
- (13) Chabner, B. A.; Roberts, T. G. Chemotherapy and the War on Cancer. *Nature Reviews Cancer*. Nature Publishing Group January 2005, pp 65–72. <https://doi.org/10.1038/nrc1529>.
- (14) Visentin, M.; Zhao, R.; Goldman, I. D. The Antifolates. *Hematol. Oncol. Clin. North Am.* **2012**, *26* (3), 629–648. <https://doi.org/10.1016/j.hoc.2012.02.002>.
- (15) Loong, H. H.; Yeo, W. Microtubule-Targeting Agents in Oncology and Therapeutic Potential in Hepatocellular Carcinoma. *Onco. Targets. Ther.* **2014**, *7*–575. <https://doi.org/10.2147/OTT.S46019>.
- (16) Liu, L. F.; Desai, S. D.; Li, T.-K.; Mao, Y.; Sun, M.; Sim, S.-P. Mechanism of Action of Camptothecin. *Ann. N. Y. Acad. Sci.* **2006**, *922* (1), 1–10. <https://doi.org/10.1111/j.1749-6632.2000.tb07020.x>.
- (17) Kannaiyan, R.; Mahadevan, D. A Comprehensive Review of Protein Kinase Inhibitors for Cancer Therapy. *Expert Review of Anticancer Therapy*. Taylor and Francis Ltd December 2, 2018, pp 1249–1270. <https://doi.org/10.1080/14737140.2018.1527688>.
- (18) Sacha, T. Imatinib in Chronic Myeloid Leukemia: An Overview. *Mediterranean Journal of Hematology and Infectious Diseases*. Catholic University in Rome 2014, p 2014007. <https://doi.org/10.4084/MJHID.2014.007>.
- (19) Chen, A. PARP Inhibitors: Its Role in Treatment of Cancer. *Chinese journal of cancer*. BioMed Central 2011, pp 463–471. <https://doi.org/10.5732/cjc.011.10111>.
- (20) Ritossa, F. A New Puffing Pattern Induced by Temperature Shock and DNP in Drosophila. *Experientia* **1962**, *18* (12), 571–573. <https://doi.org/10.1007/BF02172188>.
- (21) Ferraro, M.; D'annessa, I.; Moroni, E.; Morra, G.; Paladino, A.; Rinaldi, S.; Compostella, F.; Colombo, G. Allosteric Modulators of HSP90 and HSP70: Dynamics Meets Function through Structure-Based Drug Design. **2018**. <https://doi.org/10.1021/acs.jmedchem.8b00825>.
- (22) Powers, M. V.; Workman, P. Inhibitors of the Heat Shock Response: Biology and Pharmacology. *FEBS Lett.* **2007**, *581* (19), 3758–3769.

- <https://doi.org/10.1016/j.febslet.2007.05.040>.
- (23) Evans, C. G.; Chang, L.; Gestwicki, J. E. Heat Shock Protein 70 (Hsp70) as an Emerging Drug Target. *J. Med. Chem.* **2010**, *53* (12), 4585–4602. <https://doi.org/10.1021/jm100054f>.
- (24) Zuiderweg, E. R. P.; Bertelsen, E. B.; Rousaki, A.; Mayer, M. P.; Gestwicki, J. E.; Ahmad, A. Allostery in the Hsp70 Chaperone Proteins. *Top. Curr. Chem.* **2013**, *328*, 99–153. https://doi.org/10.1007/128_2012_323.
- (25) Wawrzynow, M. Z. A.; Wawrzynow, A. Insights into the Function of Hsp70 Chaperones. *IUBMB Life (International Union Biochem. Mol. Biol. Life)* **2001**, *51* (5), 283–287. <https://doi.org/10.1080/152165401317190770>.
- (26) Powers, M. V.; Jones, K.; Barillari, C.; Westwood, I.; Van Montfort, R. L. M.; Workman, P. Targeting HSP70: The Second Potentially Druggable Heat Shock Protein and Molecular Chaperone? *Cell Cycle* **2010**, *9* (8), 1542–1550. <https://doi.org/10.4161/cc.9.8.11204>.
- (27) Murphy, M. E. The HSP70 Family and Cancer. *Carcinogenesis* **2013**, *34* (6), 1181–1188. <https://doi.org/10.1093/carcin/bgt111>.
- (28) Vos, M. J.; Hageman, J.; Carra, S.; Kampinga, H. H. Structural and Functional Diversities between Members of the Human HSPB, HSPH, HSPA, and DNAJ Chaperone Families †. *Biochemistry* **2008**, *47* (27), 7001–7011. <https://doi.org/10.1021/bi800639z>.
- (29) Swain, J. F.; Dinler, G.; Sivendran, R.; Montgomery, D. L.; Stotz, M.; Gierasch, L. M. Hsp70 Chaperone Ligands Control Domain Association via an Allosteric Mechanism Mediated by the Interdomain Linker. *Mol. Cell* **2007**, *26* (1), 27–39.
- (30) Massey, A. J. ATPases as Drug Targets: Insights from Heat Shock Proteins 70 and 90. *J. Med. Chem.* **2010**, *53* (20), 7280–7286. <https://doi.org/10.1021/jm100342z>.
- (31) Jones, A. M.; Westwood, I. M.; Osborne, J. D.; Matthews, T. P.; Cheeseman, M. D.; Rowlands, M. G.; Jeganathan, F.; Burke, R.; Lee, D.; Kadi, N.; Liu, M.; Richards, M.; McAndrew, C.; Yahya, N.; Dobson, S. E.; Jones, K.; Workman, P.; Collins, I.; van Montfort, R. L. M. A Fragment-

- Based Approach Applied to a Highly Flexible Target: Insights and Challenges towards the Inhibition of HSP70 Isoforms. *Sci. Rep.* **2016**, *6* (October), 34701. <https://doi.org/10.1038/srep34701>.
- (32) Sherman, M. Y.; Gabai, V. L. Hsp70 in Cancer: Back to the Future. *Oncogene* **2015**, *34* (32), 4153–4161. <https://doi.org/10.1038/onc.2014.349>.
- (33) Radons, J. The Human HSP70 Family of Chaperones: Where Do We Stand? *Cell Stress and Chaperones*. 2016, pp 379–404. <https://doi.org/10.1007/s12192-016-0676-6>.
- (34) Lee, K.-J.; Kim, Y. M.; Kim, D. Y.; Jeoung, D.; Han, K.; Lee, S.-T.; Lee, Y.-S.; Park, K. H.; Park, J. H.; Kim, D. J.; Hahn, J.-H. Release of Heat Shock Protein 70 (Hsp70) and the Effects of Extracellular Hsp70 on Matric Metalloproteinase-9 Expression in Human Monocytic U937 Cells. *Exp. Mol. Med.* **2006**, *38* (4), 364–374. <https://doi.org/10.1038/emm.2006.43>.
- (35) Nylandsted, J.; Rohde, M.; Brand, K.; Bastholm, L.; Elling, F.; Jäättelä, M. Selective Depletion of Heat Shock Protein 70 (Hsp70) Activates a Tumor-Specific Death Program That Is Independent of Caspases and Bypasses Bcl-2. *Proc. Natl. Acad. Sci. U. S. A.* **2000**, *97* (14), 7871–7876. <https://doi.org/10.1073/pnas.97.14.7871>.
- (36) Kaur, J.; Kaur, J.; Ralhan, R. Induction of Apoptosis by Abrogation of HSP70 Expression in Human Oral Cancer Cells. *Int. J. Cancer* **2000**, *85* (1), 1–5. [https://doi.org/10.1002/\(SICI\)1097-0215\(20000101\)85:1<1::AID-IJC1>3.0.CO;2-O](https://doi.org/10.1002/(SICI)1097-0215(20000101)85:1<1::AID-IJC1>3.0.CO;2-O).
- (37) Frese, S.; Schaper, M.; Kuster, J. R.; Miescher, D.; Jäättelä, M.; Buehler, T.; Schmid, R. A. Cell Death Induced by Down-Regulation of Heat Shock Protein 70 in Lung Cancer Cell Lines Is P53-Independent and Does Not Require DNA Cleavage. *J. Thorac. Cardiovasc. Surg.* **2003**, *126* (3), 748–754. [https://doi.org/10.1016/S0022-5223\(03\)00703-7](https://doi.org/10.1016/S0022-5223(03)00703-7).
- (38) Nylandsted, J.; Wick, W.; Hirt, U. A.; Brand, K.; Rohde, M.; Leist, M.; Weller, M.; Jäättelä, M. Eradication of Glioblastoma, and Breast and Colon Carcinoma Xenografts by Hsp70 Depletion. *Cancer Res.* **2002**, *62* (24), 7139–7142.

- (39) Powers, M. V.; Clarke, P. A.; Workman, P. Dual Targeting of HSC70 and HSP72 Inhibits HSP90 Function and Induces Tumor-Specific Apoptosis. *Cancer Cell* **2008**, *14* (3), 250–262. <https://doi.org/10.1016/j.ccr.2008.08.002>.
- (40) Bagatell, R.; Paine-Murrieta, G. D.; Taylor, C. W.; Pulcini, E. J.; Akinaga, S.; Benjamin, I. J.; Whitesell, L. Induction of a Heat Shock Factor 1-Dependent Stress Response Alters the Cytotoxic Activity of Hsp90-Binding Agents. *Clin. Cancer Res.* **2000**, *6* (8).
- (41) Chen, I. J.; Hubbard, R. E. Lessons for Fragment Library Design: Analysis of Output from Multiple Screening Campaigns. *J. Comput. Aided. Mol. Des.* **2009**, *23* (8), 603–620. <https://doi.org/10.1007/s10822-009-9280-5>.
- (42) Evans, L. E.; Jones, K.; Cheeseman, M. D. Targeting Secondary Protein Complexes in Drug Discovery: Studying the Druggability and Chemical Biology of the HSP70/BAG1 Complex. *Chem. Commun.* **2017**, *53* (37), 5167–5170. <https://doi.org/10.1039/c7cc01376k>.
- (43) Keseru, G. M.; Erlanson, D. A.; Ferenczy, G. G.; Hann, M. M.; Murray, C. W.; Pickett, S. D. Design Principles for Fragment Libraries: Maximizing the Value of Learnings from Pharma Fragment-Based Drug Discovery (FBDD) Programs for Use in Academia. *J. Med. Chem.* **2016**, *59* (18), 8189–8206. <https://doi.org/10.1021/acs.jmedchem.6b00197>.
- (44) Ludlow, R. F.; Verdonk, M. L.; Saini, H. K.; Tickle, I. J.; Jhoti, H. Detection of Secondary Binding Sites in Proteins Using Fragment Screening. *Proc. Natl. Acad. Sci. U. S. A.* **2015**, *112* (52), 15910–15915. <https://doi.org/10.1073/pnas.1518946112>.
- (45) Onuoha, S. C.; Mukund, S. R.; Coulstock, E. T.; Sengerová, B.; Shaw, J.; McLaughlin, S. H.; Jackson, S. E. Mechanistic Studies on Hsp90 Inhibition by Ansamycin Derivatives. *J. Mol. Biol.* **2007**, *372* (2), 287–297. <https://doi.org/10.1016/j.jmb.2007.06.065>.
- (46) Nadler, S.; Tepper, M.; Schacter, B.; Mazzucco, C. Interaction of the Immunosuppressant Deoxyspergualin with a Member of the Hsp70 Family of Heat Shock Proteins. *Science* (80-.). **1992**, *258* (5081).
- (47) Schlecht, R.; Scholz, S. R.; Dahmen, H.; Wegener, A.; Sirrenberg, C.;

- Musil, D.; Bomke, J.; Eggenweiler, H. M.; Mayer, M. P.; Bukau, B. Functional Analysis of Hsp70 Inhibitors. *PLoS One* **2013**, *8* (11), e78443. <https://doi.org/10.1371/journal.pone.0078443>.
- (48) Hassan, A. Q.; Kirby, C. A.; Zhou, W.; Schuhmann, T.; Kityk, R.; Kipp, D. R.; Baird, J.; Chen, J.; Chen, Y.; Chung, F.; Hoepfner, D.; Mowva, N. R.; Pagliarini, R.; Petersen, F.; Quinn, C.; Quinn, D.; Riedl, R.; Schmitt, E. K.; Schitter, A.; Stams, T.; Studer, C.; Fortin, P. D.; Mayer, M. P.; Sadlish, H. The Novolactone Natural Product Disrupts the Allosteric Regulation of Hsp70. *Chem. Biol.* **2015**, *22* (1), 87–97. <https://doi.org/10.1016/j.chembiol.2014.11.007>.
- (49) Williamson, D. S.; Borgognoni, J.; Clay, A.; Daniels, Z.; Dokurno, P.; Drysdale, M. J.; Foloppe, N.; Francis, G. L.; Graham, C. J.; Howes, R.; Macias, A. T.; Murray, J. B.; Parsons, R.; Shaw, T.; Surgenor, A. E.; Terry, L.; Wang, Y.; Wood, M.; Massey, A. J. Novel Adenosine-Derived Inhibitors of 70 KDa Heat Shock Protein, Discovered through Structure-Based Design. *J. Med. Chem.* **2009**, *52* (6), 1510–1513. <https://doi.org/10.1021/jm801627a>.
- (50) Pettinger, J.; Le Bihan, Y.-V.; Widya, M.; Van Montfort, R. L. M.; Jones, K.; Cheeseman, M. D. An Irreversible Inhibitor of HSP72 That Unexpectedly Targets Lysine-56. <https://doi.org/10.1002/anie.201611907>.
- (51) Cheeseman, M. D.; Westwood, I. M.; Barbeau, O.; Rowlands, M.; Dobson, S.; Jones, A. M.; Jeganathan, F.; Burke, R.; Kadi, N.; Workman, P.; Collins, I.; Van Montfort, R. L. M.; Jones, K. Exploiting Protein Conformational Change to Optimize Adenosine-Derived Inhibitors of HSP70. *J. Med. Chem.* **2016**, *59* (10), 4625–4636. <https://doi.org/10.1021/acs.jmedchem.5b02001>.
- (52) Kumar, S.; Stokes, J.; Singh, U. P.; Scissum Gunn, K.; Acharya, A.; Manne, U.; Mishra, M. Targeting Hsp70: A Possible Therapy for Cancer. *Cancer Lett.* **2016**, *374* (1), 156–166. <https://doi.org/10.1016/j.canlet.2016.01.056>.
- (53) Jinwal, U. K.; Miyata, Y.; Koren, J.; Jones, J. R.; Trotter, J. H.; Chang, L.; O’Leary, J.; Morgan, D.; Lee, D. C.; Shults, C. L.; Rousaki, A.; Weeber,

- E. J.; Zuiderweg, E. R. P.; Gestwicki, J. E.; Dickey, C. A. Chemical Manipulation of Hsp70 ATPase Activity Regulates Tau Stability. *J. Neurosci.* **2009**, *29* (39).
- (54) Wadhwa, R.; Sugihara, T.; Yoshida, A.; Nomura, H.; Reddel, R. R.; Simpson, R.; Maruta, H.; Kaul, S. C. Selective Toxicity of MKT-077 to Cancer Cells Is Mediated by Its Binding to the Hsp70 Family Protein Mot-2 and Reactivation of P53 Function. *Cancer Res.* **2000**, *60* (24).
- (55) Dal Piaz, F.; Cotugno, R.; Lepore, L.; Vassallo, A.; Malafronte, N.; Lauro, G.; Bifulco, G.; Belisario, M. A.; De Tommasi, N. Chemical Proteomics Reveals HSP70 1A as a Target for the Anticancer Diterpene Oridonin in Jurkat Cells. *J. Proteomics* **2013**, *82*, 14–26.
<https://doi.org/10.1016/j.jprot.2013.01.030>.
- (56) Vasaturo, M.; Cotugno, R.; Fiengo, L.; Vinegoni, C.; Dal Piaz, F.; De Tommasi, N. The Anti-Tumor Diterpene Oridonin Is a Direct Inhibitor of Nucleolin in Cancer Cells. *Sci. Rep.* **2018**, *8* (1), 1–13.
<https://doi.org/10.1038/s41598-018-35088-x>.
- (57) Kang, Y.; Taldone, T.; Patel, H. J.; Patel, P. D.; Rodina, A.; Gozman, A.; Maharaj, R.; Clement, C. C.; Patel, M. R.; Brodsky, L.; Young, J. C.; Chiosis, G. Heat Shock Protein 70 Inhibitors. 1. 2,5'-Thiodipyrimidine and 5-(Phenylthio)Pyrimidine Acrylamides as Irreversible Binders to an Allosteric Site on Heat Shock Protein 70. *J. Med. Chem* **2014**, No. 57, 1188–1207.
- (58) Kang, Y.; Taldone, T.; Patel, H. J.; Patel, P. D.; Rodina, A.; Gozman, A.; Maharaj, R.; Clement, C. C.; Patel, M. R.; Brodsky, L.; Young, J. C.; Chiosis, G. Heat Shock Protein 70 Inhibitors. 2. 2,5'-Thiodipyrimidines, 5-(Phenylthio)Pyrimidines, 2-(Pyridin-3-Ylthio)Pyrimidines, and 3-(Phenylthio)Pyridines as Reversible Binders to an Allosteric Site on Heat Shock Protein 70. *J. Med. Chem* **2014**, No. 57, 1208–1224.
- (59) Williams, D. R.; Ko, S.-K.; Park, S.; Lee, M.-R.; Shin, I. An Apoptosis-Inducing Small Molecule That Binds to Heat Shock Protein 70. *Angew. Chemie Int. Ed.* **2008**, *47* (39), 7466–7469.
<https://doi.org/10.1002/anie.200802801>.
- (60) Evans, L. E.; Cheeseman, M. D.; Yahya, N.; Jones, K. Investigating

- Apoptozole as a Chemical Probe for HSP70 Inhibition. *PLoS One* **2015**, *10* (10), e0140006. <https://doi.org/10.1371/journal.pone.0140006>.
- (61) Hann, M. M.; Leach, A. R.; Harper, G. Molecular Complexity and Its Impact on the Probability of Finding Leads for Drug Discovery. *J. Chem. Inf. Comput. Sci.* **2001**, *41* (3), 856–864. <https://doi.org/10.1021/ci000403i>.
- (62) Hughes, J. D.; Blagg, J.; Price, D. A.; Bailey, S.; DeCrescenzo, G. A.; Devraj, R. V.; Ellsworth, E.; Fobian, Y. M.; Gibbs, M. E.; Gilles, R. W.; Greene, N.; Huang, E.; Krieger-Burke, T.; Loesel, J.; Wager, T.; Whiteley, L.; Zhang, Y. Physiochemical Drug Properties Associated with in Vivo Toxicological Outcomes. *Bioorganic Med. Chem. Lett.* **2008**, *18* (17), 4872–4875. <https://doi.org/10.1016/j.bmcl.2008.07.071>.
- (63) Leeson, P. D.; Springthorpe, B. The Influence of Drug-like Concepts on Decision-Making in Medicinal Chemistry. *Nat. Rev. Drug Discov.* **2007**, *6* (11), 881–890. <https://doi.org/10.1038/nrd2445>.
- (64) Lipinski, C. A.; Lombardo, F.; Dominy, B. W.; Feeney, P. J. Experimental and Computational Approaches to Estimate Solubility and Permeability in Drug Discovery and Development Settings. *Adv. Drug Deliv. Rev.* **2001**, *46* (1–3), 3–26. [https://doi.org/10.1016/S0169-409X\(00\)00129-0](https://doi.org/10.1016/S0169-409X(00)00129-0).
- (65) Congreve, M.; Carr, R.; Murray, C.; Jhoti, H. A 'Rule of Three' for Fragment-Based Lead Discovery? *Drug Discovery Today*. 2003, pp 876–877. [https://doi.org/10.1016/S1359-6446\(03\)02831-9](https://doi.org/10.1016/S1359-6446(03)02831-9).
- (66) Hopkins, A. L.; Keserü, G. M.; Leeson, P. D.; Rees, D. C.; Reynolds, C. H. The Role of Ligand Efficiency Metrics in Drug Discovery. *Nat. Rev. Drug Discov.* **2014**, *13* (2), 105–121. <https://doi.org/10.1038/nrd4163>.
- (67) Kirsch, P.; Hartman, A. M.; Hirsch, A. K. H.; Empting, M. Concepts and Core Principles of Fragment-Based Drug Design. *Molecules* **2019**, *24* (23), 4309. <https://doi.org/10.3390/molecules24234309>.
- (68) Murray, C. W.; Carr, M. G.; Callaghan, O.; Chessari, G.; Congreve, M.; Cowan, S.; Coyle, J. E.; Downham, R.; Figueroa, E.; Frederickson, M.; Graham, B.; McMenamin, R.; O'Brien, M. A.; Patel, S.; Phillips, T. R.; Williams, G.; Woodhead, A. J.; Woolford, A. J.-A. Fragment-Based Drug Discovery Applied to Hsp90. Discovery of Two Lead Series with High

- Ligand Efficiency. *J. Med. Chem.* **2010**, *53* (16), 5942–5955.
<https://doi.org/10.1021/jm100059d>.
- (69) Powers, M. V.; Clarke, P. A.; Workman, P. Dual Targeting of HSC70 and HSP72 Inhibits HSP90 Function and Induces Tumor-Specific Apoptosis. *Cancer Cell* **2008**, *14* (3), 250–262.
<https://doi.org/10.1016/j.ccr.2008.08.002>.
- (70) Boudesco, C.; Cause, S.; Jegou, G.; Garrido, C. Hsp70: A Cancer Target inside and Outside the Cell. *Methods Mol. Biol.* **2018**, *1709*, 371–396.
https://doi.org/10.1007/978-1-4939-7477-1_27.
- (71) Oleinikovas, V.; Saladino, G.; Cossins, B. P.; Gervasio, F. L. Understanding Cryptic Pocket Formation in Protein Targets by Enhanced Sampling Simulations. **2016**. <https://doi.org/10.1021/jacs.6b05425>.
- (72) Amaro, R. E. Will the Real Cryptic Pocket Please Stand Out? *Biophys. J.* **2019**, *116* (5), 753–754. <https://doi.org/10.1016/j.bpj.2019.01.018>.
- (73) Cimermancic, P.; Weinkam, P.; Rettenmaier, T. J.; Bichmann, L.; Keedy, D. A.; Woldeyes, R. A.; Schneidman-Duhovny, D.; Demerdash, O. N.; Mitchell, J. C.; Wells, J. A.; Fraser, J. S.; Sali, A. CryptoSite: Expanding the Druggable Proteome by Characterization and Prediction of Cryptic Binding Sites. *J. Mol. Biol.* **2016**, *428* (4), 709–719.
<https://doi.org/10.1016/j.jmb.2016.01.029>.
- (74) Lanman, B. A.; Allen, J. R.; Allen, J. G.; Amegadzie, A. K.; Ashton, K. S.; Booker, S. K.; Chen, J. J.; Chen, N.; Frohn, M. J.; Goodman, G.; Kopecky, D. J.; Liu, L.; Lopez, P.; Low, J. D.; Ma, V.; Minatti, A. E.; Nguyen, T. T.; Nishimura, N.; Pickrell, A. J.; Reed, A. B.; Shin, Y.; Siegmund, A. C.; Tamayo, N. A.; Tegley, C. M.; Walton, M. C.; Wang, H.-L.; Wurz, R. P.; Xue, M.; Yang, K. C.; Achanta, P.; Bartberger, M. D.; Canon, J.; Hollis, L. S.; McCarter, J. D.; Mohr, C.; Rex, K.; Saiki, A. Y.; San Miguel, T.; Volak, L. P.; Wang, K. H.; Whittington, D. A.; Zech, S. G.; Lipford, J. R.; Cee, V. J. Discovery of a Covalent Inhibitor of KRAS^{G12C} (AMG 510) for the Treatment of Solid Tumors. *J. Med. Chem.* **2020**, *63* (1), 52–65. <https://doi.org/10.1021/acs.jmedchem.9b01180>.
- (75) Chavanieu, A.; Pugnière, M. Developments in SPR Fragment Screening. *Expert Opin. Drug Discov.* **2016**, *11* (5), 489–499.

- <https://doi.org/10.1517/17460441.2016.1160888>.
- (76) Thoren, K. The Role of Surface Plasmon Resonance in Clinical Laboratories <https://www.aacc.org/publications/cln/articles/2019/may/the-role-of-surface-plasmon-resonance-in-clinical-laboratories> (accessed Apr 30, 2020).
- (77) Schasfoort, R. B. M. Chapter 1. Introduction to Surface Plasmon Resonance. In *Handbook of Surface Plasmon Resonance*; Royal Society of Chemistry, 2017; pp 1–26. <https://doi.org/10.1039/9781788010283-00001>.
- (78) Surface plasmon resonance <https://www.sprpages.nl/spr-overview/sensor-chips> (accessed Mar 30, 2020).
- (79) Carbodiimide crosslinker chemistry <https://www.thermofisher.com/uk/en/home/life-science/protein-biology/protein-biology-learning-center/protein-biology-resource-library/pierce-protein-methods/carbodiimide-crosslinker-chemistry.html> (accessed Apr 30, 2020).
- (80) Hall, D. R.; Kozakov, D.; Whitty, A.; Vajda, S. Lessons from Hot Spot Analysis for Fragment-Based Drug Discovery Fragment-Based Drug Discovery. *Trends Pharmacol. Sci.* **2015**, *36*, 724–736. <https://doi.org/10.1016/j.tips.2015.08.003>.
- (81) Cyclopropane ring systems <https://www.chem.wisc.edu/areas/reich/nmr/Notes-05-HMR-v26-part2.pdf> (accessed Apr 21, 2020).
- (82) Patil, P.; Madhavachary, R.; Kurpiewska, K.; Kalinowska-Tluscik, J.; Domling, A. De Novo Assembly of Highly Substituted Morpholines and Piperazines. *Org. Lett.* **2017**, *19* (3), 642–645. <https://doi.org/10.1021/acs.orglett.6b03807>.
- (83) Holder, S.; Zulch, A.; Bar, T.; Maier, T.; Zimmermann, A.; Beckers, T.; Gekeler, V.; Joshi, H. Fused Imidazoles for Cancer Treatment. WO 2009/021990 A1, August 14, 2008.
- (84) Barile, E.; Pellecchia, M. NMR-Based Approaches for the Identification and Optimization of Inhibitors of Protein–Protein Interactions. **2014**. <https://doi.org/10.1021/cr500043b>.

- (85) Fleming, I.; Williams, D. *Spectroscopic Methods in Organic Chemistry*; Springer International Publishing, 2019. <https://doi.org/10.1007/978-3-030-18252-6>.
- (86) Ariza-Castolo, A. Beyond Excitation: NMR Relaxation. *Concepts Magn. Reson.* **2008**, *32A* (3), 168–182. <https://doi.org/10.1002/cmr.a>.
- (87) Zartler, E.; Yan, J.; Mo, H.; Kline, A.; Shapiro, M. 1D NMR Methods in Ligand-Receptor Interactions. *Curr. Top. Med. Chem.* **2005**, *3* (1), 25–37. <https://doi.org/10.2174/1568026033392750>.
- (88) Reich, H. J. Relaxation in NMR Spectroscopy <https://www.chem.wisc.edu/areas/reich/nmr/notes-8-tech-1-relax.pdf> (accessed May 8, 2020).
- (89) Ludwig, C.; Guenther, U. L. Ligand Based NMR Methods for Drug Discovery. *Front. Biosci.* **2009**, *14* (12), 4565–4574. <https://doi.org/10.2741/3549>.
- (90) Bowling, J. J.; Shadrick, W. R.; Griffith, E. C.; Lee, R. E. Going Small: Using Biophysical Screening to Implement Fragment Based Drug Discovery. In *Special Topics in Drug Discovery*; InTech, 2016. <https://doi.org/10.5772/66423>.
- (91) Dalvit, C.; Fogliatto, G.; Stewart, A.; Veronesi, M.; Stockman, B. WaterLOGSY as a Method for Primary NMR Screening: Practical Aspects and Range of Applicability. *J. Biomol. NMR* **2001**, *21* (4), 349–359. <https://doi.org/10.1023/A:1013302231549>.
- (92) Zega, A. NMR Methods for Identification of False Positives in Biochemical Screens. *Journal of Medicinal Chemistry*. American Chemical Society December 14, 2017, pp 9437–9447. <https://doi.org/10.1021/acs.jmedchem.6b01520>.
- (93) Parker, C. G.; Galmozzi, A.; Wang, Y.; Correia, B. E.; Sasaki, K.; Joslyn, C. M.; Kim, A. S.; Cavallaro, C. L.; Lawrence, R. M.; Johnson, S. R.; Narvaiza, I.; Saez, E.; Cravatt, B. F. Ligand and Target Discovery by Fragment-Based Screening in Human Cells. *Cell* **2017**, *168* (3), 527–541.e29. <https://doi.org/10.1016/j.cell.2016.12.029>.
- (94) Smith, E.; Collins, I. Photoaffinity Labeling in Target-and Binding-Site Identification. <https://doi.org/10.4155/fmc.14.152>.

- (95) Zhang, Z.; Marshall, A. G. A Universal Algorithm for Fast and Automated Charge State Deconvolution of Electrospray Mass-to-Charge Ratio Spectra. *J. Am. Soc. Mass Spectrom.* **1998**, *9* (3), 225–233. [https://doi.org/10.1016/S1044-0305\(97\)00284-5](https://doi.org/10.1016/S1044-0305(97)00284-5).
- (96) Dundee Proteomics Department <http://proteomics.lifesci.dundee.ac.uk/>.
- (97) Srebalus Barnes, Catherine A. Lim, A. Applications of Mass Spectrometry for the Structural Characterization of Recombinant Protein Pharmaceuticals. *Mass Spectrom. Rev.* **2007**, No. 26, 370–388. <https://doi.org/10.1002/mas>.
- (98) Olsen, J. V; Ong, S.-E.; Mann, M. Trypsin Cleaves Exclusively C-Terminal to Arginine and Lysine Residues* □ S. **2004**. <https://doi.org/10.1074/mcp.T400003-MCP200>.
- (99) Cottrell, J. S. Protein Identification Using MS/MS Data. *J. Proteomics* **2011**, *74*, 1842–1851. <https://doi.org/10.1016/j.jprot.2011.05.014>.
- (100) Fragment Ion Calculator <http://db.systemsbio.net:8080/proteomicsToolkit/FragIonServlet.html>.
- (101) Gimeno, A.; Ojeda-Montes, M.; Tomás-Hernández, S.; Cereto-Massagué, A.; Beltrán-Debón, R.; Mulero, M.; Pujadas, G.; Garcia-Vallvé, S. The Light and Dark Sides of Virtual Screening: What Is There to Know? *Int. J. Mol. Sci.* **2019**, *20* (6), 1375. <https://doi.org/10.3390/ijms20061375>.
- (102) Massey, A. J.; Williamson, D. S.; Browne, H.; Murray, J. B.; Dokurno, P.; Shaw, T.; Macias, A. T.; Daniels, Z.; Geoffroy, S.; Dopson, M.; Lavan, P.; Matassova, N.; Francis, G. L.; Graham, C. J.; Parsons, R.; Wang, Y.; Padfield, A.; Comer, M.; Drysdale, M. J.; Wood, M. A Novel, Small Molecule Inhibitor of Hsc70/Hsp70 Potentiates Hsp90 Inhibitor Induced Apoptosis in HCT116 Colon Carcinoma Cells. *Cancer Chemother. Pharmacol.* **2010**, *66* (3), 535–545. <https://doi.org/10.1007/s00280-009-1194-3>.
- (103) Patrick, G. L. *An Introduction to Medicinal Chemistry*, Fifth.; Oxford University Press, 2013.
- (104) Wermuth, C. G.; Ganellin, C. R.; Lindberg, P.; Mitscher, L. A. Glossary of Terms Used in Medicinal Chemistry. *Pure Appl. Chem.* **1998**, *70* (5).

- (105) Rankin, S. S. Investigation of Compounds Incorporating Ribose Mimics as HSP70 Inhibitors, Institute of Cancer Research, 2016.
- (106) Rohokale, R. S.; Kshirsagar, U. A. Advanced Synthetic Strategies for Constructing Quinazolinone Scaffolds. *Synth.* **2016**, *48* (9), 1253–1268. <https://doi.org/10.1055/s-0035-1560413>.
- (107) Niementowski, S. V. No Title. *J. Fuer Prakt. Chemie* **1895**, *51* (2), 564–572.
- (108) Alexandre, F. R.; Berecibar, A.; Besson, T. Microwave-Assisted Niementowski Reaction. Back to the Roots. *Tetrahedron Lett.* **2002**. [https://doi.org/10.1016/S0040-4039\(02\)00619-6](https://doi.org/10.1016/S0040-4039(02)00619-6).
- (109) Wiemer, A. J.; Wiemer, D. F. Prodrugs of Phosphonates and Phosphates: Crossing the Membrane Barrier. *Top. Curr. Chem.* **2015**, *360*, 115–160. https://doi.org/10.1007/128_2014_561.
- (110) Meanwell, N. A. Synopsis of Some Recent Tactical Application of Bioisosteres in Drug Design. *Journal of Medicinal Chemistry*. April 28, 2011, pp 2529–2591. <https://doi.org/10.1021/jm1013693>.
- (111) Elliott, T. S.; Slowey, A.; Ye, Y.; Conway, S. J. The Use of Phosphate Bioisosteres in Medicinal Chemistry and Chemical Biology. *MedChemComm*. July 2012, pp 735–751. <https://doi.org/10.1039/c2md20079a>.
- (112) Kobayashi, S. Enantioselective Synthesis of Both Diastereomers , Including the α -Alkoxy-P-Hydroxy-P-Methyl (Pheny1) Units , by Chiral Tin (I) Lewis Acid-Mediated Asymmetric Aldol Reactions. **1994**, *50* (32).
- (113) Glomb, M. A.; Pfahler, C. Amides Are Novel Protein Modifications Formed by Physiological Sugars. *J. Biol. Chem.* **2001**, *276* (45), 41638–41647. <https://doi.org/10.1074/jbc.M103557200>.
- (114) Gill, D. M.; Iveson, M.; Collins, I.; Jones, A. M. A Mitsunobu Reaction to Functionalized Cyclic and Bicyclic N-Arylamines. *Tetrahedron Lett.* **2018**, *59*, 238–242. <https://doi.org/10.1016/j.tetlet.2017.12.017>.
- (115) Cramer, J.; Sager, C. P.; Ernst, B. Hydroxyl Groups in Synthetic and Natural-Product-Derived Therapeutics: A Perspective on a Common Functional Group. *J. Med. Chem.* **2019**, *62* (20), 8915–8930.

- <https://doi.org/10.1021/acs.jmedchem.9b00179>.
- (116) Waring, M. J. Lipophilicity in Drug Discovery. *Expert Opinion on Drug Discovery*. Taylor & Francis March 2010, pp 235–248.
<https://doi.org/10.1517/17460441003605098>.
- (117) Laurence, C.; Brameld, K. A.; Er[^] Ome Graton, J.; Le Questel, J.-Y.; Renault, E. The PK BHX Database: Toward a Better Understanding of Hydrogen-Bond Basicity for Medicinal Chemists. *J. Med. Chem* **2009**, *52*, 4073. <https://doi.org/10.1021/jm801331y>.
- (118) Rye, C.; Baell, J. Phosphate Isosteres in Medicinal Chemistry. *Curr. Med. Chem.* **2005**, *12* (26), 3127–3141.
<https://doi.org/10.2174/092986705774933452>.
- (119) Chang, C. A.; Chen, W.; Gilson, M. K. Ligand Configurational Entropy and Protein Binding. *Proc. Natl. Acad. Sci. U. S. A.* **2007**, *104* (5), 1534–1539. <https://doi.org/10.1073/pnas.0610494104>.
- (120) Steiner, M. A.; Gatfield, J.; Brisbare-Roch, C.; Dietrich, H.; Treiber, A.; Jenck, F.; Boss, C. Discovery and Characterization of ACT-335827, an Orally Available, Brain Penetrant Orexin Receptor Type1 Selective Antagonist. *ChemMedChem* **2013**, *8* (6), 898–903.
<https://doi.org/10.1002/cmdc.201300003>.
- (121) Mecinović, J.; Loenarz, C.; Chowdhury, R.; Schofield, C. J. 2-Oxoglutarate Analogue Inhibitors of Prolyl Hydroxylase Domain 2. *Bioorganic Med. Chem. Lett.* **2009**, *19* (21), 6192–6195.
<https://doi.org/10.1016/j.bmcl.2009.09.005>.
- (122) Arasappan, A.; Njoroge, George, F.; Kwong, Cecil, D. Substituted Pyridine and Pyrimidine Derivatives and Their Use in Treating Viral Infections. WO 2011/103441 A1, 2011.
- (123) Du, X.; Li, Y.; Xia, Y.-L.; Ai, S.-M.; Liang, J.; Sang, P.; Ji, X.-L.; Liu, S.-Q. Insights into Protein-Ligand Interactions: Mechanisms, Models, and Methods. *Int. J. Mol. Sci.* **2016**, *17* (144).
<https://doi.org/10.3390/ijms17020144>.
- (124) Lepori, L. Group Contributions to the Thermodynamic Properties of Non-Ionic Organic Solutes in Dilute Aqueous Solution Sergio Cabani , 1 Paolo Gianni , 1 Vincenzo. **1981**, *10* (8), 563–595.

- (125) Dominelli-Whiteley, N.; Brown, J. J.; Muchowska, K. B.; Mati, I. K.; Adam, C.; Hubbard, T. A.; Elmi, A.; Brown, A. J.; Bell, I. A. W.; Cockroft, S. L. Strong Short-Range Cooperativity in Hydrogen-Bond Chains. *Angew. Chemie Int. Ed.* **2017**, *56* (26), 7658–7662.
<https://doi.org/10.1002/anie.201703757>.
- (126) Morphy, J. R.; Harris, C. J. *Designing Multi-Target Drugs*; RSC Publishing, 2012.
- (127) Wissner, A.; Berger, D. M.; Boschelli, D. H.; Floyd, M. B.; Greenberger, L. M.; Gruber, B. C.; Johnson, B. D.; Mamuya, N.; Nilakantan, R.; Reich, M. F.; Shen, R.; Tsou, H.-R.; Upešlacis, E.; Wang, Y. F.; Wu, B.; Ye, F.; Zhang, N. 4-Anilino-6,7-Dialkoxyquinoline-3-Carbonitrile Inhibitors of Epidermal Growth Factor Receptor Kinase and Their Bioisosteric Relationship to the 4-Anilino-6,7-Dialkoxyquinazoline Inhibitors. **2000**.
<https://doi.org/10.1021/jm000206a>.
- (128) Meanwell, N. A. Fluorine and Fluorinated Motifs in the Design and Application of Bioisosteres for Drug Design. **2018**.
<https://doi.org/10.1021/acs.jmedchem.7b01788>.
- (129) Kilbourn, M. R. *Thiophenes as Phenyl Bio-Isosteres: Application in Radiopharmaceutical Design-I. Dopamine Uptake Antagonists*; 1989; Vol. 16.
- (130) Nara, H.; Kaieda, A.; Sato, K.; Naito, T.; Mototani, H.; Oki, H.; Yamamoto, Y.; Kuno, H.; Santou, T.; Kanzaki, N.; Terauchi, J.; Uchikawa, O.; Kori, M. Discovery of Novel, Highly Potent, and Selective Matrix Metalloproteinase (MMP)-13 Inhibitors with a 1,2,4-Triazol-3-Yl Moiety as a Zinc Binding Group Using a Structure-Based Design Approach. *J. Med. Chem.* **2017**, *60* (2), 608–626.
<https://doi.org/10.1021/acs.jmedchem.6b01007>.
- (131) Jonathan Clayden, N. G. and S. W. *Organic Chemistry*, 2012.
- (132) Pilcher, A. S.; Ammon, H. L.; DeShong, P. *Ppm*-19.6 ($Aí-f = 250$ Hz); *29Si NMR (CDCl3)*; UTC, 1995; Vol. 117.
- (133) Kan, X.; Liu, H.; Pan, Q.; Li, Z.; Zhao, Y. Anion- π Interactions: From Concept to Application. *Chinese Chem. Lett.* **2018**, *29* (2), 261–266.
<https://doi.org/10.1016/j.ccllet.2017.08.042>.

- (134) Gutiérrez Sanfeliciano, S. M.; Schaus, J. M. Rapid Assessment of Conformational Preferences in Biaryl and Aryl Carbonyl Fragments. *PLoS One* **2018**, *13* (3), e0192974. <https://doi.org/10.1371/journal.pone.0192974>.
- (135) Knapp, D. M.; Gillis, E. P.; Burke, M. D. A General Solution for Unstable Boronic Acids: Slow-Release Cross-Coupling from Air-Stable MIDA Boronates. <https://doi.org/10.1021/ja901416p>.
- (136) Cox, P. A.; Reid, M.; Leach, A. G.; Campbell, A. D.; King, E. J.; Lloyd-Jones, G. C. Base-Catalyzed Aryl-B(OH) 2 Protodeboronation Revisited: From Concerted Proton Transfer to Liberation of a Transient Aryl Anion. **2017**. <https://doi.org/10.1021/jacs.7b07444>.
- (137) Bellenie, B. R.; Barton, N. P.; Emmons, A. J.; Heer, J. P.; Salvagno, C. Discovery and Optimization of Highly Ligand-Efficient Oxytocin Receptor Antagonists Using Structure-Based Drug Design. *Bioorganic Med. Chem. Lett.* **2009**, *19* (3), 990–994. <https://doi.org/10.1016/j.bmcl.2008.11.064>.
- (138) Liquids, A. I.; Bian, C. Anion-Functionalized Ionic Liquids Enhance the CuI-Catalyzed Cross-Coupling Reaction of Sulfinic Acid Salts with Aryl Halides and Vinyl Bromides. **2007**, No. 19, 2951–2956. <https://doi.org/10.1055/s-2007-990778>.
- (139) Hansen, S. V. F.; Ulven, T. Oxalyl Chloride as a Practical Carbon Monoxide Source for Carbonylation Reactions. *Org. Lett.* **2015**, *17*, 54. <https://doi.org/10.1021/acs.orglett.5b01252>.
- (140) Bissantz, C.; Kuhn, B.; Stahl, M. A Medicinal Chemist's Guide to Molecular Interactions. *J. Med. Chem.* **2010**, *53*, 5061. <https://doi.org/10.1021/jm100112j>.
- (141) Ge, X.; Sun, F.; Liu, X.; Chen, X.; Qian, C.; Zhou, S. Mechanistic Aspects of Copper (II)-Catalyzed Synthesis of Sulfones from Sulfinic Salts and Aryl Halides under C-S Coupling. *Mol. Catal.* **2018**, *449*, 72–78. <https://doi.org/10.1016/j.mcat.2017.12.016>.
- (142) Bhatt, S.; Nayak, S. K. A Facile and Catalytic Method for Selective Deprotection of Tert-Butyldimethylsilyl Ethers with Copper(II) Bromide. *Tetrahedron Lett.* **2006**, *47* (47), 8395–8399.

- <https://doi.org/10.1016/j.tetlet.2006.09.073>.
- (143) Tan, Z. P.; Wang, L.; Wang, J. B. <TANG_CCL.Pdf>. **2000**, *11* (9), 753–756.
- (144) Singh, J. The Resurgence of Covalent Drugs. **2011**.
<https://doi.org/10.1038/nrd3410>.
- (145) Liu, J.; Liu, J.; Guo, S.-Y.; Liu, H.-L.; Li, S.-Z. HSP70 Inhibitor Combined with Cisplatin Suppresses the Cervical Cancer Proliferation in Vitro and Transplanted Tumor Growth: An Experimental Study. *Asian Pac. J. Trop. Med.* **2017**, *10* (2), 184–188. <https://doi.org/10.1016/j.apjtm.2017.01.020>.